

STABILITY OF EXCAVATIONS AND DESIGN OF MINING

LAYOUTS IN A DEEP LEVEL POTASH MINE

A THESIS

SUBMITTED FOR THE DEGREE OF DOCTOR OF PHILOSOPHY

in the

UNIVERSITY OF NEWCASTLE UPON TYNE

by

H.D.S. MILLER B.Sc., (Wales)

July 1980

NEWCASTLE UPON TYNE UNIVERSITY LIBRARY
ACCESSION No. 31-14114
LOCATION 71

NR

BEST COPY

AVAILABLE

Poor text in the original
thesis.

CONTENTS

Page No.

CHAPTER ONE

Introduction

1.0 Introduction	1
------------------	---

CHAPTER TWO

Geology of Evaporite Deposits with Special Reference to

Boulby Mine Geology

2.0 Geology	5
2.1 Evaporite Deposits	5
2.2 Potash Deposits	7
2.2.1 North Yorkshire Potash	8
2.3 The Geological Succession, Boulby Mine	11
2.3.1 Bunter Sandstone	14
2.3.2 The Upper Evaporites	14
2.3.3 The Carnallite Marl	15
2.3.4 The Potash Seam	15
2.3.5 The Strata Below the Potash Seam	18

CHAPTER THREE

Development of Production Panels and Layouts

3.0 Boulby Mine	19
3.1 Development of Panel Layout and Mining Method	20
3.2 Production Analysis	22
3.3 Results	23

	<u>Page No.</u>
3.3.1 East Panel and South Development	23
3.3.2 No. 1 Panel	28
3.3.3 No. 2 Panel	33
3.3.4 No. 7 Panel	38
3.3.5 No. 4 Panel	39
3.3.6 The Experimental Panel, No. 6 Panel	40
3.3.7 No. 8 Panel	45
3.3.8 Nos. 15 and 16 Panels	48
3.3.9 No. 10 Panel	50
3.3.10 No. 17 Panel	52
3.3.11 No. 19 Panel	53
3.4 Concluding Remarks	55

CHAPTER FOUR

Review of Work Concerned with Rocks Exhibiting Time

Dependent Properties

4.0 Introduction	56
4.1 Terminology	57
4.2 Creep and Creep Constitutive Models	59
4.3 General Creep Equation	64
4.4 Effect of Stress on Creep Rate	68
4.5 Applications to Excavations in Potash	68
4.5.1 Serata	68
4.5.2 Baar	73
4.5.3 Mraz	78
4.5.4 Comments	83

CHAPTER FIVE

Factors which Adversely Affect Panel Design and Layouts

5.0	Introduction	91
5.1	The Highly Variable Geology	91
5.2	The Gas Outburst Problem	96
5.3	The Water Problem	103
5.4	Concluding Remarks	106

CHAPTER SIX

Low and High Panels and Analysis of Underground Measurements

6.0	Introduction	108
6.1	Low Extraction Panels	108
6.2	High Extraction Panels	115
6.3	The Analysis of Closure Data	119
6.4	No. 8 Panel	121
6.4.1	Closure Measurements	121
6.4.2	Extensometer Measurements	126
6.5	No. 10 Panel	135
6.5.1	Closure Measurements - No. 10 Panel, A section	135
6.5.2	Microscreep Measurements - No. 10 Panel, A section	140
6.5.3	Extensometer Sites - No. 10 Panel, B section	140
6.5.4	Closure Measurements - No. 10 Panel, B section	160
6.5.5	Microcreep Measurements - No. 10 Panel, B section	163
6.6	No. 12 Panel	164

Page No.

6.6.1	Closure Measurements	166
6.6.2	Microcreep Measurements	169
6.7	No. 15 Panel	171
6.7.1	Closure Measurements - No. 15 Panel, A section, 'A' sites	171
6.7.2	Closure Measurements - B section, 'B' sites	172
6.7.3	Extensometer Sites - No. 15 Panel, B section	179
6.8	No. 16 Panel	186
6.9	No. 19 Panel	201
6.9.1	Closure Measurements	201
6.9.2	Microcreep Measurements	219
6.10	Concluding Remarks	219

CHAPTER SEVEN

The Use of Rocksalt and Saltcrete as a Fill Material

7.0	Introduction	220
7.1	Uncemented Fill - Laboratory Trials	220
7.1.1	Width to Height Ratio	223
7.1.2	Particle Size	224
7.1.3	Temperature	224
7.1.4	Water Content	224
7.1.5	Initial Density of Compaction	225
7.1.6	Conclusion on Uncemented Rocksalt Fill	227
7.1.7	Surface Trials using the Markham Stower	228
7.2	Saltcrete	229
7.2.1	Size Analysis of r.o.m. Rocksalt	229

	<u>Page No.</u>
7.2.2 Preparation of Specimens	229
7.2.3 Laboratory Testing	231
7.2.3.1 Variation of strength with time	232
7.2.3.2 Effect of varying the cement content	233
7.2.3.3 Effect of varying the particle size on the strength	234
7.2.3.4 Effect of varying the compaction	235
7.2.3.5 Effect on strength of varying the water/ cement ratio	237
7.2.3.6 Modulus of elasticity	238
7.2.3.7 Effect on tensile strength	238
7.2.3.8 Mohr envelope	241
7.2.3.9 Time dependent behaviour	241
7.2.3.10 Effect of water on saltcrete	243
7.3 Summary of Conclusions	245
7.3.1 Uncemented Fill	245
7.3.2 Cemented Fill	245

CHAPTER EIGHT

Laboratory Testing and Thin Section Analysis

8.0 Introduction	247
8.1 Test Specimens and Procedure	247
8.2 Results	250
8.3 Upper Halite Results and Thin Section Analysis	252
8.4 Summary of Conclusions	270

CHAPTER NINE

Conclusions Drawn from Results of Measurements and Proposed
High Extraction Panel Deformation Model

9.0	Introduction	271
9.1	The Proposed Model	271
9.1.1	Mechanism of Plastic Flow of Roof Rock	273
9.1.2	The Mechanism of the Deformation of the Upper Anhydrite	275
9.1.3	Combined Mechanism of Panel Deformation	276
9.1.4	Change of Slope of Strain/Convergence Rate Curves	279
9.1.5	The Upper Anhydrite as an Elastic Plate	281
9.1.6	Deformation with Distance Mined	284
9.1.7	The Stability of Yield Pillars	286
9.1.8	The Water Problem	287
9.2	Summary of Conclusions	288

CHAPTER TEN

Panel Design and Layout

10.0	Introduction	291
10.1	The Concept of Stability	292
10.1.1	Roadway Stability Criterion	293
10.1.2	Pillar Stability Criterion	298
10.2	The Design of a Stable Standard High Extraction Panel Layout	299

	<u>Page No.</u>	
10.3	Monitoring of No.15 Panel (B Section) Performance	310
10.3.1	Site 17 15 B, BH2 and BH3	310
10.3.2	Site H15B, BH 03	313
10.3.3	Site H15B, BH 01	317
10.3.4	Site H15B, BH 02	317
10.4	Discussion of Pillar Extensometer Results	322
10.5	Photography as a Monitoring Aid	324
10.6	Finite Element Analysis	324
10.6.1	Results of Finite Element Analysis	326
10.6.2	General Comments on Finite Element Analysis	331
10.7	Stress Relief vs. High Extraction	331
10.8	Conclusions and Recommendations for Mining	332
10.9	Recommendations for Rock Mechanics Investigations and Monitoring	333
10.10	Concluding Remarks	334

LIST OF FIGURES

Figure No.		Page No.
2.1	Generalised Sequence of Evaporite Deposition	6
2.2	Location of Deep Exploration Boreholes	10
2.3	General Geological Succession, Boulby Mine	12
2.4	Near Seam Geological Succession	16
2.5	Ore Type Classification	17
3.1	Production Layouts	21
3.2	South Development Layout and Results	25
3.3	Strain Rates between J and H Roadways	27
3.4	Log Strain Rate vs. Time, 40m Potash and Salt Pillars	27
3.5	Gas Blow Zone - South Development	29
3.6	Pillar Extensometers, East Panel	31
3.7	Roof Extensometer, East Panel	32
3.8	Pillar Extensometer, No.2 Panel	35
3.9	Roof Extensometer, No.2 Panel, BH05	36
3.10	Roof Extensometer, No.2 Panel, BH02	37
3.11	Roof Deformation over Narrow Section of No.2 Panel	37
3.12	No.6 Panel Instrumentation Sites	42
3.13	Strain Rate vs. Time Curve for 25,30 and 40m Pillars	42

Figure No.		Page No.
3.14	Geological Sections, Sites H15 and H16	43
3.15	No.19 Panel Designed and Actual Layouts	54
4.1	Rheological Constitutive Model - Serata	69
4.2	Stress Relief - Serata	71
4.3	Parallel Room Method - Serata	72
4.4	Time Control Method - Serata	74
4.5	Stress Relief - Baar	77
4.6	Geological Successive - Rocanville	84
4.7	Typical Strain vs. Distance into Pillar - Boulby Mine	87
4.8	Stress vs. Distance into Pillar, IMC	87
5.1	Geological Sections showing Stratigraphic Variability	92
5.2	Plan showing Longhole Intersections	93
5.3	Plan showing Location of Gas Blows	98
5.4	Plan of No.2 Panel - Gas Blows	100
5.5	Relationship between Outburst Tonnages and Roadway Width	101
5.6	Monthly Production tonnes	103
5.7	Plan showing Water Sites	105
5.8	Plan showing Overfold Zone	106

Figure No.		Page No.
6.1	Mohr's Envelope for Potash	111
6.2	Plan of Mine showing High Extraction Panels	118
6.3	No.8 Panel, Instrumentation Sites	122
6.4	No.8 Panel, Roadway Closure	125
6.5	No.8 Panel, RA1 Sidewall Extensometer Site	127
6.6	Site H13 Pillar Extensometers 30m Pillar	128
6.7	No.8 Panel, Site RCA4 Pillar Extensometer	130
6.8	No.8 Panel, Site RC6 Pillar Extensometer	131
6.9	No.10 Panel, Instrumentation Sites	136
6.10	No.10 Panel, Closure and Closure Rates	136
6.11	Geological Sections at C43E and C43B	139
6.12	No.10 Panel, Section A Microcreep	142
6.13	No.10 Panel, Site CEA BH1	144
6.14	No.10 Panel, Site CEA BH2	147
6.15	No.10 Panel, CEA BH4	149
6.16	No.10 Panel, CFA BH1	151
6.17	No.10 Panel, CFA BH2	152
6.18	No.10 Panel, CGA BH1	155
6.19	No.10 Panel, CGA BH3	157
6.20	No.10 Panel, CGA BH03	159
6.21	No.10 Panel, GHA BH02	161
6.22	No.12 Panel, Instrumentation Sites	165
6.23	No.12 Panel, Convergence Results	168
6.24	No.12 Panel, Roof Deformation	170
6.25	No.15 Panel, Instrumentation Sites	171

Figure No.		Page No.
6.26	No.15 Panel, A Section - Convergence Graphs	173
6.27	No.15 Panel, A Section - Convergence Rate	175
6.28	No.15 Panel, Closure and Closure Rates	178
6.29	No.15 Panel, B Section - Convergence	180
6.30	No.15 Panel, B Section - Convergence Rate	182
6.31	No.15 Panel, Convergence and Convergence Rates	185
6.32	No.16 Panel, Sites and Convergence Graphs	187
6.33	No.16 Panel, Closure Profiles	199
6.34	No.16 Panel, Site K16A Marl Exposure	200
6.35	No.19 Panel, Instrumentation Sites	202
6.36	No.19 Panel, Convergence and Convergence rates	204
6.37	No.19 Panel, Convergence Graphs	206
6.38	No.19 Panel, Microcreep and Closure Rates	218
7.0	Reduction in Roadway Area with Time	223
7.1	Effect of Initial Compaction on Fill Properties	226
7.2	Effect of Variation in Curing Time on Saltcrete	231
7.3	Saltcrete Compressive Strength vs. Curing Time	232
7.4	Saltcrete-Cement Content vs. Strength	233
7.5	Increase in Density vs. Cement Content	234
7.6	Particle Size vs. Strength	235
7.7	Compaction vs. Strength	236
7.8	Compaction vs. Increase in Density	236
7.9	Water/Cement Ratio vs. Strength	237

Figure No.		Page No.
7.10	Mohr Envelope	241
7.11	Creep Test	242
7.12	Water Immersion Results	243
8.1	Load at 20% Strain vs. Log of Strain Rate for Different W:H Ratios	250
8.2	Stress vs. Log of Strain Rate	251
8.3	Orientation of Salt Cubes Relative to Borehole Core	252
9.1	Section Through No.10 Panel	272
9.2	Distribution of Stresses Along a Beam	274
9.3	Deformation vs. Distance into Ribside	274
9.4	Mechanism of Panel Deformation	277
9.5	Log of Strain Rate vs. Time	279
9.6	No.10 Panel, A Section Closure Rates	280
9.7	Sub-critical and Critical Panel Widths	283
9.8	Mechanism of Deformation Along a Panel	285
10.1	Change in Roadway Area with Time	295
10.2	Distribution of Strain in 30m Pillars	300
10.3	Panel Layouts With and Without Stubs	303
10.4	Split panel Layout	304
10.5	Load Redistribution Around a Split Panel	305

Figure No.		Page No.
10.6	Relationship of B/W to R_B/R_A for Different Extraction Ratios	308
10.7	No.15 Split Panel Layout	309
10.8	Site 17 15 B Extensometer Results	311
10.9	Instrumentation Layout at H 15 B	314
10.10	Site H 15 B Pillar Extensometer Results	315
10.11	Site H 15 B Roof Extensometer Results	318
10.12	Site H 15 B, 45° Degree Hole, Extensometer Results	320
10.13	Deformation into the Roadway at H 15 B	323
10.14	Change in Vertical Stress	327
10.15	Change in Horizontal Stress	328
10.16	Change in Deviator Stress	329

LIST OF TABLES

Table No.		Page No.
2.1	World Potash Supply	7
2.2	Exploration Borehole Results	13
3.1	Production Analysis	22
3.2	Manning Levels	24
3.3	% Roof Sag Due to Strata Movement	44
4.1	Primary Creep Constitutive Equations	66
4.2	Secondary Creep Constitutive Equations	67
4.3	Closure Distribution in Pillar	80
4.4	Pressure Distribution in Pillar	82
4.5	Limit of Elastic Behaviour of Rock Salt	89
5.1	Summary of Near Seam Mechanical Properties	95
5.2	Mean Values Obtained for Mechanical Parameters of Middle Potash Rocks	96
5.3	Gas Analysis and Size of Gas Blows	99
5.4	Water Inflow Sites	104
6.1	Low Extraction Panels	110
6.2	High Extraction Panels	117
6.3	No.8 Panel Closure Data	123

Table No.		Page No.
6.4	No.8 Panel, Extensometer Data	133
6.5	No.10 Panel, Closure and Closure Rates	137
6.6	No.10 Panel, Microcreep Data	141
6.7	Closure Data, No.10 Panel B Section	163
6.8	Microcreep Data, No.10 Panel B Section	164
6.9	No.12 Panel, Closure and Closure Rates	167
6.10	No.15 Panel, A Section, Closure and Closure Rates	177
6.11	No.15 Panel, B Section, Closure and Closure Rates	184
6.12	No.16 Panel, Closure and Closure Rates	198
6.13	No.19 Panel, Closure and Closure Rates	203
7.1	% Volume Rock Salt Tests	222
7.2	Size Analysis of R.O.M. Rock Salt	230
7.3	Modulii of Elasticity, Saltcrete	239
7.4	Tensile Strengths, Saltcrete Specimens	240
7.5	Mechanical Properties, Near Seam Rocks, Boulby Mine	240
7.6	Effect of Water on Saltcrete Specimens	244
8.1	Test Specimens and Results	249
8.2	Grain and Fracture Spacings - Thin Sections	255
8.3	Recalculated Spacings	256

Table No.		Page No.
8.4	Orientations of Fracture Planes	258
9.1	Average Initial 20 Day Closure Rates	278
10.1	Relationship Between Change in Roadway Area and Time for Various Sites	296
10.2	Time to 10% and 20% Area Closure for Various High Extraction Panels	297
10.3	Classification of Pillar Stability	299
10.4	Rock Strength Parameters for Finite Element Model	325

LIST OF APPENDICES

- APPENDIX 1 Mining Layouts
- APPENDIX 2 Gammatrol Portable Potash Assaying Equipment
- APPENDIX 3 Summary of Results of Laboratory Testing of
Potash and Near-Seam Rocks, Boulby Mine
- APPENDIX 4 Constant Deformation Rate Test Results on
Salt and Potash
- APPENDIX 5 Finite Element Contour Plots
- APPENDIX 6 Weekly Face Advances

ACKNOWLEDGEMENTS

The writer wishes to express his thanks to:

- Professor E.L.J. Potts for introducing him to evaporite mining and the Boulby Project, and for his subsequent guidance and assistance.

- The Management of Cleveland Potash Ltd. for making the project possible and for providing the necessary funding. A special thanks here to Messrs. R.A. Pettit, H.J. Head, P. Squirrel and P. Green for their most valuable co-operation at and in the mine.

- Mr. Tom Shepherdson and all the members of the Technical staff in the Mining Engineering department for their willingness to help whenever it was required. A sincere word of praise is due to Mr. M. Paisley for his truly professional photography.

- Post graduate students, Mr. P. Ashworth and Mr. G. Evans for doing much of the donkey work.

- A special note of appreciation to Mrs. R. Lose and Miss S. Cree for their hard work during and after hours in getting the typing done.

- Last but not least, the writer wishes to acknowledge the devoted support of his wife and three daughters, particularly during the final two months.

CHAPTER ONE

INTRODUCTION

CHAPTER ONE

1. Introduction

The shafts at Boulby Potash Mine were sunk between 1969 and 1974 and the first potash was put through the processing plant in 1973. The decision to mine the deposit was based on the results obtained from fifteen exploration boreholes put down from surface. Since the first potash was mined, the mine has been faced with a number of problems. Many of these result from the seam and near seam geology which has turned out to be far more variable over short distances than was at first anticipated. Not only has the thickness and strength of the ore itself varied considerably, but also the proximity to, and thickness of, the overlying shale and marl formations. These latter two play a vital role in the stability or otherwise of the immediate roof of the rooms and roadways. The combination of the above factors has made it very difficult to maintain long term roadways in potash. Due to the cost and other short term disadvantages of driving development roadways in halite beneath the potash seam, alternatives in the form of "stress relief" and high extraction development in potash have been implemented.

Perhaps the most significant single factor hindering high production rates has been the occurrence of "gas blows" when mining in secondary potash ore. This is a shaley ore which occurs widely throughout the mine often containing relatively high grade potash. Unfortunately, apart from being of a lower strength and exhibiting higher creep rates than primary ore, secondary potash has associated with it lenticular shale inclusions containing gas, possibly adsorbed,

which when mined near to, or into, gives rise to a fairly rapid and sometimes violent release of pressure. This has resulted on occasion in damage to the excavations and injury to personnel. The introduction of mechanised mining techniques has meant that mining personnel are constantly exposed to the hazard, as opposed to the situation when the rooms were driven by drilling and blasting. As a result of these difficulties, the Mining Inspectorate have imposed severe restrictions that result in frequent halts to carry out cover drilling and to install support.

These constraints, in addition to the highly variable geology, have made it extremely difficult for the mine management to optimise production from regular layouts or to use the mechanical equipment in the best possible way. Production in shaley ore which at present accounts for 75% of the mine's production has to be sequenced in the operations of drilling and blasting, loading and profiling the rooms, installing support and finally probe drilling. The loading and profiling is carried out by the Heliminer mechanical miners, a function for which the machine was not strictly designed. This has meant that a minimum of three headings, but preferably four, is required for a viable production unit. Concentrated mining layouts in the form of high extraction panels have therefore become more attractive, regardless of other considerations.

This thesis looks at the geology, both anticipated and actual, and the mining layouts adopted. Comparisons are made of the production achievements from the various layouts. The stability of

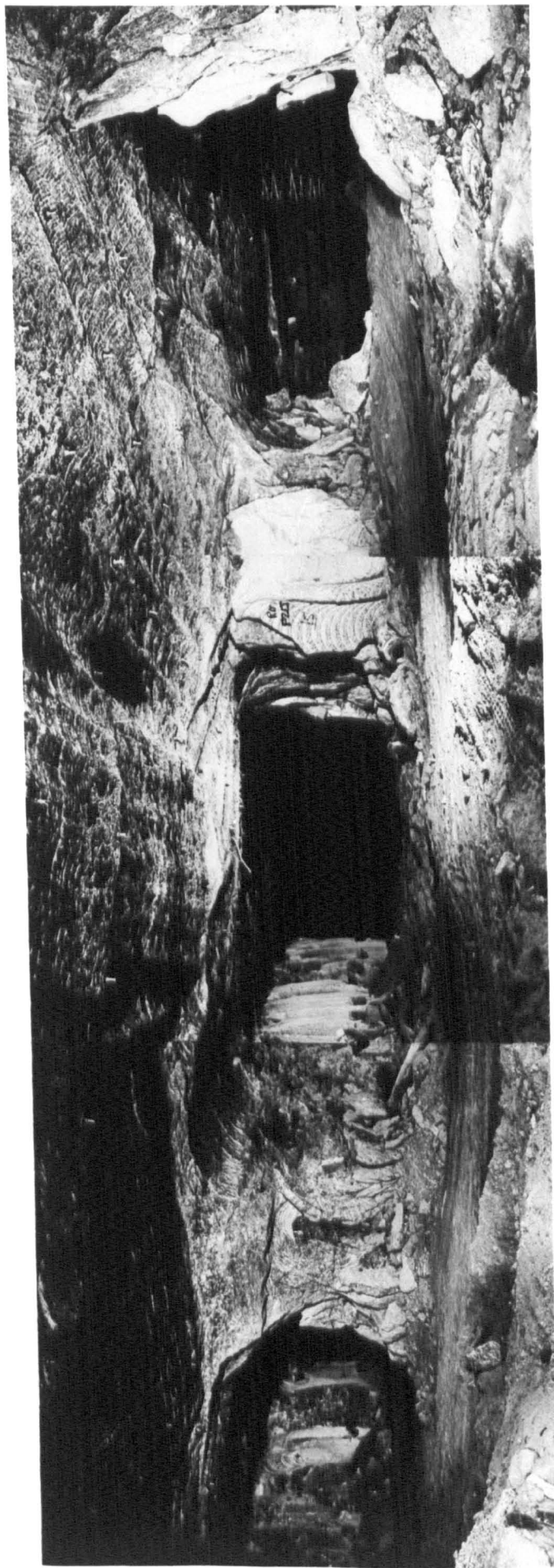


PLATE 1 NO. 22 HIGH EXTRACTION PANEL.

excavations in both salt and potash, including roadways, panels and pillars is investigated and the mode of failure in and around these excavations is examined. The instrumentation used to measure deformations is discussed together with the relative merits of the different instrumentation types and the resulting measured data. The gas blow problem and the difficulties that arise from it are described. At one stage it was felt that the salt derived from the mining of salt roadways could be utilised as a fill material to stabilise potash excavations in areas where the potash seam thickened. The properties of salt as a fill material have been examined in the laboratory. In addition, results from tests on saltcrete samples where cement has been added to improve the early strength characteristics of the fill, are also given.

Laboratory trials were carried out on potash and near seam rocks in order to determine the behaviour of pillars of various sizes under different loading conditions.

Thin sections were made of salt and potash rock samples strained to different amounts at various orientations, and the effect of anisotropy observed. A full description of these results is given and the possible practical significance discussed.

Finally, an attempt is made to describe the mechanism of move-

ment around the high extraction panels which in some instances has led to water entering the mine workings.

CHAPTER TWO

GEOLOGY OF EVAPORITE DEPOSITS WITH SPECIAL REFERENCE TO BOULBY MINE

GEOLOGY

CHAPTER TWO

2.0 Geology

2.1 Evaporite Deposits

Evaporite deposits are those deposits formed by the evaporation of seawater, and depositional phases occurred from Cambrian times through to the present. Deposits are currently accumulating in such areas as Hungary, Israel, Turkey and Central Asia in the northern hemisphere, and Argentina, Southern Africa and Australia, in the southern hemisphere⁽¹⁾.

Both the deposition and the distribution of different minerals within an evaporite succession depend primarily on the climatic conditions prevailing at the time of deposition. The repetitive occurrences of similar mineral beds are termed rhythm, and may be small or large scale, the latter probably being due to earth movements, rather than seasonal variations in temperature and rainfall. The precise nature of evaporite deposition appears to be extremely complex and many geologists have spent much time in trying to analyse and interpret the evidence presented by the numerous evaporite deposits exposed by mining and exploration drilling. An extensive bibliography of relevant authors is given by Borchert and Muir⁽¹⁾ and Baar⁽²⁾. A very generalised sequence of deposition would appear to be that given in Figure 2.1, with the possible occurrence of gypsum and limestone as indicated. Gradation from one bed to another is very common.

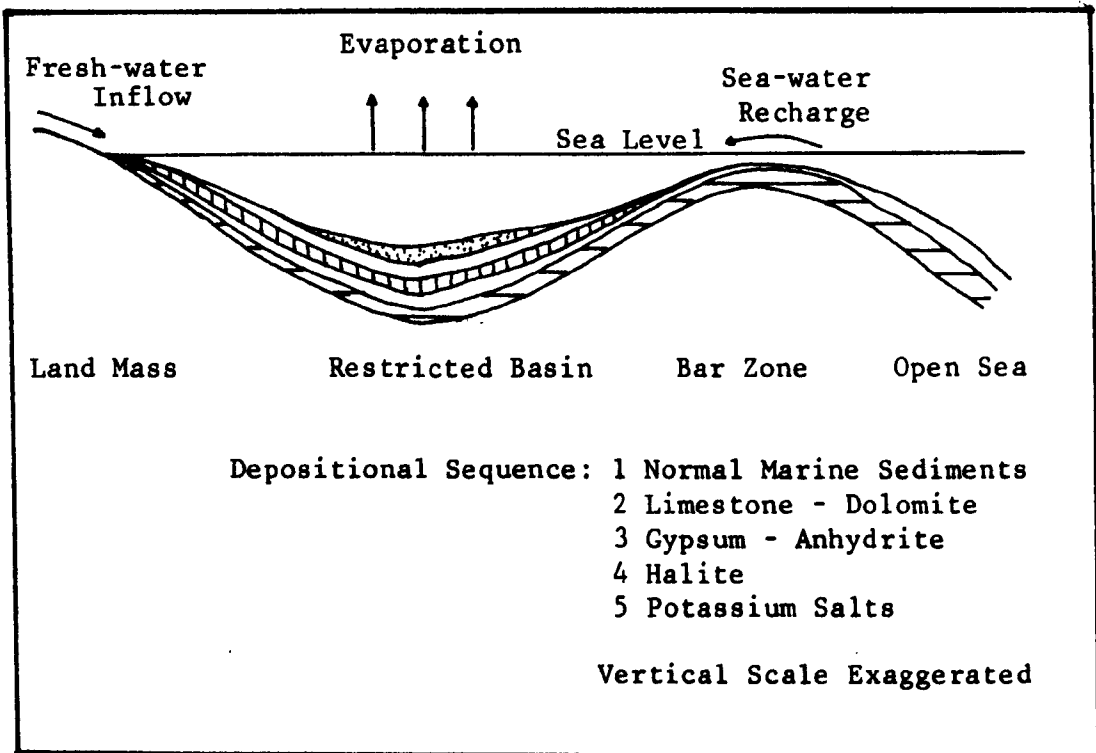


Figure 2.1 Generalised sequence of evaporite deposition

The most commonly occurring of the evaporite salts, excluding dolomite and magnesite, which are not normally regarded as evaporite minerals, despite the fact that they must often have precipitated as a result of the evaporation of seawater, are gypsum ($\text{CaSO}_4 \cdot 2\text{H}_2\text{O}$) and anhydrite (CaSO_4). Next in order of abundance comes halite (NaCl), often known as rock salt or common salt. The potash salts are much scarcer, the most important among this group being sylvite (KCl), carnallite ($\text{KCl} \cdot \text{MgCl}_2 \cdot 6\text{H}_2\text{O}$), langbeinite ($\text{K}_2\text{SO}_4 \cdot 2\text{MgSO}_4$) and kainite ($4\text{KCl} \cdot 4\text{MgSO}_4 \cdot 11\text{H}_2\text{O}$). Other magnesium salts, particularly the sulphates kieserite, epsomite, etc., often occur in association with potash salts.

An association of minerals which have formed together is known

as a paragenesis, and such an association is named by arranging the constituent minerals in order of abundance, e.g. Halite-carnallite. Two sylvite parageneses are sufficiently common and important to have been given separate and unique names. An association of sylvite and halite is known as sylvinite and that of sylvite in combination with anhydrite and/or kieserite is termed hartsaltz.

2.2 Potash Deposits

Potash is mined in the U.S.S.R., North America, the Middle East and Europe. The largest single producer outside of the U.S.S.R. is Canada, where the huge deposits of the Middle Devonian Prairie Evaporites are being exploited by nine major mining operations in the province of Saskatchewan⁽³⁾. The latest available figures on world potash production are given in Table 2.1.

TABLE 2.1

World Potash Supply

(Millions Short Tons K₂O)

	1979	1980	1985
U.S.S.R.	10.8	14.0	16.0
U.S.A. and Canada	9.8	10.5	12.5
Western Europe	6.8	7.8	8.0
Eastern Europe	3.7	3.9	4.3
Other (Mainly Israel)	1.2	1.4	2.4

Source: Engineering & Mining Journal, March 1980

2.2.1 North Yorkshire Potash

The description by Hebblethwaite and Woods⁽⁹⁾⁽⁶⁾ of the Boulby succession is given in full as it is felt that this could not be bettered, as they are both geologists working at Boulby Mine.

"The formation of evaporite deposits and the processes by which their original character can become severely modified have been outlined. Their relative significance in any assessment of the composition and structure of the Boulby evaporite succession is obviously of tremendous importance, not only to the incidence of gas bearing strata, but to an understanding of the nature of the deposit. The following geological model is offered as a contribution to the knowledge of the Boulby deposit.

The halite and potash salts of the Boulby evaporite succession were formed approximately 225 million years ago at the margins of the Zechstein Sea either in shallow water or under Sabkha conditions. The thickness of the potash seam increased with increasing depth of water which in this case was to the south-east. Within this general saucer shaped basin there existed many smaller evaporating ponds where variations in brine or clay content would produce differing environmental conditions. The basin eventually dried out completely and was covered by a layer of fine wind-born sediment, similar in many respects to the clay but laid down in oxidising conditions. The basin was again flooded and the next cycle of evaporation took place. For the next 160 million years the Boulby evaporites were buried under a continually increasing thickness of over-lying sediments until approximately 65 million years ago, when they lay at a depth of 8000 metres, equivalent to a pressure of 2000 kilobars and a temperature of 90°C. Thereafter the depth increased due to the processes of erosion until the present day where the Boulby succession is at a depth of 1100 metres, equivalent to an overburden pressure of 300 kilobars at a temperature of 41°C.

The post depositional changes which have taken place in the chemical composition of the Boulby evaporites may be grouped into early and late diagenetic effects. The early diagenetic effects being the downward percolation of brines causing replacement of anhydrite and halite by polyhalite, of carnallite by sylvite and the leaching and reconcentration of magnesium sulphates and borate minerals. Late diagenetic effects are the veining of the overlying shales and marls. Many of these chemical processes are obscured by successive episodes of physical deformation and only the most recent are preserved.

The processes of physical modification of the Boulby evaporites commenced with a series of major faults during the Jurassic period, by which time the evaporites were sufficiently deeply buried to accommodate this movement by plastic flowage. Subsequent movements have been superimposed on these early structures until a regional pattern developed whereby isolated remnants of comparatively undisturbed ground were interspersed with zones of disturbance. By the end of the Cretaceous or early Tertiary when the deposits had attained their maximum depth and temperature, the overburden pressure exceeded the yield points of evaporites (more particularly that of the potash) and a series of gravity driven structures were developed in the Boulby succession.

The disharmonic nature of these mechanical structures interfere to produce an extremely complex pattern of thinnings and thickenings as well as undulations of the sylvinite seam. Due to the nature of the geological interfaces within the Boulby succession, the large-scale or regional undulations are best preserved along the potash footwall - halite contact, whereas the potash hanging-wall - shale contact reflects the small scale perturbations caused primarily by gravity tectonics. It is for this reason that any attempts at extrapolating potash seam characteristics from wide-spaced intersections is considered highly spurious, however desirable that may be in terms of mine planning".

Potash was first discovered in the Whitby area of North Yorkshire in boreholes drilled in 1938 - 1939 by the D'Arcy Company which is now part of British Petroleum⁽⁴⁾. World War II interrupted the exploration programme, and it was not until 1948 that exploration in the area recommenced. By 1952, I.C.I. in conjunction with Fisons Ltd., had proved mineable reserves in excess of 400 million tons in an area of 40 square miles centred slightly to the west of Whitby, but at a depth of well over 1300m.

Development was deferred until in the early 1960s I.C.I. put down two further boreholes to the north of Whitby. These boreholes Newton Mulgrave No. 1 (MN1) and Staithes No. 1 (S1), proved the

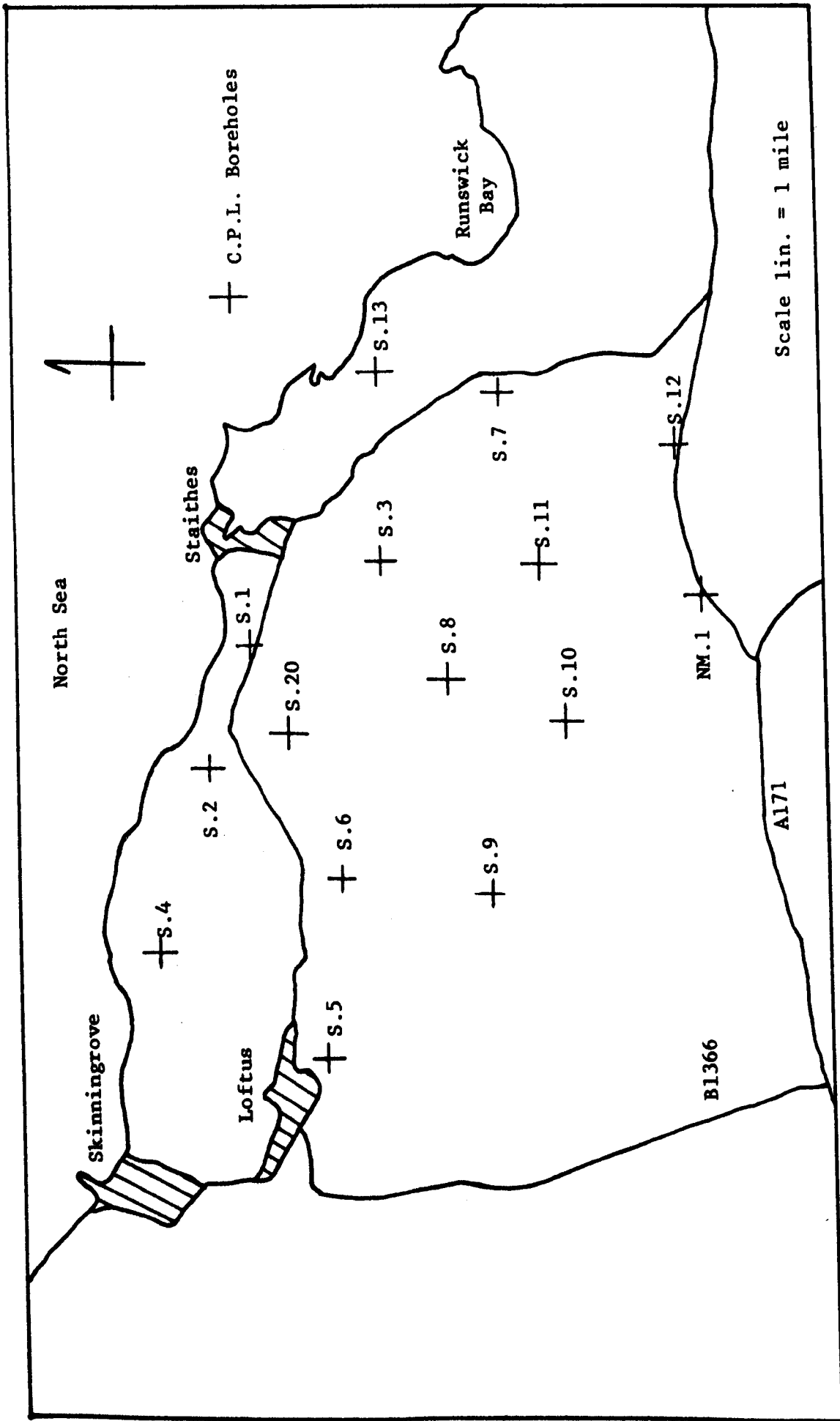


Figure 2.2 Location of deep exploration boreholes

existence of a potash seam equal in quantity and quality to that found around Whitby. Another thirteen boreholes were sunk to further explore and prove the deposit. These fourteen boreholes are regularly spaced across the mining area, and a further hole, S20, was put down in the line of the proposed Boulby mine shafts (Figure 2.2). The fifteen boreholes constituted the sole source of rock materials upon which the rock testing programme was carried out in order to determine the initial design parameters for Boulby mine⁽⁵⁾.

2.3 The Geological Succession, Boulby Mine

The strata containing and overlying the potash seam at Boulby consists of marine sediments and evaporites, and a general geological column is shown in Figure 2.3, and the near-seam succession in Fig. 2.4. Only the near-seam strata will be considered here as they are of immediate interest to the mining engineer and the design of excavations associated with the potash horizon. Patchett⁽⁵⁾ and Woods⁽⁶⁾ give more detailed descriptions of the geological succession.

Details of the different strata from all the boreholes from the Bunter sandstone down to the Middle Halite are given in Table 2.2. The strata are generally flat and fairly regular in composition, although the thickness of various beds varies considerably within the area of the C.P.L. lease.

Ironstone mines were worked in much of the lease area of Boulby mine. These were high extraction extensive room and pillar workings

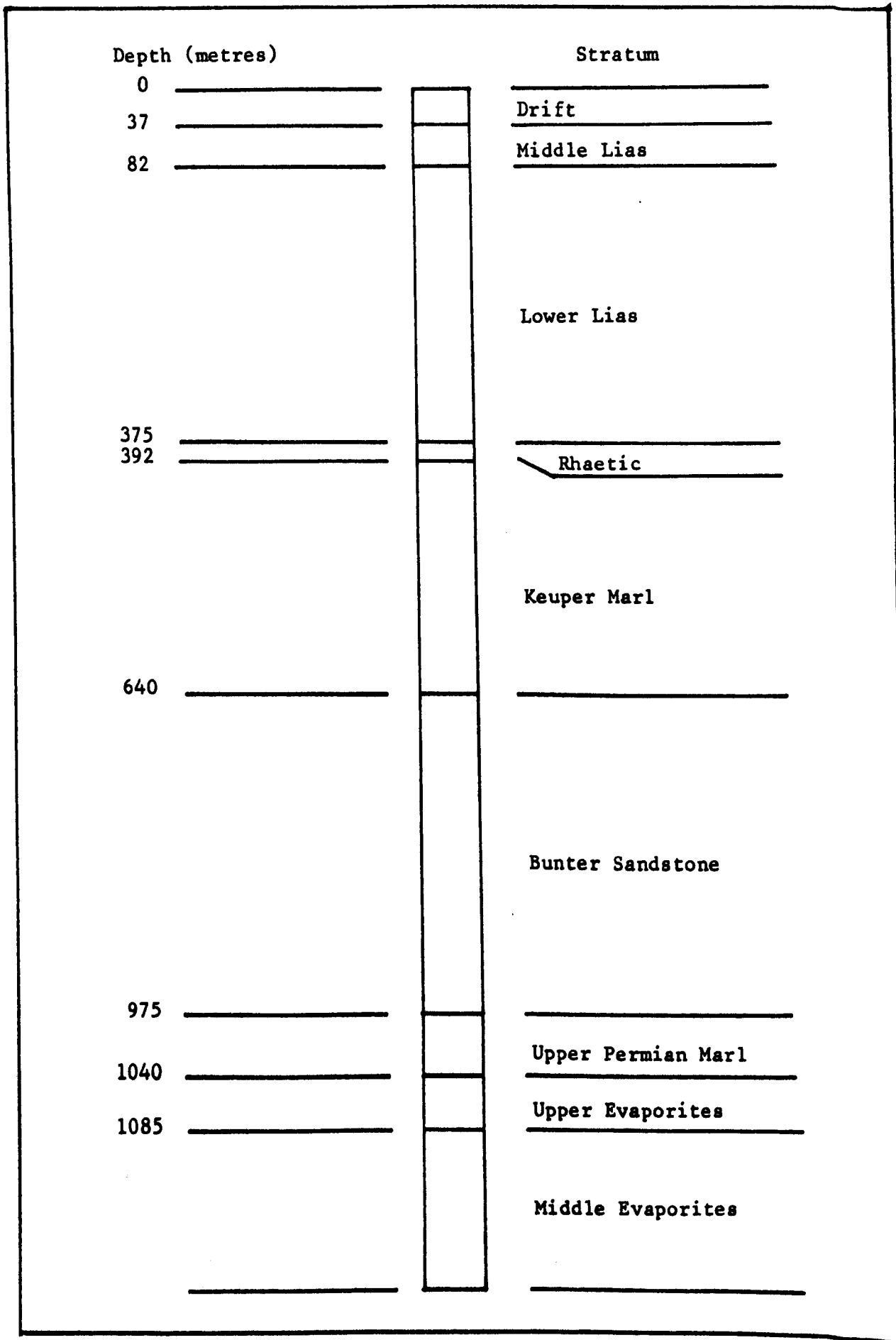


Figure 2.3 General geological succession, Boulby Mine

TABLE 2.2

Exploration Borehole Results - Top of the Bunter Sandstone to

the bottom of the Middle Halite

Thickness of beds expressed in metres

Borehole Formation	NM1	S1	S2	S3	S4	S5	S6	S7	S8	S9	S10	S11	S12	S13	S20	Mean	Range
Bunter Sandstone	311	277	307	316	249	265	264	294	278	268	317	250	286	258	392	289	249-392
Upper Permian Marl	82	130	92	112	123	104	126	130	129	108	88	166	139	136	16	112	16-166
Upper Halite	29	50	33	47	37	17	39	48	30	24	39	36	39	32	36	40	17-50
Upper Anhydrite	8	8	5	9	5	21	9	19	7	9	6	7	1	5	8	8.5	1-21
Carnallite Marl	9	15	8	23	12	8	5	35	5	26	13	5	1	11	10	12	1-35
Potash	7	8	7	17	5	5	6	5	24	4	5	13	9	12	4	9	4-24
Middle Halite	63	62	49	61	54	42	59	75	54	36	46	38	63	56	55	54	36-75

and were mined in the ironstone which occurs as a number of seams in the Middle Lias at a depth of about 40m below the surface. The possible instability of these old workings is a factor to be considered in terms of subsidence induced by mining the potash seam some 1000m below.

2.3.1 Bunter Sandstone

A major geological feature having a bearing on mine design is the Bunter Sandstone. These water bearing strata consist of fine grained red sandstones grading into mudstones and average about 300m in thickness. It contains a semi-saturated brine solution, movement of which is restricted by the low permeability of the strata, but which will be under high hydrostatic pressure. There is evidence of water bearing fissures from the Bunter penetrating the Upper Permian Marl. Recent geological speculations indicate that this water may approach to within 40m or even closer to the potash seam in zones where folding or faulting have taken place. The Upper Permian Marl is the major impermeable bed of significant thickness between the Bunter Sandstone and the potash workings.

2.3.2 The Upper Evaporites

The Upper Evaporite series occurs below the Bunter Sandstone, and consists mainly of the Upper Halite, which is a homogeneous halite deposit 35m thick. Below this is the Upper Anhydrite, a bed of varying thickness, averaging 10m, and which contains some halite veins. It is felt that this bed plays a major role in the stability

of the excavations some 15m below and that this role has been largely neglected in previous work, although Hebblewhite⁽⁷⁾ does refer to it. Three zones can usually be distinguished in the Upper Anhydrite which vary somewhat in thickness between individual boreholes. The uppermost zone is usually the thickest, with a moderate grain size and a fairly high halite content. Veins of sylvite also occur locally. The middle zone has much less halite or none at all, and the anhydrite is fine grained. The thickness of this section is quite variable and it is not always present. The bottom zone is thin but persistent and is almost always present.

2.3.3 The Carnallite Marl

The Carnallite Marl is the weakest rock in the sequence overlying the potash bed. It obtained its name when in the Whitby area traces of carnallite were found in the marl. Physically the Carnallite Marl consists largely of mudstones and marls, having little cohesion even when massive. Numerous veins and stringers of halite and sylvite are found throughout the stratum. When exposed in the mine it tends to "run" into the excavations and once this happens, it becomes very difficult to support. Such an area is usually isolated and alternative routes are found through that section of the mine. It has therefore become standard practice to leave an adequate cover of at least 2m between an excavation roof and the marl.

2.3.4 The Potash Seam

It was originally thought that between the marl and the potash

was a fairly uniform bed of halite, known as the Halite Parting. It occurred in this form through much of the shaft pillar area but on a wider scale this has been redefined together with the potash bed as in Figure 2.4. The gneissose potash is now known as Primary ore, while the remainder containing varying amounts of shale is termed Secondary ore, the latter frequently containing high grade sylvite. The shaley Secondary ore which is highly variable in thickness, contains varying amounts of halite, anhydrite and boracite. The Primary ore varies in thickness from 0 to 10m, averaging about 3m, while the Secondary ore can be up to 16m thick. The gas blow phenomenon appears to be mainly associated with shale inclusions in the Secondary ore zones. The base of the potash

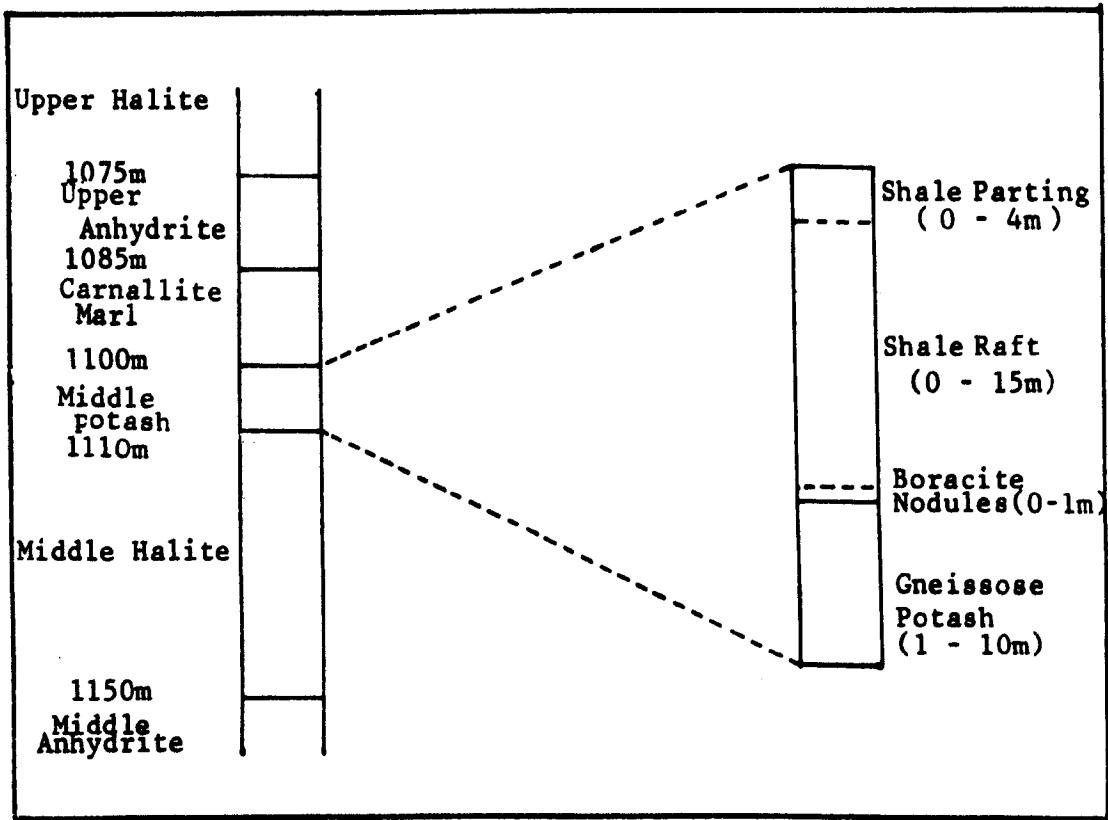


Figure 2.4 Near Seam Geological Succession

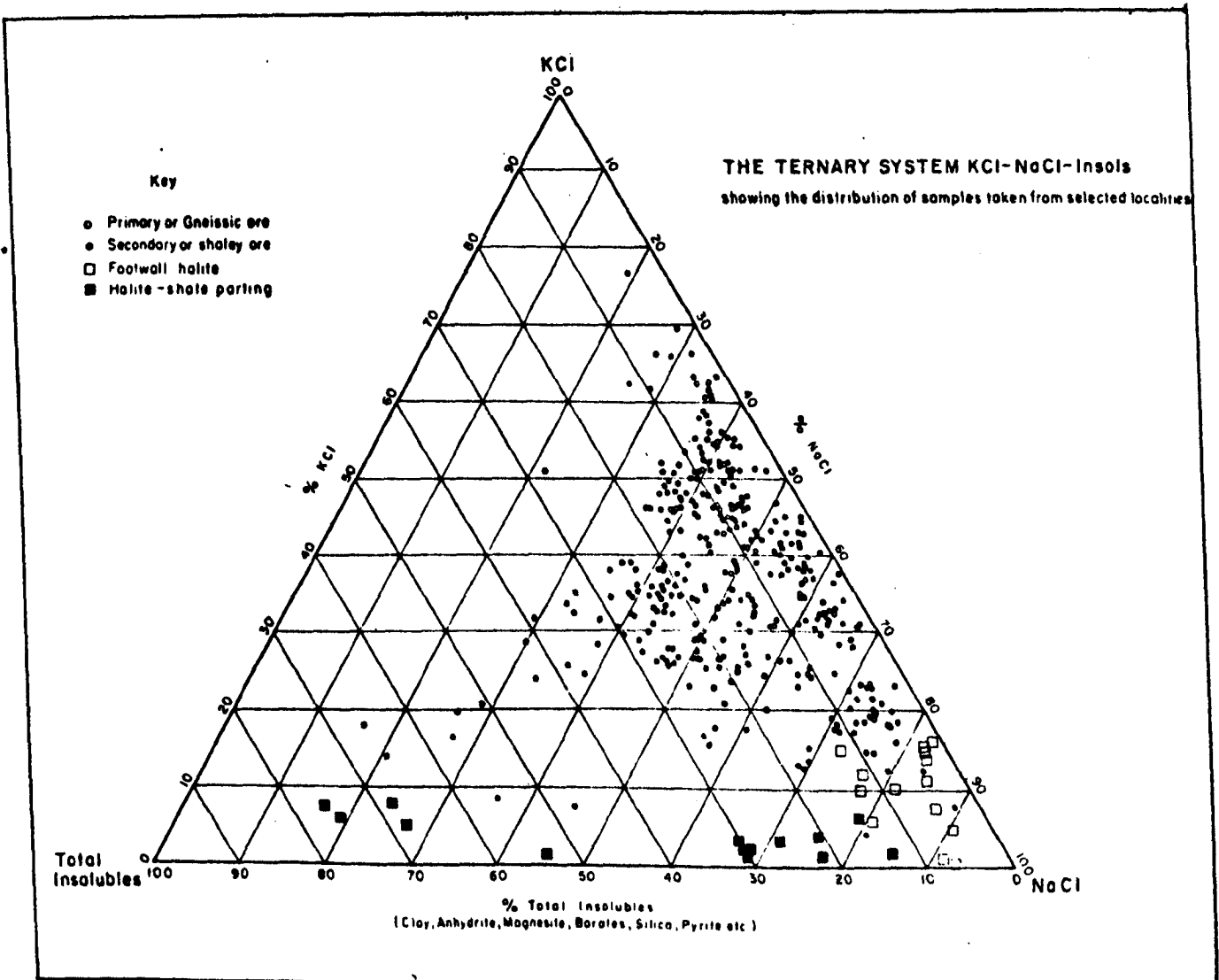
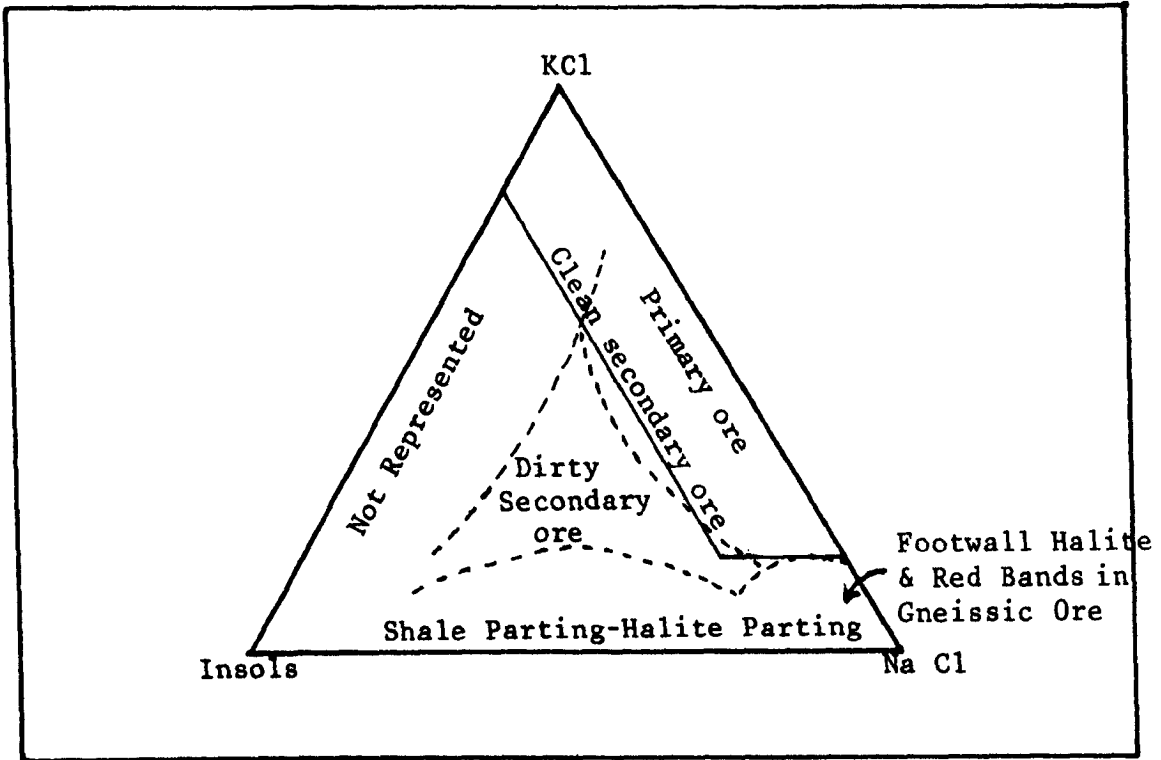


Figure 2.5 Ore type classification (after Hebblethwaite and Woods)

seam is fairly flat, but the top is extremely undulating, giving rise at times to severe difficulties in controlling the roof conditions. The low strength of the shale along with the presence of sylvinite veins as well as the marl above, cause serious roof control problems throughout the mine.

The classification of ore types as proposed by Hebblethwaite and Woods⁽⁹⁾ is given in Figure 2.5. This is based on the three component system, KCl, CaCl and Insolubles content, and was derived specifically for considering the gas blow problem. The necessity for a more comprehensive classification system arose because of the difficulty in differentiating between specific ore types as observed underground. The terms "Primary" and "Secondary" as applied to potash ore, while convenient, tend to be ambiguous, as both terms imply meanings as to both the grade and the geological origin of the ore. The various fields are drawn to a 95% confidence level for four hundred empirical and observational analyses of visibly different ore types.

2.3.5 The Strata below the Potash Seam

The bed immediately below the potash seam is a competent, 40m thick, homogeneous bed of halite, the Middle Halite. It overlies the Middle Anhydrite and the Magnesian Limestone.

CHAPTER THREE

DEVELOPMENT OF PRODUCTION PANELS AND LAYOUTS

CHAPTER THREE

3.0 Boulby Mine

Boulby potash mine is managed and run by Cleveland Potash Ltd., (CPL) now a wholly owned subsidiary of Charter Consolidated Ltd., and the Anglo American Corporation of South Africa. CPL received outline planning permission to construct a mine and plant in the North Yorkshire National Park in 1968. A twin shaft system was sunk to approximately 1150m depth through ground that was successively extremely weak, water bearing and finally liable to plastic deformation. The circular shafts are 5.5m in finished diameter, and situated 91m apart. The No. 1 shaft is designed for hoisting potash in two counter-balanced 20t skips and is the upcast ventilation shaft. The No. 2 shaft has two counter-balanced cages to handle men and material and serves as the downcast shaft. The Boulby shafts are currently the deepest in the United Kingdom. Two different methods of sinking were employed to overcome the high pressure salt water in the Bunter Sandstone. Grouting and tubbing was used in the No. 2 shaft, and freezing and steel lining in the No. 1 shaft. A full account of the shaft sinking is given by Cleasby et al⁽¹⁰⁾ in a paper to the Institution of Mining and Metallurgy in 1975.

Professor E.L.J. Potts and various researchers at the Department of Mining Engineering, University of Newcastle upon Tyne were involved in the design of layouts from the beginning, in the shaft pillar area and continuing through to the present day^(5, 7, 11, 12).

The knowledge relating to the nature of the potash seam gained from previous borehole surveys was limited, and a survey of potash mining techniques in use throughout the world led to the introduction of cyclic mining techniques in 1973. The initial method of mining employed was by undercutting, drilling and blasting. Loading and transporting was by Eimco 915 LHDs onto a conveyor. All equipment has to be approved as intrinsically safe because of the presence of various hydrocarbon gases in the secondary (shaley) ore. Since 1975, panel layout design has developed and continuous mining techniques have been tried in an effort to increase output.

3.1 Development of Panel Layout and Mining Method

Average output figures for each panel layout have been obtained and are compared and related to the overall stability of each layout. Other factors such as machine availability, labour shortages and industrial disputes have also had a varying effect on production. However, over a period of production analysis of at least three months for each layout, it is assumed that these factors have not affected production in any one layout to a great degree.

During the period July 1975 to April 1980, panel design can be differentiated into thirteen main layouts - Figure 3.1. These are shown in greater detail in Appendix 1. Four of the earlier layouts were worked by cyclic methods, employing either one or two sets of equipment. Joy 15 RV cutters and Secoma single boom drilling machines prepared the face for blasting. Ore was loaded out by

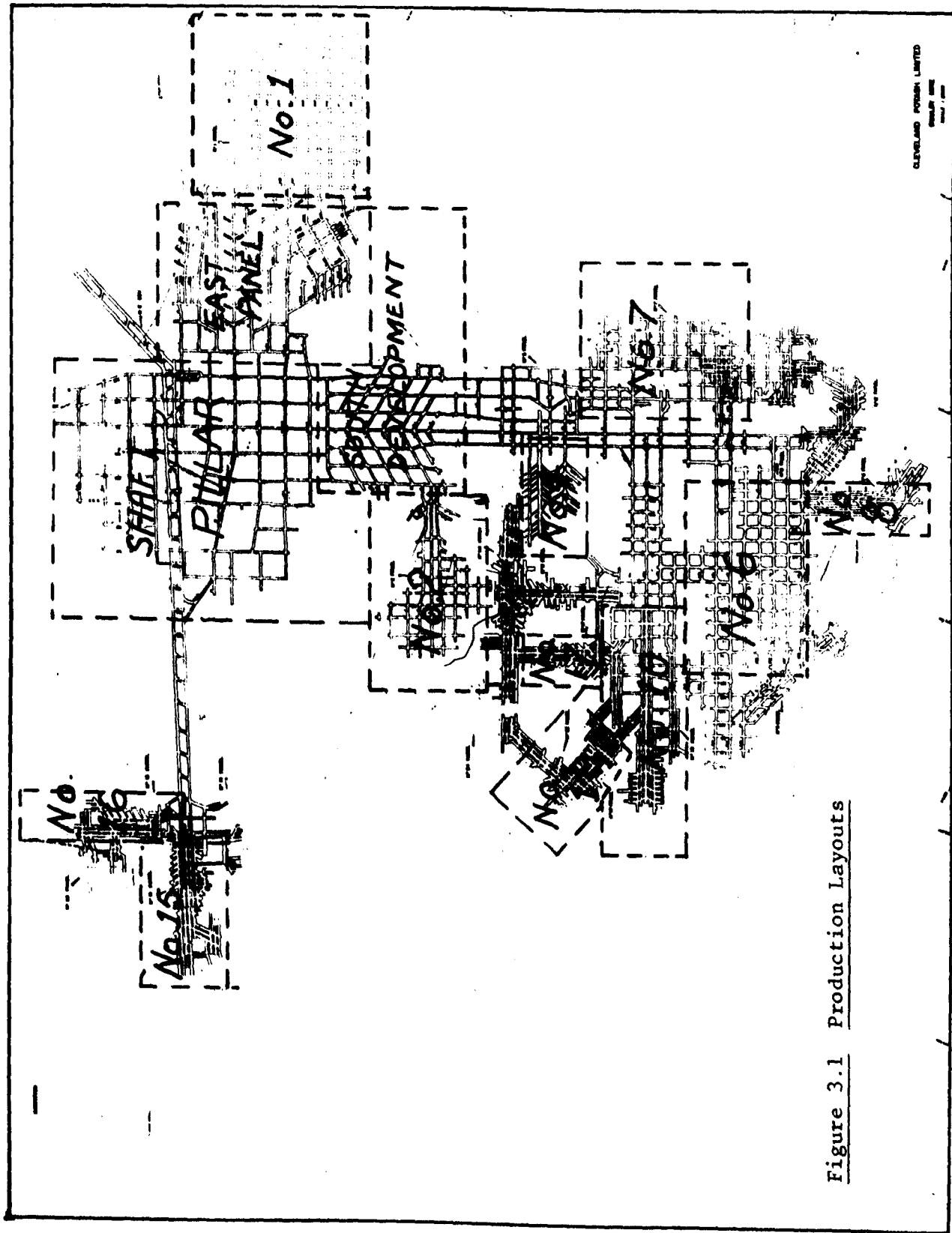


Figure 3.1 Production Layouts

Eimco 915, 5 yd³ LHD vehicles onto the belt conveying system through a Stamler feeder breaker. Support was provided by rockbolts installed by Secoma roofbolters. All machines were powered by an 1100V trailing cable supply with the exception of the LHD vehicles which were diesel engine powered, which complied with British FLP regulations (13).

With the exception of No. 7 Panel, the other panels have all been worked by continuous mining methods after initial assessment of their suitability to the conditions encountered at Boulby. The first system used a boom type - the Jeffrey dresser 120 HR Heliminer. The second system adopted a Marietta 780A Twin Rotor Borer which is the type used extensively in Canadian potash mines. No. 4 Panel was established to assess the capabilities of this particular machine.

Subsequent experience with these different machines highlighted the flexibility of the Heliminer in the variable geological conditions and in October 1978, a fleet of six Heliminers was working in the mine. Where possible the Heliminers are worked in pairs, thus gaining the benefits of lower manpower, better supervision and better operating technique. Joy shuttle cars transport the ore from the face to the conveyor belt. No secondary crushing is required at this stage. All equipment is powered by 1100V trailing cable.

3.2 Production Analysis - Table 3.1

Data for the production analysis were obtained from the monthly reports produced at the mine. Average figures for advance and output

were calculated when production was in the body of a panel and not in a development stage. Data for months when strikes and other major stoppages adversely affected production were not included in the analysis.

To enable a comparison to be made between cyclic and continuous mining methods, all production was reduced to a common basis - output per man shift (OMS). No detailed records of manning levels have been kept by the mine, so these have had to be assumed in some cases from information obtained from monthly reports and supplied by the mine staff - Table 3.2. The OMS values are therefore valid as a means of comparison between panel layouts and should not be used in any absolute sense.

3.3 Results

3.3.1 East Panel and South Development

The layout in both panels consisted of seven entries driven in the direction of the panel section with cross-cuts angled at 60° giving the characteristic herringbone type design (Figures 1 and 2, Appendix 1). Pillars were nominally 46m x 40m. It was expected that these pillars would have the same characteristics as 40m square pillars, whilst improving ventilation and vehicle handling, and also increasing the panel extraction ratio slightly, from 26% to 27.5%.

The East Panel started production with this standard layout, but subsequently contained modifications which were included to

TABLE 3.1

Panel	Pillar Size	Nom. Road Width	No. of Entries	Panel Width	% extr.	Adv/sh.	t/sh.	Analysis Period	O.M.S.
	m.	m.		m.		m.	t.	weeks	
East	46 x 40	6.0	7	282	27.5	8.55	378	24	21
Sth. Dev.	46 x 40	6.0	7	282	27.5	5.9	261	24	14.5
No. 2	25 x 25	6.0	9	254	36.5	5.6	274	32	15.2
No. 2	varied	6.0	varied	varied		3.7	170	28	11.3
No. 4	*					4.6	148	28	18.5
No. 6	30 x 30	6.5	7	225	34.4	8.0	404	20	51
No. 7	35 x 25	6.0	5	130	34.3	4.1	190	32	15.8
No. 8	*	6.5	6	62	66.0	7.8	400	8	50
No. 10	*	6.5,9	5	90		12.5	328	12	41
No. 15	*	6.5,9	5	100		11.8	272	17	34
No. 16	*	6.5,9	5	90		6.5	136	17	17
No. 17(a)	*	6.5,9	5	90		12.9	320	7	40
No. 17(b)	*	6.5,9	4	45		23	320	6	40
No. 19	*	6.5,9	5	90		10	248	15	31

TABLE 3.2

Manning Levels

1. Layouts employing cyclic mining techniques

Cutter - 1 man
Drill - 1 man
Shotfiring - 2 men
Loading - 2 men
Support - 2 men
Supervisor - 1 man

9 men per cyclic production unit

2. Layouts employing continuous mining techniques

Heliminer Driver and mate - 2 men
Shuttle car drivers - 2 men
Support - 2 men
Probe Drill - 1 man
Supervisor - 1 man

8 men per continuous mining section

Note: These are average numbers per shift. A degree of flexibility is enjoyed in each team with most men being authorised to operate more than one machine.

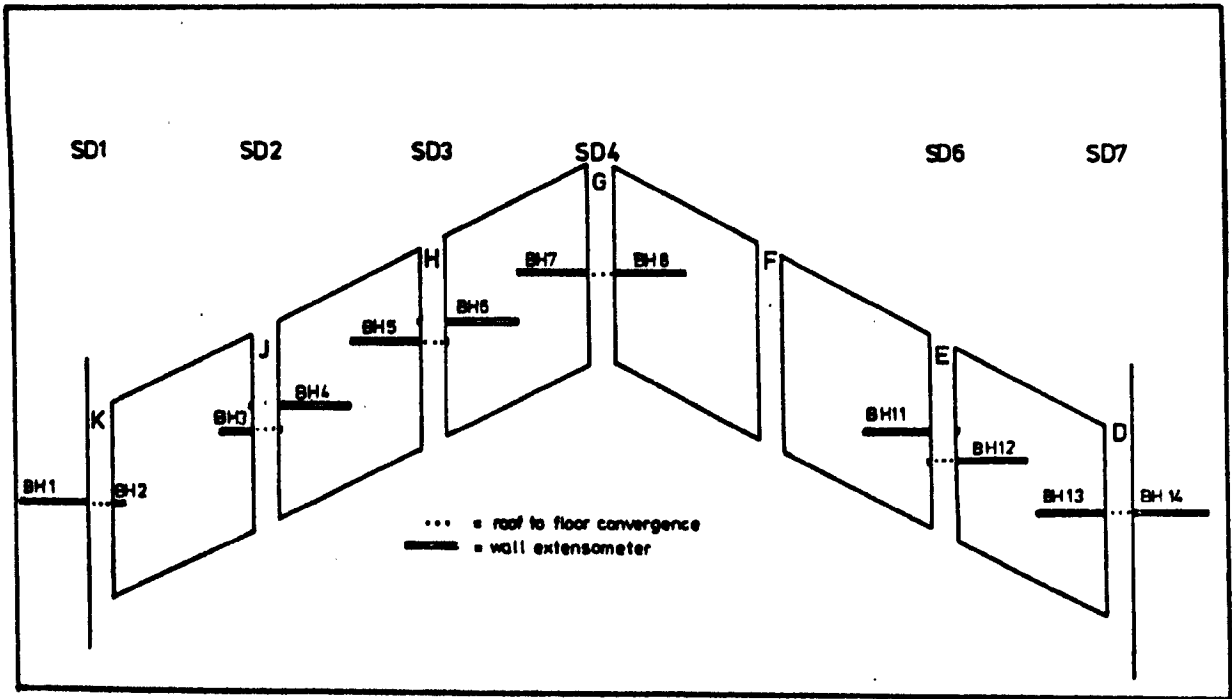


Figure 3.2 (a) South Development Layout

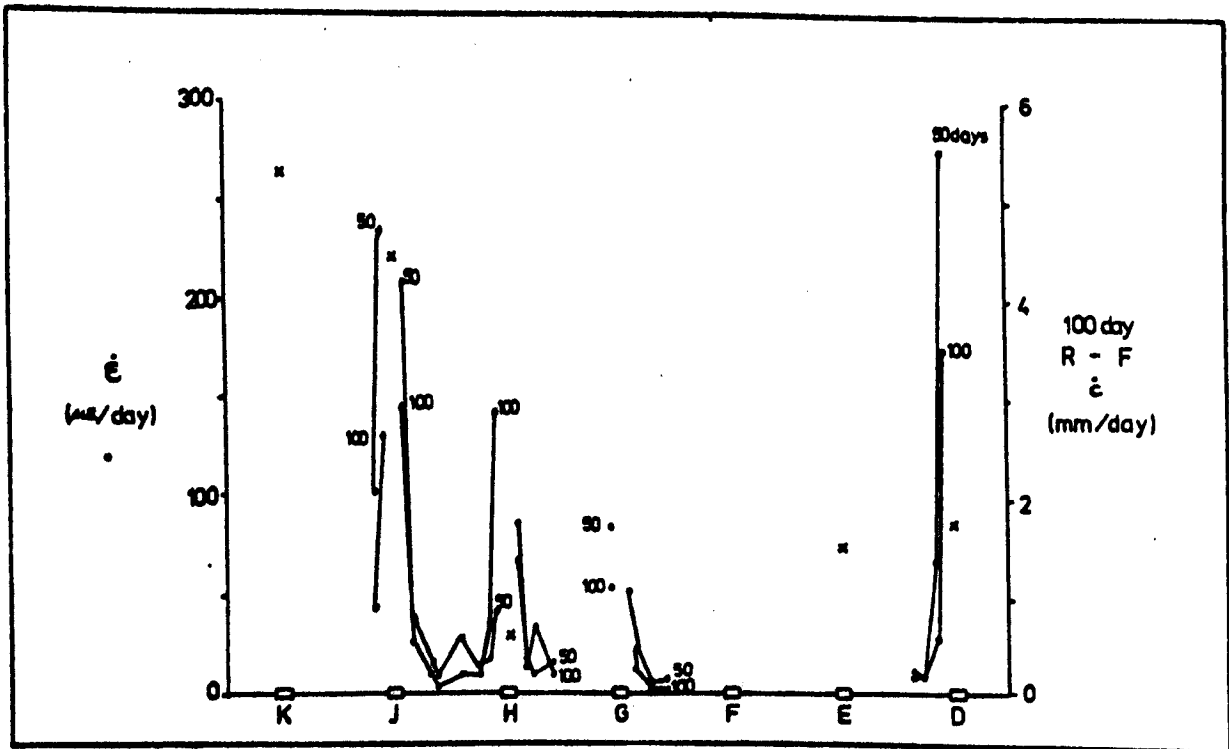


Figure 3.2 (b) South Development Results

determine the rock mechanics characteristics of different pillar designs. This programme of layout modifications included site 1P4 in early 1976, and also sites 1P7, 1P8 and 1P9 in April - May 1976. The latter sites resulted in an increase in overall panel width, but this was partly compensated for by an overall shift in the panel southwards to bypass a major marl downwarp in the north of the panel.

The South Development maintained the 46m x 40m pillar layout for most of the life of the panel, although bad ground conditions associated with marl downwarps resulted in the closure of some headings such as the East Conveyor Road (00) in the East Panel. Roadways 00 and C01 were driven in halite to ensure long term stability. This also increased the overall stability of the panel.

Rock mechanics sites were established, Figure 3.2a, in the South Development. These gave closure measurements in the roadways and horizontal deformation in the pillars. The results are shown in Figure 3.2b. Figure 3.3 shows the strain rates in the pillar between roadways J and H. This indicates that there is a central stable core in the pillar of 20m to 25m width. Figure 3.4 is a plot of the log strain rate against time for borehole 4 which is in potash, and borehole 8 which is in salt. Although borehole 8 shows some sign of reloading between 80 and 120 days, the negative slopes of both graphs illustrate continuing stability. The greater stability of the pillar in halite is also evident. The linear relationships depicted in Figure 3.4 can be described by the following equations:

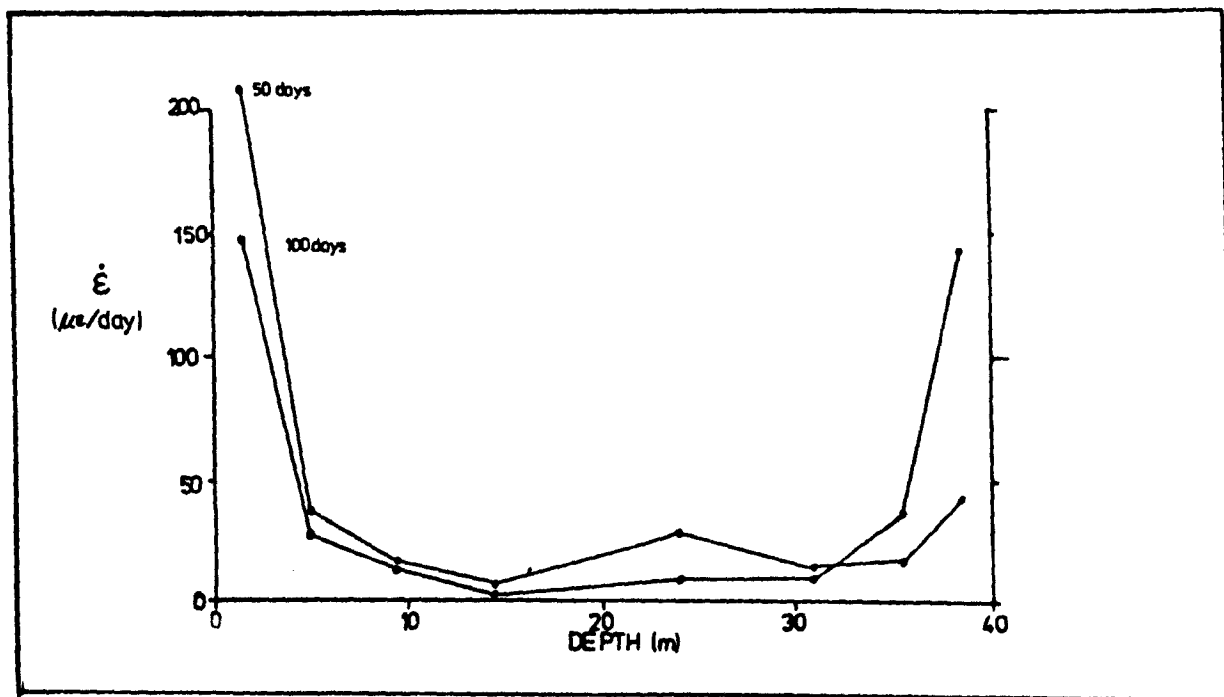


Figure 3.3 Strain rates between J & H roadways, South Development

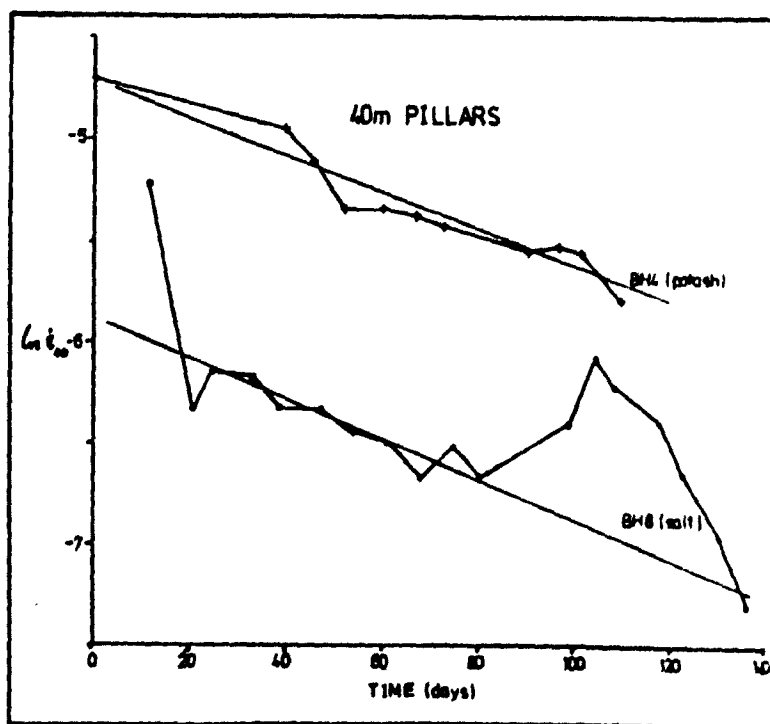


Figure 3.4 Log strain rate v. time, 40m potash and salt pillars

$$\dot{S}_{(\text{potash})} = 0.008871e^{-0.00873t}$$

and

$$\dot{S}_{(\text{salt})} = 0.002739e^{-0.00984t}$$

where S is the strain rate in mm per day and t is the time in days. A complete assessment of the rock mechanics data from these sites is given by Hebblewhite⁽⁷⁾.

It is interesting to compare the production results from the South Development and the East Panel area. The OMS values are 14.5 and 21 respectively, that is, 30% greater for the East Panel. This is accounted for by the fact that the gasblow outburst zone cuts right across the whole of the South Development, while only partly intersecting the East Panel. Figure 3.5 shows this zone as well as the geology in these areas. As well as having an increased incidence of gasblows, the South Development had the shale raft either in, or close to the roadway hanging-wall. This resulted in frequent interruptions to operations when dealing with persistent bad local roof conditions. The number of headings available for production in the South Development was limited by the actual layout and the necessity to undertake remedial work following gasblows in the previous cycle.

3.3.2 No. 1 Panel

No. 1 Panel (Figure 3, Appendix 1) was an extension of the East Panel outside the shaft pillar area, and consequently, a higher panel

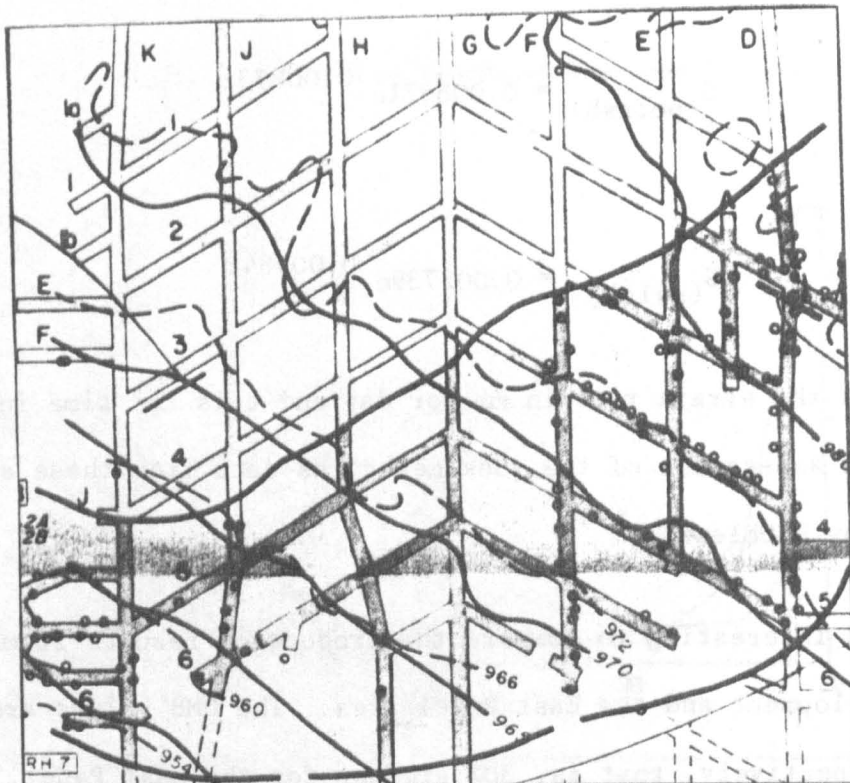


Figure 3.5 Gas blow zone - South Development

extraction ratio of 36.5% could be realised. The number of entries was increased to nine with the cross-cuts at right angles, giving 25m square pillars. The East Conveyor Road was separated from the panel by a 60m barrier pillar. Conveyor access to the panel was provided by access cross-cuts every 90m as the faceline advanced to the east.

The majority of roadways were mined in secondary ore with a shale roof and some shale or primary ore in the floor. It was originally intended to install a line of measuring stations across the width of the panel, but in the end it was only possible to establish three sites, EP1, EP4 and EP7. These were installed in the last cross-cut line before it was decided to stop the panel

altogether, due to the potash running out completely. It was possible to obtain readings only for a short period of approximately 60 days from these sites. The limited analysis that was made of the extensometers installed in the pillars indicated that a confined pillar core was developing, but that deformation was occurring throughout the pillar. Figures 3.6(a) and 3.6(b) show the pillar deformation at sites EP1 and EP4. Figure 3.7 depicts the deformations occurring along a 6m deep roof extensometer hole. The onset of roof failure can clearly be seen between 18 and 21 days after mining. The fact that anchors 1, 2 and 3 are deforming together point to bed separation somewhere between the mouth station and the first anchor 2m into the roof.

The average advance per shift over the six month period, January - June, was 5.6m with an OMS of 15.2 with two cyclic units operating in the panel. Gasblows occurred on a relatively minor scale and had little impact on production. Problems of instability associated with severe marl downwarps necessitated closure of several headings in the north-east of the panel. In addition, bad conditions were often produced by the pillars punching into the shale roof and floor. This deterioration in roadway conditions contributed largely to the loss in production by restricting vehicle movement and reducing overall machine availability. Average face effective temperatures in No. 1 Panel were 1.5°C higher than in the East Panel in the corresponding period the previous year. This higher temperature also probably had an adverse effect on the output of the panel. The

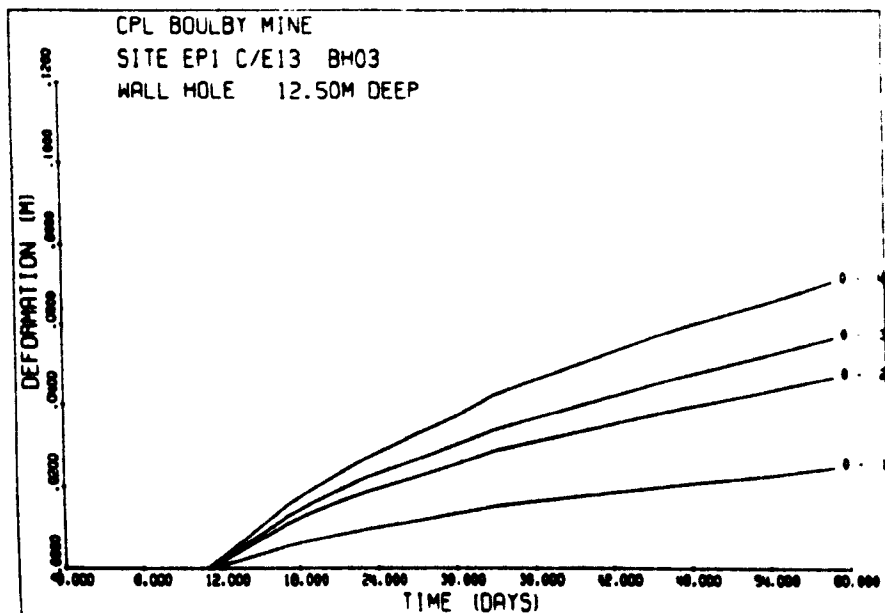


Figure 3.6(a) Pillar extensometer, East Panel

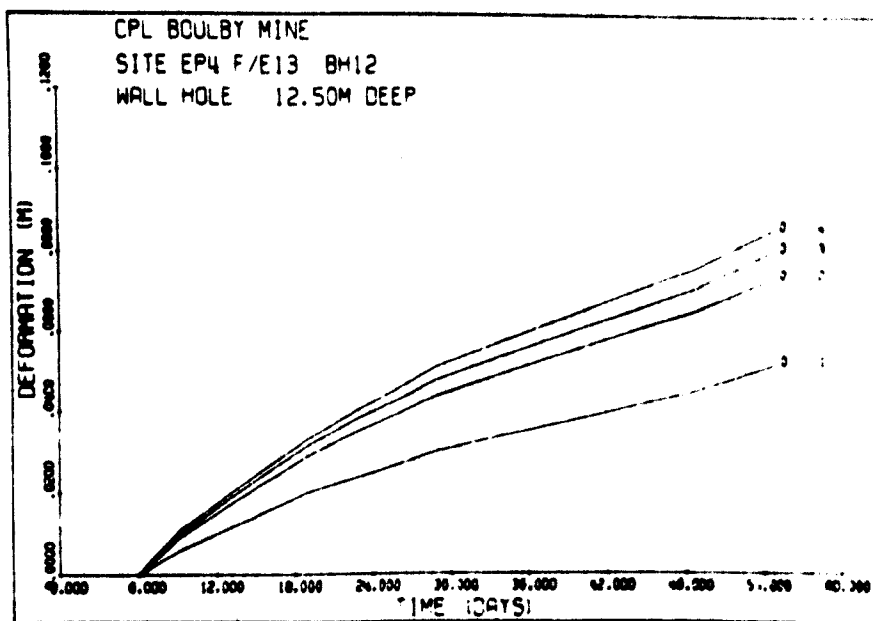


Figure 3.6 (b) Pillar extensometer, East Panel

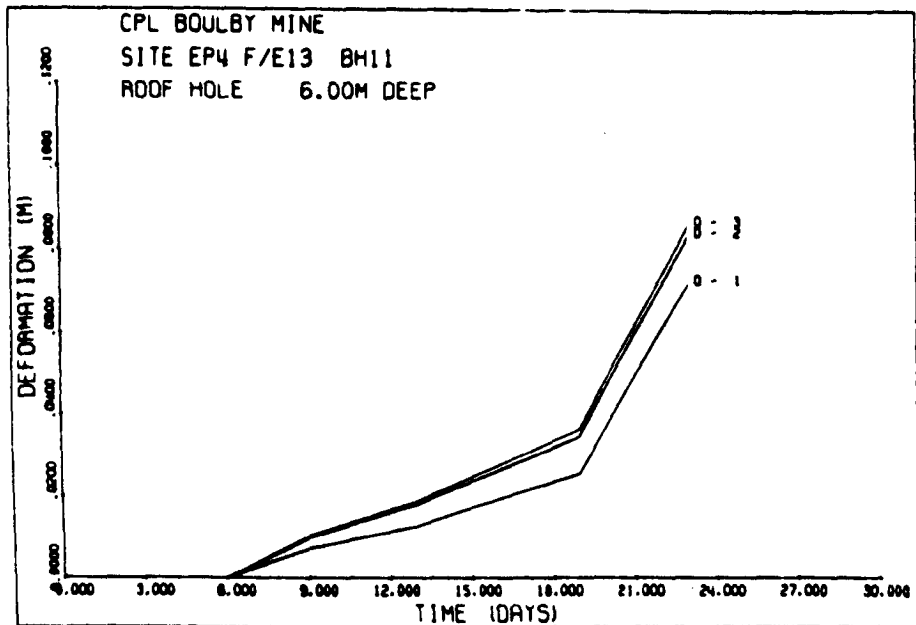


Figure 3.7 Roof extensometer - East Panel

relatively poor performance of this panel can therefore be attributed mainly to the adverse conditions produced by the proximity of the shale and marl to the roadway hanging wall, and the resultant punching of the pillars. This punching also occurred when the pillars were in primary ore and the roof in secondary ore. It was concluded on the basis of measurements made in the pillars and the panel abutments, that in panels with 25m pillars, the pillars were carrying virtually the full cover load. This remains true as long as there is a stable confined core within the pillars.

3.3.3 No. 2 Panel

No. 2 Panel (Figure 4, Appendix 1) mined into an area of uncertain geology and thus the layout did not follow any strictly defined design. It was similar to No. 1 Panel in having square or rectangular pillars, but without the symmetry. Three panel access roads were driven with the initial intention of obtaining protection of the centre roadway by means of stress relief. Unfortunately, only limited success was achieved. This was primarily because the panel was mined in massive secondary shaley ore. Two adverse results were excessive footwall heave and the occurrence of moderate to severe gasblows. This prompted the Inspector of Mines to require the mine to increase the width of the pillars from 8m to 15m. However, instead of improving matters, the wider pillars because they were stiffer, caused more floor heave as well as break-up of the immediate roof. It would have been better if the pillars had been made narrower, and thus more yielding. There was also evidence of some protection afforded by putting the wing roads C07 and C08 out ahead of the central conveyor road. The roof in the 8m pillar area remained intact, despite fairly large roof to floor closure. Extensive ripping of both floor and roof had to be carried out and steel arches were subsequently installed in various sections along the access roadways. This, as well as the increasing occurrence of major gasblows coupled with the downwarping of the marl, led to the stopping of the panel.

An advance per shift of 3.7m was achieved for the period April-

November, 1977. The average OMS was 11.3. Both of these figures were the lowest achieved in any production panel over a consistent period. This was partly due to the fact that only one drilling machine was available between two production units. Other factors were the reduced LHD availability due to severe floor heave, frequent, often severe gasblows and poor roof conditions caused by wrong pillar dimensions, and recurrent marl downwarps. Figure 3.8 shows the deformation in a 6.5m deep hole containing four anchors at depths of 1.0m, 2.2m, 3.4m and 4.5m into the sidewall. It can be seen that the bay strain between anchors 2 and 3 is greater than between 0 and 1. This indicates the opening up of a fracture due to slabbing of the sidewall some 2.5m into the pillar. The curves also show that the 8m pillar does not develop a stable core, as there is no significant drop-off in strain with distance into the pillar.

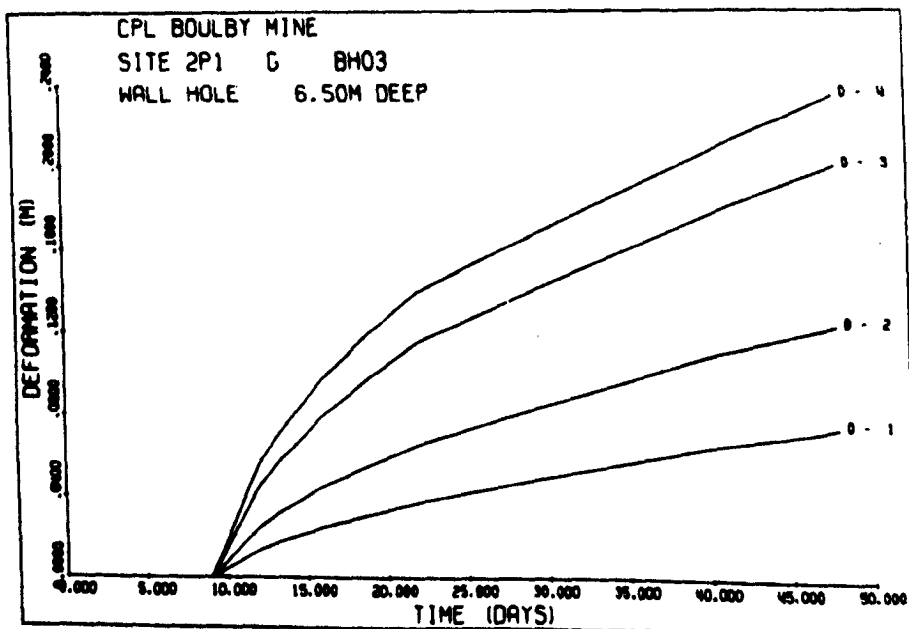


Figure 3.8 Pillar Extensometer, No. 2 Panel

Figure 3.9 shows the deformation for a 4.2m deep extensometer hole into the roof in roadway C22. The interesting feature of this hole is that there is an increase in bay strain between anchors 2 and 3 compared with 1 and 2, thus indicating bed separation some 3.5m into the roof. This can be compared with Figure 3.10 which shows the deformation in the roof in roadway C20, where it can be seen that bed separation is taking place within the first 2m. It can be deduced from the fact that the roof remained intact for nearly a year after mining, that a massive beam was formed which sheared at the outer edges of roadways C19 and C22 and then came down in one piece, due to the soft yielding of the 8m pillars. This is shown diagrammatically in Figure 3.11 and thus is significant in that it was the first indication of what was later claimed to be evidence of "stress relief" in wide high extraction panels with yield pillars.

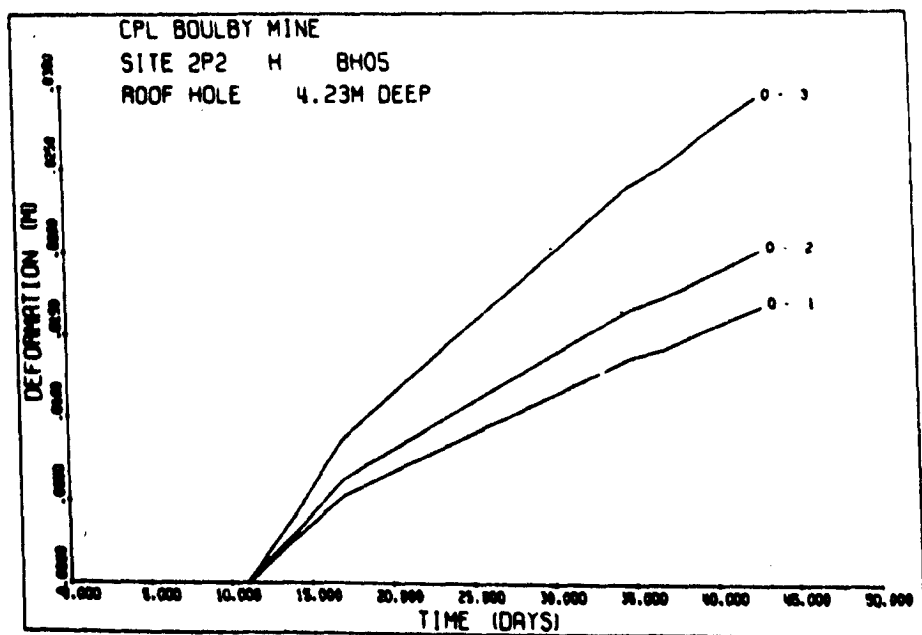


Figure 3.9 Roof extensometer, No. 2 Panel

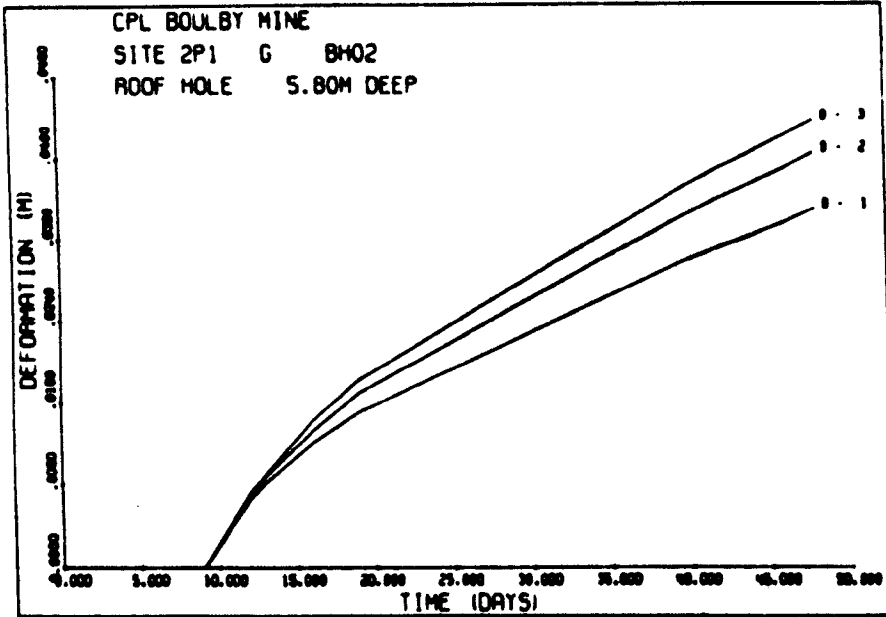


Figure 3.10 Roof extensometer, No. 2 Panel

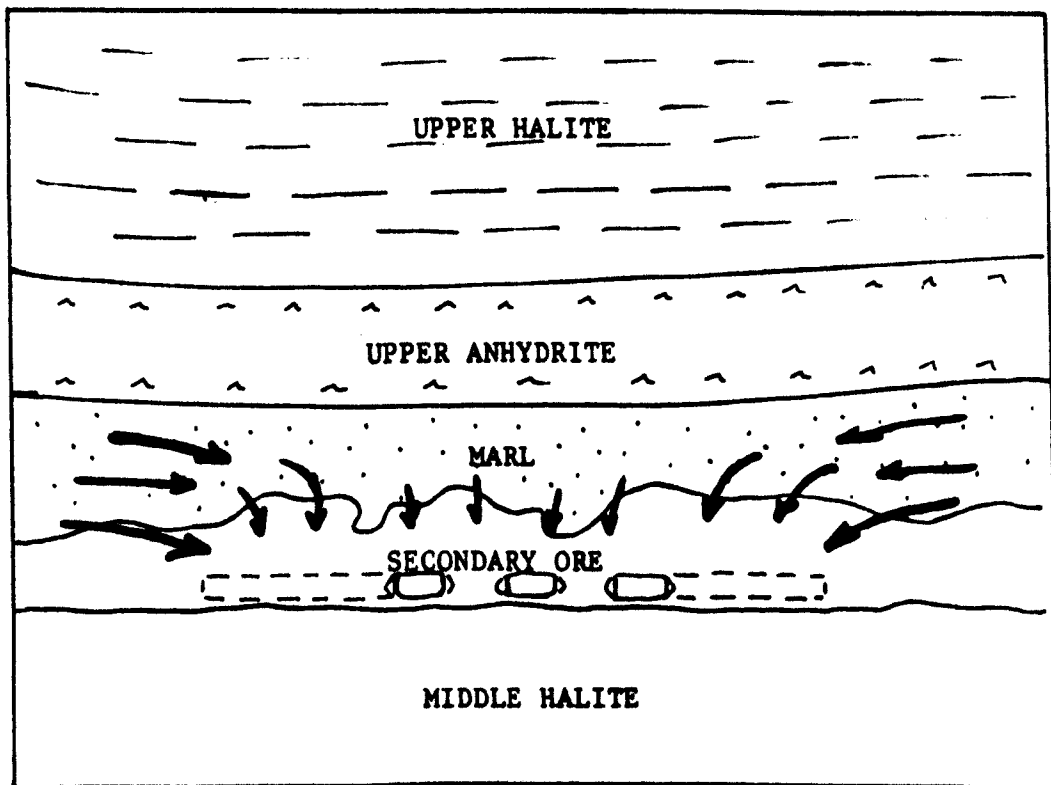
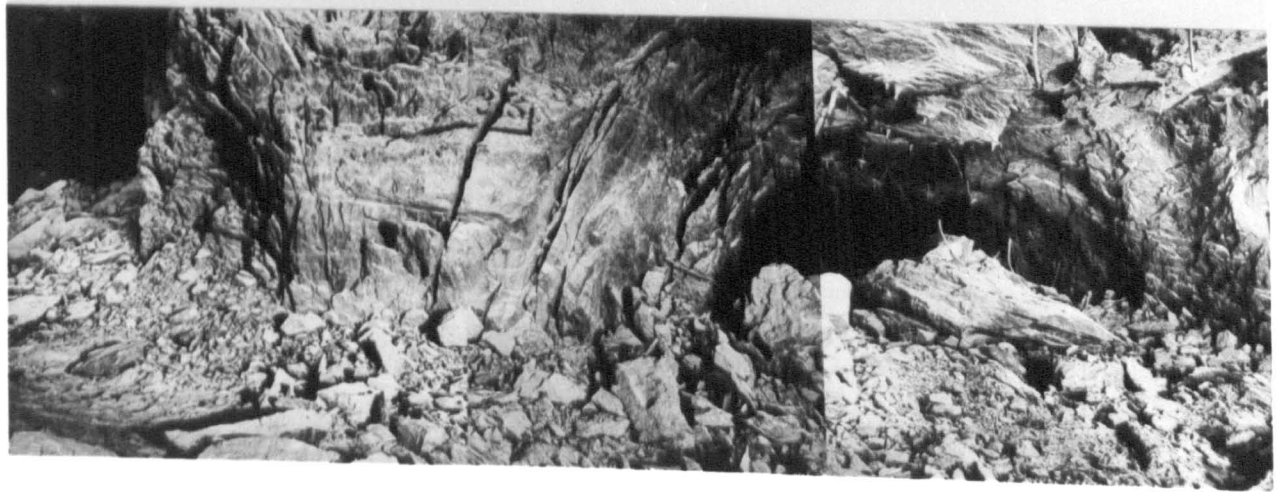
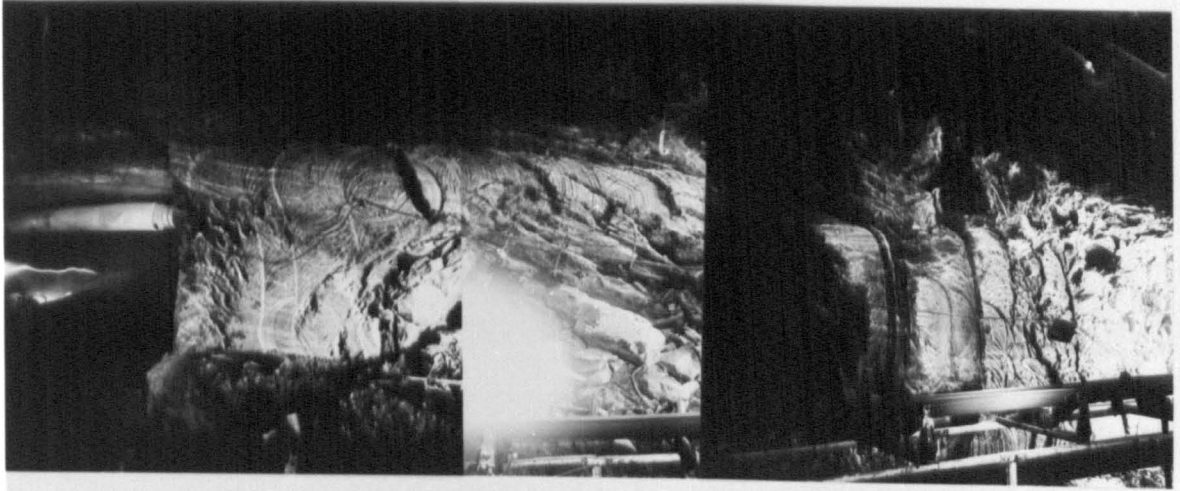
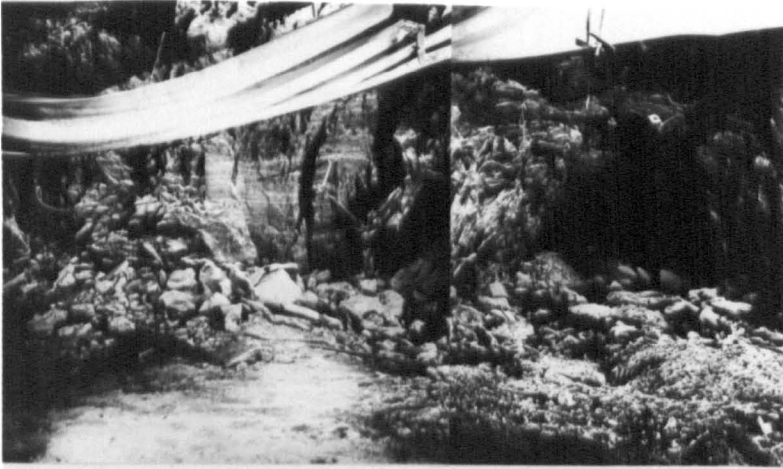


Figure 3.11 Roof deformation over narrow section of No. 2 Panel

Plate 3.1

- 1 No.7 Panel - old low extraction roadway.
- 2 No.7 Panel - new roadway looking at old workings
- 3 No.7 Panel - old roadway.



3.3.4 No. 7 Panel

The layout in No. 7 Panel (Figure 5, Appendix 1) was one having five entires with rectangular 35m x 25m pillars. The overall panel width was 130m. Panel conveyors were sited in cross-cuts to the main south trunk conveyor in roadway 00, and resited as the faceline advanced southwards. Conveyor cross-cuts were driven every 70m, so as to line up with every second set of panel cross-cuts. The eventual panel extraction ratio was 34.3%.

No rock mechanics sites were established in No. 7 Panel, due mainly to the intensive instrumentation programme being carried out in the so-called Experimental Panel, No. 6 Panel. However, observations showed that local problems occurred due to the presence of shale in the roof. Floor heave was not a problem as the majority of the floors of the panel roadways were of primary rather than secondary ore.

The average advance per shift for the period March - October 1978 was 4.1m. Two sets of cyclic equipment were in use in the panel, with each set being used as required during the shift by the same set of men. With an average number of men per shift of 12, the OMS was 15.8. Frequent gasblows, and bad roadway roof conditions due to the shale roof adversely affected the output. An average effective temperature of 30°C was an added constraint.

3.3.5 No. 4 Panel

No. 4 Panel (Figure 6, Appendix 1) was essentially an experimental panel set up to assess the suitability of a twin rotor Marietta Borer which had proved to be capable of high production rates in deep Canadian potash mines.

In order to establish a ventilation circuit, it was first necessary to drive roadway C31 to the anticipated boundary of the panel. This roadway was mined in two passes of the borer and was subsequently used as the return airway. C32 was driven parallel to C31 and stubs were mined off at an angle of approximately 40° , those to the north holing through into C31.

The borer was beset with many mechanical and operational problems during this period and was restricted to working on a single or double shift basis. The development of No. 4 Panel along C34 was stopped because of the presence of footwall anhydrite in the face. This had previously caused serious difficulties in cutting.

The availability of labour determined whether the borer was employed on a single or double shift basis. Machine availability was very poor and several modifications were made before the number of hours worked per shift was acceptable. Directional control was a major problem, both in the horizontal and vertical directions, and it took time before the machine operators were competent at turning off and driving stubs. The machine also tended to deviate downwards into the floor thus encountering the anhydrite.

During periods of production free from stoppages, very high outputs were obtained. The average advance per working shift in the period May to December 1977 was 4.6m. The average number of men in No. 4 Panel was eight, giving an average OMS of 18.5t.

No rock mechanics sites were installed in No. 4 Panel as this was essentially a project to determine the operational and mechanical capabilities of the Marietta Borer. However, excessive roof to floor closures did occur and the borer had to bore its way out when the panel was completed. It was felt that much of the excessive closure was due to incorrect sequencing of the drivage, in that the centre road was excavated in advance of the outer wing roads, and was left standing for too long while repairs and modifications were being made.

The major constraints to production during the life of the panel were poor machine availability and personnel availability, difficult ventilation and an unsatisfactory ore transportation system following behind the borer. To a lesser extent, geological features also had some adverse effect.

3.3.6 The Experimental Panel, No. 6 Panel

No. 6 Panel (Figure 7, Appendix 1) was a five entry layout with 30m square pillars and 6.5m wide roads, giving a panel extraction ratio of 34.4%. The main entries into the panel ran parallel to C50 and C52 which were driven initially in salt and rose later into the potash seam. Roadways C50 and C52 then linked up with the Experi-

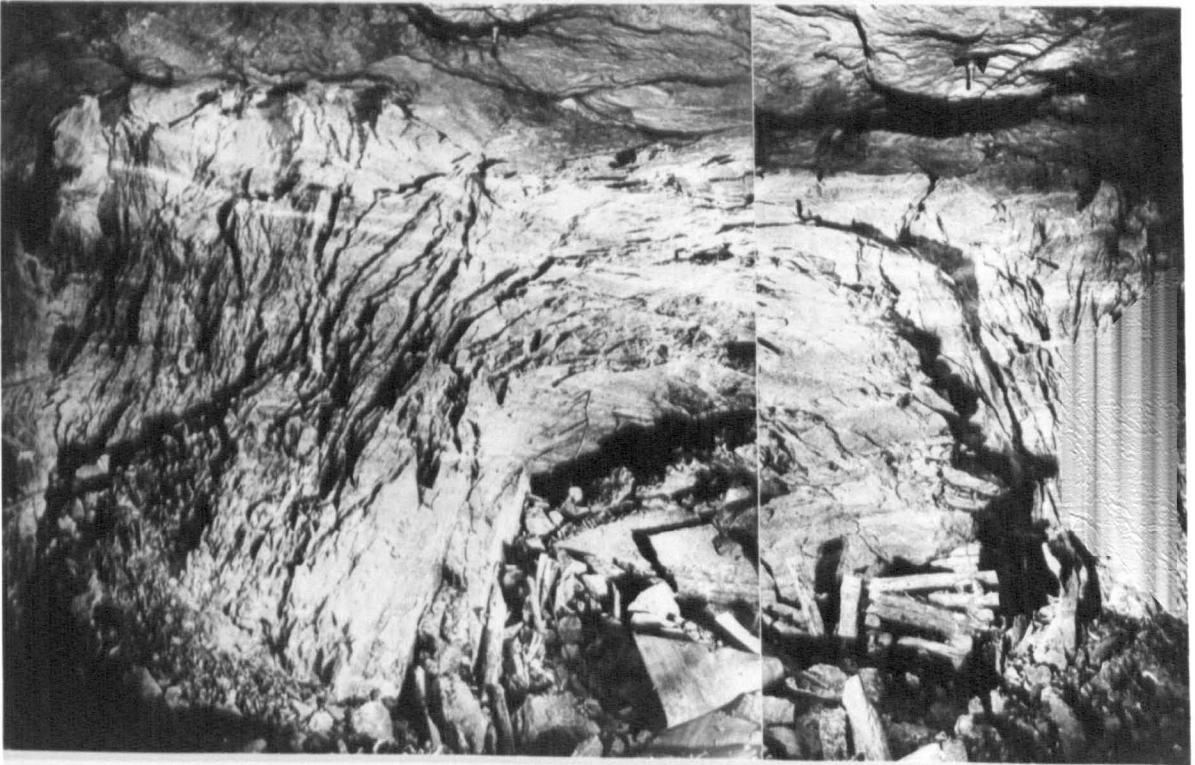
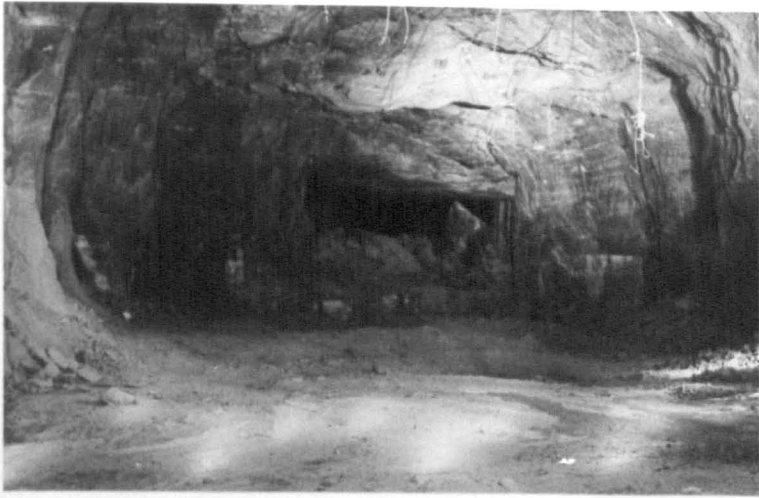
mental Panel, thus forming a seven entry panel. The conveyor was situated in C56 which was also the main return airway from the panel. No. 6 Panel was sited in a zone of thick primary potash ore and in the latter stages of development in July 1978, there were five Heliminers deployed within the area. Heliminers H1, H2 and H3 were developing other areas of the thick potash zone and were all working in a faceline with a limited number of headings. For the production analysis only data from machines H4 and H5 working in the southern part of the panel have been used. This gives a more accurate representation of a production rather than a development area.

The panel was instrumented with borehole extensometers and convergence stations at sites H9, H12, H13, H15 and H16 - Figure 3.12. Results obtained from this instrumentation have been fully reported⁽¹⁴⁾ and only the salient features will be mentioned.

Figure 3.13 shows the average strain against time for 25m, 30m and 40m pillars from different panels in the mine. The interesting feature here is that the 25m pillars exhibit less deformation with time than the 30m pillars in Panel 6. This apparently contradictory result can be explained by recourse to the geology. Hebblewhite⁽⁷⁾ concluded that as the 25m square pillars in No. 1 Panel were in an area with shaley potash in the roof and floor, they punched into the shale rather than yielding themselves. The 30m square pillars in the Experimental Panel however, are in an area that has halite and frequently anhydrite, in the floor, and thick primary ore in

Plate 3.2

- 1 Original roadway in centre showing enlargements by blasting roof and sides.
- 2 Original roadway in centre after enlargement by blasting. Note fracture pattern.
- 3 Close-up of centre road in No.1. Note formation of low angle shear fracture.



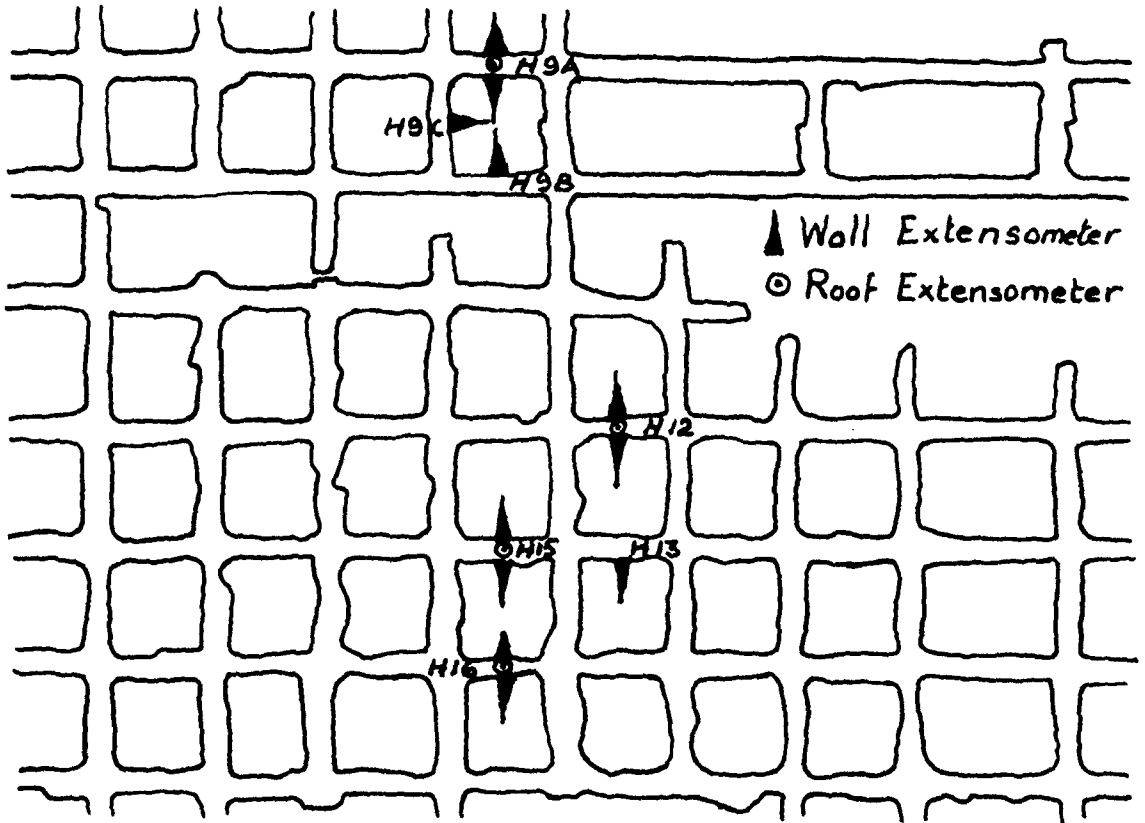


Figure 3.12 No. 6 Panel instrumentation sites

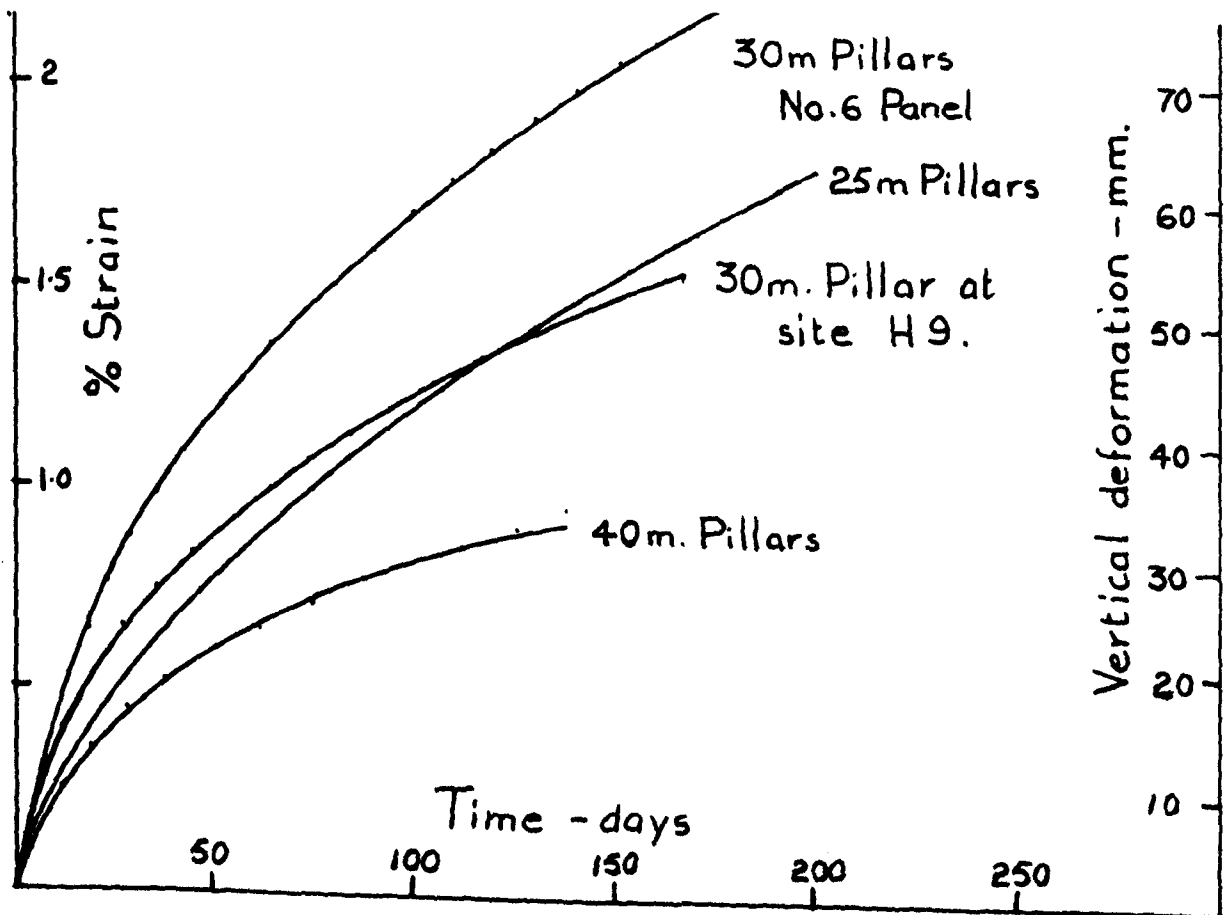


Figure 3.13 Strain rate/time curve for 25, 30 & 40m pillars

the roof. With these conditions punching does not occur and the pillar itself is forced to yield. It must be said that the primary ore was not consistently thick, and that in one or two places it thinned down so that the shale parting appeared in the roof. The shale parting was located in geological probe holes at depths from 1m upwards into the roof. Analysis of roof extensometer data indicated that a large part of the roadway closure is probably due to bed separation at the primary ore, shale parting and marl interfaces. Table 3.3 gives an analysis of roof movements at different depths for sites H15 and H16. Figure 3.14 shows the geological sections at these sites. It can be seen that a significant proportion of the roof sag takes place at a depth greater than 6m in H15, while in H16, this is much less. For example, after thirteen days the proportions are 44% compared with 5.9%.

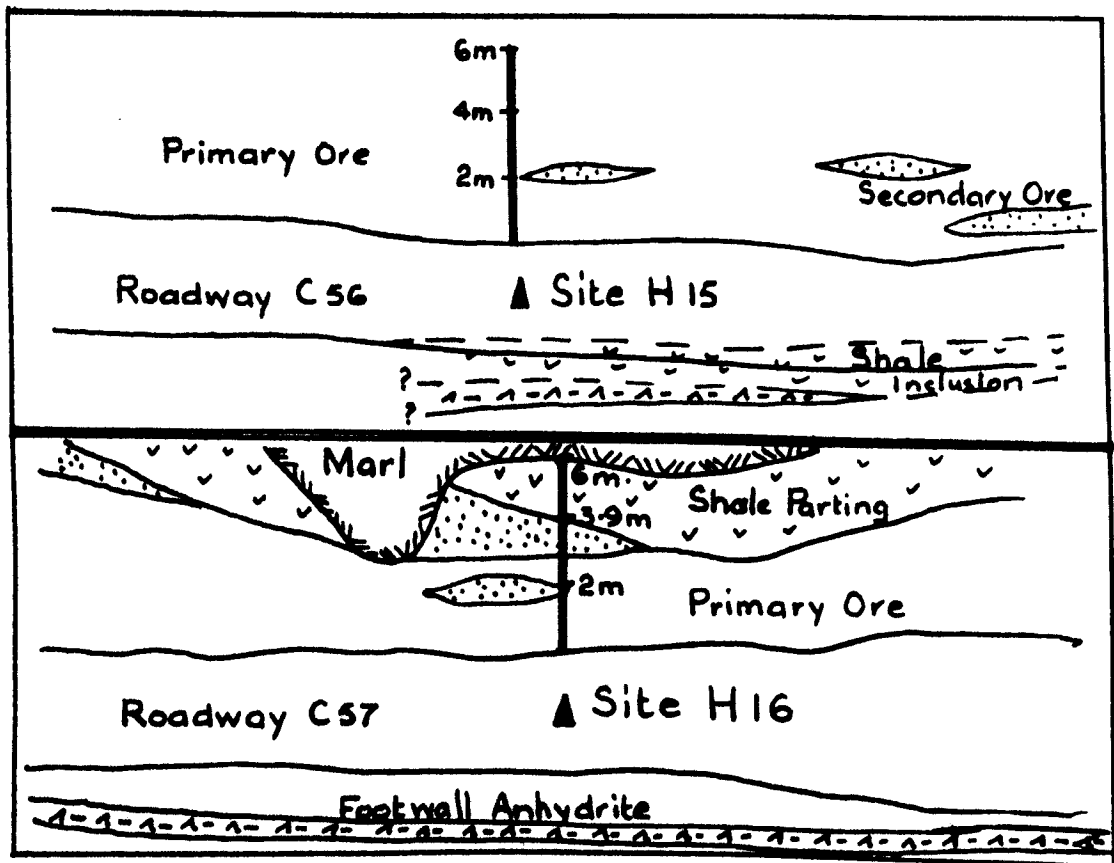


Figure 3.14 Geological sections, sites H15 and H16

TABLE 3.3

% Roof Sag Due to Strata Movement

Site	Time (Days)	Roof Sag (m)	% Roof Sag Due to Strata Movement				% Strain 0-2m
			0-2m	2-4m	4-6m	beyond 6m	
H15	13	.031	43.5	3.0	9.1	44.4	0.7
	18	.053	49.2	28.5	8.7	13.6	1.3
	26	.085	57.8	25.5	8.3	8.4	2.5
	46	.182	41.5	15.8	8.5	34.2	3.8
	60	.193	60.6	17.8	9.3	12.3	5.9
H16	41	.078	61.4	7.2	25.5	5.9	2.4
	48	.095	60.3	3.7	27.4	8.6	2.9
	53	.106	60.1	4.3	25.2	10.4	3.2
	63	.124	61.1	7.5	22.4	9.0	3.8
					* Beyond 4m		
	68	.134	60.9	8.1		31	4.1
	77	.148	62.2	12.2		25.6	4.6
	84	.158	63.9	10		26.1	5.0
	89	.165	64.2	7.1		28.7	5.3

*Note: anchor 3 (at 6m) lost after 63 days

The production analysis has been confined to the two continuous miners which were working within the Experimental Panel between April and July 1978. During this period the advance per shift for each Heliminer was 4.0m. Each pair of Heliminers was manned by one production crew, with maintenance being undertaken on one machine during the dayshift. This system ensured that it was possible for the production crew to be fully employed, since single machines manned by one crew tended to be under-utilised while waiting for headings to be supported and probe holes drilled. A team of eight men was used to man the two Heliminers, resulting in an OMS of 51t. These figures refer to the five entry panel, that is excluding C50 and C52 which had been mined separately some time before. It is likely that productivity would have been even higher had there been seven entries giving an increase in the number of available working headings. The panel ceased working in July 1978 as it encountered an overfold of halite, giving a large increase in dilution.

3.3.7 No. 8 Panel

This panel was the first in the mine to adopt the high extraction yield pillar technique, the so-called "stress relief" method described by Serata⁽¹⁵⁾. Variations of this technique are successfully used in Canadian potash mines. Heliminers H4 and H5 were transferred from the Experimental Panel to No. 8 Panel in July 1978. The panel layout, Figure 8, Appendix 1, incorporated six, 6m wide roadways with 3m yield pillars between the outer two pairs of roads. This 3m width was later increased to 4m. The outer four roads were

mined approximately 25m ahead of the inner two, giving about one week's lead in time. According to Serata, collapse of the outer roads would allow the stresses to redistribute in such a way that a protective stress free envelope would form around the inner two roadways. In this way stability of the centre roadways would be ensured. The extraction ratio of the panel was 66%. Cross-cuts were angled at 45° to take account of the mining sequence in addition to improving ventilation and shuttle car handling.

The principal measurements made in Panel 8 were those of convergence, both roof to floor and wall to wall, micro-creep and a number of extensometers were installed. The micro-creep measurements were made using a Serata micro-creepmeter. This instrument allowed accurate closure rate readings to be obtained, usually over a short time base of 30 minutes or so. It suffered from the substantial disadvantage of not giving a total closure measurement. Fortunately, some closure measurements were made at certain sites. This data is more fully analysed in Chapter Six. In addition and more meaningful, were the regular visual inspections carried out during the driving of the panel. A large number of photographs were also taken. It was unfortunate that after progressing about 40m, the panel mined into an overfold in the succession, caused by regional faulting. The potash disappeared altogether and the panel had to mine in footwall halite for a distance of some 90m in order to avoid exposing marl in the roof.

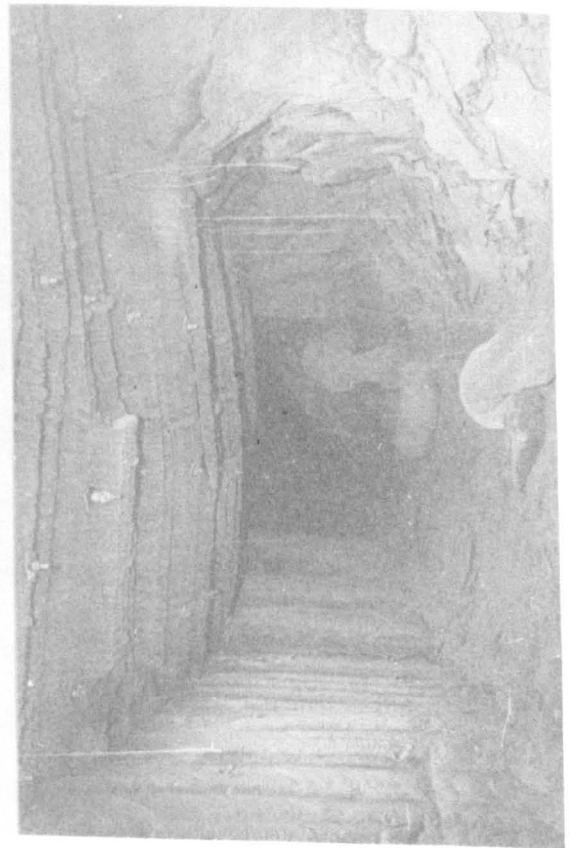
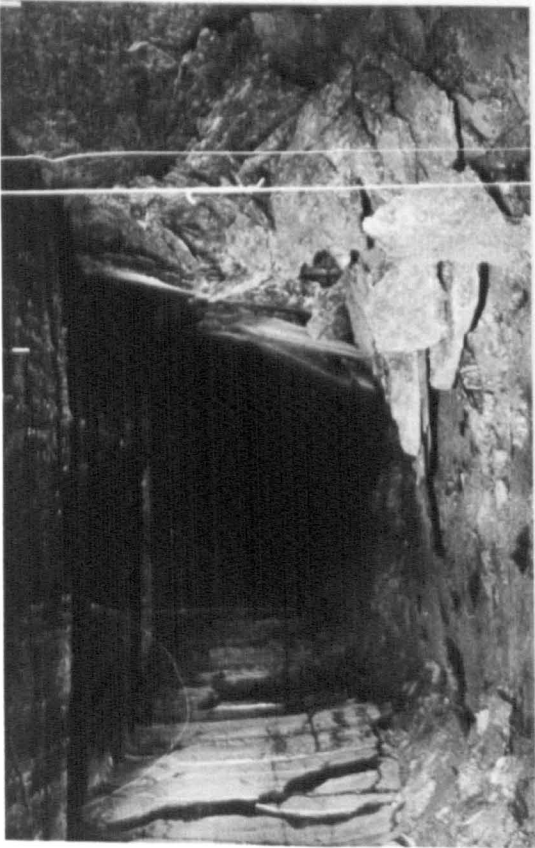
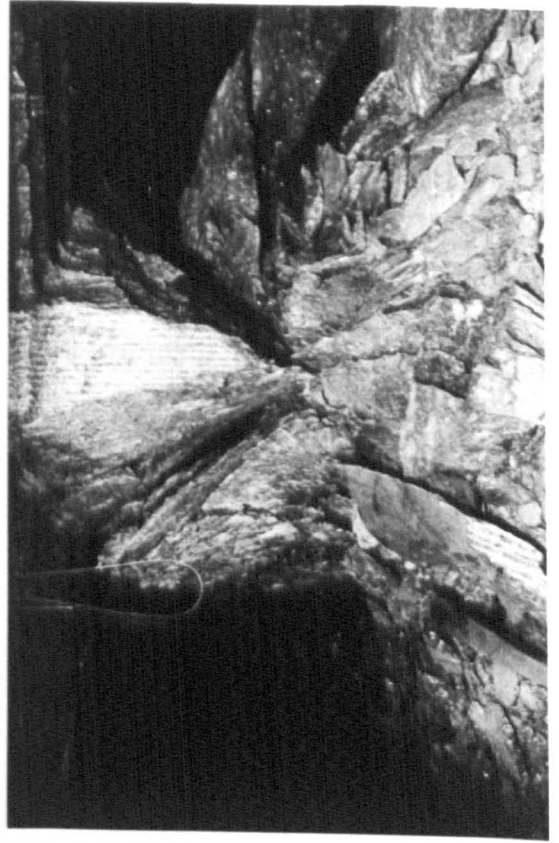
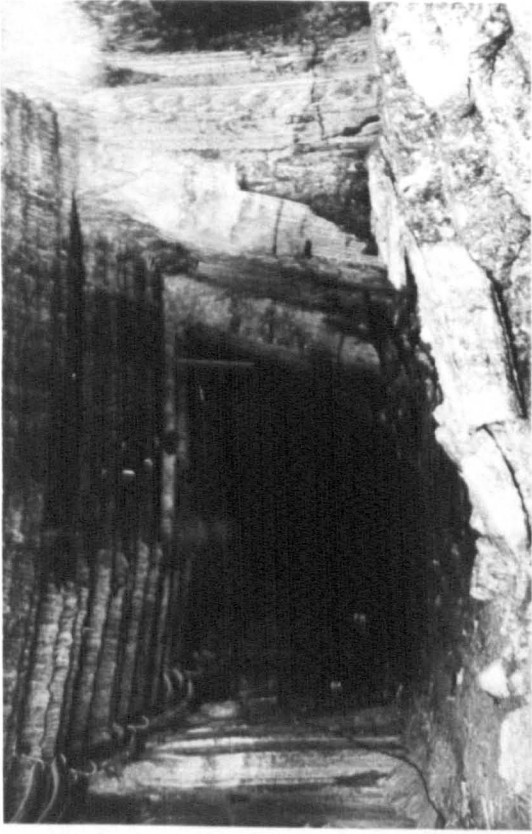
Observations showed that "stress relief" as described by

Serata did not occur, in that there was no massive failure of the outer roads. In fact, the outer roads ended up in better condition than the inner ones. No satisfactory explanation could be given for this unexpected result. Similar results have been obtained for other high extraction panels, and this phenomenon is dealt with at length in a subsequent chapter. Plate 3.3 has photographs showing conditions in various roadways.

In addition to a good roof, the intact condition of the outer sidewalls (Plate 3.3) of the panel was striking. After the panel had progressed some 230m, which took two months, it was decided to swing the panel to the south-east in order to follow what was thought to be a trend in thick potash ore. Because of deteriorating ground conditions, all travelling through the panel was stopped three months after mining had begun. Vertical closures of the order of 380mm occurred some 100 days after mining. Wall to wall movement was even more dramatic, being of the order of 520mm after 100 days. The extensometer that was installed 6m into the east abutment sidewall at RA1 is highly significant in that it shows (Figure 6.5) that the strain decays rapidly to 0.6% some 5m into the solid. This unexpected result means that very little load was being carried on the immediate abutment sidewalls. With a panel width of 62m and 66% extraction, high abutment pressures are to be expected, indeed if stress relief is to work, they are required in order to fail the outer roads. An explanation for this apparent contradiction is offered in Chapter Nine.

Plate 3.3

- 1 Note good roof, difference between intact abutment wall (left) and failed yield pillar (right).
- 2 Same as No 1.
- 3 Same as No 1 and No 2.
- 4 End-on view of failed 3m wide yield pillar.



The production analysis for the period August to October 1978 gave an advance per shift of 3.9m, and an average OMS of 50t. The mining method was found to be considerably less flexible than the conventional room and pillar method because of the necessity of maintaining the correct sequence of drivage. The benefits from the concentration of men and materials and shorter tramming distances outweighed the disadvantages and resulted in high productivity.

3.3.8 Nos. 15 and 16 Panels

Nos. 15 and 16 Panels (Figure 9, Appendix 1) were mined off the West Link development. This was a twin roadway system developed in salt west from the shaft pillar. In order to limit further development in salt, it was decided to mine a high extraction panel in potash along the line of the West Link development. The salt roadways below would then follow on if required in the protection afforded by the mined out panel above. Potash ore would be loaded into ore passes between the two levels which were approximately 8m apart in this section. The reason for the salt development was to obtain certain long-life access to the production blocks. Panel 16 was set off at right angles to the West Link, going north. This panel is intended to form an access development panel, containing long-life access roadways equipped with conveyors and major intake and return airways. These will service production panels set off to the west as Panel 16 advances and then panels will be mined to the east on the retreat. Panel 16 is intended to be

approximately 1 km long and to have a life of two to three years. It was intended that the production panels would be standardised according to the layout in the section of Panel 15 which consisted of two four-entry 40m wide sub-panels separated by a 40m pillar. This gives an overall percentage extraction of 58% and a panel (40m) extraction of 75%. The reasons for this layout are discussed in Chapter Ten.

Rock mechanics instrumentation sites have been established along the West Link and in the panels. It was anticipated that sections of the West Link salt roads in the panel abutment zone would suffer excessive loading and damage, and this area was therefore more intensely instrumented.

Roof conditions in Panel 15 were generally very good. The yield pillars with widths of 4m and 5m performed well in that they yielded as required with fairly normal closure rates and the roof has remained intact in the vital central roadways. Conditions in the outer rooms are excellent, and in the stubs in particular, except for one stub where marl was encountered. It can be said that conditions as observed are better in the stubs than anywhere else in the panel, with the small pillars between stubs showing very little signs of yielding. This indicates that roof to floor closures at the outer edges of the panel are less than the deformation in the centre of the panel. The roadways in No. 15 and No. 16 panels have been standing for some eight months since mining, and apart from one or two local roof falls due to adverse geological

Plate 3.4

West Link Salt Roads

1. Drill and blast section.
2. Cracks in concrete columns in connecting cross cut.
3. Heliminer driven section.
4. Photoprofile

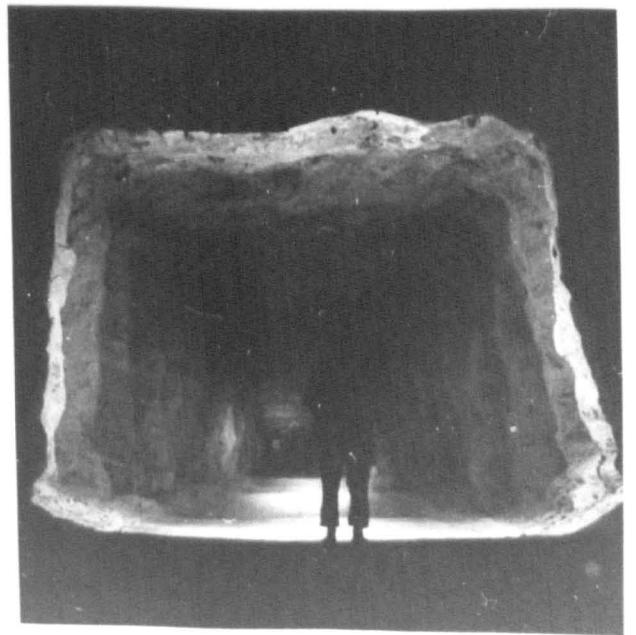
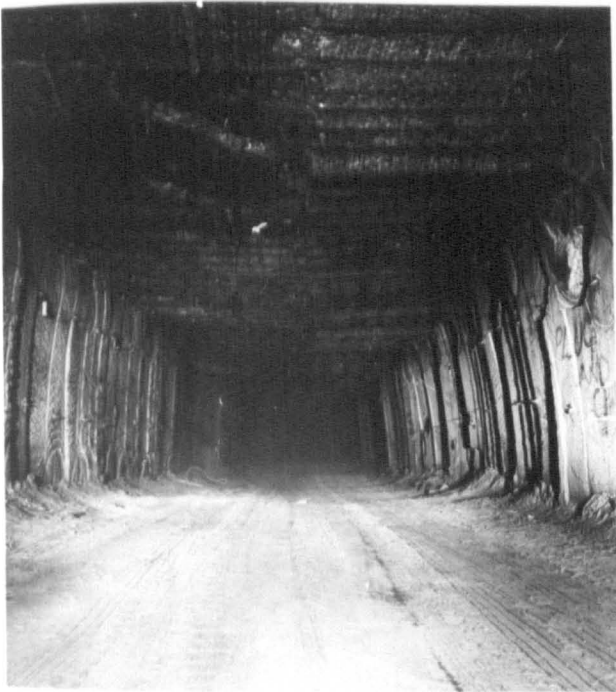
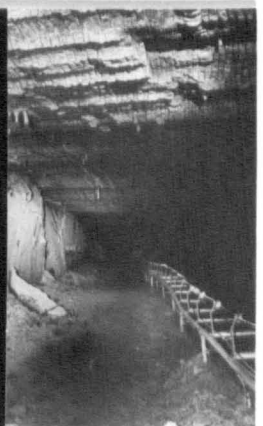
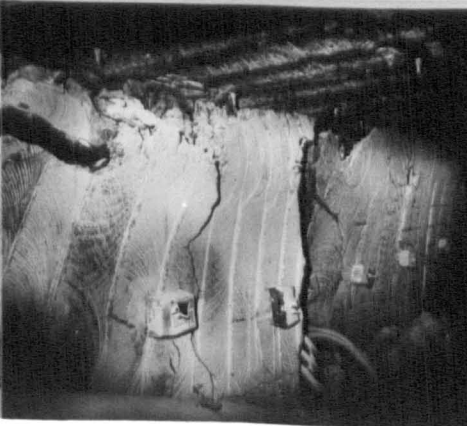
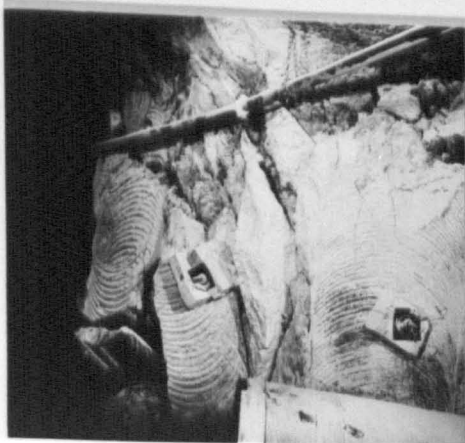
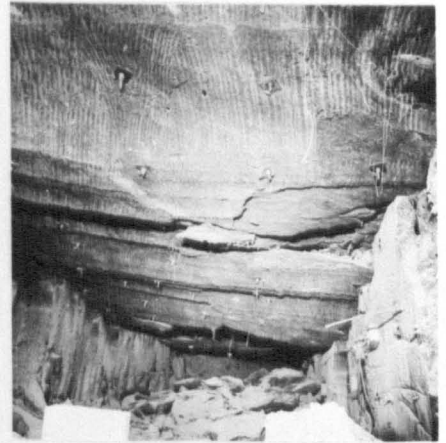
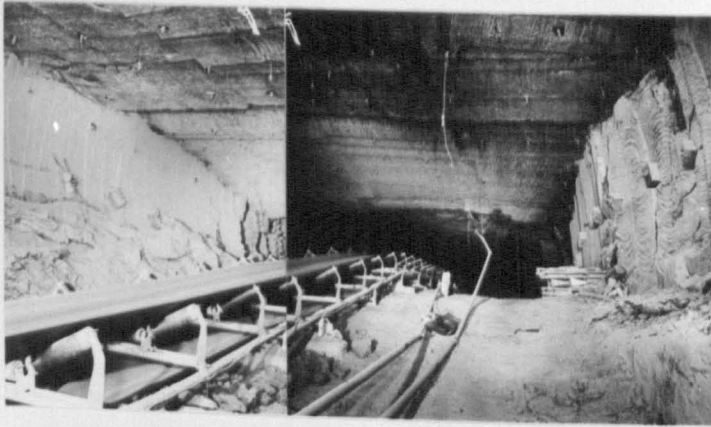
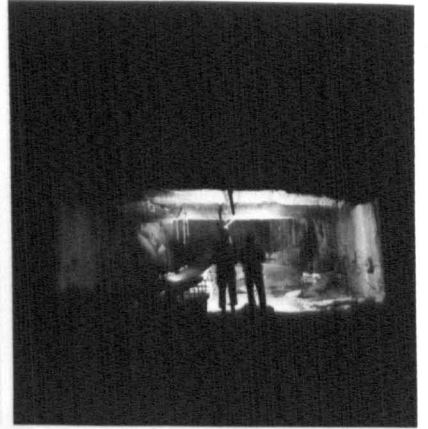
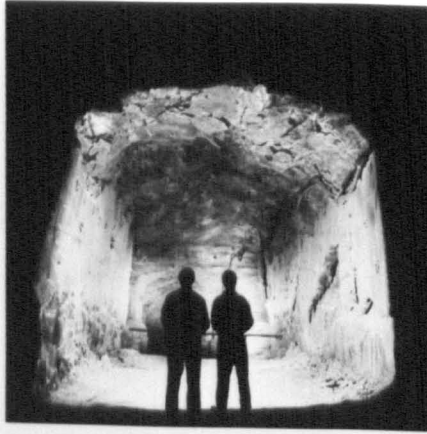


Plate 3.5

- 1 Some roof failure. Vertical shearing in roof down left-hand side - horizontal shearing on right-hand side.
- 2 Profile, roof has had to be ripped, and is failing again. Sidewalls high and in good condition.
- 3 Profile of a C43 Conveyor road.
- 4 C43, 9m wide - good roof, plenty of room for subsequent sidewall movement.
- 5 Extensive roof failure. Note support not much use.
- 6 Panoramic view down 4m wide yield pillar.



conditions such as shale or marl inclusions, conditions are good throughout the panel.

The panel advances per week for No. 15 and No. 16 panels were 11.8m and 6.5m respectively. The reason for the low figure for Panel 16 is that a number of marl downwarps and shale inclusions were encountered soon after mining commenced. These, in addition to the large stiff pillar left in cross-cut No. 3 in Panel 16, caused some severe roof collapses. The O.M.S. values which were respectively 34t and 17t were calculated on the same basis as for the low extraction panels. Because of the gasblow problem encountered as a result of mining in shaley ore, it was decided to drive the headings by undercut drilling and blasting, followed by loading out and milling to the final dimensions using a Heli-miner. This extra operation accounts for the lower O.M.S. compared with Panels 8 and 6.

3.3.9 No. 10 Panel

No. 10 Panel (Figure 10, Appendix 1) was mined as a continuation of C43 roadway. Initially it consisted of three sections; two having three roadways and one with two roads, separated by 40m square pillars. These panels were the first real attempt after No. 8 Panel at high extraction mining in potash, and as the subsequent stability of the roadways proved, it was successful. The layout suffered from the drawback that it did not provide sufficient

faces for the Heliminers to operate efficiently, and it was decided on the advice of Dr. Serata to open up the centre panel to 90m wide having five entries separated by 4m yield pillars. Stubs, 10m wide and 18m long, were driven at right angles from the outer roads with 4m pillars between them. The rooms were all 6.5m wide with the exception of the centre conveyor road which was 9m wide. It was reasoned that because the yield pillars could be expected to result in poor sidewall conditions, the wider room would give added protection to the conveyor in the event of severe slabbing. Previous work⁽⁷⁾ had indicated that high extraction panels should not be more than 60m wide if the danger of encountering water from roof strata was to be minimised.

Rock mechanics sites were established at various points in the panel, and these monitored closure rates using both the Serata Geomechanics Microcreepmeter, and direct measurement of closure. Unfortunately, it is not possible to obtain total closure measurements with the microcreepmeter. The panel had been mining for some eighty days when water began to pour from probe boreholes in E and H roadways at the points marked in Figure 6.9. Mining ceased ten days later and all men and machinery were pulled out of the panel. Water inflow had reached a flow rate of about 180 litres per minute, at which rate it appeared to stabilise.

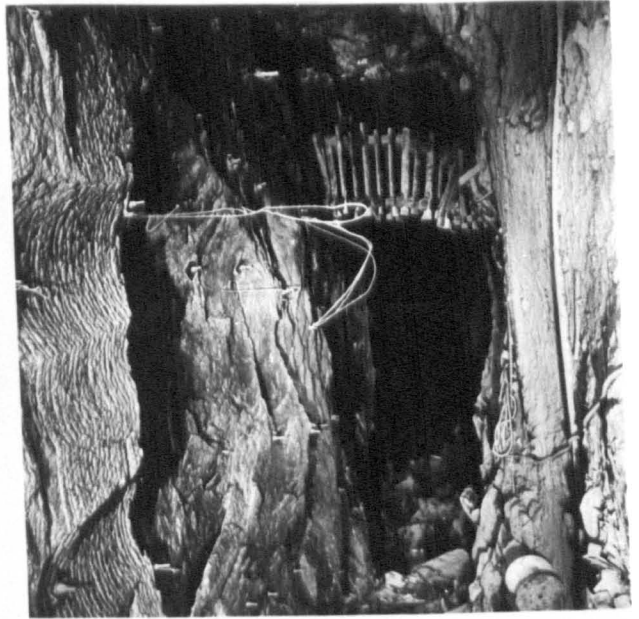
The panel advance per week averaged 12.5m over the twelve week period of production with an O.M.S. of 4lt.

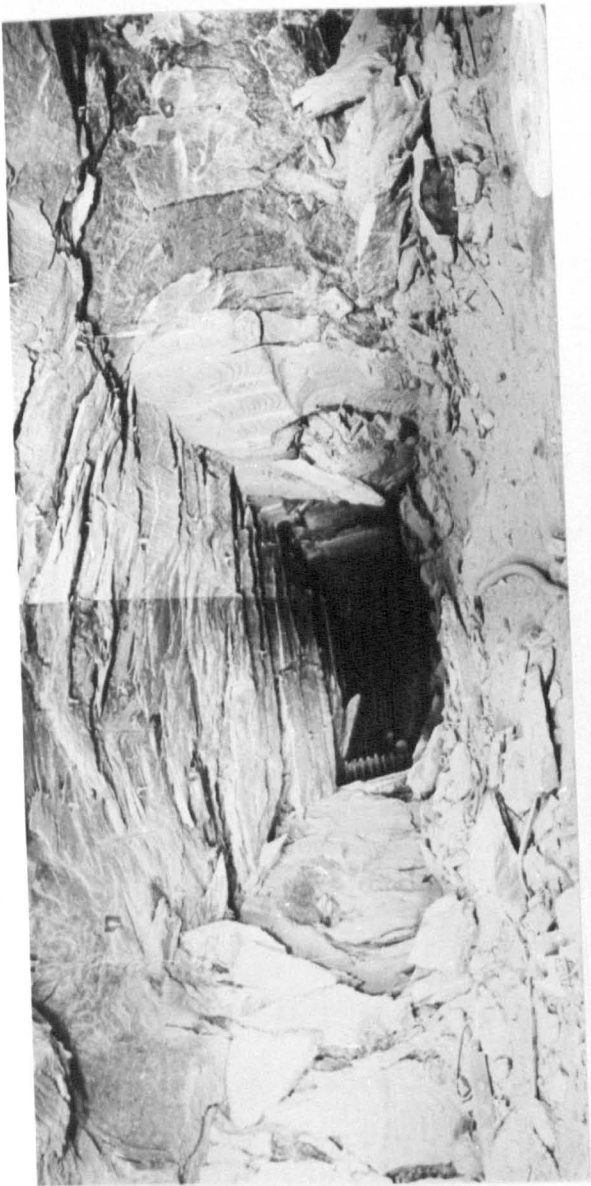
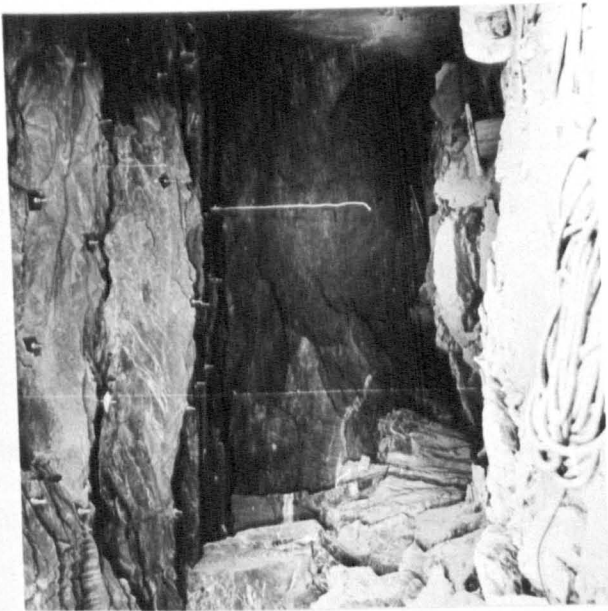
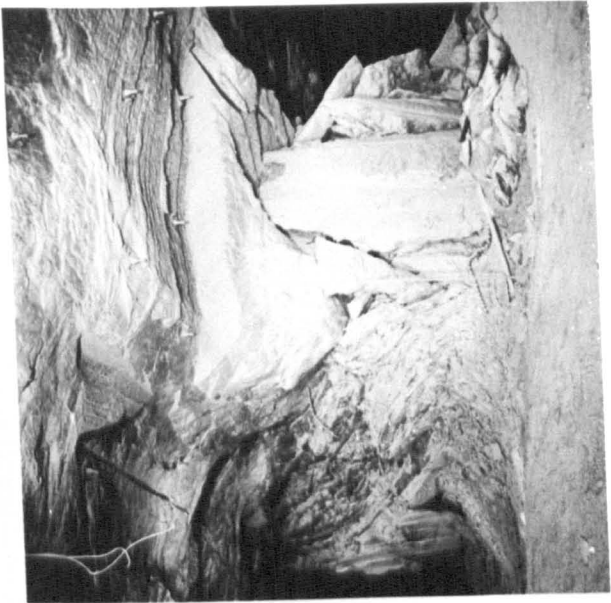
Plate 3.6

- 1 Looking west along C44 from junction
Note intact roof, sideway pillar movement.
- 2 Looking East along C44 at junction
Note high sidewall, good conditions.
- 3 Note shear failure in roof, contrast with 1.
- 5 Same view as 1 but taken 6 months before. Most noticeable effect is that of sidewall movement.

Plate 3.7

- 1 Same as 3 some 6 months later. Note increase in all round failure. Effect least on sidewall of large pillar (right). Contrast with conditions in 1.
- 2 One of the rare occurrences of footwall heave.
- 3 Extensive roof failure.
- 4 4m wide yield pillar showing yield at pillar end. Contrast with 4.





3.3.10 No. 17 Panel

No. 17 Panel (Figure 11, Appendix 1) can be divided into two sections, Section A where it was 90m wide, and B where it was narrowed down to 45m. This was done as a result of the water inflow in No. 10 and No. 19 Panels, when it was decided that the water inflow had occurred because of the excessive panel width of 90m.

The panel was driven at right angles off the northern three-entry panel of No. 10 Panel, using Heliminer H9 when it was removed from No. 10 Panel. Initially it advanced some 90m at a width of 90m before it was narrowed to 45m. Unfortunately there were no rock mechanics sites established in this 90m wide section.

An average advance of 12.9m per week was achieved, with an O.M.S. of 40t. The section was mined for seven weeks. Water was encountered in G roadway, at a flow rate of 22 litres per minute.

Section B was a continuation of Section A, but with a width of 45m, achieved by eliminating the outer two roads and the stubs. Several rock mechanics sites were installed, but only microcreep-meter data were recorded and a few wall to wall closures. The wall to wall closures recorded after 50 days were of the order of 450mm, which compared with 400mm for a similar site in No. 8 Panel. The average advance per week was 23m, and the O.M.S. achieved was 40t. Conditions in this section were very good and are reflected in the

high output achieved. It is interesting to note that the standard layout to be adopted for all new panels is basically a double unit the same as the above, separated by a 40m pillar, with a slightly narrower panel width of 40m.

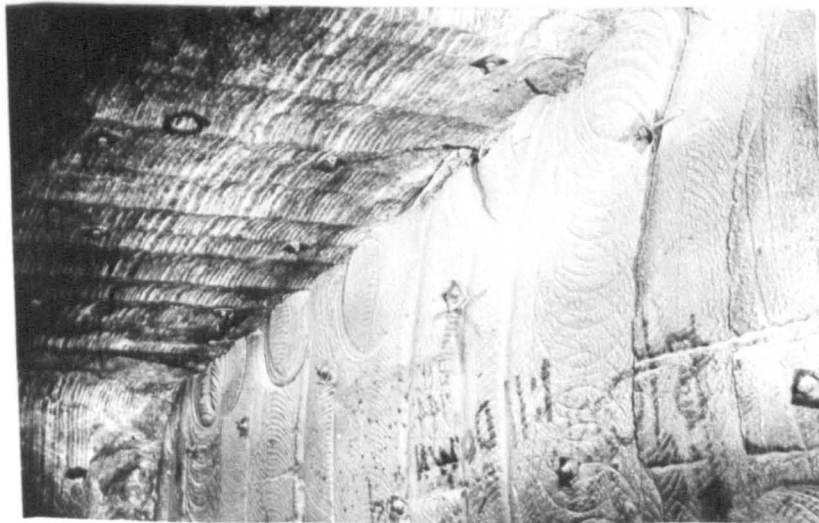
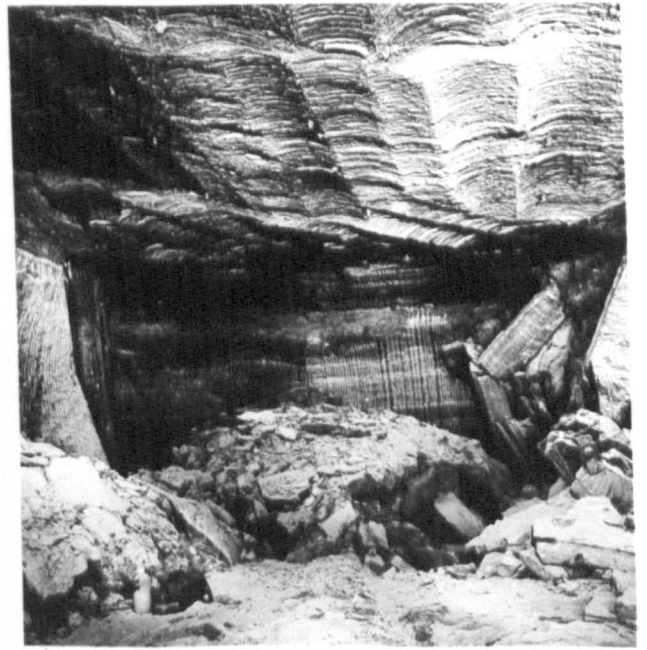
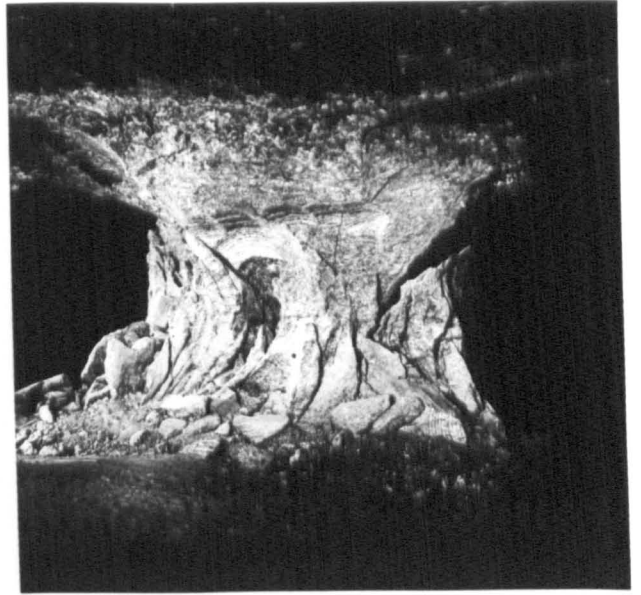
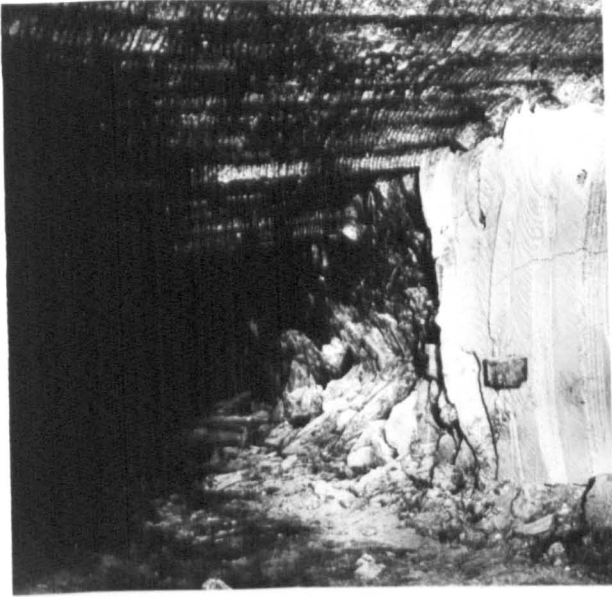
3.3.11 No. 19 Panel

No. 19 Panel (Figure 12, Appendix 1) was mined at an angle of about 45° to the north west of No. 10 Panel. It was decided to mine in this direction in order to mine parallel to a geologically disturbed zone that had been intersected by No. 6 Panel and No. 8 Panel. In this way it was hoped to avoid mining in the very mixed strata associated with the faulted ground. From the beginning, trouble was experienced in the panel. Excessive closure rates and marl downwarps did nothing to improve matters. Figure 3.15 shows how it was originally laid out and how it eventually ended up. Rock mechanics measuring stations were established as shown in Figure 6.35. "J" roadway was particularly well instrumented with a station every 20m or so along its length. Figure 6.36 gives the closures along J road for various time periods. The problems of No. 19 Panel are discussed further in Chapter Six. This was the second panel where water entered the workings in E roadway some ten days after the inrush in No. 10 Panel.

A mean advance rate of 10m per week was achieved over the fifteen weeks that the panel was mined, giving an O.M.S. of 31t. The panel ceased mining in its original direction on 22nd October

Plate 3.8

- 1 Roof in good condition, pillar failed.
- 2 End-on view of 4m yield pillars.
- 3 Site showing roof relatively intact, extensive sidewall failure due to high closures. E road water sites.
- 4 Good conditions in the stub at water site.
- 5 Top corner in stub showing increasing amounts of vertical shears.



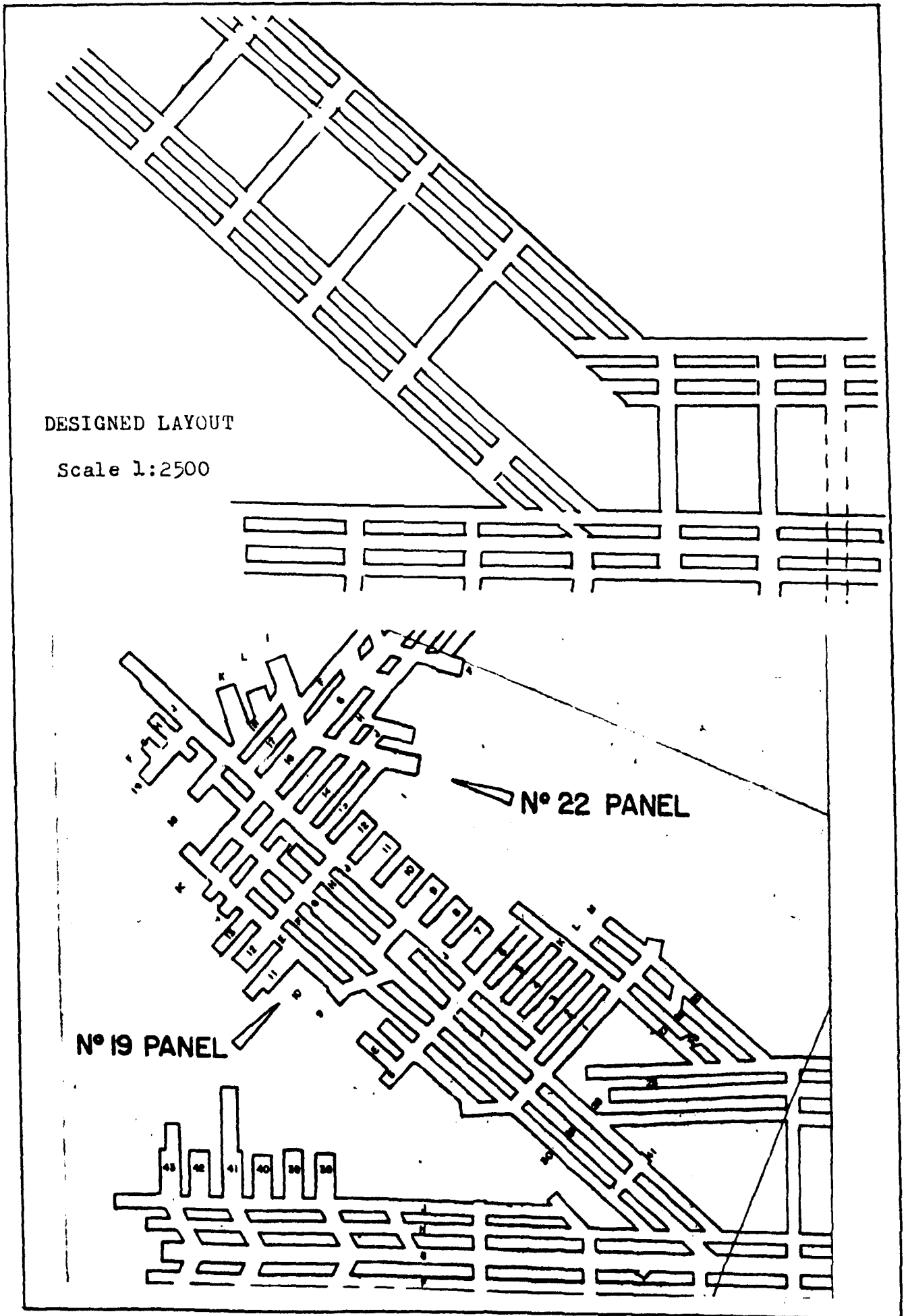


Figure 3.15 No. 19 Panel, designed and actual layouts

1979 and a new panel, Panel 22, was set off at right angles to the north east from the end of Panel 19. There is no doubt that the direction, extent, and sequencing, of mining Panel 19 relative to Panel 10 had an adverse effect on the stability of the surrounding strata. The wedge shaped pillar formed at the breakaway could not have developed a stable core until it was 30m to 40m wide. This meant that in fact the two panels could be considered to be acting as one single wide panel over a considerable distance. It is possible that this led to the failure of vital hanging wall strata which gave rise to the water entering the workings.

3.4 Concluding Remarks

This Chapter has set out the various mining layouts that have been implemented since the inception of mining. Many different geometries have been tried. Immediately prior to the water intrusions occurring, it was felt that as far as layout was concerned, the mine's problems had been solved. Subsequent inflows in other wide (>90m) panels made a re-appraisal an urgent necessity. The conflicting aims of higher productivity and safer mining layouts have not yet been satisfactorily resolved. It is hoped that by fully analysing the data available from measurements in the mine, an optimum compromise solution can be attained.

CHAPTER FOUR

REVIEW OF WORK CONCERNED WITH ROCKS EXHIBITING TIME DEPENDENT
PROPERTIES

CHAPTER FOUR

4.0 Introduction

A review of the literature has shown that the subject of rheological rocks has received much attention ever since it was realised that rocksalt could flow without fracturing. Rocksalt "glaciers" in Turkey and other arid regions have provided visual and measurable evidence of this strange phenomenon. Salt domes encountered in the ever increasing search for gas and oil have provided geologists with fertile ground for lengthy discussion, and theories abound as to the origin and mechanisms of subsequent movement of evaporite deposits. The increasing demand for the evaporite minerals, in particular salt and potash, has led to the opening of more underground mines at ever greater depths. The problems of working these deposits has demanded a deeper understanding of the behaviour of the evaporite rocks, both on a small scale and also a large scale.

Numerous papers and much research have been concerned with describing the time dependent properties of evaporites and many models have been proposed. Nearly all have been developed purely theoretically or from consideration of the behaviour of single crystals or laboratory scale test specimens. These results have often been generalised to describe the response of the rock mass surrounding mine openings, some with more success and accuracy than others. Statements made by different authorities on the subject

are often flatly contradictory. All of this makes the task of a relative newcomer to the scene extremely difficult when trying to assess and quantify the behaviour of mining excavations in a deep level potash mine such as Boulby. The added complexities arising from a highly variable non-uniform succession of geological strata make the creation of a viable and accurate model of the mine even more difficult, if not impossible.

The creep of rocksalt has been studied by numerous investigators over the past two decades. These studies have encompassed the behaviour of both single crystal and polycrystalline salt over a wide range of temperature and stress environments. Constitutive models for salt that reflect the observed creep behaviour have been formulated from the experimental data as part of many of these investigations. Some of these creep constitutive equations that have been employed in the past and are currently being employed in the analyses of the mechanical response of rocksalt will be discussed. No attempt will be made to make comprehensive comparisons of the constitutive equations. Several review articles have been published that discuss the creep experiments of various investigators from which the models are derived.

4.1 Terminology

It has been found that many of the terms associated with time dependent behaviour of rocks are often loosely used. In order to avoid ambiguity, some of the more commonly used words are defined. These definitions are similar to those given by Robertson⁽³²⁾.

The word deformation refers to all the qualitative characteristics of mechanics of materials, such as rupture, yielding, flow and fracture.

A general term for the non-linear time dependent behaviour of real materials is rheology; under rheology, large as well as small strains and the effects of heat and hydrostatic pressure are considered as a function of time.

In contrast with rheology, under viscoelasticity, only small strains at low temperatures and pressures are fitted into phenomenological equations with elasticity and viscosity coefficients.

The term elastic describes a linear stress-strain behaviour with recovery of strain on unloading and, without regard to time effects, in practical use, full recovery of strain is not important. In the behaviour of an inelastic material, strains are non-linear with stresses, and strain hardening may occur; but as in elasticity, strain rates are not considered.

The term plastic describes an ideal behaviour in which the initial deformation is elastic, and then at some yield stress, deformation continues without limit, that is, without strain hardening. No account is taken of time effects, but a linear relation is assumed between the vectors of stress and strain.

Anelasticity is a word introduced to describe the inelastic relaxation of very small deformations, usually studied as forced vibrations.

The term flow has connotations of liquid behaviour and is commonly used for inelastic deformation at nearly constant strain rate under any load.

Creep refers to inelastic deformation under a constant load, usually below the yield stress, and at any low strain rate.

4.2 Creep and Creep Constitutive Models

Creep can be defined in terms of the time dependent deformation of a material subjected to a constant stress state. Laboratory experiments are typically idealised into three stages of creep deformation for a specimen subjected to constant stress for long periods of time. These are described as:

- (1) Primary creep, where the deformation rates are decreasing (deformation rate here refers to a tensor defined in terms of the symmetric portion of the velocity gradient).
- (2) Secondary creep, demonstrating constant deformation rates,
- (3) Tertiary creep, exhibiting increasing deformation rates and usually terminating with fracture.

The relative importance of each regime is controlled by the deformation mechanisms that are active under the imposed conditions of stress and temperature. These deformation mechanisms include defectless flow, dislocation glide, diffusion creep, growth of microfractures and other (possibly yet undefined) mechanisms. Further, the rate of creep occurring as a result of a particular mechanism

is a function of the imposed environmental conditions.

Constitutive equations for materials undergoing creep deformations (frequently called creep "laws") have been developed from available experimental data. Often a creep law is determined by empirically fitting an arbitrarily chosen equation containing the necessary independent variables. In other instances, the form of the constitutive equation has been motivated from a model for the physical mechanisms dominating secondary creep. In this instance, the parameters appearing in the equations are determined such that the equations can approximate the data. Equations associated with deformation mechanisms have also been applied to primary creep without thorough physical justification.

Certain equations for primary creep and secondary creep are used most frequently. It will be helpful to review these equations in general terms before discussing specific cases. For primary creep, constitutive equations of the form:-

$$\dot{\epsilon} = f(t \text{ or } \epsilon) g(\theta) h(\sigma) \quad \dots \quad (4.1)$$

have frequently been used, where ϵ is the creep strain, t is time, θ is the temperature, σ is the stress, and f , g , and h represent functions. Creep laws using equation 4.1 assume that the effects of time, temperature and stress on the induced creep strain rate are separable. Functional forms of g that have been reported, include power laws (θ^n) and exponential law forms ($e^{-Q/R\theta}$). The

exponential forms are related to activation energies (Q) associated with deformation mechanisms, while the power law form is apparently strictly empirical. The use of time (t) or strain (ϵ) as the independent variable for f leads to the interpretations for the decreasing strain rate as a function of time, observed during constant stress creep tests. Life fraction rules for the function f have been proposed as an alternative to time and strain-hardening representations in which the proportion of total possible deformation that has occurred enters the constitutive model in place of time or strain. The stress function h , has most frequently been expressed as a power law (σ^n) to reflect the possible non-linearity associated with the stress state.

The distinction between strain-hardening and time-hardening is important in applications that have changing stress and temperature fields. Strain-hardening laws normally require that as the stress state changes, and thus moves from one constant stress and temperature creep curve to another curve, the shift occurs between points of equal times on the two constant stress curves. These two interpretations can give very different results. Life fraction rules represent a means of compromising between time-hardening and strain-hardening by moving from one constant stress curve to another, according to equal percentages of the total deformation that can be tolerated by the material. Time-hardening laws are the simplest to implement in a solution algorithm and are probably the most commonly used. They are most successfully applied when the problem involves

a stress state that is constant in time, but can produce very poor results if this is not the case. Time is not an intrinsic material property and in general, should not appear explicitly in the constitutive model.

Secondary or steady-state creep, is characterised by constant deformation rates under conditions of constant stress and temperature. Separable constitutive equations of the form:-

$$\dot{\epsilon} = f'(\theta) g'(\sigma) \quad \dots 4.2$$

have been used to model this type of creep. Weertman⁽³³⁾ has proposed that the functions f' and g' be defined as:

$$f'(\theta) = \frac{AG}{\theta} e^{-\frac{Q}{R\theta}} \quad \text{and} \quad g'(\sigma) = \left(\frac{\sigma}{G}\right)^n \quad \dots 4.3$$

where G is the shear modulus, Q is the activation energy, and R is the universal gas constant. It has been observed that the temperature dependence of G leads to the fact that the quantity $\frac{AG}{\theta} \frac{\sigma^n}{G}$, is nearly constant. At higher stress levels where slip occurs, the stress function is expressed as an exponential function such as $\sinh(B\sigma)$. At very low deformation rates and elevated temperature, where the diffusion limiting Nabarro-Herring or Coble creep mechanisms dominate, a linear dependence between stress and deformation rate is obtained.

Tertiary creep exhibits increasing deformation rates that lead to failure. Some work has been done in developing constitutive

models in terms of creep rupture theory that are appropriate for the tertiary creep regime. The onset of instability characterised by tertiary creep has been observed to be related to the total strain. However, little has been done to express either the transition from secondary to tertiary creep or creep rates in the tertiary creep range using constitutive equations for rocksalt.

Several efforts are currently being conducted to develop constitutive models for the deformation of salt. This has been partly motivated by the assumption that more than one mechanism is active for a particular combination of independent variables. This assumption has led to constitutive models having additive primary or secondary creep functions and provides a means of having multiple activation energies and stress non-linearities. Other efforts are being made to quantify where a given mechanism dominates over other mechanisms, but alone does not fully account for more than one mechanism being active at a particular stress and temperature state.

Analyses of creep deformations of salt have been provided in recent years by numerical methods using finite element or finite difference methods in the space domain, and various numerical techniques in the time domain. Some of the models were elastoplastic to predict the stress state due to the applied loads. Creep deformations are then predicted using the computed stress state in conjunction with the relevant creep law. Other analyses are formulated from a creeping flow formulation in which the elastic response is neglected.

Elastoplastic formulations normally assume linear elastic behaviour for stress states lying below the yield surface. A Mohr-coulomb failure criterion might typically be used. Once the stress reaches the yield surface, the material deforms inelastically and independently of time. The stress state resulting from the elastoplastic analysis is introduced into the creep law to predict the creep strain increment for a specified time increment. Some analyses have applied a yield surface concept to the creep law in such a way that no creep deformations occur below a certain limiting stress.

Creeping viscous flow formulations have also been applied to the analysis of creep deformations. These relate the applied stress field to the deformation rates of the material using the creep law as the constitutive model for a non-Newtonian fluid. Normally such formulations neglect the elastic portion of the deformation and thus apply to problems in which creep strain increments dominate over elastic strain increments for a given time increment.

Table 4.1 lists the primary creep constitutive equations as described by various investigators. Similarly Table 4.2 gives a list of secondary creep constitutive equations. These were derived mainly from rocksalt data.

4.3 General Creep Equation

This can be expressed as

$$\epsilon = \epsilon_e + \epsilon(t) + At + \epsilon_T(t) \quad \dots 4.4$$

where ϵ is strain, ϵ_e is elastic strain, t is time, A is a constant

$\epsilon_T(t)$ is a function expressing the accelerating creep of the tertiary stage, and $\epsilon(t)$ is a function expressing the decelerating creep of the primary stage. The elastic strain ϵ_e occurs immediately after loading; the steady state term At , accounts for linear strain with time, which occurs after the transient creep stage. No expression has been derived for $\epsilon_T(t)$ and it is therefore disregarded. Many forms for transient creep $\epsilon(t)$ have been proposed, the most common being that represented by a logarithmic relation

$$\epsilon(t) = B \ln t \quad \dots 4.5$$

Another relationship is given by the Kelvin-Voigt viscoelastic model.

$$\epsilon(t) = B \left[1 - e^{(-t/t_k)} \right] \quad \dots 4.6$$

in which t_k is the retardation time constant for transient creep.

At $t = t_k$ the strain reaches $0.632B$ where B is the maximum, asymptotic value of strain at infinite time.

The Burger viscoelastic model adds the expression for a Maxwell material to that of the Kelvin-Voigt material to account for steady state creep at constant stress:

$$\epsilon(t) + At = B (1 - e^{(-t/t_k)}) + C \left(1 + \frac{t}{t_m} \right) \quad \dots 4.7$$

where C is a constant involving the stress, and t_m is the relaxation time constant. At time $t = t_m$, stress decreases by $1/e$ at constant ϵ .

TABLE 4.1

PRIMARY CREEP CONSTITUTIVE EQUATIONS

Investigator	Primary Creep Law	Units (θ , t, σ)	Data Source
McClain and Starfield	$\epsilon = 1.3 \times 10^{-37} \theta^{-37} t^{9.5} \sigma^{0.3} \sigma_0^{3.0}$	K, hrs, psi	Lomenick's pillar studies
McClain and Starfield	$\epsilon = 6.5 \times 10^{-37} \theta^{-37} t^{9.5} \sigma^{0.37} \sigma_0^{3.0}$	K, hrs, pai	Project Salt Vault
Maxwell, Wahi and Dial	$\dot{\epsilon}_c = .4656 \left[(3.1386 \times 10^{-20}) S^{3.0} \exp\left(\frac{-4100}{\theta}\right) \right] \frac{1}{.4656} \left[\frac{1}{\epsilon_c} - 1 \right]$	K, s, Pa	SENM Salt
Ratigan and Callahan	$\epsilon_{ij} = 6.87 \times 10^{-15} \left(\frac{\theta}{295.5}\right)^{9.5} t^{0.40} J_2 \sigma^{ij}$	K, s, psi	Project Salt Vault
Hansen	$\epsilon_1 = 1.1 \times 10^{-35} \theta^{-35} t^{0.4656} \sigma^{2.475} \epsilon^{8.969}$	K, s, psi	SENM Salt
Thoms, Char, Bergeron	$\epsilon_{ij} = \frac{1.45 \sigma_{ij} - .45 \delta_{ij} \sigma_{kk}/3}{15.6 \times 10^{-38} (J_2) \cdot .974 \theta^{9.66} t^{-.75}}$ $i = j$	K, hr, psi	Weeks Island Salt
Carter	$\epsilon_t = 200 \sigma_t^{1.4} \theta^{0.55} \exp\left(\frac{-19.7}{R\theta \times 10^{-3}}\right)$	K, s, bar	LeComte data

TABLE 4.2

Secondary Creep Constitutive Equations

Investigators	Secondary Creep Law	Units (stress, temperature, time)	Data Source
Hedley	$\dot{\epsilon}_A = 15 \times 10^{-14} \sigma_0^{2.7}$	psi, -, days	Salt Mine Convergence measurements
Obert	$\dot{\epsilon}_A = D \sigma_0^{3.0}$	Coefficient D not given	Michigan Salt Kansas Salt
Thompson & Ripperger	$\dot{\epsilon} = 11.4 \times 10^{-7} \left(\frac{\Delta\sigma}{2500} \right)^{5.5}$	psi, -, minutes	Grand Saline and Hockley Texas Salt
Heard	$\dot{\epsilon} = 3 \times 10^{-6} \exp\left(-\frac{11833}{\theta}\right) (\Delta\sigma)^{5.5}$	bar, K, seconds	Artificially salt aggregates
Dawson & Tillerson	$\epsilon'_d = 1.232 \times 10^{-23} \exp\left(-\frac{5200}{\theta}\right) \sigma'_d{}^3$	Pa, K, seconds	SENM Salt

σ_0 - average pillar stress

$\Delta\sigma$ - stress difference

σ'_d - effective deviatoric stress

$\dot{\epsilon}_A$ - axial strain rate

$\dot{\epsilon}$ - strain rate

$\dot{\epsilon}_d$ - effective deformation rate

4.4 Effect of Stress on Creep Rate

The amount of strain ϵ observed in a creep test after a given time depends on the strain rate $\dot{\epsilon} = \frac{d\epsilon}{dt}$, which in turn depends on the amount of stress applied. An empirical equation commonly used to relate the variables is:-

$$\dot{\epsilon} = A\sigma^n \quad \dots 4.8$$

and approximately:

$$\epsilon = A\sigma^n t \quad \dots 4.9$$

where σ is the maximum stress difference applied, and A and n are constants.

4.5 Applications to Excavations in Potash

Having been armed with a battery of constitutive equations, it might appear that all that is now required is to select the appropriate one and (possibly with minor modifications) apply it to the underground mining situation. The following section deals with the attempts by the very limited number of investigators who have involved themselves with potash mining.

4.5.1. Serata

Serata^{(15),(19),(20)} has developed a rheological constitutive model to represent the material properties of salt rocks. This is

a complex model and is shown diagrammatically in Figure 4.1. It includes elasticity, viscoelasticity, viscoplasticity, dilatancy, strength and strength deterioration, brittle failure and post yield behaviour in terms of hydrostatic and octahedral tensors.

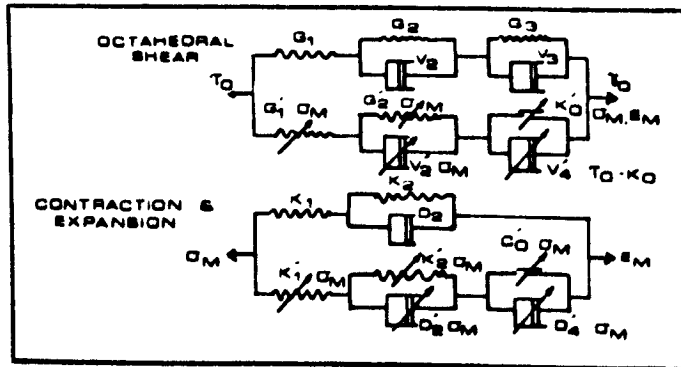


Figure 4.1 Rheological constitutive model - Serata

The claim is made that by using this method of defining material properties, all geological materials including both brittle and ductile rocks, can be represented by the constitutive models. The material properties thus defined are used to develop a rheological finite element computer program (REM). This program, it is claimed, provides the basis for both the design analysis of underground openings and the analysis of instrumental data. No details or listing of the program have so far been published.

In order to determine the behaviour of underground excavations, various instruments have been developed. These include the micro-creepmeter, a stressmeter and multiple point borehole extensometer, all of which have been patented and are described⁽¹⁸⁾.

The micro-creepmeter has been used at Boulby Mine and is a small portable electromechanical device, based on a linear variable differential transducer (LVDT). It measures the change in distance between two points by a temperature compensated wire, with a resolution claimed for it of the order of 10^{-5} inches. Closure rate measurements are made over a time base of a minimum of 30 minutes and are normally plotted against age of the opening.

From laboratory testing of salt rock specimens, and the subsequent development of this model, Serata has described (and patented) three methods of mining called:

- 1) Stress Relief,
- 2) Parallel-Room
- 3) Time-Control.

These are fully described in the references already given. A brief outline will be given here, as the initial high extraction panels at Boulby were designed on the basis of Serata's techniques.

In stress-relief, it is claimed that the wider the room is made, the greater is the stress relief created in the ground immediately above and below the opening. This is due to the circular expansion of the stress envelope as illustrated in Figure 4.2 and leads to improved room and floor stability. The increased stability

from widening the rooms is only obtained provided there are no planes in the immediate vicinity of the opening along which bed separation can occur.

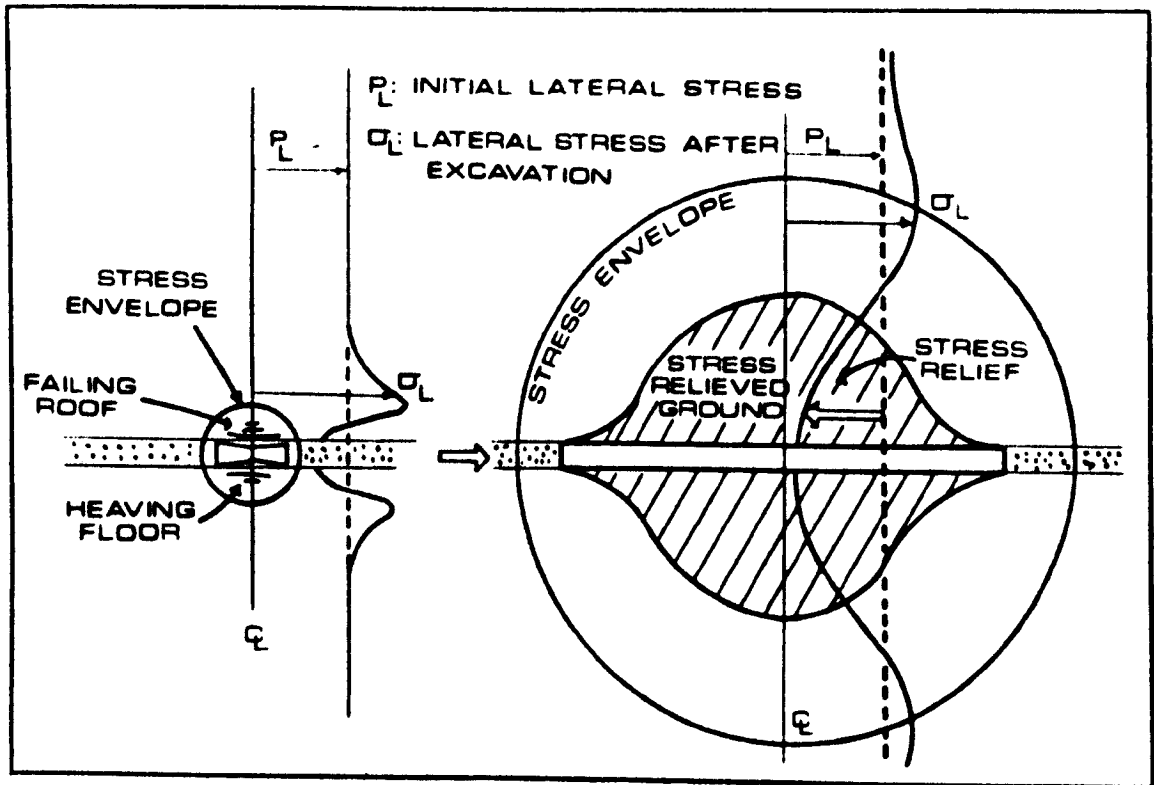
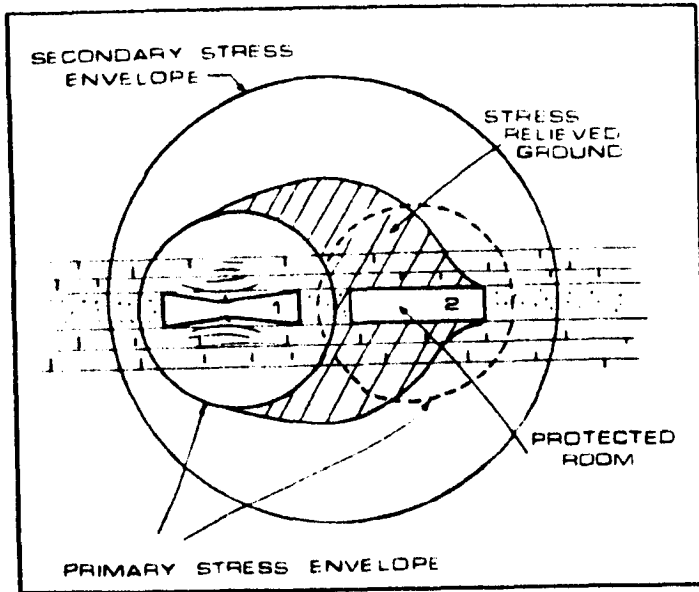
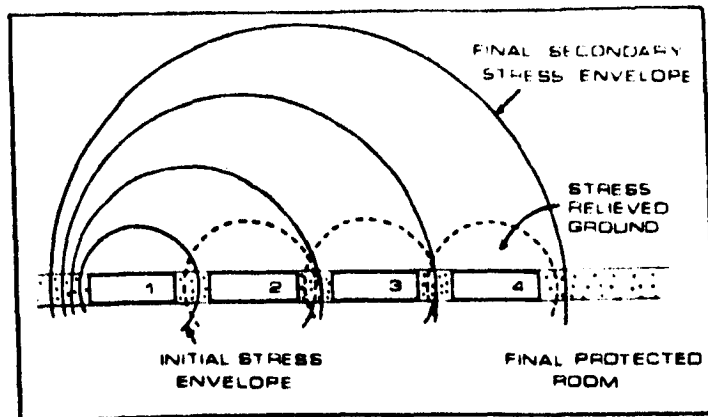


Figure 4.2 Stress Relief - Serata

The parallel-room method is applied to weak ground containing parting planes. This requires the driving of a second room parallel to the first failing room, with a very narrow yield pillar in between. The second room is then protected while the first continues to deteriorate. It is claimed that the mechanism is that of a secondary stress envelope which develops around both rooms, Figure 4.3(a).



(a)



(b)

Figure 4.3 (a) & (b). Parallel room method - Serata

The technique can then be extended by driving more rooms parallel to the first two. Figure 4.3(b). There is a limit to the number of rooms that can be driven in this way and this arises when the presence of unfavourable roof strata cause collapse of the secondary stress envelope.

The time-control method is used in extremely weak ground. It uses basically the same technique of developing stress relieved zones as for the previous methods. In addition it involves the specific time controlled sequencing of the excavation of a group of rooms. Figure 4.4 illustrates the method. Two rooms are driven far enough apart to allow separate primary stress envelopes to develop, but close enough to allow the intervening pillar to become strain hardened after a suitable time interval. A third opening is then made through the strain hardened ground. The two pillars thus formed fail rapidly, transforming the two primary stress envelopes into one larger secondary stress envelope. This counteracts the failing of the small pillars, resulting in stable equilibrium, thus protecting the inner room and substantially improving the stability of the outer rooms. The process can be used with multiple openings and optimised by setting the final protective stress envelope in the most competent geological formations overlying the excavations.

4.5.2 Baar

Baar has published⁽²¹⁾ a monograph on salt rock mechanics.

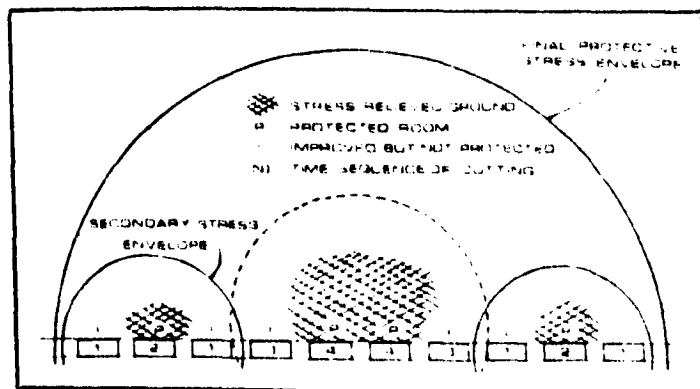
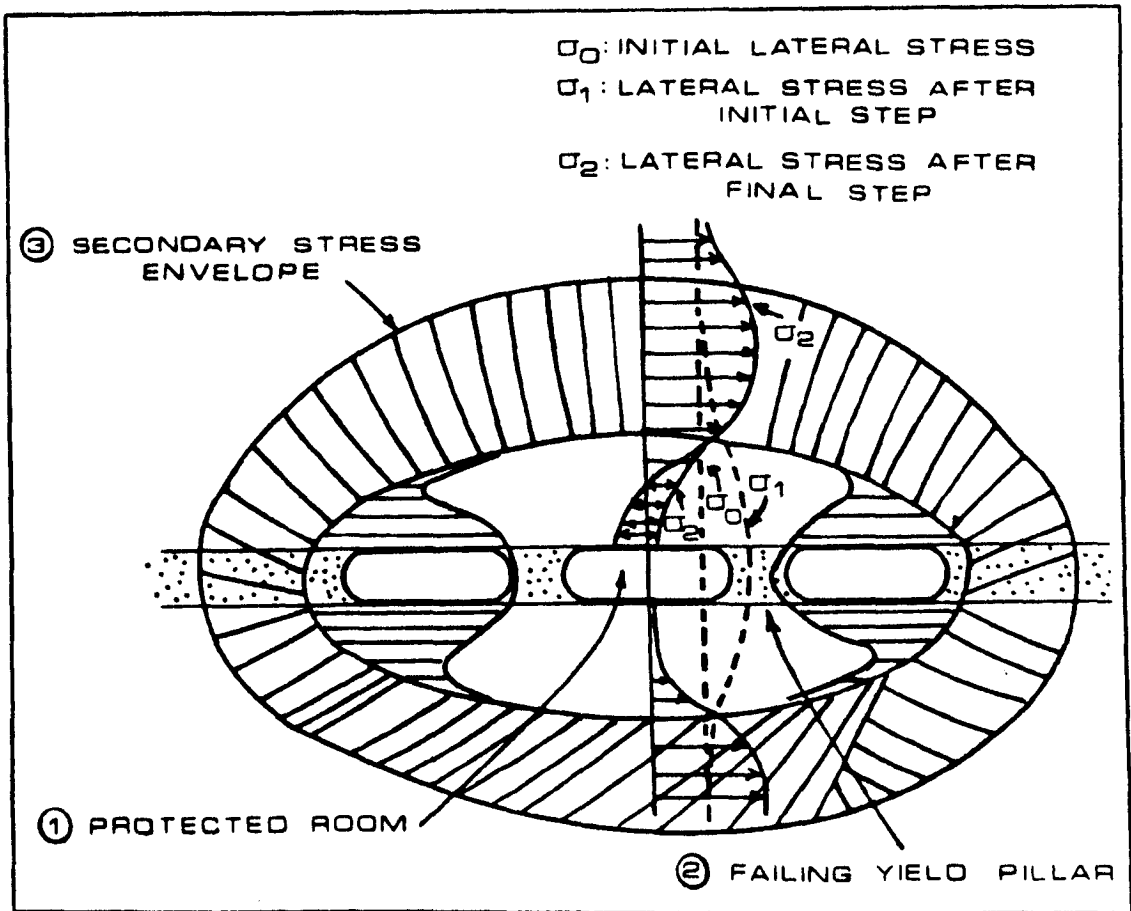
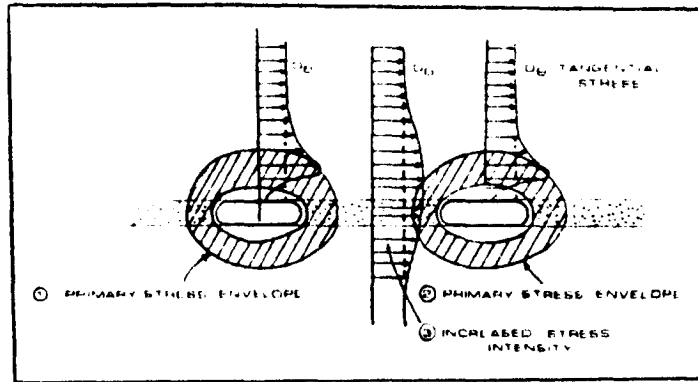


Figure 4.4 Time Control Method - Serata

This text contains discussions on the geology and physical properties of salt rocks as well as numerous references to in-situ convergence and extensometer measurements in salt and potash mines. He calls attention to questionable assumptions made in formulating creep laws from laboratory data of creep rates.

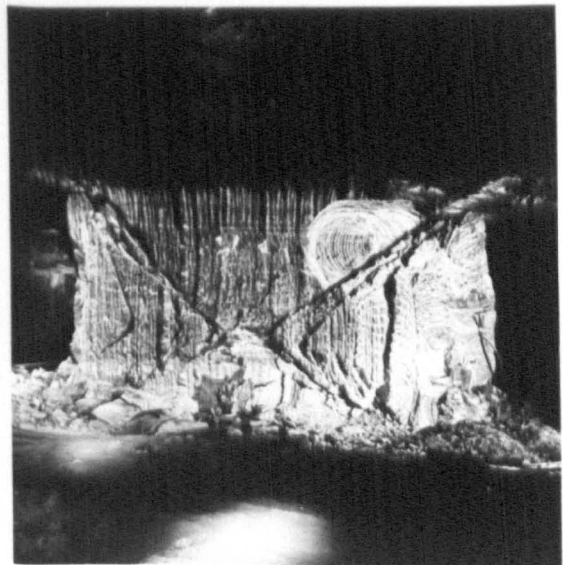
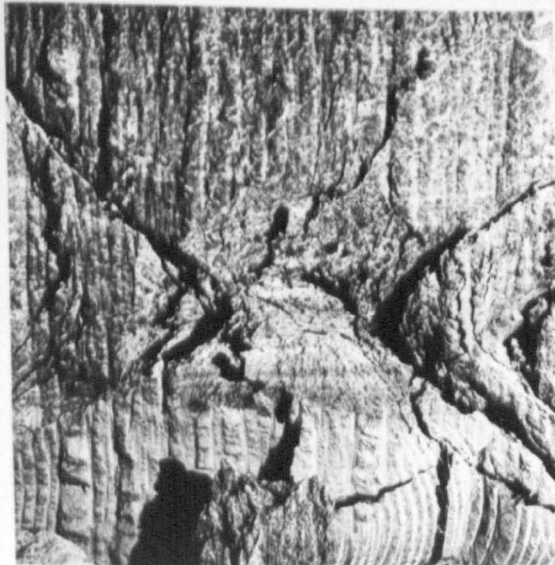
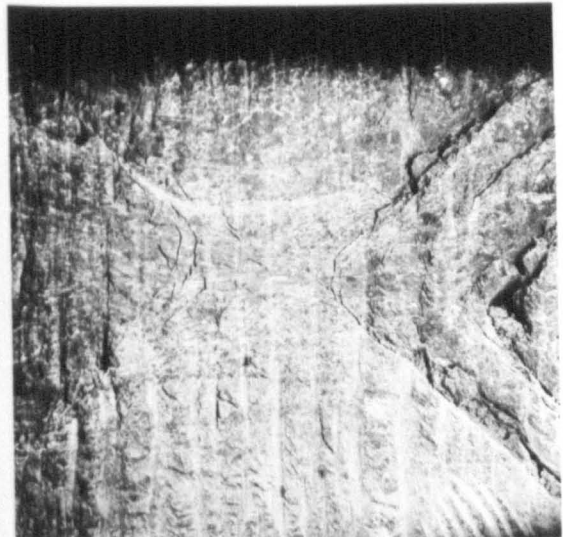
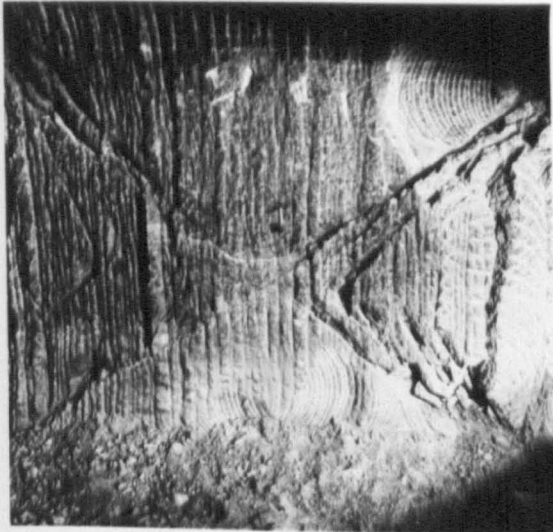
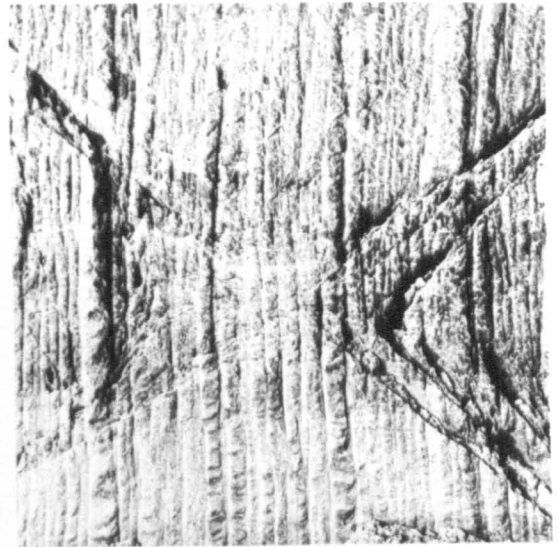
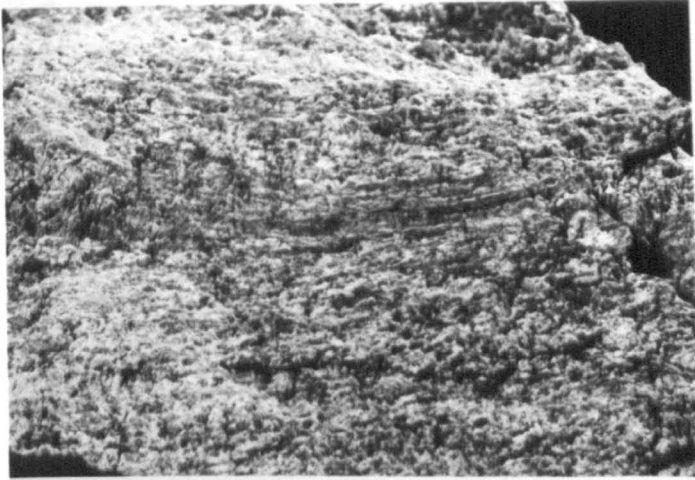
Baar's perception⁽²²⁾ from mine observations is that strain hardening observed in the laboratory does not exist in-situ. He assumes that salt rocks will reach the secondary creep regime very soon after being loaded and will then demonstrate constant strain rates for constant stress conditions. The primary creep regime is embodied in what Baar terms stress relief creep. Creep rates decrease rapidly for a few days until the original stresses in large zones around the openings are sufficiently adjusted to the very low creep limits of salt rocks. Reloading of stress relieved zones depends on overburden subsidence which can be prevented by appropriate design to keep the long term constant creep rates small. Baar attributes the occurrence of severe rock bursts in salt and potash mines to the overlapping of subsidence tension zones which approached one another from opposite directions. This can only be controlled by the careful planning of mining sequences. He further makes the very important point that surface subsidence measurements carried out over long periods of time, cannot be reconciled with "hypothetical stable stress arches postulated in some recent publications". This is an obvious reference to work by Serata. Some of the statements made by Baar do not reflect the situation as

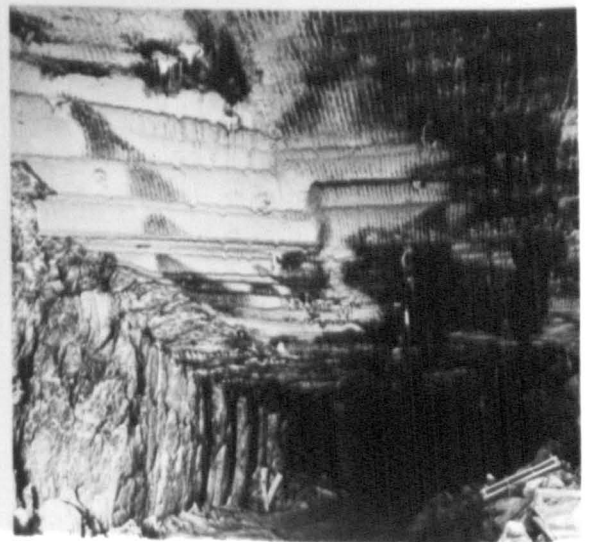
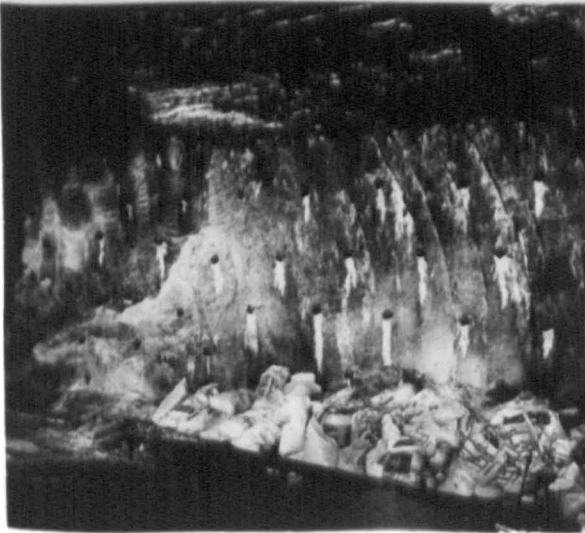
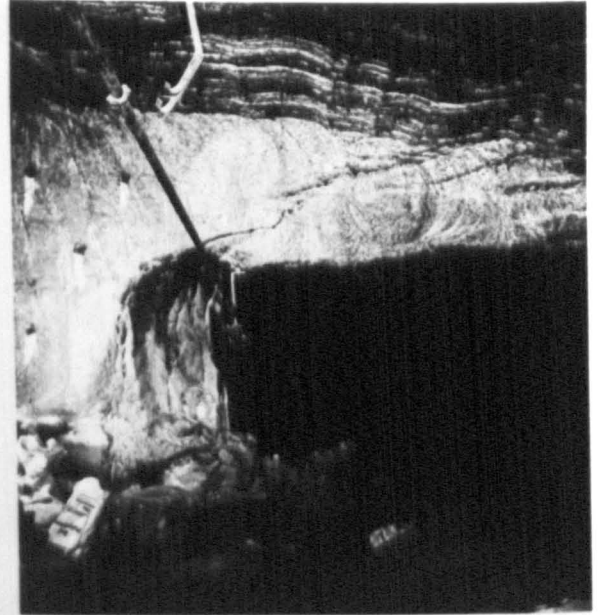
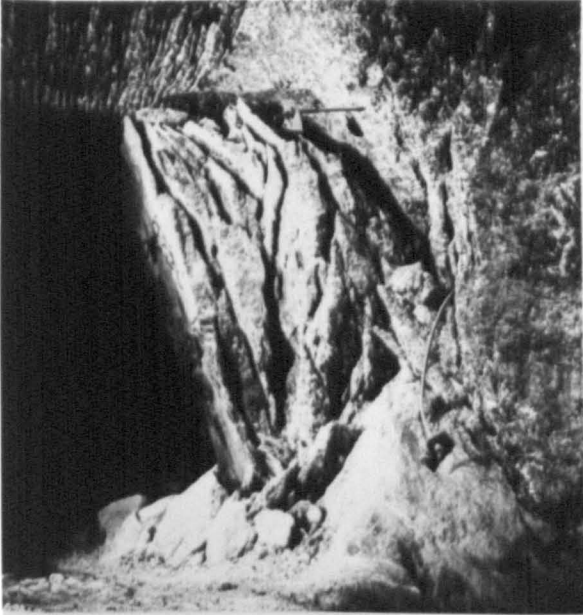
Plate 4.1

- 1 Section of rock taken from pillar as it was when 5 and 6 were taken, showing plastic flow.
- 2 No.12 pillar 120 days after it had been mined.
- 3 35 days later. Note formation of slabs.
- 4 Central core from No. 3 showing plastic flow.
- 5 380 days after mining showing central core breaking up due to brittle failure.
- 6 Taken same time as No.5. Note lateral displacement of slabs, and increase in W:H ratio.

Plate 4.2

- 1 Showing extensive sidewall fracturing with formation of elliptical opening.
- 2 Low angle fracture and sidewall slabbing leading to elliptical shape in salt roadway.
- 3 Brine weeping from rockbolt holes in salt road after entry of water in No.12 Panel.
- 4 Wet patches on roof of salt roadway. Note failure of sidewalls indicating high loading on this section of salt roadway.





experienced at Boulby Mine. For example, in (22), he states that under normal mining conditions, creep deformations around underground openings in salt rocks prevent any stress concentrations near the openings that could possibly result in fracture as it is observed in the laboratory when specimens and models are loaded too fast. He goes on to say that the only two conditions known to cause fracturing of salt rocks in-situ, arise from gas occlusions and rock bursts due to sudden loading of mine pillars. The failure of narrow yield pillars would appear to contradict this particular statement. Plates 4.1 to 4.2 show typical failure patterns observed in potash yield pillars and further examples are given in other chapters.

Baar's explanatory statement which is meant to prevent misunderstandings, only serves to increase the confusion. He says:

"It may be emphasised that the detachment of segments or slabs from the surface of salt rocks around openings with non-ideal cross-sections is caused by different mechanisms; the term, 'destruction by fracturing' as used means 'brittle fracture' with little or no plastic flow".

This is a good example of the difficulties that arise when an attempt is made to relate physical observations to a theoretical concept. Unfortunately the practice of rock mechanics constantly requires this process and may account for some of the bitter disputations that have occurred with the presentation of many research papers.

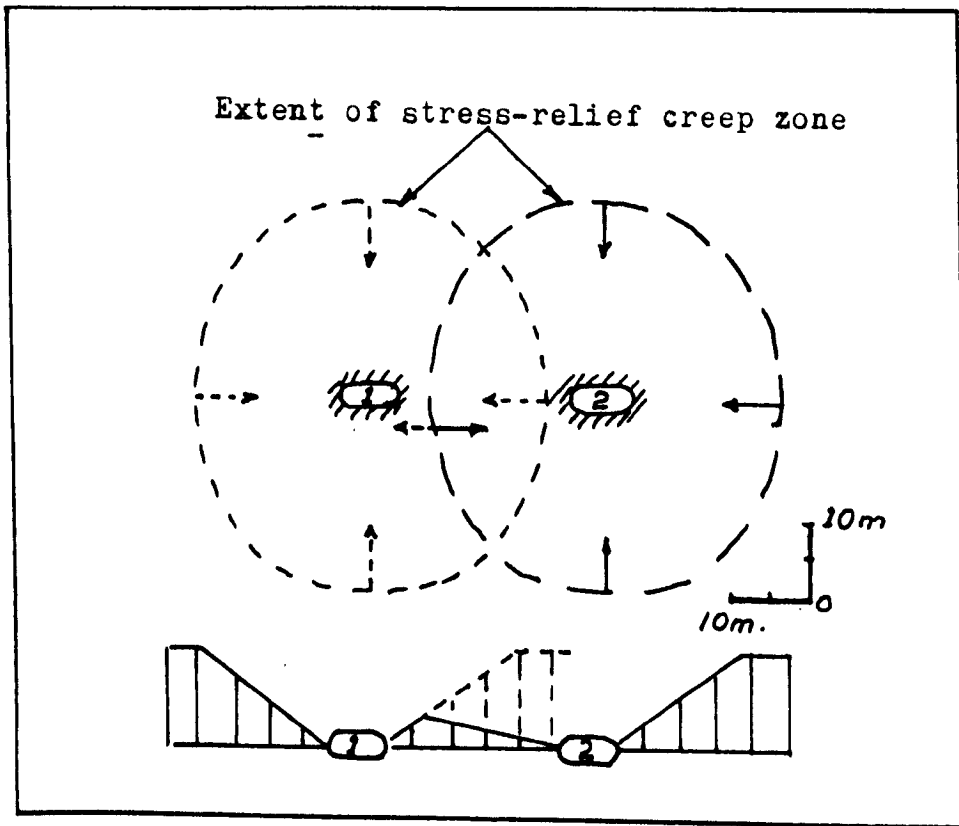


Figure 4.5 Stress-relief - Baar

Figure 4.5 illustrates Baar's hypothesis of how stress-relief works in potash mines in the Saskatoon area in Saskatchewan, Canada. Overlapping stress-relief creep zones as shown in Figure 4.5, are created by advance excavation of two stress relief openings. A third opening is excavated in the stress relieved ground between the two stress relief openings. He is emphatic that there is no 'prestressing loading' by what he calls 'imaginary stress envelopes' that result in stabilisation by strain hardening as postulated by Serata.

Baar constantly refers to the inadequacy of laboratory scale testing as a means of accurately simulating in-situ conditions. The large dimensions of stress-relief creep zones estimated to be 20m to 30m in diameter, that are reached prior to any reloading due to overburden subsidence cannot be adequately simulated. He is also sceptical that the actual conditions - first, unloading by creating a hole in highly stressed salt rock, then reloading according to the expected overburden reaction, can be simulated.

4.5.3 Mraz

Three papers by Mraz^{(23), (24), (25)}, discuss his ideas concerning the flow of salt rocks. In (24) and (25), he compares the theoretical results with measurements obtained in the I.M.C. potash mine near Esterhazy, Saskatchewan. Mraz bases his conclusions on the observation that under the conditions prevailing at the I.M.C., K1 mine, the salt rock behaves in accordance with the concept of a generalised perfectly plastic substance, and does not exhibit any strain-hardening effects. The deformation of the salt rock is that of a quasi-isotropic, polycrystalline structure having a well defined yield point. This means that its material elements start and continue indefinitely to deform permanently whenever the maximum shear stress τ_{\max} reaches a well defined limit dependent on the confinement.

$$\tau_{\max} = \frac{\sigma_t - \sigma_r}{2} = \Delta\sigma \quad \dots 4.10$$

This limit increases with confinement and its minimum value is equal to the limit of elastic behaviour, σ_E

$$\Delta\sigma = \sigma_E \frac{r}{a} \quad \dots 4.11$$

where a is the radius of curvature of the ellipse, acting around a mine opening and r is the distance from the centre of curvature.

The value of σ_E calculated from observations is found to be $\sigma_E = 1.46$ MPa.

The rate of plastic flow of salt rock, ϕ across an area A , is formulated as being equal to a proportionately constant ζ (the ductility) multiplied by the pressure gradient at the point of interest.

$$\phi = \zeta A \frac{d\sigma_r}{dr} \quad \dots 4.12$$

This leads to the result that for an elliptical surface acting around an isolated mine room, the rate of flow at the point of interest is inversely proportional to the distance of the point from the centre of curvature of the opening:

$$\epsilon_r = \epsilon_R \frac{R}{r} \quad \dots 4.13$$

When applied to measurements of horizontal and vertical closures around a mined room the results given in Table 4.3 were obtained. These show a remarkably good fit between calculated and measured values.

TABLE 4.3

Closure Distribution in Pillar

Cumulative Closure - %

Distance from		Cumulative Closure - %				
Wall - feet		0	5	10	15	20
Time	117	100	40	25	20	15
Since	440	100	41	25	20	15
Excavation-	1196	100	45	28	22	16
days	2924	100	39	28	23	17
Actual Average		100	41	26	21	16
Calculated from						
Equation 4.13		100	44	26	21	16
<u>Closure Distribution in Roof</u>						
Cumulative Closure - %						
Distance from		Cumulative Closure - %				
Roof - feet		1.75	5	10	15*	20
Time	117	100	88	74	-	64
Since	440	100	84	69	-	57
Excavation-	1196	100	81	64	-	52
days	2924	100	80	60	-	45
Actual Average		100	83	67	-	54
Calculated from						
Equation 4.13		100	85	70	59	51

* This station was not installed

Similar results are obtained in respect of the stress distribution around an isolated opening. The equation

$$\Delta\sigma_p = \frac{a}{2} \frac{\epsilon_0}{\zeta} \dots 4.14$$

is derived from the analysis of a thick walled cylinder and when combined with

$$\sigma_r = \frac{R}{\zeta} \frac{\epsilon}{R} \ln \frac{r}{R} \dots 4.15$$

for an elliptical surface acting around a room, the result

$$\Delta_p = \frac{\sigma_i}{2 \ln \frac{r_i}{a}} \dots 4.16$$

is obtained. These are then used to compute the values $\Delta\sigma_p$, σ_{rp} and r_p . When substituted in the equations derived to calculate stress to the left and to the right of a point p,

$$\sigma_r = \frac{a}{\zeta} \frac{\epsilon_0}{a} \ln \frac{r}{a} \dots 4.17$$

and

$$\sigma_r = \sigma_0 - D\sigma_p \frac{r_p^2}{r^2} \dots 4.18$$

values are obtained which are compared with measured values, Table 4.4.

Using the same basic functional relationships, Mraz further develops equations to describe the stress distribution in pillars between rooms and sets of rooms. A yielding pillar between two rooms was instrumented with three SRC omni-directional stress cells.

TABLE 4.4

Pressure Distribution in Pillar

Distance from Wall - feet	Pressure as % of $\sigma_{r(p)}$					
	2	5	10	13.4	15	20
Measured	3.5	43.3	82.2	-	106.1	116.9
Calculated	4.5	43.7	82.1	100	106.4	118.4

$\sigma_{r(p)}$ - radial pressure at point -'p'

Again there was good agreement between measured and computed values, except for the vertical stress at five feet which was significantly higher than the calculated value.

Finally he derives a series of equations that can be used for the design of stable room and pillar systems. His fundamental design criterion is that the salt cover over the entire area will remain competently supported until the excavated openings close by creep. In addition the stress gradients and closure rates must stay within the limits preventing excessive expansion of brittle failure zones or a brittle failure of the entire pillars as has occurred elsewhere⁽²¹⁾. At the same time, the salt cover slab must not fail either by shear or by bending due to an excessive span over a single room or group of rooms.

His concluding remarks in (25) are felt to be extremely pertinent:

"... the underground observations and measurements are the single most important tool in understanding the behaviour of salt rock in a deep mine".

4.5.4 Comments

Consideration of the above three sections illustrates the difficulty in arriving at a consensus view of the behaviour of salt rocks both in laboratory and in-situ underground.

Most, if not all, the work done by the above three rock mechanics engineers has been concerned with salt and potash deposits in Canada, the U.S.A. and Germany. Here the geological successions immediately above and below the salt and potash beds are nearly all fairly massive competent strata. This means that they are reasonably homogeneous and isotropic over relatively large distances, and are thus amenable to mathematical treatment. It is felt that much of the stability in the Canadian potash mines can be attributed to the presence of the massive competent Dawson Bay limestone bed, which lies between 10m and 30m above the potash. Figure 4.6 shows the stratigraphic succession at the Rocanville Mine in the Esterhazy district of Saskatchewan. Conditions in rooms up to 25m wide that have been standing for some seven years, are excellent with hardly any signs of deterioration of either roof or sidewalls. Similar observations and comparisons have been made by several visitors to the Canadian potash mines^{(26), (27)}. The consensus of opinion is that the far better ground conditions in Canadian potash mines are

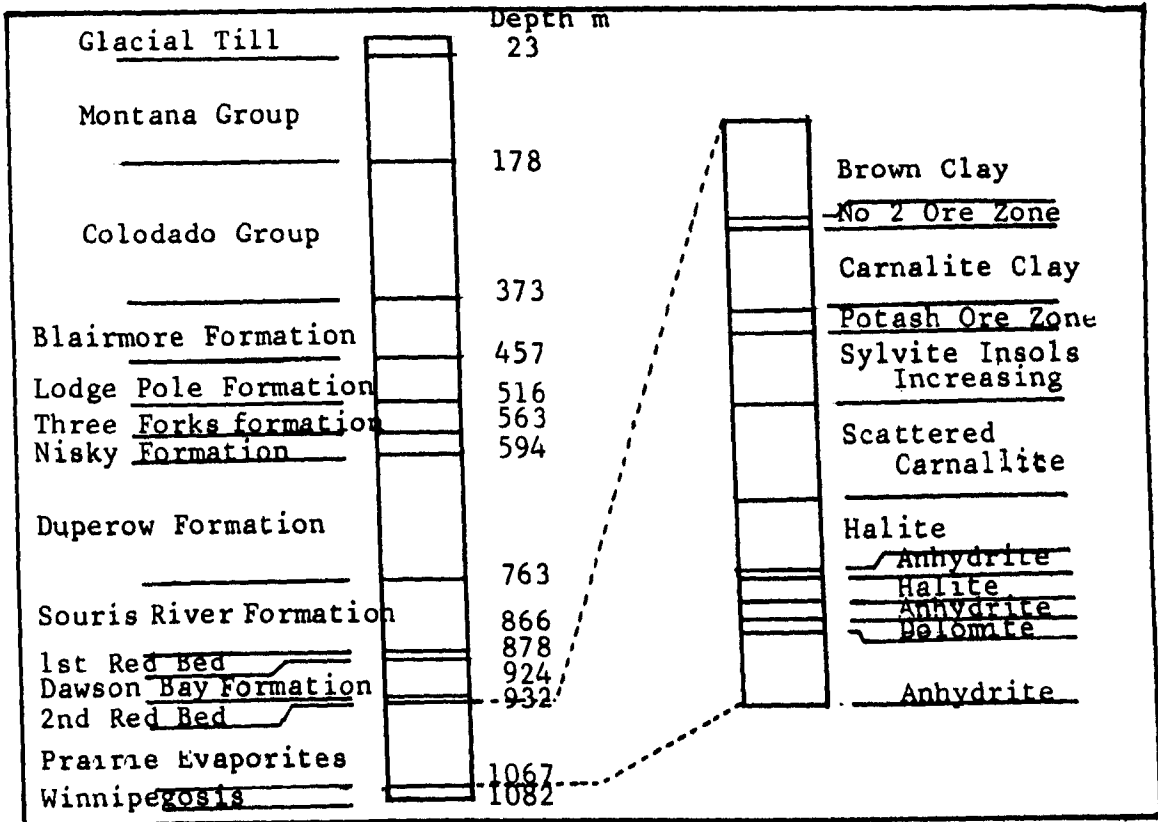


Figure 4.6 Geological succession, Rocanville

due almost entirely to the advantageous geological succession, with competent halite in the immediate roof. Indeed, the significant difference between the stability of the strata at a mine such as Rocanville in the Esterhazy district of Saskatchewan, compared with Lanigan Mine, some 250 miles away near Saskatoon, is attributed solely to the presence at Rocanville of a 30m thick halite bed in the roof. The 10m or so thick halite which contains clay partings that overlies the Saskatoon potash, gives rise to greater instability and it is found that rooms deteriorate faster and cannot be driven as wide as in the Esterhazy district. The major problem

encountered in Canadian potash mines is floor heave - see Plate 4.3. The major points of variance that arise between Serata and others, can be summarised in the form of a number of questions:

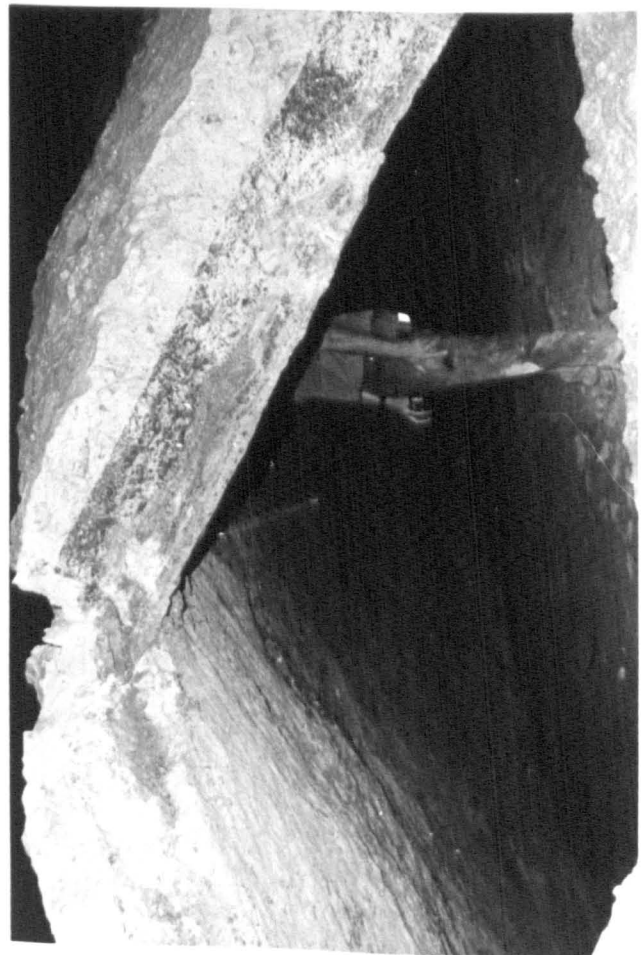
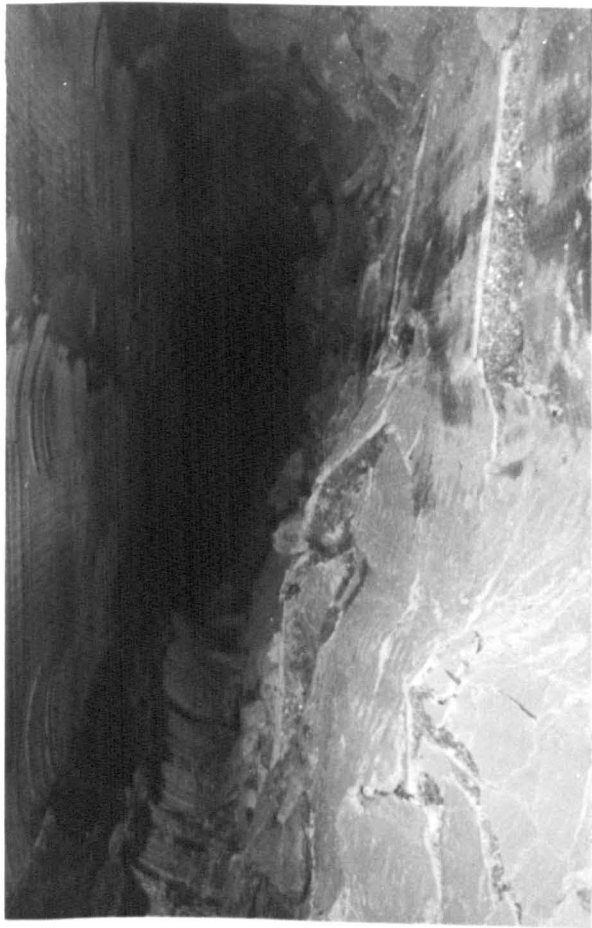
- 1) Does strain hardening occur in-situ?
- 2) Is primary creep significant in determining the stability of mine openings?
- 3) Does a stable stress arch form over excavations?
- 4) What is the in-situ elastic limit of strength of salt rocks?
- 5) Can salt rocks be assumed to be perfectly plastic substances?

After a number of years in which numerous in-situ and laboratory measurements have been made, as well as constant observation of conditions underground in the mine, the author has come to the overall conclusion that the differences are more relative than fundamental. To take each point separately:

- 1) There is no doubt that in small yield pillars that are rapidly and highly loaded, strain-hardening of the material in the core does take place. It is doubtful whether this occurs in the larger load bearing pillars, certainly no direct evidence can be found. Laboratory trials in which separate specimens were loaded under different constant strain rates indicate that as the strain rate decreases, a point is reached where the conditions described by Baar hold true - constant strain rate for constant stress. The general conclusion is that whether strain-hardening takes place or not, depends on the pillar width and height and the rate at which

Plate 4.3

Footwall heave in a Canadian Potash Mine.



it is loaded. The author's opinion is in agreement with that of Baar that strain hardening does not contribute greatly to the stability of a third room driven between two stress relief rooms as claimed by Serata, Figures 4.3(a) and (b).

2) The problem in answering this particular question is that when considering in-situ rock structures it is very difficult to tell what stage of creep is occurring. Primary creep is characterised by a decreasing stress to strain ratio, whereas for secondary creep, this ratio is constant. In order to evaluate which stage is taking place, it is therefore necessary to determine both the stress and strain at a given location in the mine. Both of these have been measured separately, but not together. A typical strain curve against distance into a pillar at Boulby Mine is shown in Figure 4.7. Mraz⁽²⁵⁾ shows the distribution of stress with time at different distances into a pillar, Figure 4.8. From this graph it can be seen that the stress increases with time, but at a decreasing rate. Without precise knowledge of the stresses and strains at one point, it is impossible to tell when primary creep changes to secondary.

Obert⁽²⁸⁾ agrees with Mraz and Baar and is of the opinion that primary or transient creep is short lived, possibly lasting 24 hours. Laboratory tests by Patchet⁽⁵⁾ indicate that constant rate creep occurs after about 50 days in rocksalt and potash specimens.

If it is assumed that primary creep is of short duration, then

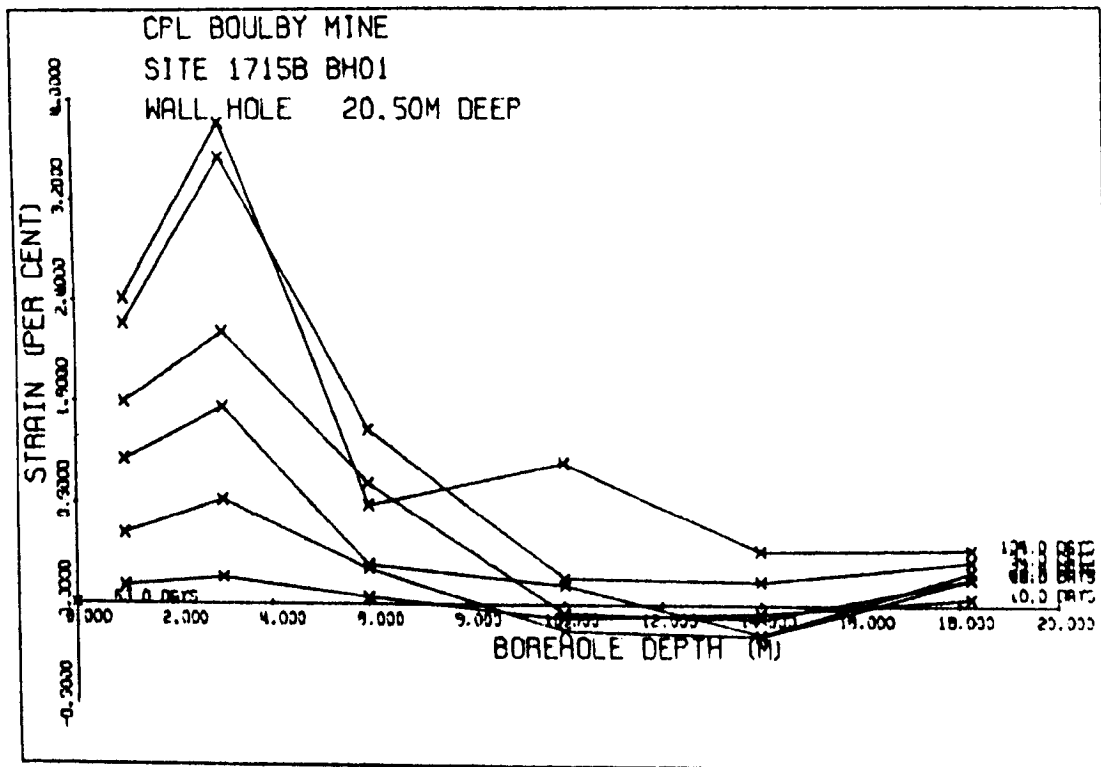


Figure 4.7 Typical strain vs. distance into a pillar, Boulby Mine

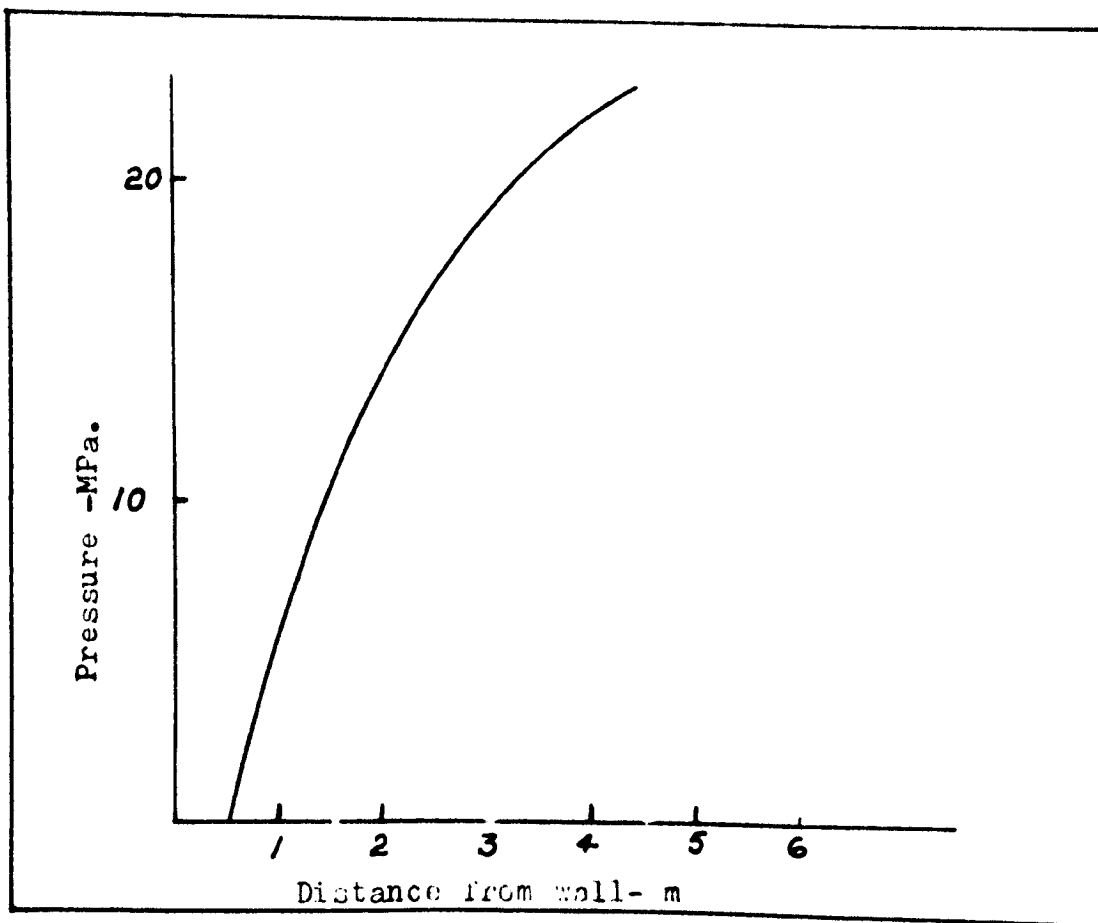


Figure 4.8 Stress vs. distance into pillar, IMC

the strain/time graphs obtained from measurements in Boulby Mine indicate that the stresses into the pillars are being redistributed over a fairly long time period.

3) The existence of a stable stress arch requires an associated high stress arch zone. If this did really exist, it is to be expected that stressmeters could have been installed to locate it. So far this has not been done. In addition, the subsidence associated with the formation of the proposed stress envelopes could also be monitored. Once the stable arch has formed, subsidence outside the stress relieved zone can be expected to reduce, if not cease altogether. All the available evidence^{(29), (30)} implies that this is not the case. Mackintosh⁽³¹⁾ suggests that failure in the 'sacrificial' stress relief rooms deflects the horizontal stresses away from the subsequent protected room. The protected room is thus isolated and the stresses are transferred to deeper, more competent beds. Yield pillars then allow these competent beds to deform at rates low enough not to produce fractures due to bending yet quickly enough to eliminate shearing.

It is felt that this latter explanation is more acceptable than hypothetical stress arches and it will be shown in a later chapter that it is supported by further evidence from Boulby Mine.

4) Much seems to depend on the elastic strength of the salt rock. Once this is exceeded, non-elastic yield takes place and one enters the dimly illuminated field of creeping rocks. Table 4.5 lists the range of values published by various authors.

TABLE 4.5

Limit of Elastic Behaviour of Rocksalt

<u>Author</u>	<u>Value</u>
	MPa
Adachi, Serata and Sakurai	6.18
Albrecht and Langer	7.35
Coolbaugh	10.30
Serata	4.41 - 8.24
Gimm	14.71
Höfer	14.71
Ode	0.49 - 0.98

Baar maintains that the true creep limits of salt rocks are of the order of 5-10 kp/cm² or less. The variations in these values explain the difference between theoretical predictions and in-situ creep measurements. The probability exists that creep is taking place at far lower stress levels than expected and is therefore more extensive. Horseman⁽³⁶⁾, who carried out extensive, very carefully controlled laboratory tests on rocksalt, states:

"The most important source of non-linearity (and of permanent set) is creep deformation which occurs even at low stress levels...".

He does not quote a figure for the limit of elastic behaviour because of the difficulty in being able to determine it precisely. This factor, of the limit of elastic behaviour is closely related

to the question of whether strain-hardening occurs or not.

5) The whole problem of describing the in-situ behaviour of salt rocks would be simplified if they could be classified as being perfectly plastic. Results obtained by Mraz show that this appears to be a realistic assumption under certain conditions. Problems arise when, as at Boulby, a 10m thick bed of elastic anhydrite rock overlies the potash. However, it is felt that it may be possible to apply the theory of plastic flow to the intervening rock and to the potash itself. The complexities introduced by highly variable geology make the precise solution of stresses and displacements in a mine such as Boulby, impossible in the absolute sense. Therefore a more relativistic approach is required where what is obtained are trends rather than absolute values. This method is adopted in attempting to describe the mechanism of rock behaviour in the mine, rather than the doubtless more intellectually satisfying one of solving the impossible.

CHAPTER FIVE

FACTORS WHICH ADVERSELY AFFECT PANEL DESIGN AND LAYOUTS

CHAPTER FIVE

5.0 Introduction

There are three major factors which have determined the basic mining layouts and subsequent operations and each in different ways has forced constraints upon the mine planning personnel. These three factors are:

1. The highly variable nature of the mine geology.
2. The problem of gas outbursts.
3. The inflow of water into mine workings.

5.1 The Highly Variable Geology

A few of the problems arising from varying strata have been touched on in previous chapters. These variations can be in strata type, thickness or because of features such as overfolds or inclusions of shaley material. The possible influence of post depositional flow has also been examined.

At present every roadway in the mine is surveyed by the mine geology department. In addition to visual examination of the exposed rock surface, probe holes are drilled into the roof at regular intervals. These are examined by means of a gamma ray probe, the "Gamma Trol", which locates changes in stratigraphy by measuring the emitted gamma radiation. A description of this instrument is given in Appendix 2.

The resulting data is used to draw 1 : 250 scale sections. Figure 5.1 shows a number of these sections from various parts of

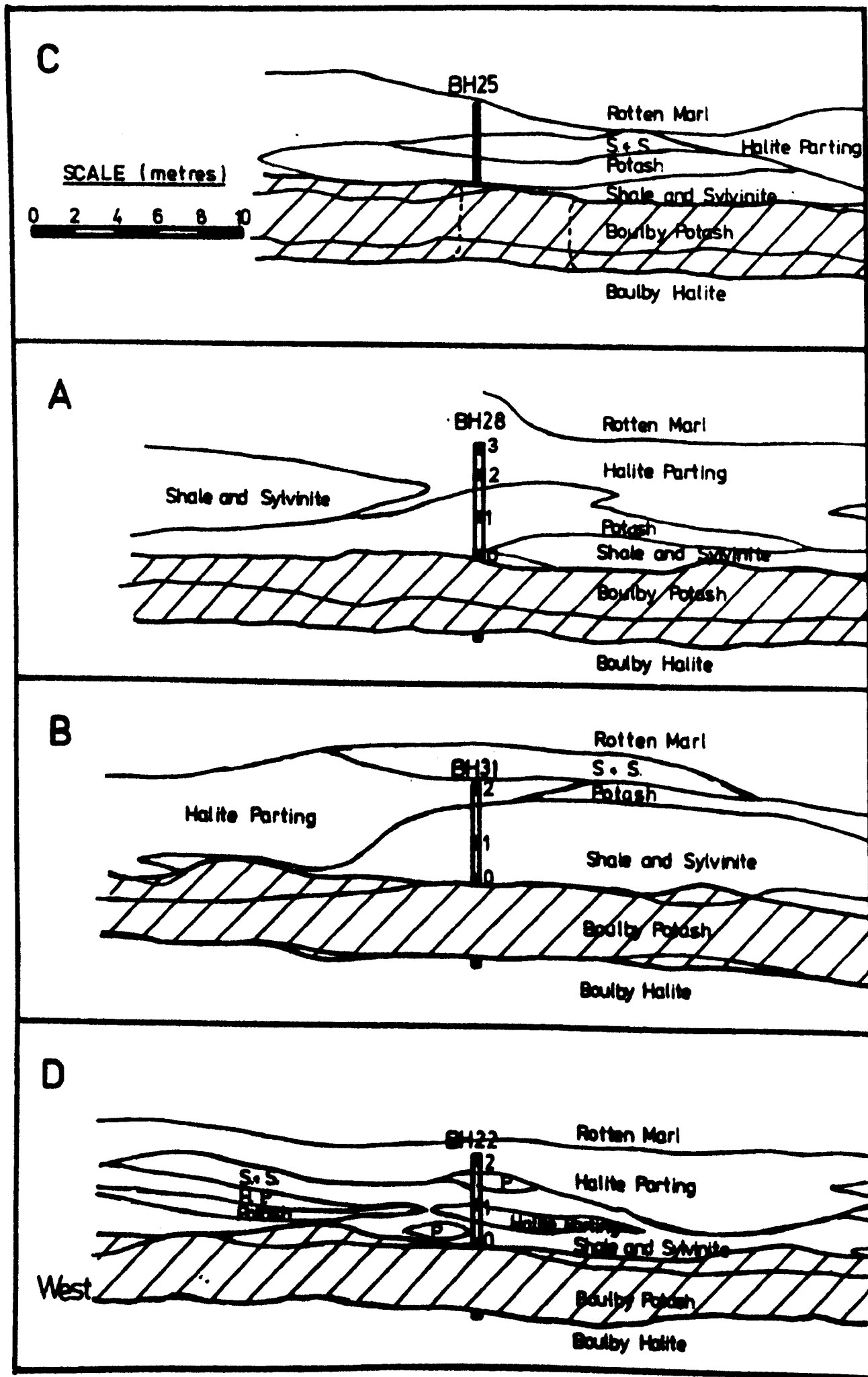


Figure 5.1 Geological Sections showing stratigraphic variability

the mine, and these illustrate the highly variable nature of the seam and immediate roof strata.

In addition to the above geological survey methods, longhole probe drilling is also carried out. This is a highly skilled drilling operation that was originally developed on the South African goldmines, and adapted for use at Boulby Mine.

Briefly, a drill bay is established in some convenient roadway and a diamond core drill set up, Plate 5.1. It then drills horizontally or slightly below the horizontal with the coring bit being deflected upwards wherever a seam intersection is required. The bit is subsequently retracted to a position before the turn-off point and drilling is recommenced in the original direction. Distances up to 1.5 km have been drilled with as many as six intersections being achieved. The flushing fluid is saturated brine solution. The method has been highly successful, even though fairly costly. Figure 5.2 shows a plan of the mine with the longhole intersections. The data thus acquired provides the main information on which longer term planning is based.

The biggest local problem arises with the presence of down-warps in the marl. These have occurred virtually throughout the mine and Plates 5.2 to 5.3 show various roof collapses that have taken place as a result of mining too close to the marl. 'Collapse' is probably not quite the right descriptive term. Although occasionally there are fairly large scale sudden collapses of

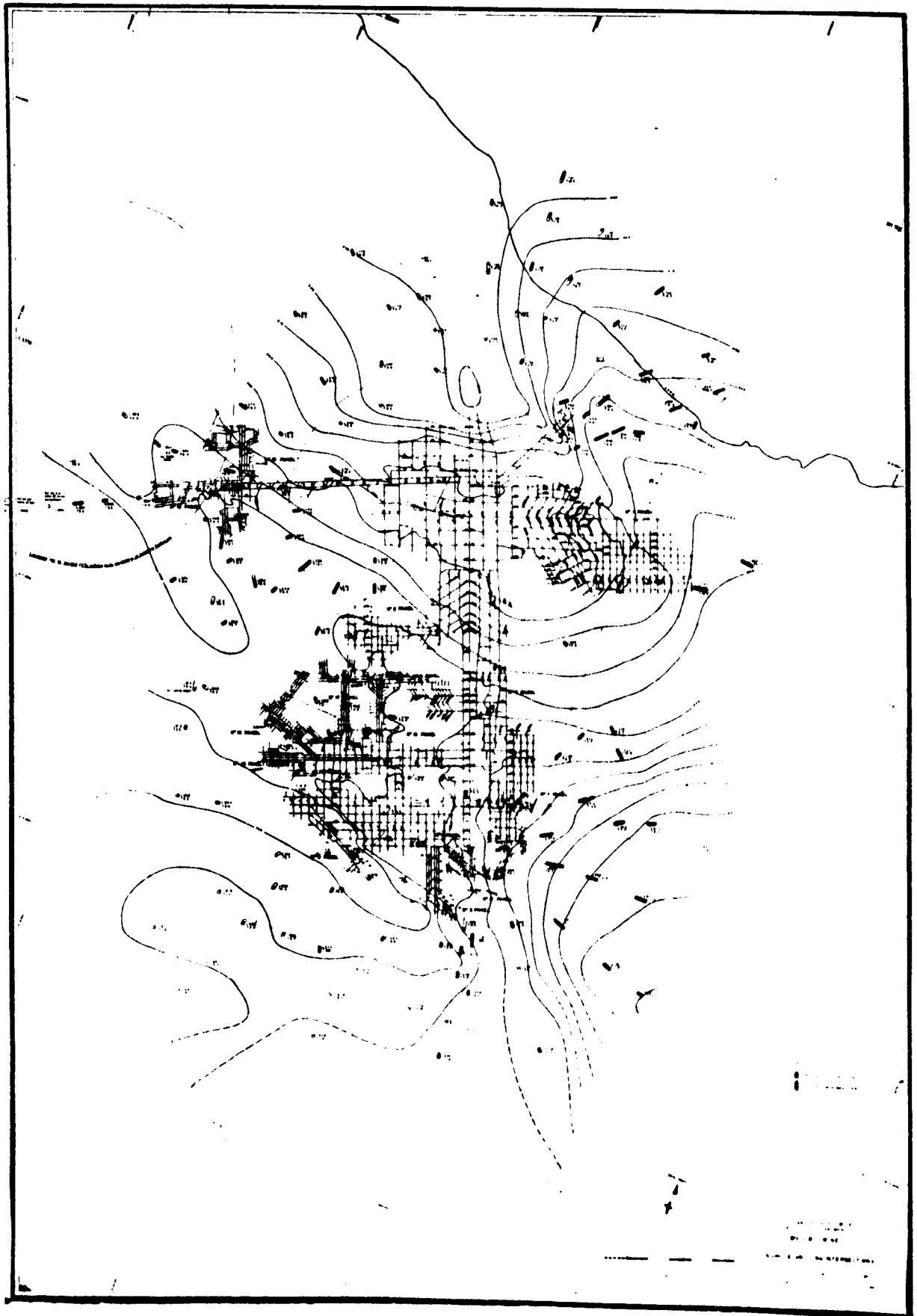
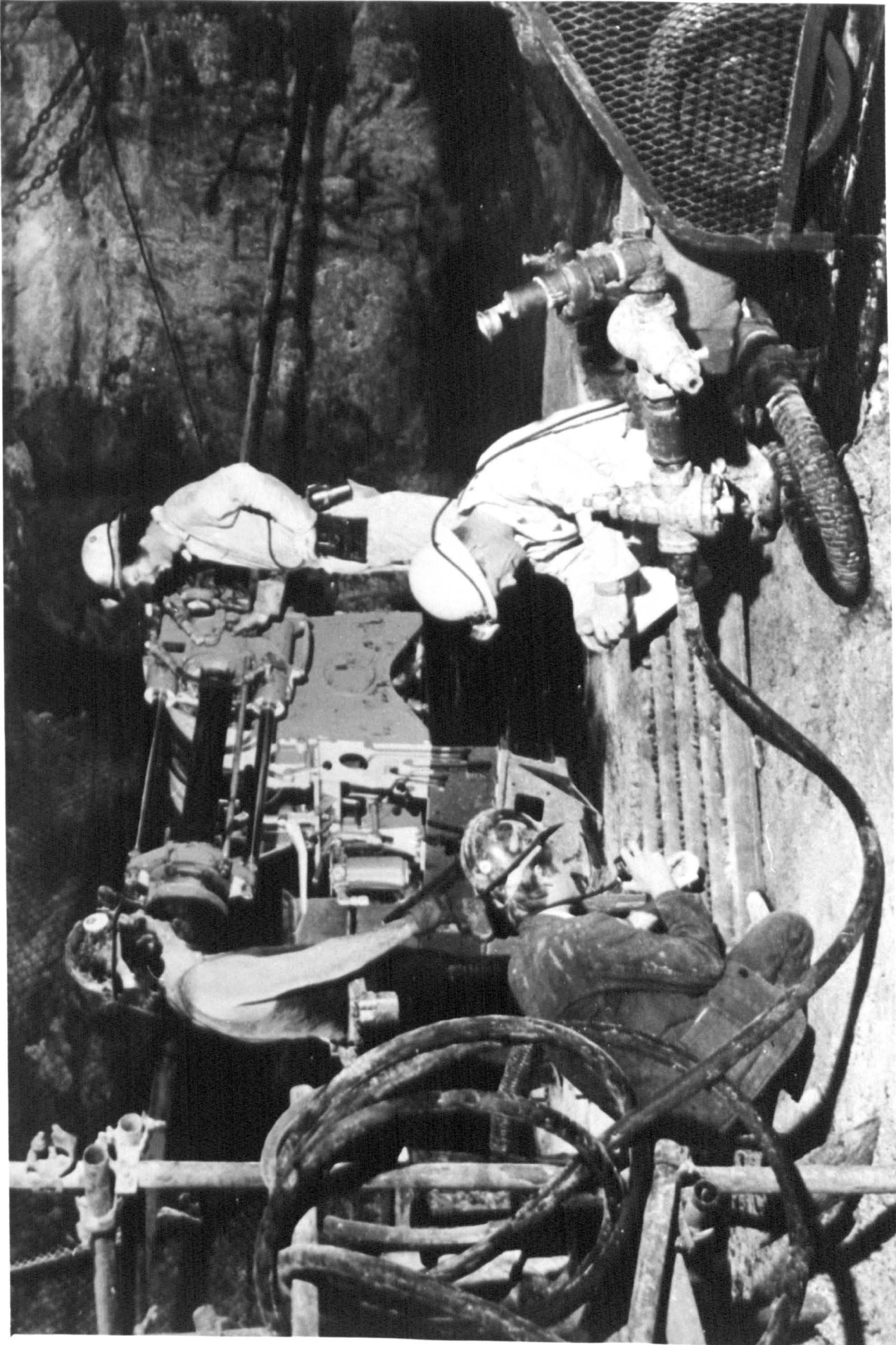


Figure 5.2 Plan showing longhole intersections

Plate 5.1

Longhole drilling rig.



hanging, the more usual event is that once the marl is exposed, it 'runs' into the excavation and over a period of days the hole in the roof becomes enlarged until the entire excavation is choked with fallen marl. Steel sets with shielding and timber chocks can sometimes control small exposures, particularly if they are caught in time, but more often the roadway has to be stopped and an alternative route found around the fall. Serious large scale collapses have occurred where a large stiff pillar has been left adjacent to a high extraction zone. Shearing along the pillar edge with subsequent complete and fairly sudden collapse takes place. This has happened in No. 16 Panel and No. 10 Panel. Downwarps of the marl are nearly always accompanied by a thinning of the ore and this caused No. 1 Panel to be stopped altogether. It is extremely difficult to drill through the marl because of the rapidity with which the drill hole closes. The probe holes therefore go no further than the lower marl interface, which means that very little is known about the actual thickness of the marl itself.

Another major variation that occurs is in the type of ore. Apart from the direct connection with the gas outburst problem, described in the next section, differences in the ore result in different strength and time dependent properties. This can affect the stability of both roadways and pillars. The variations arise mainly from the presence of shale or clay in the potash, and it has been shown that the ultimate strength is decreased the greater the proportion of shale present. In addition the presence of shale increases the creep rate. Another parameter that has similar

effects on performance is the crystal size. The larger the crystal size, the weaker the rock is and the greater the creep rate. Table 5.1 is a summary of the mechanical properties of near-seam rocks as obtained by various investigators. A full list of these test results is given in Appendix 3.

TABLE 5.1

Summary of Near-Seam Mechanical Properties

Material Type	Young's Modulus GPa	Poisson's Ratio	U.C.S. MPa	Tensile Strength MPa
Carnallite Marl	7.01	0.20	14.66	1.24
Shale	11.02	0.24	12.20	1.18
Potash*	7.44	0.37	39.66	1.79
	22.42			
Middle Halite*	4.20	0.28	26.77	1.63
	23.66			
Upper Anhydrite	19.14	0.22	82.95	6.08
Upper Halite	-	0.24	31.07	1.59

* The two values quoted for Young's Modulus are those with cycling and without cycling

Plate 5.2

- 1 Roof collapse along geological discontinuity. Note roof bolts pulled out.
- 2 Experimental roof 'truss bolts'.
- 3 Steel arch sets coping with extensive sidewall and roof failure.
- 4 Roof slabbing, mechanical anchors pulled out.
Notr good sidewall.

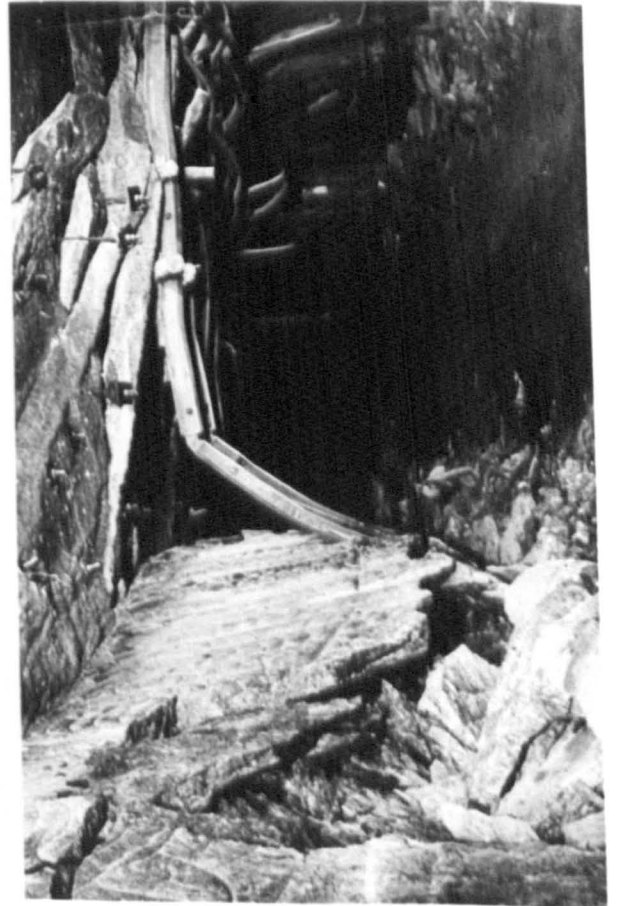
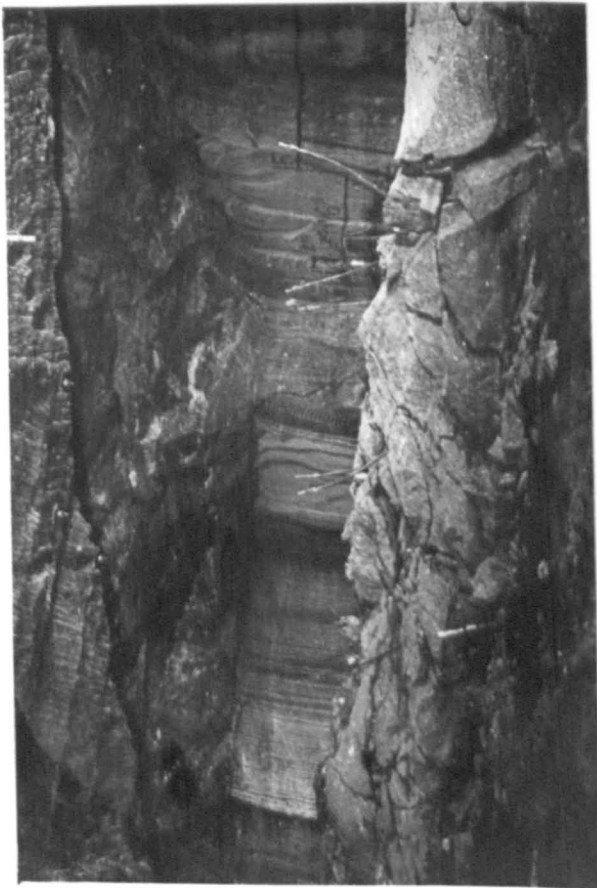
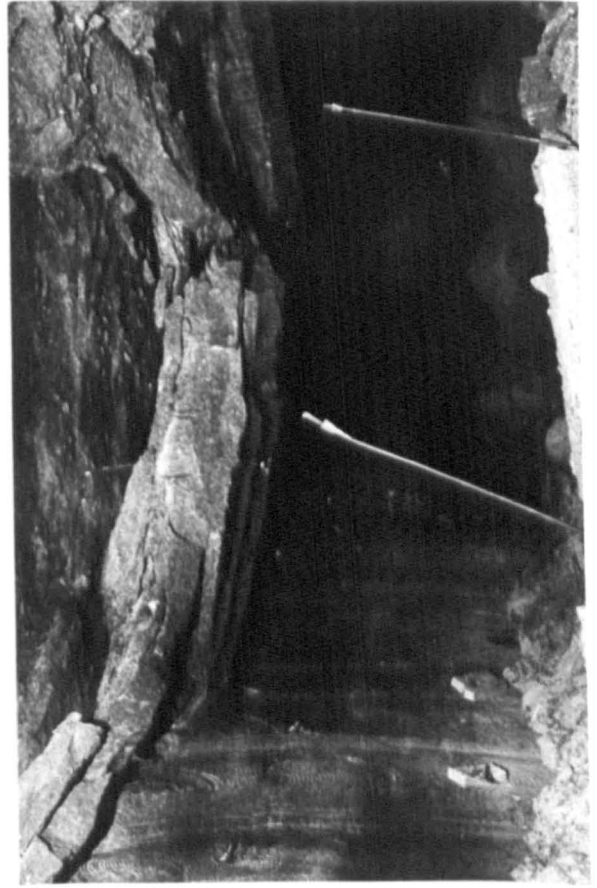
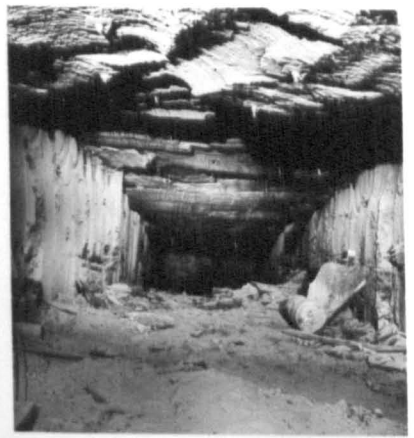


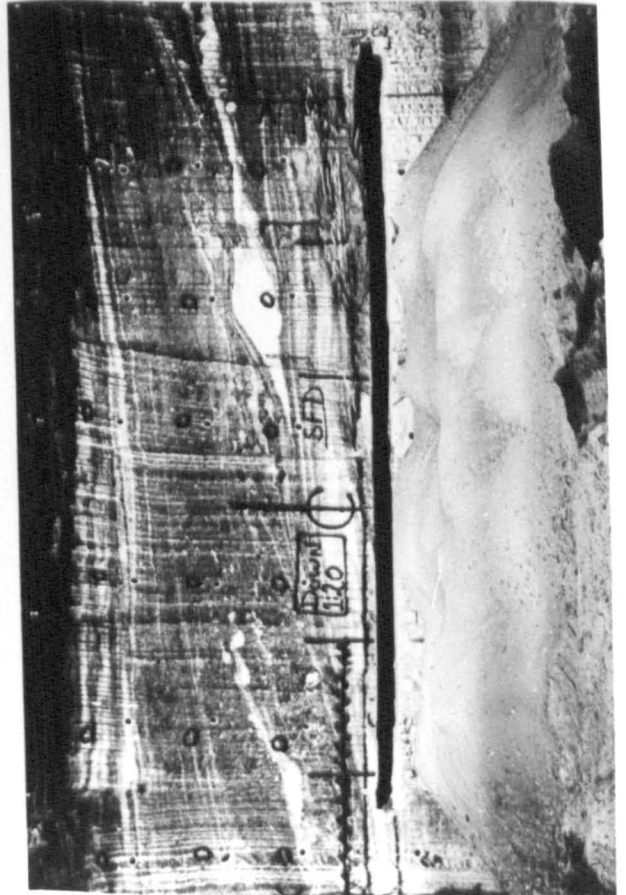
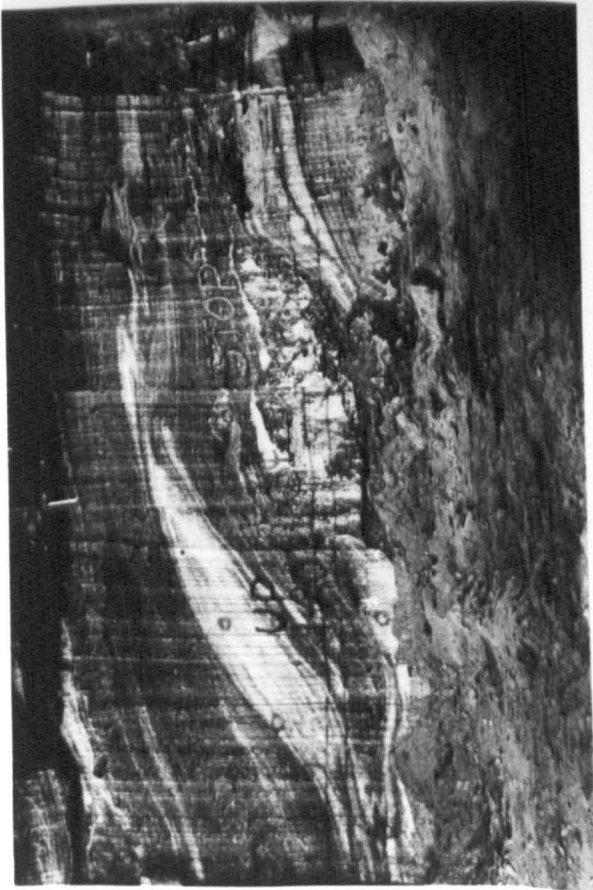
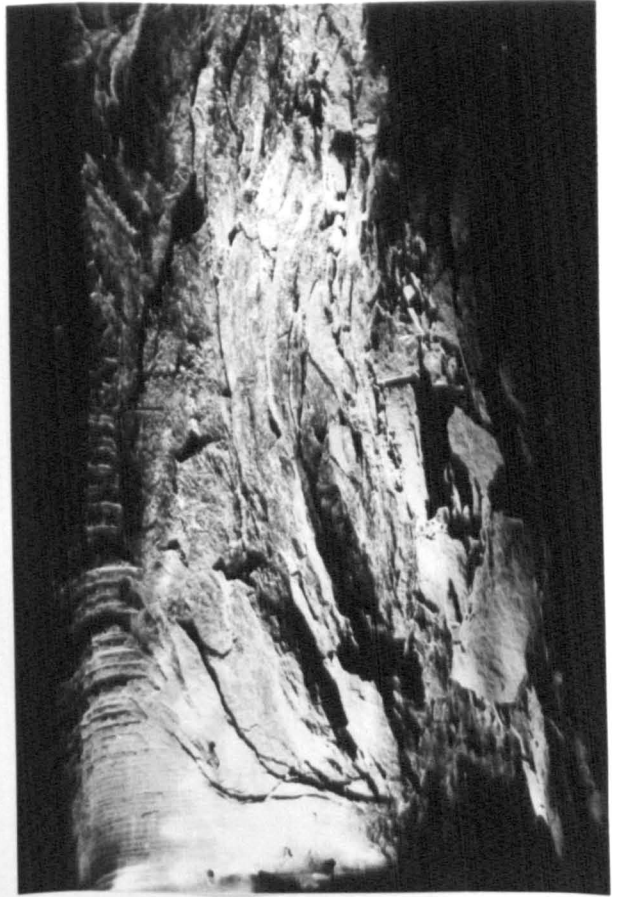
Plate 5.3

- 1 Slight roof slabbing.
- 2 Roof beginning to break up due to lateral movement of yield pillar on the left. Vertical shearing on the right, conditions otherwise good. No evidence of stress relief.
- 3 Roof breaking up.
- 4 Sidewall failure due to lateral movement.
- 5 Vertical shear, roof breaking up.
- 6 Same roadway as in 1, conditions generally good. No evidence of stress relief.
- 7 Lateral movement of yield pillars, horizontal shear.
- 8 'Chippings' from upper corner failure.
- 9 Marl exposure.

Plate 5.4

- 1 Pure sylvite (white) in high grade but increasingly geologically disturbed zone. Face after profiling with Heliminer.
- 2 Face marked for drilling and drill at left.
- 3 Undercut slot, face drilled for blasting.
- 4 Face after blasting.





The effect of increasing shale content on the mechanical properties can be seen from Table 5.2.

TABLE 5.2

Mean Values obtained for Mechanical Parameters of Middle Potash Rocks

(after Wiggett)

Rock Type	Young's Modulus kN/m ² x 10 ⁷	Poisson's Ratio	Uniaxial Comp. Strength kN/m ²	Tensile Strength kN/m ²	Shear Strength kN/m ²
Primary Potash	2.428	0.385	41220	-	-
Shaley Potash	1.500	0.320	38100	-	-
Potash Shale	1.142	0.252	10430	1280	10650
Boracitic Shale	1.066	0.276	12280	1100	9970
Anhydritic Shale	0.825	0.125	13920	1200	10540

5.2 The Gas Outburst Problem

Gas outbursts or gas 'blows' as they are known on the mine, arise basically from the release, usually fairly rapid, of gas that has been trapped by some as yet unknown mechanism in the rock surrounding the mine openings. Although gas exists in virtually all the strata that are exposed during mining, gas blows are always associated with zones of shaley ore. Very often these shaley pockets consist of highly fragmented rock which may even be largely in the form of dust.

Hebblethwaite and Woods⁽⁹⁾ claim that at a distance of 5m from the location of the gas blow, 20% of the fragments are centimetre size, 60% millimetre size and the remainder, fine shale dust. Eighty per cent of the shale and 60% of the gas are released within seconds of the event, thereafter a steady release occurs at a continually decreasing rate. This latter phase may continue for minutes. Gas continues to seep into the excavation for periods lasting hours, days or even weeks after the blow took place.

Two types of outburst have been identified. Ninety per cent of gas blows that occur are of the "throat" type, in which the shape of the resulting cavity is cylindrical or conical. These cavities are randomly orientated and can occur anywhere around the excavation. It would appear that there is an upper limit on the size of throat type gas blows, probably in the region of 100 m³ representing about 200 tonnes of rock. This type of gas blow is by far the most frequent that occurs in the mine.

The second type of gas blow has completely different characteristics, in that the dimensions and tonnages expelled are much greater. The mechanism would appear to involve a chain type of reaction where the initial shock wave from blasting initiates a series of rapidly advancing rock fractures. Table 5.3 lists the composition and size of the two types of outburst. Figure 5.3 is a plan of Boulby Mine showing gas blow zones and geological sections.

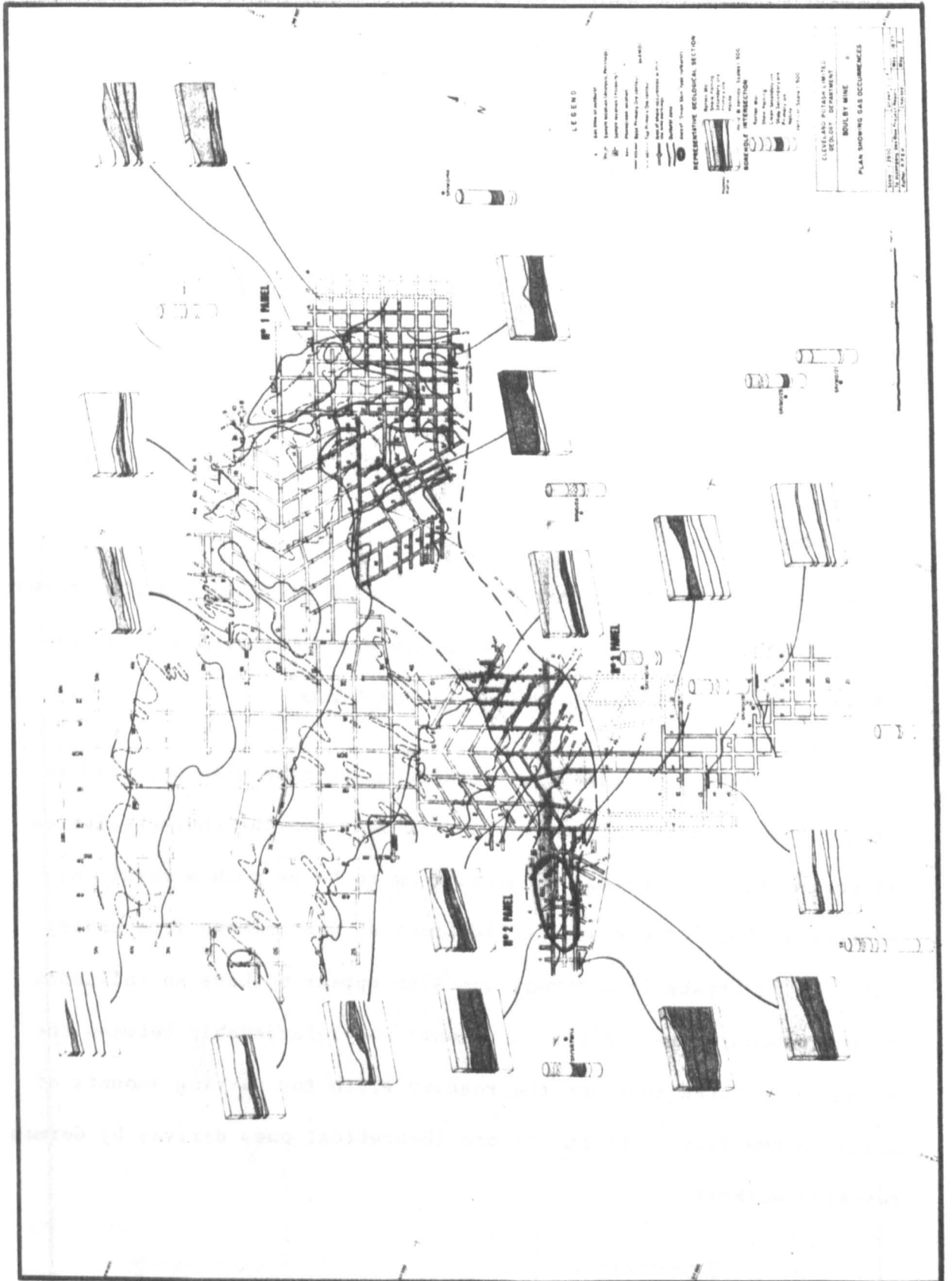


Figure 5.3 Plan showing location of gas blows

TABLE 5.3

Gas Analysis and Size of Gas Blows

Type 2 ('Throat' Type)

	<u>Composition</u>	<u>Range</u>
Gas	20% Hydrocarbon, 80% Nitrogen	50-500 m ³
Rock	20.6% KCl; 27.7% NaCl; 51.7% Insols.	20-170 tonnes

Type 2 ('Onion Skin' Type)

Gas	20% Hydrocarbon; 80% Nitrogen	100 - 10000 m ³
Rock	54.3% KCl; 35.6% NaCl; 10.1% Insols	300 - 1000 tonnes

Type 2 gas blows tend to have an ellipsoidal shape and the only area where they have occurred has been in No. 2 Panel and they appear to be associated with massive secondary ore. Figure 5.4 is a plan of No. 2 Panel with the locations of gas blows.

Outbursts in potash and rocksalt mines have also occurred in European and Russian mines and exhibit many similar characteristics although the West German outbursts seem to be as much a result of brittle failure of carnallite-rich rock as gas release from shaley ore. Large crystalline formations also appear to have an influence on their occurrence. Figure 5.5 shows the relationship between the volume of ejected rock and the roadway width for varying amounts of shale in the face. The curves are theoretical ones derived by German research workers.

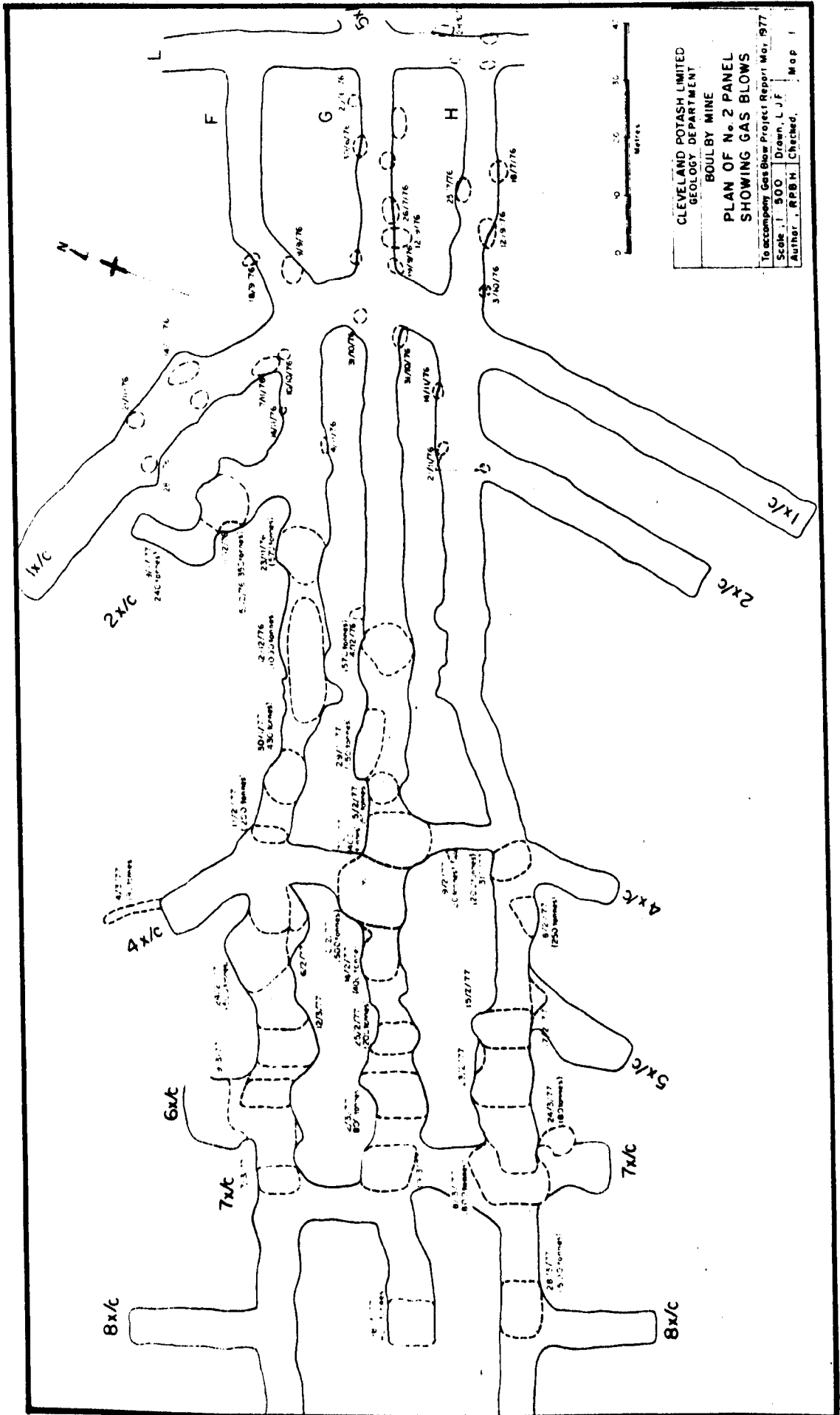


Figure 5.4 Plan of No. 2 Panel gas blows

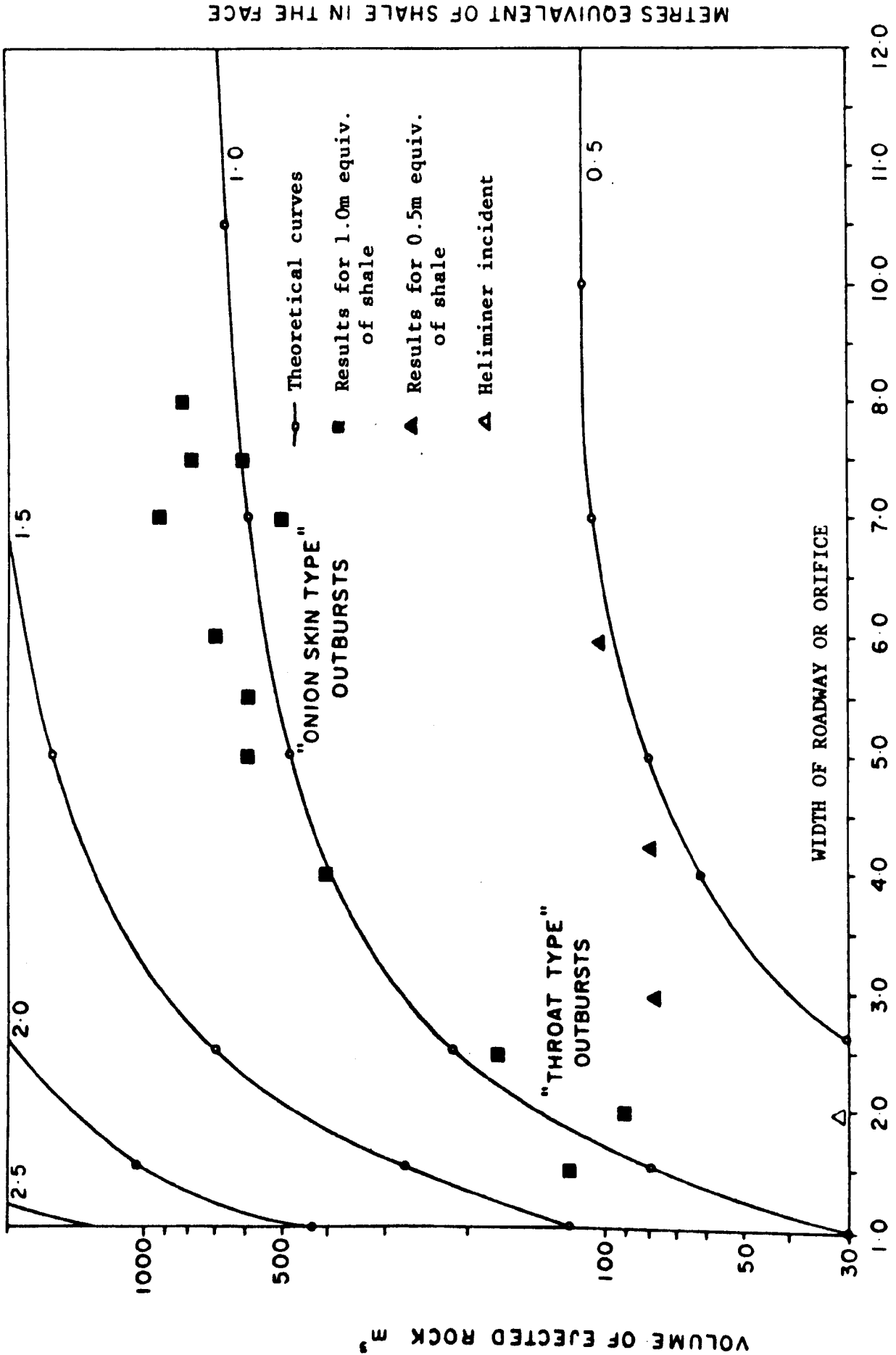


Figure 5.5 Relationship between outburst tonnage, and roadway width

In terms of discharge of rock and gas into the excavation, the results of mining into potential gas blow sites are independent of whether the method of mining is by conventional drill and blast or by mechanical miners. However, when the excavation is created by blasting, no men are present, and if a gas blow is initiated there is no chance of injury to persons. With mechanical miners, the machine operators are at risk if a gas blow zone is exposed.

The Mines' Inspectorate therefore, found it necessary to impose severe operational constraints when a fatality in which a Heliminer operator was killed, occurred that was directly attributable to a gas blow. These constraints require the mine to leave no more than 6m of roof unsupported, and to carry out probe drilling ahead and around the advancing heading. The mine was also required to drill and blast headings where shaley secondary ore was intersected. This was originally done by undercutting with the Heliminers and blasting down the brow that was left. A gas blow that occurred while undercutting was in progress caused the Heliminer and shuttle car behind it to be moved forcibly backwards a distance of about 6m. Fortunately, no-one was badly injured. The mine then altered the excavation routine so that the faces are undercut by means of a jib cutter, drilled and blasted, and then a Heliminer is used to muck out and cut the final profile. As can be expected, the full potential of the Heliminers are not being realised by using them in this manner.

5.3 The Water Problem

By September 1979, the mine appeared to have solved most of their layout problems; No. 10 Panel was going well and Panels 15, 16, and 19 looked like improving on the already steadily increasing monthly tonnage figures, which are depicted graphically in Figure 5.6.

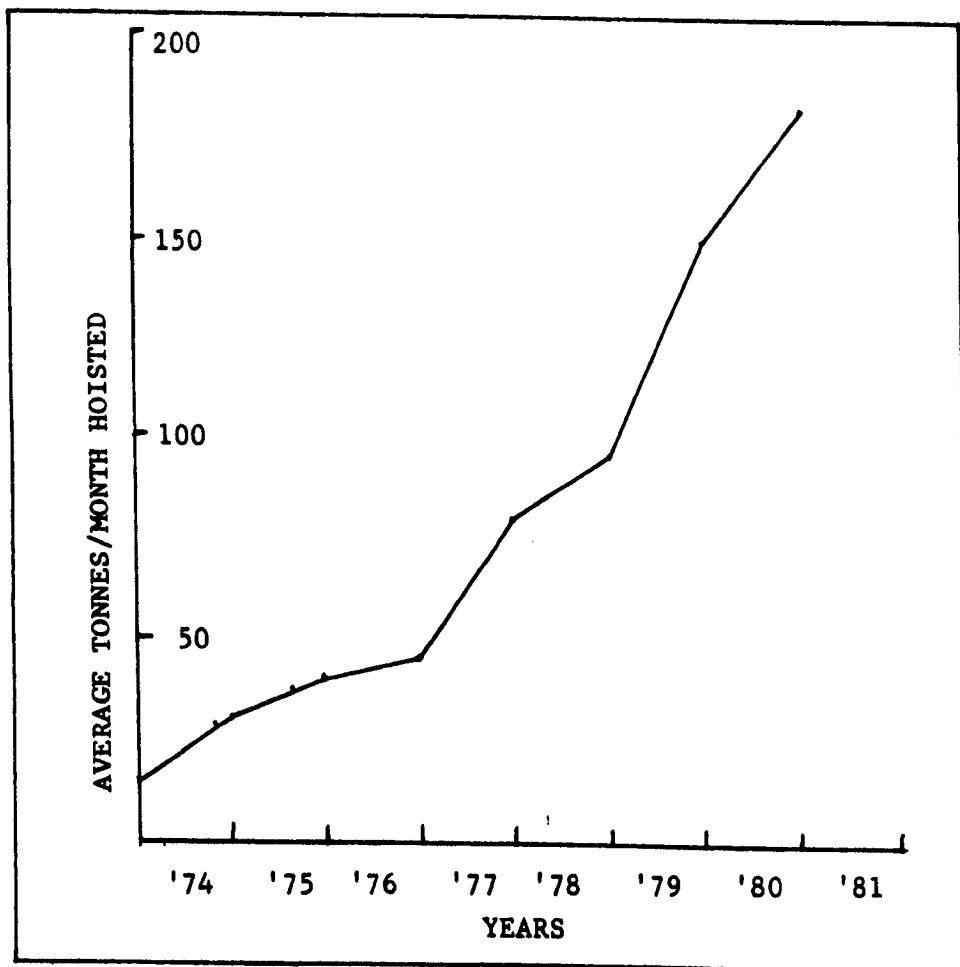
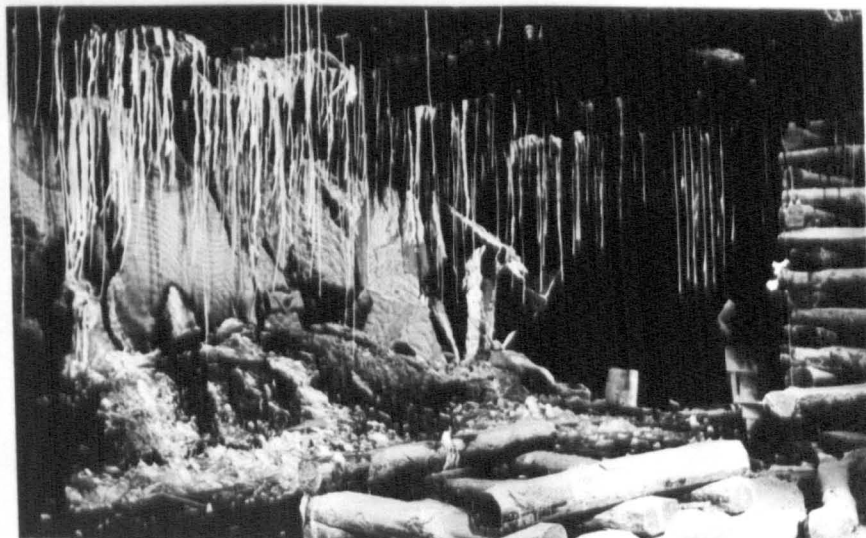
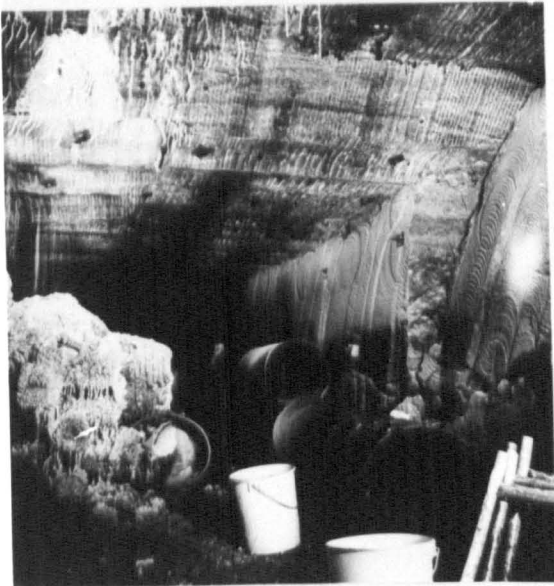
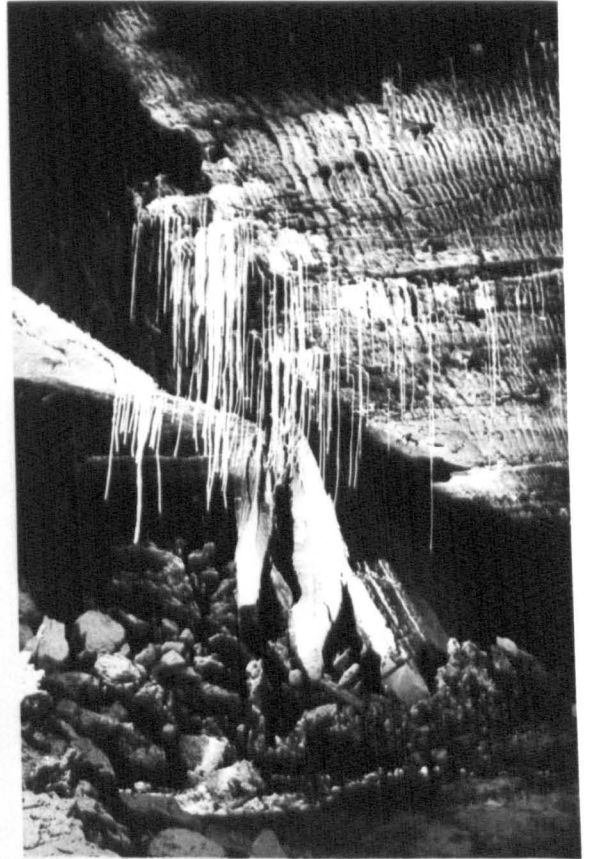


Figure 5.6 Monthly production - tonnes

Wide (>90m) high extraction panels had apparently provided the much needed solution. Then came, if not disaster, great misfortune. Water started pouring from a geological probe hole in H roadway, No. 10 Panel, on 23rd October 1979, to be followed by a similar

Plate 5.5

Showing different views of water ingress site.
No 3 shows the vertical shear fracture running
along the roof across the mouth of the stub.
Conditions in the stub were good.



event in E roadway in the same panel. The inflow rate increased within the first few days to about 100 litres per minute and appeared to stabilise at that level. It was difficult to establish the precise volume entering the workings as after a day or so, it was coming through numerous additional cracks and fissures. When the flow rate did not decrease, No. 10 Panel was stopped and the resources deployed into No. 17 Panel. No. 19 Panel was the next panel where water entered, followed by Nos. 12, 17 and 11 Panels. Table 5.4 lists the panels and sites with the dates, flow rates in litres/minute. These are also located on the plan in Figure 5.7.

TABLE 5.4

Water Inflow Sites

Panel Site	Date of Water	Flow Rate litres/min.
No. 10 E	23.10.79	123
H	22.10.79	55
No. 11	18.4.80	18
No.12-16/5	6.12.79	5
20/7	6.12.79	2
21/8	6.12.79	2
No. 17 G/4	7.1.80	11
H/5	9.1.80	11
No. 19 G/9	12.12.79	5
E	16.12.79	55

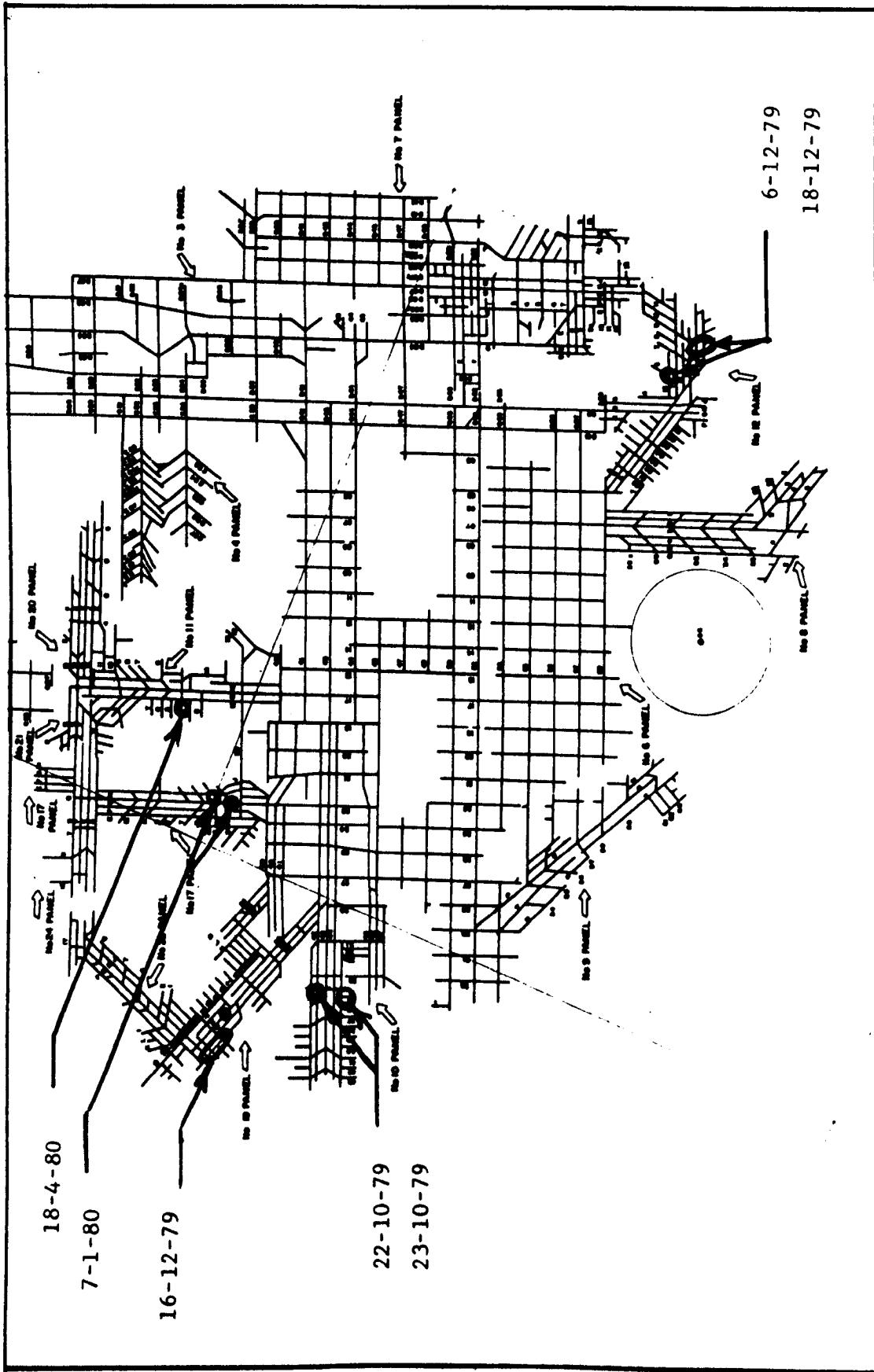


Figure 5.7 Plan showing water sites

Plate 5.6

- 1 Newly mined heading in good primary ore.
- 2 Roadway coming up out of salt into potash, with extensive roof slab. Note that it is the halite that has broken away on the sidewall due to its lower failure strain.
- 3 C43 Conveyor road approximately 15 days after mining - excellent conditions.



The features common to the water sites were that they had all occurred where the panel width was 90m or greater and that they were all reasonably adjacent to a fairly well defined geological anomaly. This was the salt overfold, the trend of which is shown in Figure 5.6. It has been established that this overfold is associated with faulting in the Magnesian Limestone below the Middle Halite and potash horizons. Other similarly trending disturbed zones probably containing salt overfolds have been identified elsewhere in the mine. These are shown in Figure 5.8.

The latest available evidence is that the flow rates are decreasing everywhere with the exception of No. 11 Panel. The probable reason for this is that the large area of high extraction at the conjunction of Nos. 11, 20 and 21 panels is deforming to the extent that failure of the roof strata will probably occur. This is to be expected. If the criterion for water inflow is high extraction at a critical width, then certain other areas must have a high probability of encountering water as time passes and deformation inexorably continues. These areas are, the junction of No. 7 and No. 18 Panels, Panel Nos. 15 and 16 and possibly No. 4 Panel and the junction of Panels 26, 27 and 28.

5.4 Concluding Remarks

The intention of this chapter was to describe the main features giving rise to problems in panel design and layout. Although these features have been described as three separate entities, they are

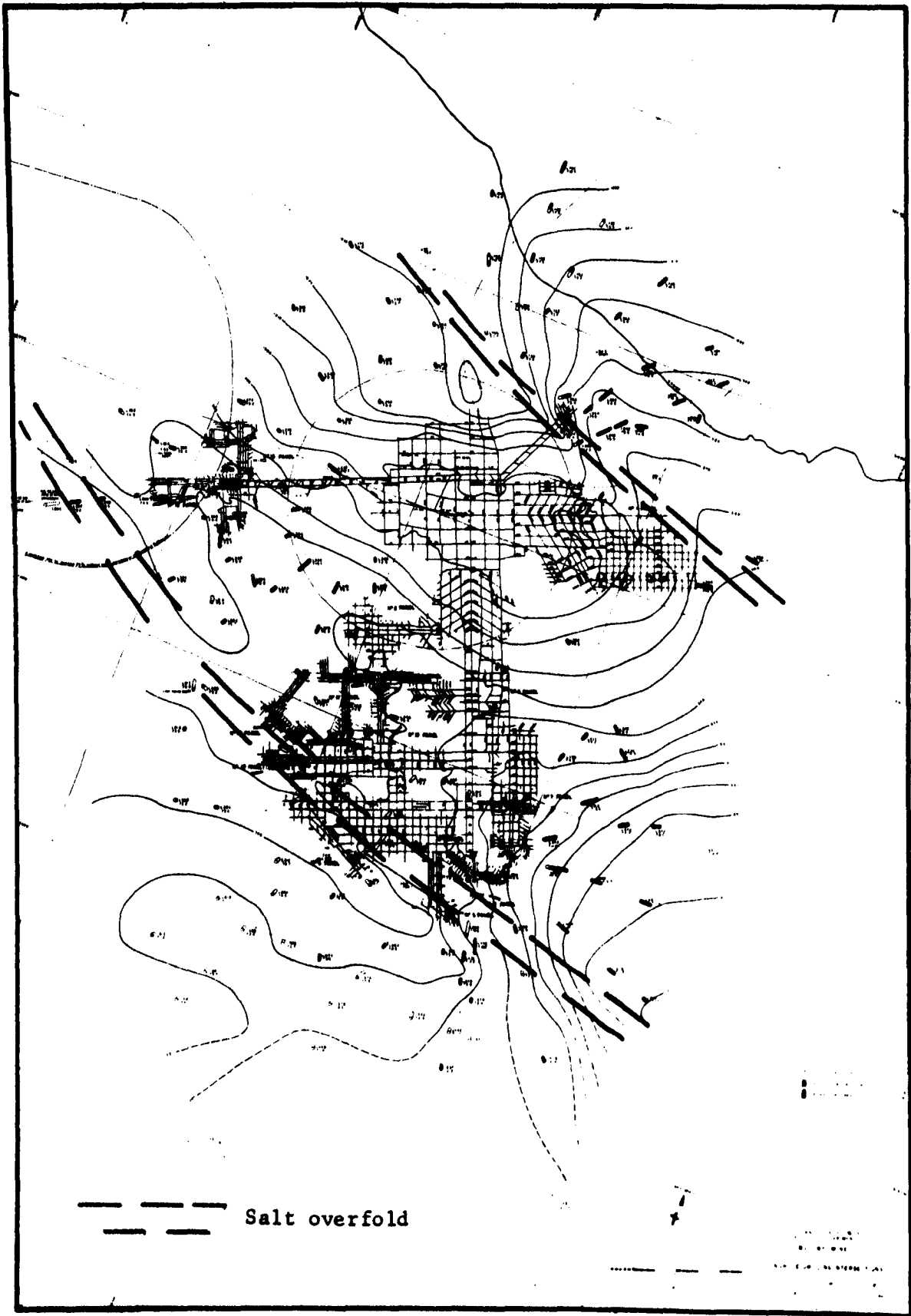


Figure 5.8 Plan showing overfold zones

in fact different aspects of the same overall phenomenon. This is the non-uniform nature of the potash seam and the surrounding strata. From a potash mining point of view the geology at Boulby is uncompromising and inflexible and as such is testing the ingenuity, not to say the patience and purse strings, of the mining company to the limit. Any layout at Boulby, to be successful, has to be flexible and yet when changed must not alter fundamentally. In the end, though, it must provide sufficient headings so that the mechanical equipment available can be used with optimum efficiency and productivity.

CHAPTER SIX

LOW AND HIGH EXTRACTION PANELS AND ANALYSIS OF UNDERGROUND MEASUREMENTS

CHAPTER SIX

6.0 Introduction

The original concept of mining layouts was based on the accepted European practice in rocksalt and potash, mainly in East and West Germany as well as rocksalt mines in Great Britain. This utilised a standard room and pillar system with square or rectangular pillars laid out in panels with between 5 and 11 entries. Percentage extractions of up to 60%⁽¹⁶⁾ were achieved. Because of the unknown nature of the geology and the likely response of the rock to mining, the initial layouts were implemented largely on a basis of "try it and see". Model studies and laboratory trials were carried out by Patchet⁽⁵⁾, Buzdar⁽³⁷⁾, and Peggs⁽³⁸⁾ and others and the results obtained were applied to the initial design of roadway and pillar dimensions. Mining in the shaft area where 60m square pillars were used with an extraction of 21% gave only a few clues as to what to expect with higher extraction production panels. After mining in the shaft pillar area for some 36 months on a 60m square grid, it was decided to increase production by setting off two panels, the East Panel going east, and the South Development Panel, going south. These two panels set the main directions of development that have been followed up to the present apart from one or two attempts to follow geological trends with high extraction panels.

6.1 Low Extraction Panels

The term "low extraction panels" is used to refer to panels

that have an overall percentage extraction of up to 35%. These panels range in width from 150m to 450m and it was intended to obtain long term stability over a large area of the panel. Table 6.1 lists the low extraction panels together with the salient features. The shaft pillar area is included for completeness, although it never was a production panel. Long term in this context refers to at least several years. It was hoped that stability could be achieved by designing the panels, pillars and roadways in such a way that the pillars would contain triaxially confined stable cores. In this way the pillars would be able to carry the full redistributed cover load as based on the tributary area theory.

Hebblewhite⁽⁷⁾ discusses the results of a number of finite element analyses of different low extraction panel layouts. The panel geometries were drawn up by the mine staff at Boulby Mine.

In order to assess the relative stability of the pillars within each panel on the basis of strength, a relative safety factor was derived. The stress levels at Boulby Mine exceed the uniaxial strength of the rock due to the great depth, and therefore pillar stability depends on the formation of a triaxially confined core. The safety factor was therefore based on the triaxial strength of the rock. This was established from the Mohr envelope for potash established by Patchet⁽⁵⁾, Figure 6.1, and is defined as:

$$F_s = \sigma_1(\text{fail}) / \sigma_1 \quad \dots 6.1$$

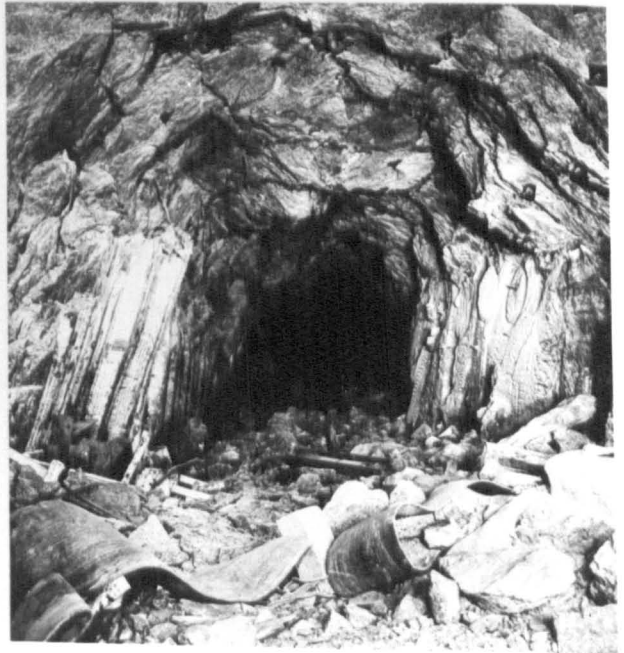
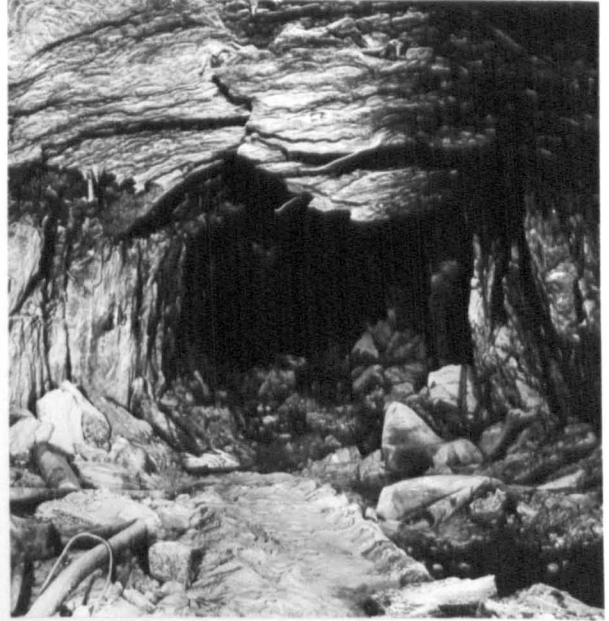
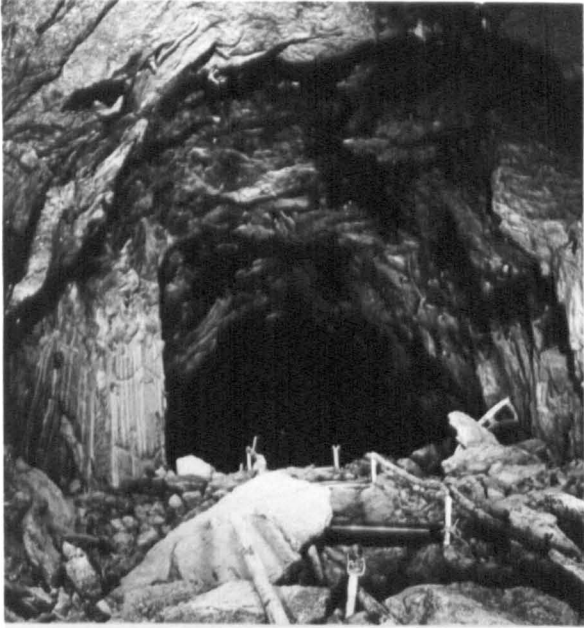
Plate 6.1

No.6 Low Extraction Panel

- 1 to 4 Note extensive roof failure due to excessive wall to wall closure, causing 'overthrust' shear fractures.

Plate 6.2

- 1 Shows profile after enlarging with the Dosco roadheader in No.6 Panel.
- 2 Sidewall to be blasted to soften it sufficiently for Dosco to mine it.
- 3 Large tensile failure of the immediate roof beam.
- 4 Shows the difficulty of maintaining good ventilation seal around vent doors because of rock creep.



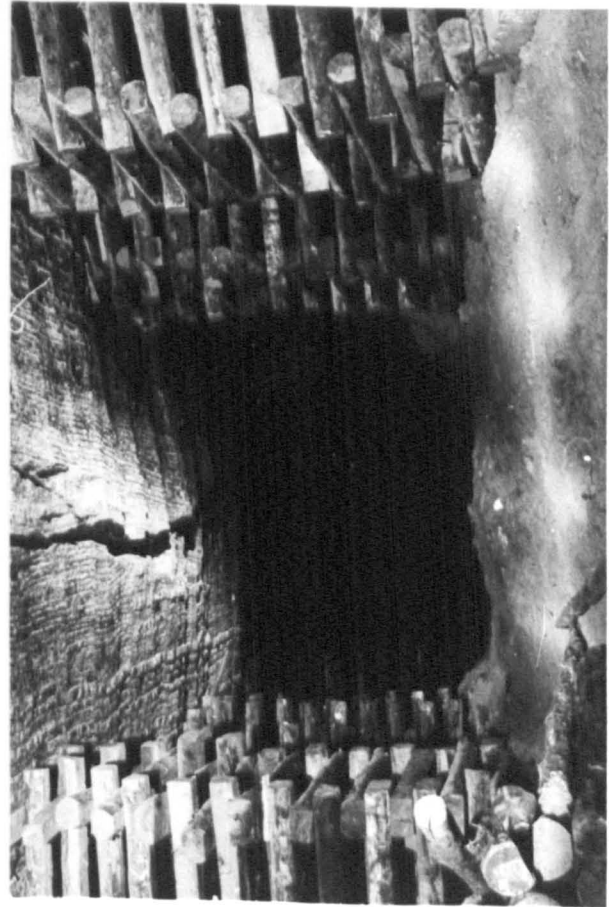
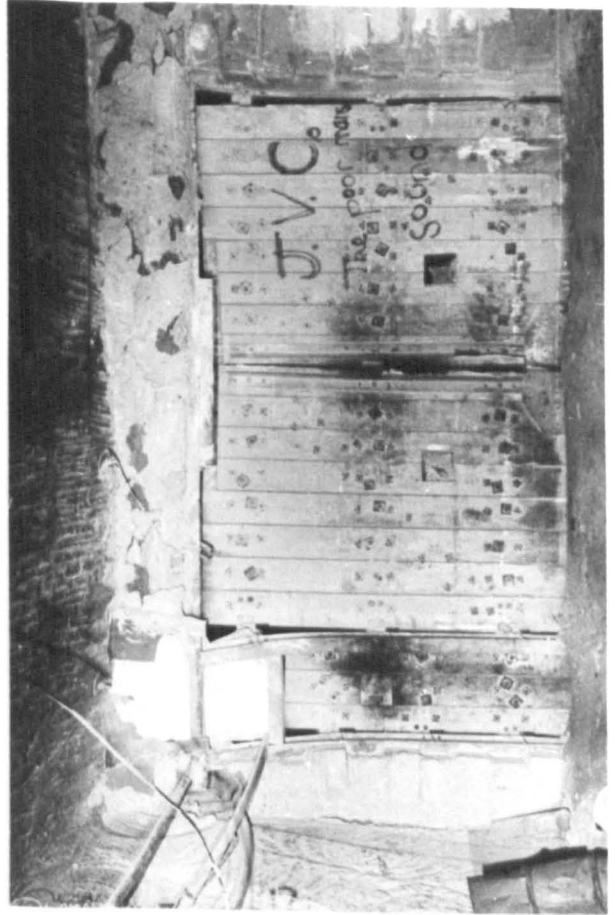
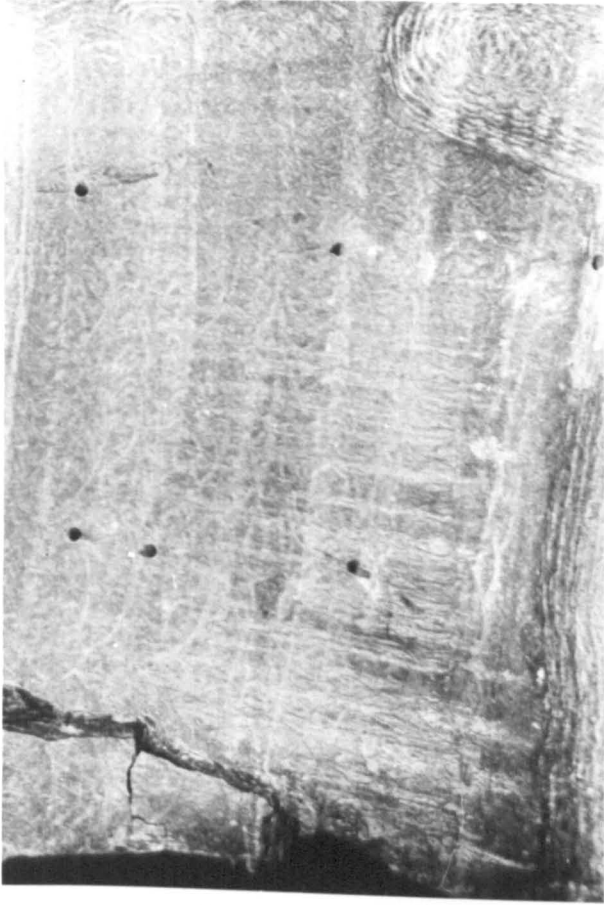


TABLE 6.1

Low Extraction Panels

	Panel Width (m)	Pillar Dimensions (m)	Distance Worked (m)	Time Worked (months)	Type of Ore	No. of Rock Mech. Sites	O.M.S. tonnes/man shift
Shaft Pillar	600	60 x 60	600	36	Salt Potash	16	-
East Panel	450	diamond 40 x 40	400	20	Salt Potash	7	21
No. 1 Panel	350	25 x 25	450	20	Primary Potash	3	15.2
No. 2 Panel	300	25 x 25 25 x 40 15 x 35	250	14	Secondary Potash	3	11.3
South Devel.	300	40 x 40 diamond	280	12	Primary & Secondary Potash	6	14.5
No. 6 Panel	250	30 x 30	500	14	Primary Potash	7	51
No. 7 Panel	150	25 x 30	350	12	Primary & Secondary Potash	0	15.8

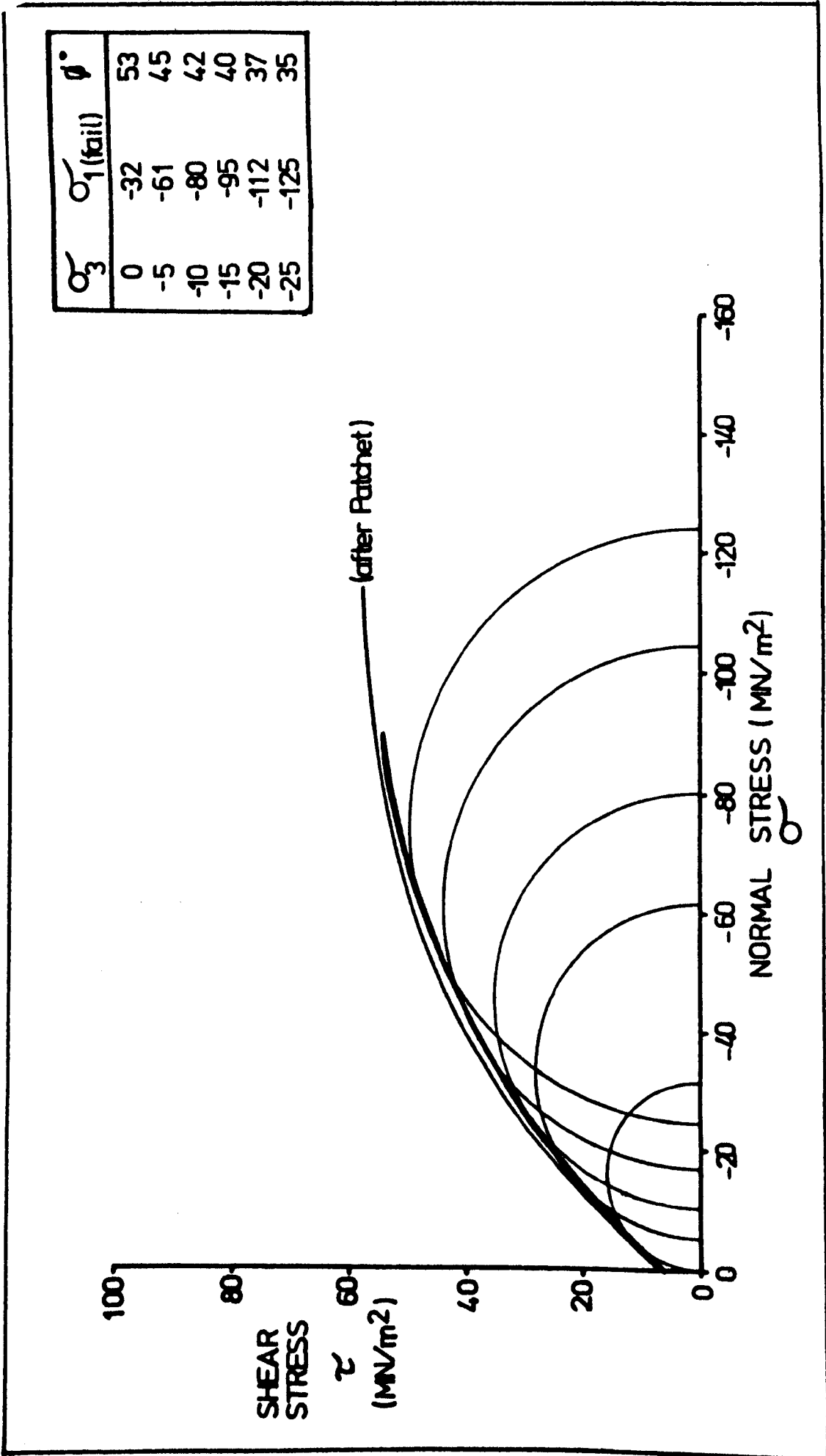


Figure 6.1 Mohr's Envelope for Potash

for a given σ_3 , where σ_1 (fail) is the major principal stress which, in conjunction with σ_3 forms a Mohr's circle in contact with the Mohr's envelope for potash. This suffers from the disadvantage that it does not take into account the time-dependent behaviour of the rock. Hebblewhite arbitrarily defined a pillar safety factor to take into account time dependent behaviour. This was based on a deviator stress of 16 MN/m^2 representing infinitely stable conditions, giving a safety factor of 10, and a value of 27 MN/m^2 having a safety factor of 1. This latter stress represents the limiting value for long term stability.

The ultimate criterion in the initial design of panel layouts was that of not exceeding the tensile failure strain of a fairly thin (<1m) anhydrite layer 120m above the potash seam. It was assumed that the Upper Permian Marl above this bed would be water bearing, and that fracturing the anhydrite would lead to water entering the mine workings. That this criterion was valid is evidenced by the fact that to date no water intrusions have occurred in any of the low extraction panels.

The low extraction panels however, suffered from the major drawback that it was not possible to achieve long term stability of roadways in potash in these panels. This means that either massive and expensive re-ripping and supporting of these areas has to be carried out at frequent intervals, or the panels have a limited life. Plates 6.1, 3.1 and 3.2 show various aspects of low

extraction panel conditions. Also the long cross-cuts meant that the advantages of concentrating men and machines was lost.

Because of the expense involved as well as the dilution of ore, it was decided not to site long term panel access roads in the salt below the potash. This had been recommended by the research team at Newcastle University, led by Professor Potts.

A further constraint on the design of layouts was that no damaging subsidence could be allowed to occur at the surface. Since mining began, subsidence troughs have developed and have been surveyed and reported on (7), (17). The conclusions reached are summarised below.

- (i) The maximum vertical subsidence measured to date is 80mm over the South Development and No. 2 Panel area.
- (ii) The maximum horizontal tensile strain measured on surface is 100 microstrains. Higher strains are probable over areas of high extraction, possibly as high as 200 micro-strain, but as no measuring stations exist above these areas, no direct measurements have been obtained.
- (iii) There is an apparent time lag of about 9.5 months between mining taking place and the associated subsidence appearing on surface. This is assumed to be a result of the time dependent deformation of the pillars and strata below.

- (iv) The angle of draw for surface subsidence is approximately 54° with the maximum tensile strains occurring between 32° and 36° over the ribside.
- (v) A subsidence trough with an associated vertical subsidence of 22mm has been monitored along a line approximately 1500m from the nearest potash workings. It is possible that the presence of old ironstone room and pillar workings underlying this area could be influencing the movement.

The main factors which had been found to influence the design of low extraction panels can be enumerated as follows:

- (a) All long term stable pillars exhibit high strains in the first 5m to 10m, depending on their size, but a stable core exists beyond this zone. Generally speaking, the stable core is about 15m narrower than the minimum pillar width.
- (b) Pillars below 25m width should not be used for stable low extraction panels.
- (c) All pillar sizes investigated (including 60m pillars) have shown significant yield which would result in measurable surface subsidence. This includes the very low extraction (21%) shaft pillar area.

- (d) Pillars mined in halite are up to four times as rigid or stiff as the equivalent pillars in potash.
- (e) Low extraction panel widths should not be greater than 290m if excessive loading of ribside pillars and therefore subsidence at the critical anhydrite bed, is to be avoided.
- (f) Four-way road intersections are stress relieved and stable if they contain at least 1.5m of competent potash in the roof. T junction intersections are not stress relieved, and behave as normal roadways.
- (g) Shaley roof conditions do not give stress redistribution around intersections for any length of time.

6.2 High Extraction Panels

The term "high extraction panel" refers to a panel where the extraction ratio within the panel is greater than about 60%. In order to achieve this at Boulby Mine, use has to be made of narrow pillars, usually between 3m and 6m wide, that exhibit high rates of yield. These still have to have some load bearing capability in order to provide local support for the immediate roof across the width of the panel. This roof then sags uniformly without breaking up, thus maintaining good conditions for a reasonable period of time.

These high extraction panels were initially designed according

to the criteria given by Serata. He describes his theories in various papers^{(15), (18), (19), (20)} (described in Chapter Five) and attributes protection of the inner roadways to so-called "stress relief". These methods had their origin in the Canadian potash mines where it is felt that Serata's theories are one way of describing what is occurring. However, because of the presence of highly variable rock strata within the first 30m of roof material at Boulby the successful application of these theoretical ideas in this mine is precluded. Although high extraction layouts have generally resulted in good roadway roof conditions, it will be shown that this has not come about by "stress relief" in the Serata sense, but by another mechanism altogether. One of the results of making panels wider, which is a basic tenet of the concept of stress relief mining, is that water has entered the mine workings. It is felt that this could have been avoided even though still using high extraction panels, but with a limit on the panel width.

To date, some twelve high extraction panels have been mined. These have been of varying width and extension, having an average panel extraction ratio of 66%. Table 6.2 lists these panels and some of their more pertinent features. It can be seen from the above table and the plan of the mine showing the panels - Figure 6.2, that the layouts were often very irregular. The main reason for this was that adverse ground conditions were frequently encountered. In the earlier panels, experimentation caused a

TABLE 6.2

High Extraction Panels

Panel	Rock Mech. Instrumentation	Width m	Length m	No. of roads	Yield Pillar width	Stubs m x m	% Extraction	Comments
No. 8	MC, Ext, Conv.	67	200	6	3, 4, 6	-	61.6	90 in salt
No. 9	-	Varied	300	Varied	Varied	-	45*	Unsuccessful expt.
No. 10	MC, Ext, Conv.	90	200	5	4	9 x 20	73.6	Water
No. 11	Conv.	70-80	250	3	4	Varied	64.8	Erratic, water
No. 12	MC, Conv.	80-90	270	3, 6	4	9 x 20	69.5	Water
No. 15	MC, Ext, Conv.	100	200	5	4, 5	9 x 20	65.8, 62.8	Undermined by salt roads
No. 16	MC, Ext, Conv.	85	150	5	4	9 x varied	65*	
No. 17	Conv.	100, 45	90, 150	5, 4	4	varied	60, 73.1	Water in wide section
No. 19	MC, Ext, Conv.	75-100	250	5	4	9 x 20	73.6	Water
No. 20	Conv.	40-70	200	5, 4	4	-	65.9	Erratic
No. 21	Conv.	40	200	4	4	-	76.9	Mined in salt
No. 22	Conv.	40-75	170	3, 4	4	Erratic	74.3	At rt. angles to No. 19 Panel

* Estimated

MC - Microcreep; Ext. - Extensometer; Conv. - Convergence

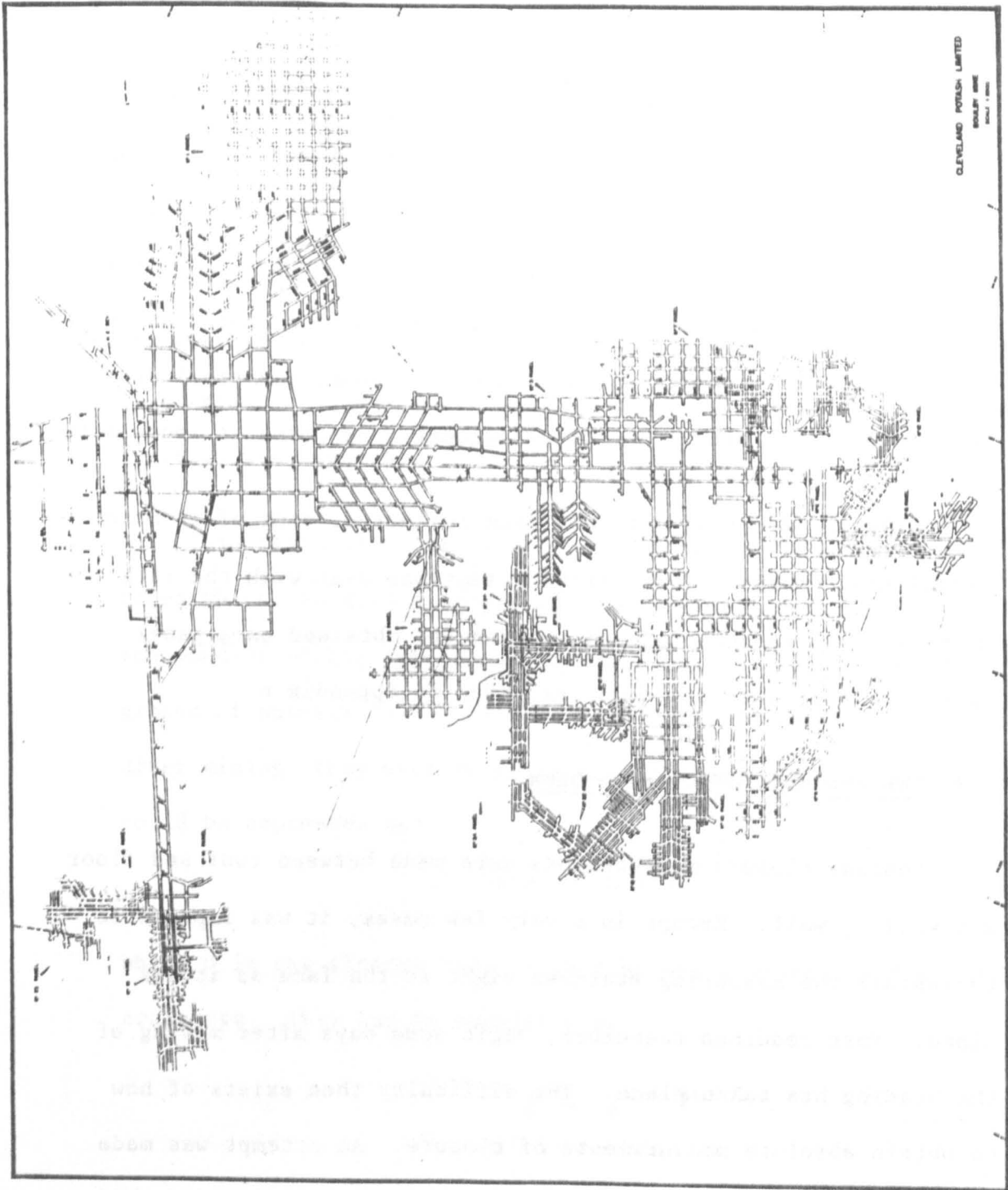


Figure 6.2 Plan of mine showing high extraction panels

certain amount of erratic development. Water was encountered in five of the major high extraction panels, all where the panel width was of the order of 90m.

The rock mechanics instrumentation installed (and the subsequent recording of data) was somewhat erratic, consisting of micro-creep, convergence (both roof to floor and wall to wall) and extensometer (roof and pillar) stations either singly or in combination. It was intended to have stations sited in lines across panels as well as down the lengths of roadways. However, the presence of both bad ground conditions and the installation of support or equipment such as conveyors, sometimes precluded the installation altogether or subsequently rendered it inoperative.

A large amount of data has been collected, some of it more useful than others. The following sections deal with the rock mechanics instrumentation and the results obtained on a panel basis. Weekly face advances are given in Appendix 6.

6.3 The Analysis of Closure Data

Roadway closure measurements were made between roof and floor and wall to wall. Except in a very few cases, it was impossible to install the measuring stations right at the face as it was mined. Most readings therefore, begin some days after mining of the heading has taken place. The difficulty then exists of how to obtain absolute measurements of closure. An attempt was made to fit curves to the measured data using the curve fitting program,

CURFIT, which fits data to six different functions:

1. $y = A + Bx$
2. $y = Ae^{Bx}$
3. $y = A(x-B)$
4. $y = A + B/x$
5. $y = 1/A + Bx$
6. $y = A + B \ln x$

Where y is the closure and x , time since mining.

The sixth function, $y = A + B \ln x$, gave the best fit, with an index of determination generally greater than 0.90. However, since the function was undefined for $x = 0$, it could not be used.

This difficulty can be partially overcome by using closure rates which, because they are not cumulative, are essentially independent of the initial reading but not of time. When the graphs of natural log of closure rate were plotted against days after mining, they were found to have a linear relationship, and could be expressed as:

$$\ln \dot{c} = A + Bt \quad \dots 6.2$$

where \dot{c} is the closure rate, t is time after mining, and A and B constants. This can be rewritten as:

$$\dot{c} = e^{A + Bt} \quad \dots 6.3$$

Integrating with respect to time gives:

$$c = e^{A + Bt} + D$$

when $t = 0$, $c = 0$, therefore,

$$c = \frac{1}{A} (e^{At + B} - e^B) \quad \dots 6.4$$

As long as log of closure rate has a linear relationship with time since mining, equation 6.4 will give the closure curve with time.

This functional relationship was applied to a number of the sets of closure data, and the results were found to be in close agreement.

The constants A and B were then obtained for all closure data sets and total closures and closure rates were evaluated for 20 day intervals. These results are given in tabular form in the respective sections to which they apply.

6.4 No. 8 Panel

6.4.1 Closure Measurements

This panel was extensively instrumented as shown in Figure 6.3, but as the life of the panel was only about 70 days, the readings, particularly of the later sites, did not cover a very long period. Table 6.3 gives the closure measuring sites and the closure data that was available. These consist of total closures

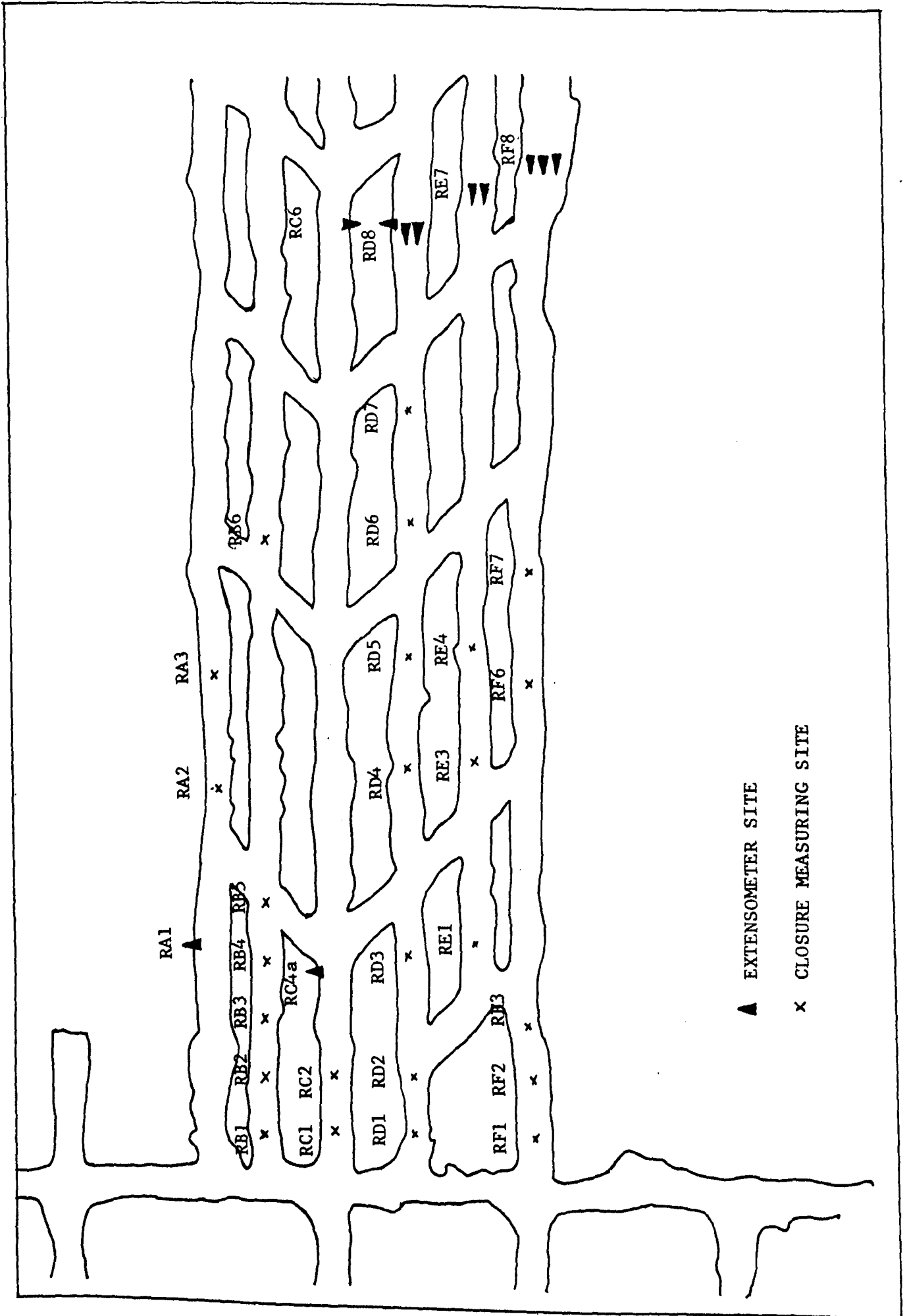


Figure 6.3 No. 8 Panel Instrumentation Sites

TABLE 6.3
No. 8 Panel Closure Data

Total Closure

Closure Rate

Site	20 w/w	20 r/f	40 w/w	40 r/f	60 w/w	60 r/f	Ratio w/w : r/f (20days)	20 w/w	20 r/f	40 w/w	40 r/f	60 w/w	60 r/f
RA2	350							17.5					
RA3	190							9.5					
RB1	190	85	305				2.24	9.5	4.3	5.75			
RB2		120		180					6.0		3.0		
RB3	290	140	440	210			2.01	14.5	7.0	7.5	3.5		
RB4	330	190	492	268			1.74	16.5	9.5	8.1	3.9		
RB5	330							16.5					
RB6	130		180					6.5		2.5			
RC1	180		310					9.0		1.5			
RC2	230		330					11.5		5.0			
RD1	136	106	230	170			1.28	6.8	5.3	4.7	3.2		
RD2	190	170	296	290	364	396	1.12	9.5	8.5	5.3	6.0	3.4	5.3
RD3	226	72	340	134	384	162	3.13	11.3	3.6	5.7	3.1	2.2	1.4
RD4	120		200					6.0		4.0			
RD5	226		345		415			11.3		6.0		3.5	
RD6	125		200		265			6.3		3.8		3.3	
RD7	295	165	388	240	455	300	1.79	14.8	8.3	4.7	3.8	3.4	3.0
RE1	200	135	290	185			1.48	10.0	6.8	4.5	2.5		
RE3	265	130	380	195			2.03	13.3	6.5	5.8	3.3		
RE4	390							19.5					
RE7	330							16.5					
RF1	105		170		220			5.3		3.3		2.5	
RF2	155	135	248	235	315	310	1.15	7.8	6.8	5.7	5.0	3.4	3.8
RF3	180	170	290	250			1.06	9.0	8.5	5.5	4.0		
RF6	310		410					15.5		5.0			
RF7	245		380					12.3		6.8			
RF9	95	70	165	92			1.36	4.8	3.5	3.5	0.6		
RFB1	90	80	145	140			1.13	4.5	4.0	2.8	3.0		
RFB2	100	80	160	160			1.25	5.0	4.0	3.0	4.0		

and closure rates 20, 40 and in some cases, 60 days after mining. In some cases only wall-to-wall closures were measured, while at others, both wall-to-wall and roof-to-floor convergences were obtained. In the latter cases, the ratio of wall-to-wall to roof-to-floor closure was calculated. The conveyor was located in C roadway whilst D roadway served as the main travelling way. The instrumentation sites located in the latter road gave the best data. However, when all the data is plotted, Figure 6.4, an overall picture emerges. The wall-to-wall closures plotted are those for 20, and 40 days after mining for each measurement site. The graphs along roadway D show an initial increase in closure with distance from the start of the panel. This closure rate drops off rapidly somewhere between 42m and 77m. This cycle is repeated with a minimum again being reached approximately 120m from the start of the panel. A similar picture as far as the initial build up is concerned, emerges from B, C and F roadways. The lower initial closures experienced in F and D roads arise almost certainly as a result of the large pillar located between them at the entrance to the panel. This pillar also affected the initial behaviour of E roadway where its build up phase coincided with a drop in closure, at least in D roadway. A maximum closure is reached in E probably coinciding with the second maximum in D, round about the 120m distance mark. This cyclic pattern of behaviour is felt to be highly relevant in explaining the response to loading of the "plate" of elastic anhydrite above the panel.

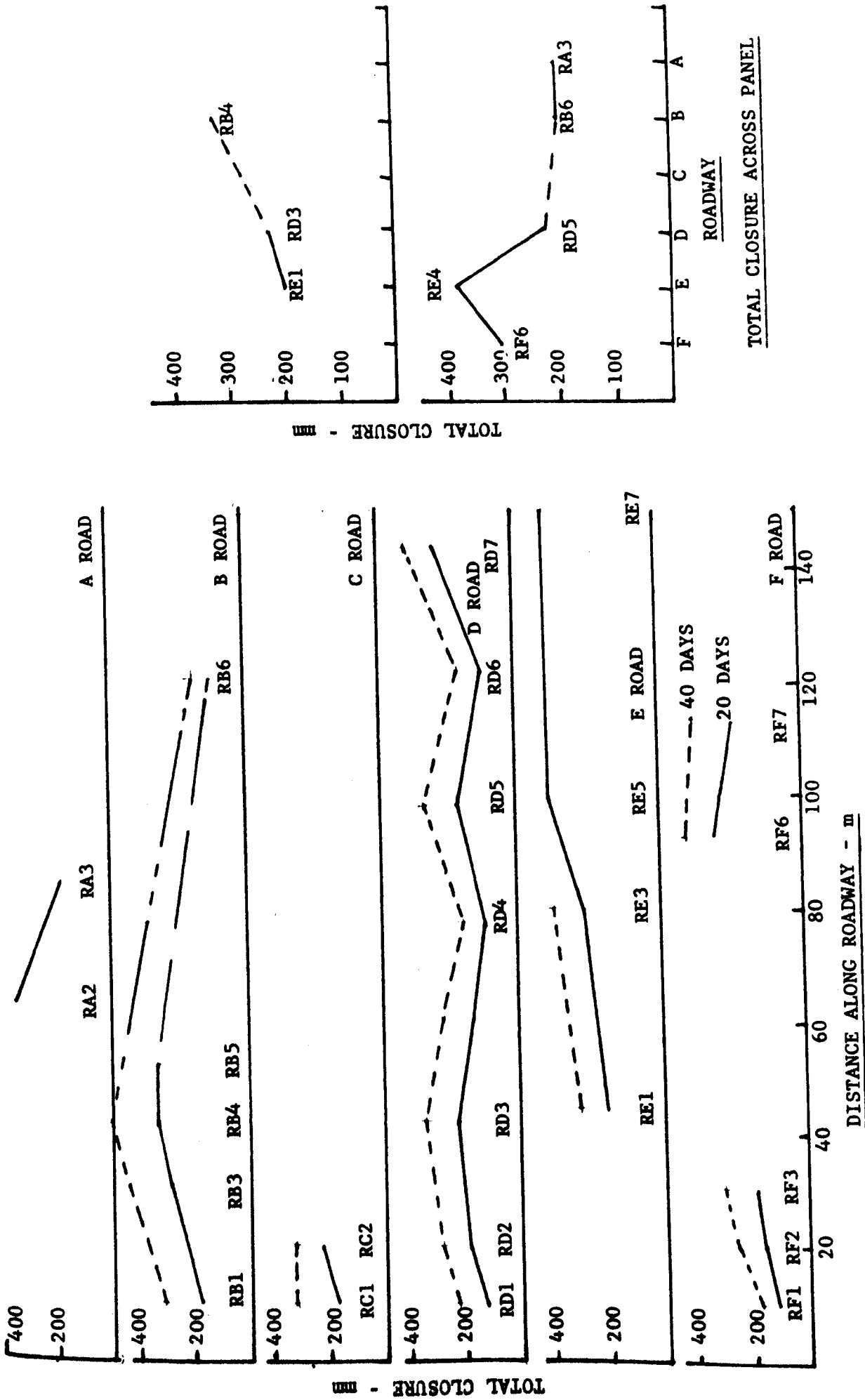


Figure 6.4 No. 8 Panel - Roadway closures

6.4.2 Extensometer Measurements

Site RA1 - Abutment extensometer

This site consisted of a horizontal hole drilled into the east abutment equipped with a multiple point borehole wire extensometer having anchors at depths of 2m, 4m and 6m. The deformations obtained were plotted in Figure 6.5, both as a function of time as well as borehole depth. The interesting feature of these results is the similarity when compared with those obtained from a typical wall extensometer in a 30m square pillar in a low extraction panel, Figure 6.6. These show that there is not a great deal of difference in deformation with time or distance into the sidewall between the sites. This was an unexpected result, as the site in Figure 6.6 was located in a 6.5m wide roadway, 3.5m high, with a 30m wide pillar on either side. RA1, on the other hand, was in the abutment sidewall of a 60m wide panel containing only narrow highly yielding pillars. It could therefore have been expected that high abutment load in the latter case would have given rise to much greater sidewall deformation. In fact, as Plates 3.3, 6.3 and 6.4 show, it was the abutment sidewalls that showed the least signs of damage or deformation throughout the whole of Panel 8. This significant effect, both observed and measured, leads to the conclusion that in a wide extraction panel, the cover load which arises from mining the panel is redistributed very rapidly away from the immediate abutment. The phenomenon described must be due to the rock in the

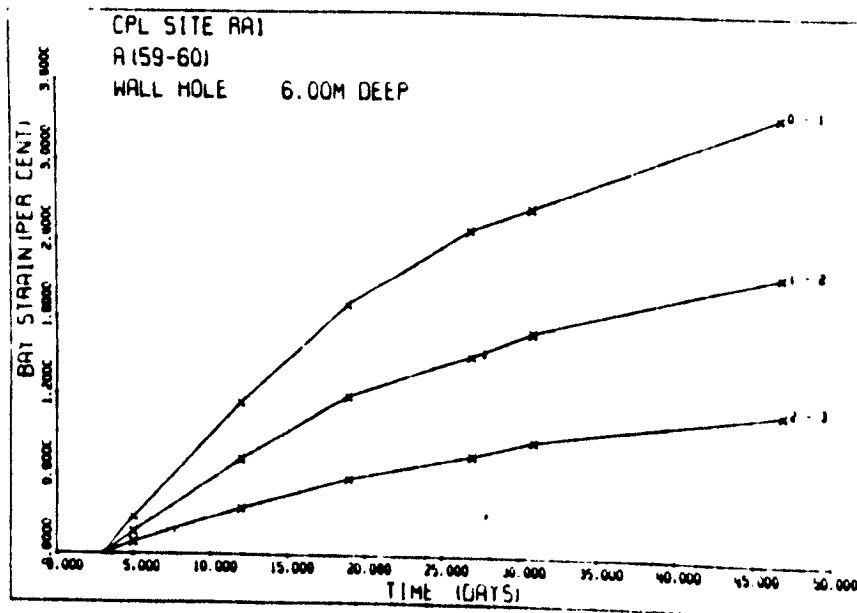
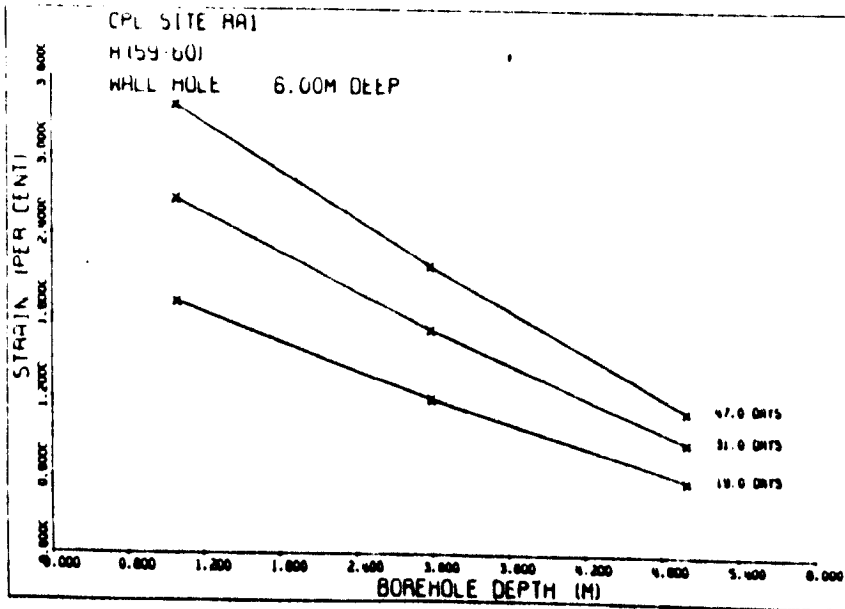
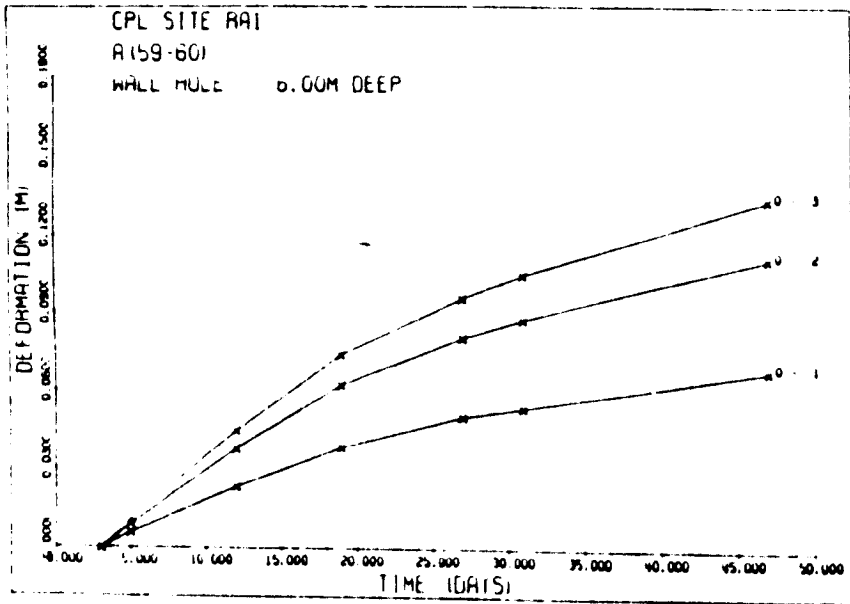


Figure 6.5 No. 8 Panel RA1 sidewall extensometer site

Plate 6.3

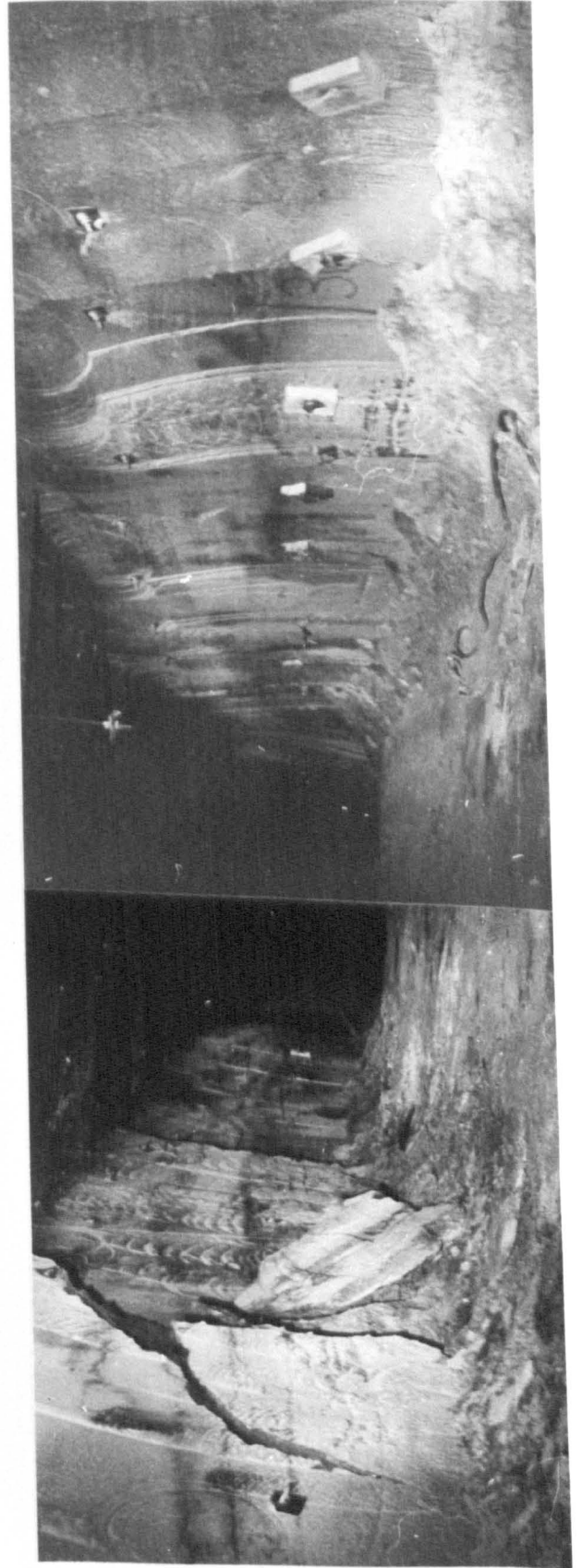
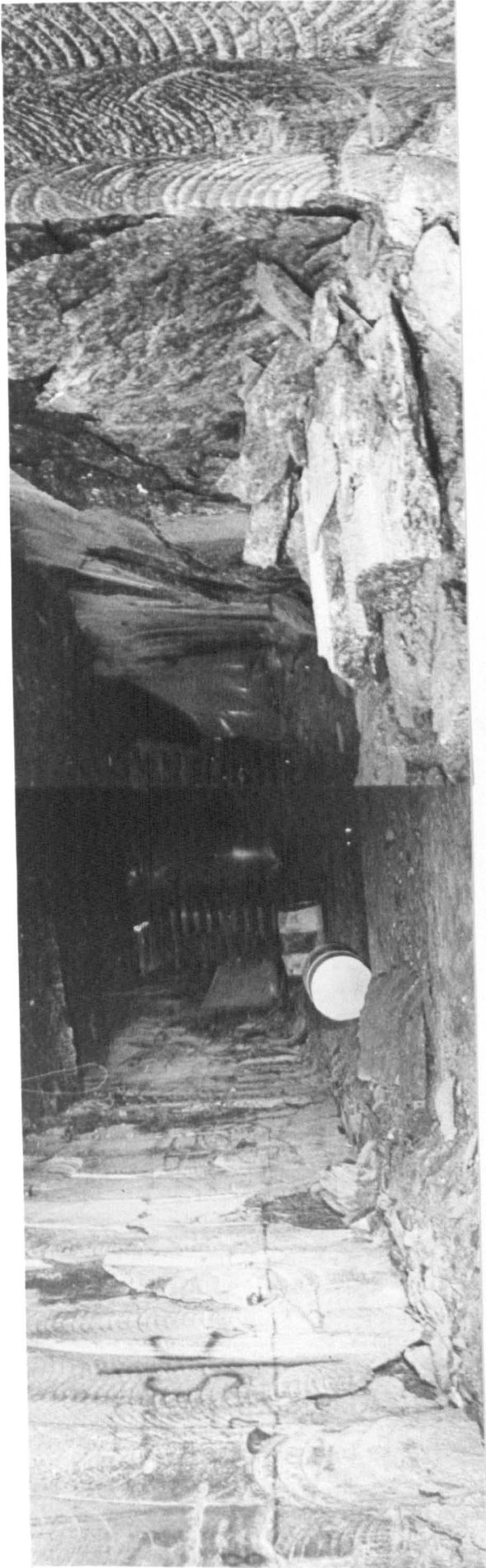
No.8 Panel Conditions

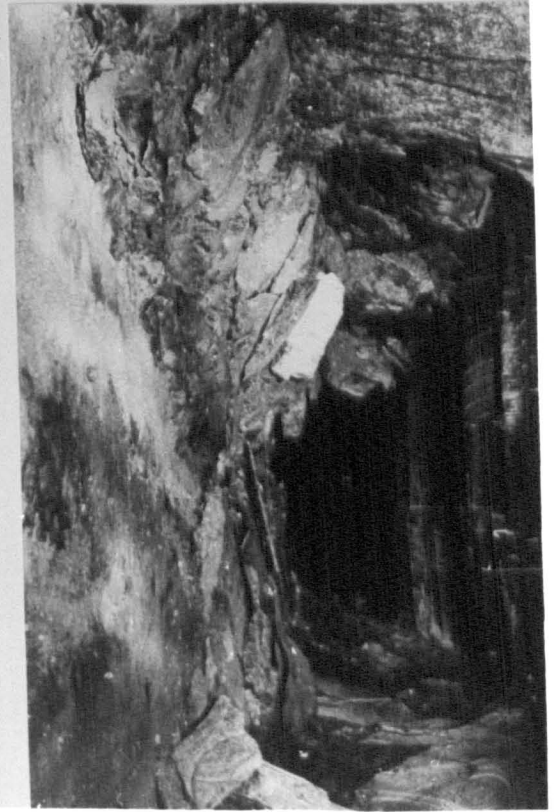
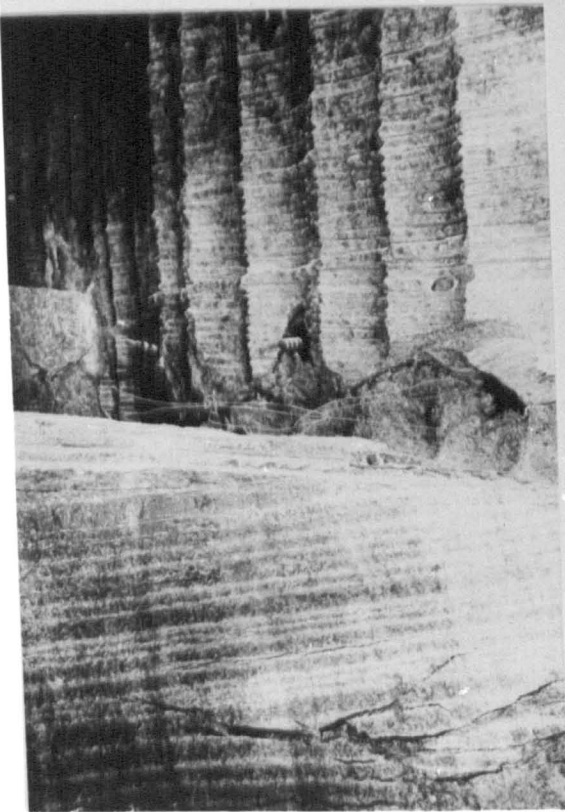
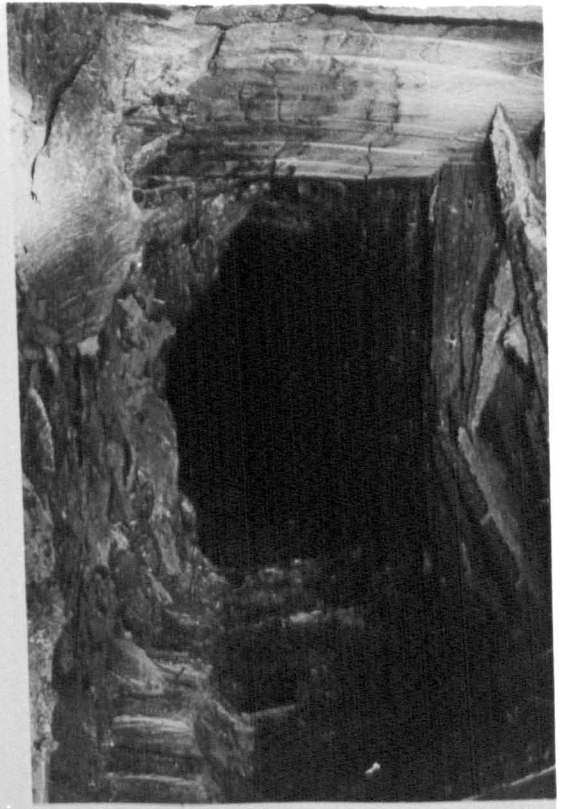
- 1 Showing difference in conditions between outer (abutment) sidewall and yield pillar sidewall (right). No evidence of stress relief.
- 2 Same as No .1. Conditions in these outer roads very good.

Plate 6.4

No.8 Panel Conditions

- 1 View down A roadway.
- 2 View down C roadway.
- 3 E roadway 25m in from start of panel.
- 4 Vertical shearing along ribside abutment in E roadway.





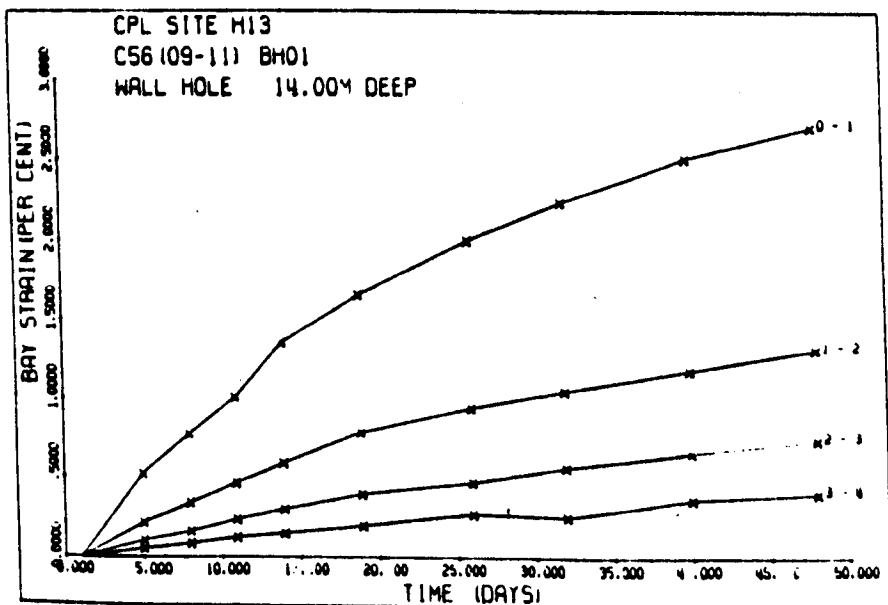
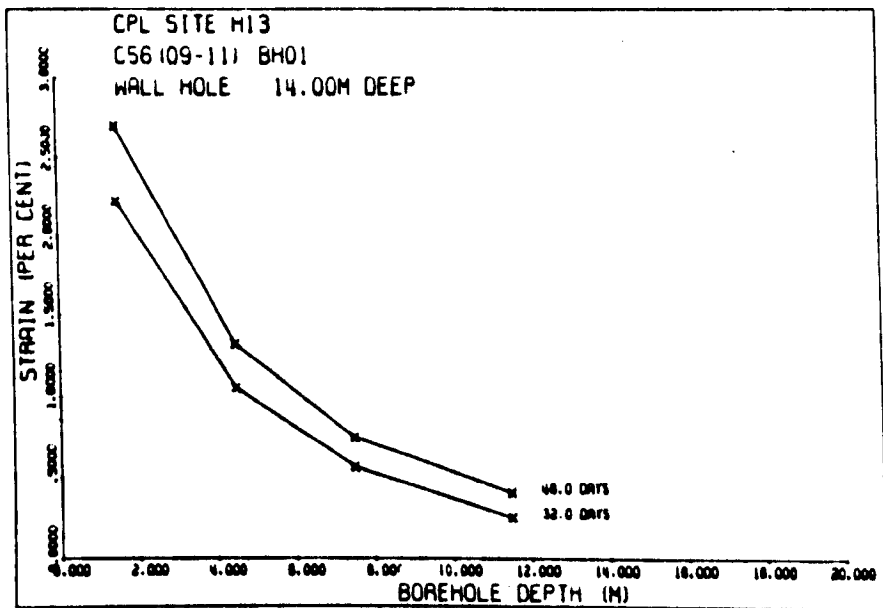
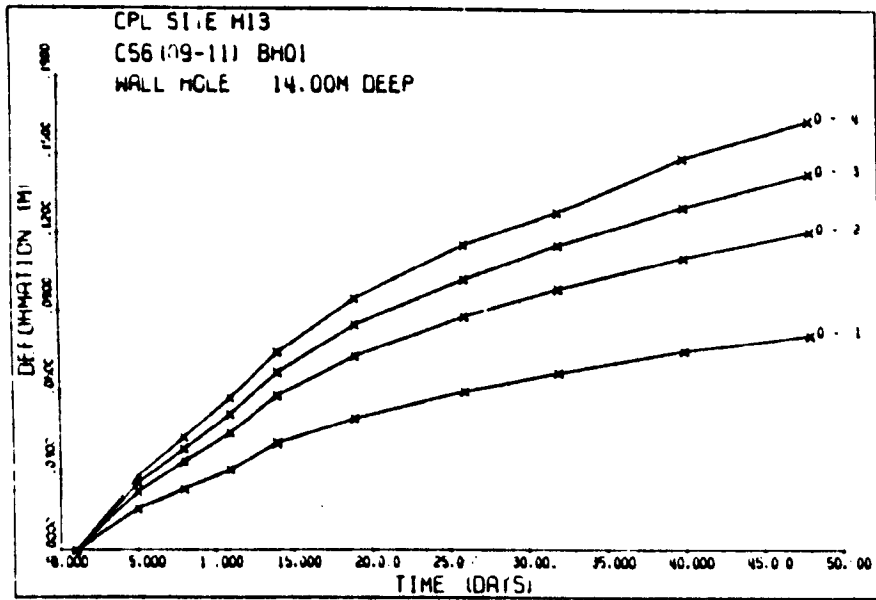


Figure 6.6 Site H13 Pillar extensometer, 30m Pillar

immediate vicinity of the excavation deforming rapidly, although not necessarily massively, with time. Evidence from other panels supports this conclusion, and it is discussed further later in the chapter. This is a similar conclusion to that reached by Baar⁽²²⁾.

Sites RCA4 and RC6 - yield pillar extensometers

A multiple point wire borehole extensometer was installed at site RCA4 into the sidewall of the 6m wide yield pillar between B and C roadways with anchors at 2m, 4m, and 6m. The results are given in Figure 6.7.

These show that virtually all the movement took place within the first two metres into the sidewall. The picture is somewhat complicated by the difference in elevation of the roadways on either side of the pillar. It is this difference that accounts for the fact that most of the deformation (in the direction of the borehole) occurs on the one side of the pillar only.

A similar installation was made at site RC6, with the anchors being located at 1m, 2m and 3m into the 6m wide yield pillar between C and D roadways. The results are given in Figure 6.8 and are very similar to those for RCA4 in that about 90 per cent of the deformation takes place within the first metre. This indicates the formation of slabs, an actual case of which can be seen in Plate 4.1

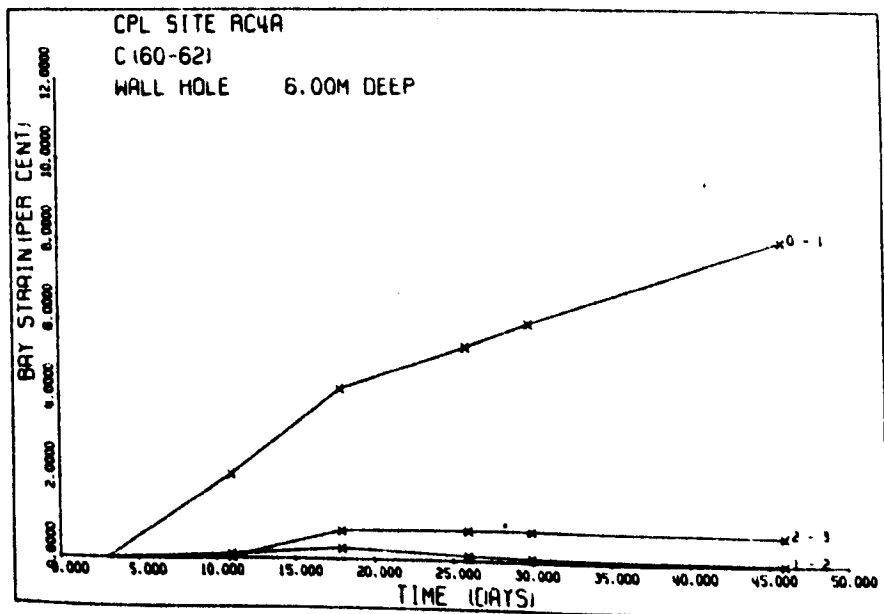
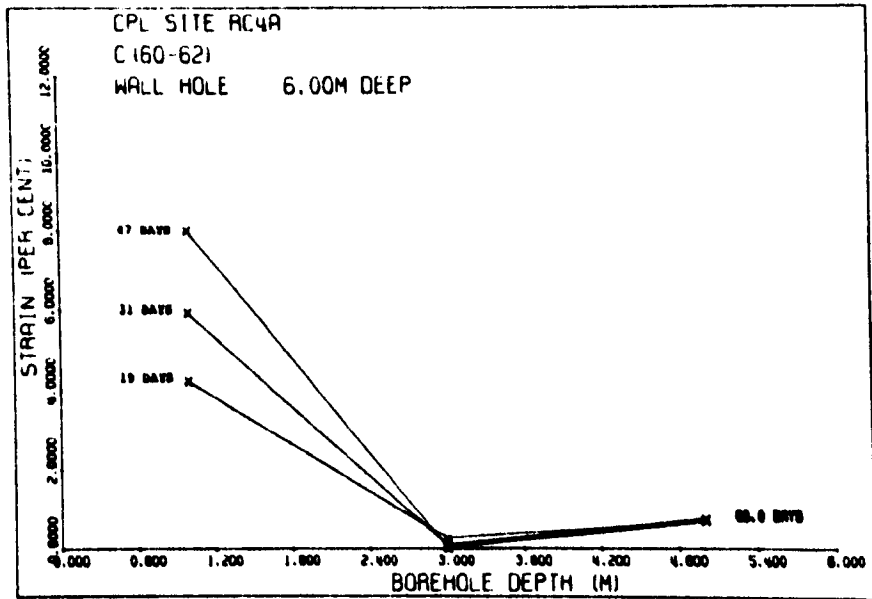
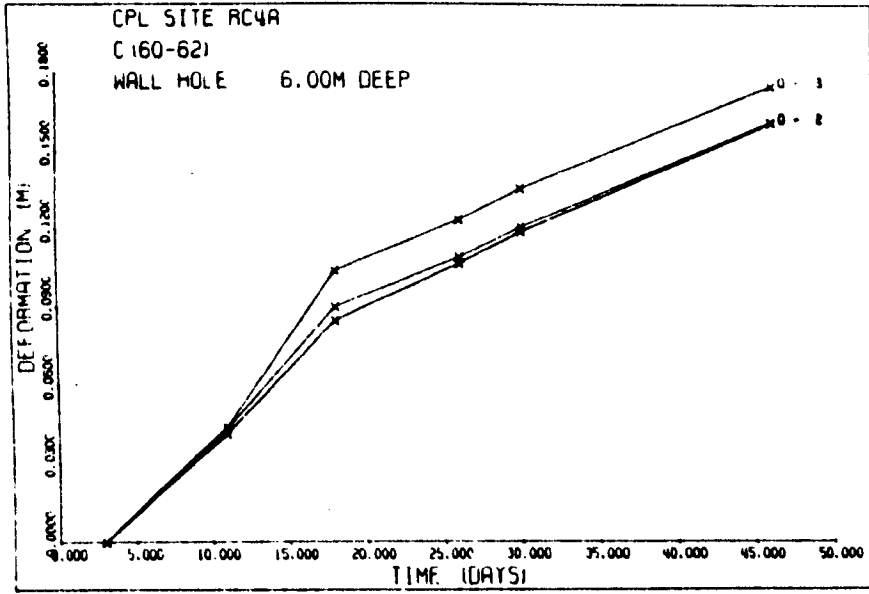


Figure 6.7 No. 8 Panel - Site RCA4 pillar extensometer

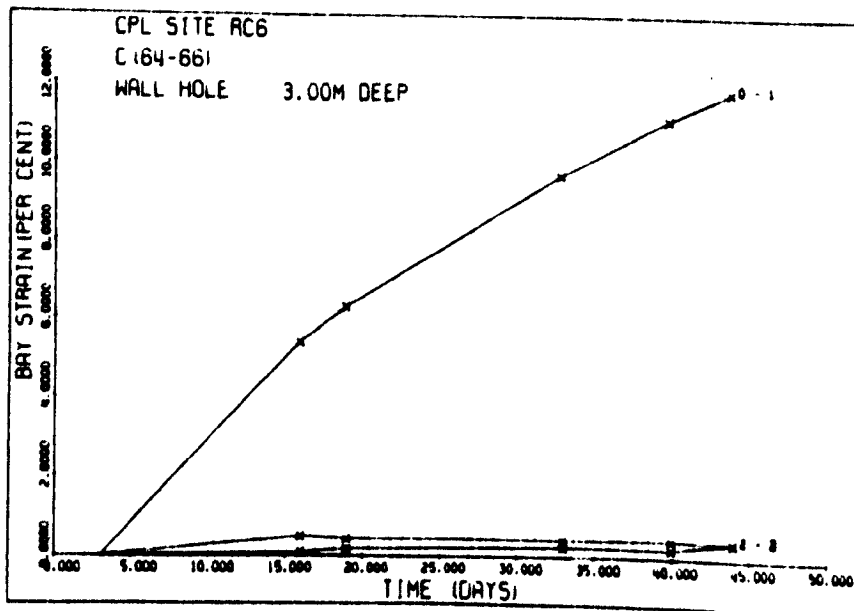
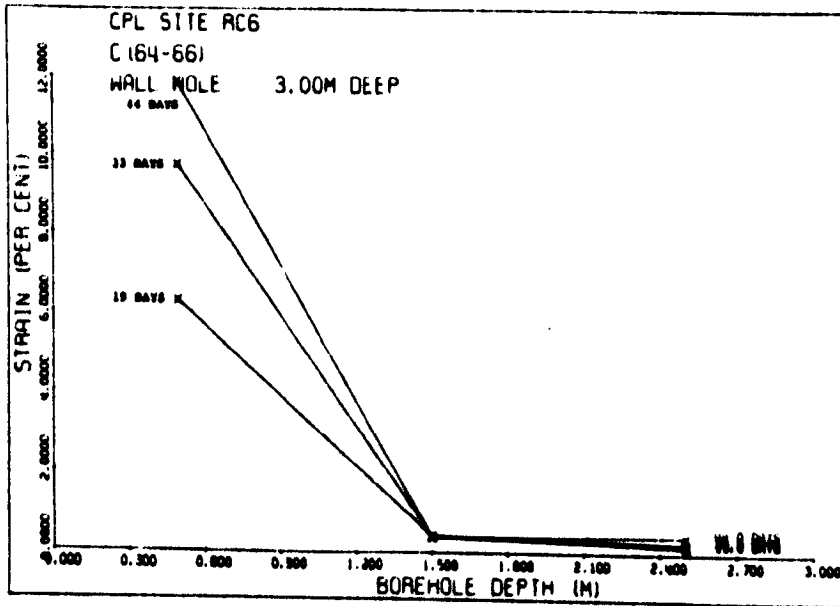
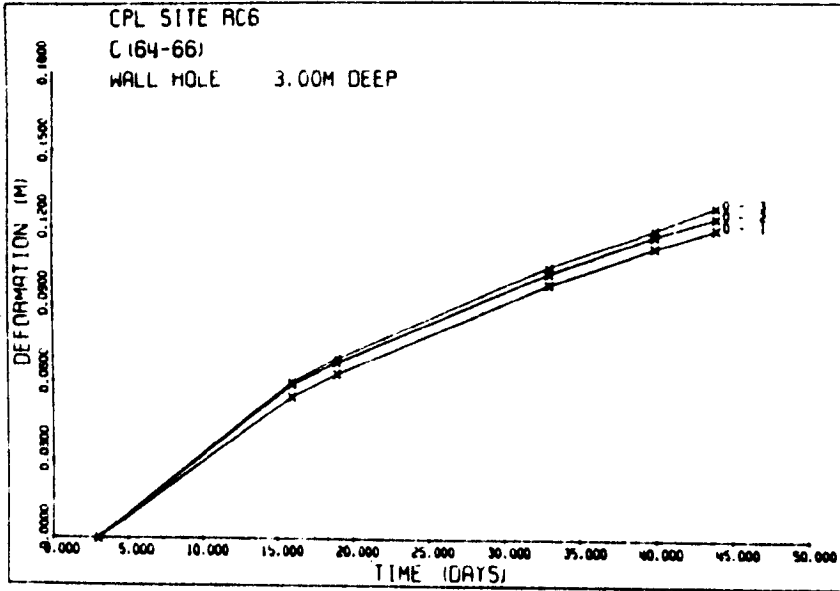


Figure 6.8 No. 8 Panel - Site RC6 pillar extensometer

It would appear that the 0-1 anchor bay is largely in a brittle fracture zone, bay 2-3 is in a zone of plastic flow, and bay 1-2 showing the relatively small strain of about 1% could still be within the elastic limit of the pillar rock. It is interesting to compare these results with those for site RA1 where the deformation is much more evenly distributed into the rock. The brittle failure of the outer skin of the pillar is no doubt due to an extremely high initial strain rate. Similar results have been achieved in laboratory tests, described in Chapter Eight.

Sites RD8, RE7, RF8 - roof extensometers

Roof extensometers were installed at the above sites in roadways D, E and F with anchors at various depths into the roof. The results are tabulated in Table 6.4 together with those from sites RA1, RCA4 and RC6 for comparison. It can be seen that the deformations in roadways D and E are similar, with E being slightly higher. This can be accounted for by the thicker 6m wide yield pillars on either side of roadway D which can be expected to be somewhat stiffer. Roadway E had a 3m wide pillar which yielded more readily thus explaining the difference in roof deformation. The extensions in the RF8 boreholes are significantly lower, being 3 to 4 times less than the corresponding ones in roadways D and E. All boreholes show a similar trend in that over 80 per cent of the deformation takes place in the first 2m. The significance of the RF8 measurements lies in the fact that the total roof to floor convergence in

TABLE 6.4

No. 8 Panel Extensometer Data

Anchor depth	1m		1.5m		2.0m		3m		4m		4.5m		6m		7m		7.5m		9.5m	
	20	40	20	40	20	40	20	40	20	40	20	40	20	40	20	40	20	40	20	40
Days	20	40	20	40	20	40	20	40	20	40	20	40	20	40	20	40	20	40	20	40
Extensometer																				
RA1			39	60							64	100	76	120						
RCA4			90	145							118	146	133	160						
RC6	73	115			78	120	100	145												
RD8 - 1	115	172			115	180	138	197												
RD8-3					105	157			110	160					121	175				
RE7 - 1					130				130						155					
RF8 - 1 & 2					27				31								36			40
RF8 - 3					38				42				75							

All readings in mm.

F roadway (the outer road) is similar if not greater than that at a corresponding position in E and D roadways. Either bed separation of more than 100mm is taking place at a depth into the roof greater than 9.5m in F roadway, or another explanation must be found for these results. It is to be expected that if it occurs, bed separation at any depth into the roof would become less the closer the abutment is approached, unless it is purely surface spalling which is taking place. No surface slabbing was noted. Therefore it is suggested that the roof in the outer road is coming down as a result mainly of plastic flow of the roof strata above the ribside. If this is true, then the most likely bed where it is taking place is the Carnallite Marl. Both laboratory tests and in-situ observation of this particular rock show that it is extremely weak and liable to flow. These characteristics arise from the presence of numerous randomly orientated veins of halite and/or sylvinite. The day to day experience gained in the mine has been that once exposed, Carnallite Marl will continue to flow or deform into the excavation. It can be said that most of the practical mining problems experienced in the mine are due to the presence of the marl.

A further piece of evidence is the occurrence in the outer roads of a vertical shear fracture in the upper corner of the abutment sidewall running parallel with the road, Plate 6.4. This could be due to the flow in the marl exerting a downward pressure immediately over the abutment, thus creating a shear stress large enough to cause failure.

6.5 No. 10 Panel

Measuring stations were established in No. 10 Panel as shown in Figure 6.9. A brief history of the development of the panel is given in Section 3.3.9, and it can be seen that there are two distinct sections to the panel; one before and the other after it was widened to 90m. Prior to being widened, it (A section) consisted of a 30m wide centre panel of three roadways separated by yield pillars, with a similar parallel set to the north and a parallel twin roadway heading to the south. The outer panels were separated from the central panel by 40 m wide pillars. The middle road in the centre panel was a continuation of C43 roadway and contained the main conveyor belt. Cross sections of these two different panel layouts are given in Figure 6.9. The widened section of No. 10 Panel (B section) had been mined for just on 60m when water first entered the workings, first at site W1 and then at W2, shown in Figure 6.9. A steady rate of approximately 100 litres per minute was established.

6.5.1 Closure Measurements - No. 10 Panel, A section

Table 6.5 lists the closures and closure rates obtained after 20 day intervals at the various sites. These closure sites were mainly located in the narrower 30m wide central panel. The closures and closure rates are plotted in Figure 6.10. Because the sites were located halfway between successive crosscuts, the

TABLE 6.5

No. 10 Panel - A section Closures (c), mm, and Closure Rates (ĉ), mm/day

Site	20		40		60		80		100		120	
	c	ĉ	c	ĉ	c	ĉ	c	ĉ	c	ĉ	c	ĉ
C 42 C	142	5.6	230	3.5	286	2.2	220	1.3	341	0.8	355	0.5
C2	122	5.2	212	3.8	278	2.8	326	2.1	362	1.5	388	1.1
C3	198	7.9	326	5.1	408	3.2	460	2.1	494	1.3	516	0.9
C4	319	13.6	554	10.0	727	7.4	855	5.4	949	4.0	1018	3.0
C 42 D	242	9.9	408	6.8	521	4.7	599	3.2	652	2.2	688	1.5
C4	244	8.6	371	4.5	437	2.3	471	1.2	489	0.6	498	0.3
C 43 A	189	7.2	301	4.3	368	2.6	408	1.5	431	0.9	446	0.5
C3	98	4.4	172	3.6	244	3.0	299	2.5	344	2.0	381	1.7
C 43 B	53	2.5	100	2.3	144	2.1	183	1.9	219	1.7	251	1.5
C1	61	2.9	116	2.6	164	2.3	207	2.0	246	1.8	280	1.6
C3	77	3.7	148	3.4	212	3.1	272	2.8	326	2.6	375	2.4
C4	128	6.3	252	6.2	374	6.0	403	5.9	609	5.7	722	5.6
C 43 C	272	11.3	461	7.8	593	5.5	684	3.8	748	2.6	792	1.9
C4	78	3.1	146	3.2	207	2.8	260	2.5	307	2.2	348	1.9
C1	84	3.9	157	3.4	221	3.3	277	2.6	327	2.3	370	2.0
C3	212	9.0	365	6.5	476	4.7	557	3.4	616	2.5	658	1.8
C4	45	2.3	92	2.4	141	2.5	192	2.6	244	2.7	300	2.8
C 43 E	53	2.5	102	2.3	146	2.1	187	2.0	225	1.8	259	1.6
C3	148	6.3	255	4.6	333	3.3	390	2.4	432	1.8	462	1.3
C4	147	5.9	242	3.8	304	2.4	343	1.6	369	1.0	385	0.7
C 43 F	165	6.9	283	5.0	368	3.5	428	2.5	471	1.8	502	1.3
C4	112	5.6	225	5.7	340	5.8	456	5.9	574	5.9	694	6.0
C 45 E	124	5.2	212	3.7	275	2.6	320	1.9	352	1.3	375	1.0
C1	228	8.3	353	4.6	422	2.5	460	1.4	481	0.8	492	0.4
C4	150	5.8	242	3.6	298	2.2	332	1.3	353	0.8	366	0.5

C1, C2, C3 are roof to floor measuring stations equally spaced across the roadway

C4 is a wall-to-wall measuring station, located midway up the sidewalls

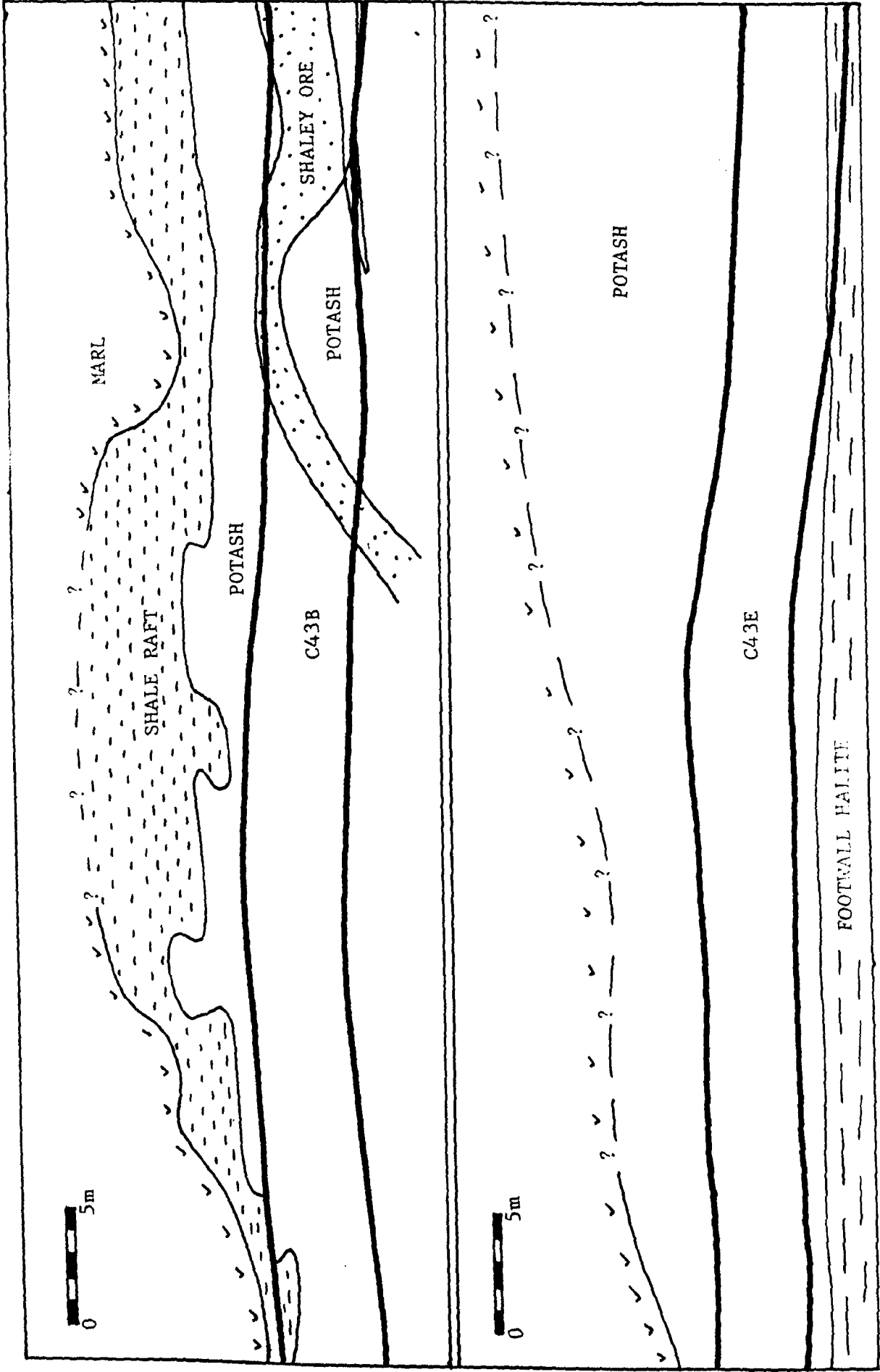
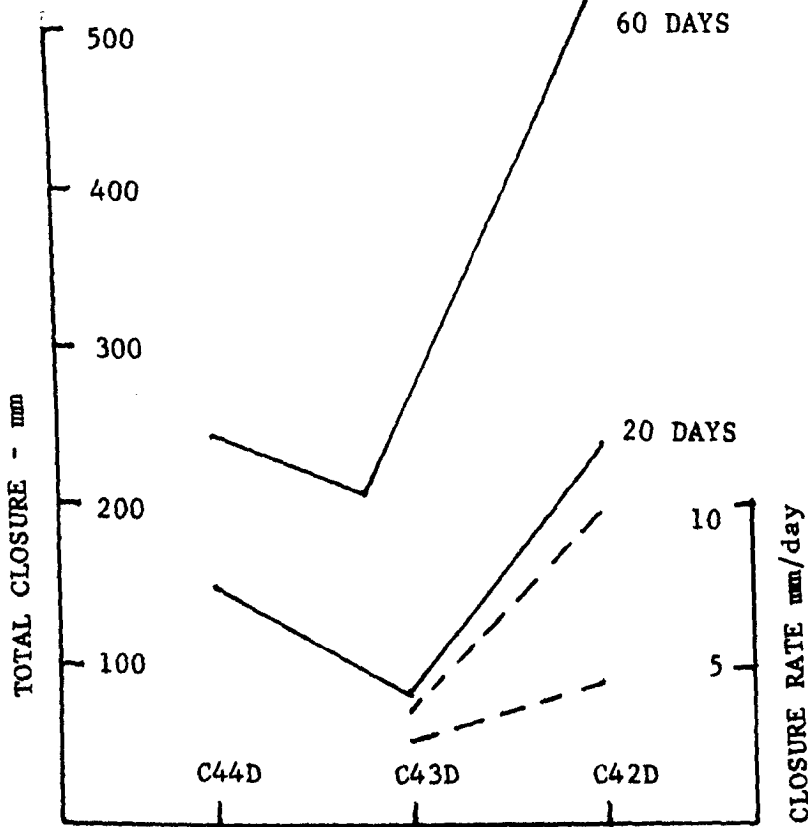


FIGURE 6.11 GEOLOGICAL SECTIONS C43B and C43E

resulting spacing of approximately 50m was too great to give a clear picture of closure along the roadway. It would appear that there is a low point at the 'B' station site. This is about 60m from the start of the 30m section. The next discernible trough occurs a further 120m down D roadway at the 'E' station. Whether this is significant or not is open to question. In view of the irregular geometry arising from the mining of major crosscuts through the adjacent large pillars, plus the fact that these pillars vary in size, and that there is airway in the salt passing directly beneath the 'D' sites, it is felt that no clear conclusions can be drawn.

When looking at the closure across the panel, which is only partially possible at sites 'D' and 'C', a slightly contradictory picture emerges. At site 'D', the outer road, C42 closed more than the inner road, C43, whereas at the 'E' sites, the opposite was true. The closure rate graphs give essentially the same picture. This would indicate that no Serata type stress relief is taking place. This apparent contradiction can possibly be explained by the presence of the undermining salt roadway at 'D'. The closure rates at C43 E and C43 B are extremely low, the initial 20 day rates being 2.3mm per day, which is about half that experienced in most other comparable sites. The geological sections, Figure 6.11, show thick primary ore (>8m) in the roof at C43 E and this could explain the low closure rate. Nothing much can be said about the geology at C43 B except that a thick shale parting is indicated, with possibly thick primary ore in the floor.



CLOSURE ACROSS PANELS

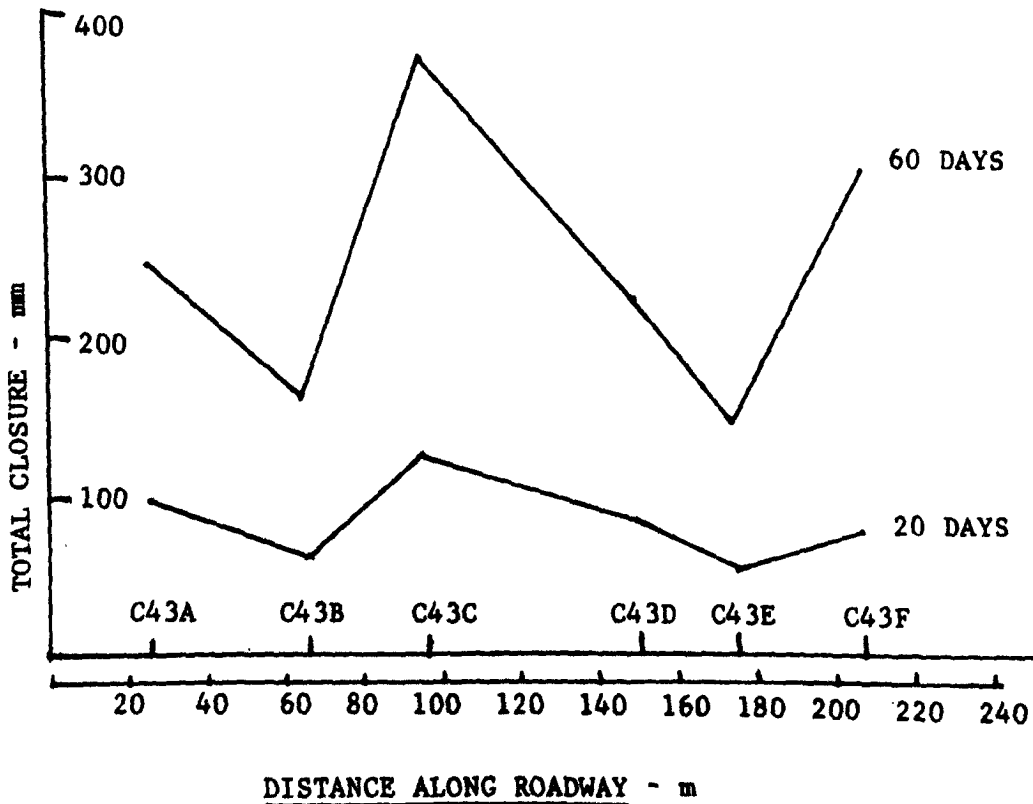
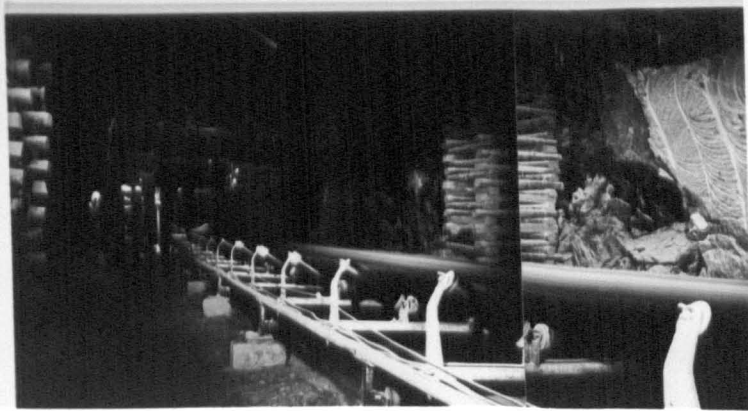
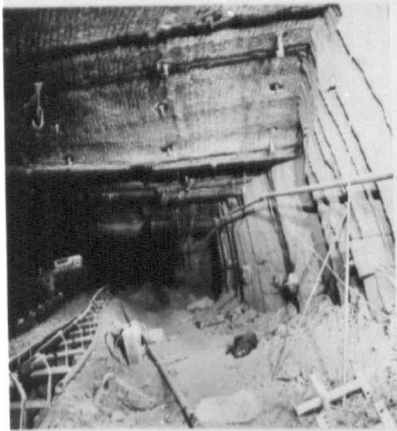
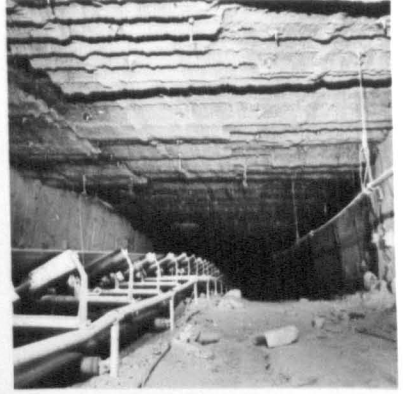


Figure 6.10 No. 10 Panel, A section roadway closures and closure rates

Plate 6.5

- 1 Extensive roof failure in low extraction section. Sidewalls relatively intact.
- 2 Start of high extraction section.
- 3 High extraction section looking in the opposite direction to No.2. Excellent conditions.
- 4 Note 'chipping' at bottom of right hand wall, coming from the movement and failure in the upper corner.
- 5 Roadway profile.
- 6 Extensive roof failure due to proximity to marl. Marl exposed.
- 7 Sidewall failure of yield pillar. Usefulness of 9m wide conveyor road.



This latter fact is probably the important one, as the wall-to-wall closure rate is also very low (3.7mm/day), showing that the pillar sidewalls are not deforming very much. The geological features at E and B are peculiar to these two sites, whereas the rest of the sites have similar geological conditions.

6.5.2 Microcreep Measurements - No. 10 Panel, A section

Microcreep measurements using the Serata Microcreep meter described in section 4.5.1, were made at various sites. Deformation was monitored over a 30 minute period and from this, a closure rate in mm per day was calculated. The results are given in Table 6.6. The relevant results have been plotted in Figure 6.12.

There appears to be a general agreement between the microcreep closure rates and those obtained from direct measurement of closure. The generalised curve in Figure 6.12 indicates that there is an initial drop off in closure rate in the first 24 hours, followed by an increase which peaks at about Day 3. After this, there is a steady decline. There is no clear picture of higher closure rates occurring in the outer roads as would be expected if "stress relief" were taking place.

6.5.3 Extensometer Sites - No. 10 Panel, B section

Extensometers were installed as shown in Figure 6.9 both in the roof and in sidewalls, and provide data prior to the inflow

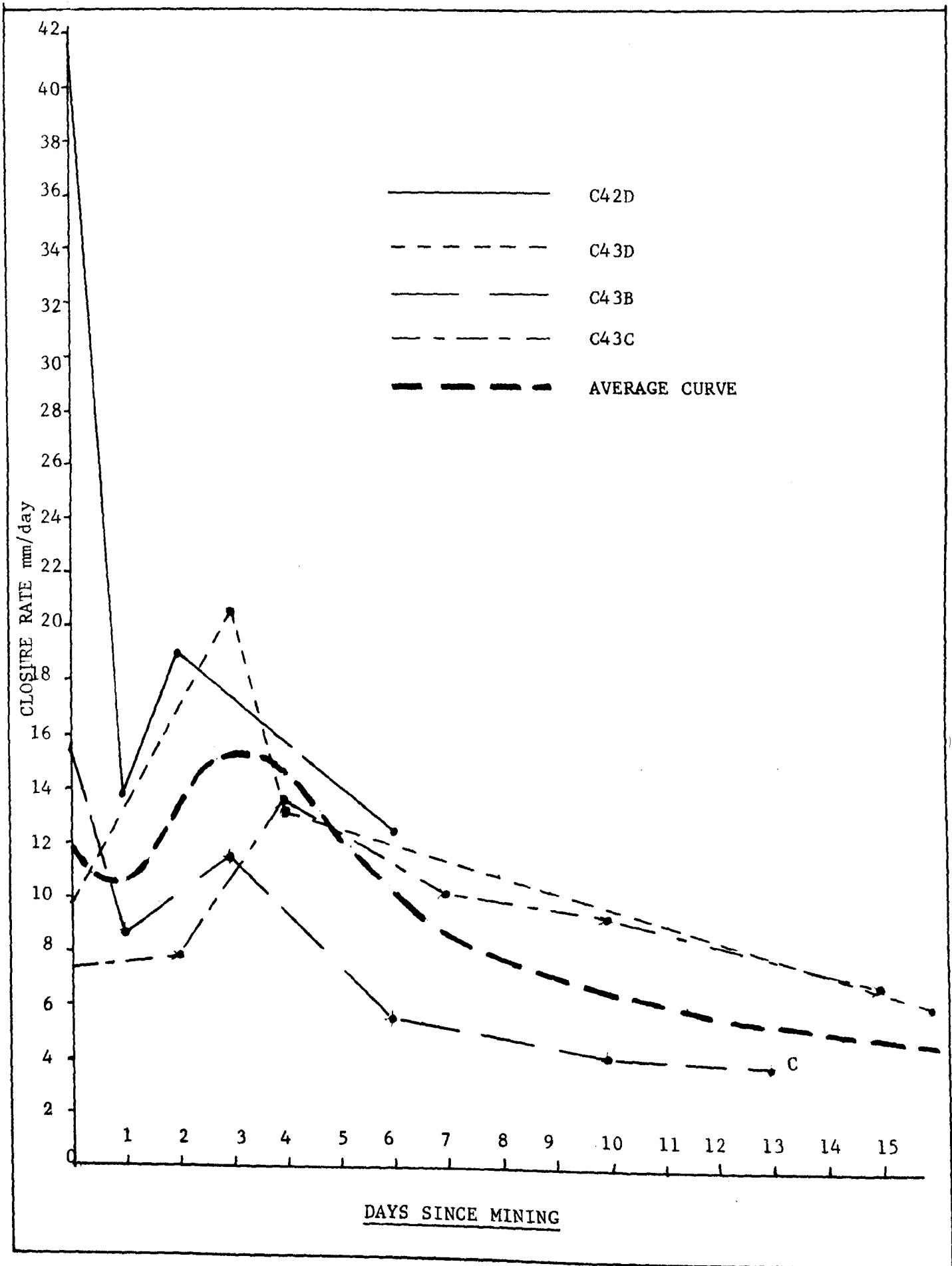


Figure 6.12 No. 10 Panel, A section - Microcreep

of water which occurred at the sites shown approximately 30 days after most of the extensometers were installed.

Site CEA, BH Ø1 - Wall Hole

This was a wall extensometer with anchors installed at 27.5m, 20m, 10m and 5m depths into the abutment at the end of the No. 39 south stub. Figure 6.13 show the deformations of the different anchors plotted against both time and depth into the solid.

As with extensometer RA1 in No. 8 Panel, virtually all the deformation occurs within the first 6m, and by 15m into the abutment, the strain is less than 1%. This again indicates rapid dissipation of load into the solid away from the opening. Hebblewhite⁽⁷⁾ found that failure in unconfined specimens occurred in the laboratory at strains as low as 2%, and therefore if a critical failure strain of 2% is assumed, then slabbing is probably occurring within the first 5m.

The graph of log strain rate against time shows an increasing strain rate virtually from when the instrument was installed. This is particularly noticeable in the deeper bays where a fairly significant increase in strain rate begins to take place some 42 to 48 days after mining, by which time the panel had advanced some 60m. Water entered the mine in H roadway 54 days after mining and in E road 55 days after mining of the CEA site.

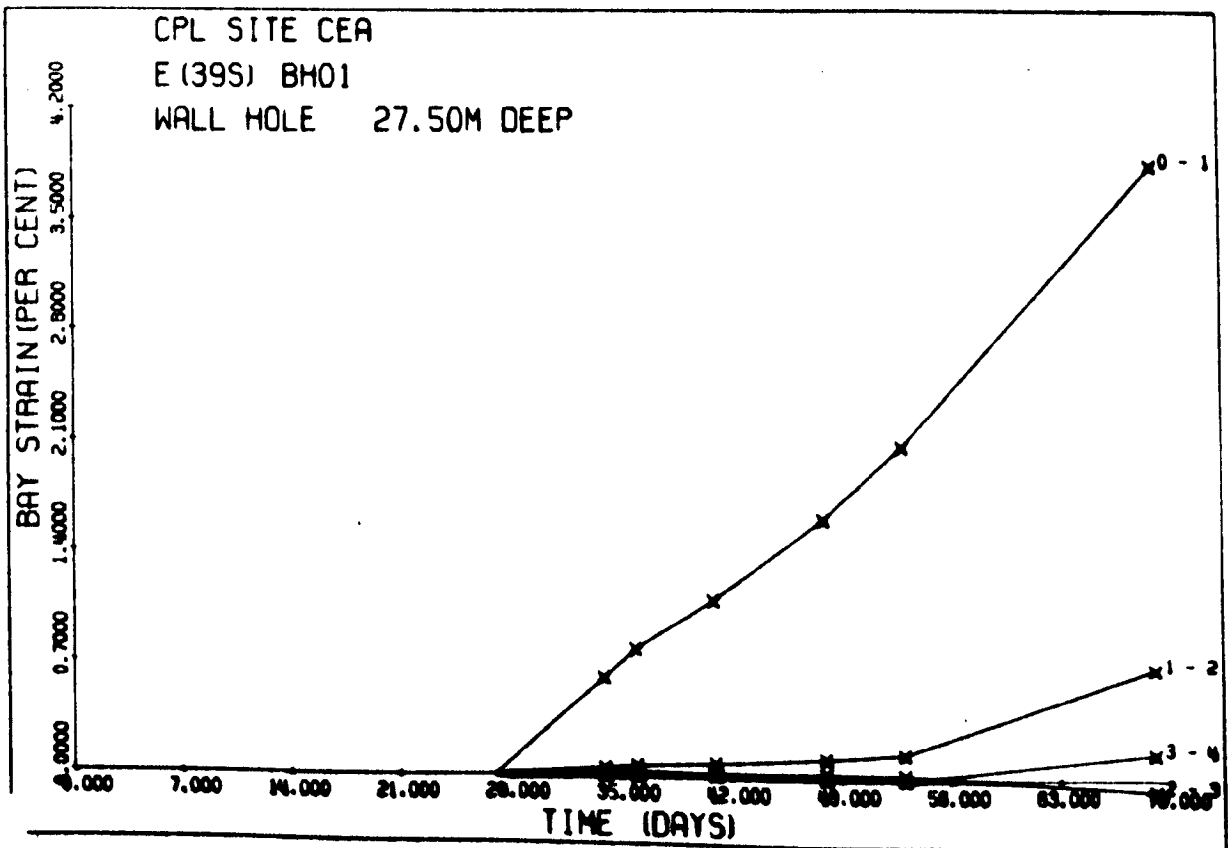
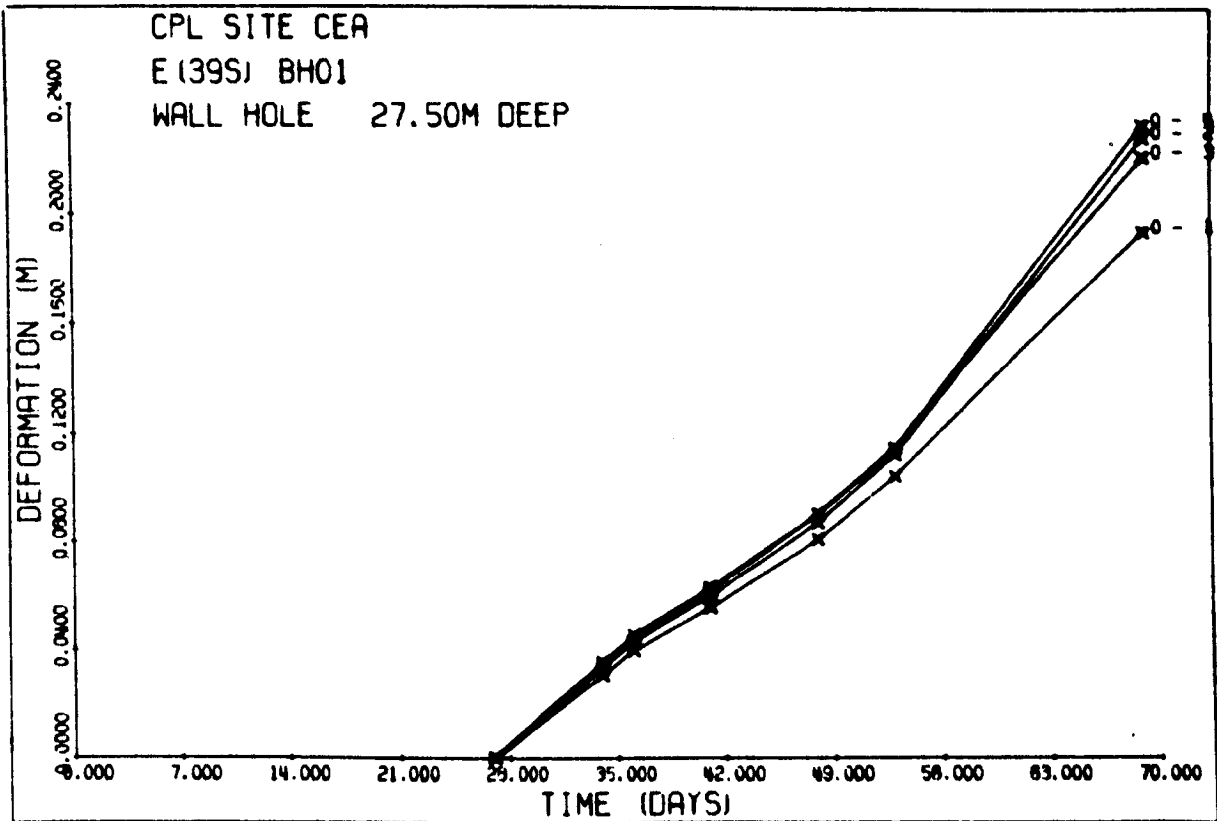


Figure 6.13 No.10 Panel, Site CEA BH1

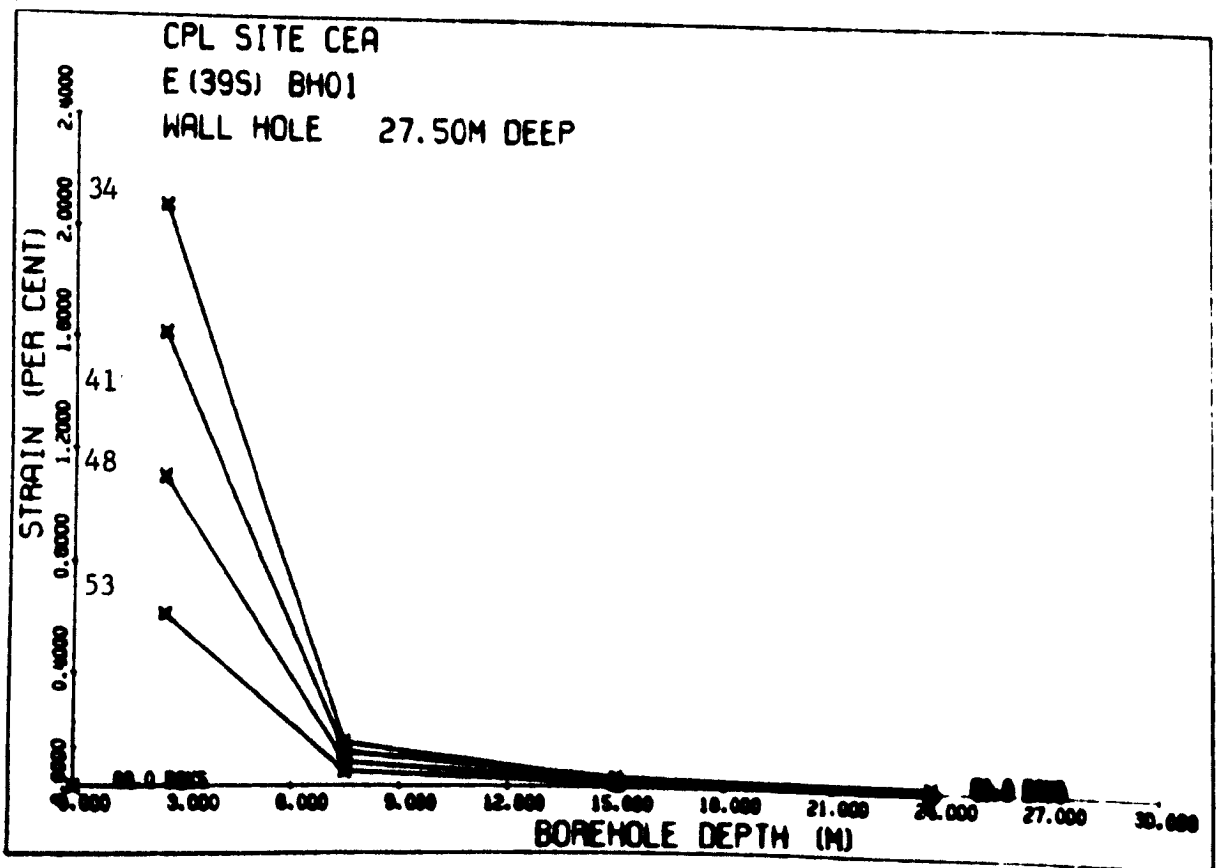
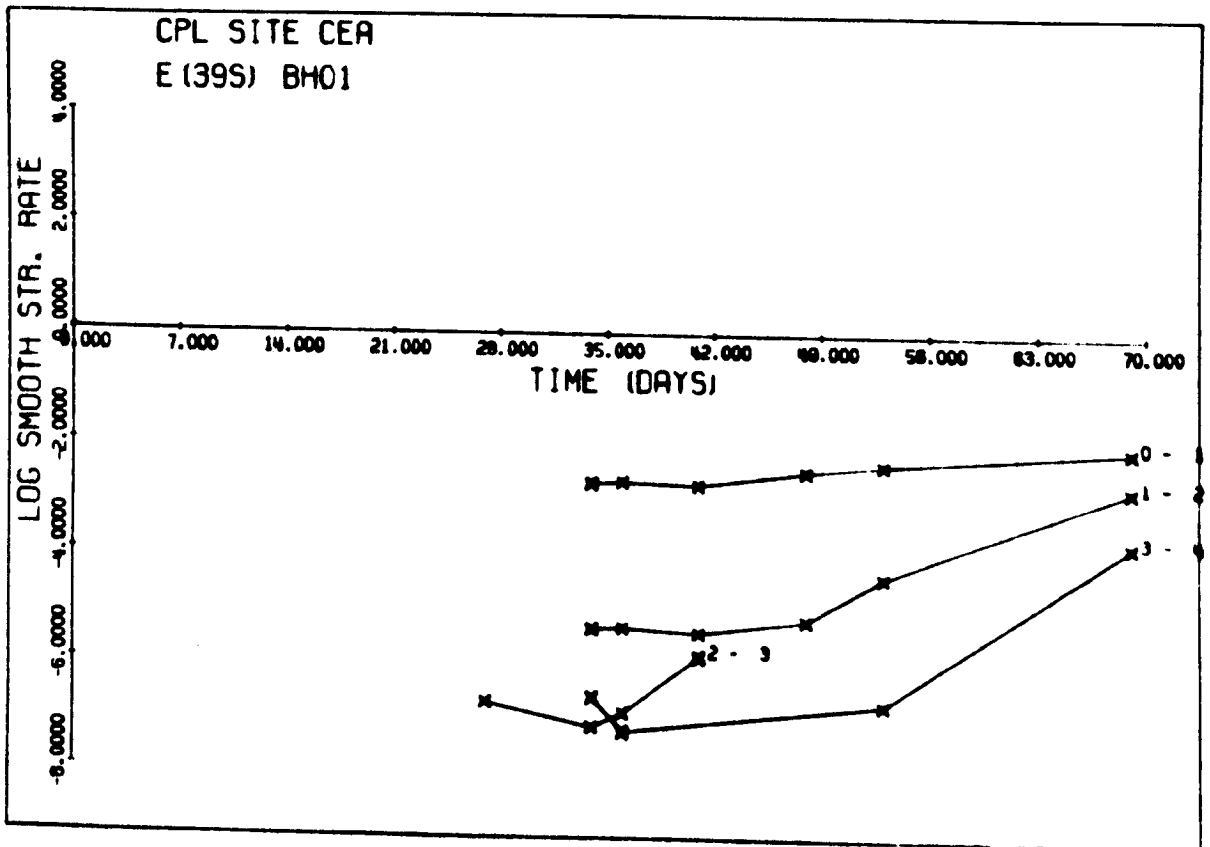


Figure 6.13 No. 10 Panel, Site CEA BH1 (Contd.)

Plate 6.6

- 1 Profile using stationery cap lamp exposure. Note good conditions - no stress relief although slight roof slabbing.
- 2 Note good roof and sidewalls.
- 3 Slight sidewall break-up - sidewalls high.
- 4 Same view as No1 and No2.



Site CEA BH Ø2 - Roof Hole

This extensometer situated in the No. 39 south stub had anchors at 3m and 1.5m into the roof. The graphs of deformation and strain rate are given in Figure 6.14. These show even more dramatically than BH Ø1 the change at about 48 days after mining. It can also be seen that nearly all the measured deformation is taking place within the first 1.5m, and the strains are probably great enough to produce bed separation, particularly if the strain prior to installation is included. The strain rate increases to a maximum some 56 days after mining which coincides with the water inrush in E roadway and by 69 days had dropped significantly.

Site CEA BH Ø4 - Roof Hole

This had a roof extensometer installed in the southern outer roadway with anchors at 6m, 4m and 2m. The graph of deformation with time, Figure 6.15, shows that there are two zones of increased strain, one between the mouth station and anchor 1 (first 2m) and the other between anchors 2 and 3 (4m to 6m deep). There is little movement between anchors 1 and 2. This effect can be seen even more clearly in the graph of % strain vs. borehole depth where, although the strains are still fairly small, incipient bed separation is indicated. Strain rates, which had been steadily decreasing, suddenly began to increase somewhere between 42 and 48 days after mining, which is 14 to 8 days before the water in H roadway, and 15 to 9 days before K roadway.

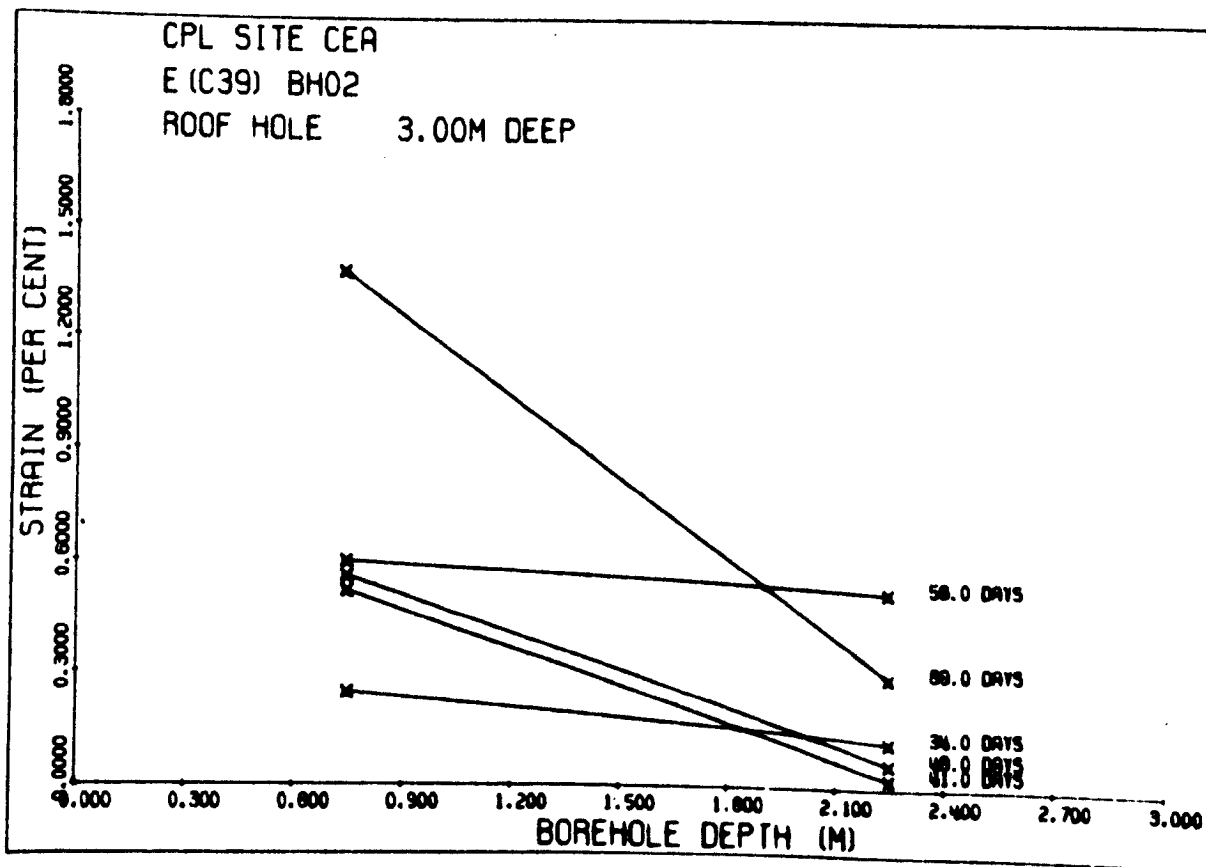
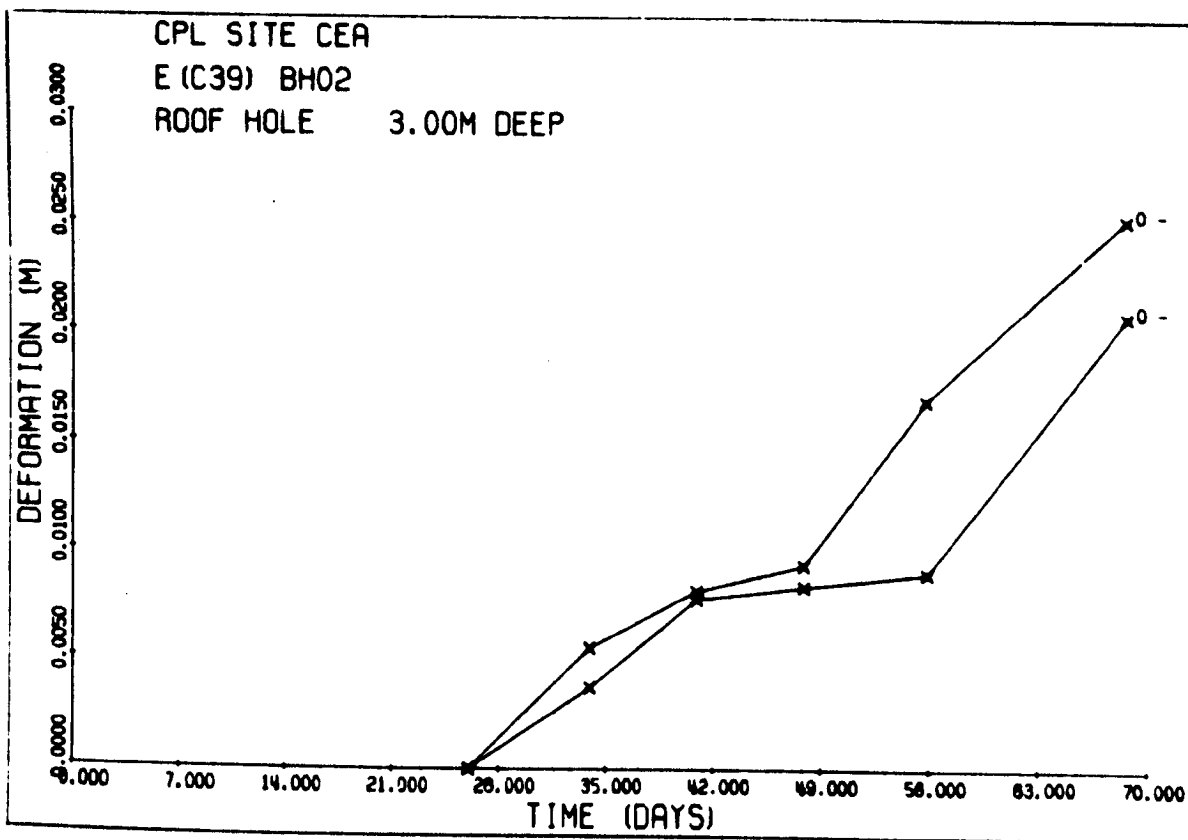


Figure 6.14 No.10 Panel, Site CEA BH2

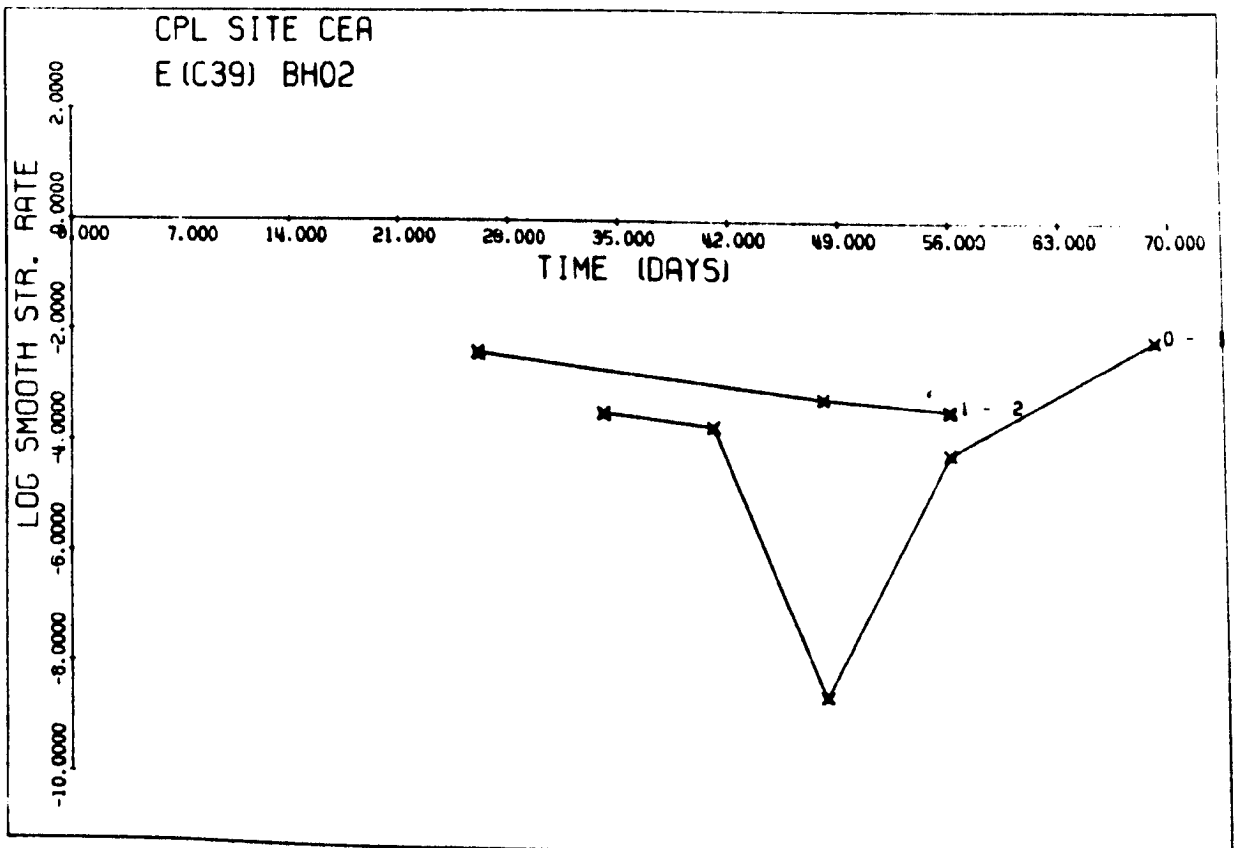
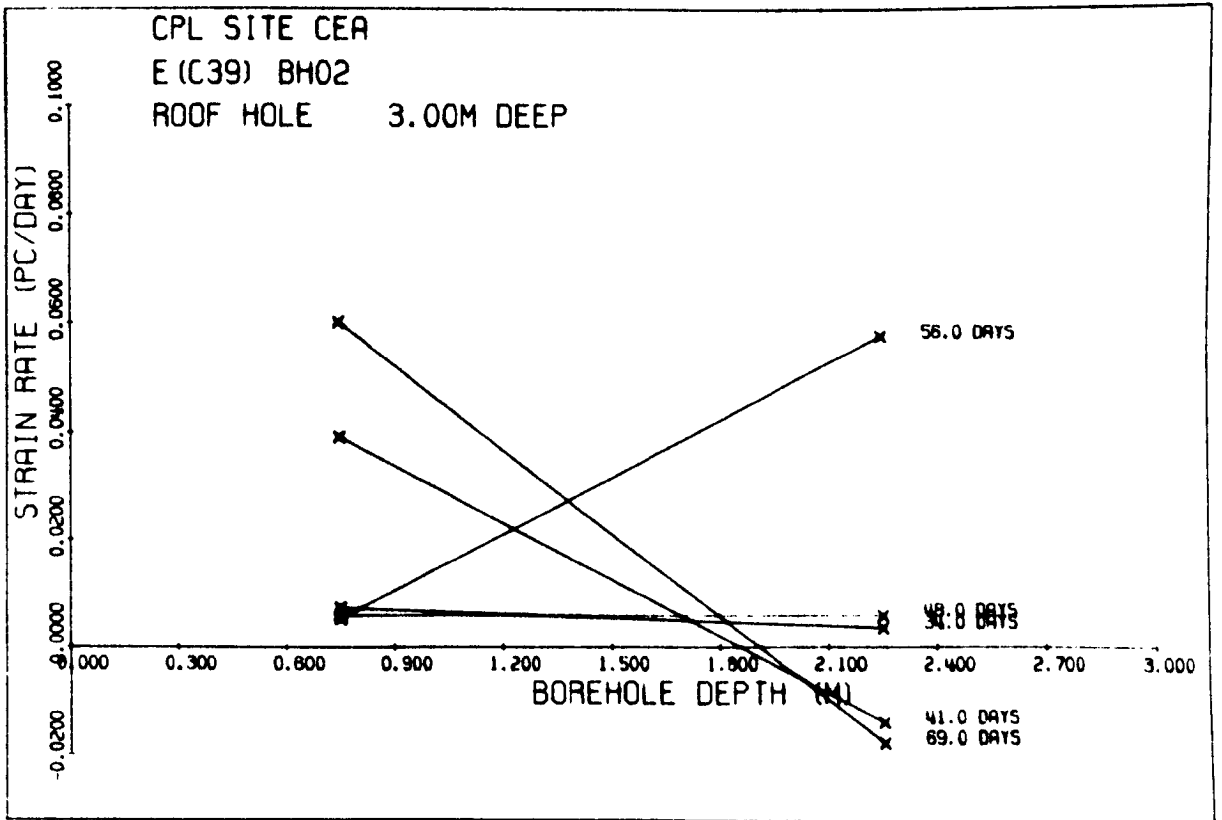


Figure 6.14 No. 10 Panel, Site CEA BH2

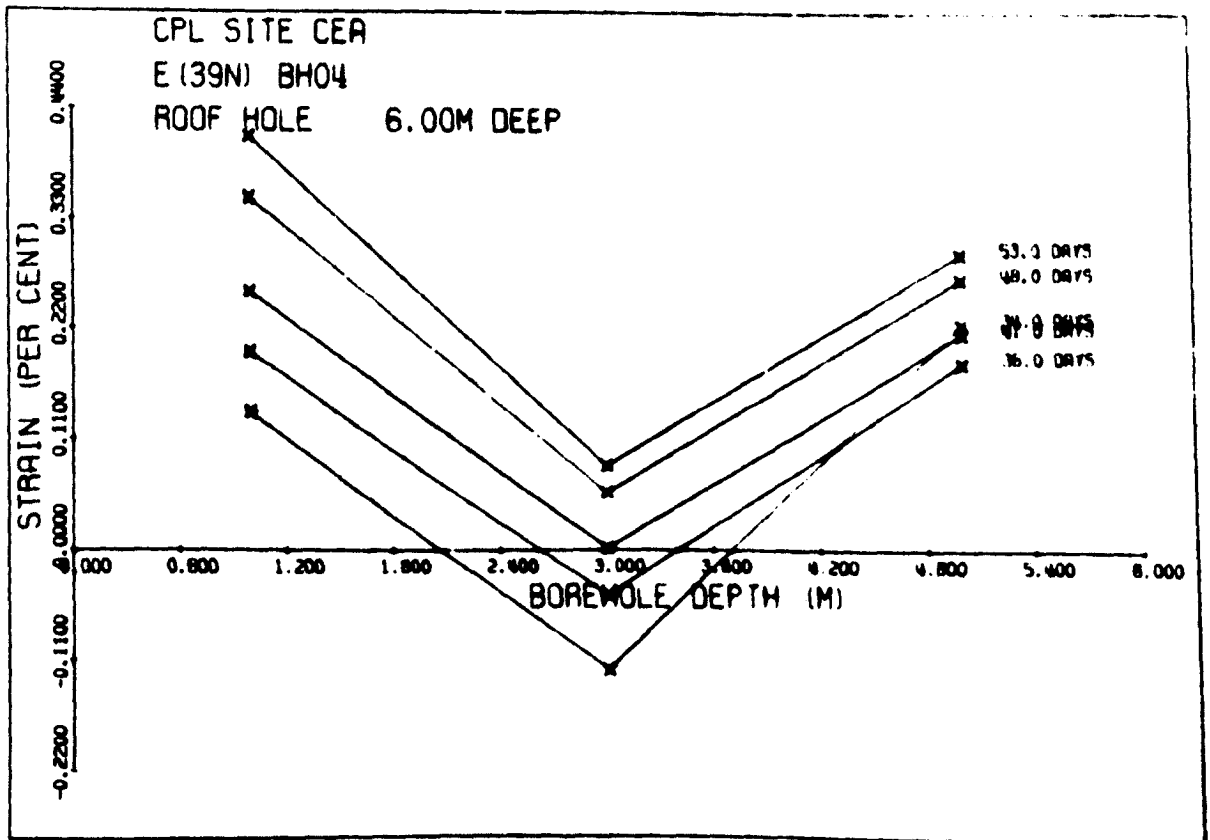
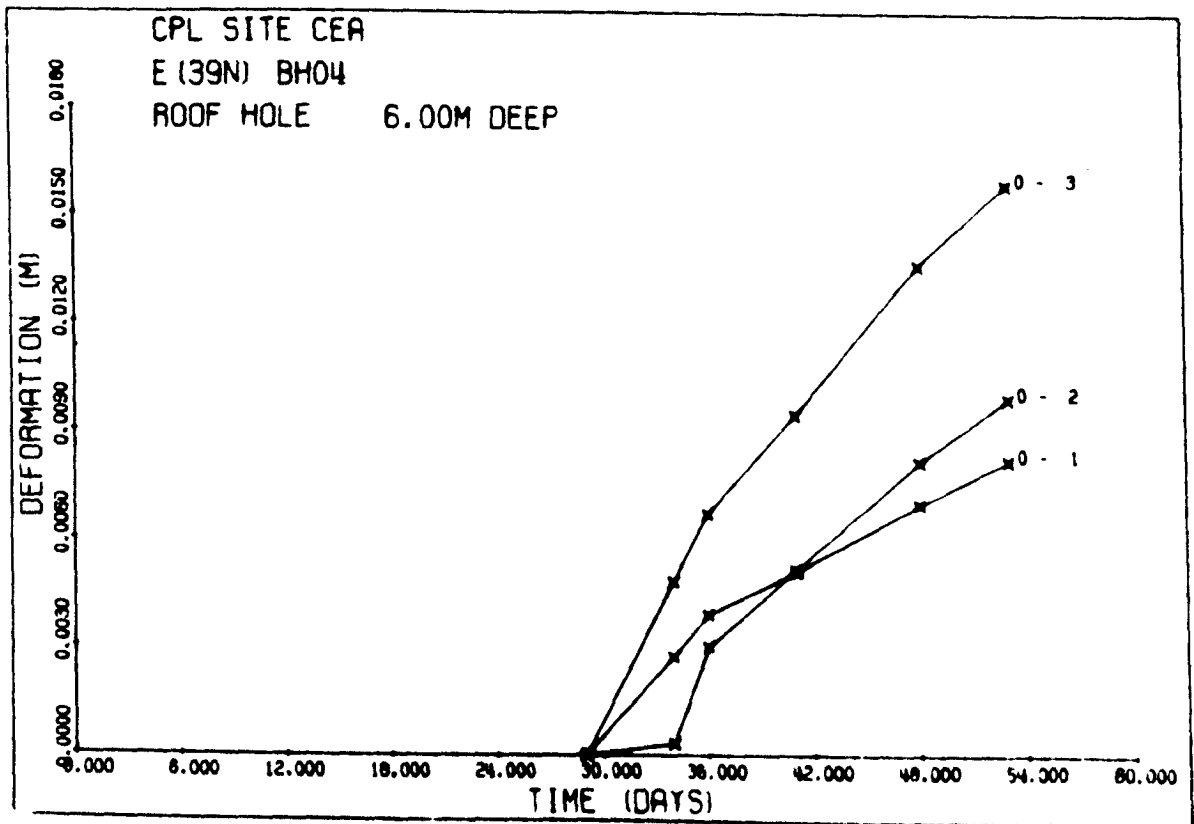


Figure 6.15 No. 10 Panel, Site CEA BH4

Site CFA, BH Ø1 - Wall Hole

This extensometer was sited in a horizontal hole in the 4m wide yield pillar between roadways F and E, with anchors at 2.5m and 1m depths. The results are given in Figure 6.16. It can be seen that initially the strain rates were extremely high, of the order of 0.8% per day. After three days it would appear that fracturing takes place with the formation of sidewall slabs. Referring to Plate 6.5, the explanation must be that the anchors are both located within the intact zone. This is a similar result to that obtained for sites RCA4 and RC6 in No. 8 Panel. The strain in both bays is greater than 2.5% between three and six days after mining.

Site CFA BH Ø2 - Roof Hole

This was a roof extensometer with anchors at 3m and 1.5m depth, and was installed 33 days and 34 days before the water inrush occurred in H and E roadways respectively. The results of the measurements are given in Figure 6.17. These show that the strain in both bays is less than 0.5%, a figure well below the critical strain required for fracturing. It can therefore be concluded that no bed separation is taking place within the first 3m into the roof. The strains and strain rates in the two bays are very similar, which indicates that the roof material is deforming uniformly in this region. There is no apparent increase in strain rate as the date of the water inflow is approached.

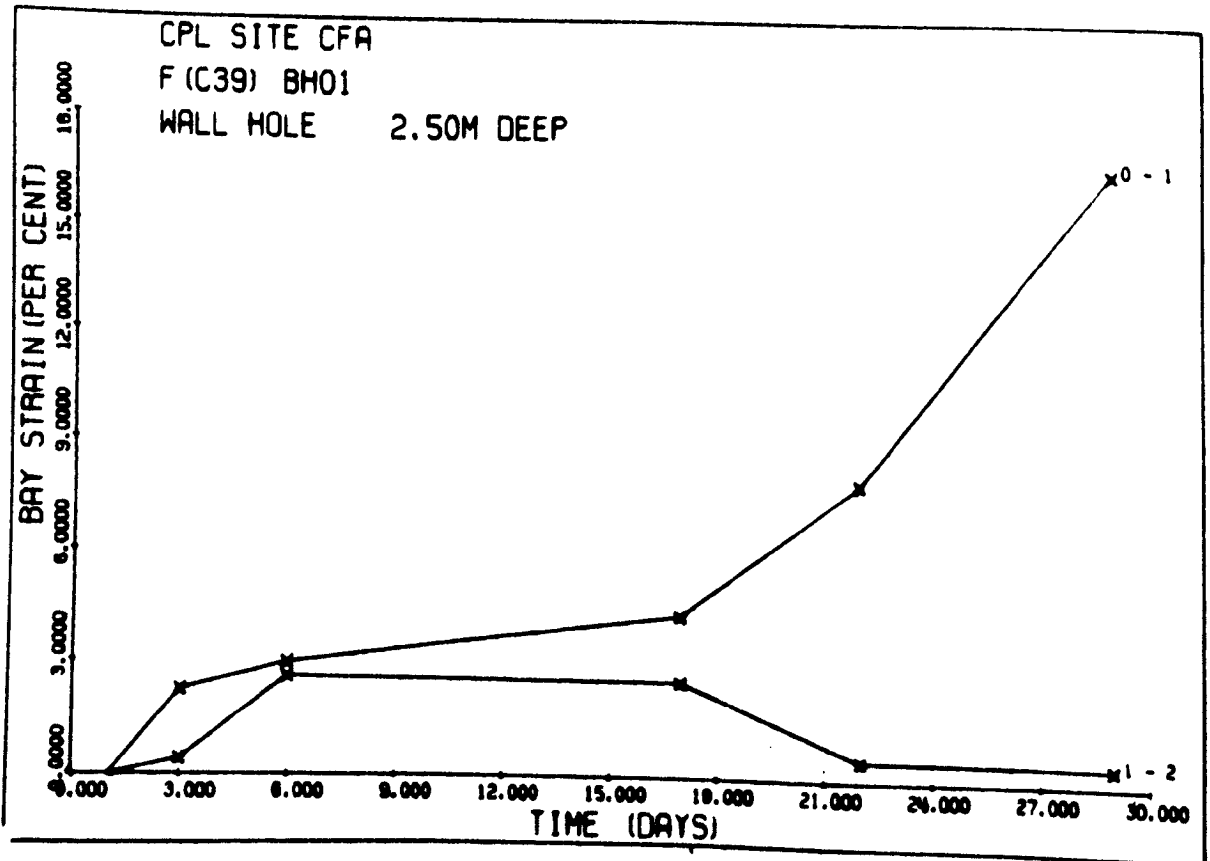
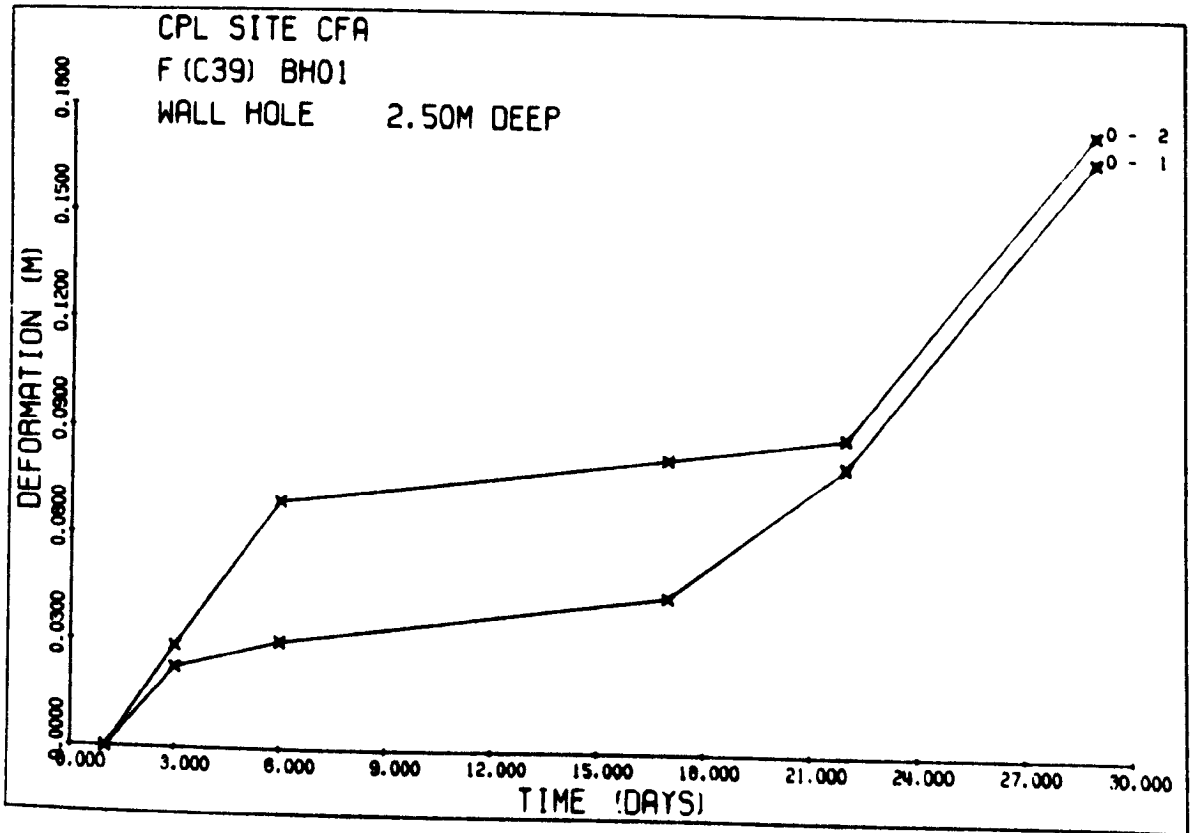


Figure 6.16 No.10 Panel, Site CFA BH1

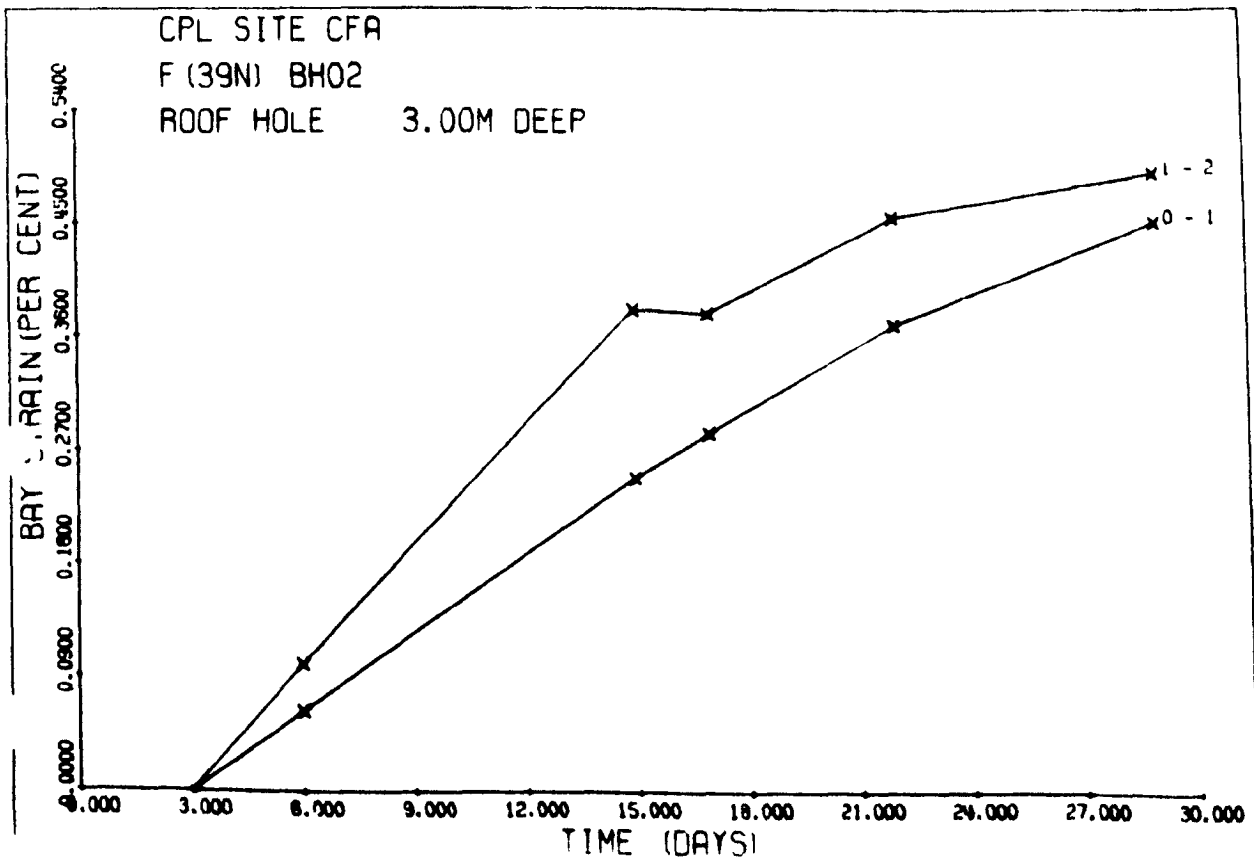
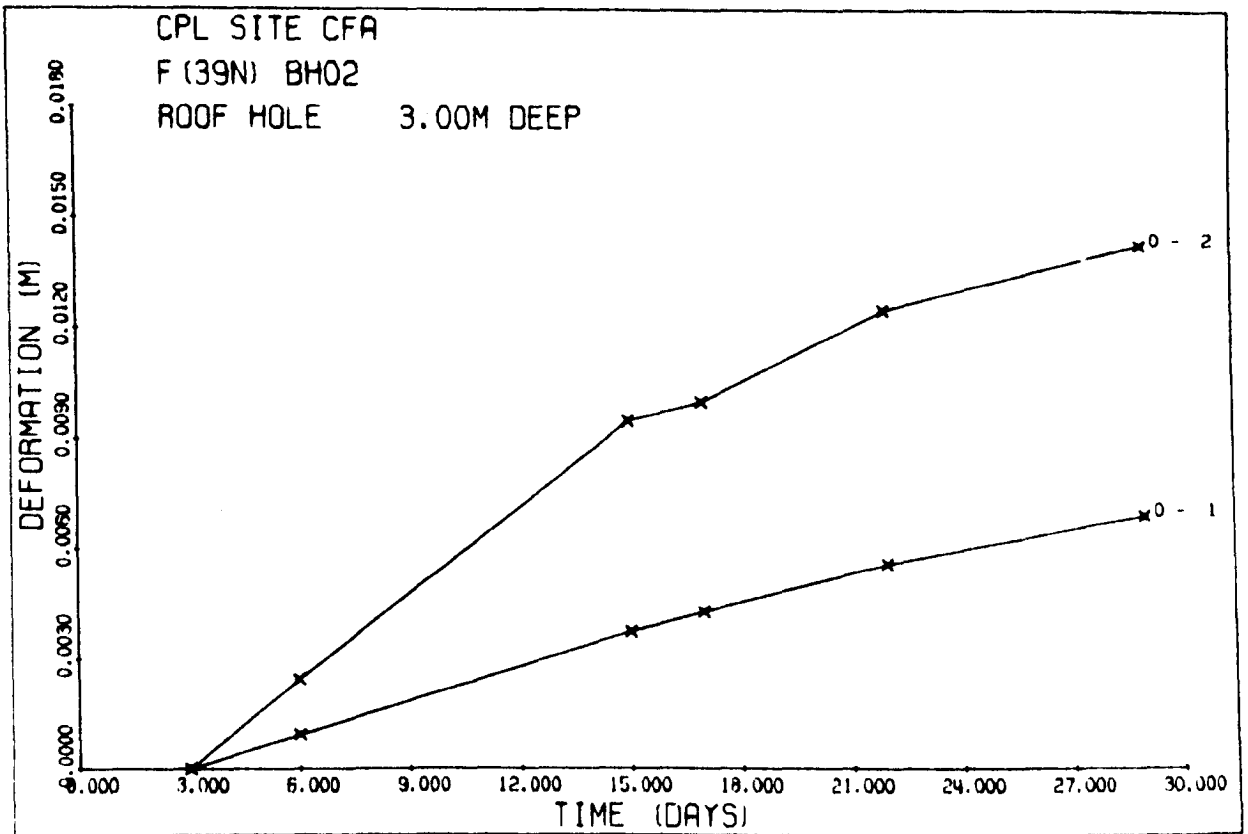


Figure 6.17 No. 1C Panel Site CFA BH2

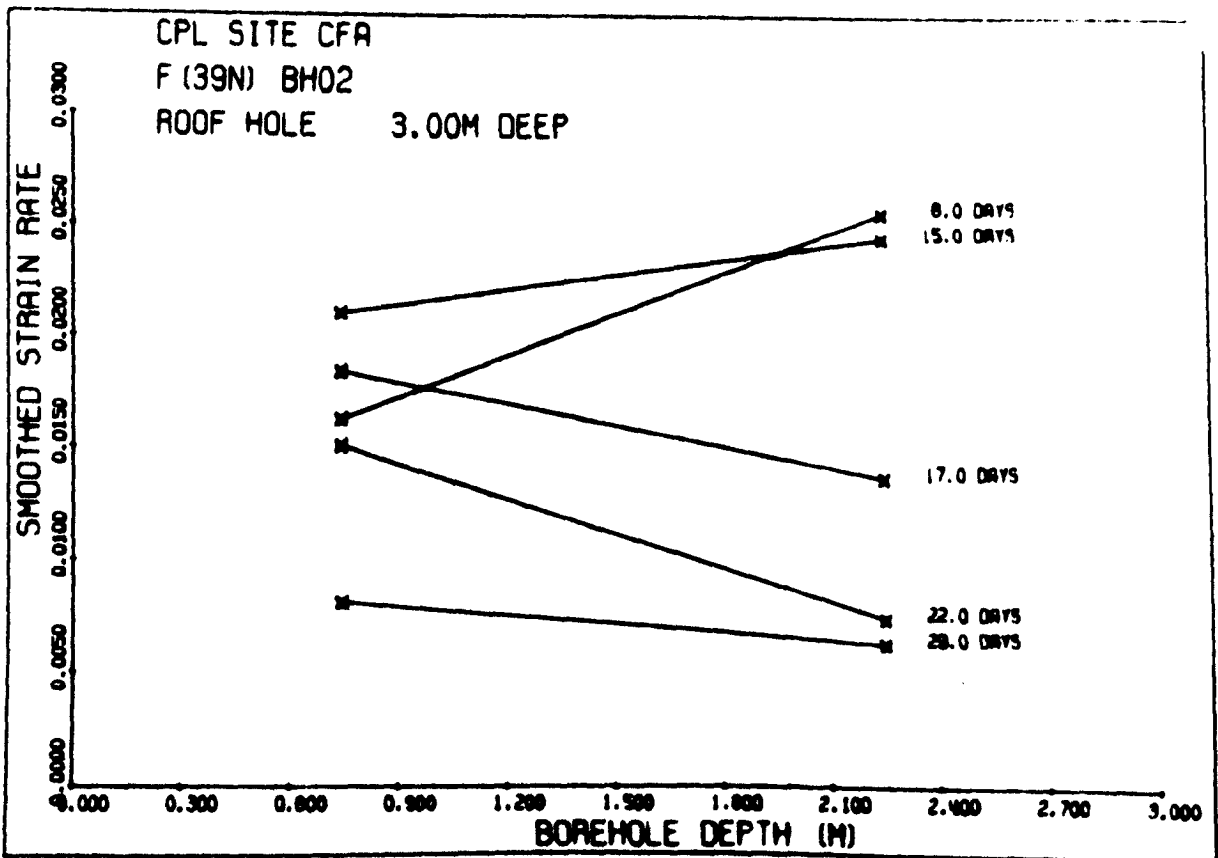
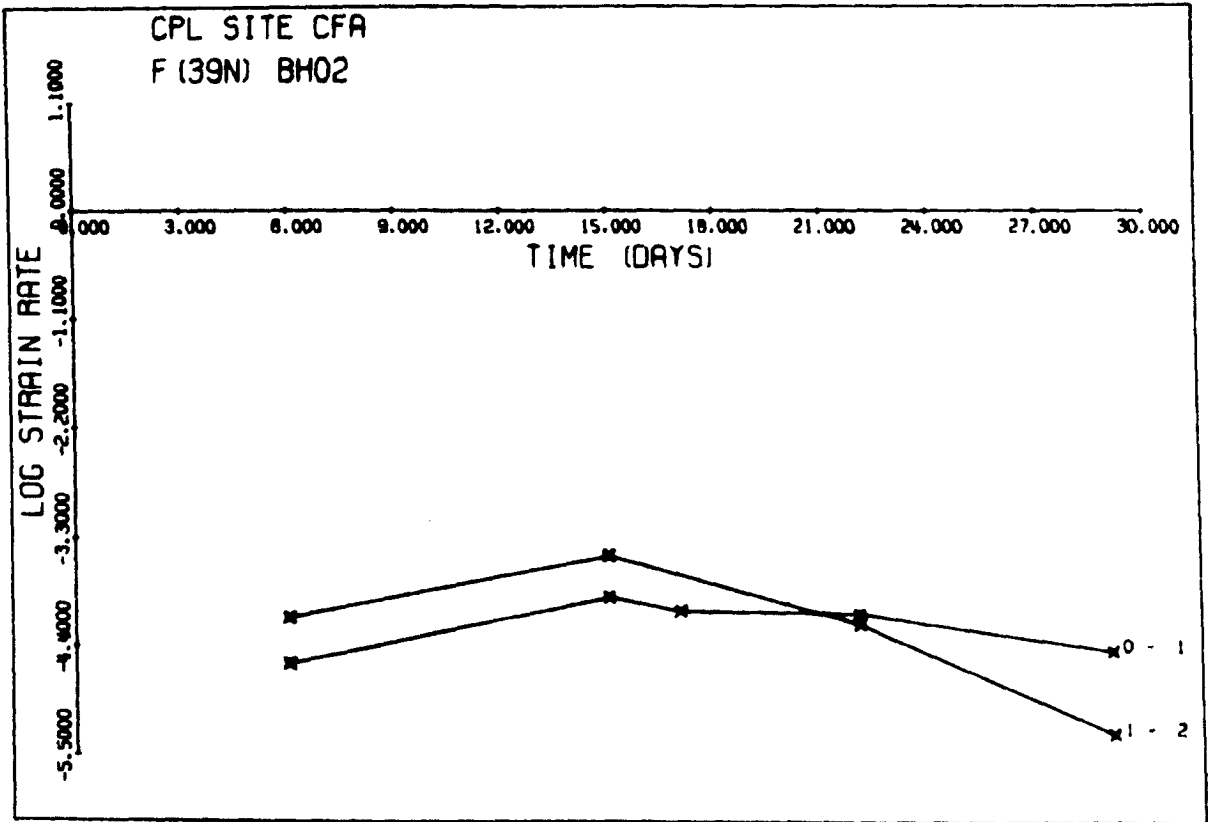


Figure 6.17 No.10 Panel Site CFA BH2

Site CGA BH Ø1 - Wall Hole

This extensometer was installed horizontally into the 4m yield pillar between G and F roadways with anchors at 3.6m, 2.4m and 1.2m depth. The resultant graphs are given in Figure 6.18. The water inflow in H and E roadways occurred 16 and 17 days, respectively, after mining of this site. Strain rates are shown as increasing as these dates are approached, then decreasing rapidly initially and tailing off some 20 days later. Most of the deformation takes place within 32 days of mining, with a bay strain in the 1 - 2 bay (1.2 to 2.4m) of over 25%. Again, the major fracture zone must lie between 1.2m and 2.4m into the pillar. Bay Q-1 (0-1.2m) has over 5% strain, indicating open fracturing, whereas bay 2-3 (2.4 to 3.6m) has a fairly constant strain of about 2%, indicating that these two anchors are in the intact zone.

Site CGA, GH Ø3 - Wall Hole

This extensometer was installed in G roadway horizontally into the sidewall of the nominally 4m wide yield pillar between roadways G and H. G roadway was the continuation of C43 and was a 9m wide conveyor road. The resulting data are plotted in Figure 6.19. Anchors were located at depths of 1m, 2m, 3m and 4m along the length of the borehole, and were installed on 2nd October 1979. Water entered the workings in H and E roadways 19 and 20 days later, 24 and 25 days after this site was mined. The results show that the strain in each bay is roughly the same, which suggests

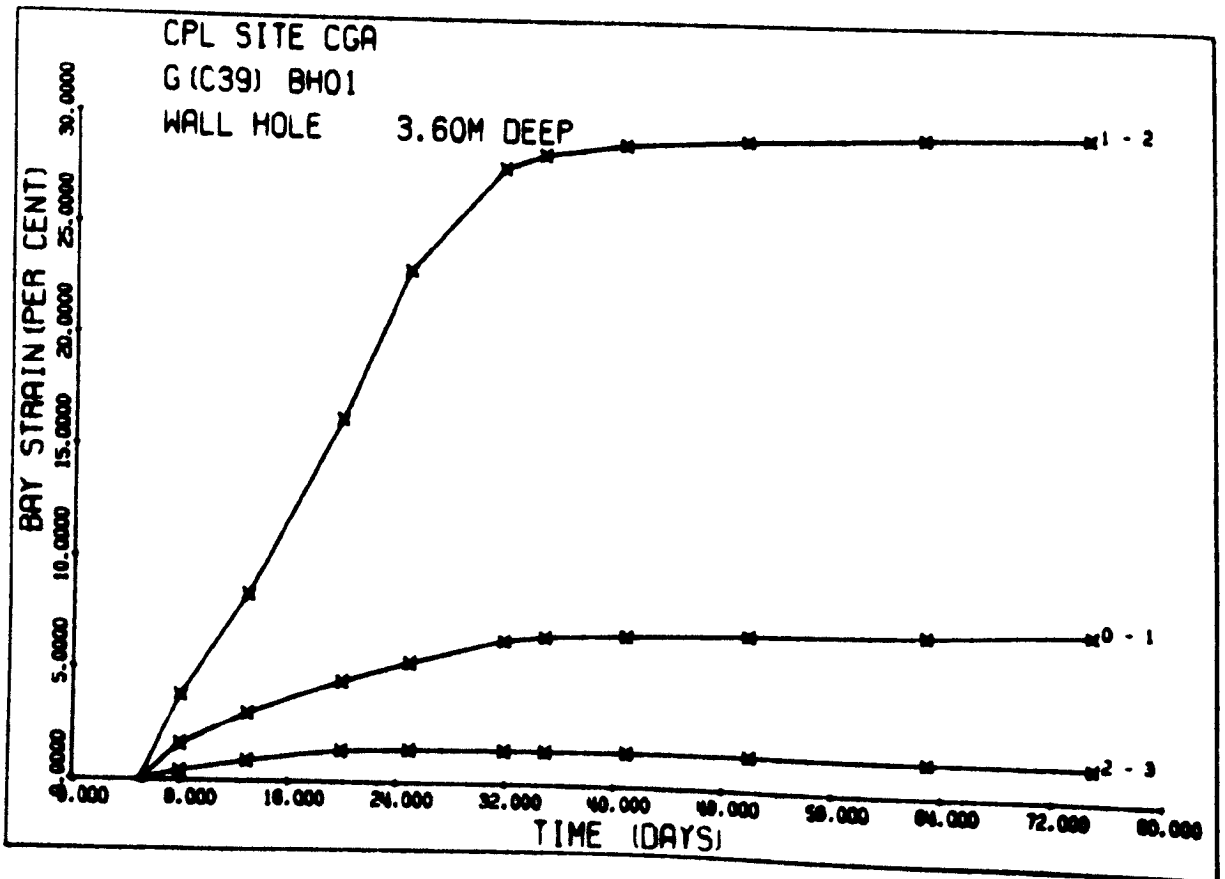
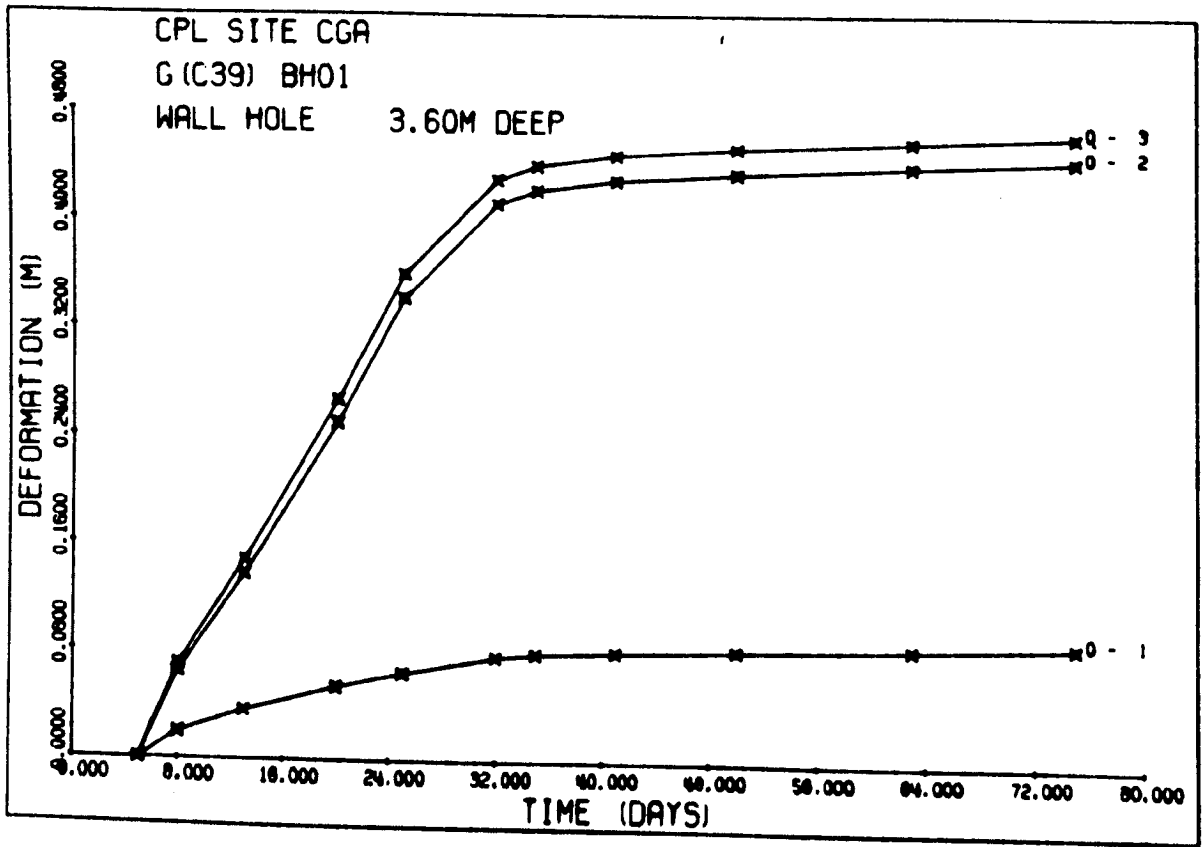


Figure 6.18 No. 10 Panel, Site CGA BH1

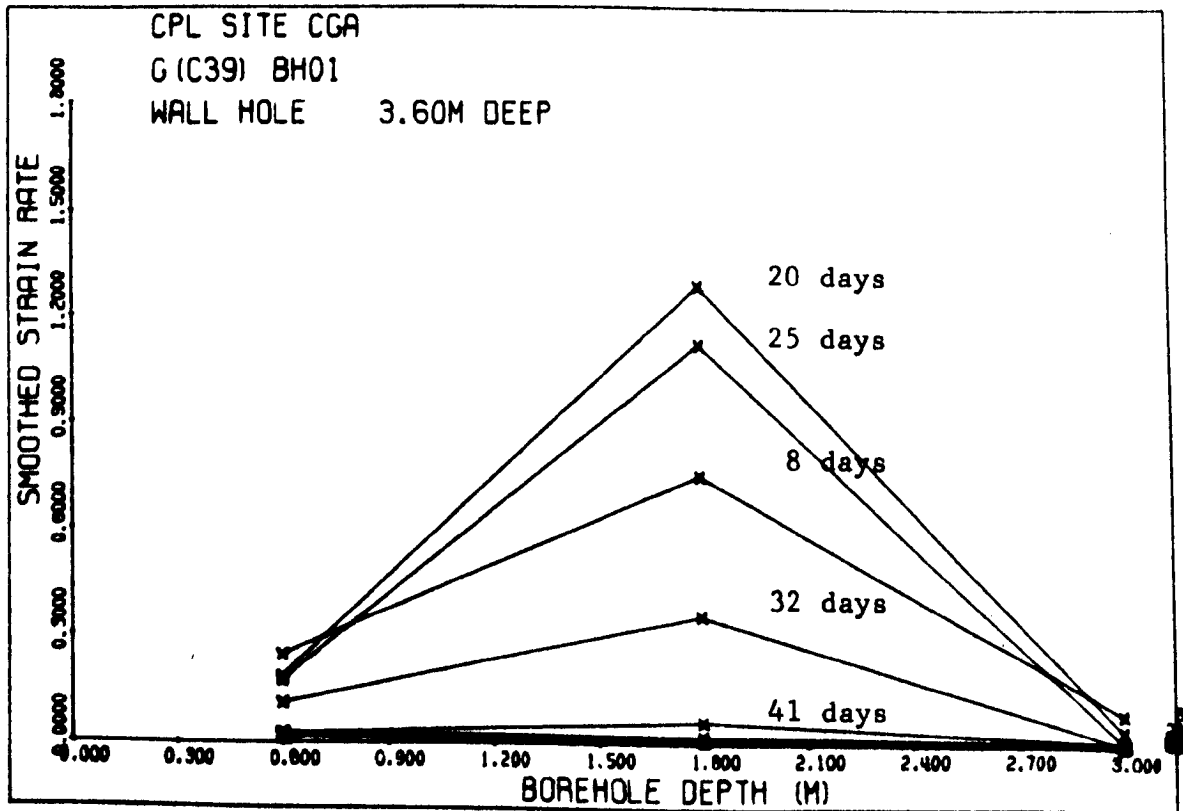
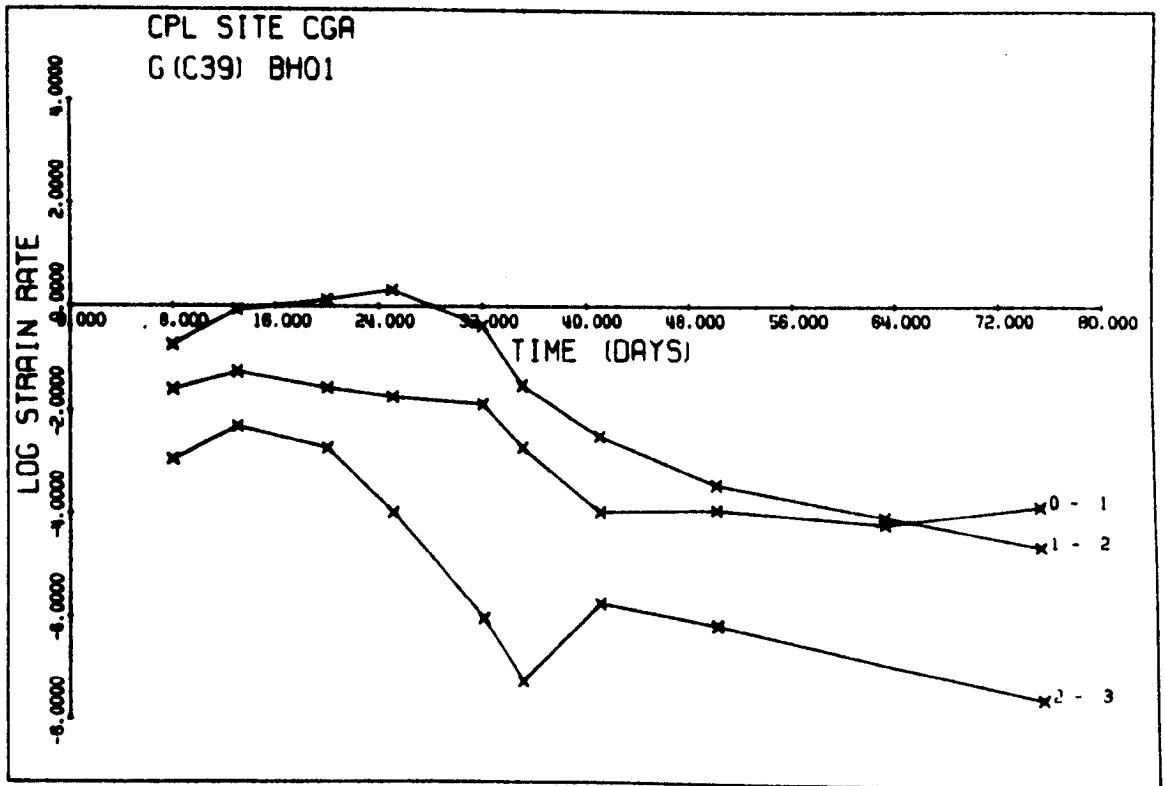


Figure 6.18 No.10 Panel, Site CGA BH1 (Contd.)

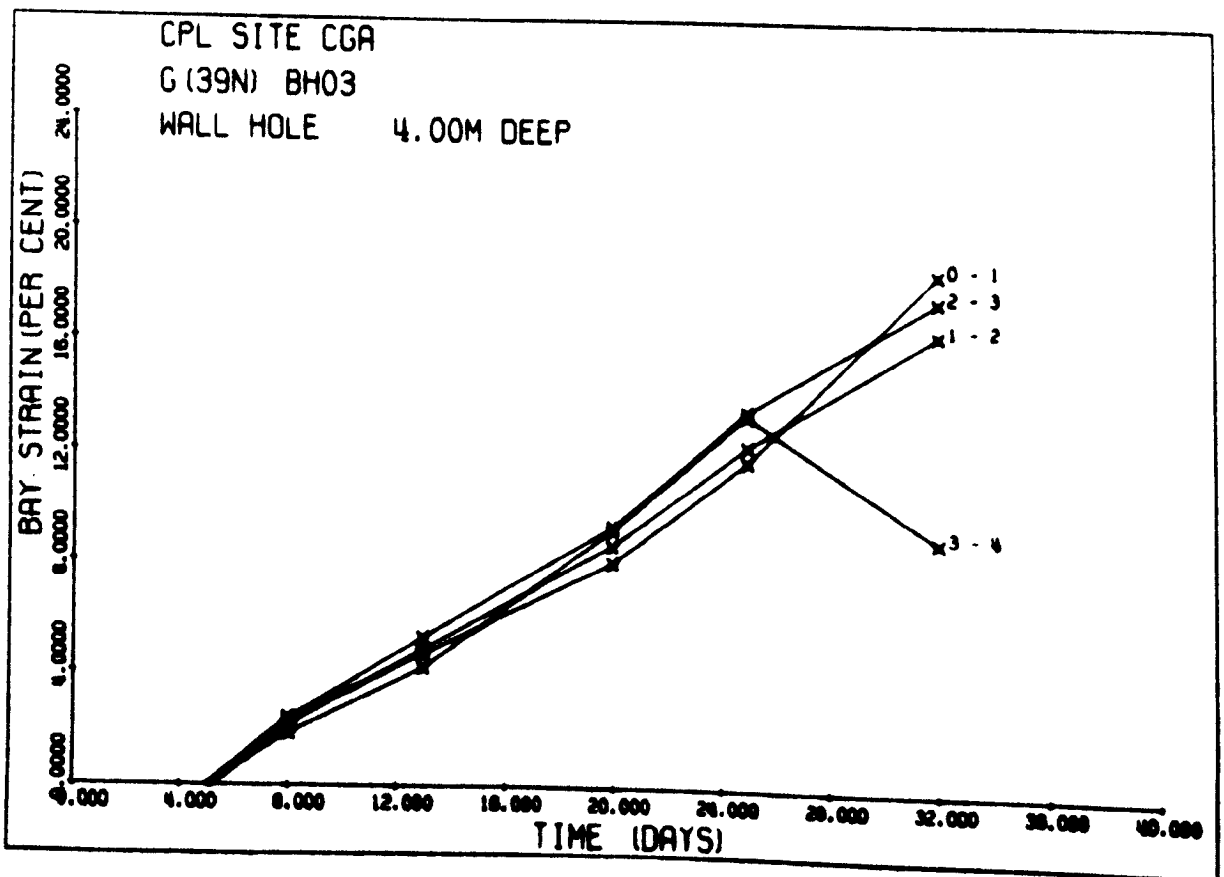
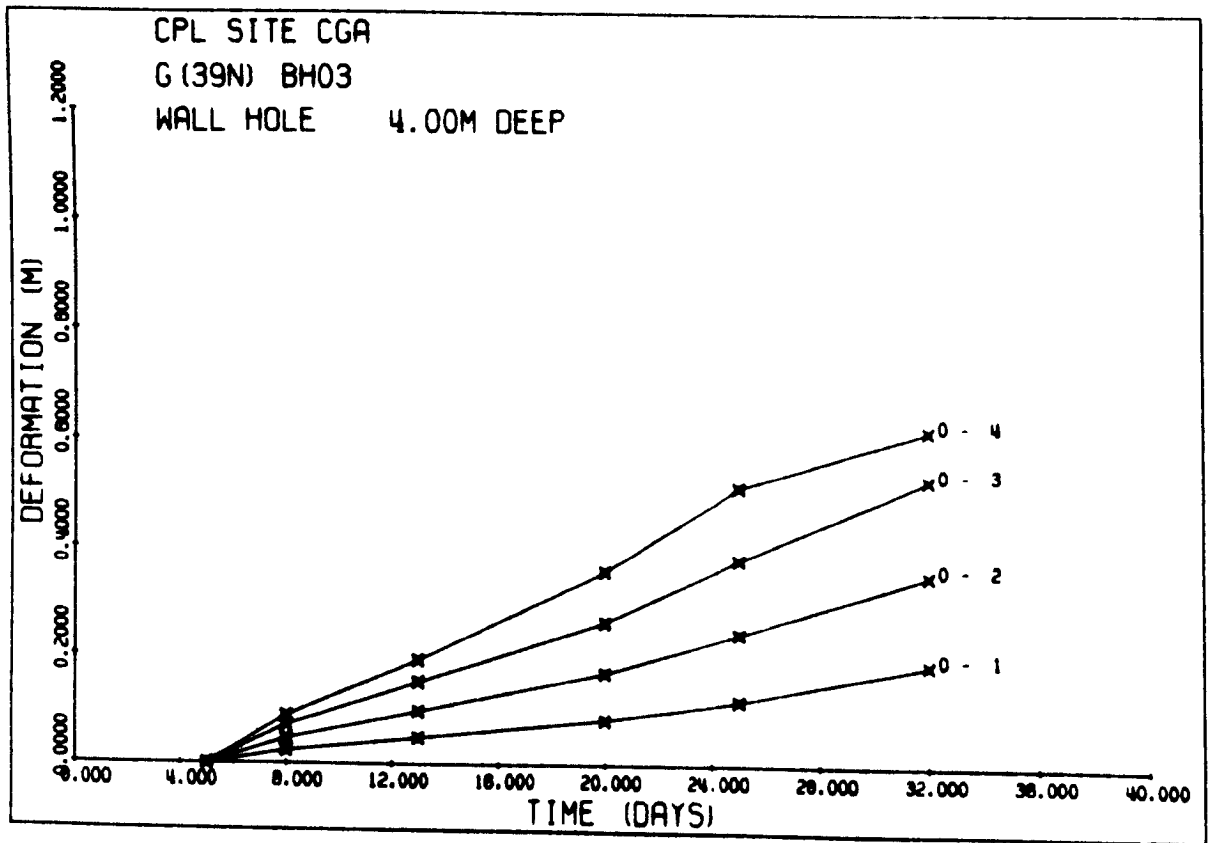


Figure 6 .19 No. 10 Panel, CGA BP3

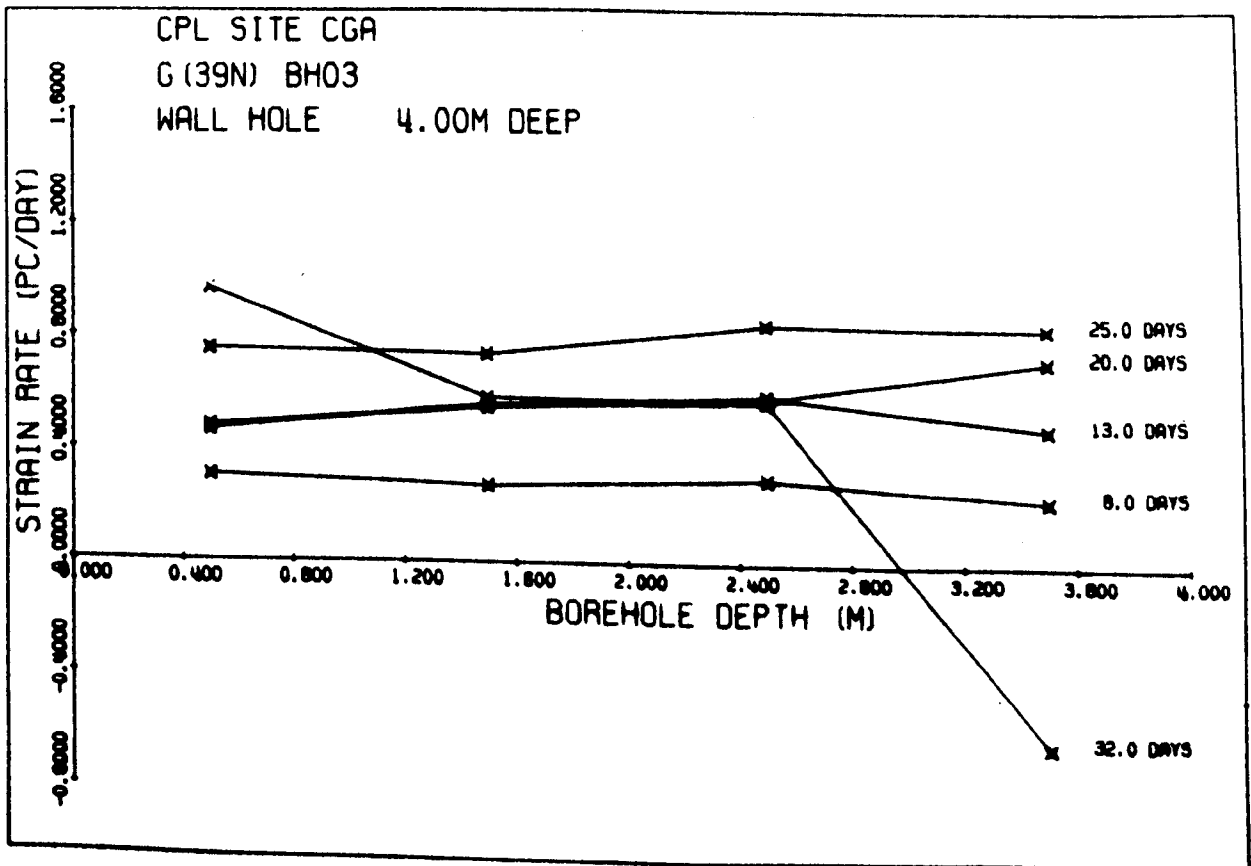
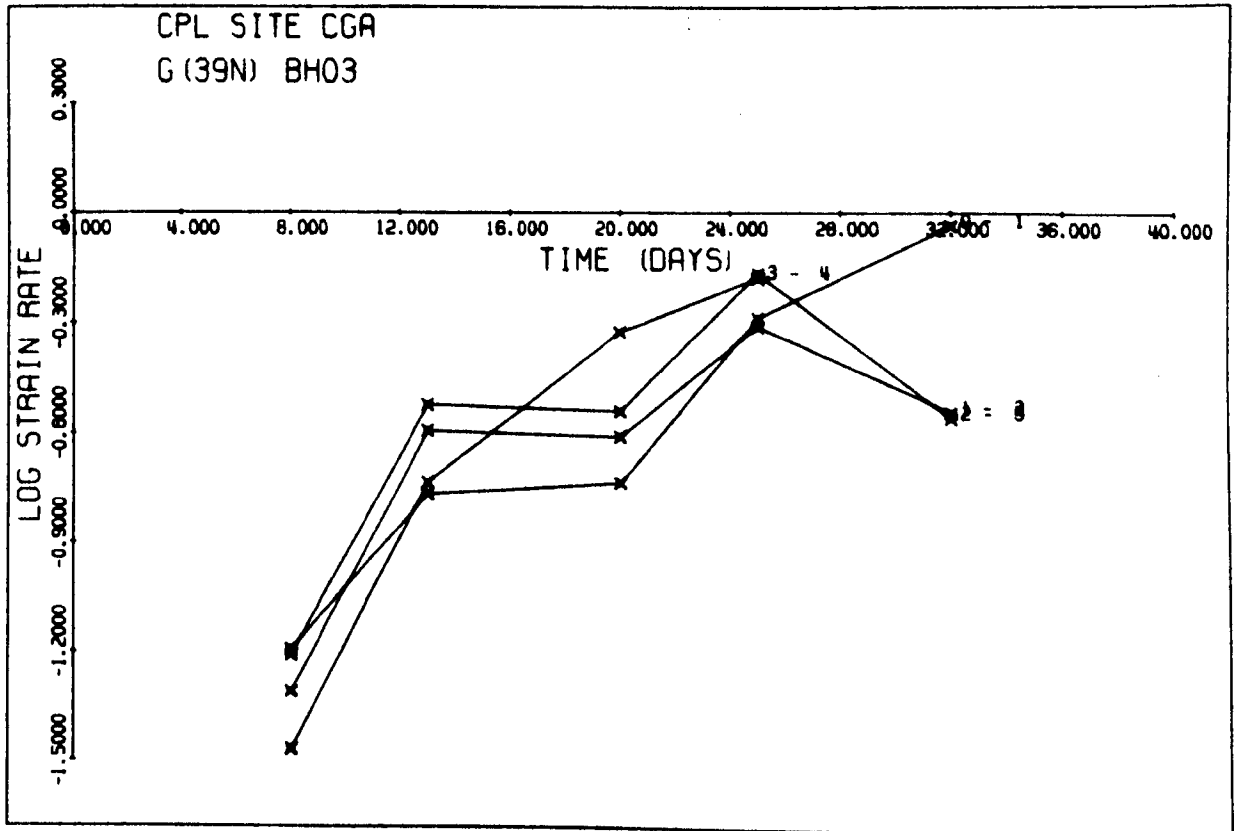


Figure 6 .19 No. 10 Panel CGA BH3 (Contd.)

that the anchors must be located as in Figure 6.20. That is virtually through the centre of the pillar. The high strains all well in excess of 2% after 8 days or possibly sooner, further suggest that this pillar is failing, not by plastic deformation, but by vertical fracturing throughout.

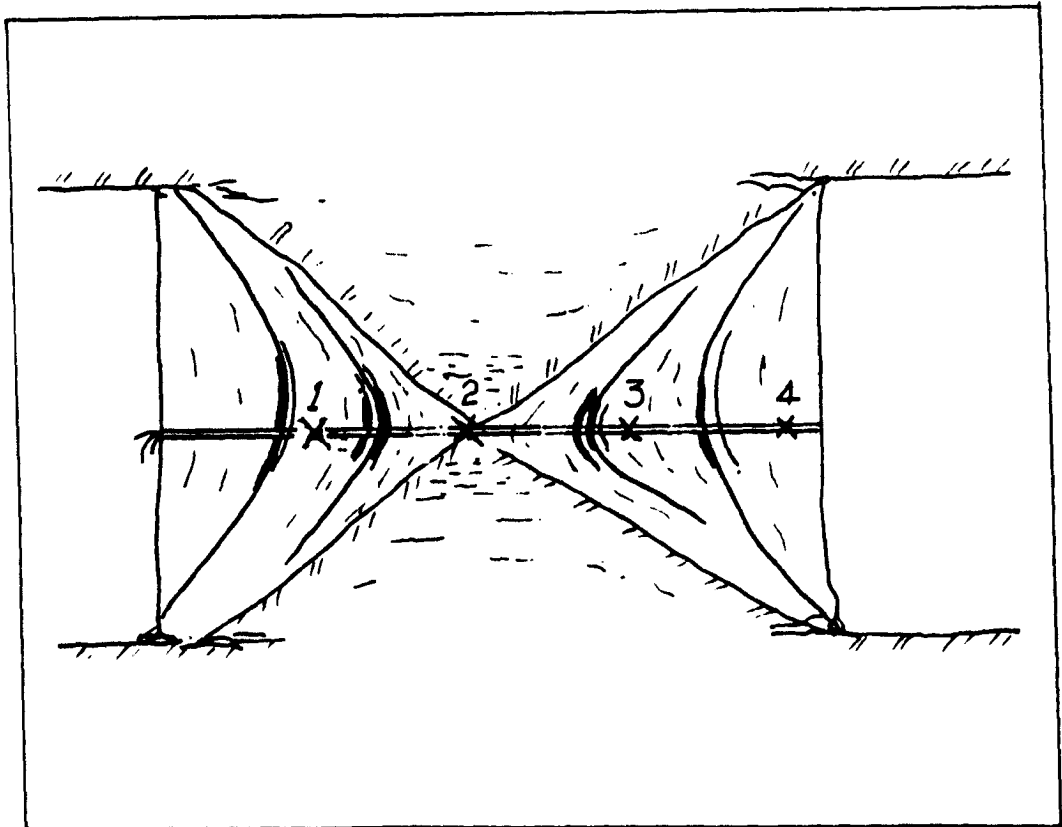


Figure 6.20 No. 10 Panel, site CGA BH Ø3 - diagram showing anchors in relation to fracturing

The graph of strain rate vs. time shows a rapidly increasing strain rate from the date of installation up to day 25, the day after water inflow in H roadway. This is followed by an equally rapid decrease in strain rate, which is a similar picture to that from the other yield pillars.

Site CHA BH Ø2 - Roof Hole

The extensometer was installed in the roof of H roadway with anchors at 6m, 4m and 2m depths. The site had been mined on 5th September 1979 and water entered H roadway 55m behind this point 48 days later, and in E roadway 49 days later. The results are depicted graphically in Figure 6.21. They show that the strain in bay 1 (0-2m) is great enough to indicate bed separation, whereas in bay 1 - 2 (2m-4m) this is unlikely. There is virtually no movement occurring between anchors 2 and 3 (4m-6m). Similarly with the roof extensometer in CFA, there was no increase in strain rate except a small one in bay 0-1, as the water date approached. However, there is an increase in strain rate up to about 18 days after mining, this effect appearing to hit a peak sooner the deeper the anchor. There would seem to be a change in the rate of decrease of strain rate from about 30 days after mining which could be due to the approaching water.

6.5.4 Closure Measurements - No. 10 Panel, B section

The only closure measurements made in No. 10 Panel in the wide section, were at sites CEA, CGA and CJA. These were subsequent to the water inflow, and only two readings were obtained from each site. The data is therefore very limited, and allows only an estimate of the total closure to be made by assuming a constant closure rate. Table 6.7 lists the estimated closures and the closure rate, the latter being the mean over a 40 day period

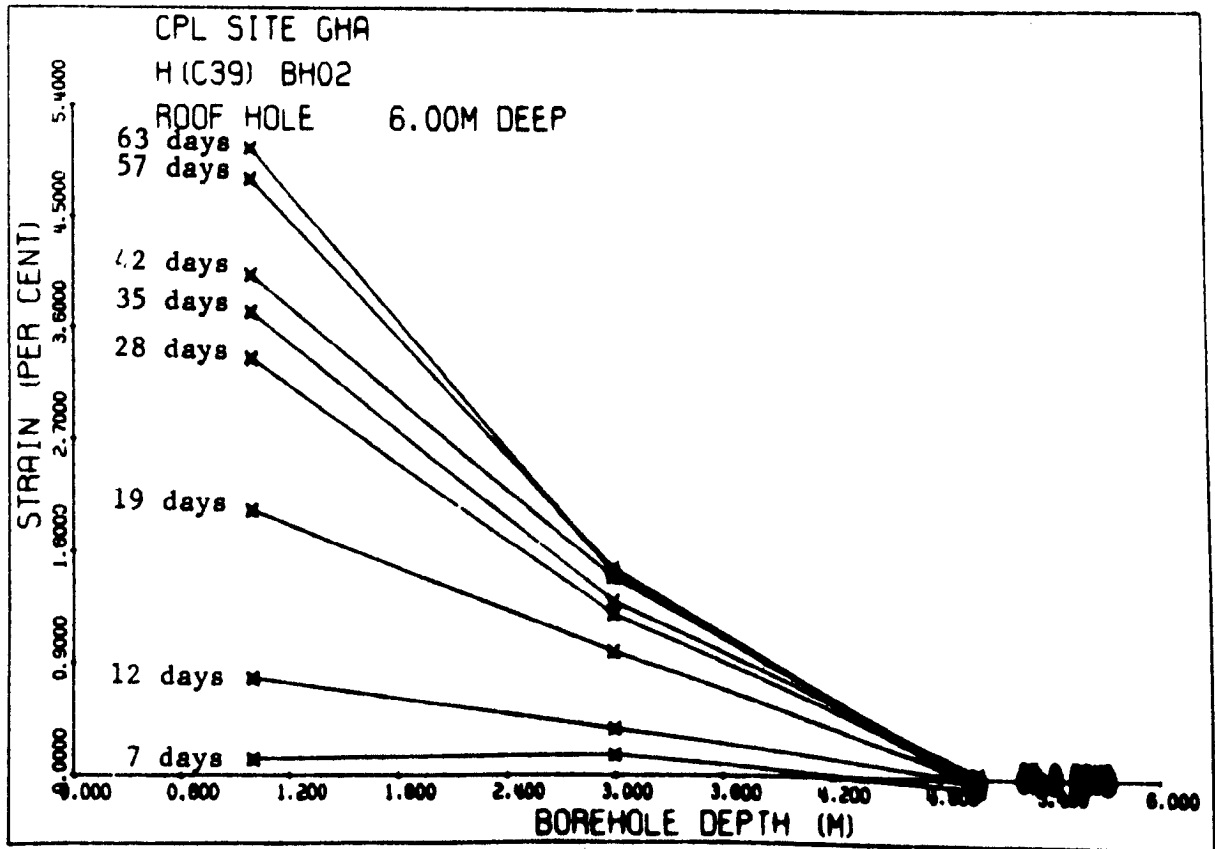
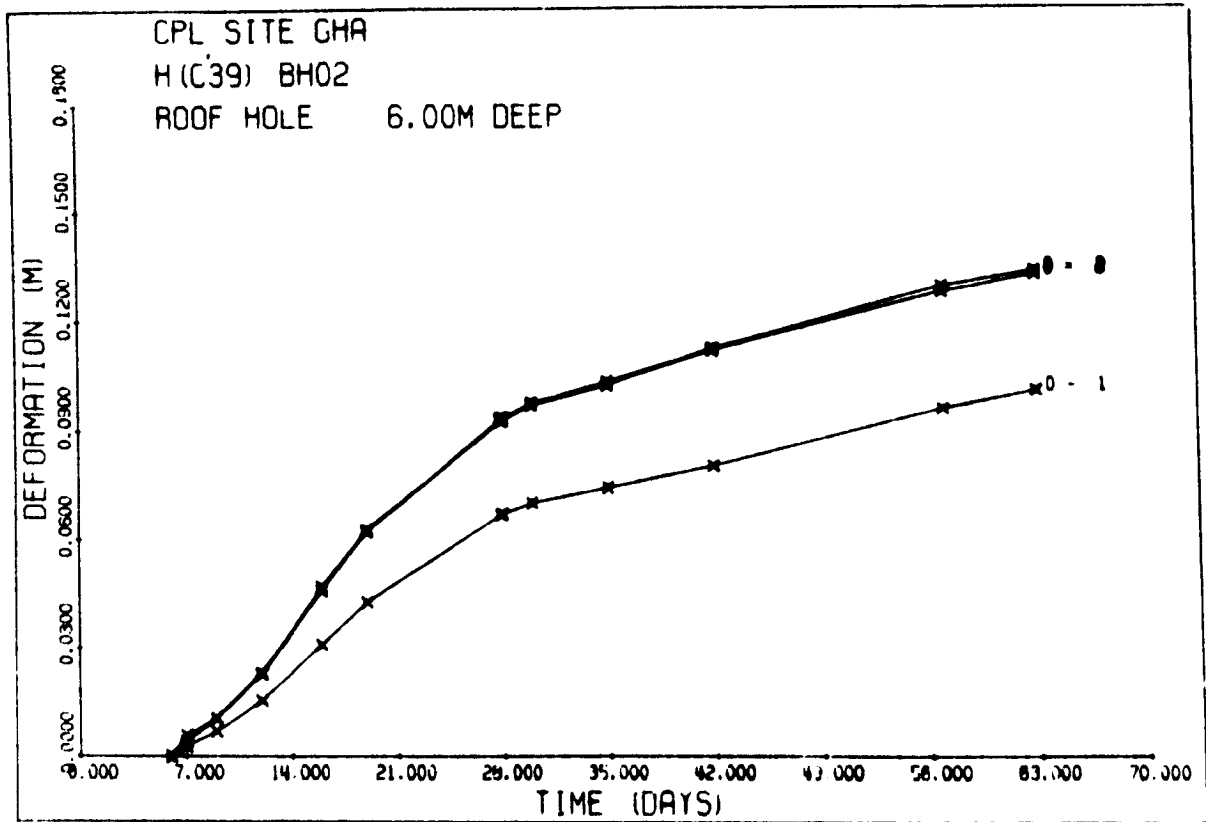


Figure 6.21 No.10 Panel Site CHA BH02

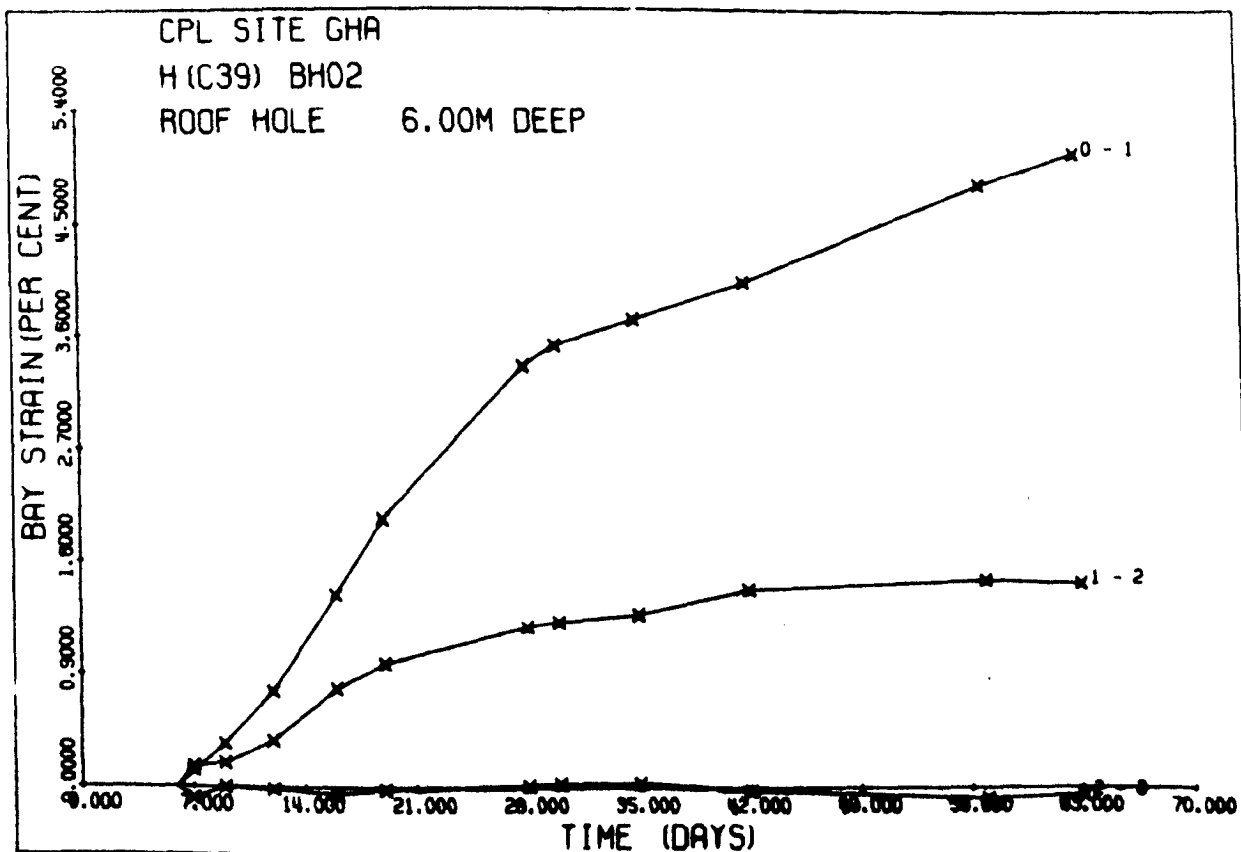
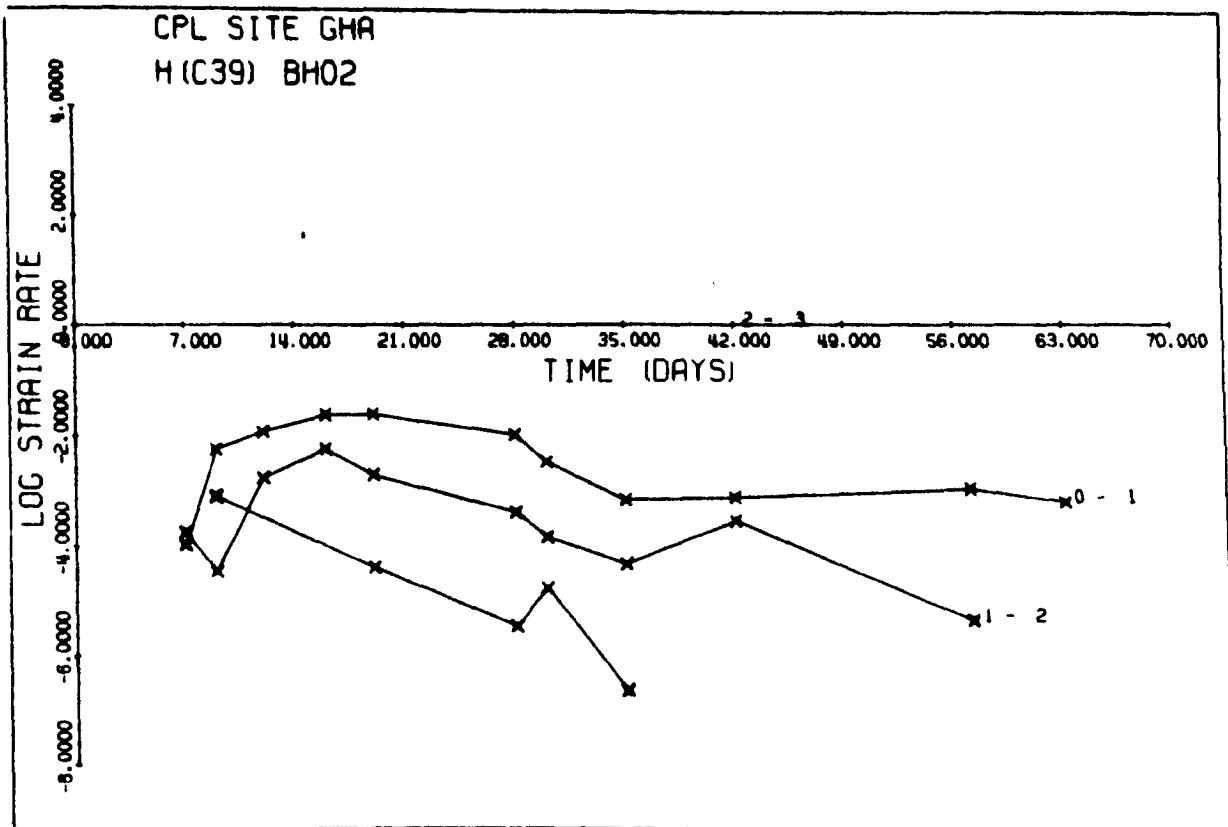


Figure 6.21 No.10 Panel, Site GHA BH02 (Contd.)

beginning five days after the water inrush. These appear to be reasonable when compared with the microcreep readings which were taken from about eight days before the water entered the mine for a period of approximately sixteen days. The total closures are definitely on the low side, and the actual closure may well be twice as high as the estimated values given in the table.

TABLE 6.7
Closure Data, No. 10 Panel, B section

Site	60 days mm	100 days mm	Closure rate mm/day
CEA	475	775	7.8
CGA	425	715	7.1
CTA	300	500	5.0

6.5.5 Microcreep Measurements - No. 10 Panel, B section

Table 6.8 lists the closure rate data obtained with the Serata Geomechanics Microcreep meter, six days before the water, on the same day as the water and six days after the water in H roadway.

There is a sharp increase in closure rate before the water inflow followed by a less rapid decline afterwards, at all the sites except CJA, which is situated in the northern-most flank road. The closure readings also show that site CJA has a lower

closure rate and total closure relative to the other adjacent sites. The reason for this probably lies in the fact that the projected position of the salt overfold (marked on Figure 6.9) passes close to site CJA. Massive salt in the roof could account for the lower closure and closure rate.

TABLE 6.8

Microcreep Data, No. 10 Panel, B section

Site	6 days before water mm/day	Same day as water mm/day	6 days after water mm/day
CEA	6.3	19.6	15.1
CGA	13.1	19.0	17.4
CHA	13.5	17.8	13.9
CJA	13.8	13.3	13.0

6.6 No. 12 Panel

This panel was developed in a south-easterly direction off the south east corner of No. 6 Panel. A number of closure measuring sites were established as given in Figure 6.22. Panel 12 was similar to Panel 19 in that it was mined parallel to and on the up-dip side of the same salt overfold. Mining began in March 1979 and it advanced approximately 100m in two months.

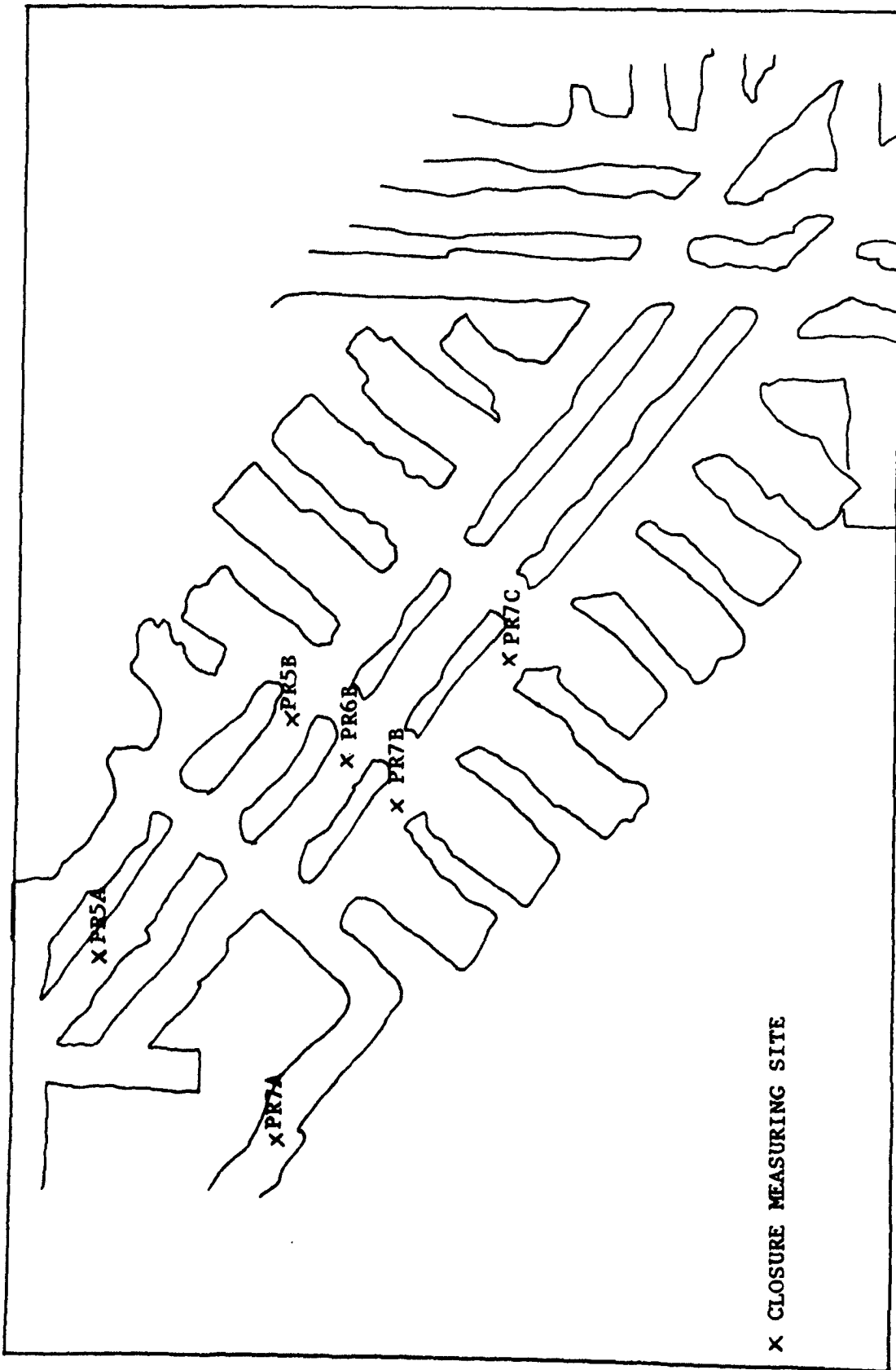


Figure 6.22 No. 12 Panel Instrumentation sites

It consisted of three 6m wide roadways separated by 4m wide yield pillars, with the conveyor located in the centre roadway. Stubs 25m long by 9m wide were driven at right angles off the outer road. The stubs were also separated by 4m yield pillars. The overall panel width was between 70m and 80m.

6.6.1 Closure Measurements

Of the convergence measuring sites installed, only six were operational. The total closures and closure rates for 20 day intervals are given in Table 6.9. It was possible to get back into this panel in April 1980 and establish some new sites as well as to measure two of the original closure sites. The new sites are designed PR C1 to PR C4. One of the intentions was to measure the variation in closure rate along a stub, as visual inspection showed that general conditions deteriorated with distance from the end of the stub. A series of photographs was taken in April 1980 at various sites and looking in different directions. These are shown in Plates 6.8 to 6.9, and their location is indicated in Figure 6.22. The varying conditions are shown very clearly, and it can be seen that the centre (conveyor) road is in the worst condition of all. Consideration of the results in Table 6.9 shows that there is not a great deal of difference in closure rate between the different sites. The outer roads appear to close at a faster rate initially, but slow down sooner, and after about 60 days, there is very little difference in closure rates. The convergence results are given in Figure 6.23. (a) to (f). The

TABLE 6.9

No. 12 Panel Closures (c), mm, and Closure Rates (ċ), mm/day

	20		40		60		80		100		120	
	c	ċ	c	ċ	c	ċ	c	ċ	c	ċ	c	ċ
PR5A C1	120	5.1	209	3.8	275	2.8	324	2.1	360	1.6	388	1.2
C4	177	8.2	328	7.0	457	6.0	568	5.1	661	4.4	743	3.7
PR5B C1	259	10.6	435	7.2	554	4.9	634	3.3	689	2.2	725	1.5
C4	307	12.6	315	8.5	657	5.8	753	3.9	818	2.8	862	1.8
PR6B C1	196	8.2	334	5.8	432	4.1	501	2.9	551	2.1	585	1.5
PR7A C1	79	3.6	145	3.0	201	2.6	248	2.2	288	1.8	321	1.5
C4	106	4.9	197	-4.2	276	3.7	343	3.1	402	2.7	453	2.3
PR7B C1	178	7.9	320	6.4	434	5.1	526	4.1	599	3.3	658	2.6
PR7C C1	228	9.4	385	6.5	494	4.5	569	3.1	621	2.1	657	1.5
C4	338	14.2	578	10.0	748	7.1	868	5.1	954	3.6	1014	2.5

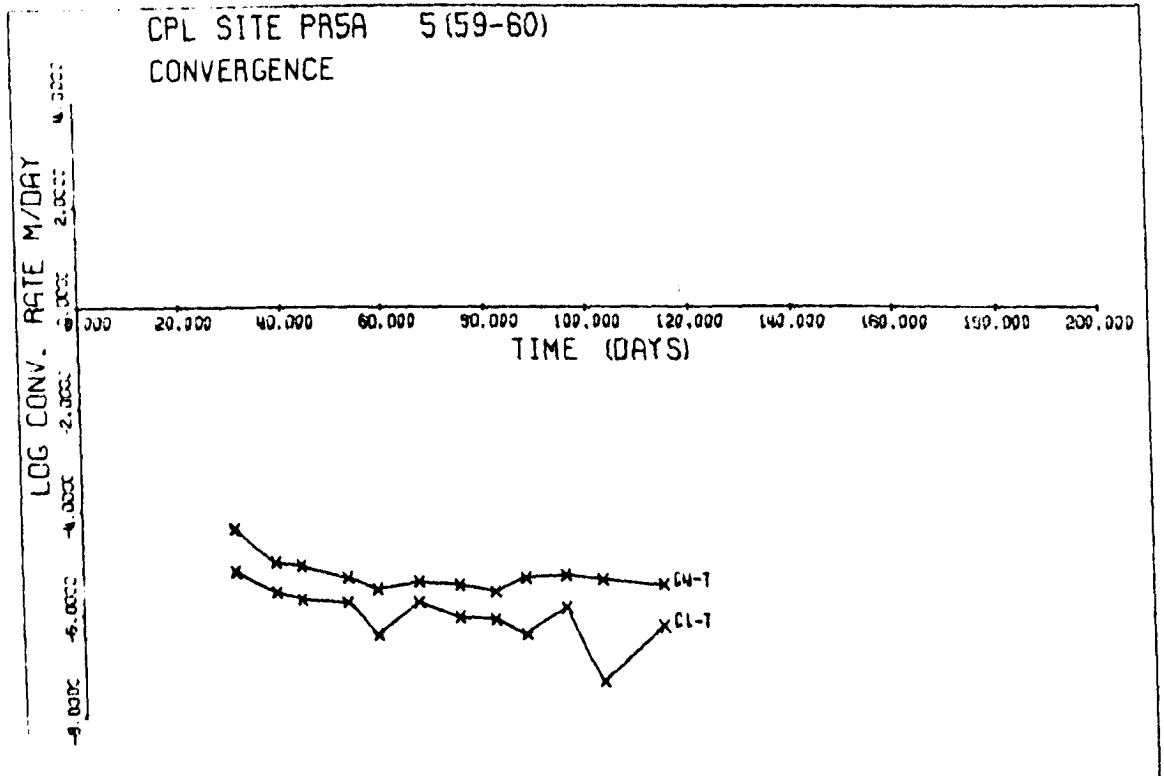
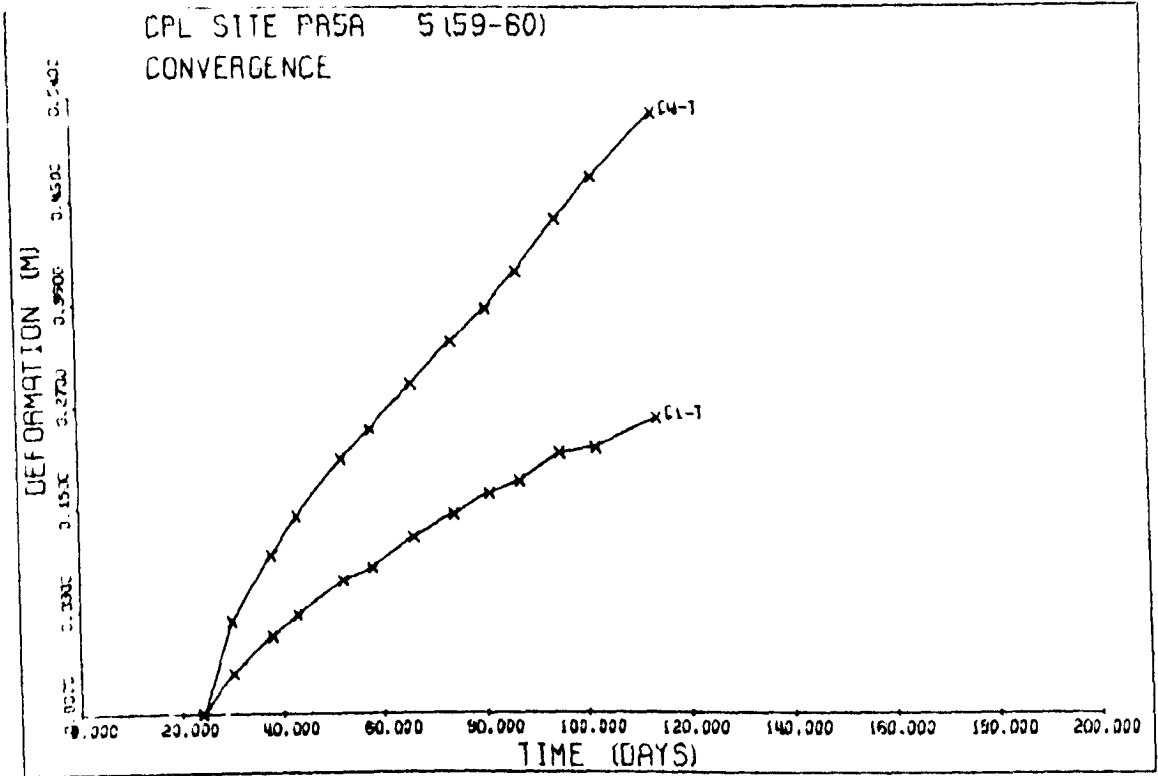


Figure 6.23 (a) No.12 Panel Closure and Closure Rates

closure rates measured in PR C1 to PR C4 show that these get progressively less with distance into the stub. This is born out by physical examination. The overall picture of how the roof is deforming across the panel is given diagrammatically in Figure 6.24. Plates 6.8 and 6.9 show conditions in the panel.

Water began entering the workings in No. 12 Panel at the sites marked in Figure 5.7 on the 6/12/79, some six months after that particular section had been mined. The total maximum inflow rate was about 9 litres per minute and this rate has steadily decreased to the point where by the 1/6/80, it had been reduced to a mere trickle. The section where inflow occurred was over 90m wide, and the main points of entry were to the sides of the panel. Plate 6.7 was taken at the site of the water inflow.

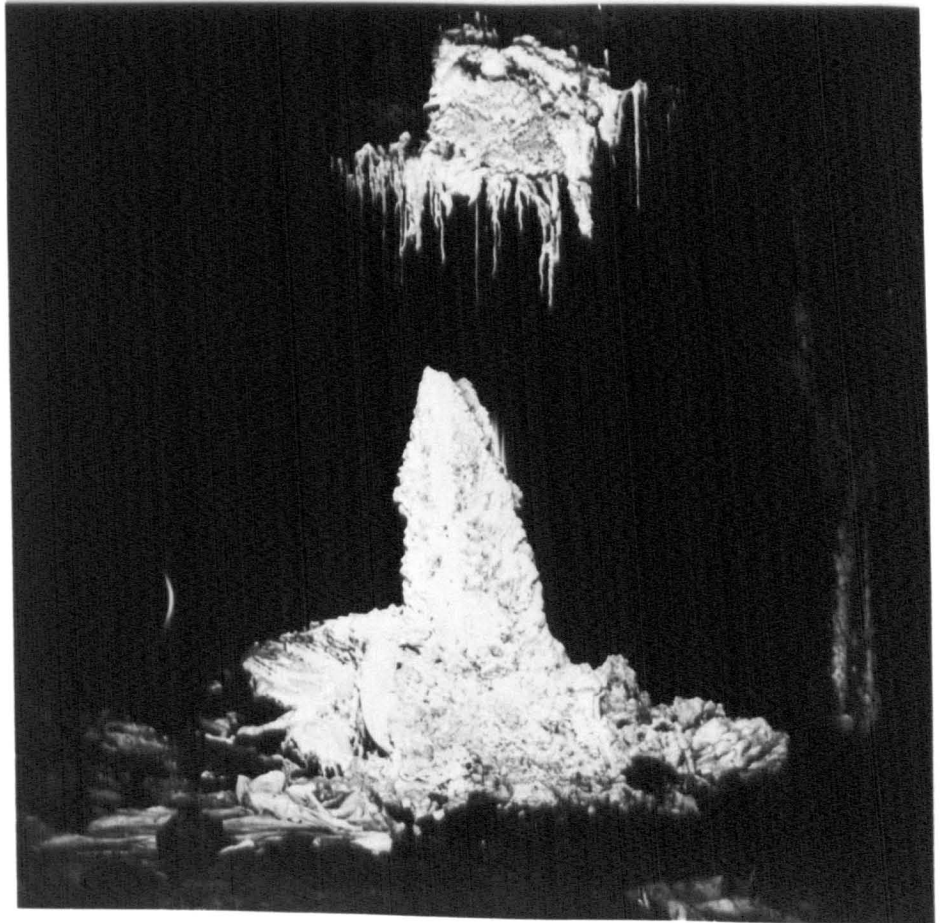
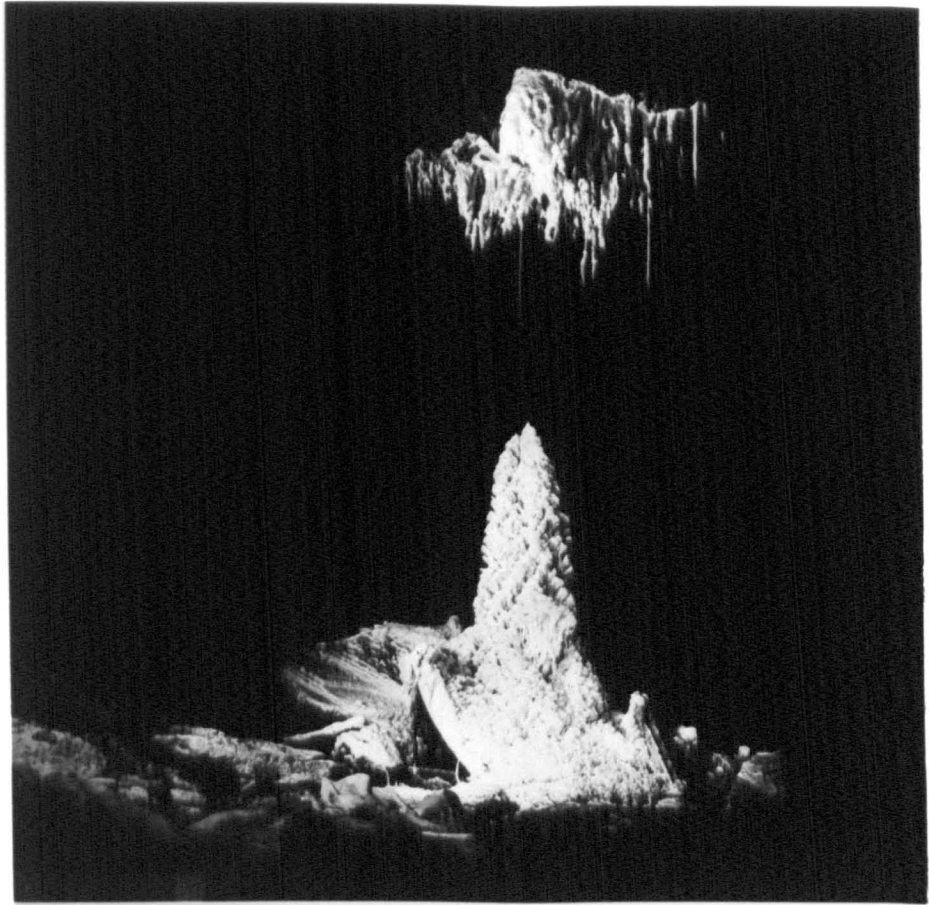
The first sites to be instrumented, PR5A and PR7A, exhibit much lower closure rates than the next set of stations, the 'B' sites. Unfortunately, there are not sufficient sites along the line of the panel to produce a meaningful graph of closure with distance down the panel.

6.6.2 Microcreep Measurements

An attempt was made to take microcreep readings at PRC1 to PRC4. It was found that even when the instrument had been left in-situ for over 20 hours, stable readings could still not be obtained. These were therefore ignored.

Plate 6.7

- 1 Stalactite/stalacmite 60 days after appearance of water.
- 2 30 days later.



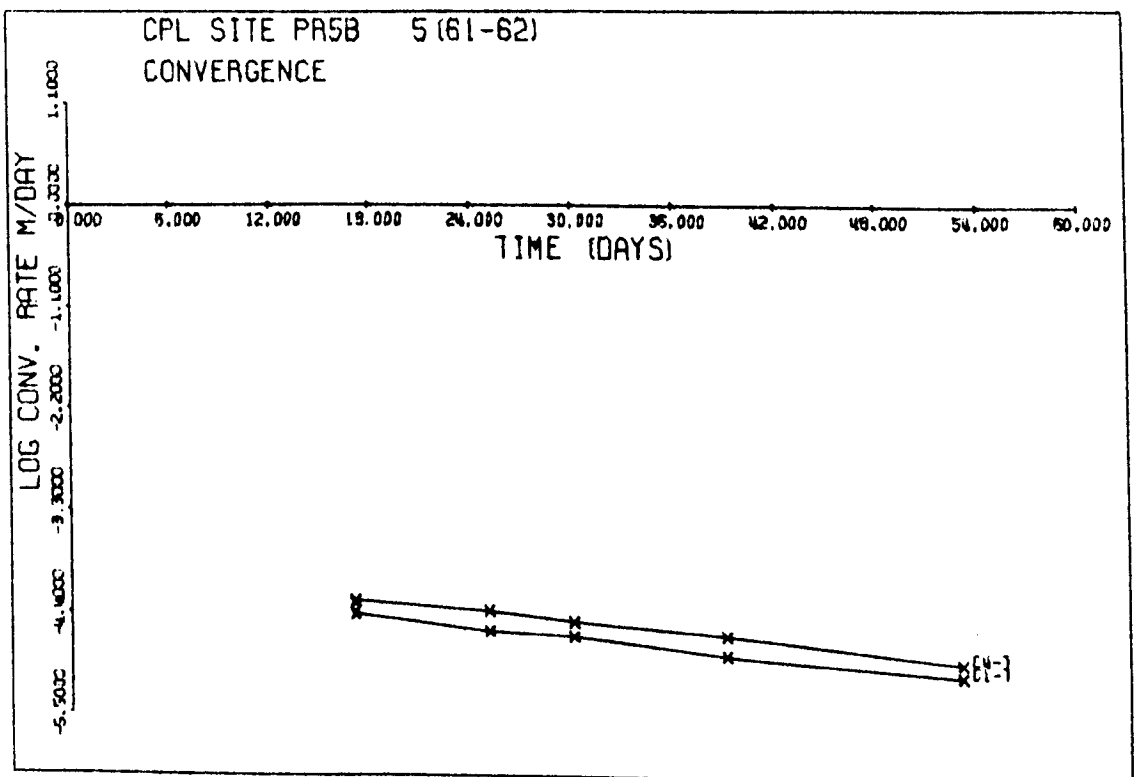
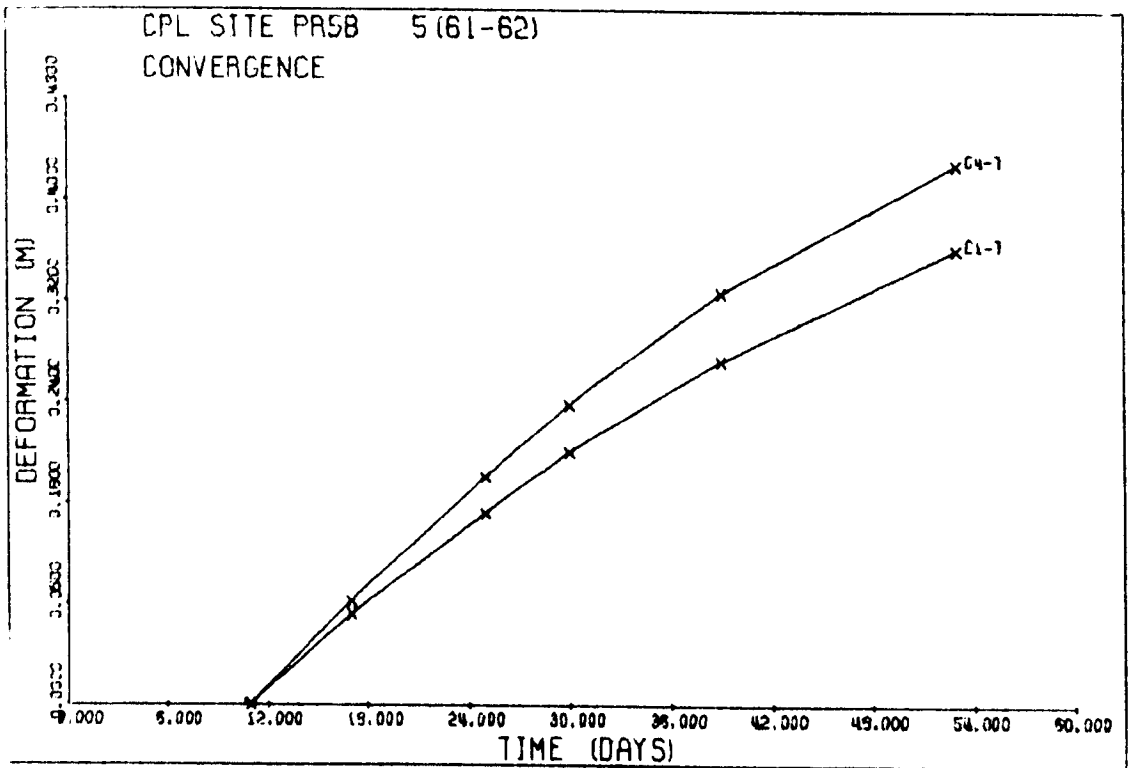


Figure 6.23 (c) No.12 Panel Closure and Closure rates

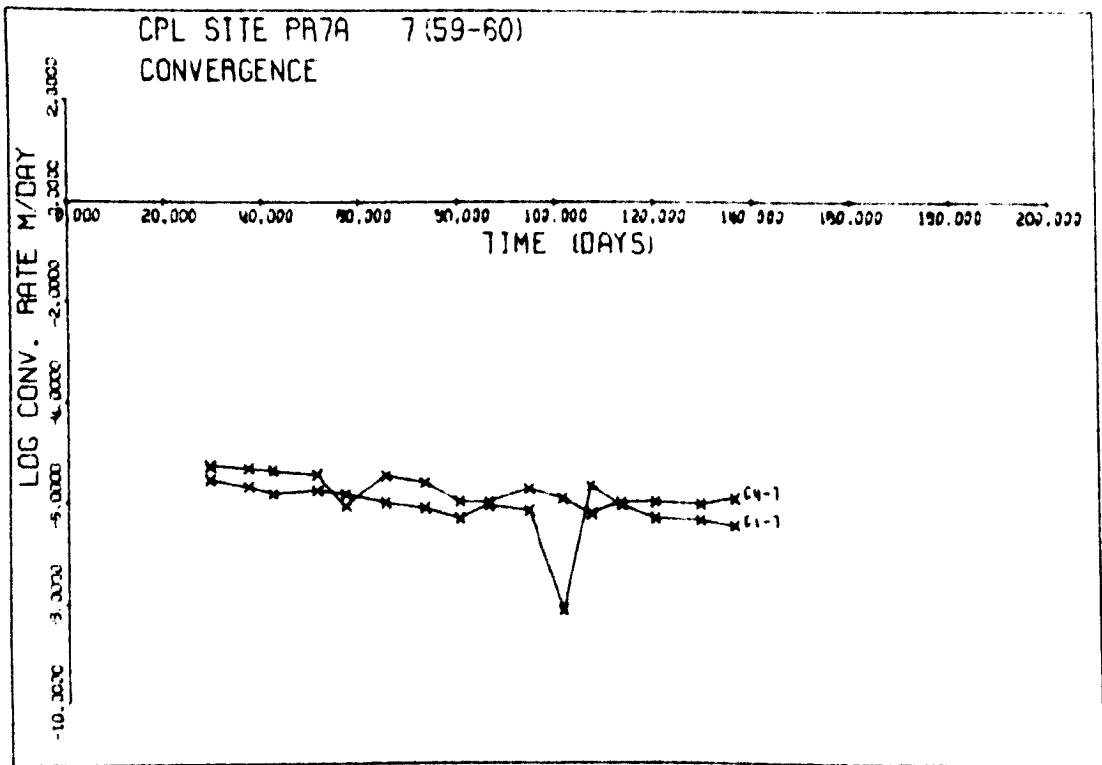
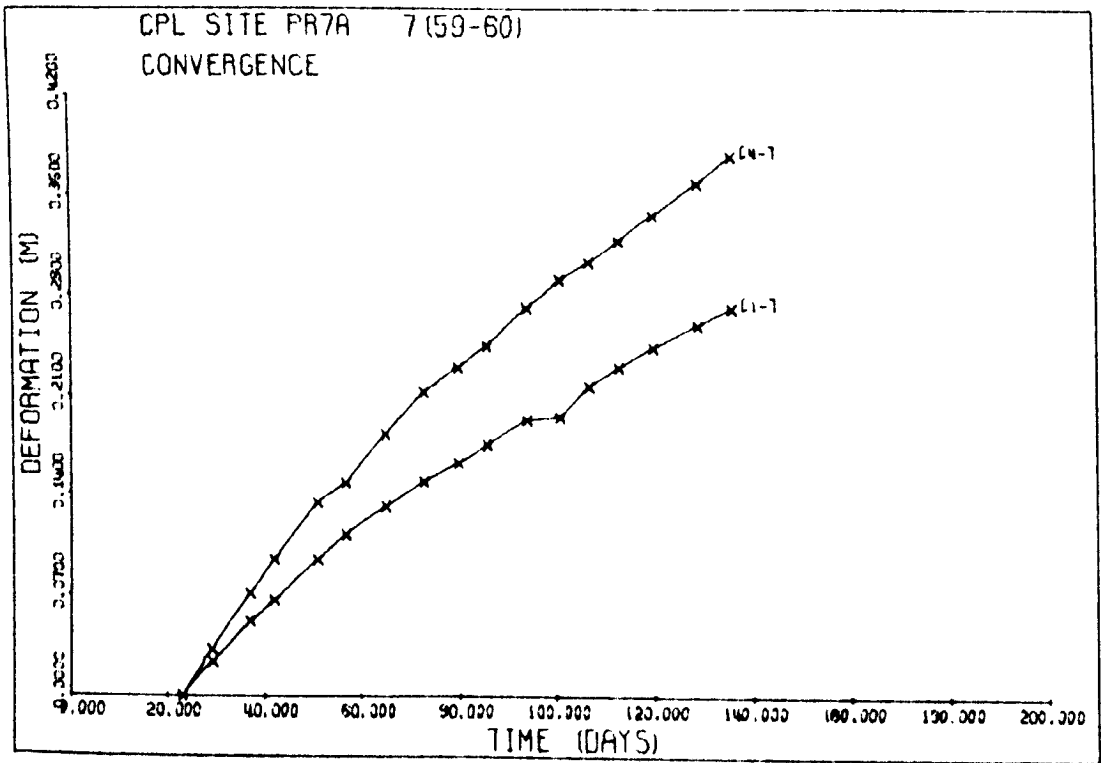


Figure 6.23 (d) No.12 Panel Closure and Closure Rates

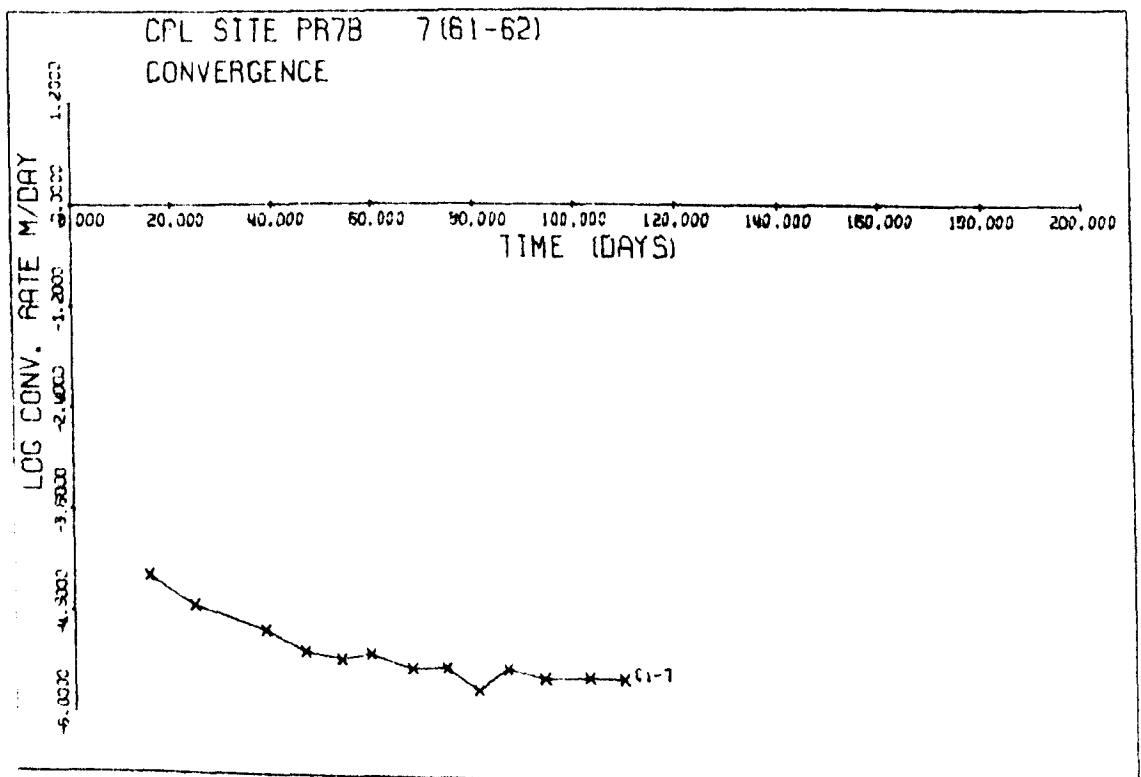
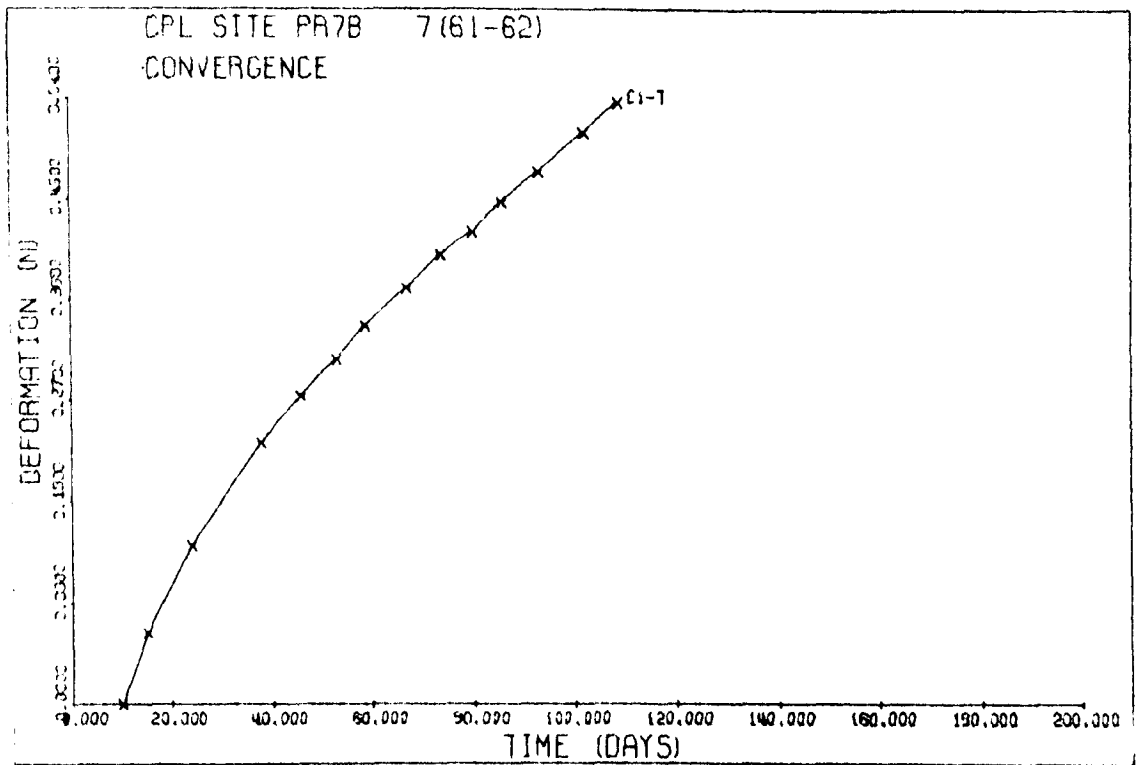


Figure 6.23 (e) No.12 Panel Closure and Closure Rates

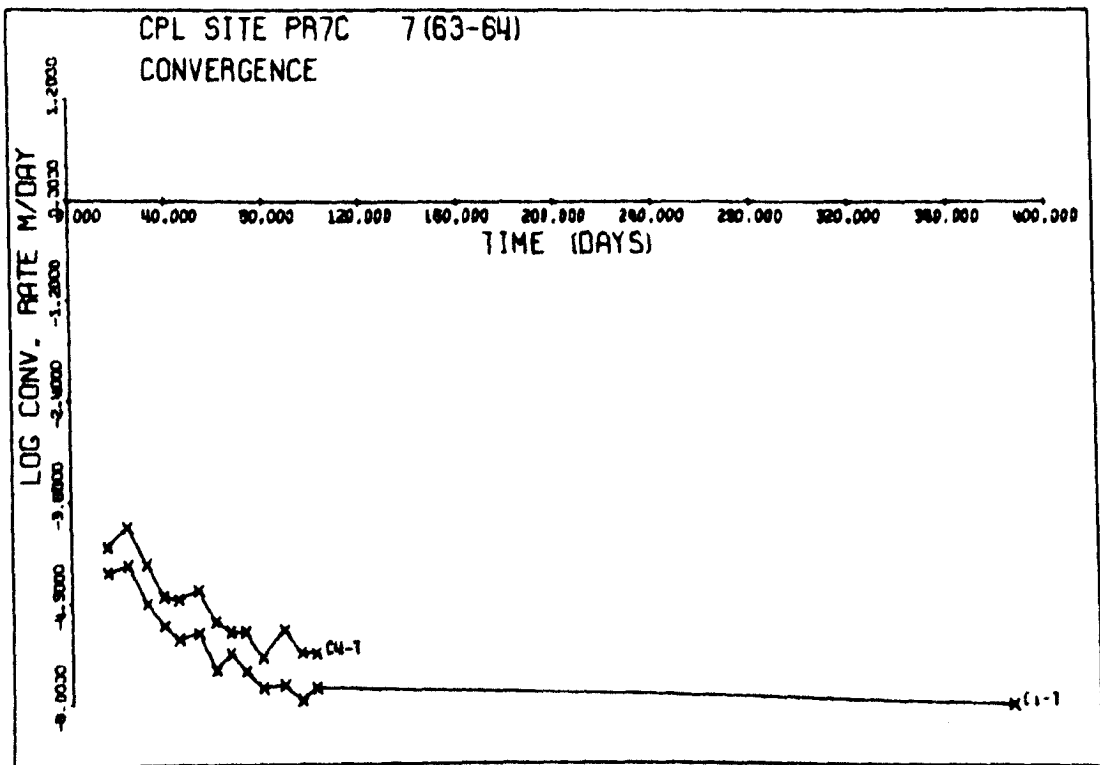
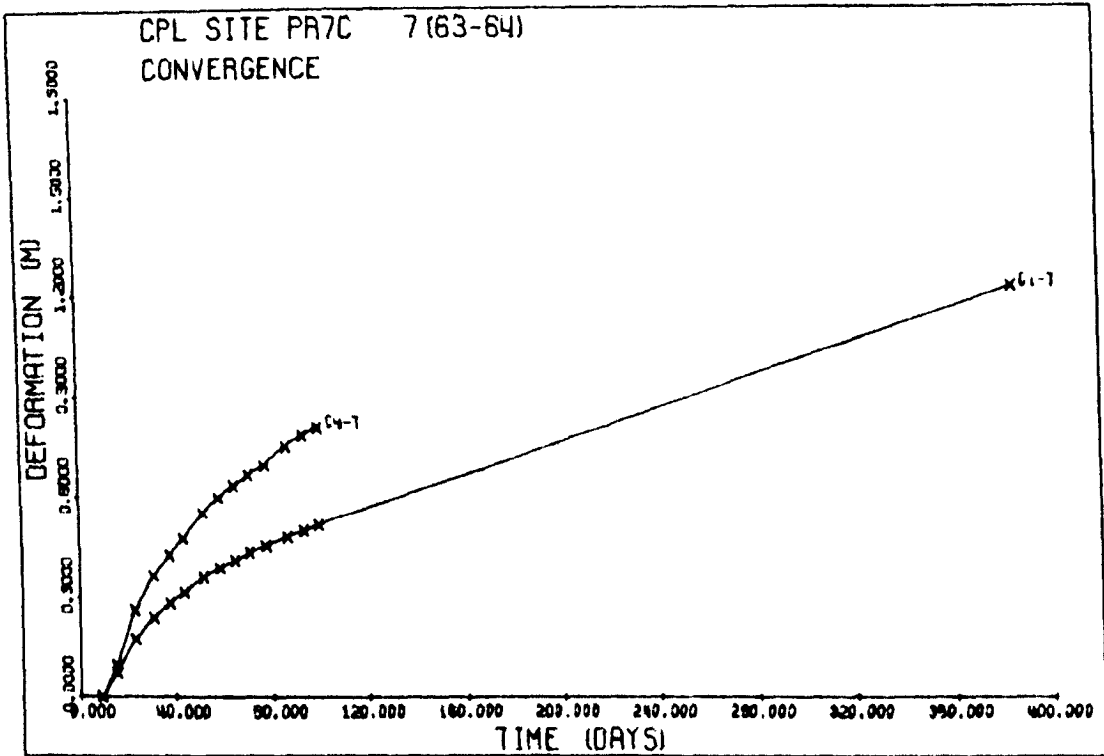


Figure 6.23(f) No 12 Panel Closure and Closure Rates

Plate 6.8

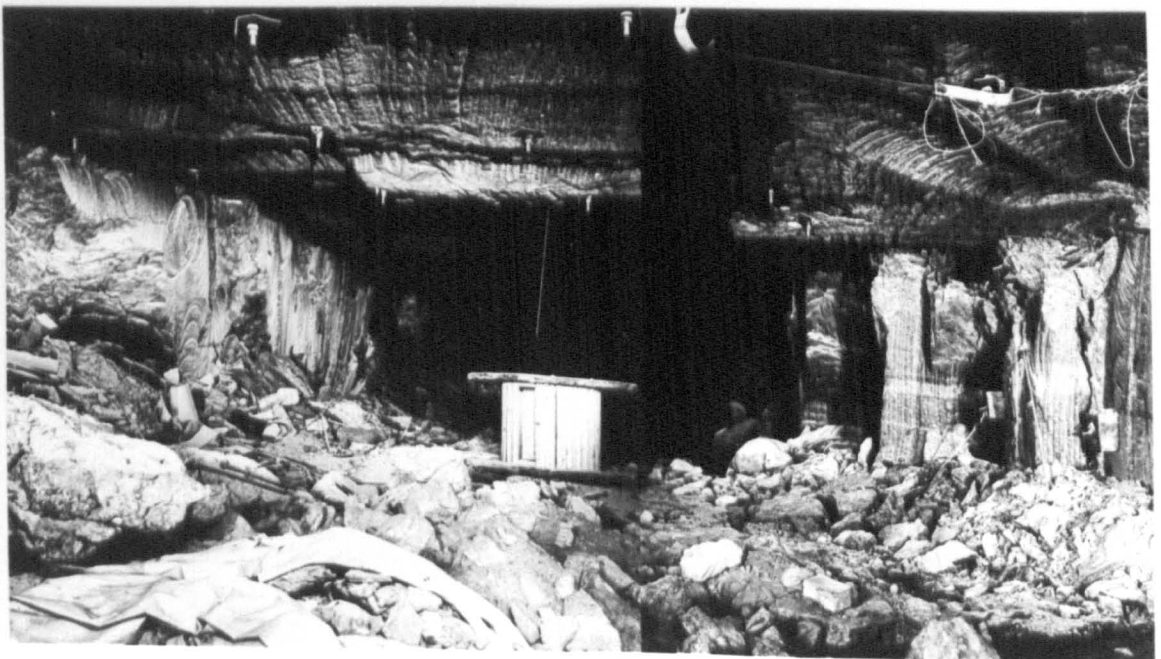
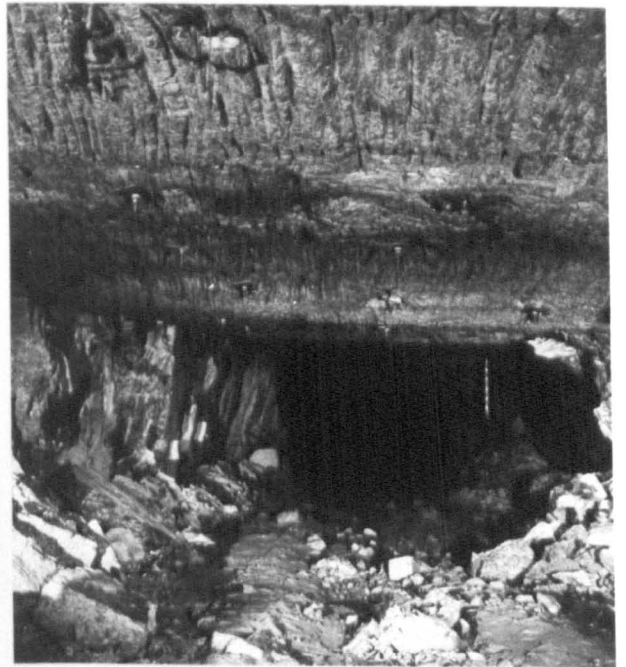
No.12 Panel 24/4/1980

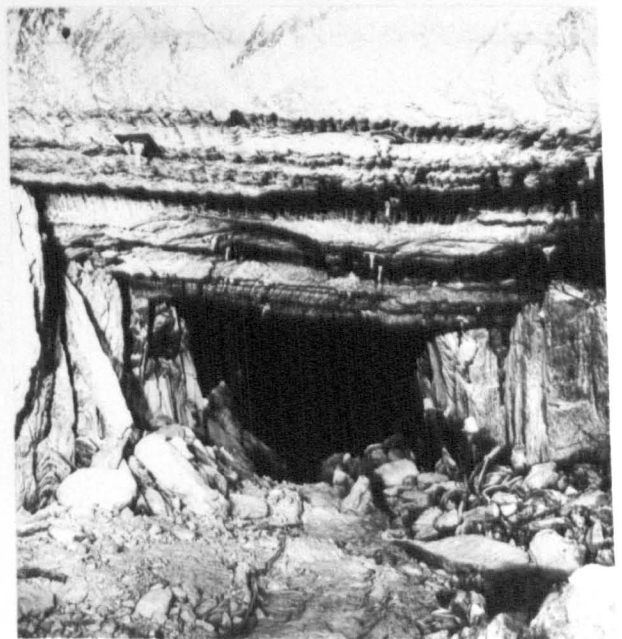
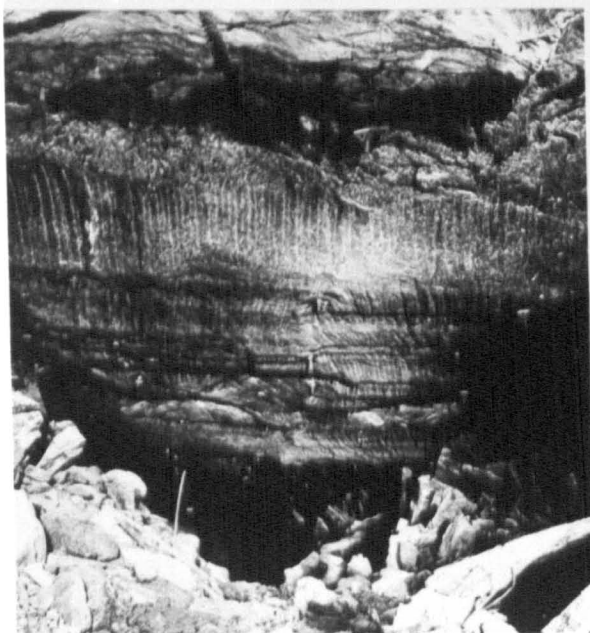
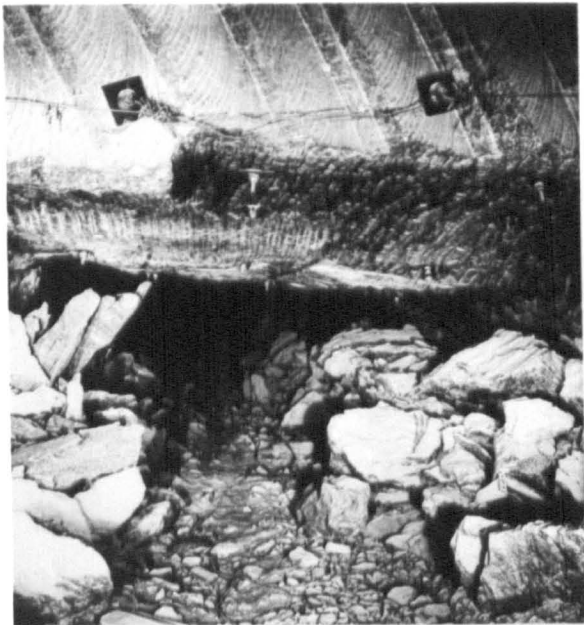
- 1 07/64 Looking West
- 2 07/64 Looking East
- 3 07/64 Looking South into stub.

Plate 6.9

No.12 Panel 24/4/1980

- 1 06/64 Looking West
- 2 06/64 Looking West
- 3 06/64 Looking North into stub.
- 4 06/64 Looking East





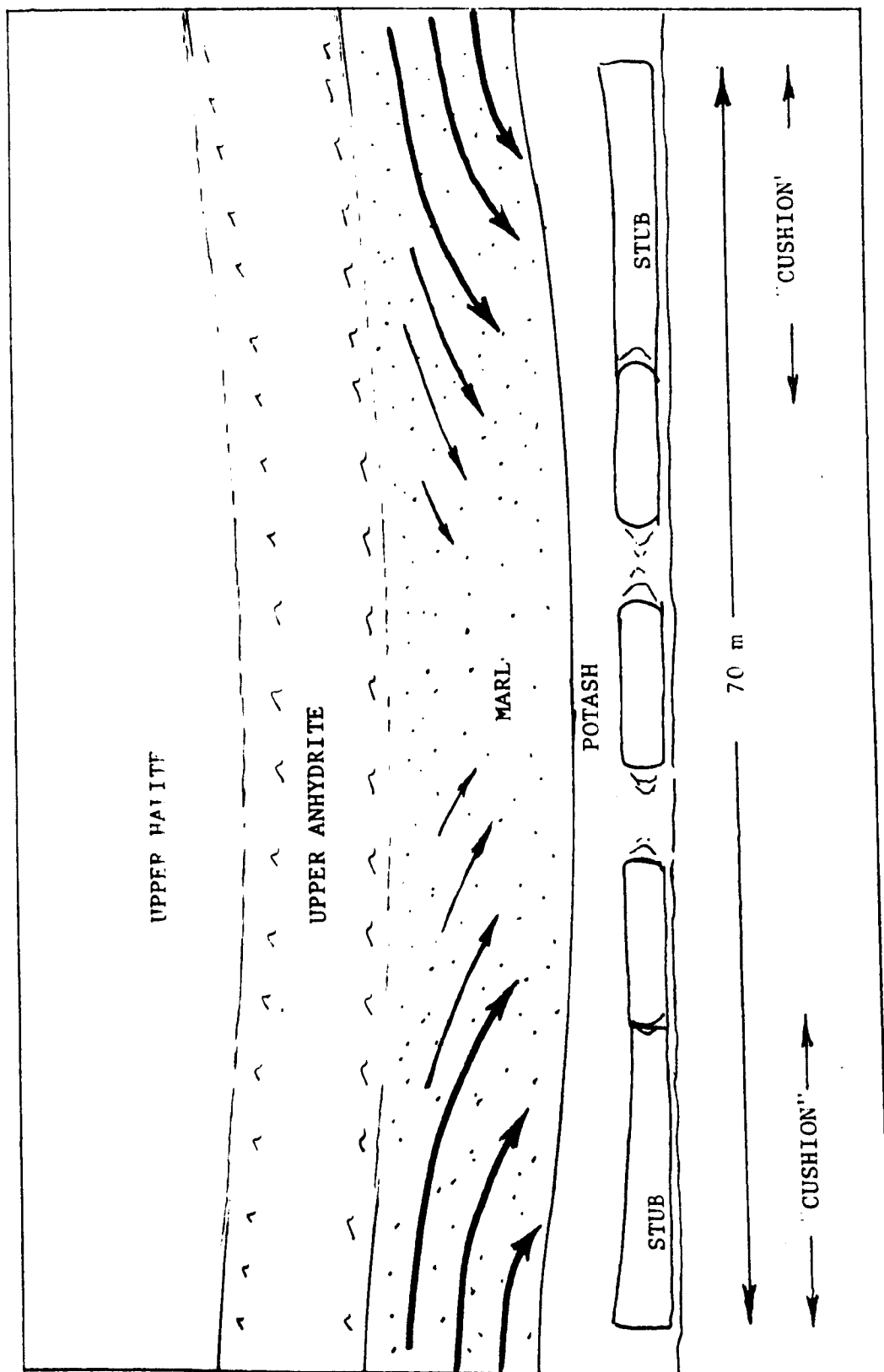


Figure 6.24 No. 12 Panel, Roof Deformation

6.7 No. 15 Panel

No. 15 Panel was set away westwards above the West Link (WL) twin salt road development. Instrumentation sites were created as shown in Figure 6.25. It was planned to continue with the West Link salt roads under the cover of the overmining by No. 15 Panel. The halite middling is generally of the order of 8m thick, It was when the panel had been mined a distance of approximately 160m with a width of more than 90m, that water was encountered in No. 10 Panel and shortly afterwards in No. 19 Panel. The decision was then taken to reduce the overall width of No. 15 Panel. A further alteration was then made to the layout, the result of which was similar to the original No. 10 Panel layout (A section) in that there were two 40m wide high extraction sub-panels having four roadways. These two sub-panels were separated by a 40m wide pillar. Twin cross-cuts were driven through these pillars every 40m, with one of them being driven before the other in order to provide a measure of stress relief to the second roadway. The outer roads in the sub-panels were kept about 20m ahead of the inner roads. The roads were all 6.5m wide and the yield pillars between them had a nominal width of 4m. In order to differentiate between them, the wide section is termed the A section, and the section containing the sub-panels is the B section.

6.7.1 Closure Measurements - No. 15 Panel, A section, 'A' sites

The graphs of convergence and convergence rates are given in

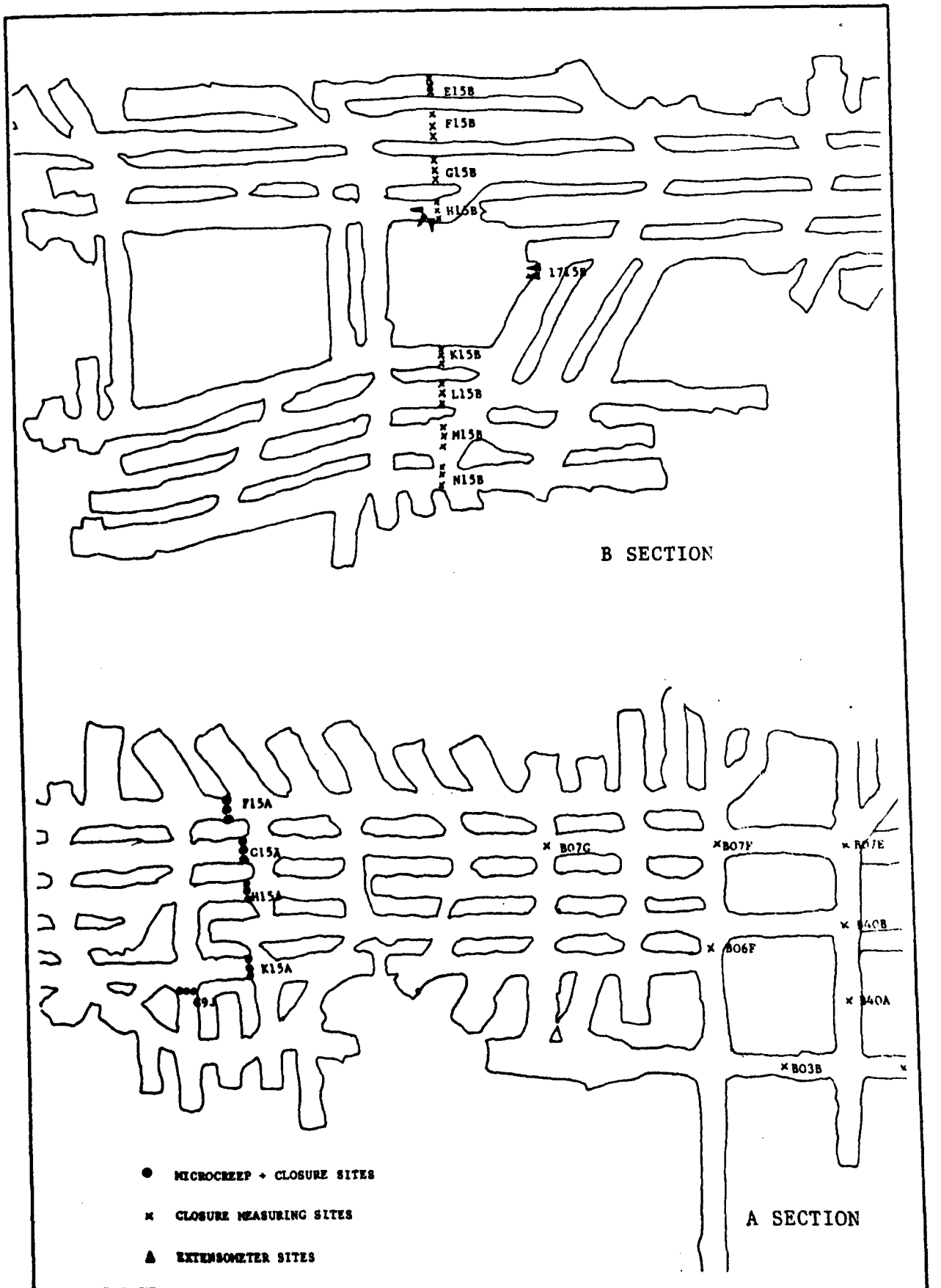


Figure 6.25 No.15 Panel Instrumentation Sites

Plate 6.10

- 1 F roadway at 09 Cross cut looking at R.M. site F15A
- 2 G/08 Looking West at R.M. site G15A
- 3 G/08 Looking East from R.M. site G15A

Plate 6.11

No.15 Panel 'A' sites
15/5/1980

- 1 F/08 Looking South across G (conveyor)
- 2 F/08 Looking East
- 3 F/08 Looking North into stub

Plate 6.12

No.15 Panel 'A' sites
15/5/1980

- 1 K/08 Looking East
- 2 K/08 Looking West at R.M. site K15A
- 3 K/08 Looking South

Plate 6.13

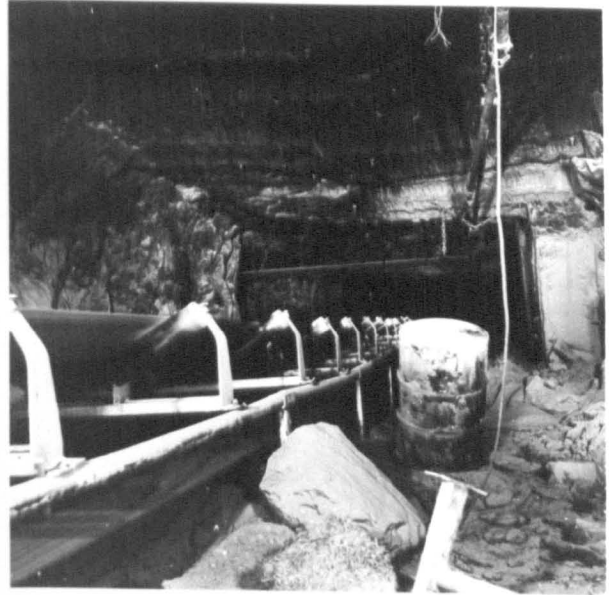
No.15 Panel 'A' sites
15/5/1980

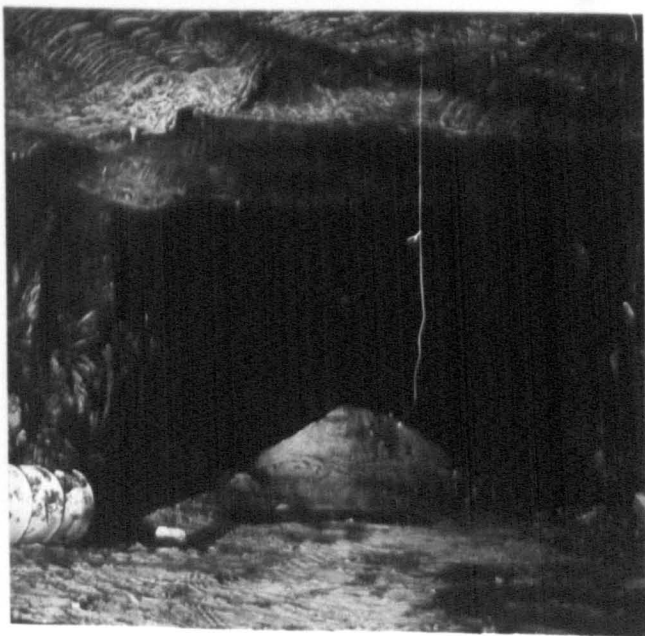
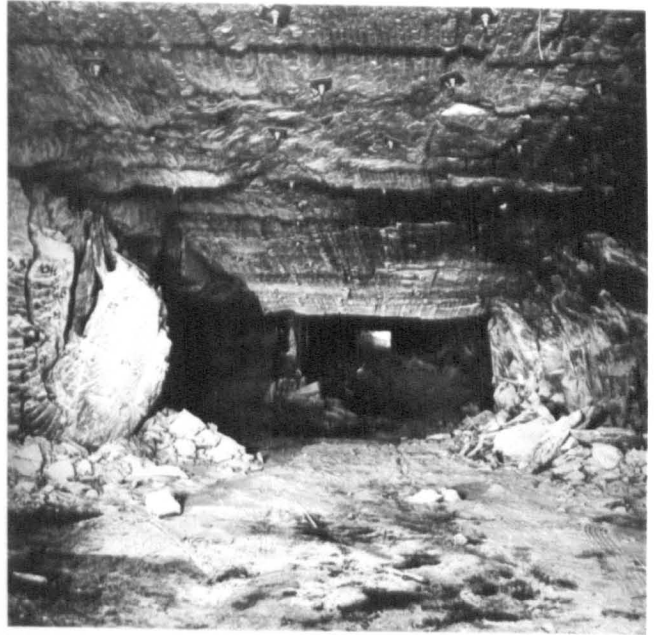
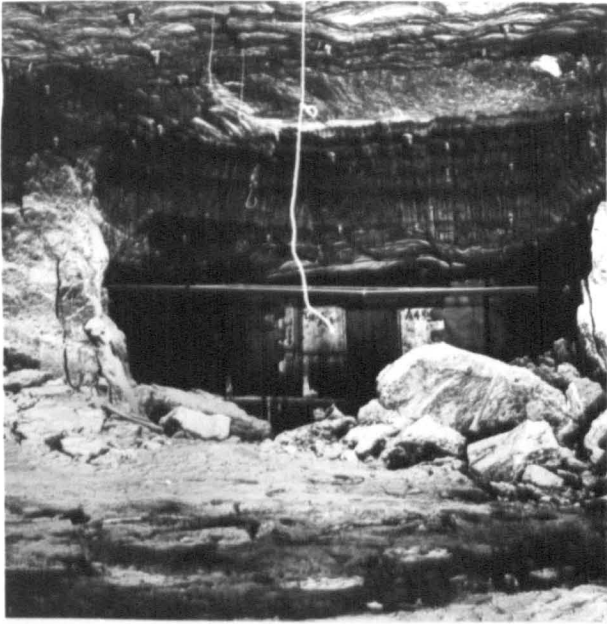
- 1 H/08 Looking East
- 2 H/08 Looking North
- 3 H/08 Looking West

Plate 6.14

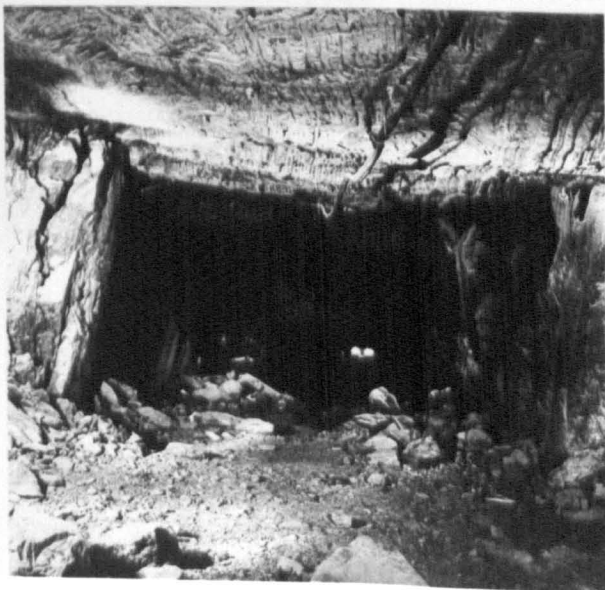
No.15 Panel 'A' sites
15/5/1980

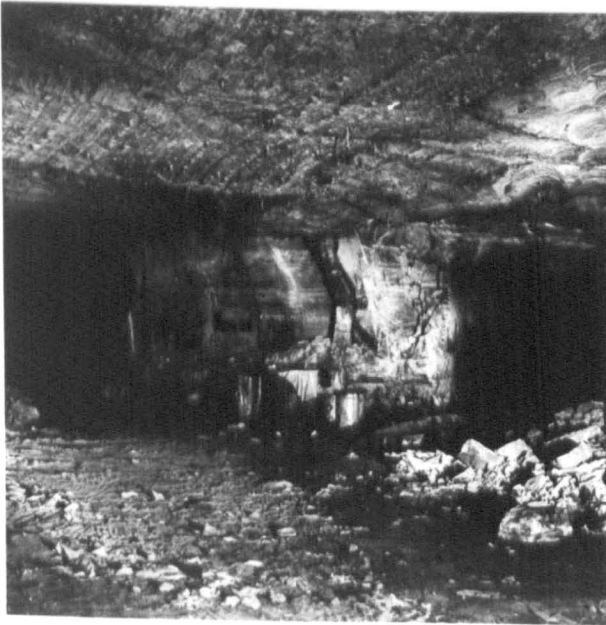
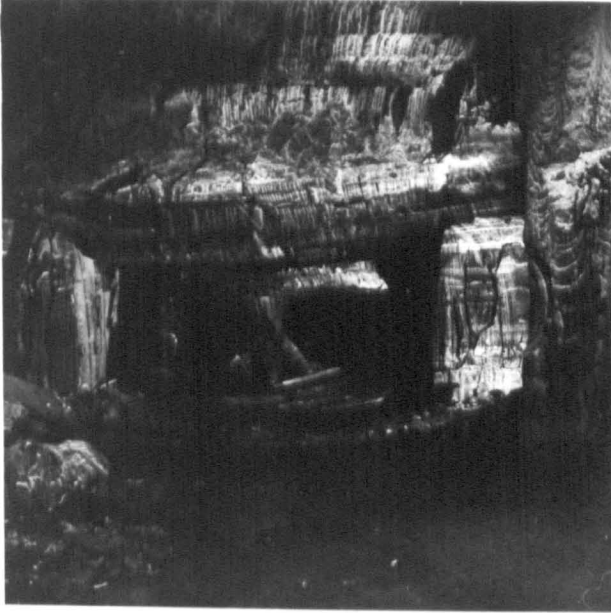
- 1 L/08 Looking West
- 2 L/08 Looking North
- 3 L/08 Looking East
- 4 L/08 Looking South at No.8 stub











Figures 6.26 and 6.27 and the total closures and closure rates for 20 days intervals are given in Table 6.10. These show that all the sites in this section exhibit relatively low initial closure rates, which then decrease further with time. In addition, the graph of closure across the panel depicted in Figure 6.28 shows that the roof is closing uniformly across this section. Again, as in the other high extraction panels, the outer roads which were driven ahead of the inner ones, do not have a significantly higher closure rate. Therefore it can again be concluded that Serata-type stress relief is not the mechanism that explains what is occurring. The lower closure and initial closure rate of site G15 A, is almost certainly due to the fact that it lies directly above the \emptyset 7 salt roadway. However, the important feature is that after about 60 days the closure rates at all sites become very similar at about 3mm per day, with only F15 A being slightly higher. Plates 6.10 to 6.14 were taken at the 'A' sites in No. 15 Panel some three months after they had been mined, and illustrate what the conditions are like across the panel.

6.7.2 Closure Measurements - B section 'B' sites

The graphical representations of closures and closure rates at the 'B' sites are shown in Figures 6.29 and 6.30, and the total convergences and convergence rates derived from these graphs are given in Table 6.11. The initial closure rates at the 'B' sites are somewhat lower than those at the 'A' sites, but more significant is the fact that they decrease subsequently more rapidly.

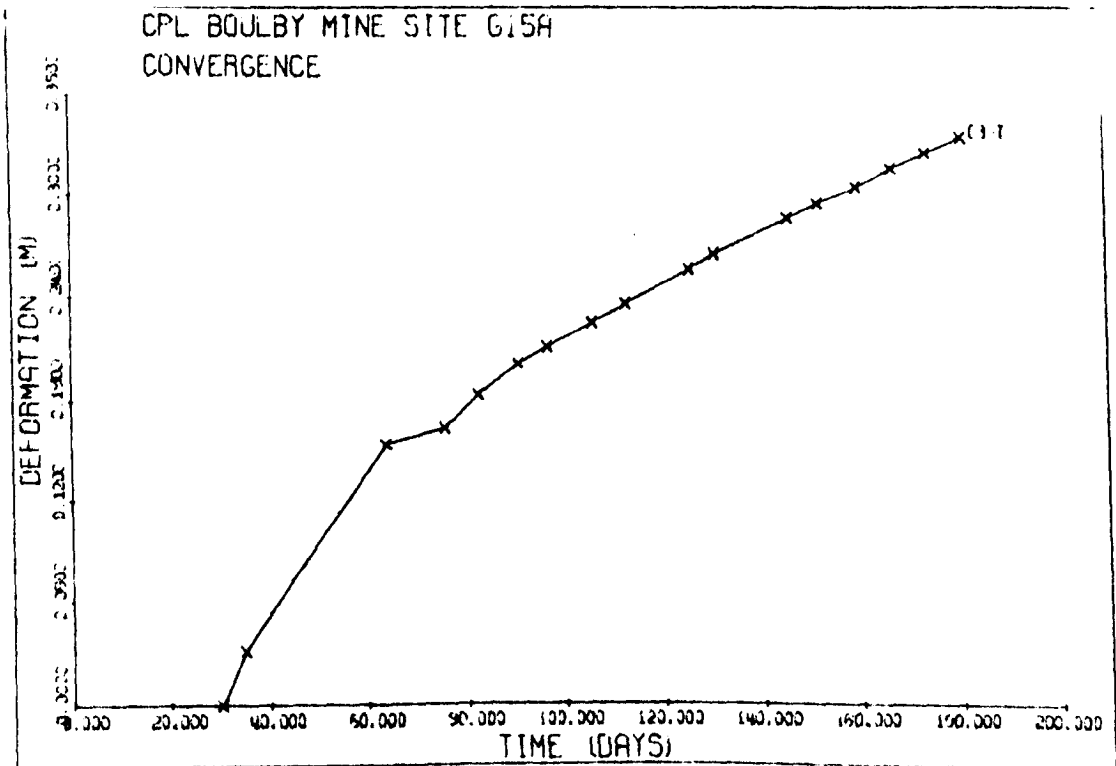
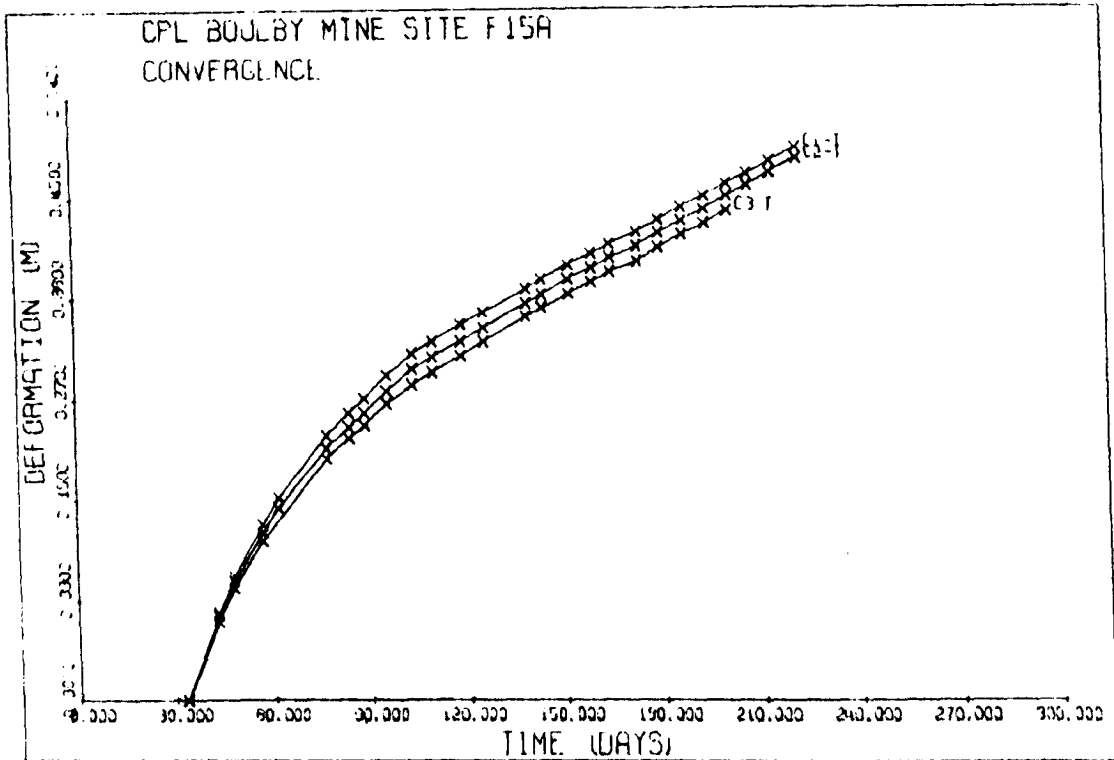


Figure 6.26 No. 15 Panel, A section - Convergence graphs

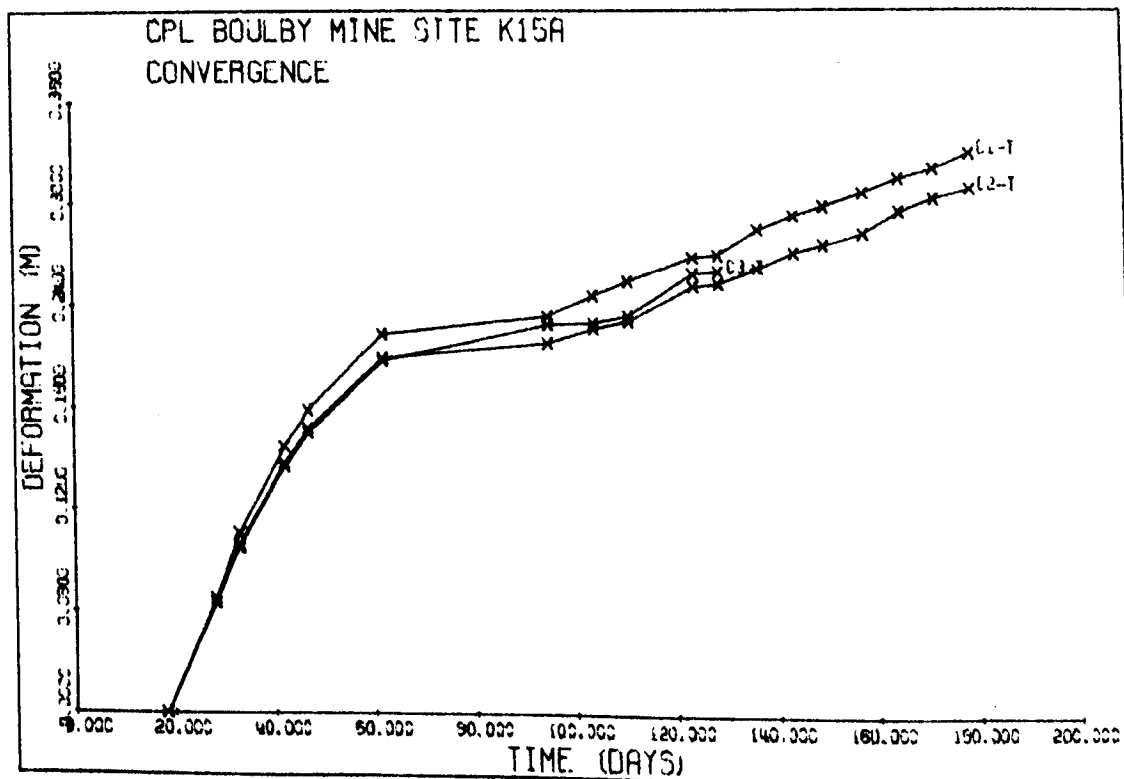
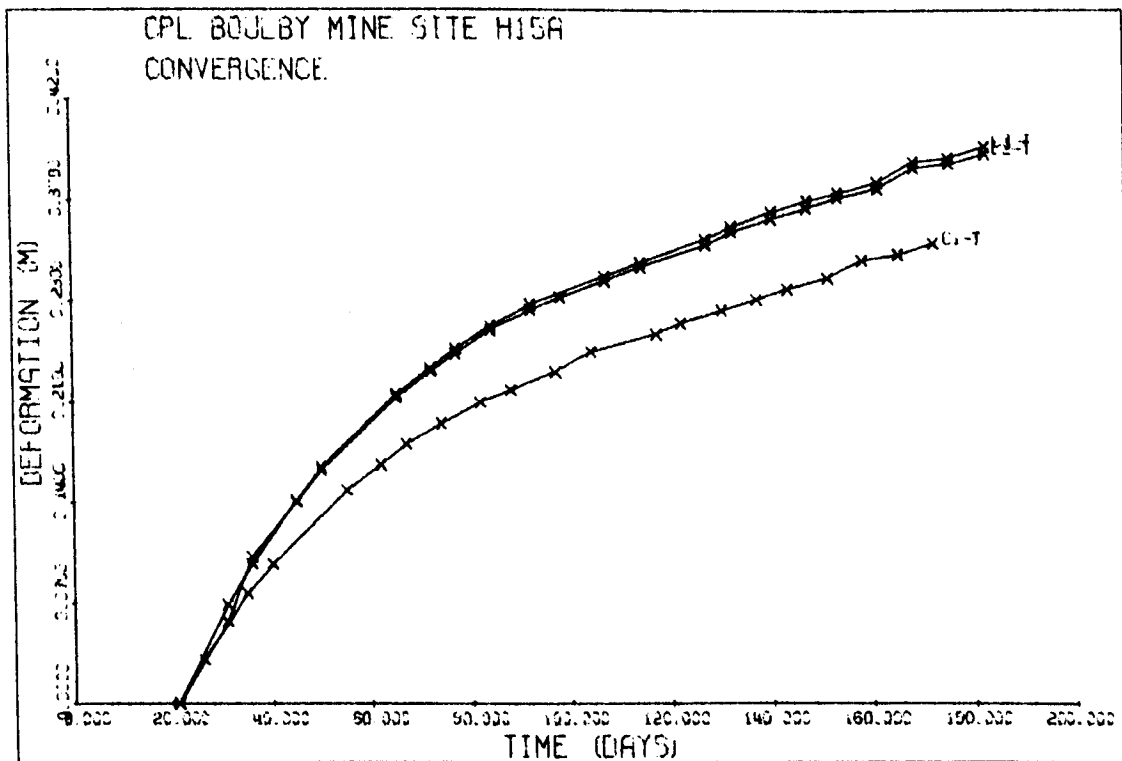


Figure 6.26 No. 15 Panel, A section - Convergence graphs
(Contd.)

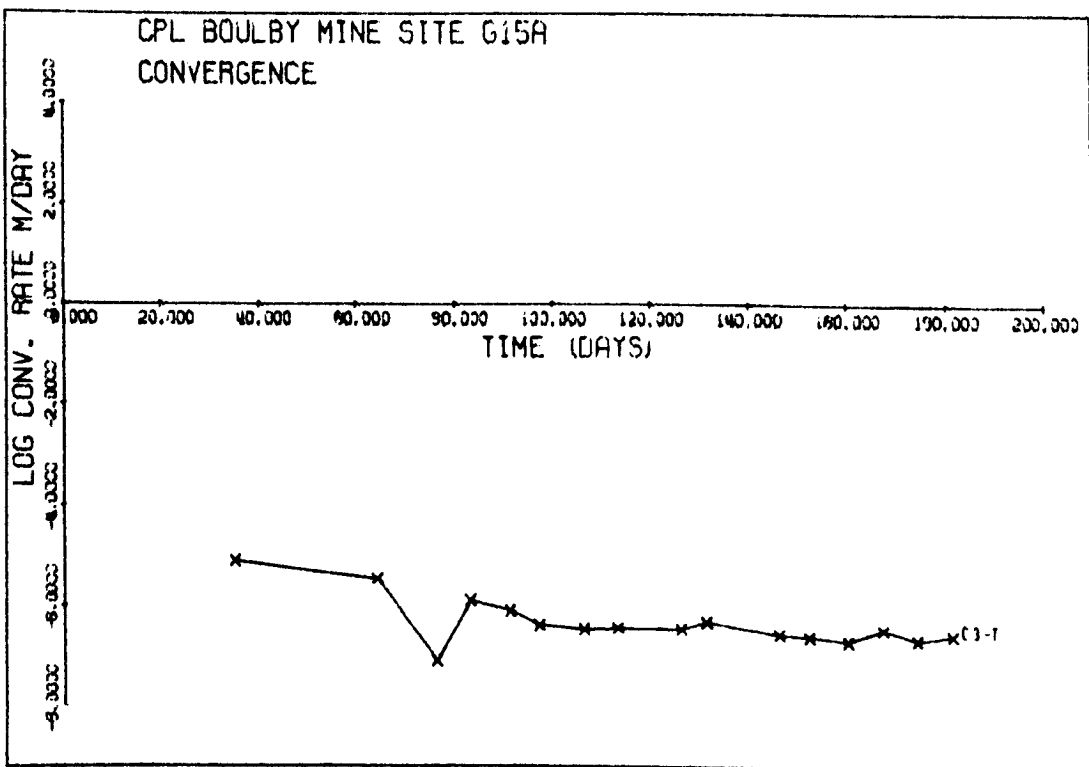
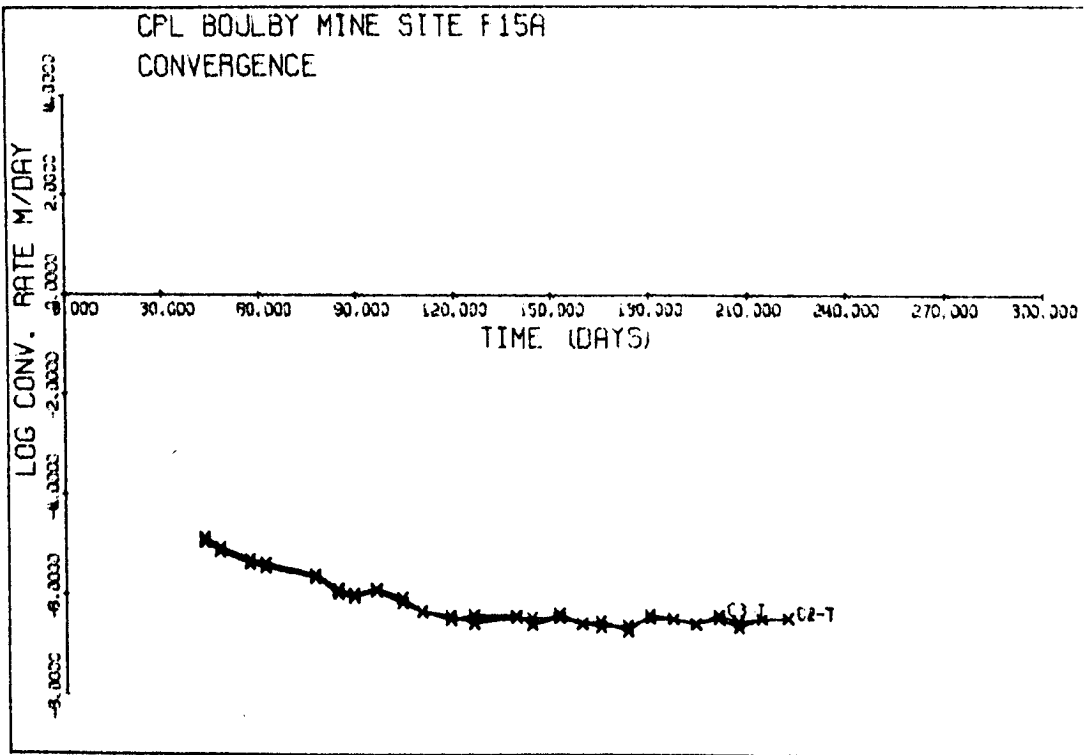


Figure 6.27 No. 15 Panel, A section - Convergence Rate

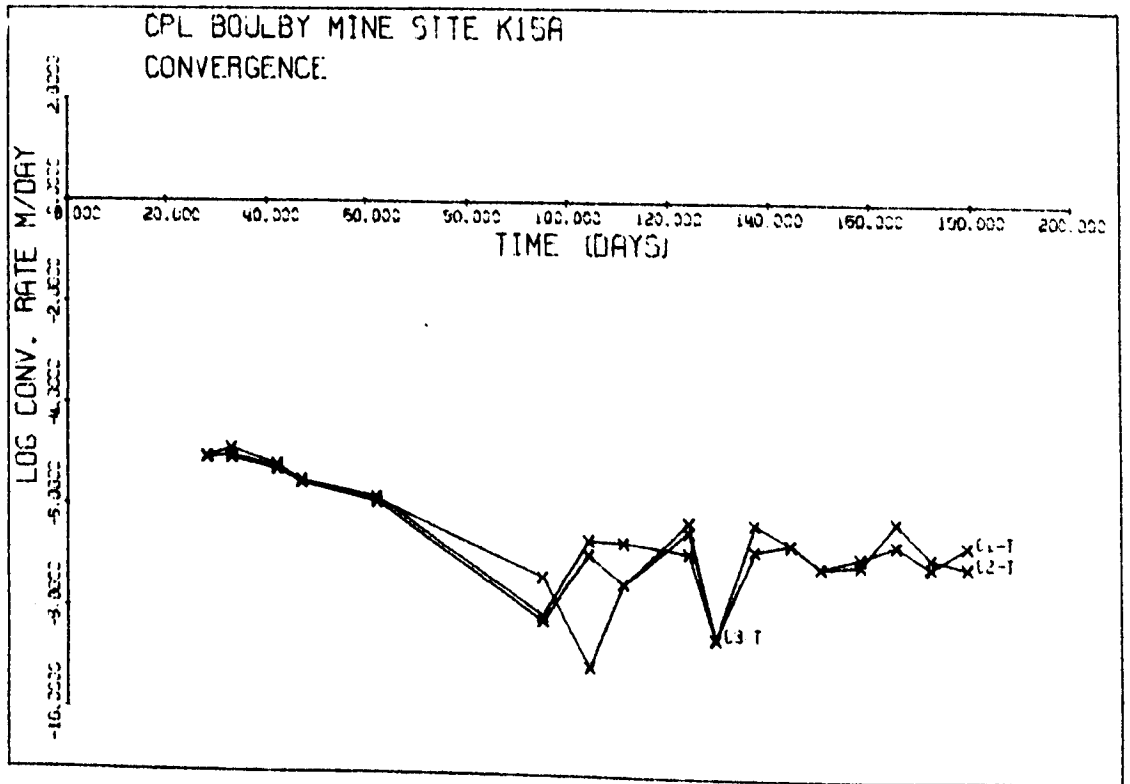
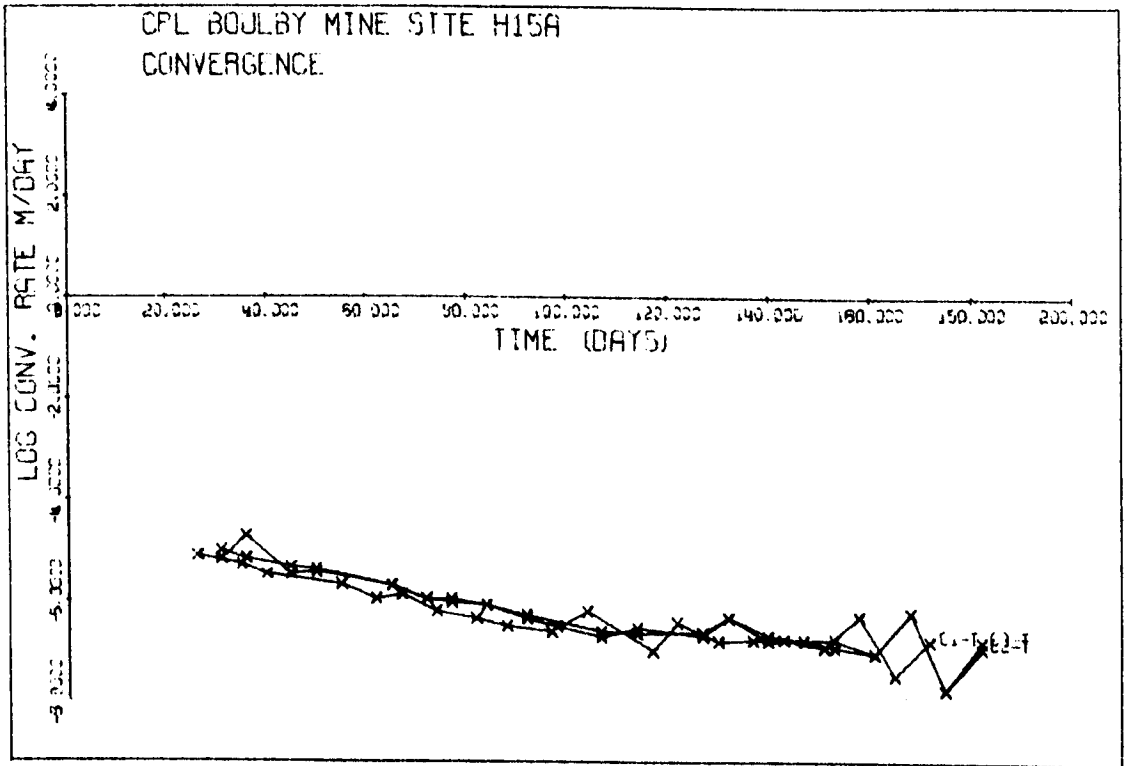


Figure 6.27 No. 15 Panel, A section - Convergence rate (Contd.)

TABLE 6.10

No. 15 Panel, A section, Closures (c), mm, and Closure Rates (ċ), mm/day

Days	20		40		60		80		100		120	
	c	ċ										
E 15 B C1	126	4.7	197	2.7	238	1.5	261	0.9	274	0.5	282	0.3
C2	141	5.0	213	2.5	250	1.3	269	0.7	279	0.3	283	0.2
C3	217	7.6	328	3.9	286	2.0	415	1.0	431	0.5	438	0.3
F 15 B C1	145	5.1	221	2.7	260	1.4	281	0.7	292	0.4	298	0.2
C2	114	4.4	183	2.7	225	1.6	251	1.0	266	0.6	276	0.4
C3	146	5.2	222	2.7	262	1.4	282	0.7	293	0.4	299	0.2
C4	127	4.7	199	2.6	239	1.5	261	0.8	274	0.5	282	0.3
H 15 B C1	178	5.8	257	2.6	292	1.1	308	0.5	315	0.2	218	0.1
C2	194	5.9	270	2.3	300	0.9	312	0.4	317	0.1	319	0.1
C3	189	5.8	265	2.3	297	0.9	309	0.4	314	0.2	316	0.1
C4	111	4.8	193	3.5	254	2.6	298	1.9	331	1.4	355	1.0

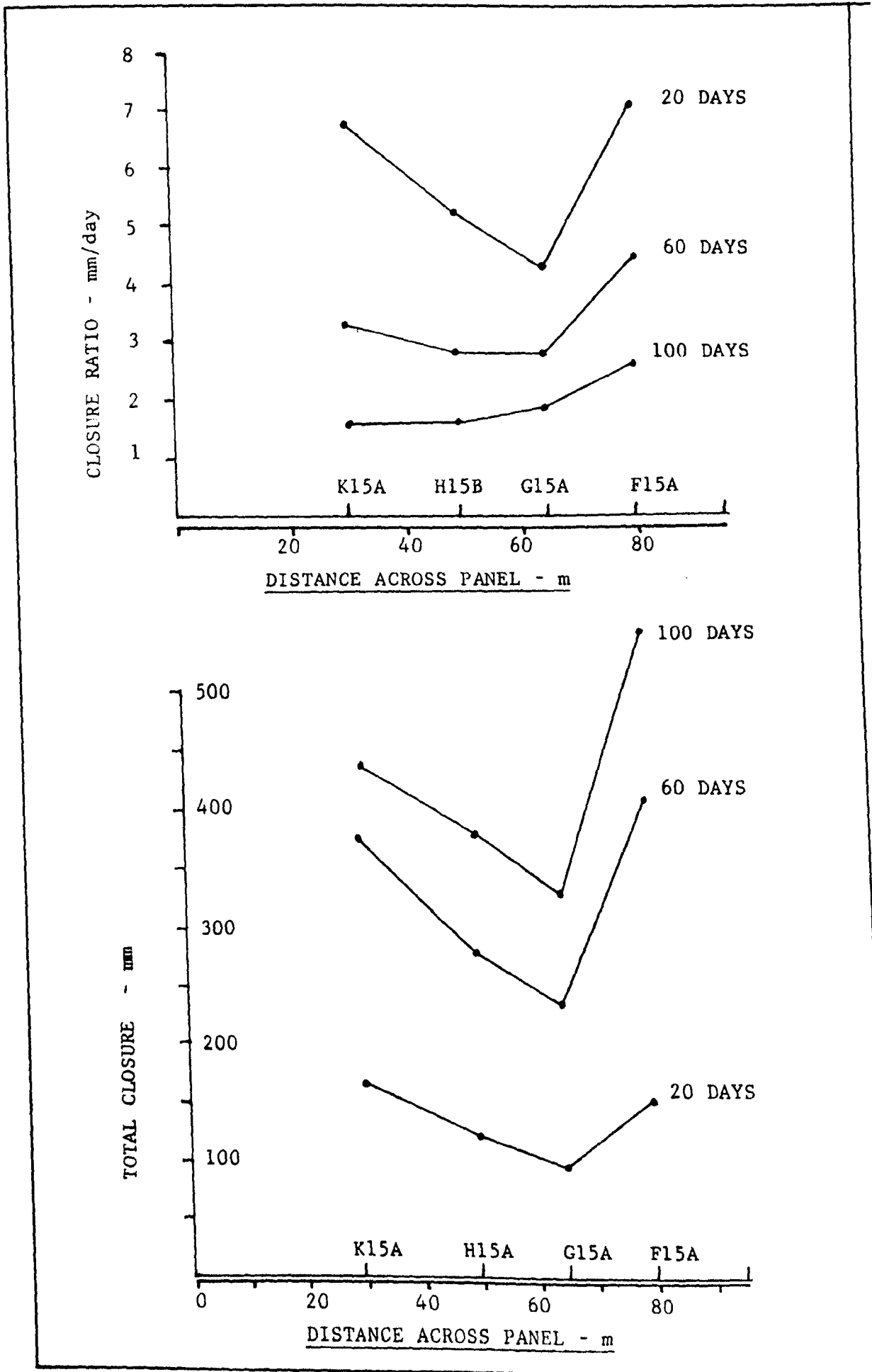


Figure 6.28 No. 15 Panel, Closure and closure rate across the panel

After 20 days the mean roof to floor closure rate at the 'A' sites is 6.42mm per day, and at the 'B' sites, 5.5mm per day. This result shows that the 'B' sites are achieving stability more rapidly than the 'A' sites. From the graphs of closure and closure rate across the panel, Figure 6.31, it can be seen that the roof sag is very even across the panel. At this point the panel is 41m wide.

6.7.3 Extensometer Sites - No. 15 Panel, B section

Extensometers were installed at two sites, designated H 15 B and 17 15 B. The purpose of this instrumentation was to monitor the performance of the 40m central pillar in order to ascertain whether, when, and to what extent, it was developing a stable core. This was important as the pillar was designed to be load bearing.

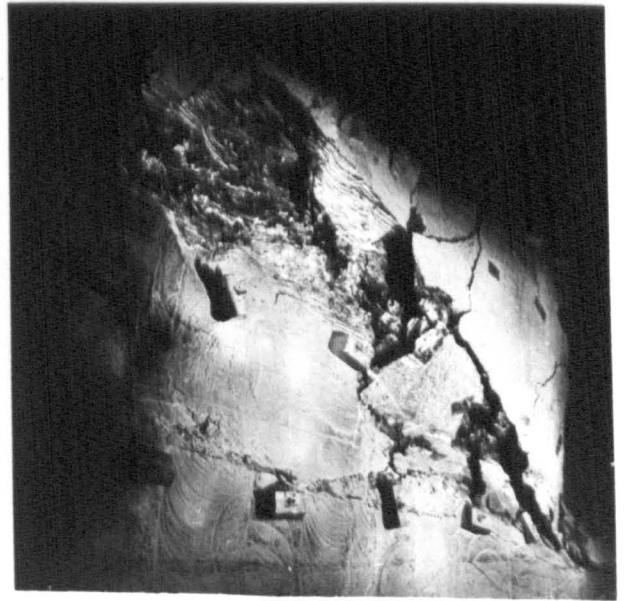
Site 17 15 B

Two boreholes were used in this installation with a total of six anchors installed. Experience had demonstrated that the maximum number in any one hole should not exceed four. This was mainly to prevent the monel wire from intertwining and giving false readings. The anchor depths in borehole 01 were 4m and 8m and in borehole 02, they were at 2m, 12m, 16m and 20.5m. Installation was carried out eight days after mining and the resulting combined graphs are given in Figure 10.8. The results from these boreholes are discussed further in Chapter 10 where they form part of the design and monitoring of the panel layout in this section of No. 15 Panel.

Plate 6.15

No.15 Panel B Section
15/5/1980

- 1 F road at R.M. site looking East
- 2 J/17 Cross cut looking South at R.M. Ext. site 17 15 B
- 3 E roadway at 16 Cross cut looking West
- 4 Looking East at North sidewall at 16 Cross cut



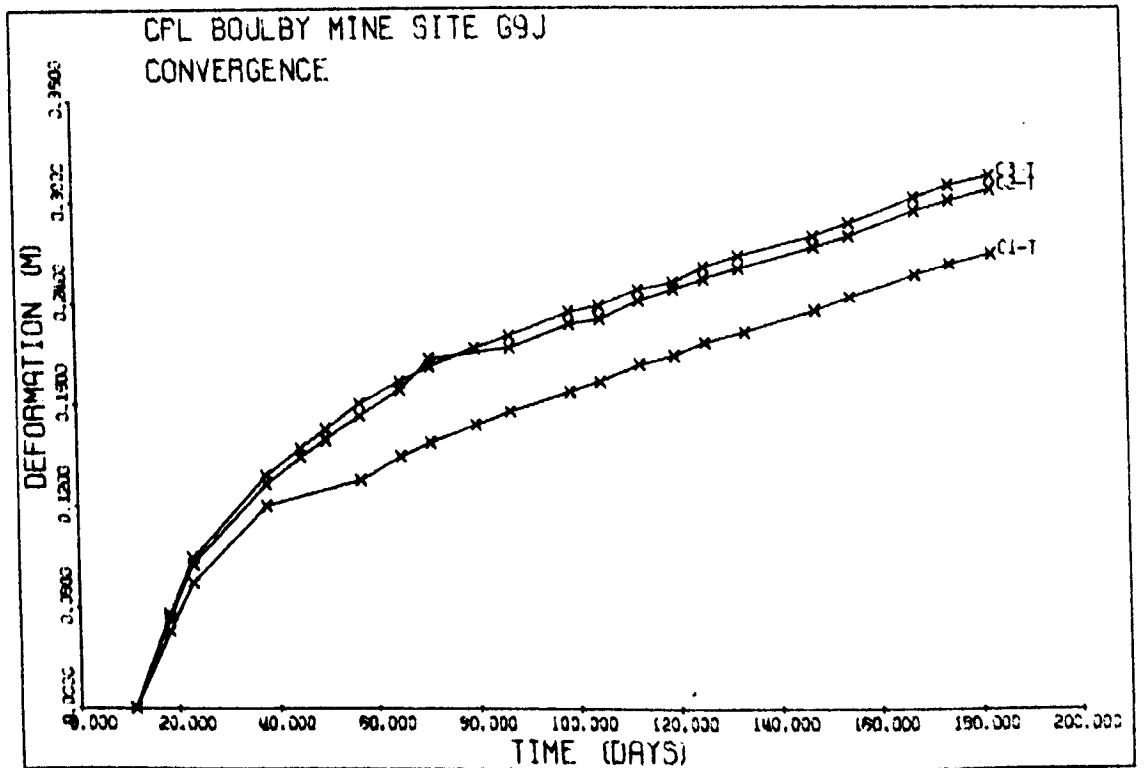
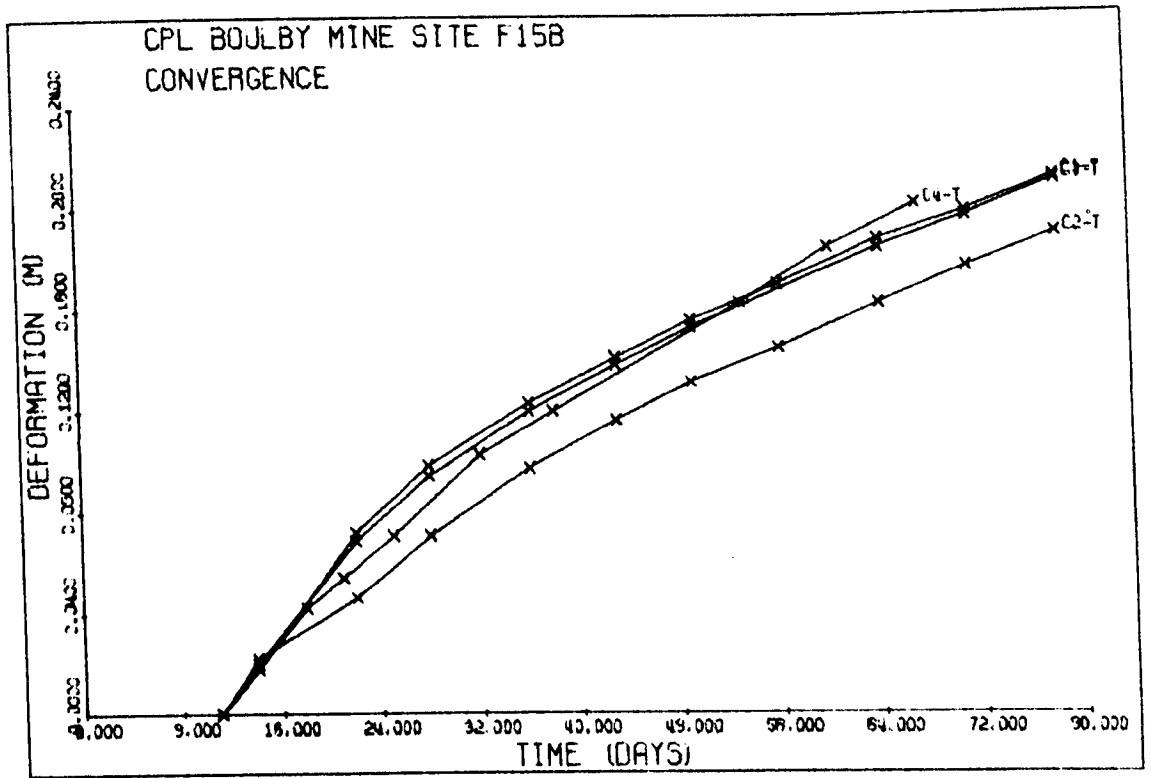


Figure 6.29 No. 15 Panel, B section - Convergence

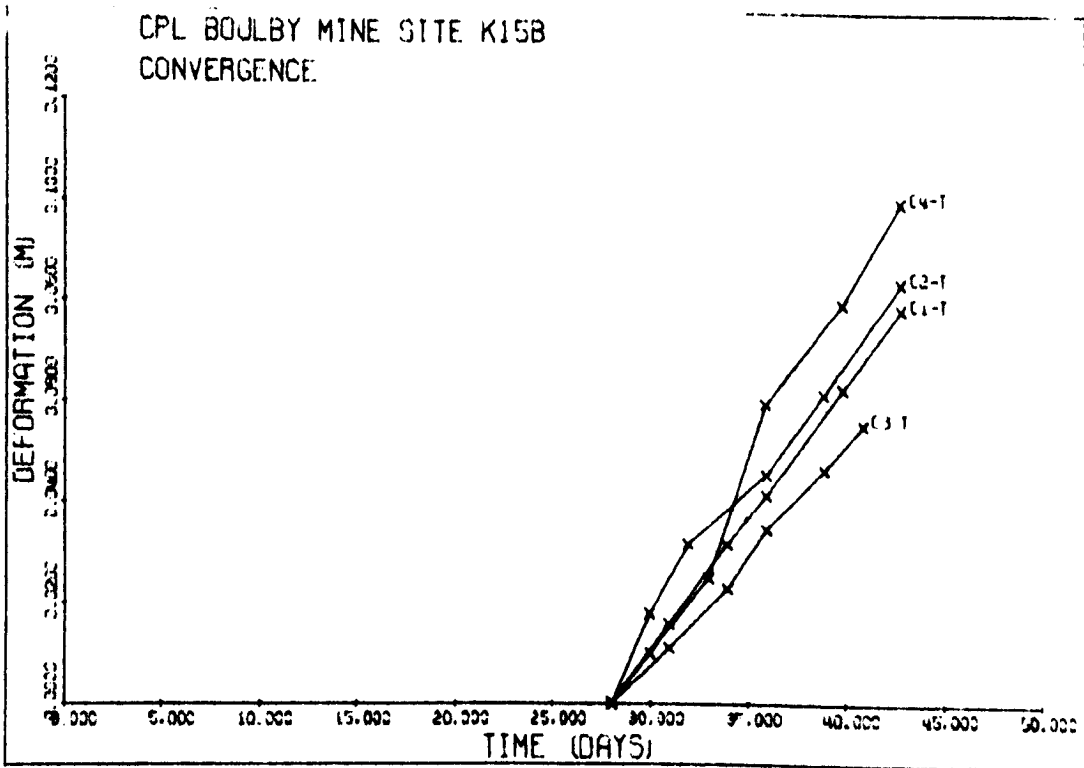
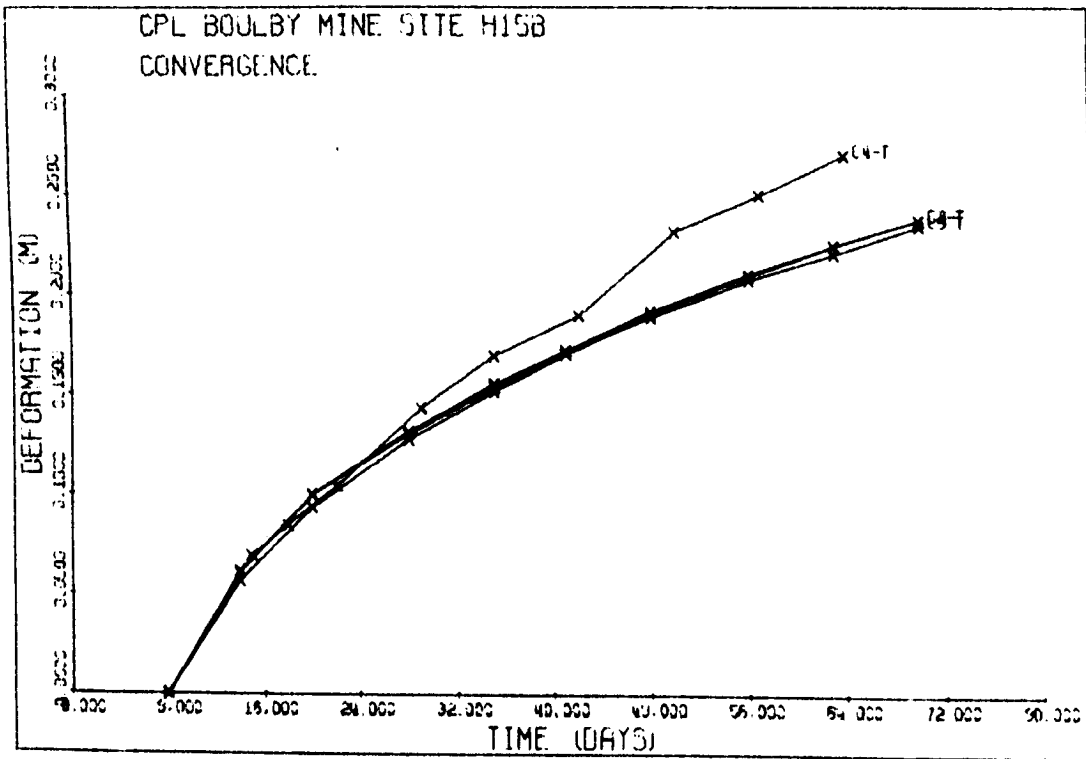


Figure 6.29 No. 15 Panel, B section - Convergence (Contd.)

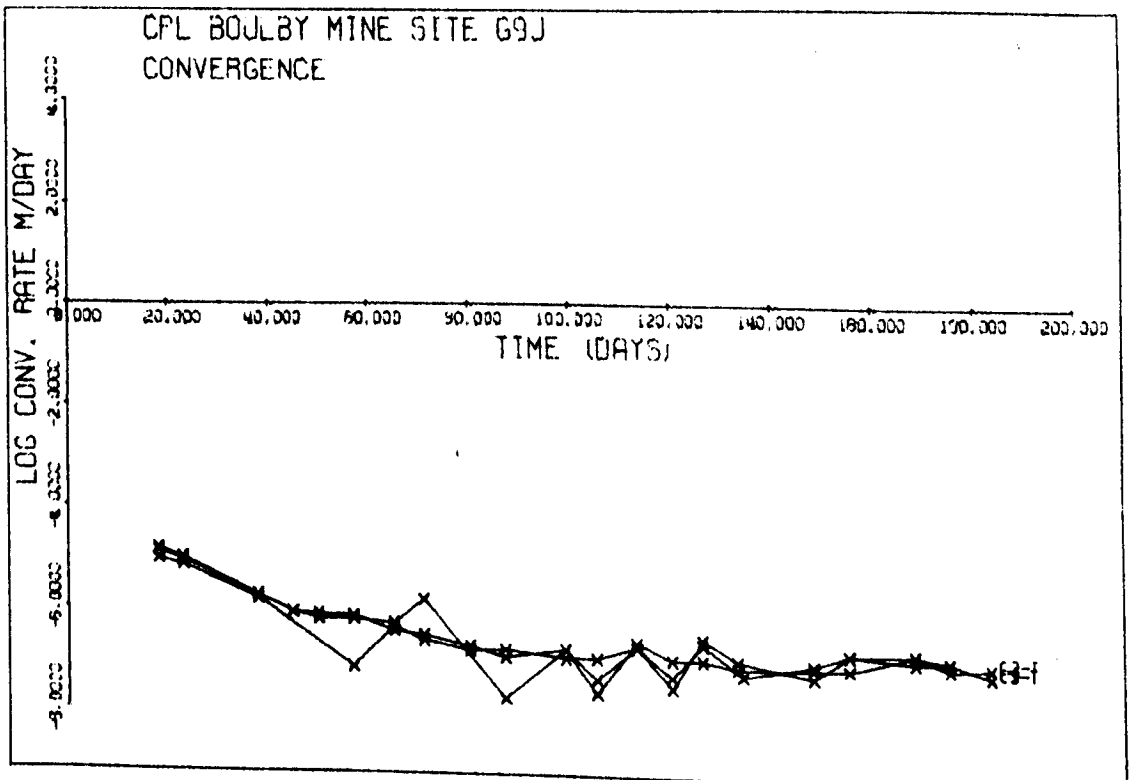
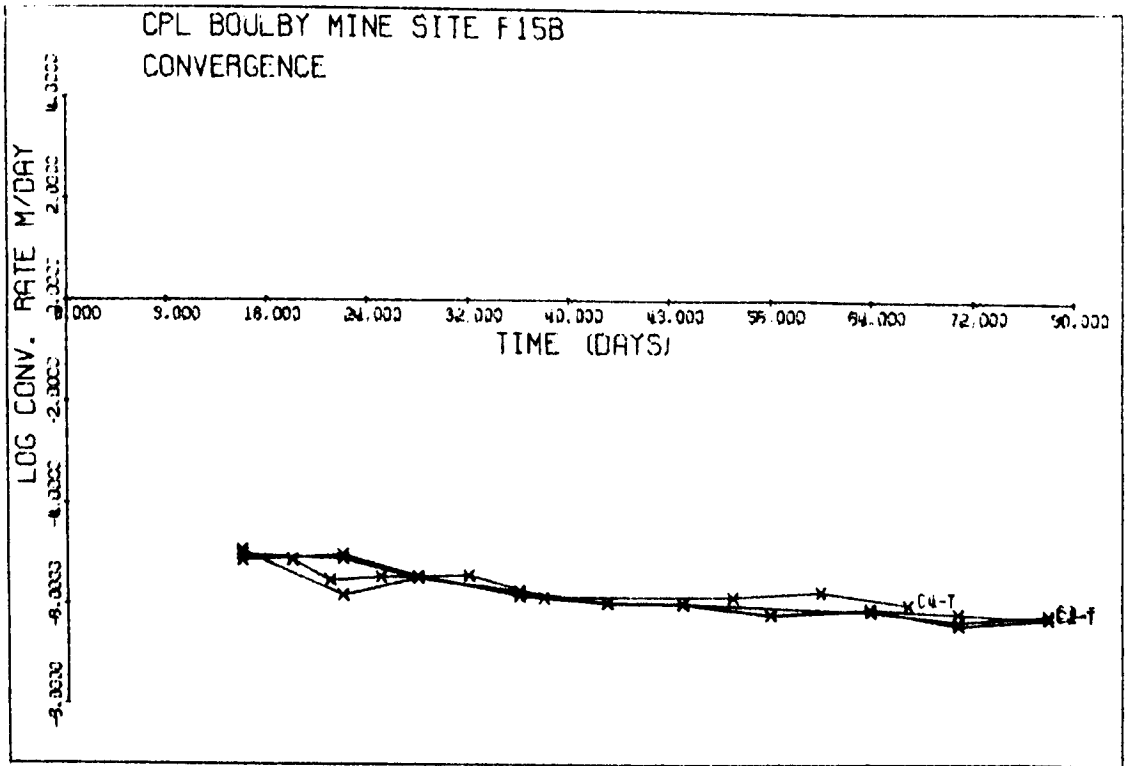


Figure 6.30 No. 15 Panel, B section Convergence rate

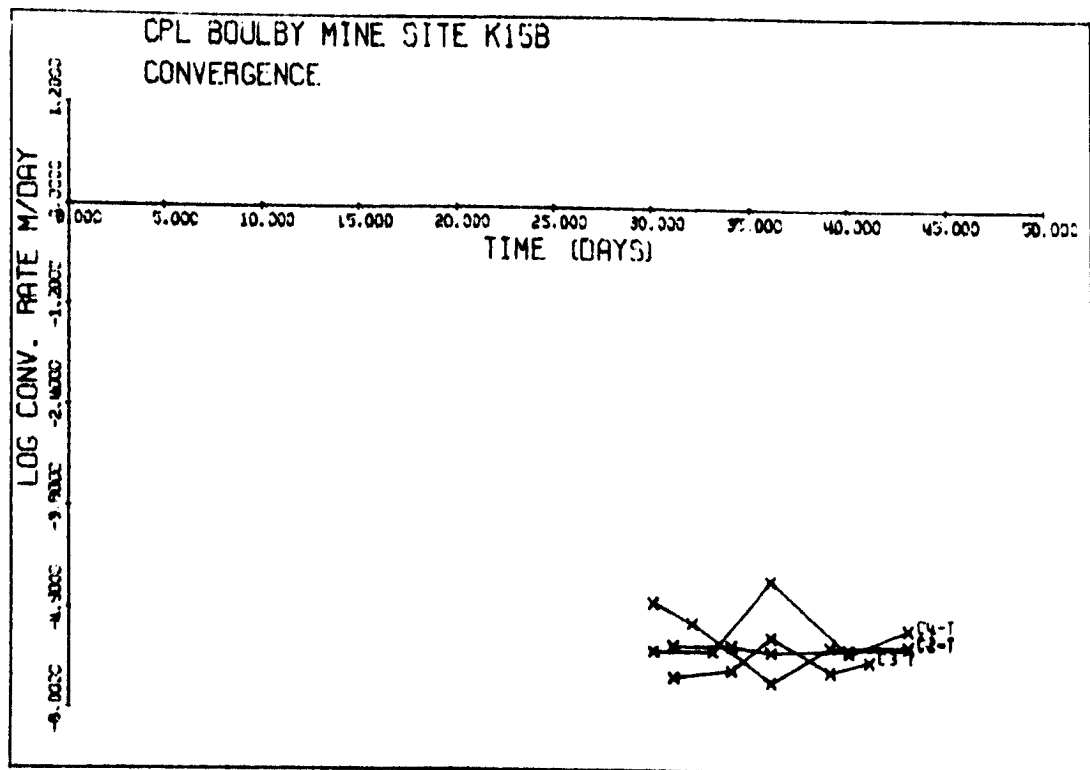
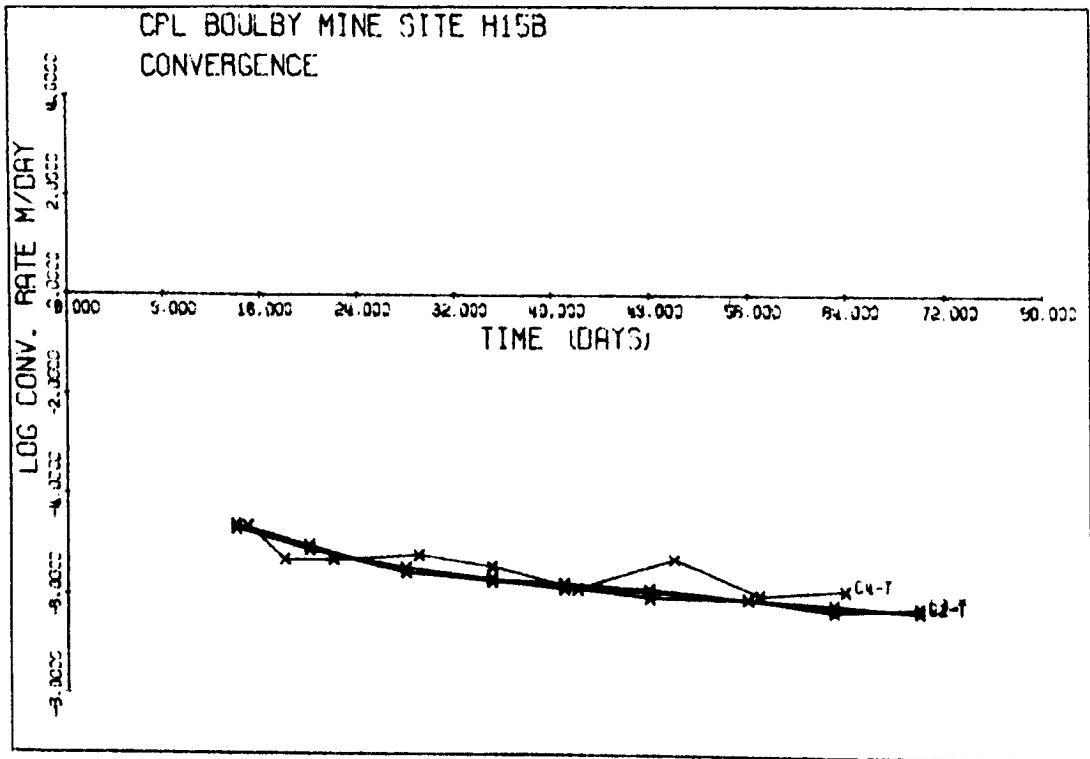


Figure 6.30 No. 15 Panel, B section - Convergence (Contd.)

TABLE 6.11

No. 15 Panel, B section, Closure (c), mm, and Closure Rates (\dot{c}), mm/day

Days	20		40		60		80		100		120		
	c	\dot{c}											
F 15 A	C1	178	7.7	313	5.9	416	4.5	494	3.4	553	2.6	598	2.0
	C2	163	7.1	288	5.5	385	4.3	460	3.3	518	2.5	563	3.0
	C3	153	6.7	272	5.2	365	4.1	437	3.2	493	2.5	537	1.9
6 15 A	C3	95	4.3	172	3.5	235	2.8	286	2.3	328	1.9	362	1.5
	C1	122	5.2	213	3.9	280	2.9	330	2.1	366	1.6	393	1.2
C2		127	5.4	220	4.0	289	2.9	339	2.2	376	1.6	404	1.2
	C3	117	5.1	205	3.8	272	2.9	322	2.2	359	1.6	388	1.2
K 15 A	C1	176	7.2	296	4.9	378	3.4	434	2.3	473	1.6	499	1.1
	C2	170	6.8	281	4.5	355	3.0	404	2.0	436	1.3	457	0.9
C3	236	8.7	367	4.8	440	2.7	481	1.5	503	0.8	516	0.5	

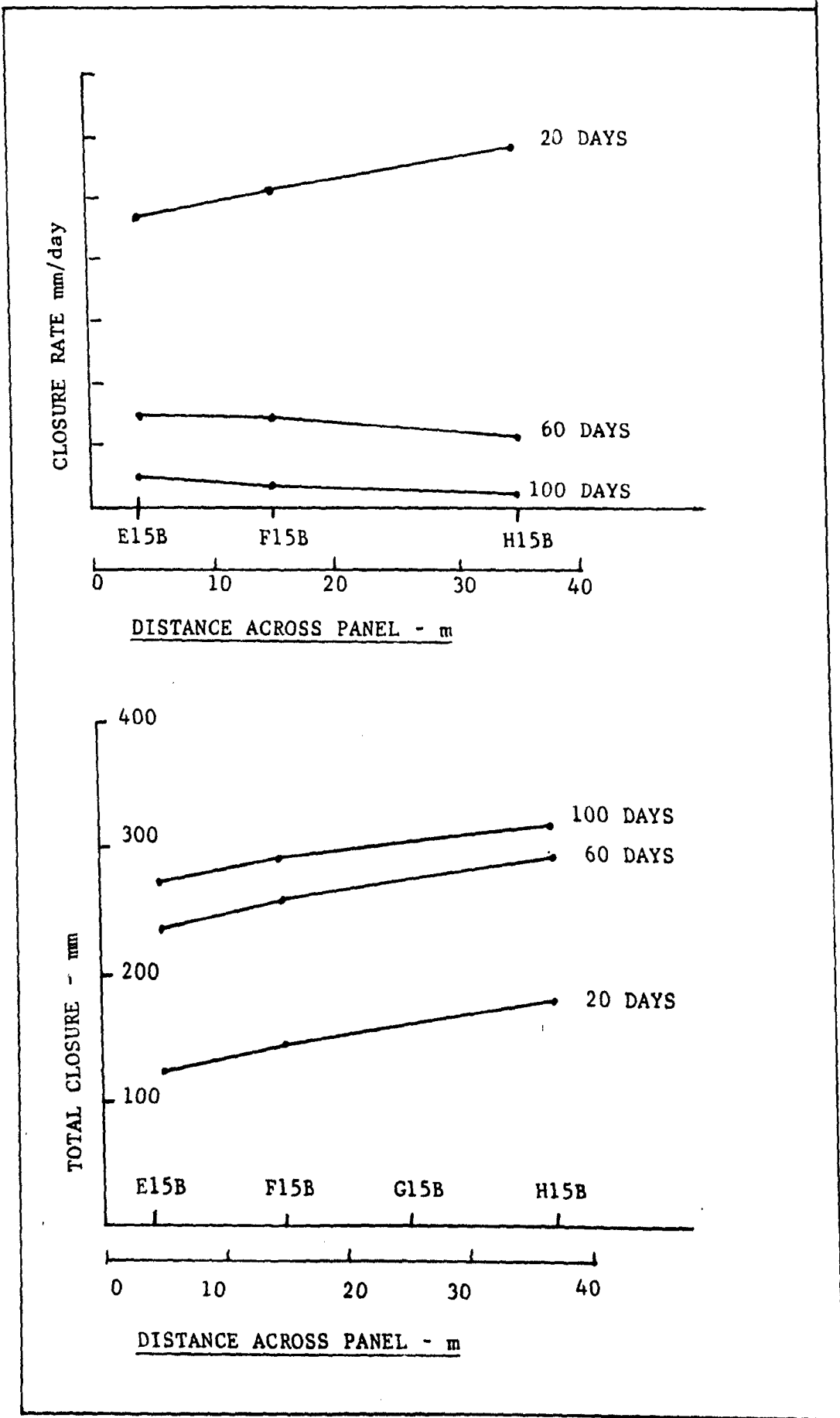


Figure 6.31 No. 15 Panel, B section - Convergence and convergence rate
across the panel

Site H 15 B, BH \emptyset 1, BH \emptyset 2 and BH \emptyset 3

As with the 17 15 B extensometers, these results are discussed in Chapter Ten and the graphical output is given in Figure 10.10 10.11 and 10.12 .BH \emptyset 1 is a roof hole with anchors at depths of 2m and 4m. Borehole \emptyset 2 is installed at 45° to the horizontal in the top corner over the pillar ribside, and has anchors at 4m and 7.5m. Borehole \emptyset 3 is a wall hole installed horizontally into the pillar with anchors at depths of 2m, 11m, 15m and 19m.

6.8 No. 16 Panel

No. 16 Panel was driven north off the West Link salt development at the same time as No. 15 Panel was started. Instrumentation sites were established as shown in Figure 6.32. Convergence measurements only were made as the microcreepmeter was found to be unstable, and constant readings could not be guaranteed. Table 6.12 gives the total closures and closure rates for 20 day intervals. Graphical output is given in Figures 6.32(a) to (j).

It was fortunate that two lines of sites were obtained across the panel, as well as a line of three sites down the panel. These have been plotted in Figure 6.33. If the closure profiles across the panel are considered it can be seen that the roof is closing uniformly. The weekly face advances are given in Appendix 6. The line down the panel shows a large increase in closure and closure rate from K 16 A to K 16 B, and it can be seen that K 16 C initially closes faster than K 16 B, but after about 80 days, the total closure is less and the closure rate much reduced. This would

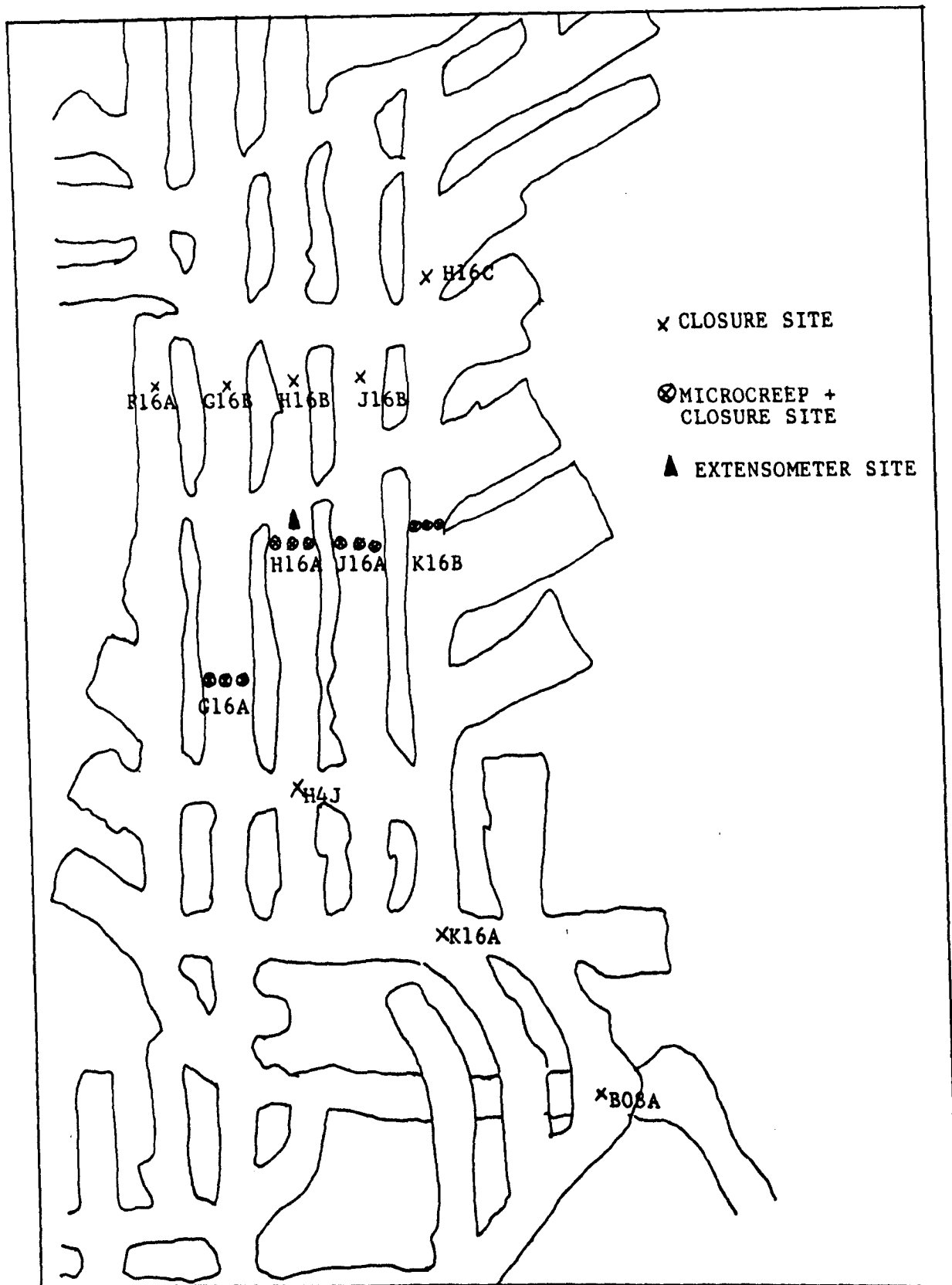


Figure 6.32 No. 16 Panel, instrumentation sites

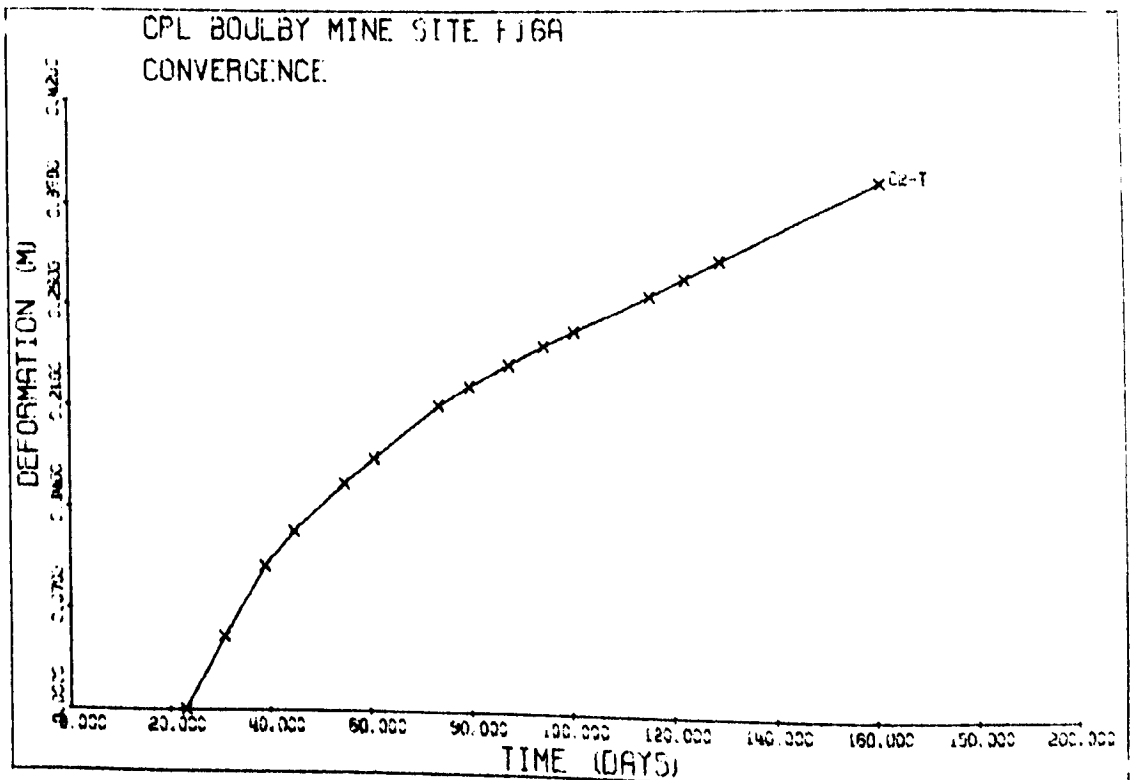
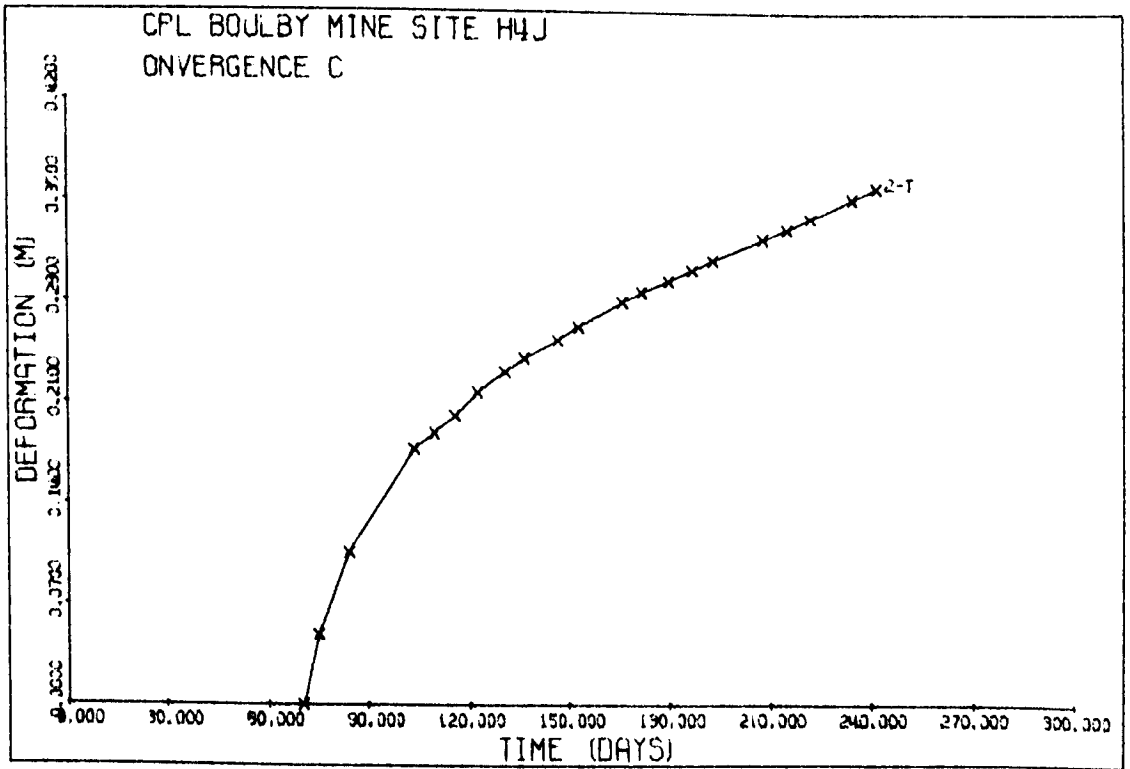


Figure 6.32 (a)

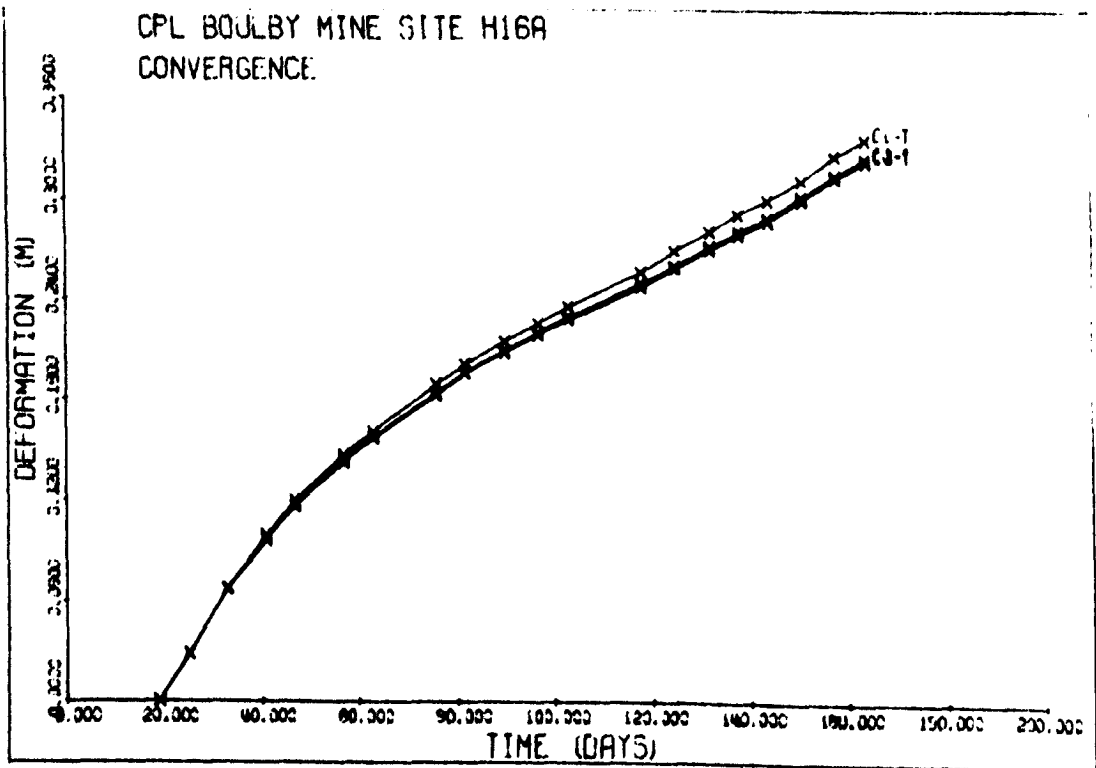
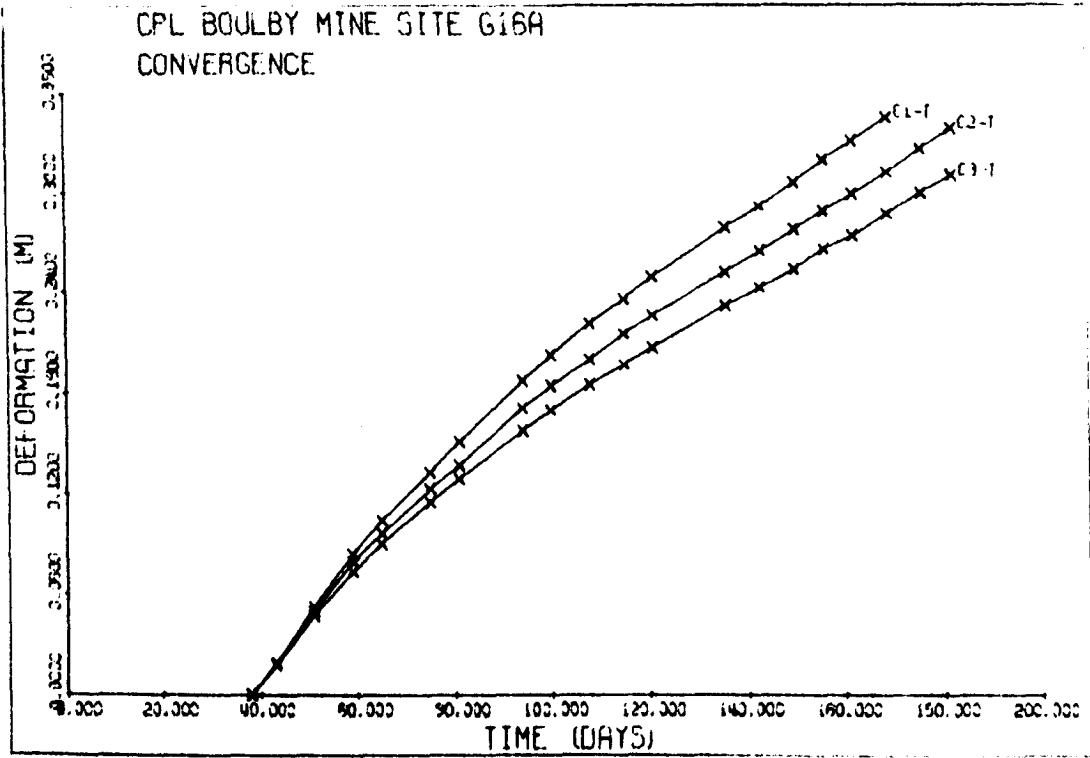


Figure 6.32 (b)

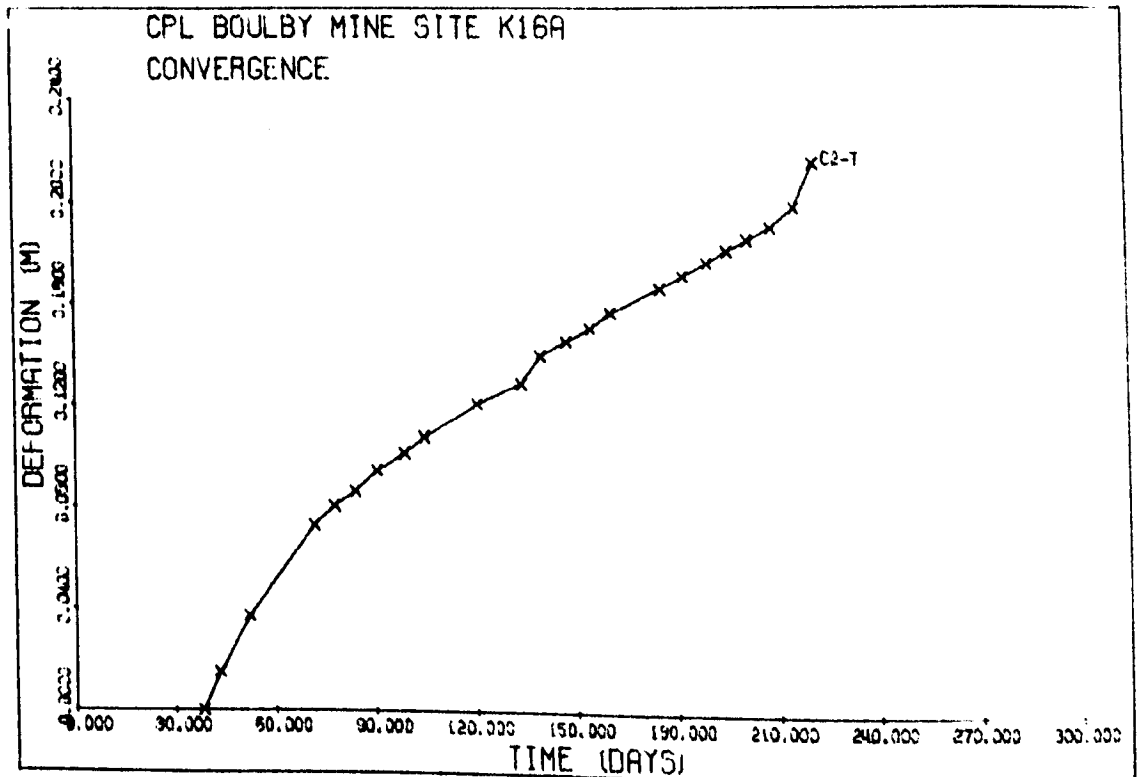
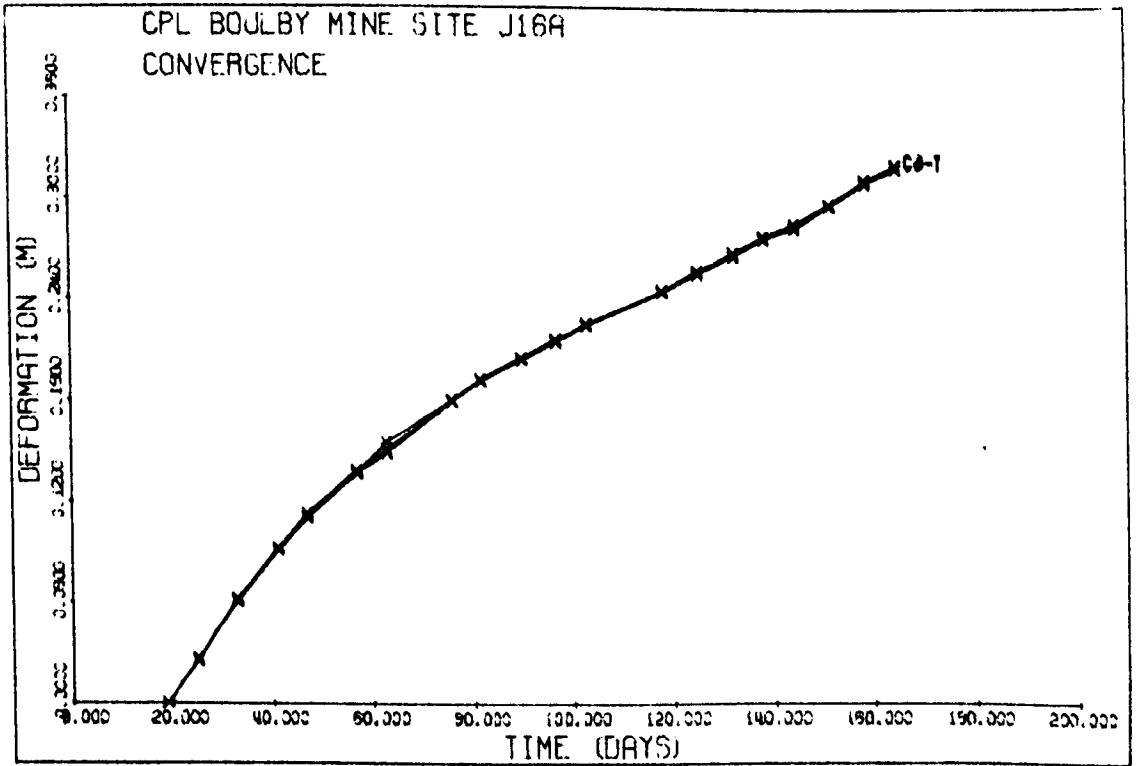


Figure 6.32 (c)

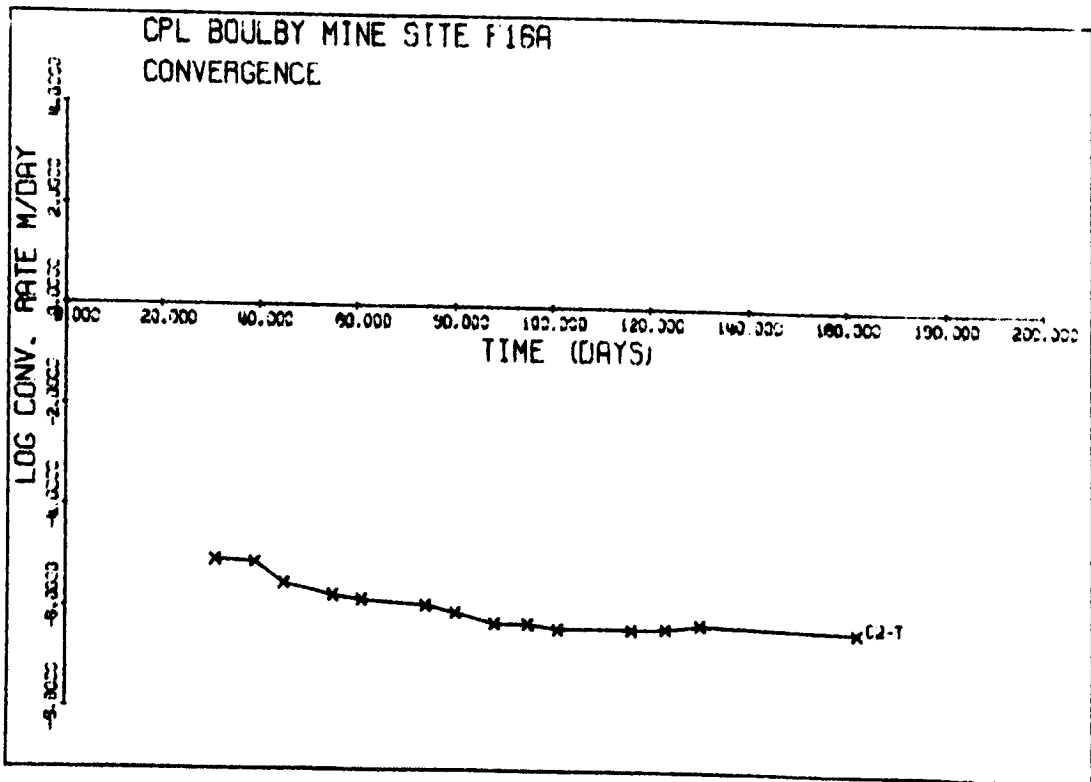
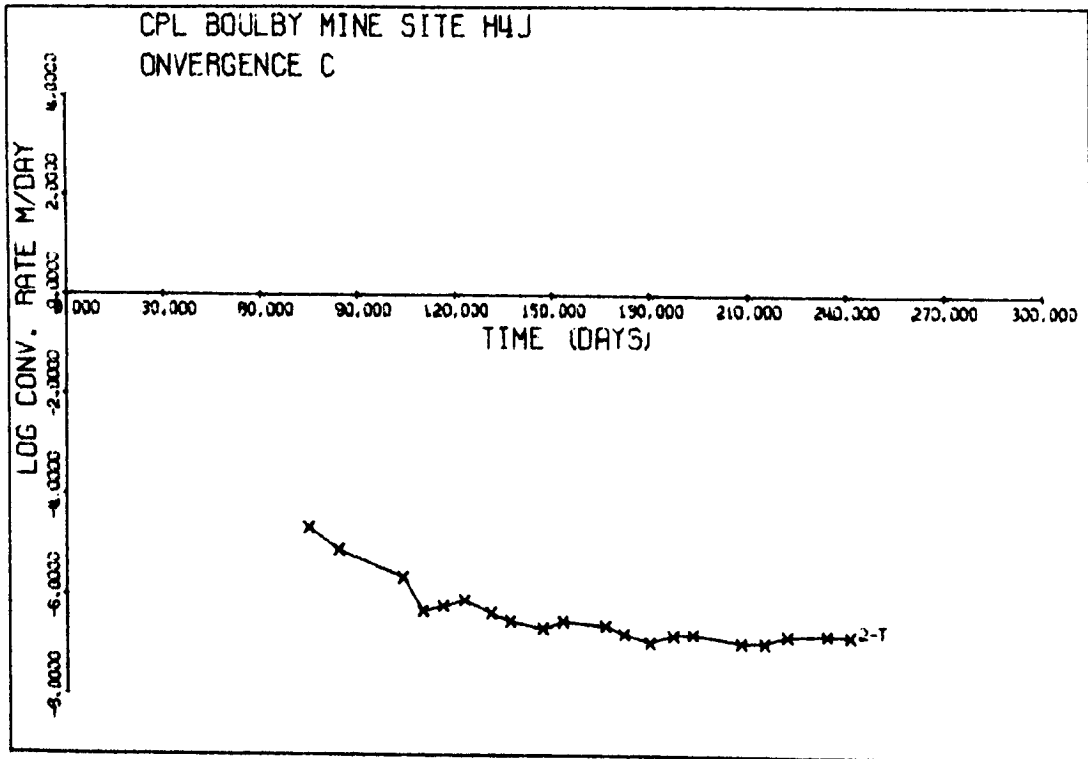


Figure 6.32 (d)

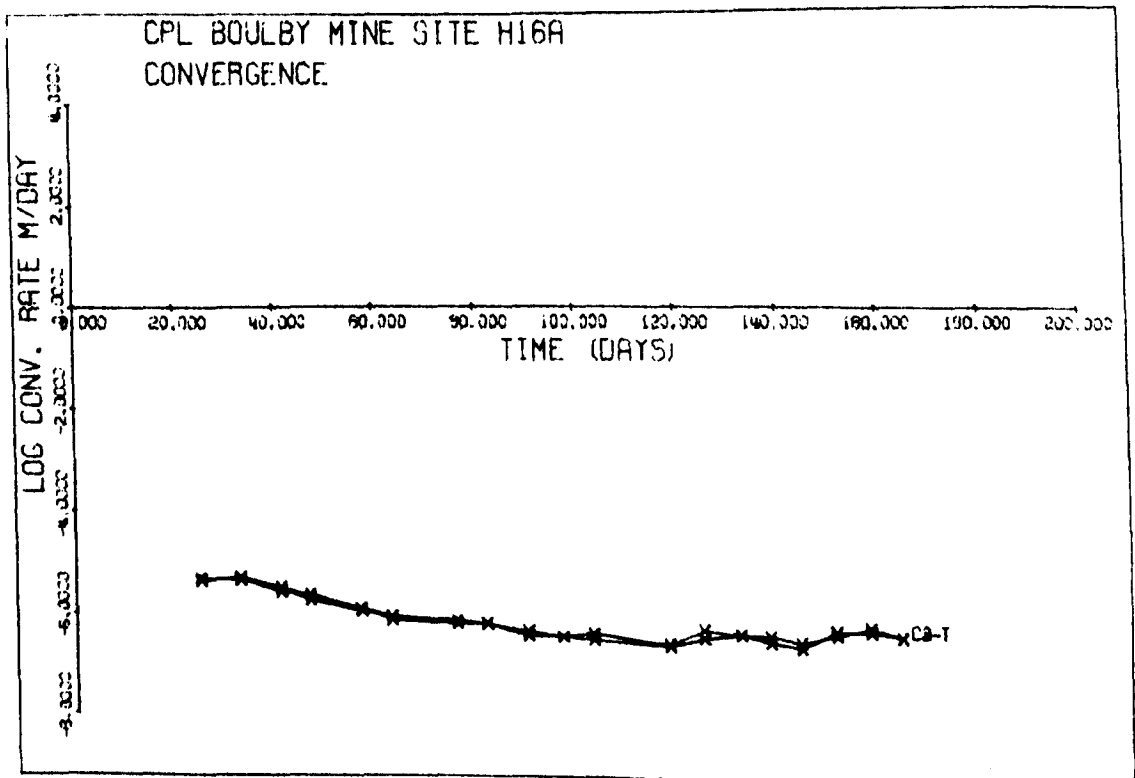
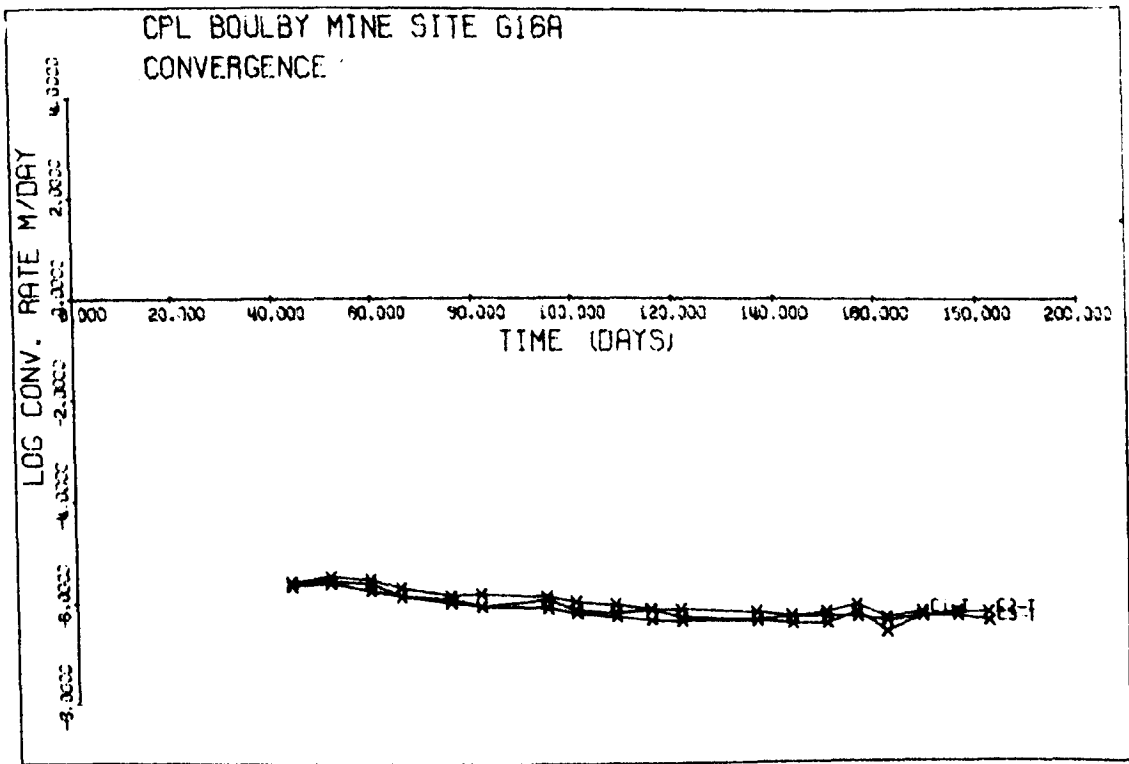


Figure 6.32 (e)

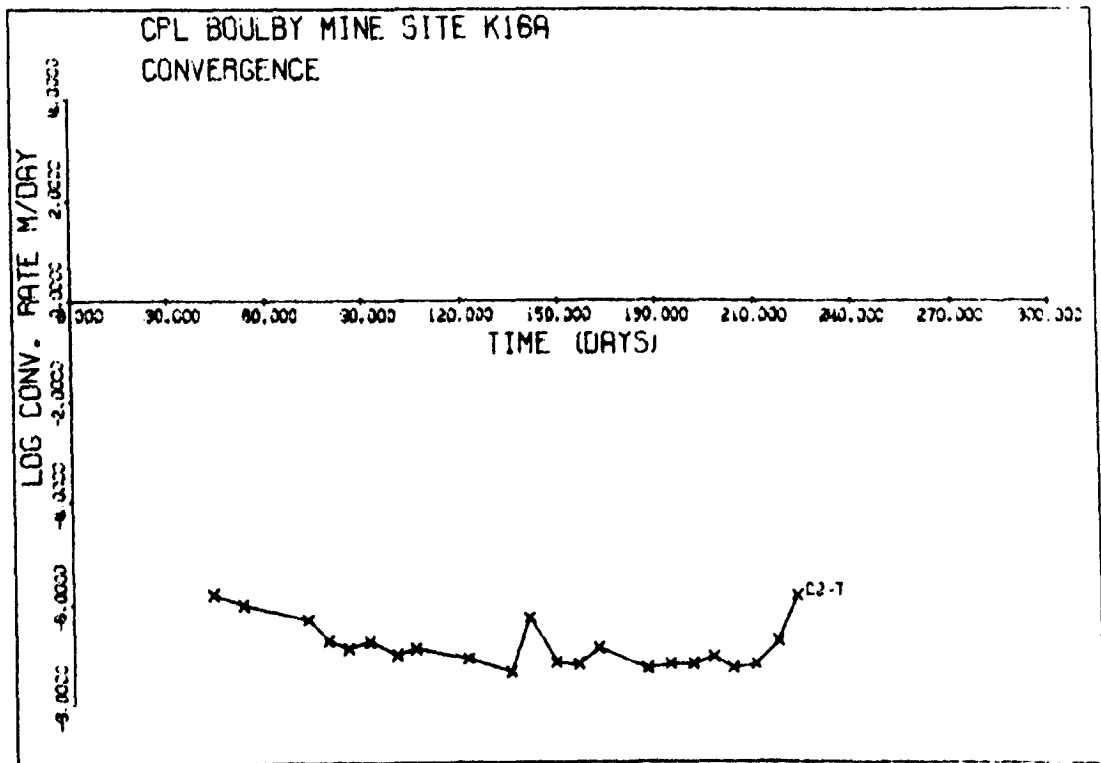
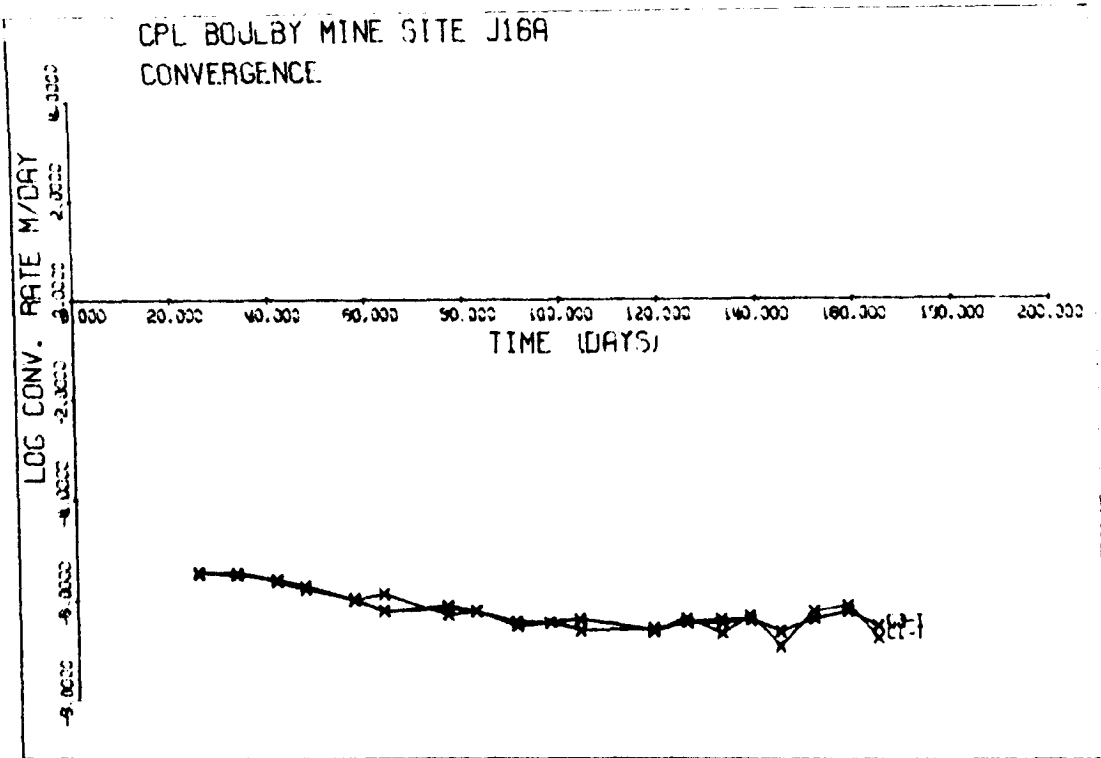


Figure 6.32 (f)

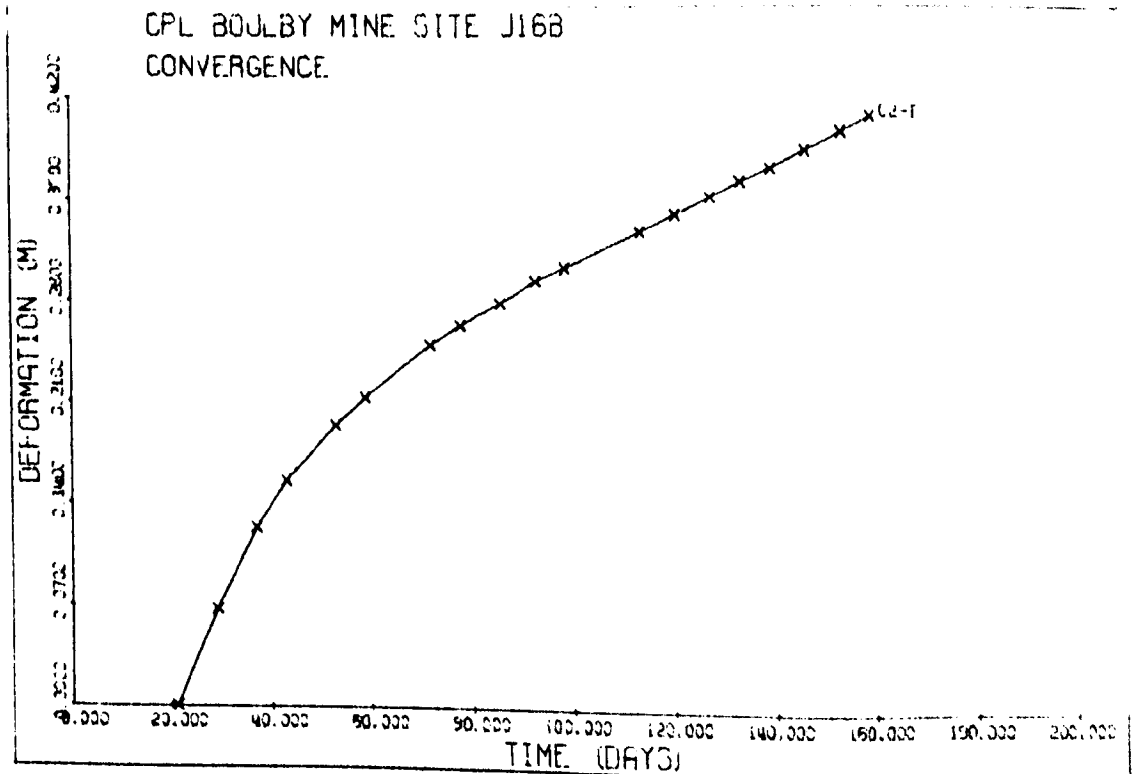
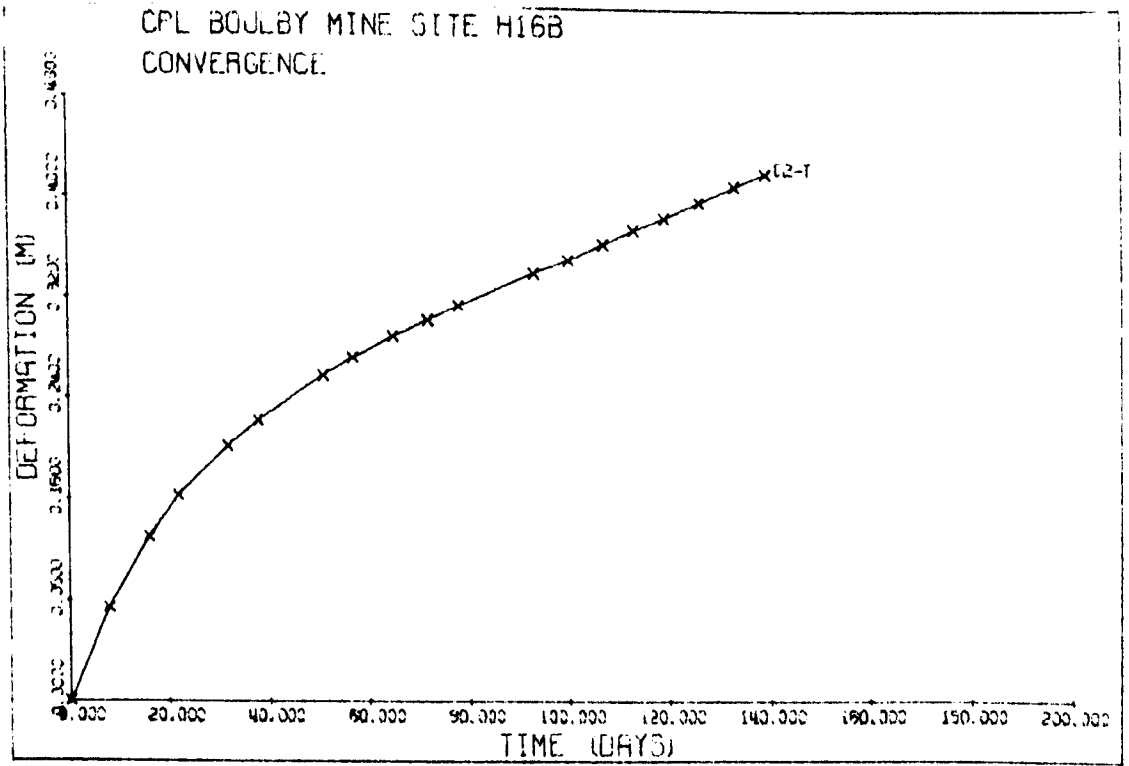


Figure 6.32 (g)

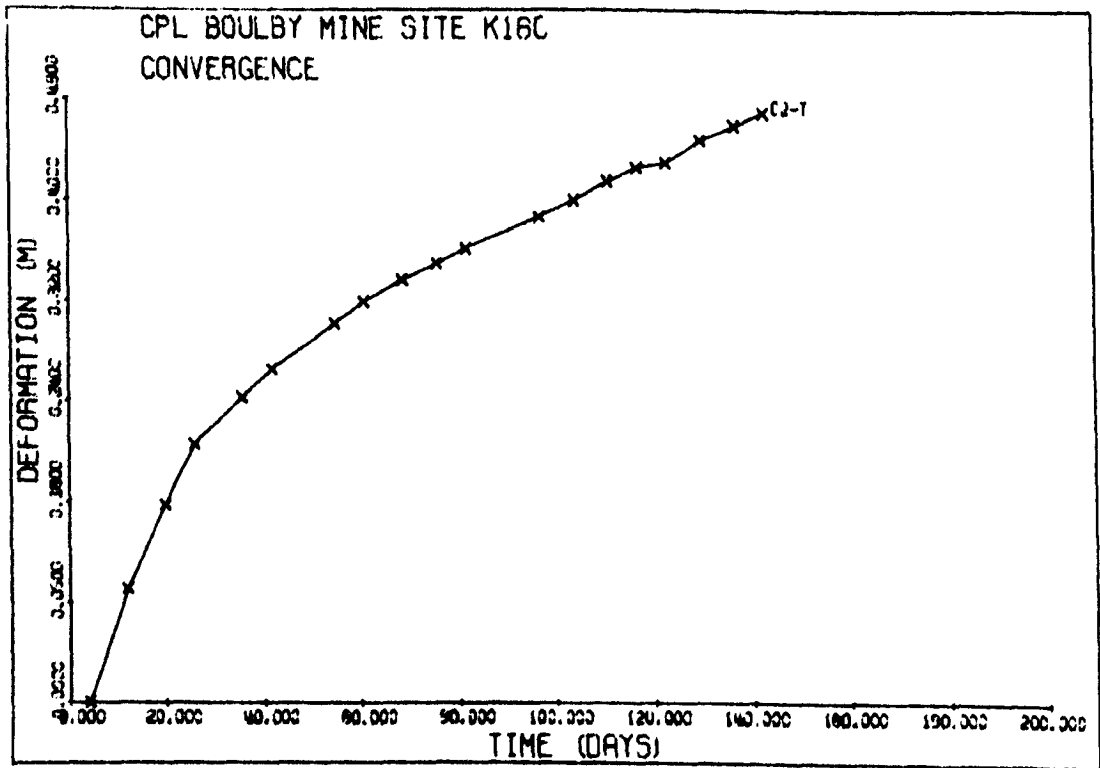
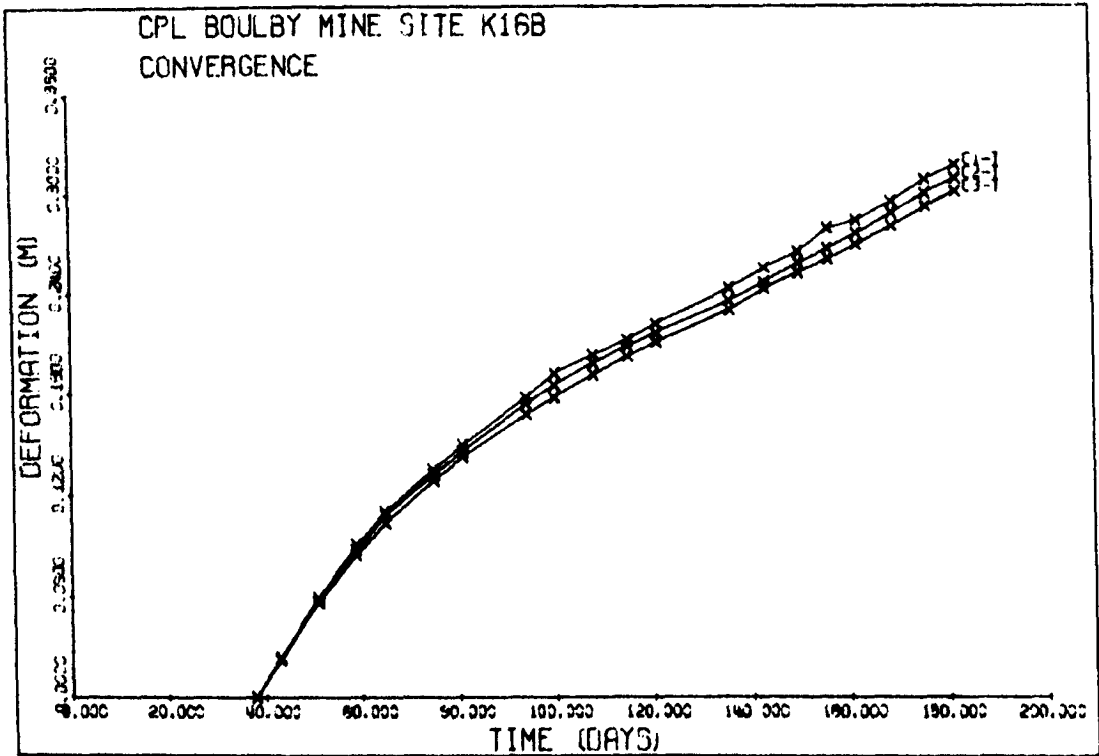


Figure 6.32 (h)

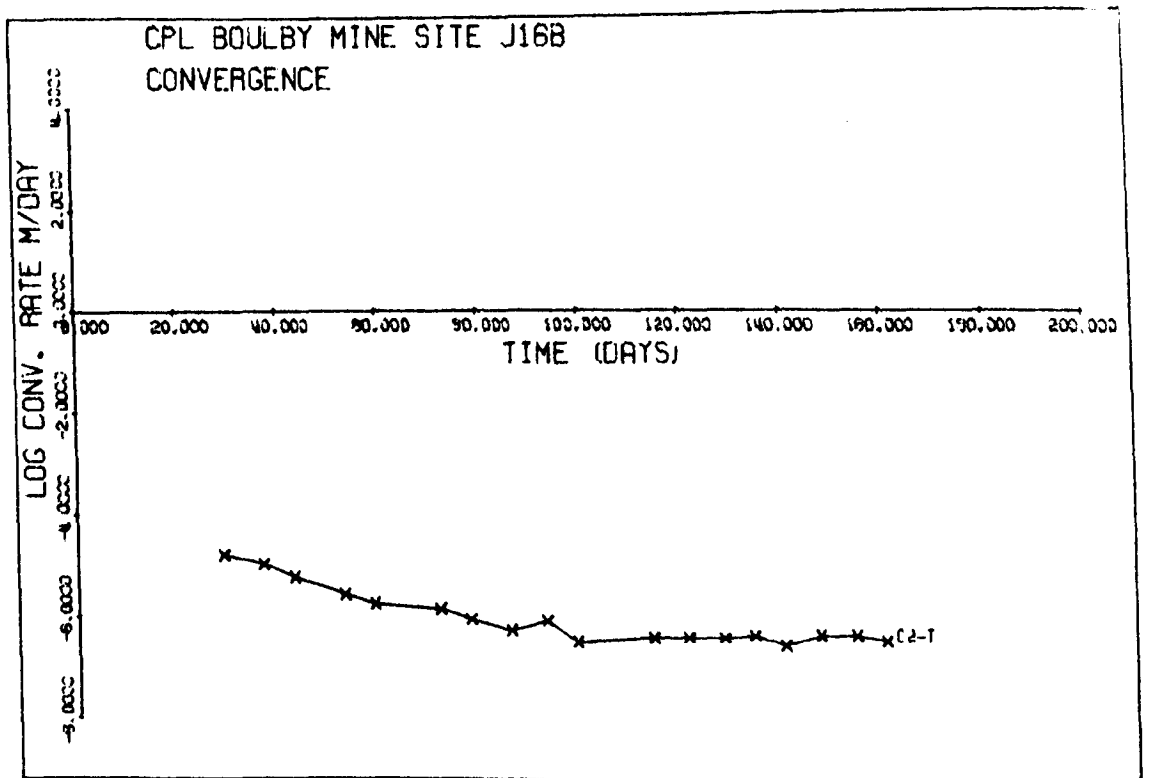
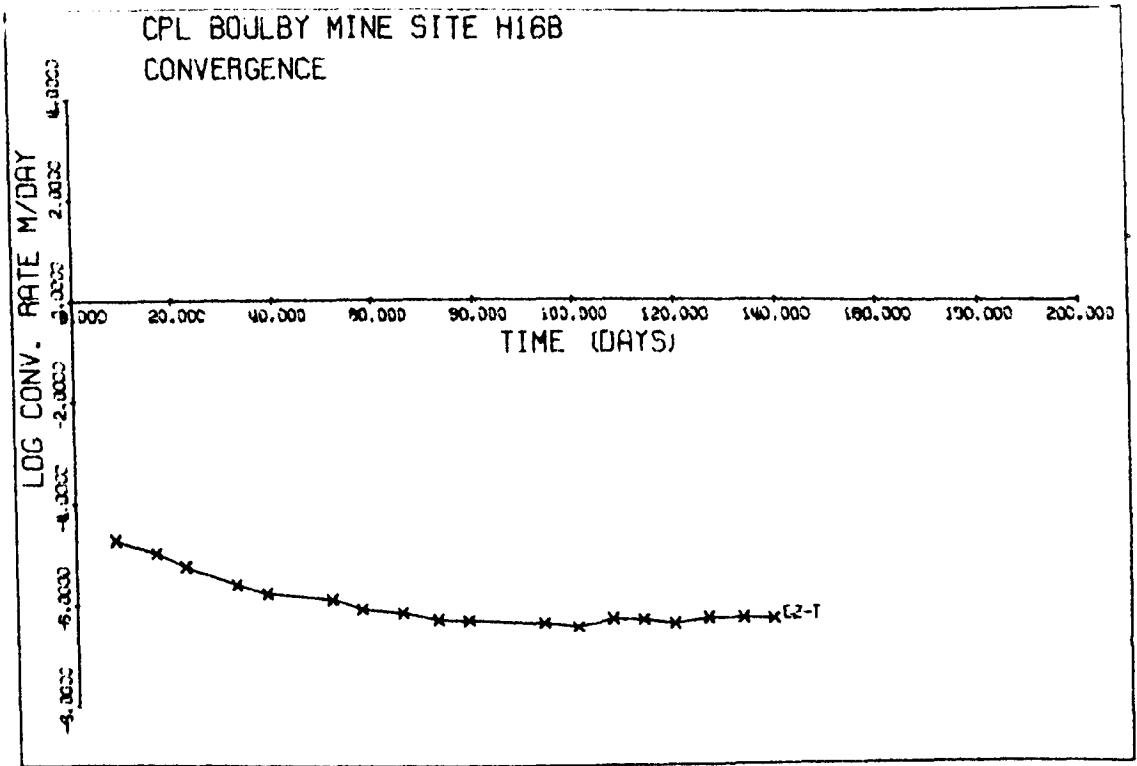


Figure 6.32 (i)

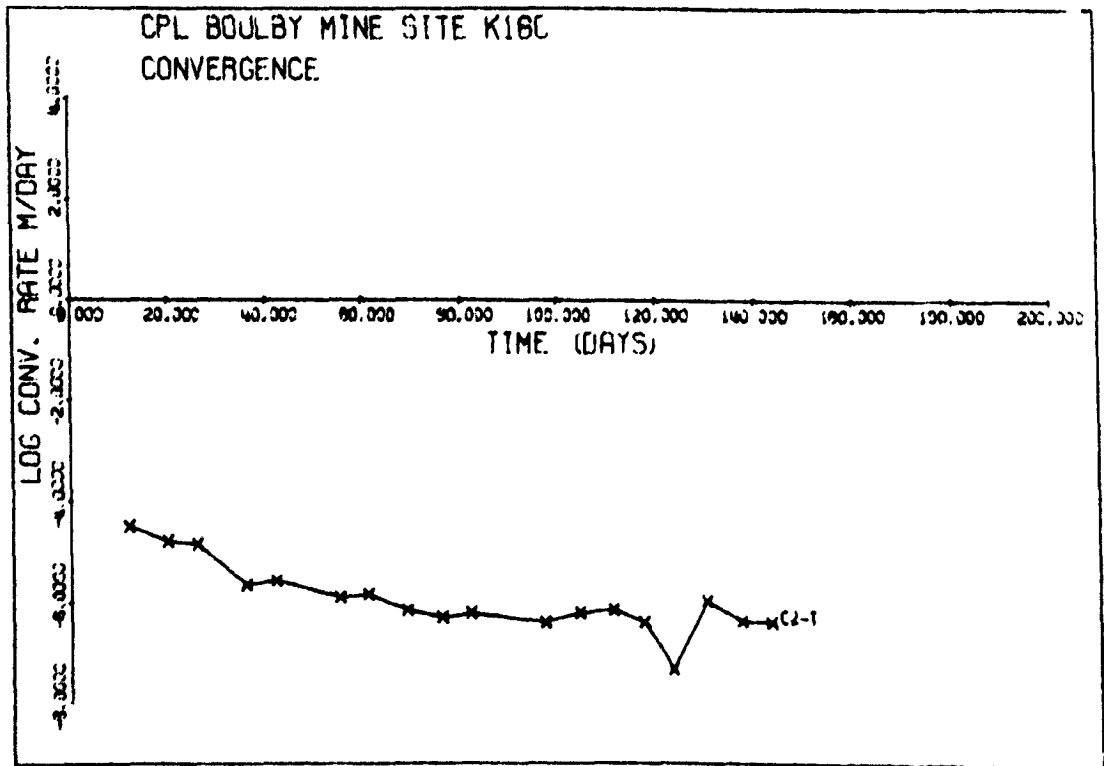
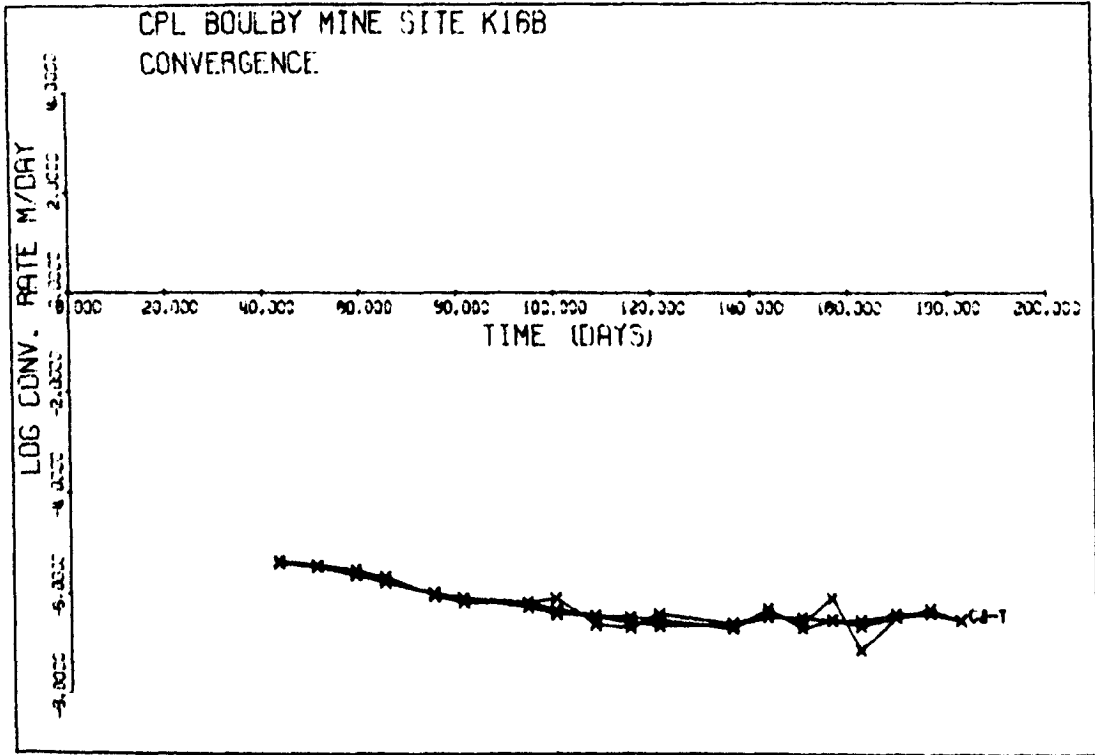


Figure 6.32 (j)

TABLE 6.12

No. 16 Panel, Closure (c), mm and Closure Rates (ċ) mm/day for 20 day intervals

Days	20		40		60		80		100		120	
	c	ċ	c	ċ	c	ċ	c	ċ	c	ċ	c	ċ
E 16 A C2	163	6.7	275	4.6	351	3.2	404	2.2	440	1.5	464	1.0
6 16 A C1	108	5.0	199	4.2	275	3.5	339	2.9	393	2.4	438	2.1
C2	103	4.7	188	3.8	258	3.2	315	2.6	363	2.2	402	1.8
C3	102	4.6	185	3.7	251	3.0	305	2.4	348	1.9	383	1.6
H 16 A C1	115	4.9	199	3.6	261	2.7	307	2.0	341	1.4	366	1.1
C2	113	4.8	196	3.5	257	2.6	302	1.9	334	1.4	358	1.0
C3	114	4.8	197	3.5	258	2.6	302	1.9	334	1.4	357	1.0
K 16 A C2	51	2.3	94	2.0	131	1.7	161	1.4	187	1.2	208	1.0
J 16 A C1	107	4.6	186	3.4	245	2.5	289	1.9	321	1.4	345	1.0
C2	112	4.8	195	3.5	254	2.5	298	1.8	329	1.3	352	1.0
C3	104	4.5	182	3.4	240	2.5	284	1.9	317	1.4	341	1.1
H 16 B C2	135	5.3	221	3.4	276	2.2	311	1.4	323	0.9	347	0.6
K 16 B C1	156	6.6	268	4.7	349	3.4	407	2.5	450	1.8	480	1.3
C2	156	6.6	267	4.7	347	3.4	403	2.4	444	1.7	473	1.2
C3	140	6.0	244	4.4	319	3.2	375	2.4	416	1.7	446	1.3
J 16 B C1	211	8.3	345	5.3	431	3.4	485	2.2	520	1.4	542	0.9
K 16 C C2	184	7.0	294	4.3	361	2.6	401	1.5	425	0.9	440	0.6
H 4 J C2	103	4.4	178	3.2	232	2.3	272	1.7	301	1.2	322	0.9

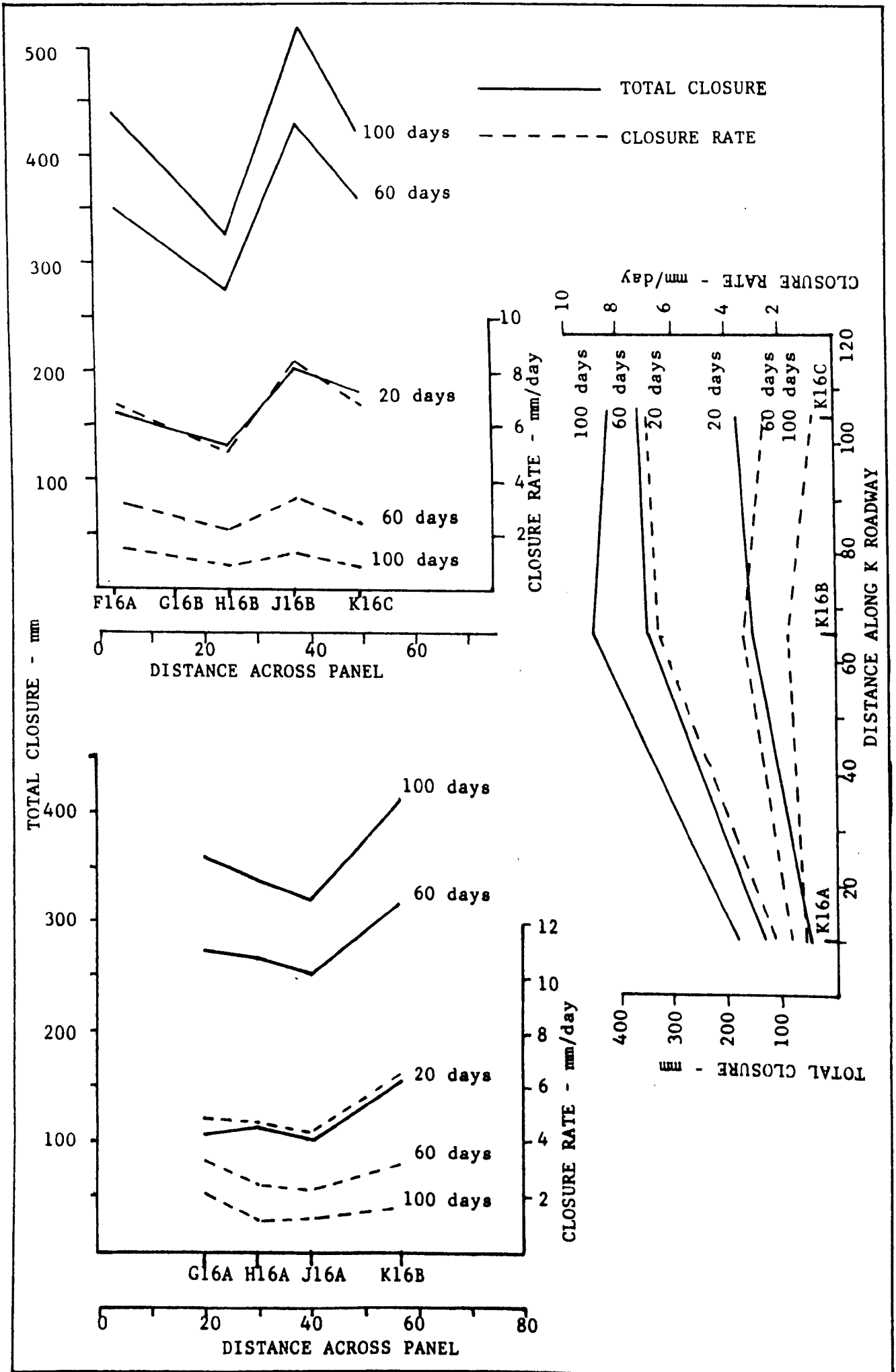


Figure 6.33 No.16 Panel, Closure Profiles

seem to indicate that there is greater instability in the area where K 16 B is located. If the distance from the start of the panel is measured, K 16 B lies some 65m away. Again this ties in with the evidence from the other panels. It is quite likely that the low closure at K 16 A is partly a result of large scale roof collapses in No. 3 crosscut and east stub. Marl was exposed and this has continued to flow into the excavations. The marl would creep or flow preferentially into these collapsed areas, thereby relieving the pressure above K 16 A, and thus reducing the closure. This is diagrammatically shown in Figure 6.34.

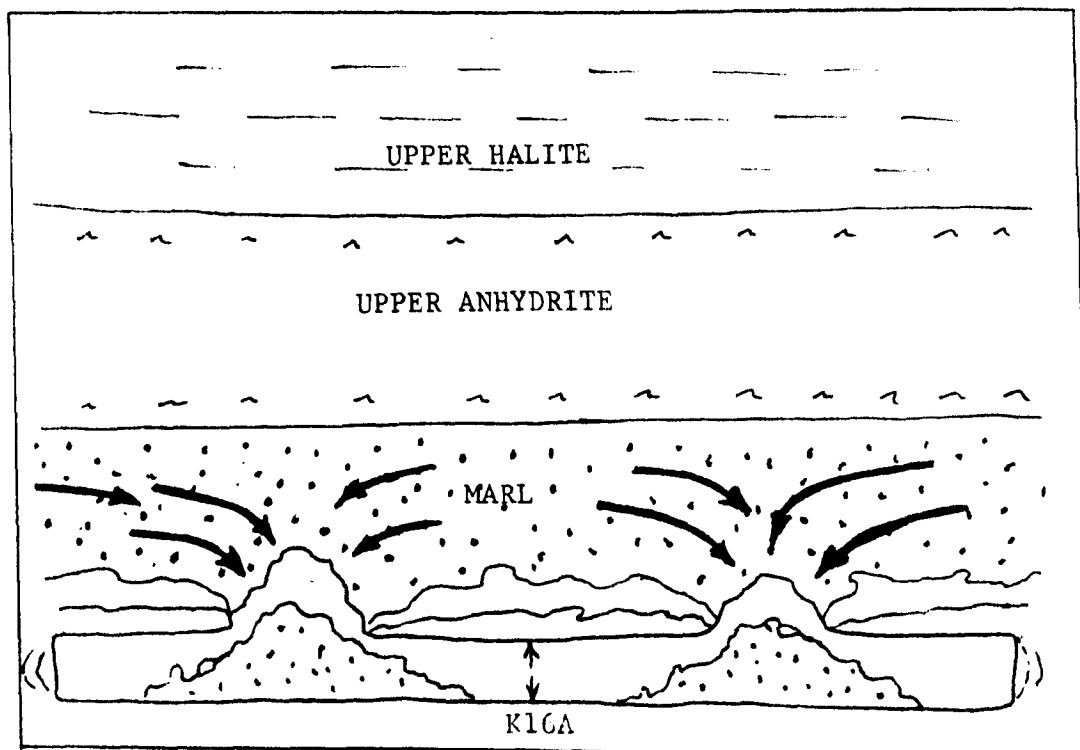


Figure 6.34 No. 16 Panel, site K16A - Marl Exposure

6.9 No. 19 Panel

No 19 Panel was set off at an angle of 45° to the line. No. 10 Panel: it was intended that this panel would mine parallel and to the east of the salt overfold. From the beginning the panel experienced fairly high closure rates. After water was encountered in No. 10 Panel and was stopped, the decision was made to carry on with No. 19 Panel. It ran into barren ground with highly variable geology, and was therefore turned at right angles to the north-west and designated No. 22 Panel. Water entered No. 19 Panel in E roadway on 16/12/79 some 25 days after that in No. 10 Panel.

It was only after the water inflow that instrumentation sites were installed. These were mainly down 'J' roadway, and consisted of closure sites. A few microcreep sites were also installed. The locations of all the sites are shown in Figure 6.35.

6.9.1 Closure Measurements

Even though the closure measurements were begun in the case of J 19 A as much as 138 days after mining, by applying the method explained in section 6.2, it was possible to obtain values for total closure as well as closure rate. These values for 20 day intervals are tabulated in Table 6.13, and plotted in Figure 6.36. Extremely high closure rates ($>20\text{mm/day}$) were experienced at sites J 19 F, J 19 6 and J 19H. It is interesting that site G 19 A

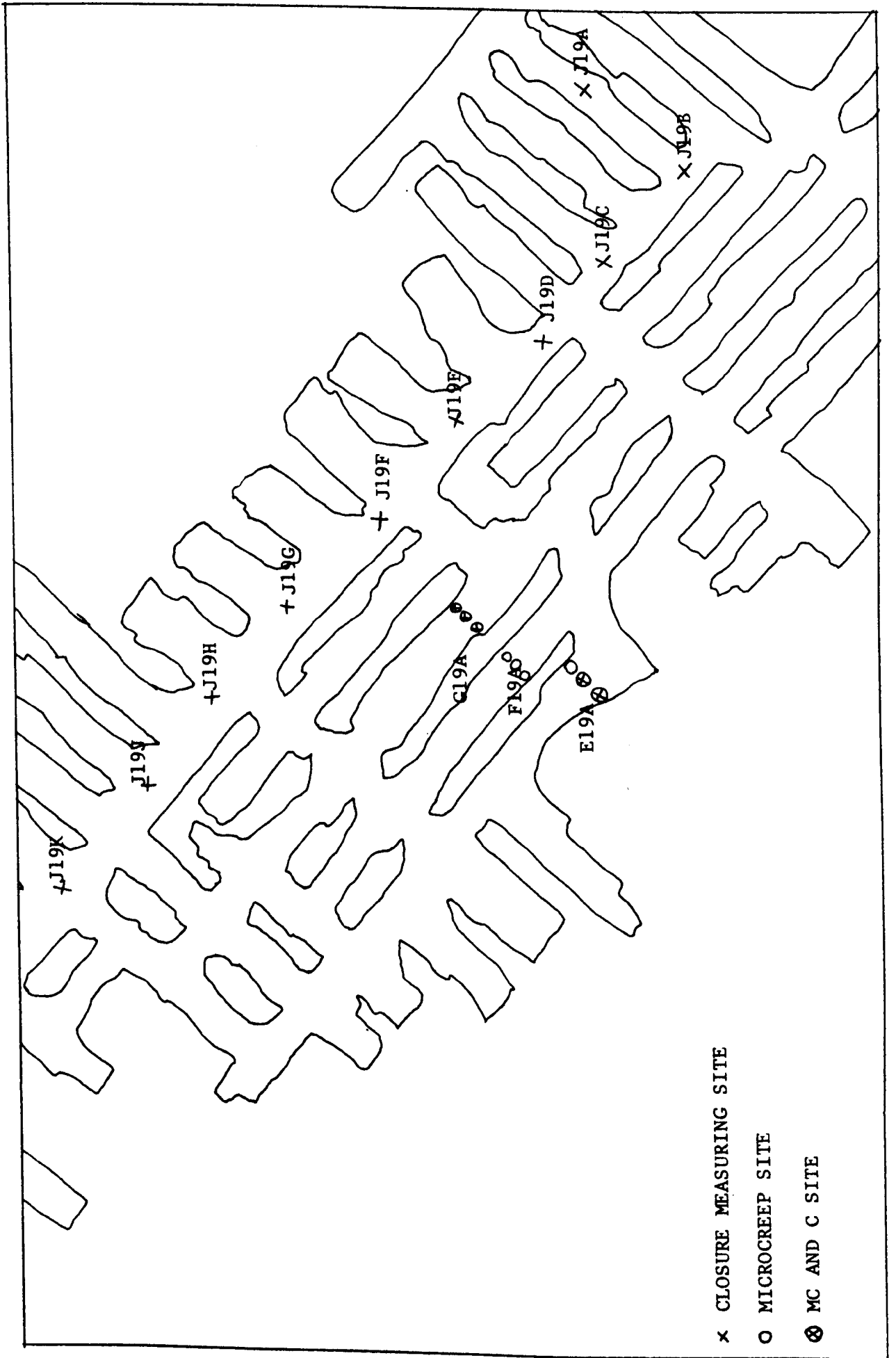


Figure 6.35 No. 19 Panel, Instrumentation sites

TABLE 6.13

No. 19 Panel Closures (c), mm, and Closure Rates (ĉ), mm/day for 20 day intervals

Days	20		40		60		80		100		120	
	c	ĉ	c	ĉ	c	ĉ	c	ĉ	c	ĉ	c	ĉ
G 19 A C1	207	9.4	379	7.9	523	6.5	643	5.5	743	4.5	826	3.8
C2	232	10.4	420	8.4	571	6.8	694	5.5	793	4.4	873	3.6
C3	238	10.6	429	8.5	582	6.8	704	5.5	803	4.4	882	3.5
J 19 A C2	227	10.1	408	8.0	552	6.4	666	5.1	757	4.0	829	3.2
J 19 B C2	198	8.8	357	7.1	483	5.6	584	4.5	665	3.6	729	2.9
J 19 C C2	277	12.3	495	9.7	667	7.6	802	6.0	909	4.7	993	3.7
J 19 D C2	337	14.8	597	11.4	798	8.8	954	6.8	1074	5.3	1157	4.1
J 19 E C2	295	13.2	531	10.5	720	8.5	872	6.8	993	5.4	1091	4.3
J 19 F C2	481	20.7	840	15.5	1109	11.6	1310	8.6	1460	6.5	1572	4.8
J 19 G C2	516	21.9	892	15.9	1165	11.6	1364	8.4	1508	6.1	1614	4.5
J 19 H C2	509	21.6	877	15.6	1144	11.3	1338	8.2	1478	5.9	1580	4.3
J 19 H C2	277	12.3	496	9.7	669	7.7	807	6.1	916	4.8	1002	3.8
J 19 K C2	298	13.0	524	9.9	697	7.5	829	5.7	929	4.4	1006	3.3

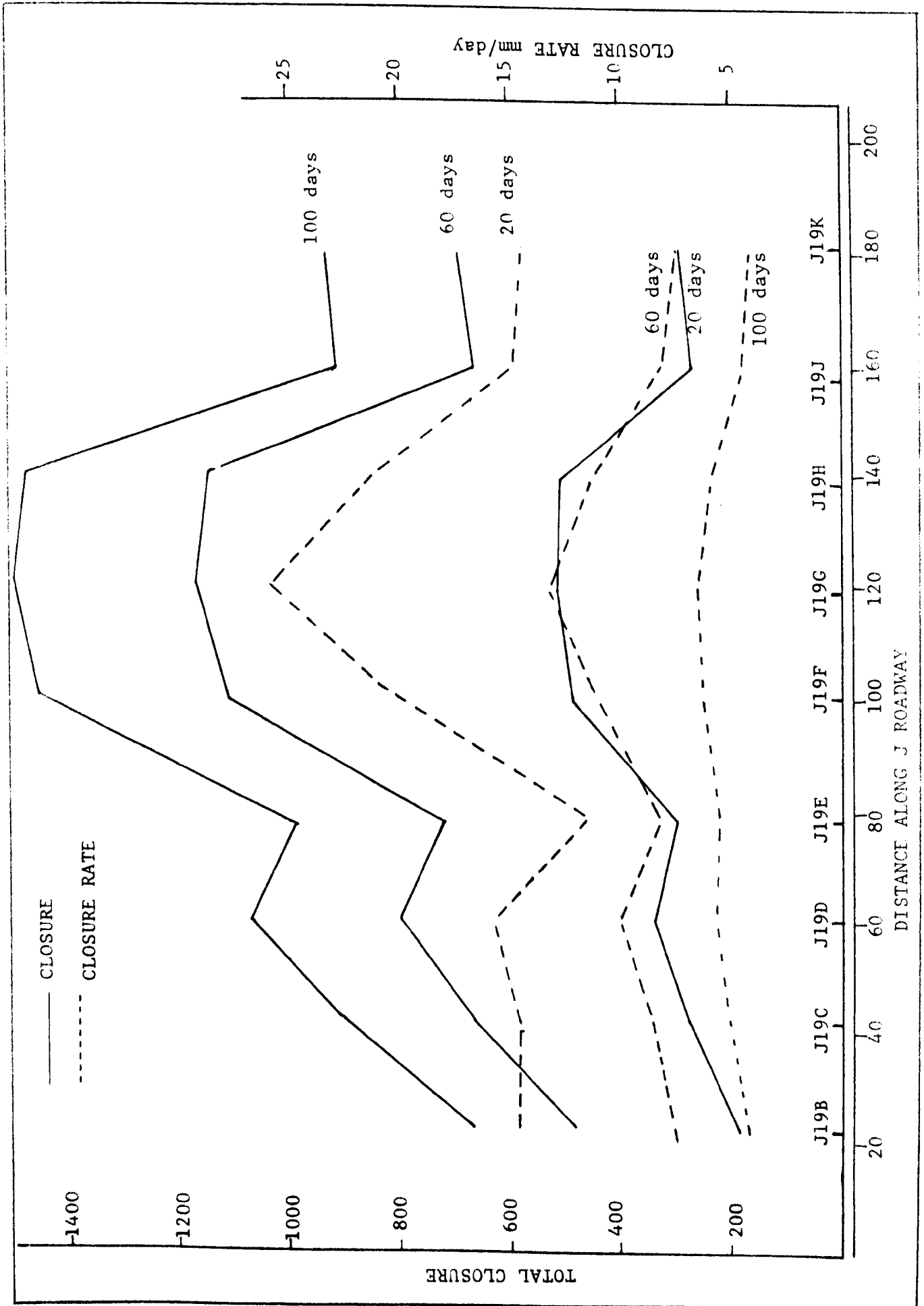


Figure 6.36 No.19 Panel, Convergence and Convergence Rates

which is located approximately the same distance down the panel, but in the centre roadway, had closure rates almost exactly half of those mentioned. This can be explained by excessive creep or flow of the marl over the north-east ribside. Even so, when compared with the other high extraction panels, all the 19 panel sites exhibited significantly higher closure rates.

Another interesting feature is that after the very high initial closure rates, all the sites had by 120 days, settled down to fairly similar rates of between 3 and 5 mm/day. Again these are still high when compared with other panels after a similar period had elapsed, and indicate continuing overall uniform deformation into the panel.

From the graph of deformation along J roadway, Figure 6.36, it can be seen that there is a fairly rapid increase in closure with distance along the panel, with a peak at D. This decreases to E, followed by another very rapid increase to a second peak at C. The distances of D and C from the start of the panel are 60m and 120m respectively.

Closure measurements were obtained at the various sites and convergence and convergence rate graphs are given in Figure 6.37(a) to (1). Water entered the workings in E roadway, No. 19 Panel 75 days after site G 19 A had been mined. This can clearly be seen in Figure 6.37 (a) where an abrupt increase in closure rate occurs between days 70 and 75, followed by an almost equally rapid decrease and by 92 days after mining, the closure rate is decreasing at the same rate as before the water.

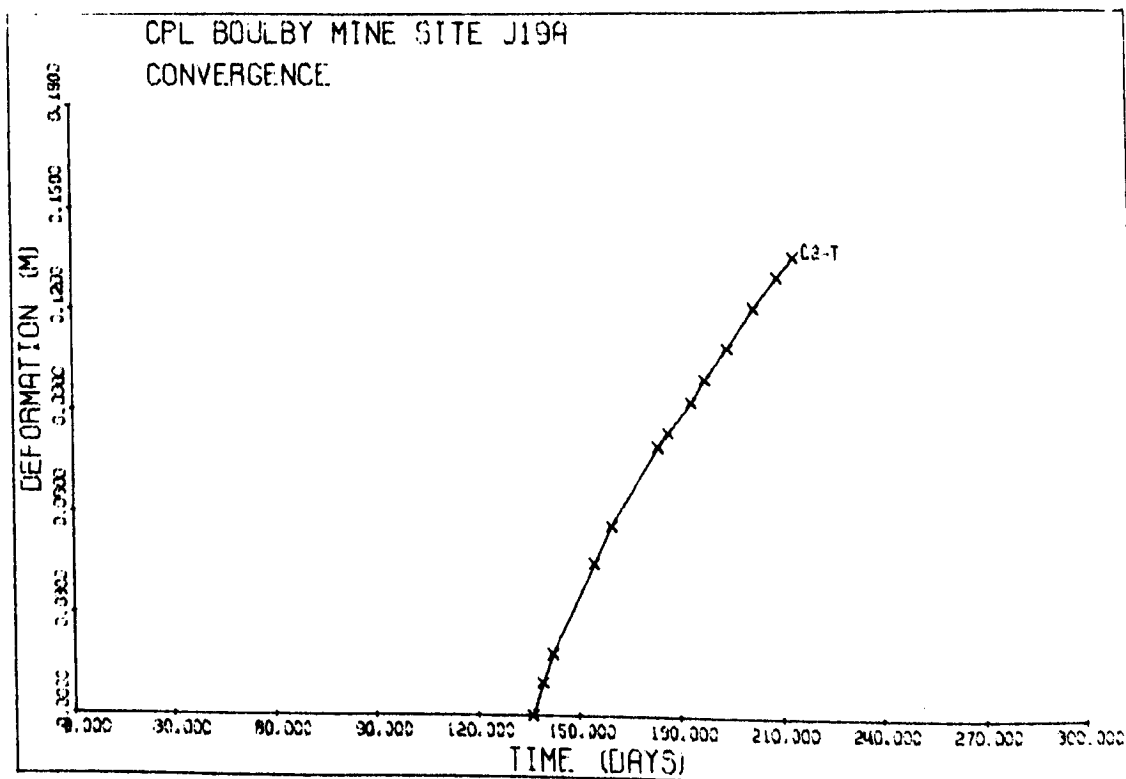
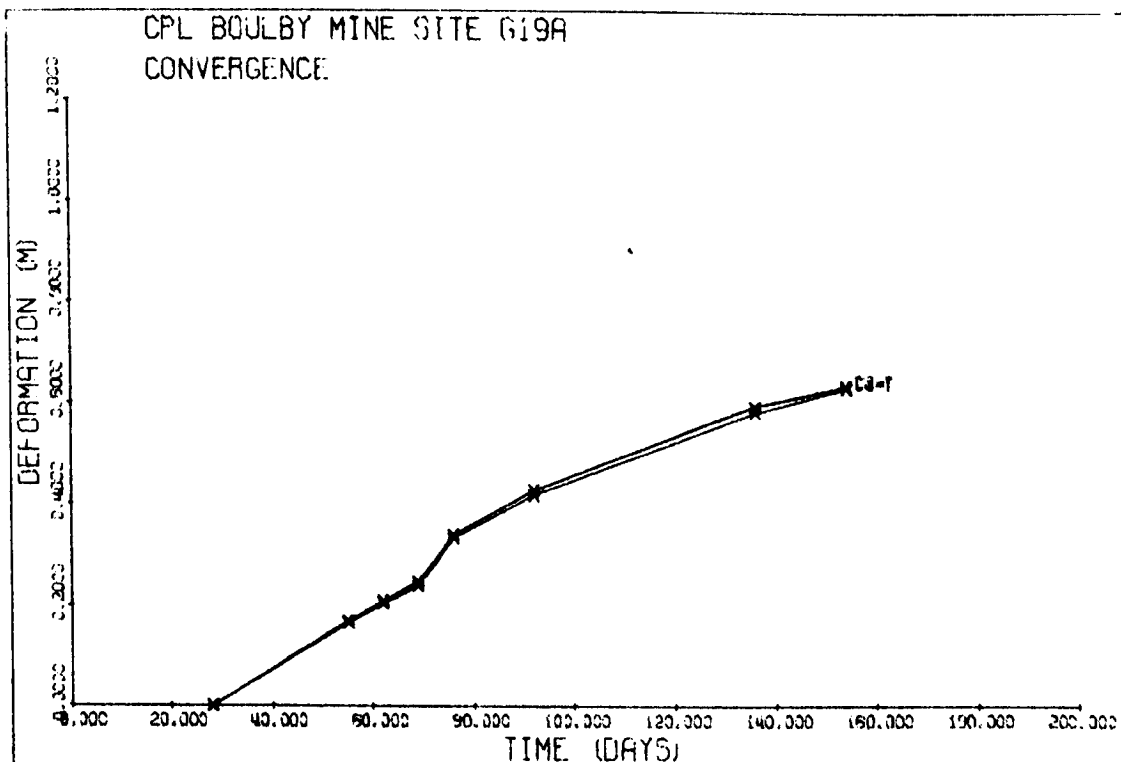


Figure 6.37 (a)

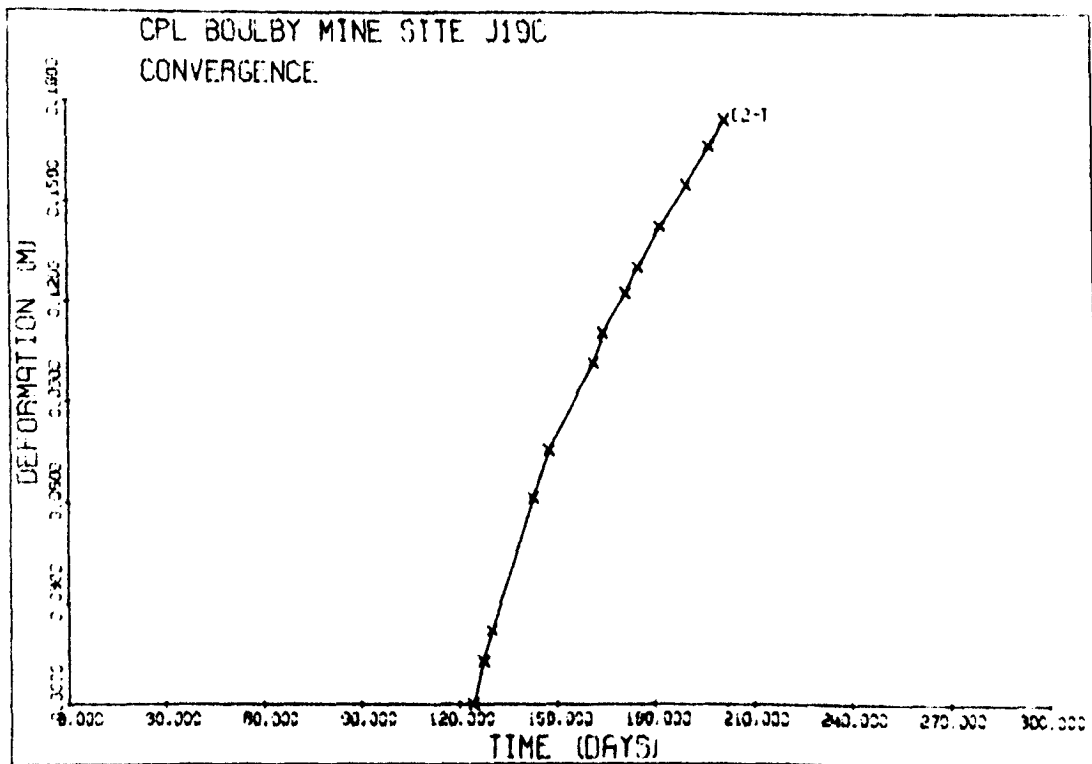
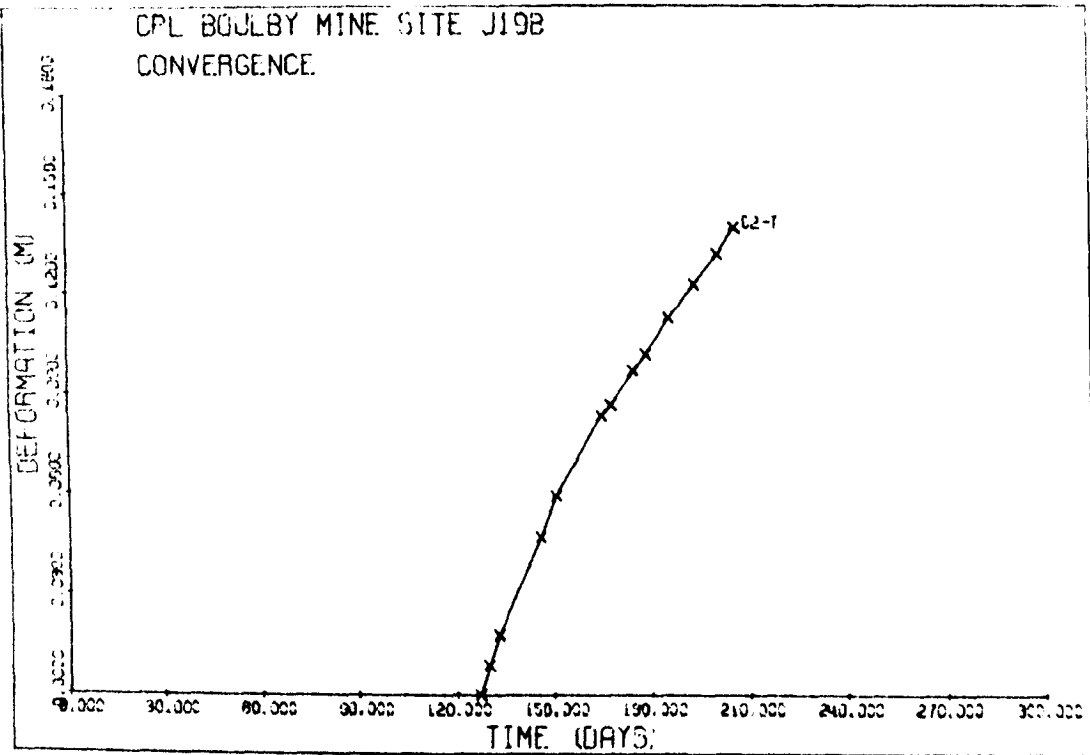


Figure 6.37 (b)

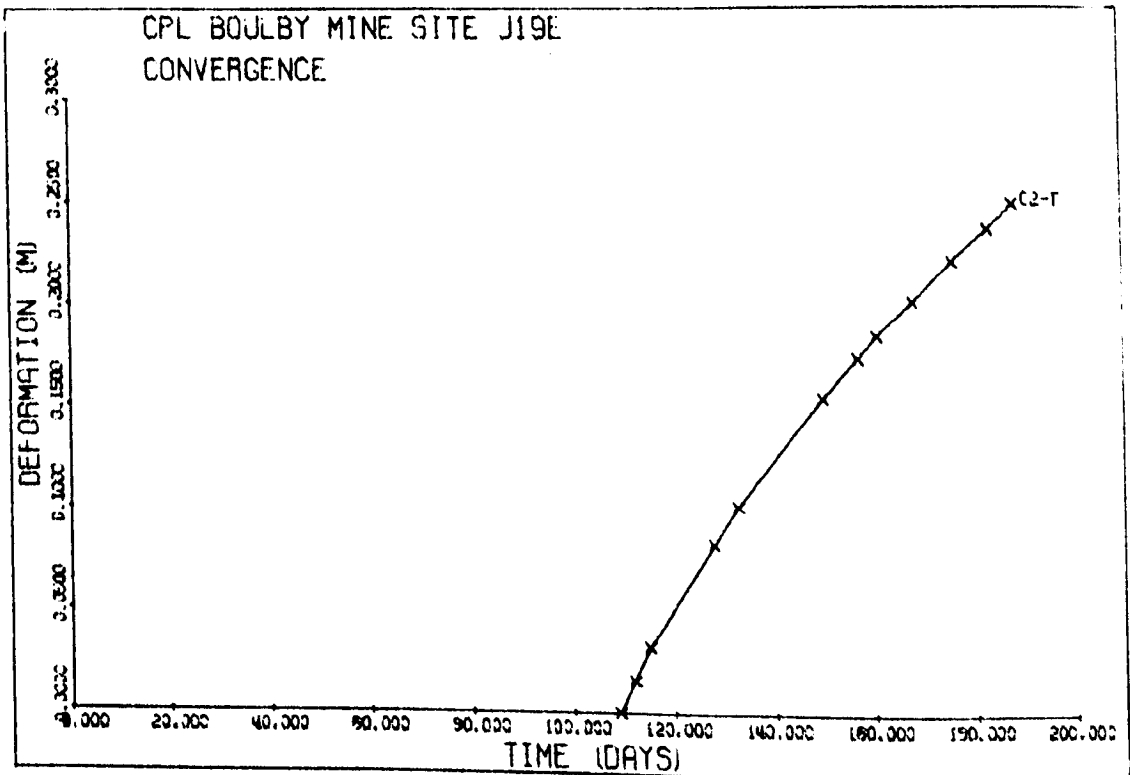
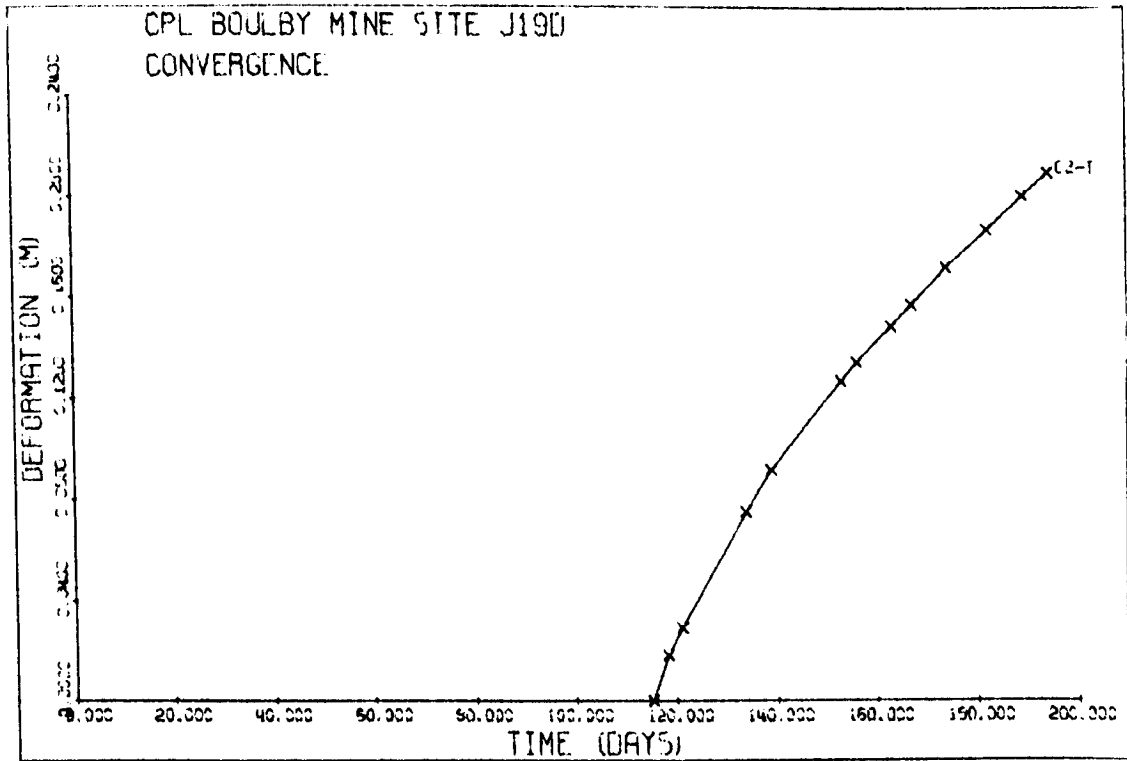


Figure 6.37 (c)

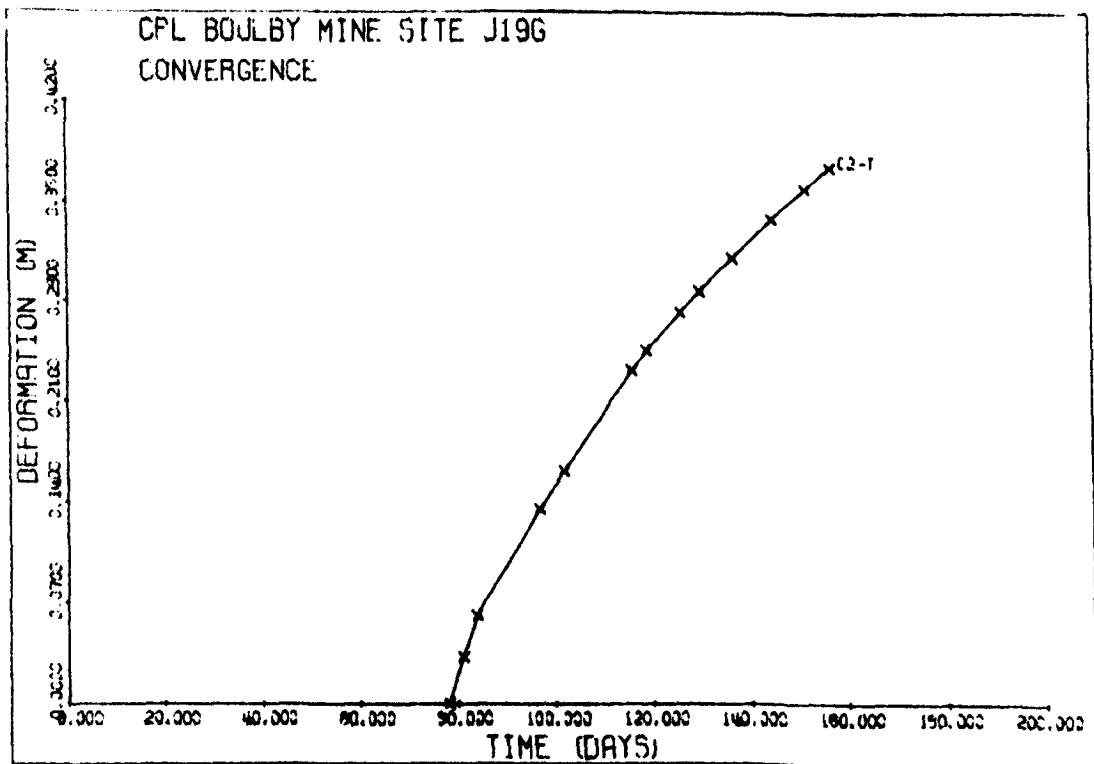
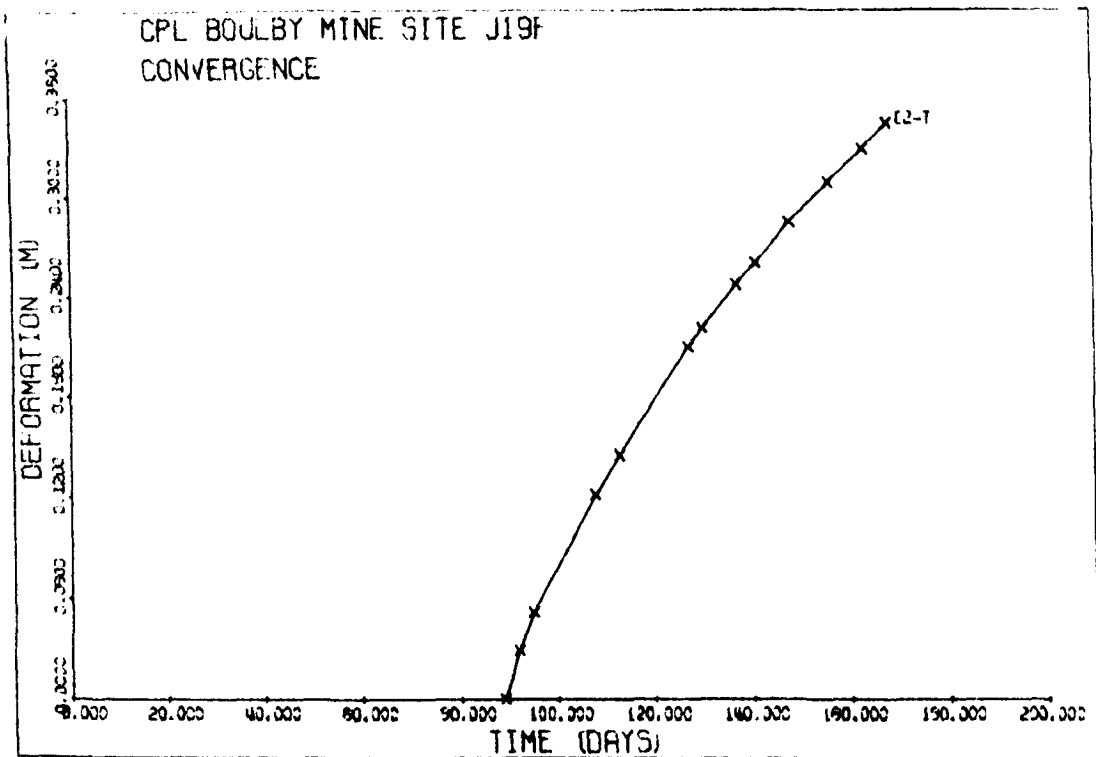


Figure 6.37 (d)

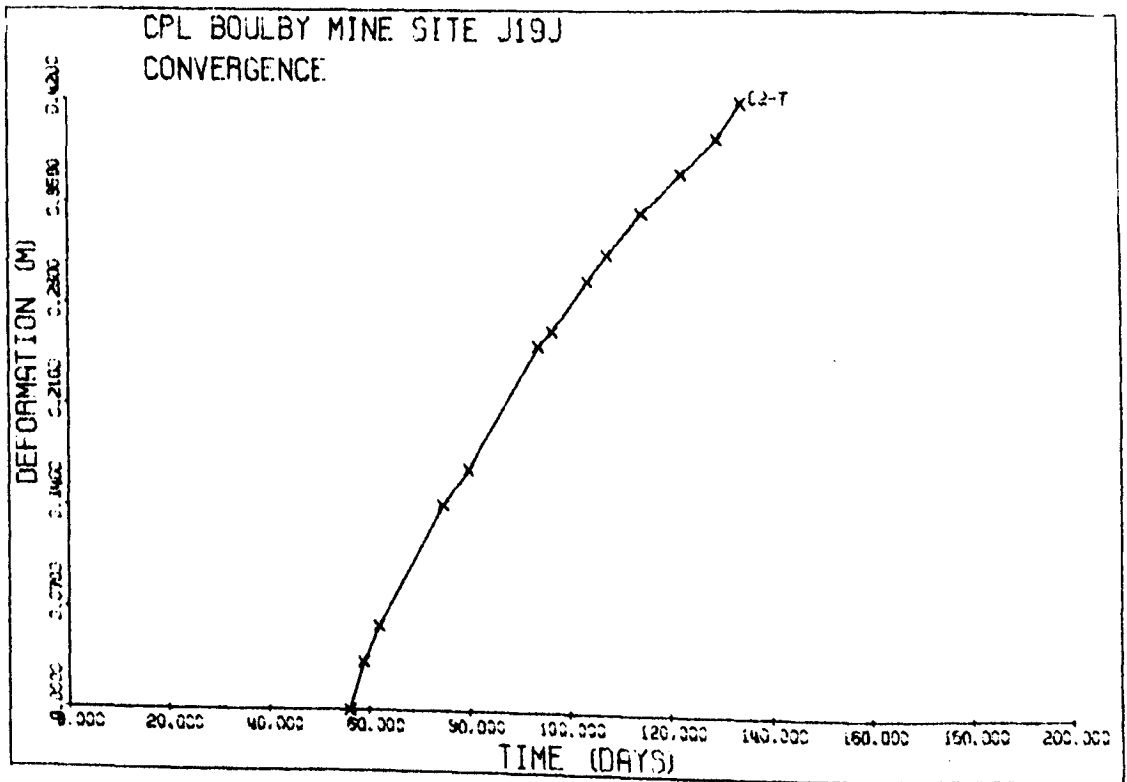
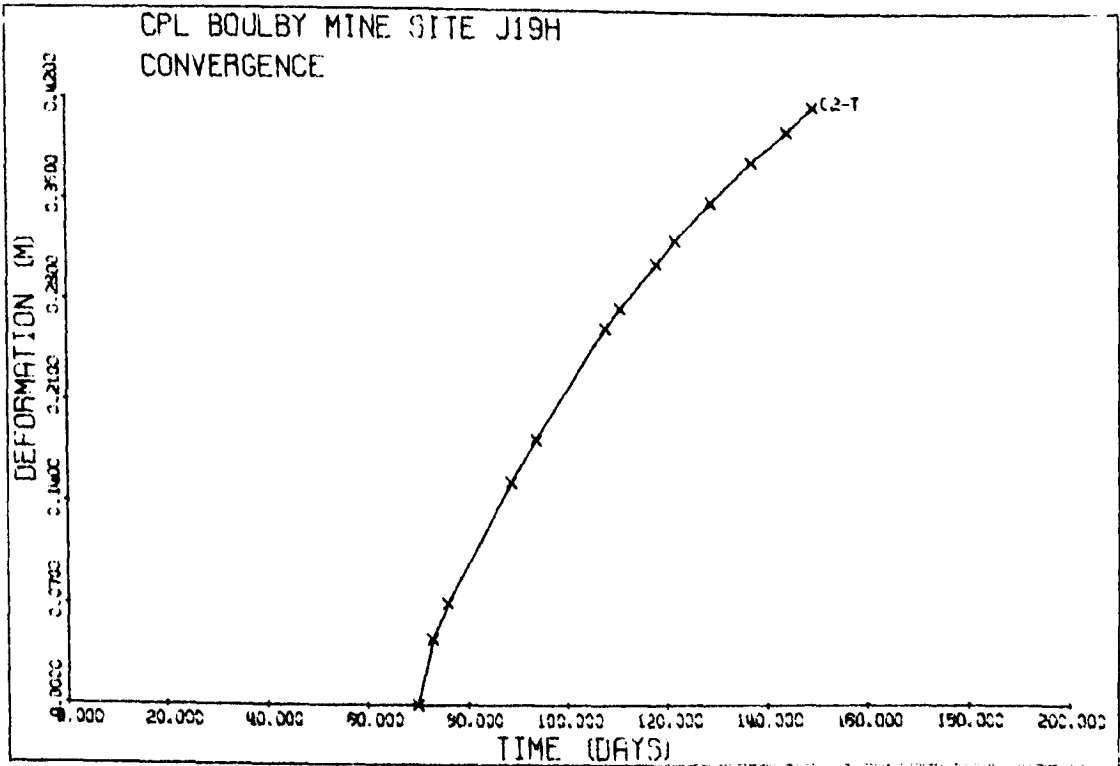


Figure 6.37 (e)

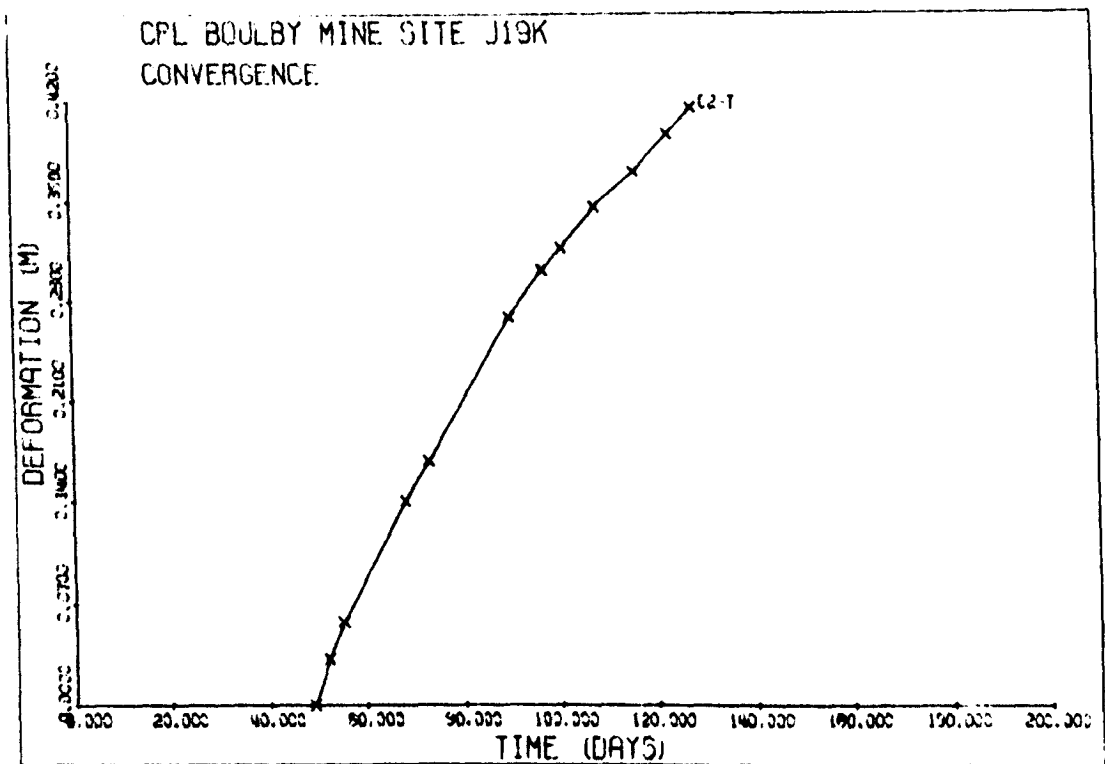


Figure 6.37 (f)

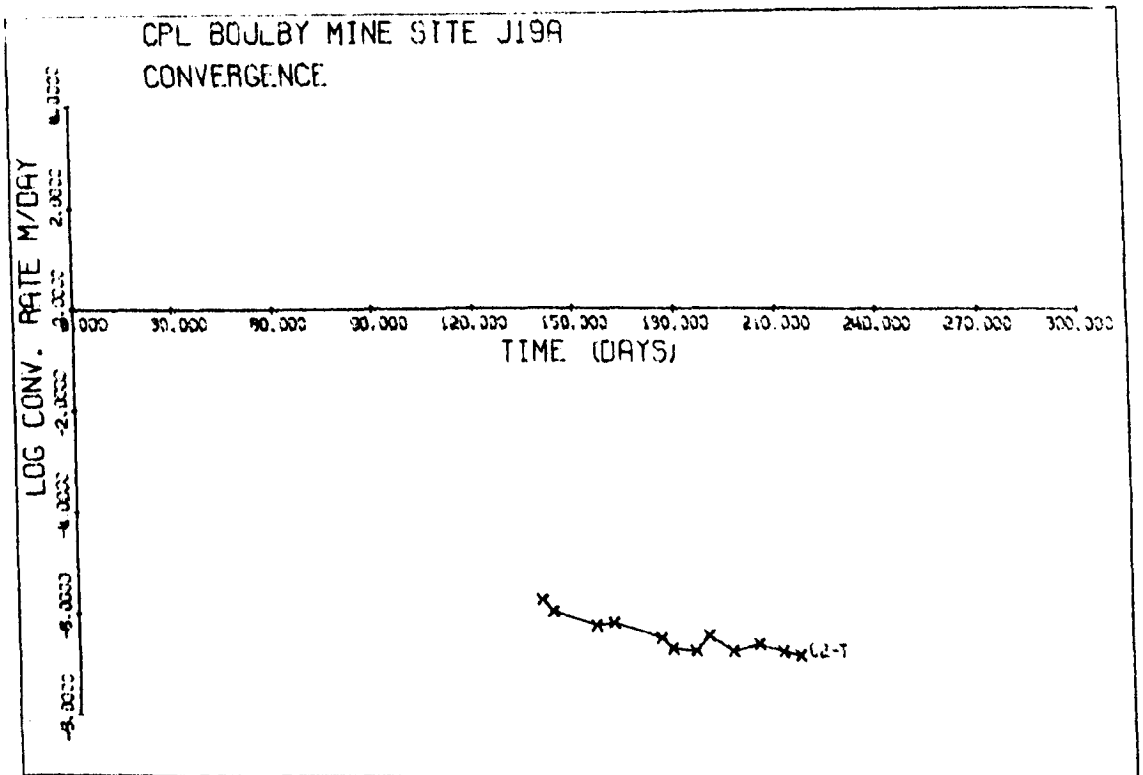
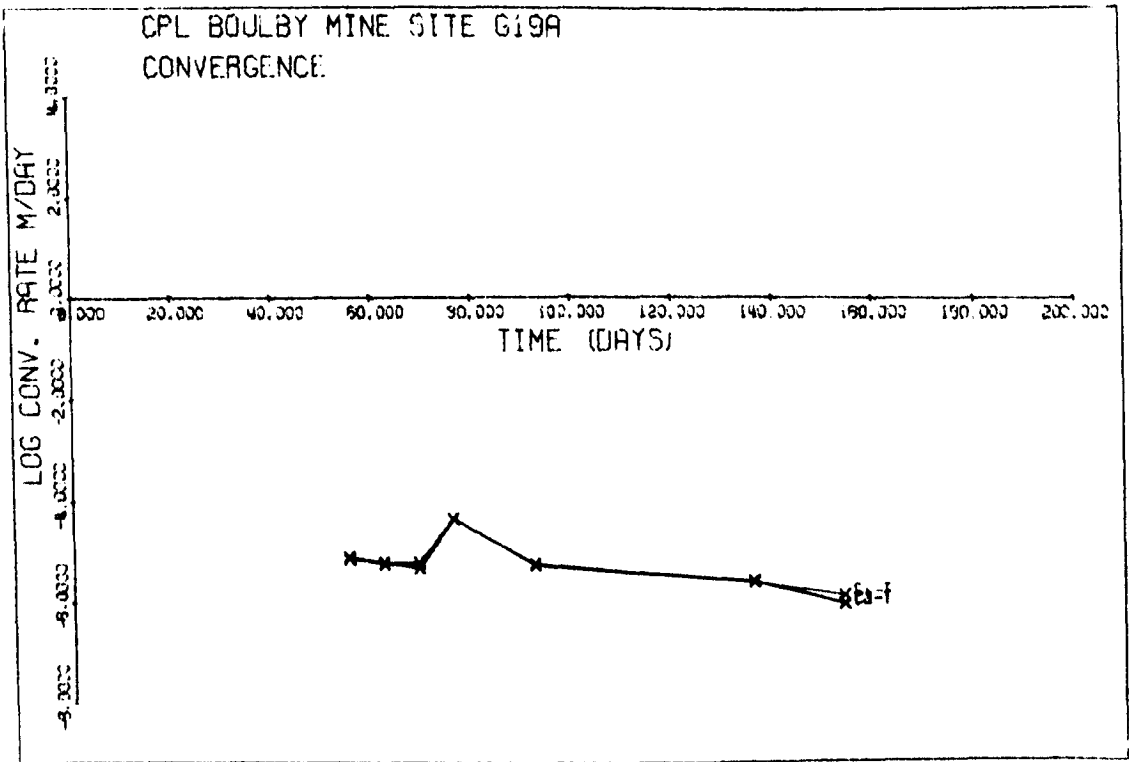


Figure 6.37 (g)

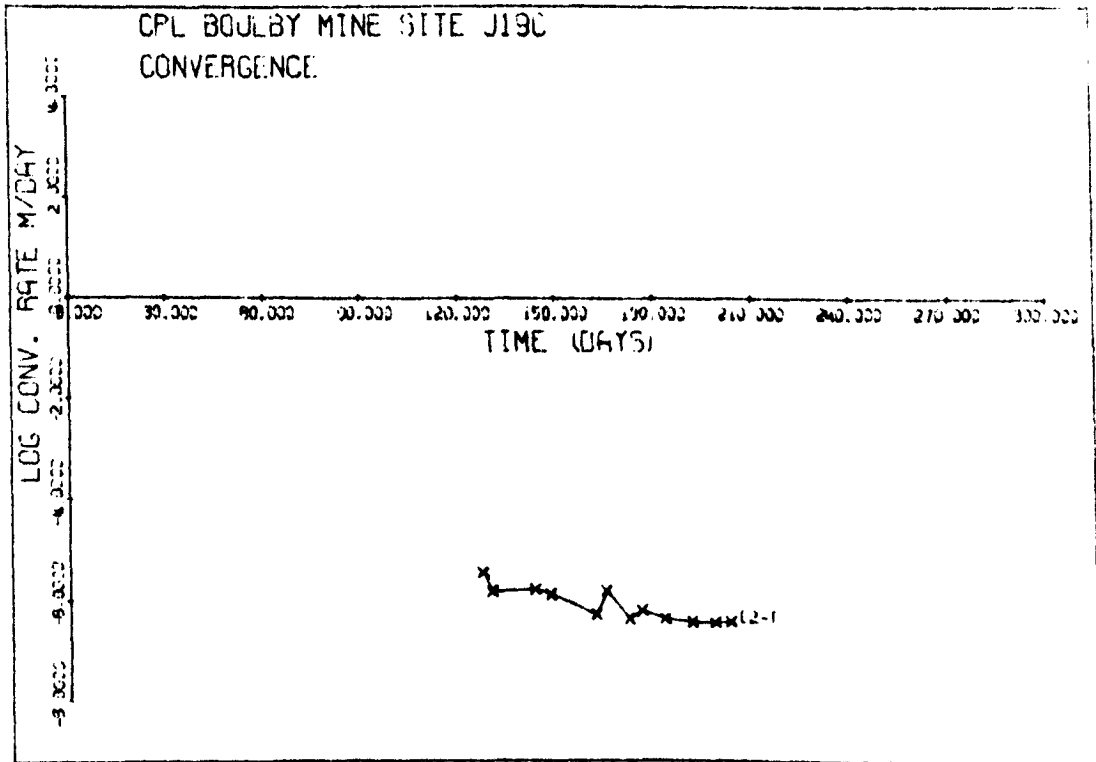
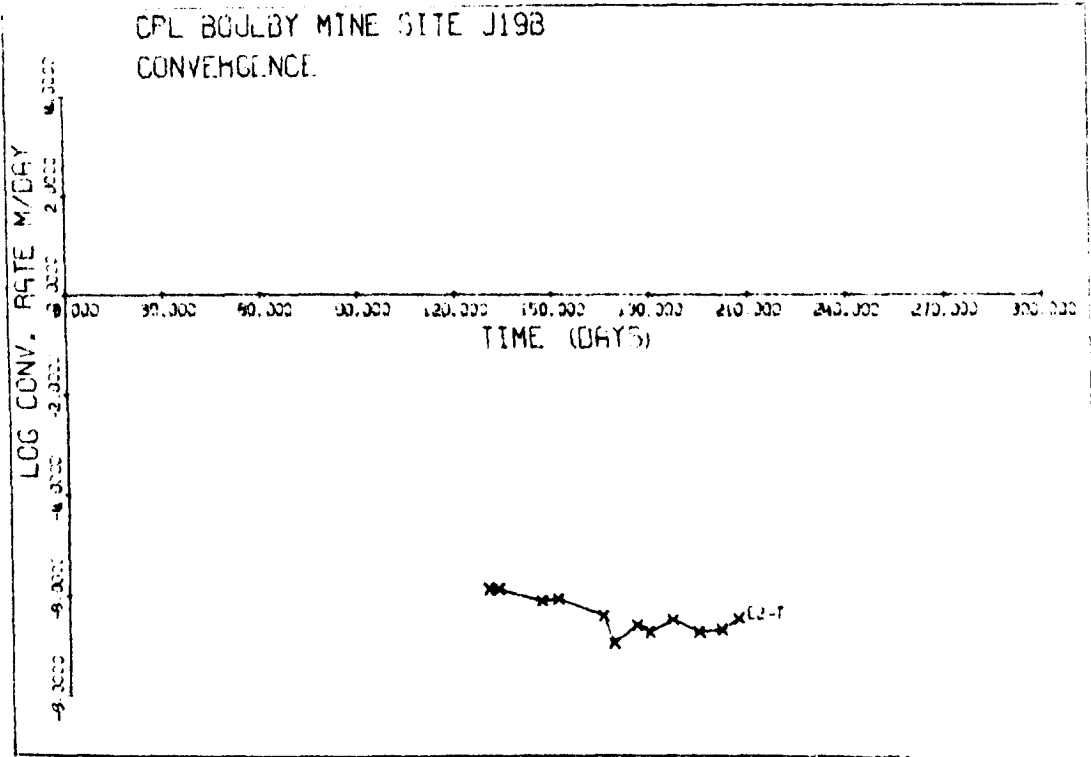


Figure 6. 37 (h)

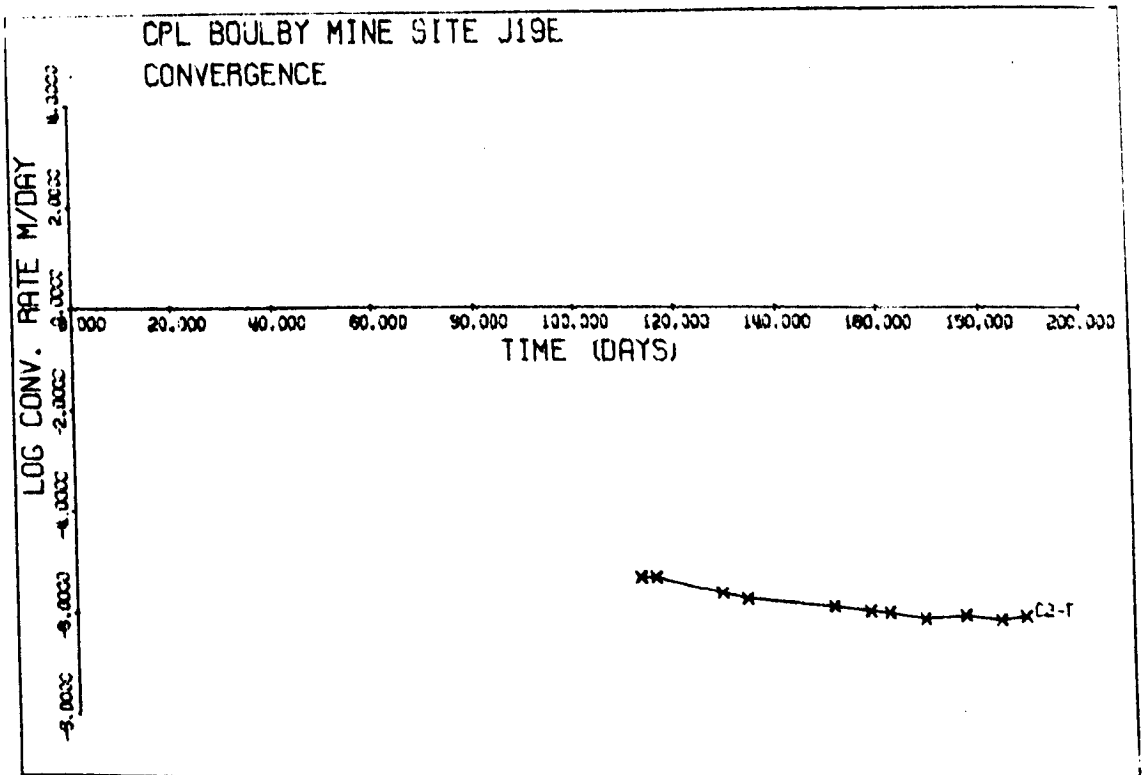
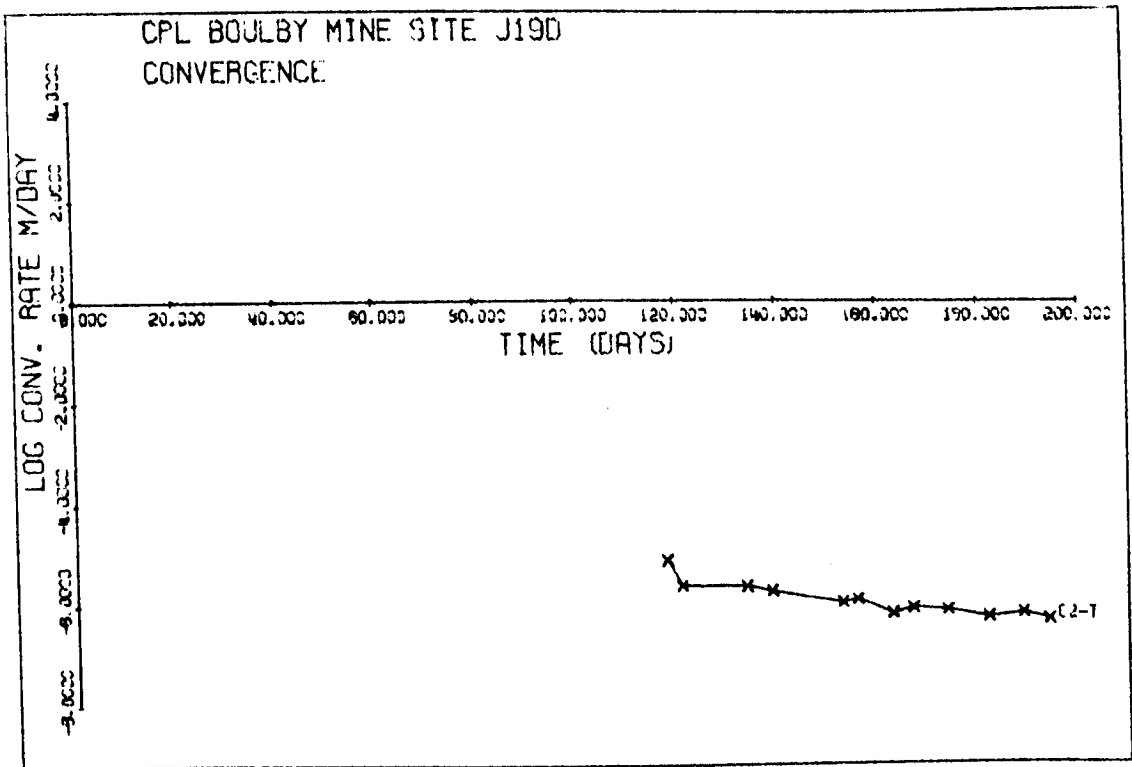


Figure 6.37 (i)

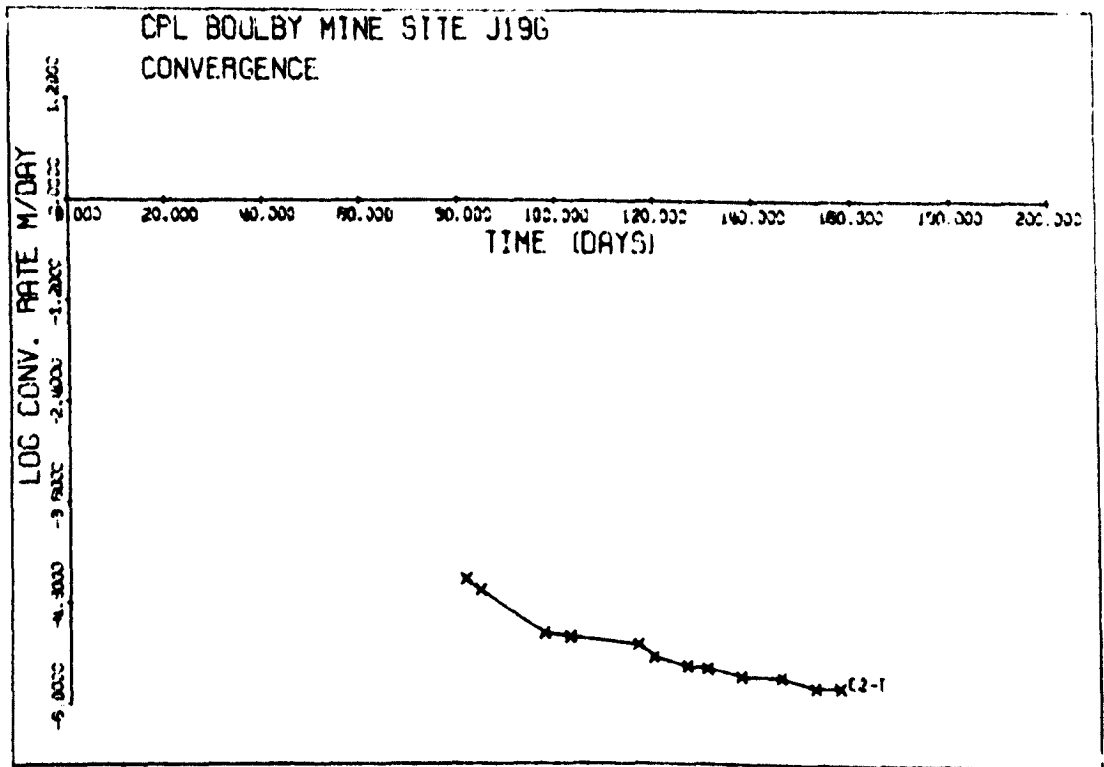
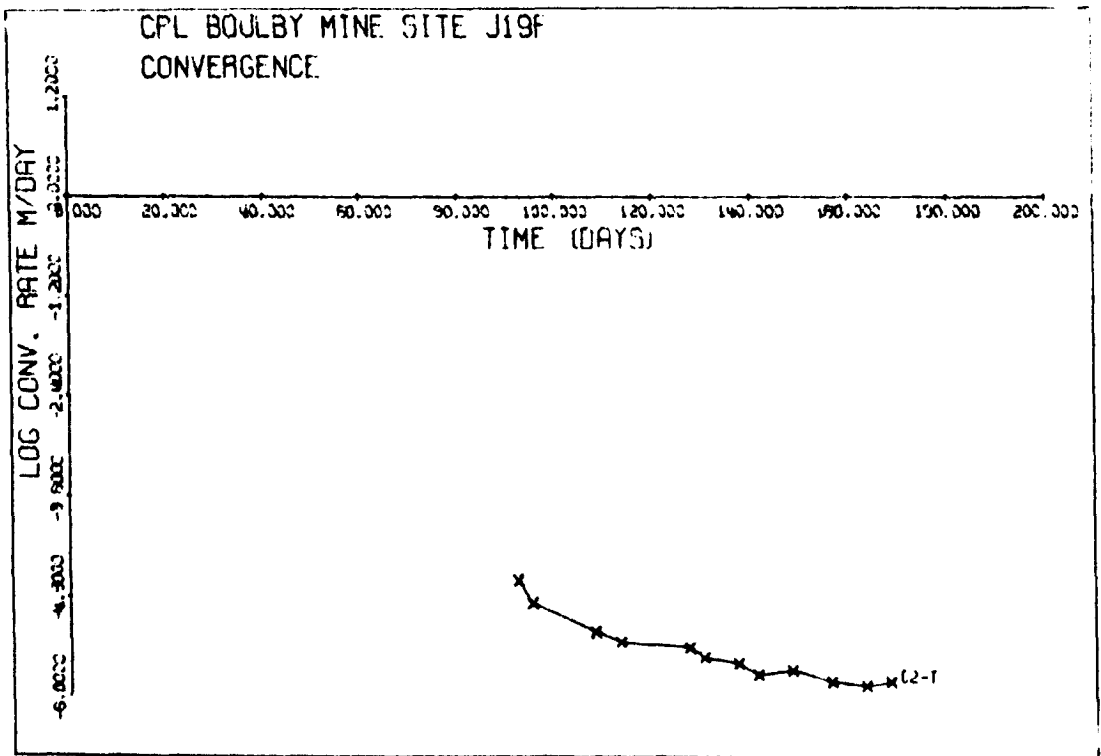


Figure 6.37 (j)

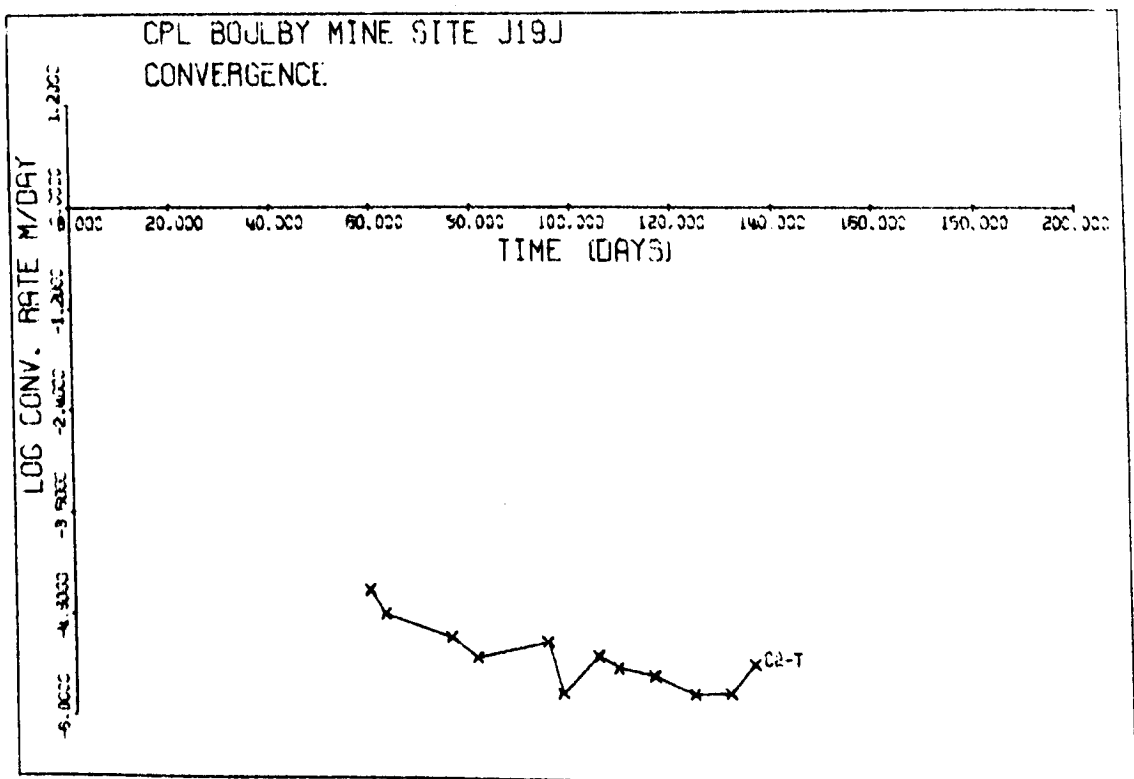
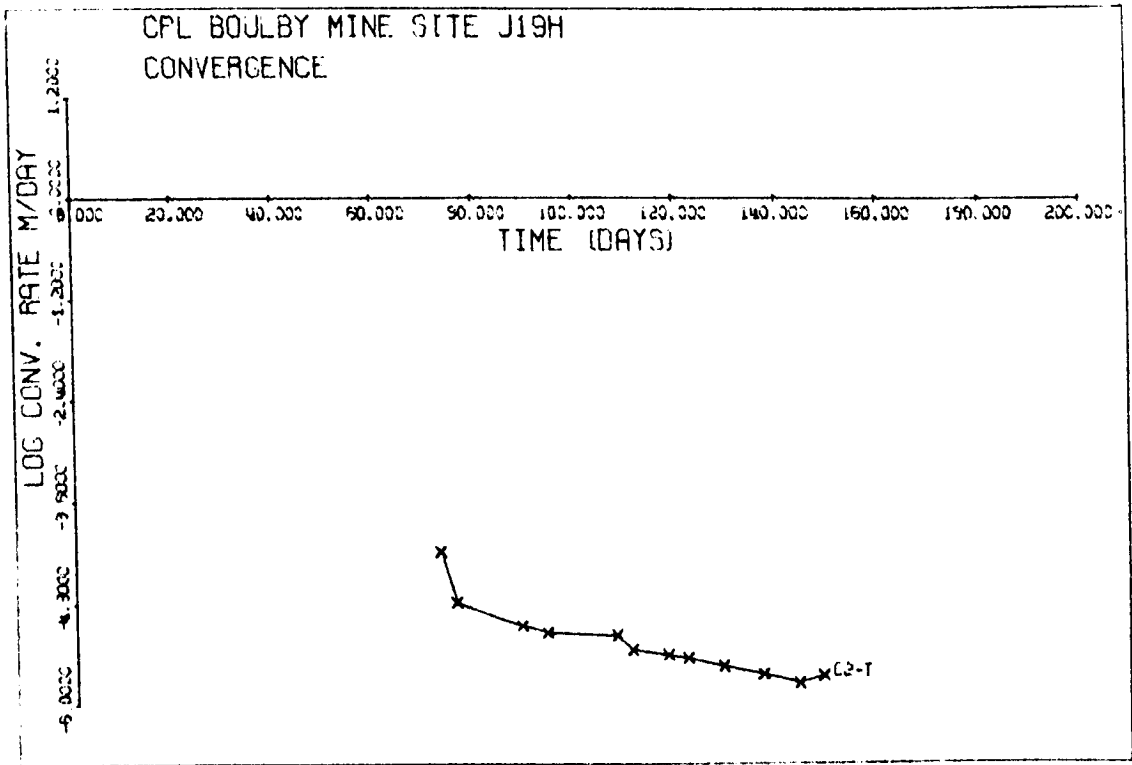


Figure 6.37 (k)

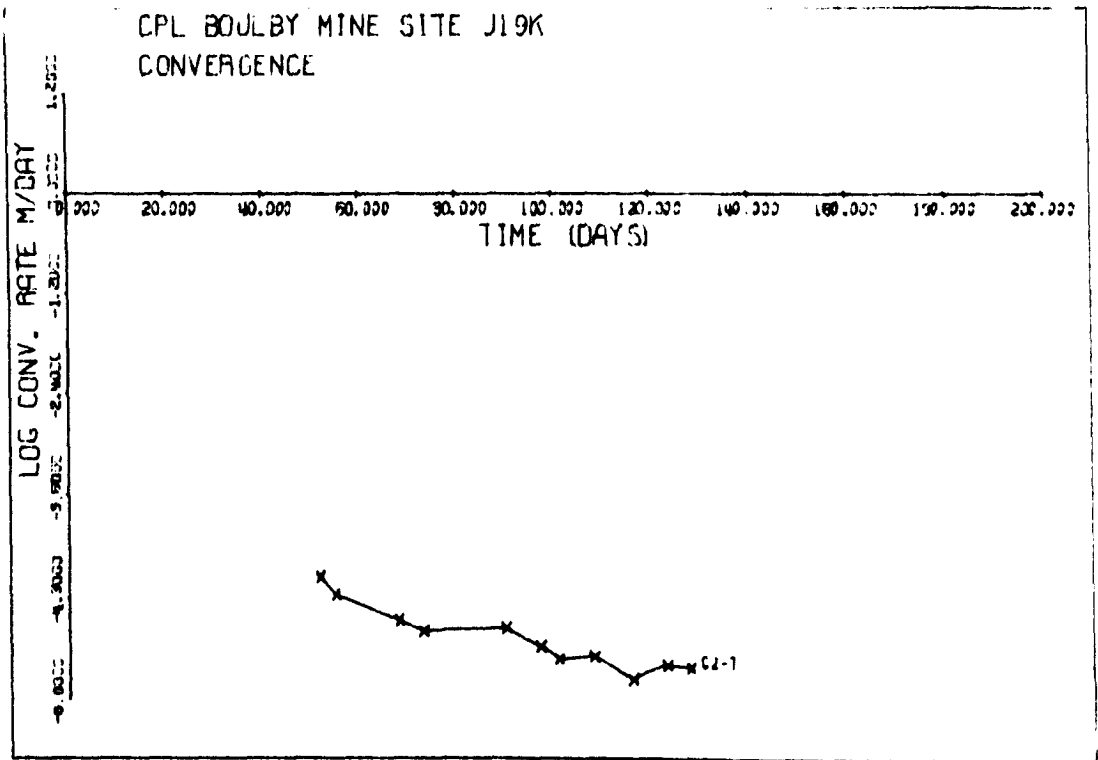


Figure 6.37 (1)

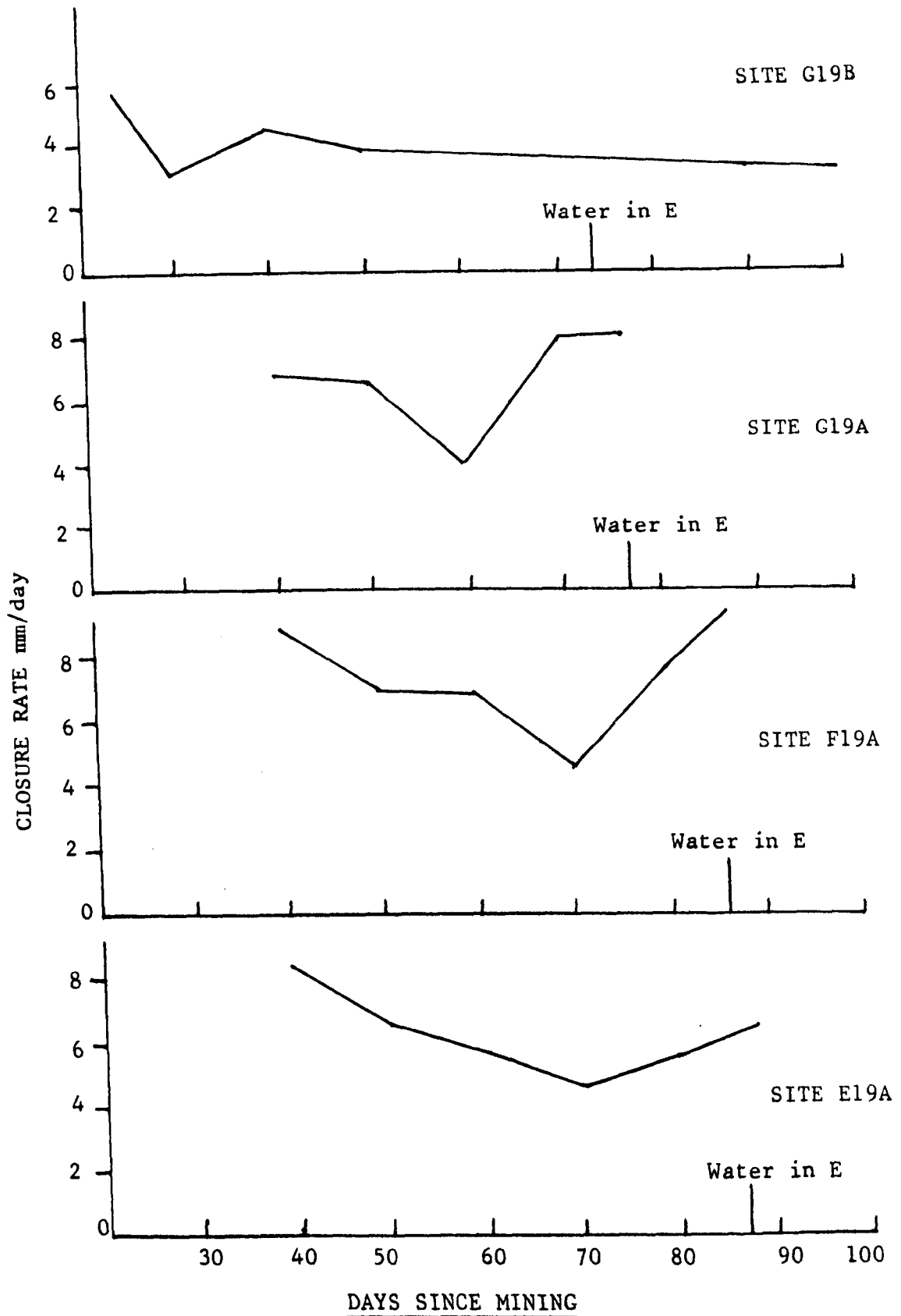


Figure 6.38 No. 19 Panel, Microcreep closure rates at E19A, F19A, G19A and G19B

The picture here is somewhat different to that obtained from No. 10 Panel, where increases in closure rate were observed up to 40 days before the water entered the workings. It is therefore concluded that the water in No. 19 Panel came from No. 10 Panel, and not from some source above No. 19 Panel itself.

6.9.2 Microcreep Measurements

The microcreep measurements that were obtained at sites E 19 A, F 19 A, G 19 A and G 19 B, are given in Figure 6.38. These show that an increase in closure rate is evident from between 10 and 15 days before the entry of the water in E roadway. Site G 15 B does not appear to have been affected by the advent of the water and this could be due to it being some 87m away.

6.10 Concluding Remarks

The data obtained from the measurements made in the high extraction panels and presented in this chapter, are the result of a determined and continuing effort by the mine to monitor the effects of various layouts that have been implemented. Unfortunately, it was not always possible to install and maintain measuring sites and stations where they were most required. What remains then, is a series of bits and pieces of information, some of which are connected, others not. An attempt has been made to fit these pieces together to form a coherent picture which will explain the behaviour of the excavations after they are mined. In addition it is anticipated that the results acquired will allow predictions to be made of the future stability of the mining excavations.

CHAPTER SEVEN

THE USE OF ROCKSALT AND SALTCRETE AS A FILL MATERIAL

7.0 Introduction

It was decided to investigate the use of rocksalt mined as waste as a stabilising fill material. The rocksalt would be obtained from the mining of long term access roads in the Middle Halite below the potash seam. Apart from the strata control aspects of stowing the waste rock, other economic benefits would also accrue. A Markham Stower was purchased for this purpose.

The project was executed in a number of different stages. Laboratory tests were done in order to determine the properties of ordinary run of mine rocksalt, as well as rocksalt stabilised by the addition of cement. Surface trials in a tunnel mock-up were carried out in order to test the stowing equipment and to estimate various stowing parameters, such as distance of throw, compaction, etc. Finally a finite element model was used to test the effects of fill of different characteristics in openings of varying size, but as these results were derived for the elastic solution they have been omitted.

7.1 Uncemented Fill - Laboratory Trials

The purpose of these trials was to establish the response to loading of run of mine rocksalt when the following parameters were varied:-

1. Width to height ratio
2. Particle size
3. Water content
4. Temperature

The material was placed in a thick walled steel cylinder having close fitting pistons inserted at both ends in order to ensure that load was applied equally from both sides. A 25 tonne Avery compression testing machine was used for the trials and a standard loading rate of 25 kN/min was applied for all specimens tested. The internal cross-sectional area of the cylinder was 51.5 cm^2 (internal diameter, 80.5mm). All the specimens were loaded to 180 kN, giving a stress of 34.9 MPa which slightly exceeded the expected in-situ vertical stress.

The samples for the water tests were prepared by spraying a previously determined volume of water over a 10mm thick layer of rocksalt. The amount of water was calculated as a percentage of the weight of the dry rocksalt sample.

The load/deformation curves were recorded. It was found that within the range 5kN to 180 kN, the deformation of the filling material expressed as a function of the load applied, followed a pattern represented by the logarithmic function:

$$y = A + B \log x$$

Table 7.1 gives the results of the tests with the percentage volume change at 180 kN. Percentage volume change was calculated as this could be related to the roof to floor and wall to wall closures measured in roadways in the mine.

TABLE 7.1

% Volume Change, rocksalt tests

Sample	Condition	W:H Ratio	Volume Change at 180 kN (%)
-10mm	Dry, room temperature	2:1	26.4
		1:1	28.8
		1:2	28.5
-2mm	Dry, room temperature	2:1	29.9
		1:1	31.3
		1:2	28.3
-10mm	Dry, 50°C	2:1	28.1
		1:1	32.2
		1:2	31.9
-10mm	5% H ₂ O, room temperature	2:1	40.1
		1:1	39.4
		1:2	35.7
-10mm	2.5% water, 50°C.	2:1	36.9
		1:1	34.5
		1:2	35.0
-10mm	5% H ₂ O, 50°C.	2:1	35.1
		1:1	31.5
		1:2	33.0

7.1.1 Width to Height Ratio

Tests were done using three width to height ratios, namely, 1:2, 1:1, and 2:1, the latter being the one which approximates the situation of a normal roadway driven with a Heliminer. The results indicate that there is a somewhat small random variation in the percentage volume change for different width to height ratios. It can be concluded that width to height ratio is not a significant factor in determining the load bearing properties of salt fill. However, the W:H ratio of a roadway will affect the rate at which it closes and therefore the build up of load in the fill. Figure 7.0 shows the change in area of roadways in the mine after different times have elapsed.

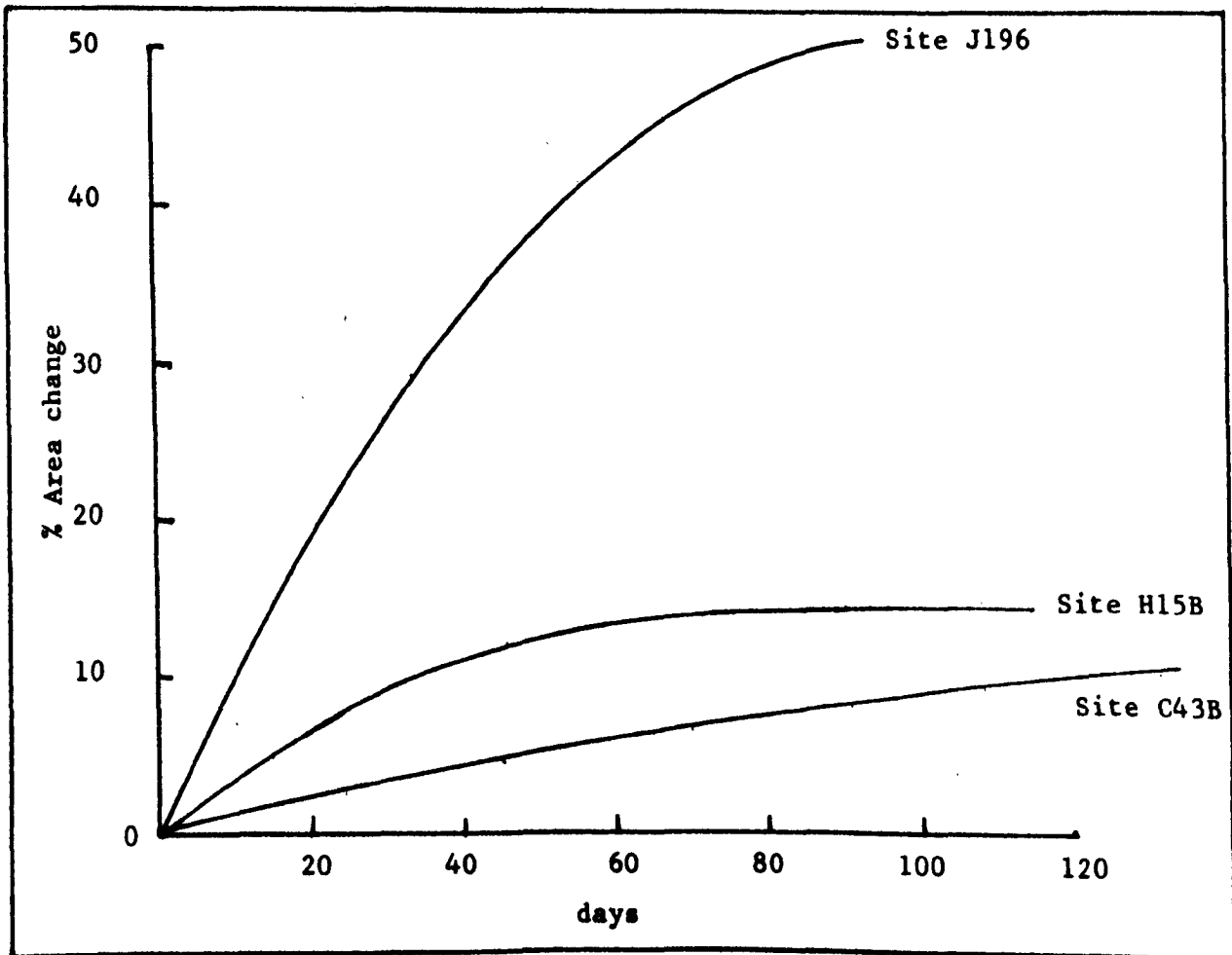


Figure 7.0 Reduction in roadway area with time

7.1.2 Particle Size

Two particle size ranges, -10mm, and -2mm, were tested. The variation in the resulting volumetric closure at 180 kN was again fairly small, being slightly greater (av. 29.8% as against 27.9%) for the -2mm size fraction sample. It can be concluded that from a practical point of view, these results are not significant. The test particle size fractions that were chosen had similar ratios of particle size to test cell diameter as the ratio of actual lump size to excavation width (0.02 and 0.124). These ratios represent lump sizes of 12cm and 75cm.

7.1.3 Temperature

Samples of the -10mm size range were tested at room temperature (19°C) and at 50°C. with different width to height ratios. Although the average value obtained at 50°C. was slightly higher than that at room temperature (30.7% compared with 27.9%), this difference is not felt to be practically significant. It is possible that the creep properties of the rocksalt fill may change with temperature, but this effect may not be significant at the expected virgin rock temperature.

7.1.4 Water Content

Tests were carried out on rocksalt at room temperature containing 5% water and at 50°C. containing 2% and 5% water. The addition of water at room temperature had a marked effect on the

volumetric closure at 180 kN. The average closure increasing from 27.9% with dry salt to 38.4% with 5% water. This can be attributed to a decrease in friction between rocksalt particles due to the lubricating effect of brine formed on the particle surfaces. In addition there is some evidence that greater instantaneous creep occurs with wet rocksalt particles under load.

The rocksalt material which was initially dry, was observed to be unable to absorb more than about 2% of water without a saturated brine solution appearing. When the 5% mixture was tested, a certain amount of brine was squeezed out of the cylinder as the load was increased. An attempt was made to make a 10% mixture, but the results were meaningless due to the formation of a great deal of brine.

Two sets of tests were also done on wet rocksalt at 50°C., one with 2.5% water and the other with 5%. The mean volumetric closure values were 35.5% and 33.2%. These appear to be significantly higher than those obtained from dry samples and similar to the values for the 5% water sample at room temperature.

It is concluded that dry material will develop load more rapidly than fill containing water since even an amount as small as 2.5% appears to be able to lubricate the particles sufficiently to accelerate the closure process.

7.1.5 Initial Density of Compaction

The effect of increasing the initial compaction and therefore

the density of the stowed material can be seen by reference to Figure 7.1. The average curve for the -10mm, dry, W:H = 1.2 sample has been drawn. Successive curves representing density increases of 5, 10, 15 and 20 percent were obtained by transferring the origin to the required point on the original curve to stimulate increases in density.

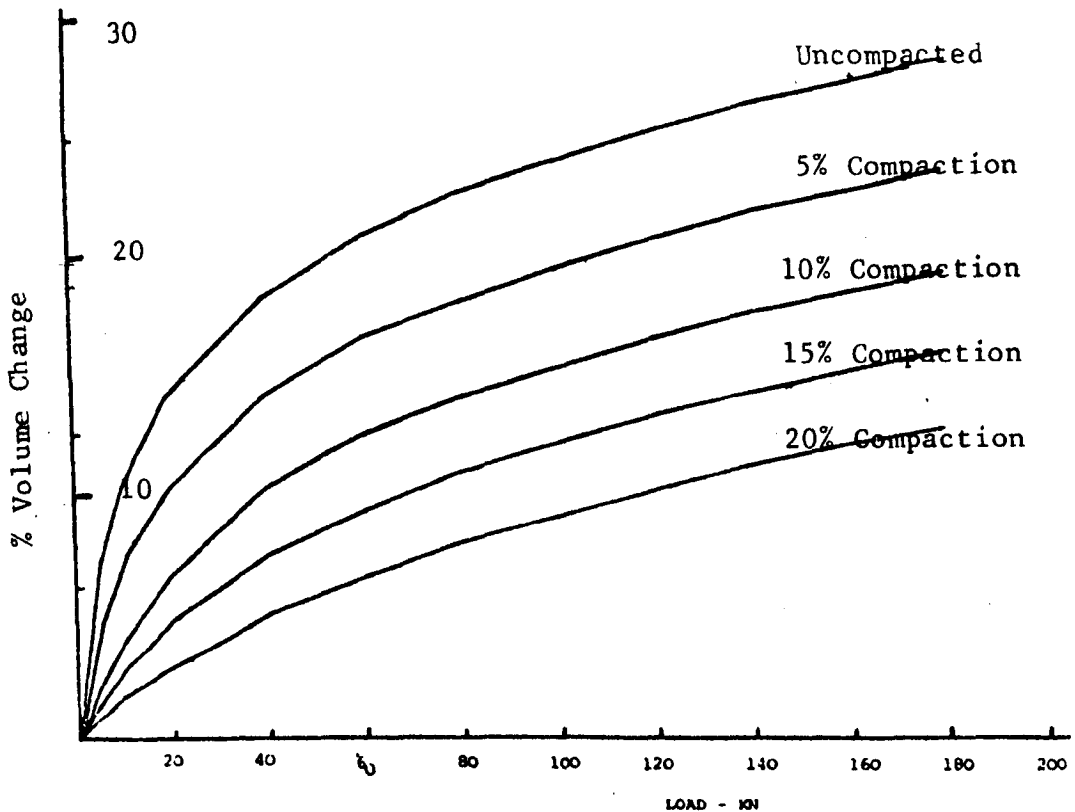


Figure 7.1 Effect of initial compaction on fill properties

The new origins were obtained by calculating how much the piston would have to compress the original volume and therefore decrease the height of the salt sample, since the cross-sectional area remains constant, in order to increase the density the required amount. The density of the uncompacted fill was calculated

to be 1.383 gr/cm^3 . It can be seen from Figure 7.1 that if the density of the stowing material can be increased by 20%, the volumetric closure required to achieve 180 kN load is 12.9%. This is a considerable improvement over the 28.5% for uncompacted fill. If this could be achieved in practice, it would mean that the filled excavations would not only stabilise in a shorter time, but also subsidence effects due to roadway closure would be considerably reduced.

There is no doubt that apart from the addition of cement, precompaction of the fill by increasing its density, produces the best results in terms of stiffening the stowed material.

7.1.6 Conclusion on Uncemented Rocksalt Fill

1. The presence of even small amounts of water decreases the effectiveness of fill to develop load when increasingly confined.
2. Roadway width to height ratio has no significant effect on the performance of the fill material.
3. Particle size in the range tested has a marginal effect on fill performance. Further tests should be carried out, particularly on material that has passed through the stower.
4. Small temperature variations (19°C. to 50°C.) appear to have a marginal effect on fill performance and more tests are required to fully evaluate its effects.

5. Initial compaction and therefore density of the fill when it is stowed, is the most important parameter leading to rapid load development. Every effort should be made to increase the initial stowing density.

7.1.7 Surface Trials using the Markham Stower

The Markham Stower acquired by the mine was set up on surface in the r.o.m. potash storage shed and a test tunnel erected nearby. This was constructed of precast concrete segments, Plate 7.1. As r.o.m. rocksalt was not available, it was decided to use r.o.m. potash instead. Drums were set at different positions in the tunnel and potash stowed into them in order to try to assess the stowing density. From the eleven drums of stowed potash, the average stowed density was calculated to be 1.44 gr/cm^3 , with values ranging from 1.38 to 1.58. No correlation between the drum location and density was found. The uncompacted density of r.o.m. salt was found to be 1.28 gr/cm^3 and that of r.o.m. potash, 1.37 gr/cm^3 .

The trials showed that the stowed density did not vary with distance from the stower's nozzle, nor with the amount of water added at the stower inlet. It was also found that the stowed material did not form a vertical face, but ran down to form a natural angle of repose. This was found to be a fairly consistent 32° . It must be said that the Markham Stower is not designed to compact material, but merely to place it, and in this regard the machine performed satisfactorily. The high velocity and fairly large air volume resulted in much rebound which is a problem that will have to be attended to.

7.2 Saltcrete

The possible use of saltcrete, a mixture of rocksalt, cement and water, as an alternative to uncemented fill material, was investigated by assessing its physical and mechanical properties in the laboratory.

Consistent specimens were obtained by careful hand mixing of ingredients. Because of the limited time available, it was possible to repeat only some of the tests to check results and accuracy. Test specimens were made by casting in a cylindrical mould. It is interesting to note that test work involving cement and concrete is carried out on cubes in Britain and much of Europe. However, there is a trend towards greater use of cylinders, and this is the standard adopted in the U.S.A., France, Canada, Australia and New Zealand.

7.2.1 Size Analysis of r.o.m. Rocksalt

The run of mine rocksalt obtained from a heading in the north-east development at Boulby was subjected to a particle size analysis. Only the -8mm size fraction was considered, as this was the fraction that was used in the tests. The mean results of several separate analyses are given in Table 7.2.

7.2.2. Preparation of Specimens

In order to obtain a good mix, in which the surface of all the rocksalt particles would be coated with cement paste, the

Plate 7.1

- 1 Mock up roadway on surface.
- 2 Markham Stower.
- 3 Bin for catching fill materail.
- 4 Stowing nozzle.

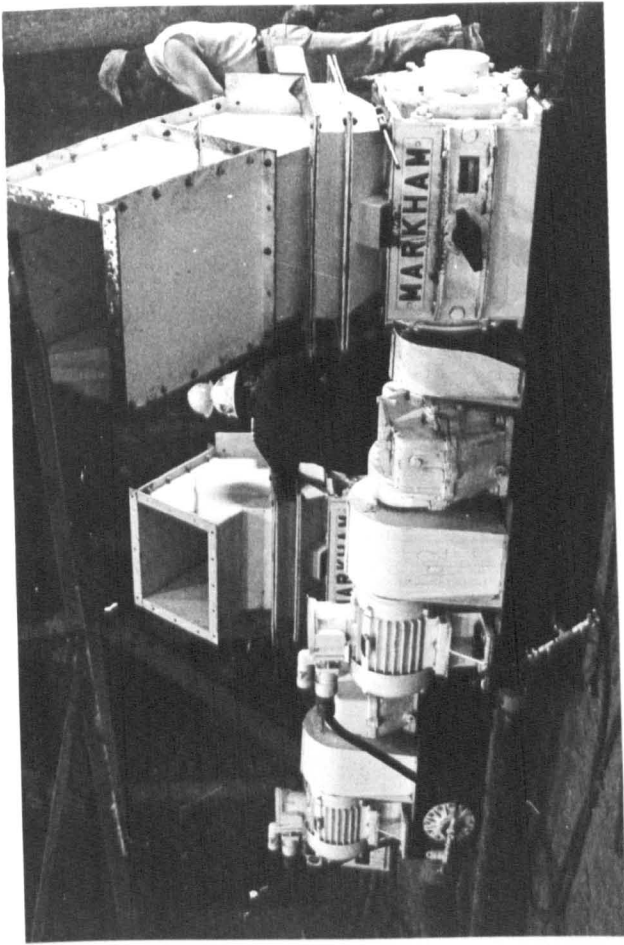


TABLE 7.2

Size Analysis of r.o.m. Rocksalt

Size Fraction	Weight (g)	%
-8mm + 4mm	2516.6	39.95
-4mm + 2mm	1646.9	26.15
-2mm + 1mm	1429.9	22.70
-1mm	705.3	11.20
Total	6298.7	100

rocksalt sample was thoroughly mixed by hand, with the correct proportion of Portland cement before the addition of any water. Water was then slowly added, while continuing the mixing process until the desired water/cement ratio was achieved. Mixing was carried out on a plastic sheet, after which the saltcrete was put into the plastic cylindrical moulds and placed on a vibratory table vibrating at 60 cycles/sec. for a minimum of 20 minutes in order to achieve maximum compaction. The moulds were coated with grease to promote easy removal.

After curing at 19^oC. and 40% humidity for five days, the specimens were removed from their moulds by pressing and then cut to the appropriate length and allowed to continue to cure. The effect of curing at different temperature following removal from the mould can be seen in Figure 7.2 which shows the loss in weight

with time as a result of different rates of hydration. Hydration is the diffusion and subsequent chemical reaction of moisture throughout the saltcrete. More rapid hydration produces accelerated setting which generally results in lower strength.

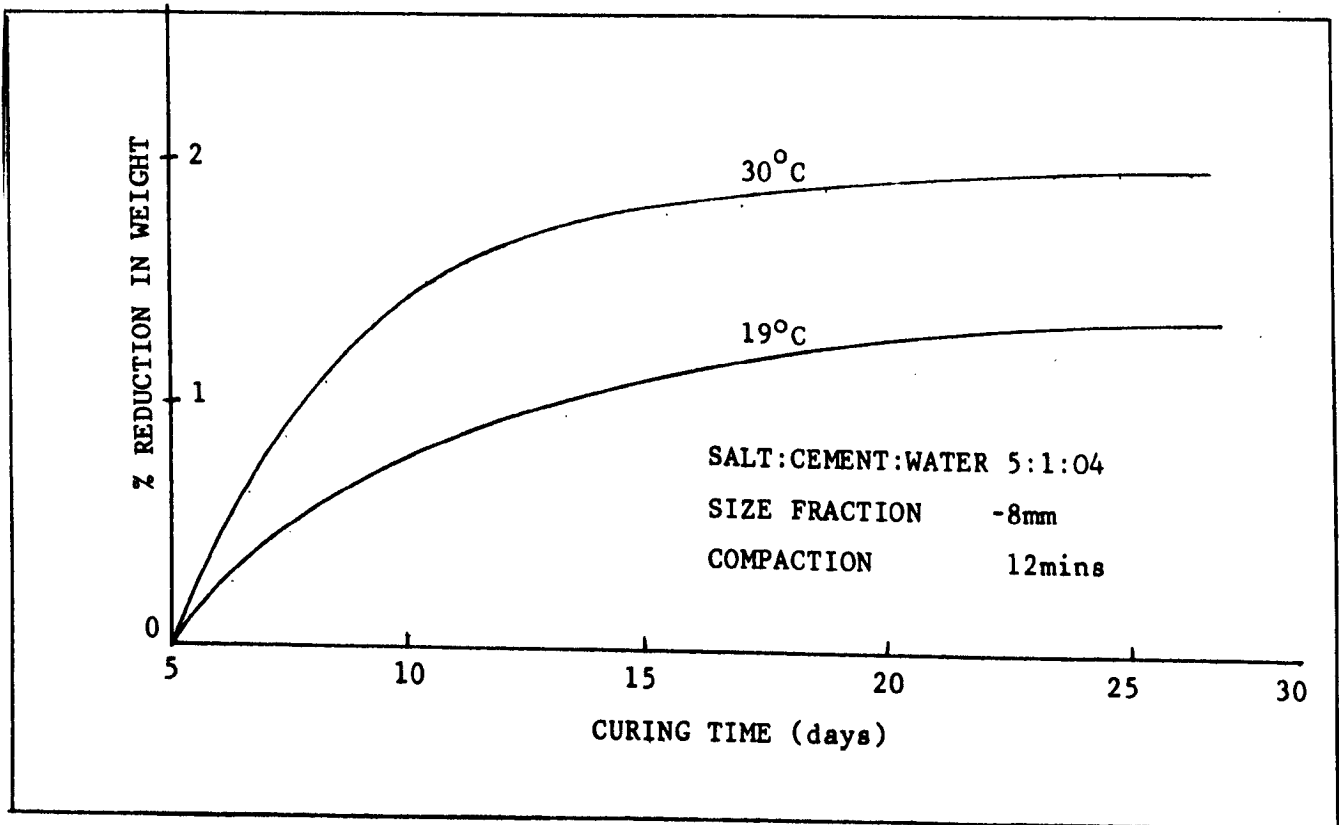


Figure 7.2 Effect of variation in curing time on saltcrete

7.2.3 Laboratory testing

Various properties of saltcrete were determined in a number of tests carried out in the laboratory. Instantaneous compressive tests were carried out at a loading rate of approximately 1 MPa per second.

The properties investigated were:

- (1) Increase in strength with age.
- (2) Effect of varying the cement content.
- (3) Effect of particle size.
- (4) Effect of different compaction.
- (5) Effect of varying the water/cement ratio.
- (6) Modulus of elasticity.
- (7) Tensile strength.
- (8) Mohr failure envelope.
- (9) Time dependent behaviour.

7.2.3.1 Variation of strength with time

From Figure 7.3 it can be seen that similarly to concrete,

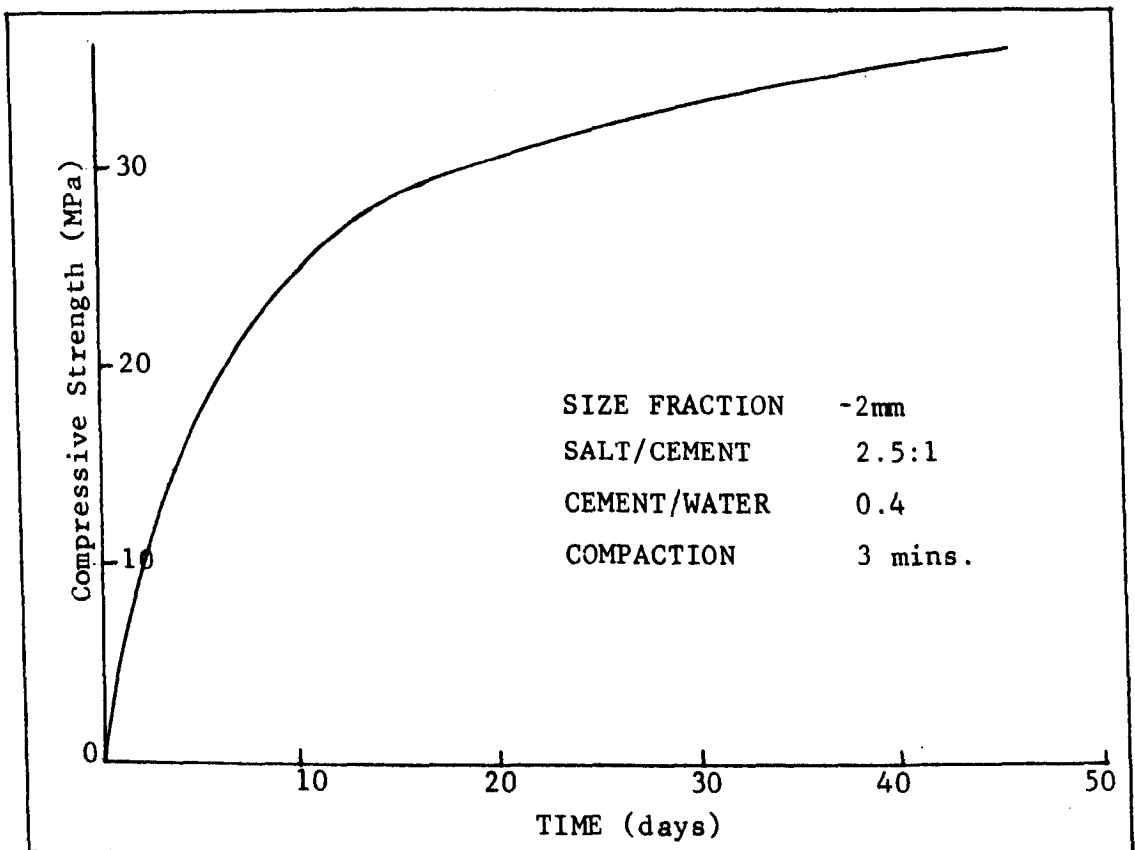


Figure 7.3 Saltcrete - Compressive strength vs. curing time

the compressive strength increased with time of curing. This time dependent property could be important if the saltcrete is to be used in excavations that themselves exhibit time dependent deformation.

7.2.3.2 Effect of varying the cement content

Different salt/cement ratios were tested after 36 day and 45 day curing periods, on specimens with two size fractions. Water /cement ratio, temperature and compaction were kept the same. The results are shown in Figure 7.4.

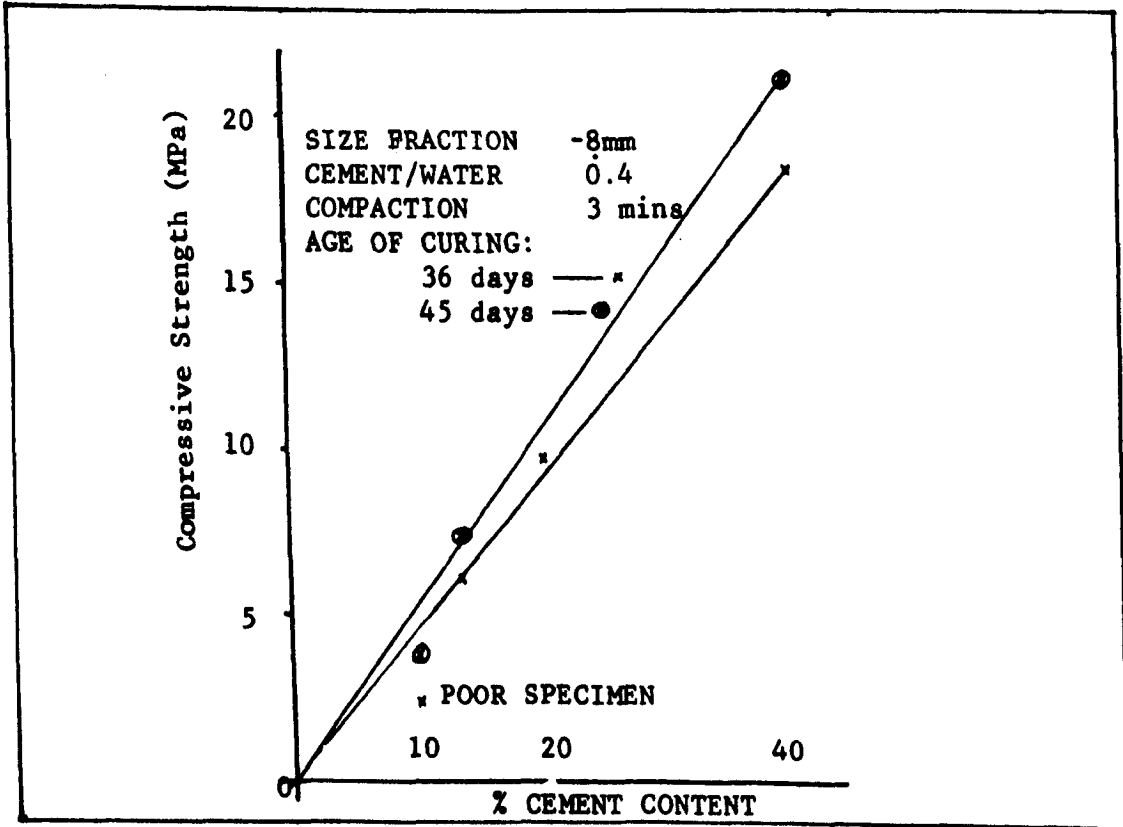


Figure 7.4 Saltcrete - Cement content vs. strength

As expected, increased cement content resulted in an increase in strength. The mix itself was also more workable. Figure 7.5 shows

the increase in density that occurred with an increase in cement content. This is due to the fine cement particles filling voids in the matrix, thus reducing the void ratio, giving higher strength. At higher cement/salt ratios, the increase in density was greater with the finer particle specimens.

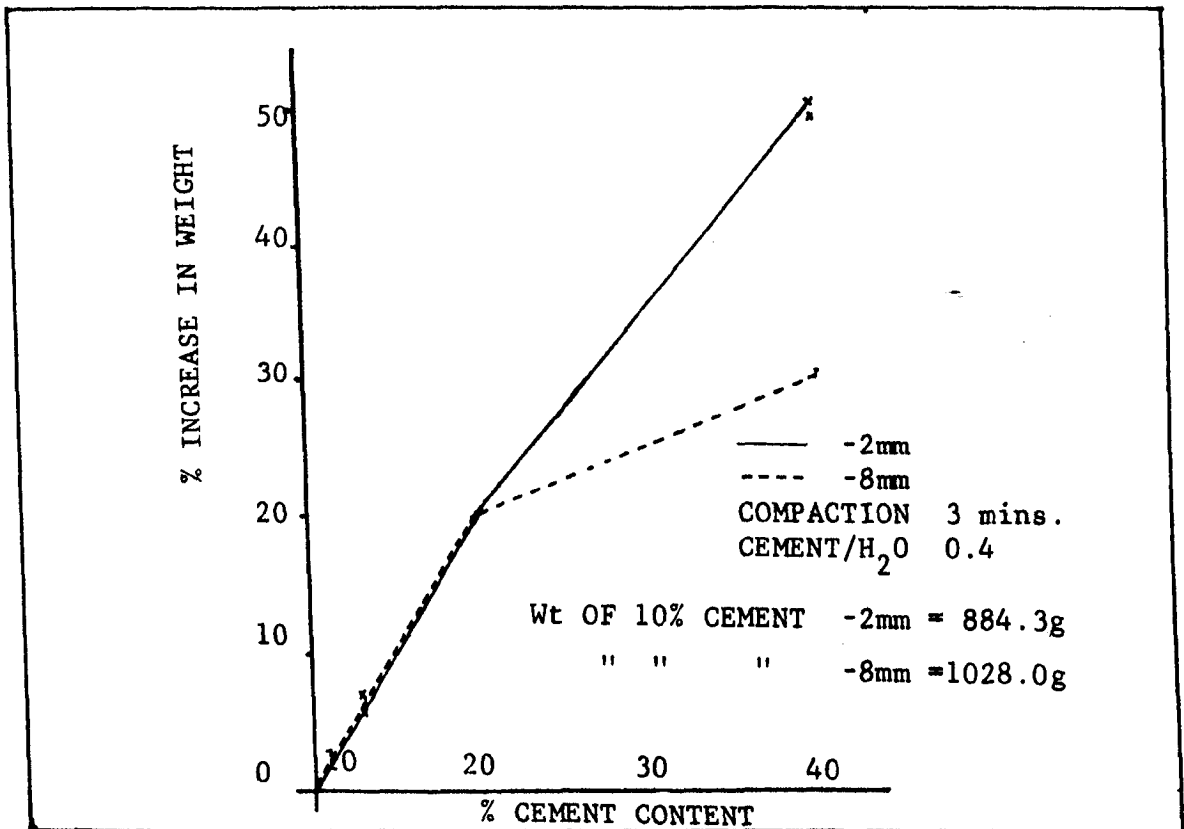


Figure 7.5 Increase in density vs. cement content

7.2.3.3. Effect of varying the particle size on the strength

Specimens using -8mm, -4mm, -2mm and -1mm size fractions and with the same salt/cement/water ratio, and degree of compaction, were made and strength tested. The results are shown in Figure 7.6.

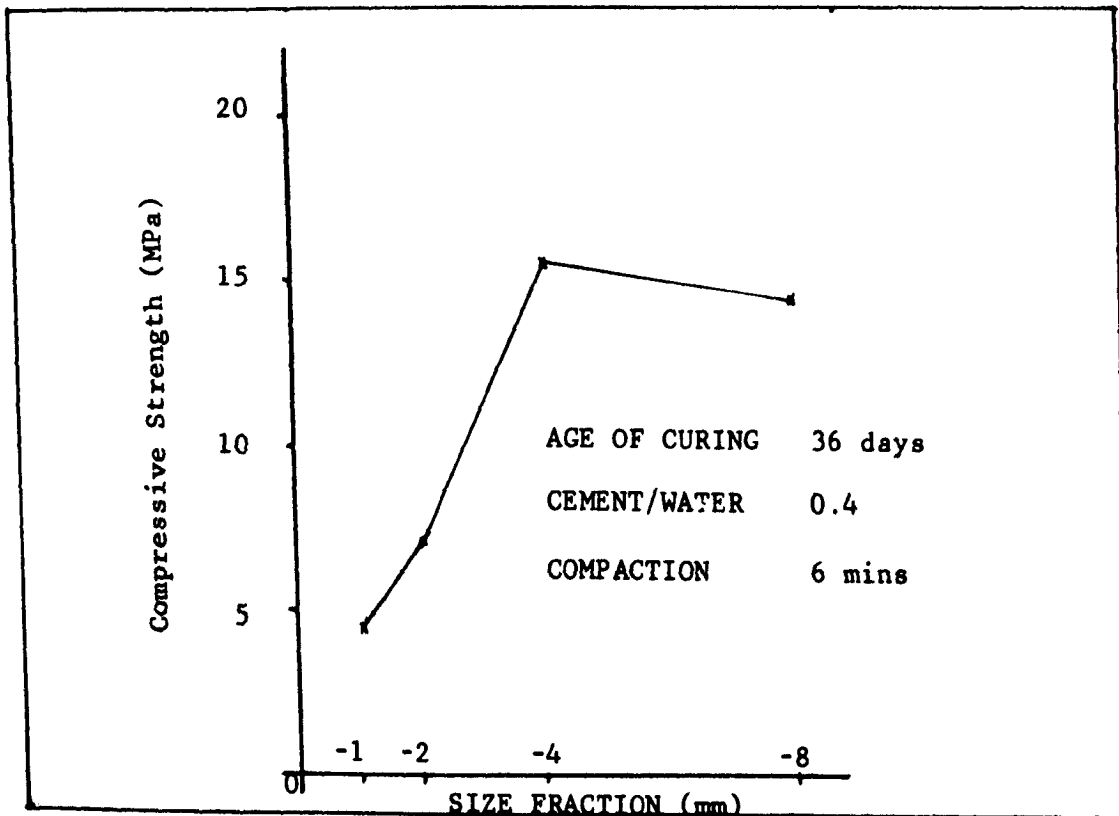


Figure 7.6 Particle size vs. strength

Clearly the particle size has an influence on the strength of the saltcrete. With the increase in particle size, there was an increase in apparent dampness and also workability of the mix. This can be explained by the greater surface area available on the samples with smaller particle size.

7.2.3.4 Effect of varying the compaction

The effect of increasing the time of vibration and thus compaction on the strength is illustrated in Figures 7.7 and 7.8. It can be seen that the major effect is achieved within the initial 20 minutes, after which the relative benefits of further vibration decrease rapidly.

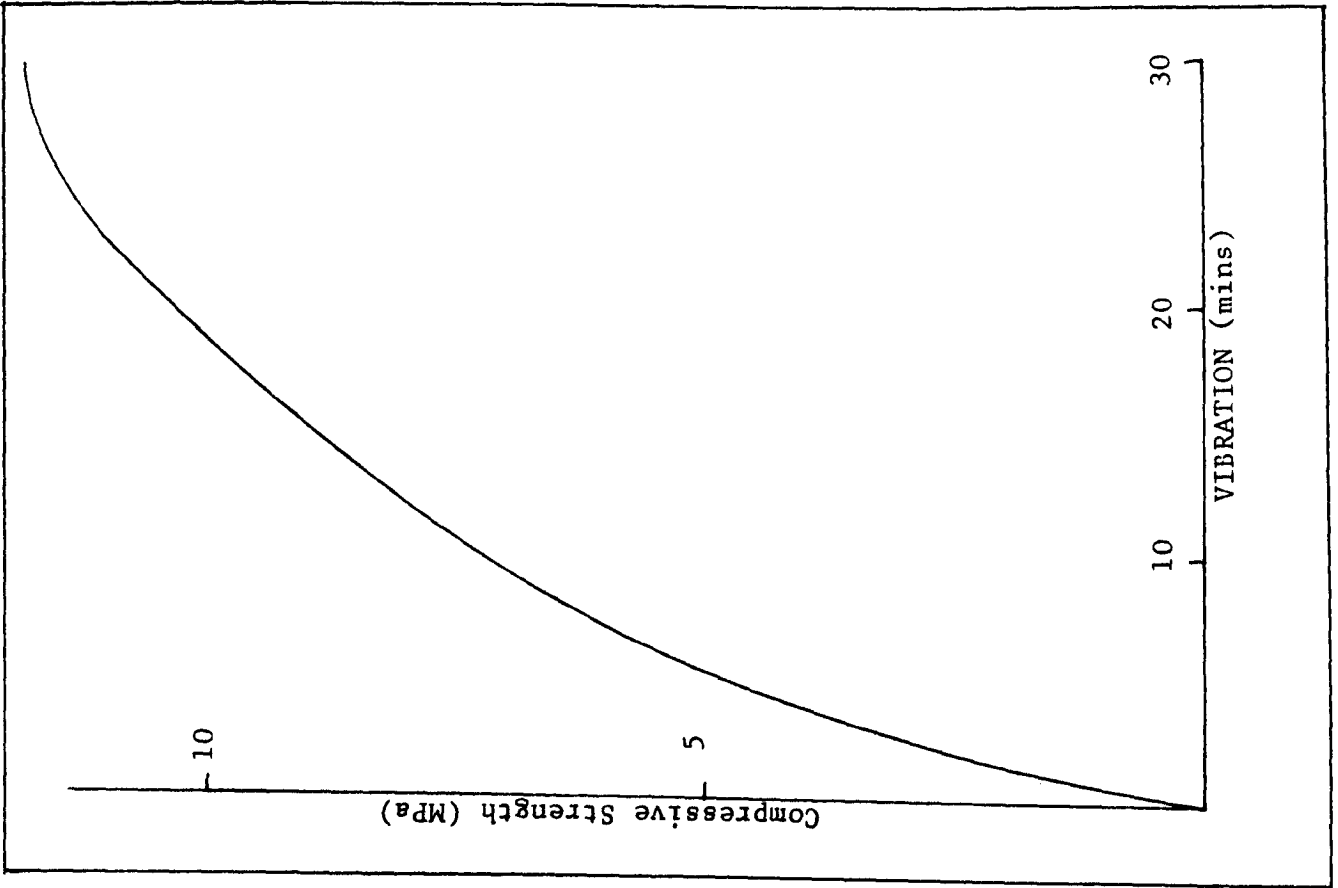


Figure 7.7 Compaction vs. Strength

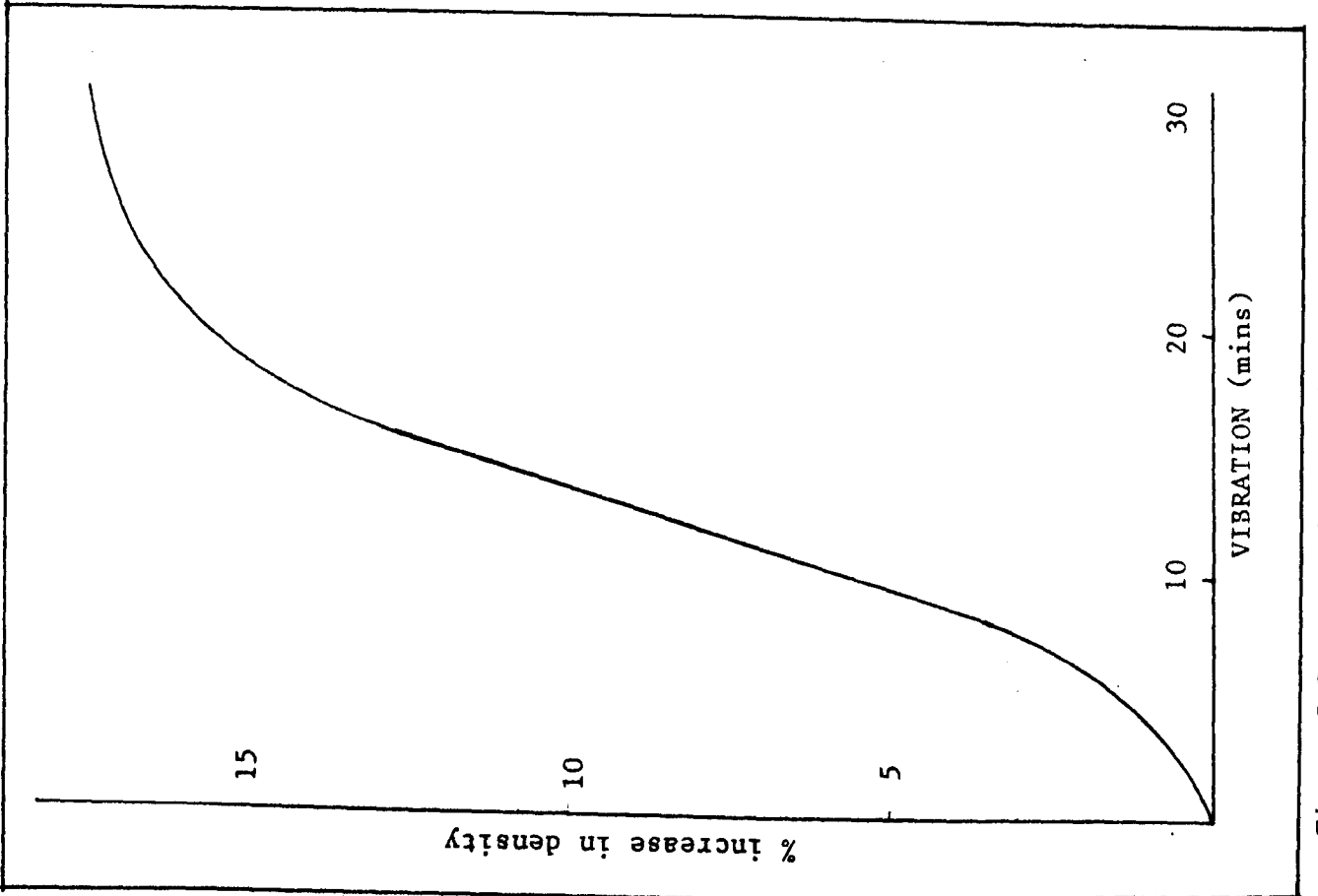


Figure 7.8 Compaction vs. increase in density

7.2.3.5. Effect on strength of varying the water/cement ratio

For normal Portland cement, one part by weight of cement requires 0.26 parts by weight of water for complete hydration⁽³⁵⁾. However, this mix would be very dry and exceedingly difficult to work. Extra water is therefore added to lubricate the mix. As all excess water evaporates when the saltcrete dries, leaving voids, it is important that this excess is kept to a minimum. Figure 7.9 gives the results of varying the water/cement ratio on the strength of saltcrete specimens. A marked increase is noted from a ratio of 0.25 to 0.5. It was noted that with the increase in water/cement ratio, water tended to separate out when being vibrated. The optimum ratio would appear to be between 0.4 and 0.5, a result which is in agreement with Forster⁽³⁴⁾.

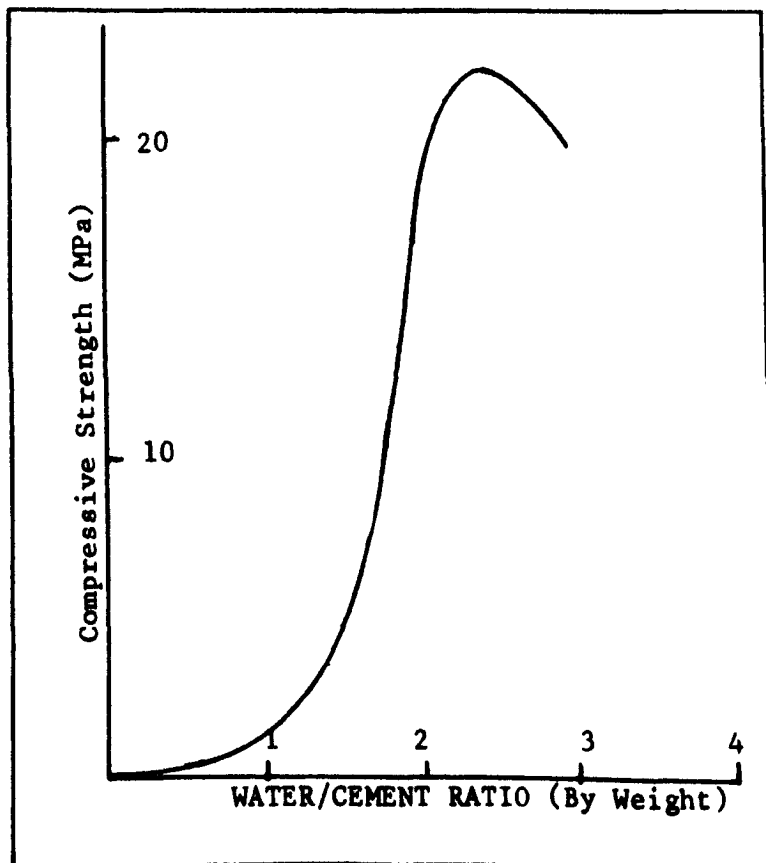


Figure 7.9 Water/cement ratio vs. strength

7.2.3.6 Modulus of elasticity

In order to determine a modulus of elasticity, the samples were loaded and unloaded four times to 35 kN, then loaded to failure. Deformation was recorded by means of dial gauges. The secant modulus was calculated at approximately half the uniaxial compressive strength on the fourth loading cycle. Table 7.3 summarises the results of the tests done, while the full set of graphical results are given in Appendix 5. It would appear that even at the loading rate of 1 MPa/sec. creep occurred between loading cycles. The plastic strain diminishes at each repeated loading, although the total plastic deformation increased. Specimens 3 and 4 were cured at higher temperatures and it can be seen that the modulus was increased, but the ultimate strength decreased. The modulus is also increased with increase in compaction, specimens 5 & 6. This is most likely due to a decrease in the void ratio.

7.2.3.7 Effect on tensile strength

The tensile strengths of six samples were determined using the Brazilian disc method. Three discs were cut from each of two cylindrical specimens made in the normal way. The three discs were taken from the top, middle and bottom of the cylinders. The results are given in Table 7.4 and reflect that compaction is better near to the base of the specimen. It is interesting to compare the results for saltcrete with those for the near seam

TABLE 7.3

Results of Determination of Modulus of Elasticity
of Samples of Saltcrete

Specimen No.	Modulus of Elasticity	Remarks
	GPa	
1	5.22	
2	4.92	3 min. vibration
3	8.85	curing temperature 30°C.
4	7.32	curing temperature 30°C.
5	4.92	10 min. vibration
6	8.19	30 min. vibration
7	2.24	Loading Modulus
7	4.85	Unloading Modulus

All except specimen No. 7 were measured after four loading cycles

Mean secant modulus 6.57 GPa

rocks at Boulby after Hebblewhite⁽⁷⁾ - Table 7.5.

TABLE 7.4

Tensile Strengths, Saltcrete Specimens

Particle Size	Position in specimen	Weight (g)	Tensile Strength (MPa)
- 2mm	Base	278.9	2.49
	Middle	269.9	2.01
	Top	266.6	1.89
			Av. <u>2.13</u>
- 8mm	Base	329.2	3.76
	Middle	312.6	3.23
	Top	303.9	2.85
			Av. <u>3.28</u>

TABLE 7.5

Mechanical Properties, near seam rocks, Boulby Mine

Material Type	Young's Modulus GPa	Poisson's Ratio	Compressive Strength MPa	Tensile Strength MPa
Carnalite Marl	7.01	0.20	14.66	1.24
Shale	11.02	0.24	12.20	1.18
Potash		0.37	39.66	1.79
Middle Halite		0.28	26.77	1.63

7.2.3.8 Mohr Envelope

The Mohr envelope was obtained from testing three specimens in a triaxial cell. Confining pressures of 5.17 MPa and 10.34 MPa were used. The results are shown in Figure 7.10. An extra point on the curve can be obtained if the tensile strength value is included.

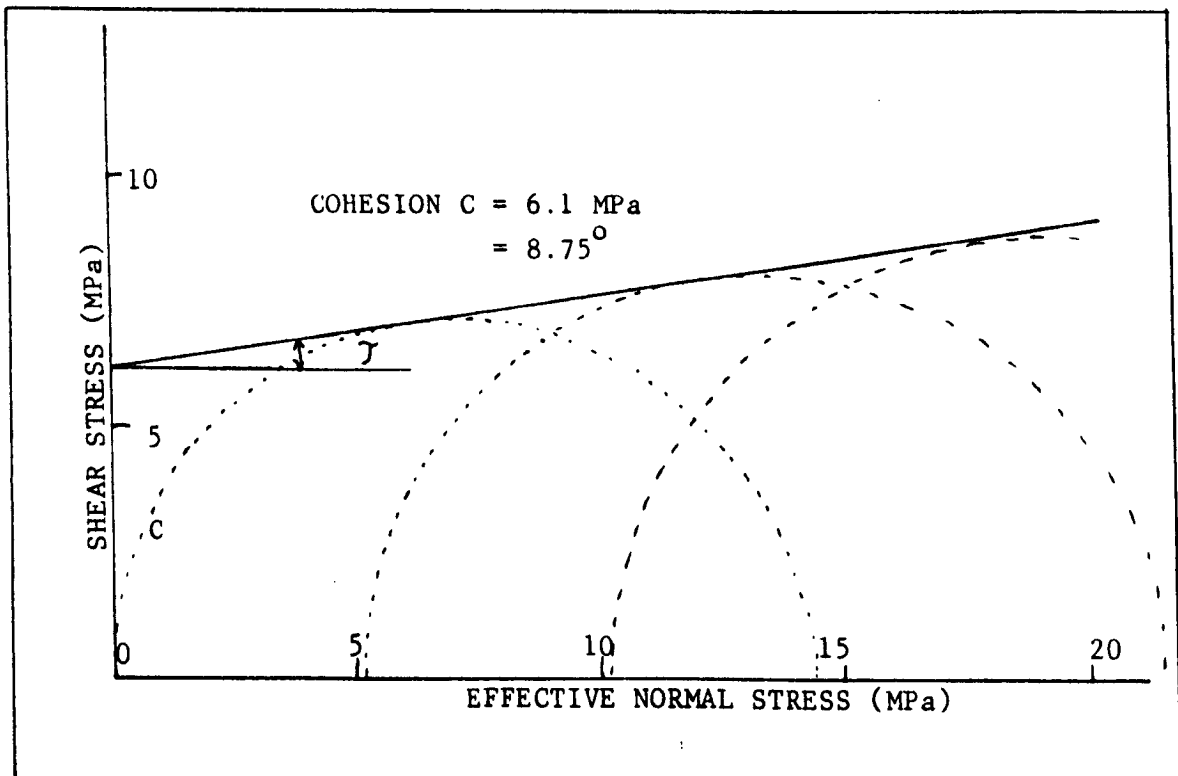


Figure 7.10 Mohr envelope

7.2.3.9 Time Dependent Behaviour

It was possible to conduct a creep test on only one specimen which had been cured for 36 days. The creep rig is shown in

is shown in Plate 7.2. The specimen was loaded uniaxially to approximately 50% of its ultimate compressive strength, and was sleeved with rubber to prevent a loss of water due to evaporation. To simulate underground conditions, the test was conducted at 40°C. The results are given in Figure 7.11. It would appear that under the test conditions prevailing, the saltcrete was still in a state of primary creep after 28 days, following a curve of the general form $\dot{c} = A \log B$. The test was terminated after 28 days and a modulus of 4.85 GPa was obtained when the specimen was unloaded.

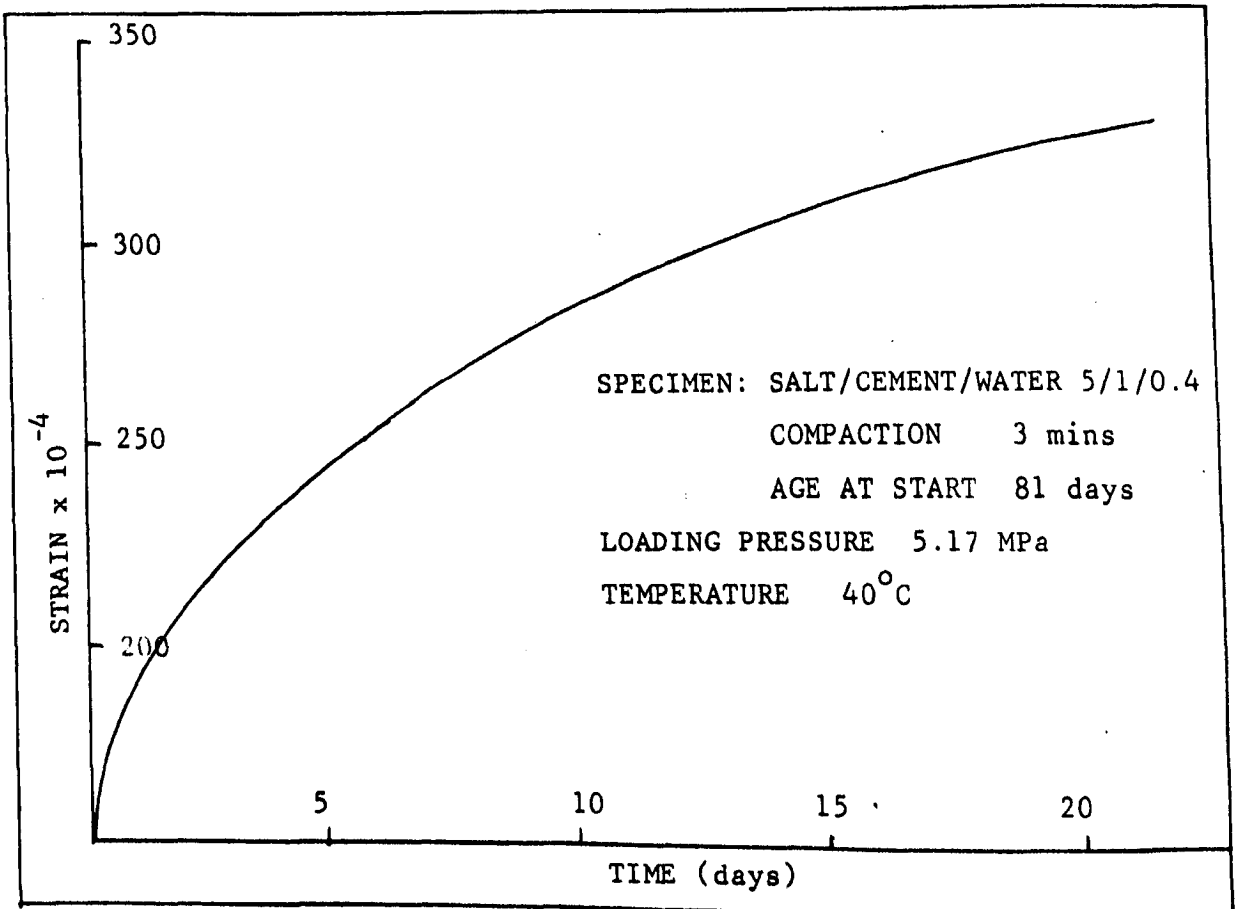


Figure 7.11 Creep Test

7.2.3.10 Effect of Water on Saltcrete

Because of the presence of water in the mine, it was decided to assess the possible effects of water on saltcrete. Tests were carried out on specimens using tap water. This is a worse case than could be expected underground, where any free water would probably be saturated or near saturated brine. Specimens of different particle sizes and salt/cement ratio, were immersed in water at room temperature for a week, weighed and allowed to dry out and reweighed after different time intervals. The resulting loss in weight due to evaporation was then calculated. The results are shown in Figure 7.12 and Table 7.6.

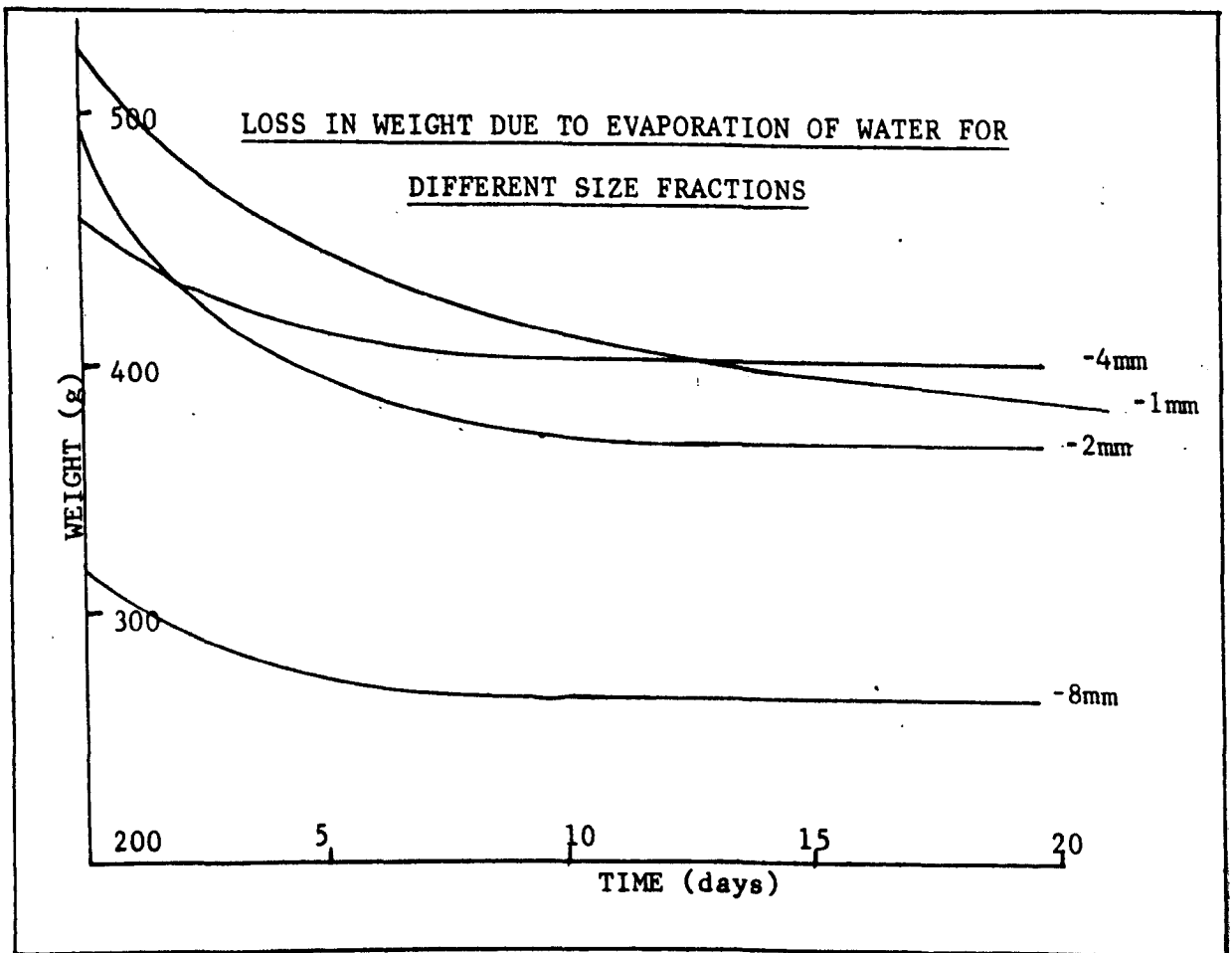


Figure 7.12 Water immersion results

Plate 7.2

Creep Rig

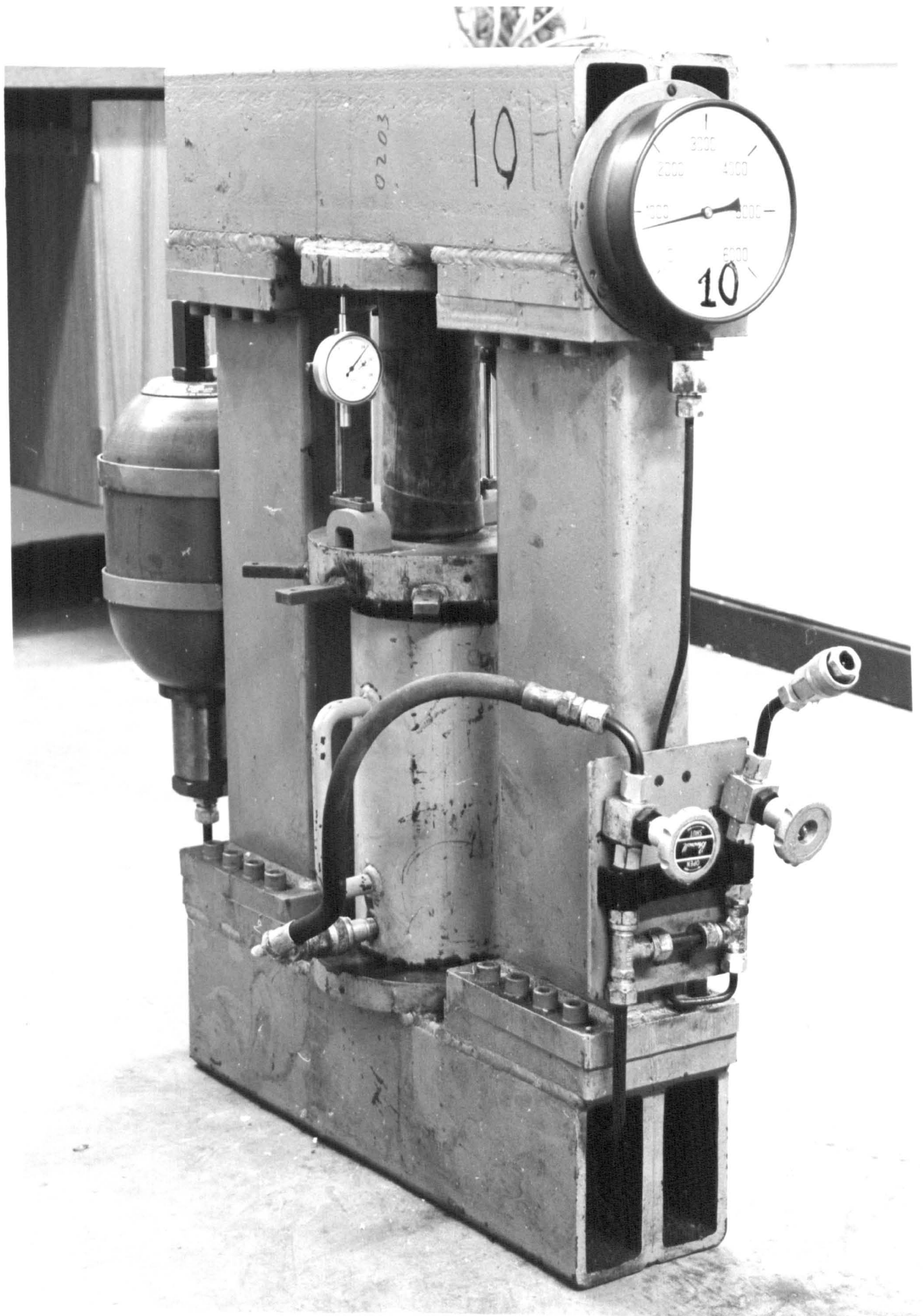


TABLE 7.6

Effect of Water on Saltcrete Specimens

Salt:Cement Ratio	Particle Size	Orig. Wt.	After 1 week 50° C.	Wt. after drying out	% H ₂ O Uptake	% Break -down
2.5:1	-8	446.4	390.1	337.8	13.4	24.3
5:1	-8	580.0	471.2	380.1	19.3	34.5
7.5:1	-8	530.4	CRUMBLLED			
10:1	-8	676.9				
2.5:1	-2	768.8	700.4	631.2	9.9	17.9
5:1	-2	626.2	582.5	400.1	31.3	36.1
5:1	-8mm	375.4	322.2	266.0	17.4	29.2
5:1	-4mm	517.7	468.3	402.1	14.1	22.3
5:1	-2mm	540.9	440.0	370.1	31.5	31.6
5:1	-1mm	441.3	512.2	371.5	27.5	12.9

It would appear that the smaller the particle size, the greater the water uptake, and the larger the particle size, the greater is the total breakdown of the saltcrete. The effect of increasing the amount of cement in the mix is also clearly evident. The 7.5:1 and 10:1 tests showed about half the resistance to attack as the 2.5:1 tests. It was also clear that the elevated temperature had a marked effect on the ability of the water to dissolve the salt in the saltcrete. One specimen was loaded uniaxially

after immersion in water and subsequent drying out and its compressive strength was found to be 0.3 MPa. This showed a great reduction from the expected normal value of 17 MPa.

7.3 Summary of Conclusions

7.3.1 Uncemented Fill

The effectiveness with which uncemented rocksalt will develop load is influenced most strongly by water content and initial compaction. Even small amounts (2.5%) of water, decrease this effectiveness. Initial stowed density is the single most important factor influencing the subsequent load bearing capability of the fill material. This derives from the fact that the load/compaction curve follows an exponential path.

The Markham Stower, although suitable for placing rocksalt fill material, is not able to increase the initial stowed density to any significant degree.

7.3.2 Cemented Fill

1. Saltcrete increases in strength with age and the effect is most marked up to 15 days after the onset of curing.
2. In order to achieve a reasonable strength, the cement content has to be at least 20%. For a given salt/cement ratio, generally the larger the particle size, the weaker the specimen.

3. There is a marked increase in strength as the water/cement ratio goes from 0.25 to 0.5, with the optimum being between 0.4 and 0.5.
4. The tensile strength increases with an increase in particle size, and with the density of compaction.
5. Saltcrete would appear to exhibit a fair degree of time dependent deformation. This could be as much a function of the presence of voids as the creep properties of salt itself.

CHAPTER EIGHT

LABORATORY TESTING AND THIN SECTION ANALYSIS

Chapter Eight

8.0 Introduction

The validity of testing rocks that exhibit time dependent behaviour in the laboratory and then applying the results to the design of excavations in such rocks has been strongly questioned by Baar⁽²¹⁾ and others. Baar's main objection to this type of approach has been that because the rates at which rocks are loaded in-situ are much slower than in the laboratory, the resulting stress/strain/time behaviour is not comparable. An attempt has been made to verify whether this is so or not. Baar disputes the occurrence of in-situ strain hardening, also on the grounds of differences in loading or strain rate, and this problem is also investigated.

8.1 Test Specimens and Procedure

The tests were carried out in a 100t compression testing rig that had an electronic control console for controlling the loading of the specimens so as to obtain constant strain rates.

One of the difficulties in obtaining true stress/strain relationships from laboratory trials arises from the problem of measuring the change in loaded area as the specimen undergoes deformation. By cleaning away failed material from the test specimen as it deforms and measuring the diameter of the remaining core, an estimate of the bearing area could be obtained. The relationship between area and deformation was found to be linear

and by knowing the initial and final areas of the test specimens, the stress corresponding to any deformation and therefore strain, could be calculated. This enabled stress/strain curves to be constructed from the load/deformation graphs obtained directly from the tests.

Table 8.1 lists the test specimens and some of the results. Specimens 1, 2 and 3 were rocksalt from Winsford Salt mine, Cheshire, and were included partly for comparison with Boulby Upper Halite and partly because they were samples that were readily available for early trials to gain confidence in the use of the test rig.

Specimens 4, 5 and 6 were obtained from the S1 surface borehole core which had been kept in air conditioned storage by the mine geologists. The section of core from which the tests specimens were cut came from a depth of 1042.4m below surface. This section was chosen, not only because it came from Upper Halite, but because its polycrystalline structure showed a well defined direction of flow. It was felt that this preferential crystal alignment may well result in strengthening of the rock in one direction rather than another. Observations of both this salt as well as potash specimens in thin section, before and after straining, have been made and are discussed in Section 8.3.

Strain rates were determined by setting the maximum closure and the time over which this had to take place. Deformation was

TABLE 8.1

Test Specimens and Results

Spec. No.	Rock Type	W:H	Duration of test	Strain Rate	Maximum Load	Strain at max Load	Stress at max. Load	Load at 10% strain	Stress at 10% strain
1	Winsford Salt	1:1	5 x 10 ⁴	2.70	172	3.6	37.19	107	34.39
2	Winsford Salt	1:1	1 x 10 ⁴	12.16	173	3.7	34.86	128	31.30
3	Winsford Salt	1:1	1 x 10 ³	132.14	172	1.5	35.15	46	29.93
4	Boulby Upper Halite	1:1	1 x 10 ⁴	16.0	160	4.2	46.30	135	65.78
5	Boulby Upper Halite	1:1	1 x 10 ⁴	16.0	146	5.9	47.25	125	49.55
6	Boulby Upper Halite	1:1	1 x 10 ⁴	16.0	119	4.4	38.51	75	26.47
7	Primary Potash	1:1	2 x 10 ³	100	318	2.8	37.27	202	21.13
8	Primary Potash	1:1	3 x 10 ²	333	325	2.8	37.73	271	28.51
9	Primary Potash	1:1	2 x 10 ⁴	10.0	329	3.2	37.45	249	25.88
10	Primary Potash	1:1	1 x 10 ⁴	10.0	355	3.4	41.50	256	26.74
11	Primary Potash	2:1	2 x 10 ³	200	513	7.7	57.94	496	58.27
12	Primary Potash	2:1	2 x 10 ³	200	507	2.5	53.15	400	49.04
13	Primary Potash	2:1	2 x 10 ⁴	20	473	8.0	50.57	456	49.61
14	Primary Potash	2:1	3 x 10 ⁵	2.0	473	7.2	50.34	473	51.63
15	Primary Potash	1.5:1	2 x 10 ³	152	393	7.7	48.74	359	48.90
16	Primary Potash	1.5:1	2 x 10 ⁴	15.2	397	7.5	47.80	366	47.28
17	Primary Potash	1.5:1	2 x 10 ⁵	1.5	382	6.9	41.28	366	40.26

measured by means of an L.V.D.T. located between the loading platens, the maximum deformation being set to 10mm for most of the tests. Some of the specimens were reloaded for a second, and in the case of specimen No. 14, a third time, so that total deformations of up to 30mm were obtained. The time settings that were used were 10^3 , 10^4 and 10^5 seconds, giving deformation rates of 10×10^{-6} m/s, 1×10^{-6} m/s and 0.1×10^{-6} m/s, respectively. The resulting strain rates that occurred were dependent on the initial height of the specimen.

8.2 Results

Figure 8.1 shows the relationship between load at 20% strain and log of strain rate for the different width to height ratios

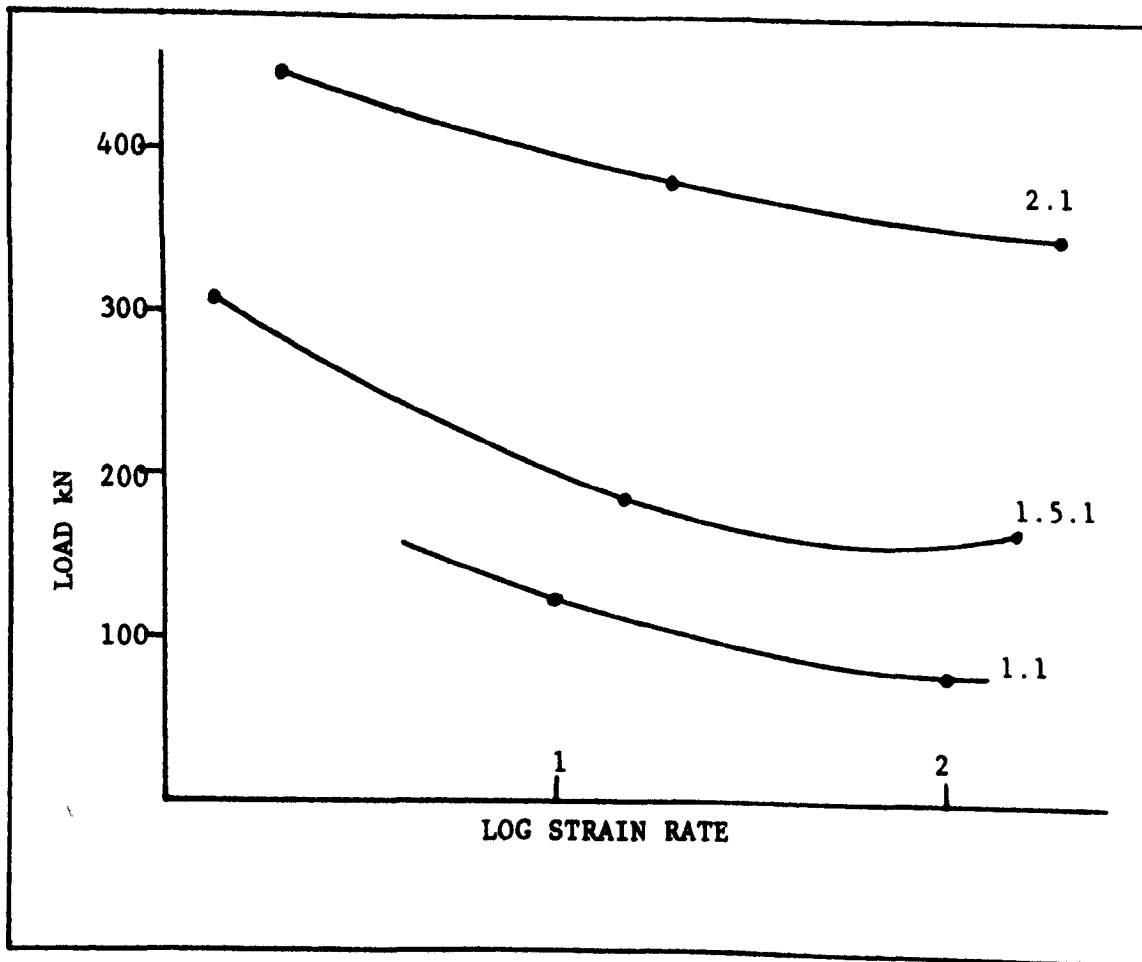


Figure 8.1 Load at 20% strain vs. log strain rate for different W:H ratios

used, namely, 2:1, 1.5:1 and 1:1. These show quite clearly for all three W:H ratios, that as the strain rate is increased, there is a decrease in the load bearing capacity of the rock. However, the maximum load attained by the specimens appears to be relatively unaffected by variations in rate of deformation, and in fact, the maximum load achieved is similar for each set of specimens with the same W:H ratio.

If, instead of load, the stresses are plotted against log of strain rate, a different relationship is obtained. It can be seen from Figure 8.2 that, as the deformation rate is increased on the specimens, and after they have been strained by the same amount of 10%, they are able to withstand a higher level of stress. The results shown in Fig. 8.2 and load/deformation curves given in

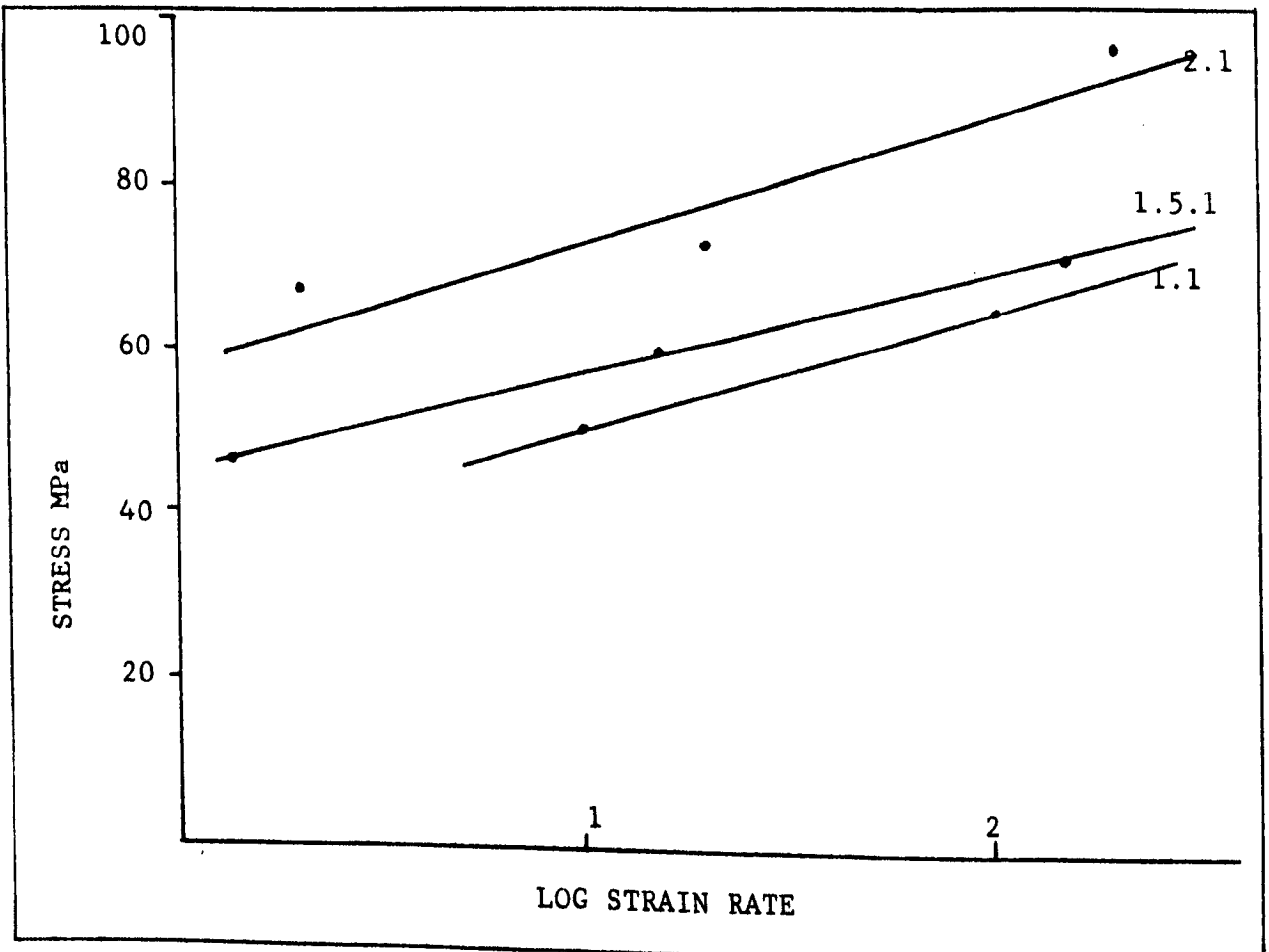


Figure 8.2 Stress vs. log strain rate

Appendix 4 indicate that strain hardening is taking place. The other effect worth mentioning is the obvious one of the increase in load carrying ability as the W:H ratio, increases. This refers of course to the initial W:H ratio, since as the specimen deforms, this ratio will increase. It would appear that a solid core will only develop with a W:H ratio of about 2:1 or greater. Again, this is a result borne out by observation and measurement in the mine on actual pillars, and reported on in other chapters.

8.3 Upper Halite Results and Thin Section Analysis

Specimens 4, 5 and 6 already referred to in Section 8.1, were cubes cut from a section of S1 borehole core, as shown in Figure 8.3, with faces parallel and at right angles to the direction of

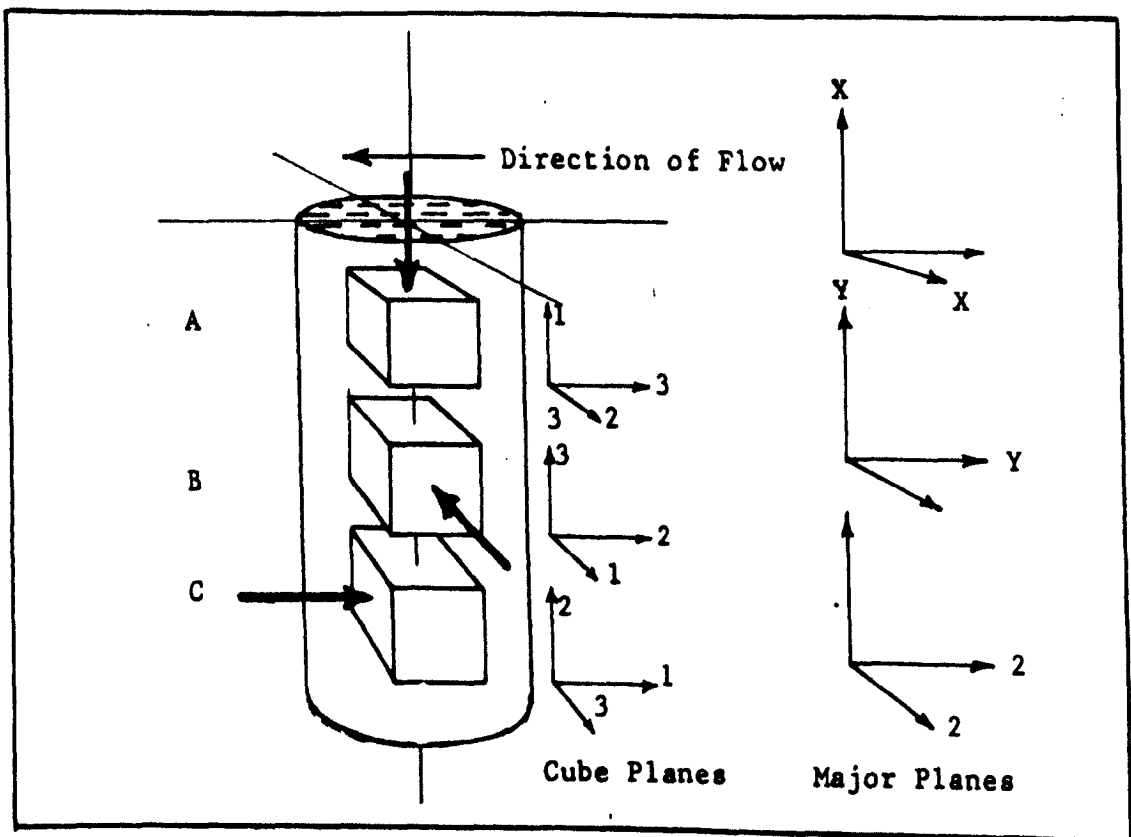


Figure 8.3 Orientation of salt cubes relative to borehole core

flow. These were all tested at a constant strain rate of 16 micro-strain per second, and the total deformation was 10mm, giving a total strain of 16%.

Thin sections were made in the same set of orthogonal planes as referred to above, i.e. parallel and at right angles to the direction of flow, from all three specimens after testing as well as from an untested sample from the same piece of core.

An inspection of these thin sections was made in order to investigate the effect of the loading and straining on the rock fabric. The technique used was similar to geotechnical line logging. With the slide correctly mounted on the petrographic microscope, it was slowly traversed across the stage and all discontinuities in it were recorded along with their distance from the left hand side of the mounted section. This was taken as the zero datum point.

The discontinuities were divided into two categories; grain boundaries (G) and fractures (F). In addition to distinct boundaries, which were often annealed, major cleavage partings, often with clay inclusions, were included in the category of grain boundaries.

The objective was to place all the features due to sedimentary and diagenetic processes in the first category. All other fractures were included in the second category. These were predominantly cleavage partings which were assumed to be due to tectonic stresses

and the test loading. In addition to cleavage partings, which were dominantly planar, a small number of conjugate Reidel type shears were found to be present in the tested specimens.

Because the maximum length of sample line was 42.9mm, it was realised that the presence of exceptionally large grains or clusters of small grains could significantly affect the results. The length of line sampled varied from 24.9mm to 42.9mm, the sample population varied from 43 to 105. The total sample taken was 322 grain boundaries and 546 fractures. From these it was possible to calculate the mean grain separation (G) and mean fracture spacing (F), and thus fractures per grain, $(\frac{F}{G})$; this is shown in Table 8.2.

From these results it can be seen that a number of significant variations exist along the same axial direction. Since the grain boundary spacings are only related to sedimentary and diagenetic processes, it is to be expected that this factor should be similar for both the tested and untested specimens. In order to standardise the grain boundary spacings, a standard grain size distribution method was used where all grain separations below 0.5mm were rejected from the sample. Although this encompassed 20% of all the grains, it made up less than 0.05% of the total rock volume. Similarly, all grains greater than 5mm were rejected. This comprised 2% of the total grains sampled but less than 0.5% of the volume.

Based on the new figures obtained, F, G and F/G were recalculated and the resulting values are given in Table 8.3. If the

TABLE 8.2

Spec. No.		Mean Grain Separation, G	Mean Fracture Spacing, F	Grain over Fracture
Un-tested	x - y	19.4	12.932	1.5
	y - y	13.272	14.600	0.909
	x - x	10.043	13.111	0.766
4	A ₂₃	13.0	5.342	2.433
	A ₁₃	10.875	6.858	1.583
	A ₁₂	21.545	6.583	3.273
6	B ₁₃	10.065	8.211	1.226
	B ₂₃	14.286	7.500	1.905
	B ₁₂	14.727	5.229	3.77
5	C ₁₃	7.4	6.033	1.229
	C ₁₂	13.368	6.35	2.105
	C ₂₃	10.333	5.741	1.800

x - y, y - y, and x - x are the untested specimens.

The subscripts A₂₃, etc., refer to the planes.

TABLE 8.3

Recalculated Spacings

Spec. No.		Mean Grain Separation, G	Mean Fracture Spacing, F	Grain over Fracture
Un-tested	x - y	14.32	12.15	1.18
	y - y	15.368	14.600	1.05
	x - x	14.303	13.111	1.09
4	A ₂₃	15.00 (5)	5.690 (46)	2.636 (223)
	A ₁₃	14.50 (6)	6.868 (47)	2.111 (208)
	A ₁₂	15.111 (6)	6.476 (49)	2.333 (214)
6	B ₁₃	13.00 (7)	8.210 (67)	1.58 (134)
	B ₂₃	14.286 (7)	7.500 (51)	1.905 (190)
	B ₁₂	17.000 (18)	5.333 (40)	3.188 (292)
5	C ₁₃	13.632 (5)	6.023 (49)	2.263 (192)
	C ₁₂	13.478 (6)	5.849 (45)	2.304 (211)
	C ₂₃	14.941 (3)	6.350 (48)	2.353 (224)

The figures in brackets are the % change from the untested sample

grain boundary spacings are now compared, a remarkably good agreement is obtained (maximum variation 12%), considering the natural anisotropy and inhomogeneity of the rock.

The mean fracture spacing, however, shows a considerable variation from the datum with a marked decrease in fracture spacing. Specimens A and C (4 and 5) have the most isotropic grain distribution (variation 4% in A and 9% in C). In both cases the fracture spacing is decreased by just under 50% in all directions and the F/G ratio approximately doubled. This shows a markedly isotropic fracture development with a strong correlation between load, strain and fracturing. Specimen B (No. 6) is markedly more anisotropic than the others with a grain axial variation of 24%, and this specimen failed at a considerably lower load than the other two specimens.

In order to estimate the orientations of the fractures, these were plotted on stereographic nets. The major recorded orientations of the fracture planes are shown in Table 8.4,

These show that there is a definite preferred fracture orientation in all the specimens, striking approximately E-W and dipping between 50° and 70° to both N and S. There is not an apparent new fracture set induced by the testing, suggesting that fracturing has taken place on pre-existing weakness planes. These were probably induced in geological time by loading and flow of the material.

TABLE 8.4

Orientations of Fracture Planes

Spec. No.	Slide No.	Plane Dip/Direction(s)
	x - y	50/004, 73/250, 60/170
4	A	50/038, 66/158, 70/128, 80/024
6	B	50/030, 70/170, 72/224, 80/240
5	C	70/360, 70/156, 70/176, 84/296

Many of the rocksalt crystals exhibit a phenomenon known as anomalous interference. This occurs when cubic optically isotropic crystals such as salt, exhibit apparent anisotropic optical properties. This effect can best be seen if a mica $\frac{1}{4}$ wavelength plate is placed in the optical path between the two microscope polars. This results in all the isotropic materials appearing with the colour of the mica plate first order mauve, whereas the anisotropic minerals undergo a wavelength shift of approximately 570nm. Second order yellows and blues result.

The reason for the anomalous interference is an alteration of the atomic structure. Halite or potash crystals are cubic with identical physical properties in all directions. If the atomic crystal structure is deformed, a loss of symmetry results and among other changes, the mineral develops two (in any plane) different refractive indices, which in turn gives the different colours at the eye piece. Plates 8.1 to 8.5 are the results obtained from both the salt and potash specimens.

The most likely deformation mechanism that has occurred to give the above effect is kinking. This is most marked at cleavage partings where anomalous interference colours are produced along the fracture boundary. Crystal distortion is indicated, almost certainly caused by the testing. About 40% of all fractures present show this effect. Anomalous interference colours are also obvious at grain boundaries, particularly at sharp points and triple junctions, indicative of high stress concentrations giving rise to crystal distortion.

PLATE 8.1

Photomicrographs Untested Specimens

- A. View field of large crystal in the x-y plane from untested specimen. Poorly developed cleavage and anomolous interference colours.

- B. General field of view of slide cut from untested sample in the y.y plane. The slide shows typical grain boundaries and undefined cleavage planes.

- C. General field of view of slide cut from untested sample in the x-x plane from untested specimen. Again typical grain boundaries and anomolous interference colours.

All photomicrographs at x 50 if not otherwise marked

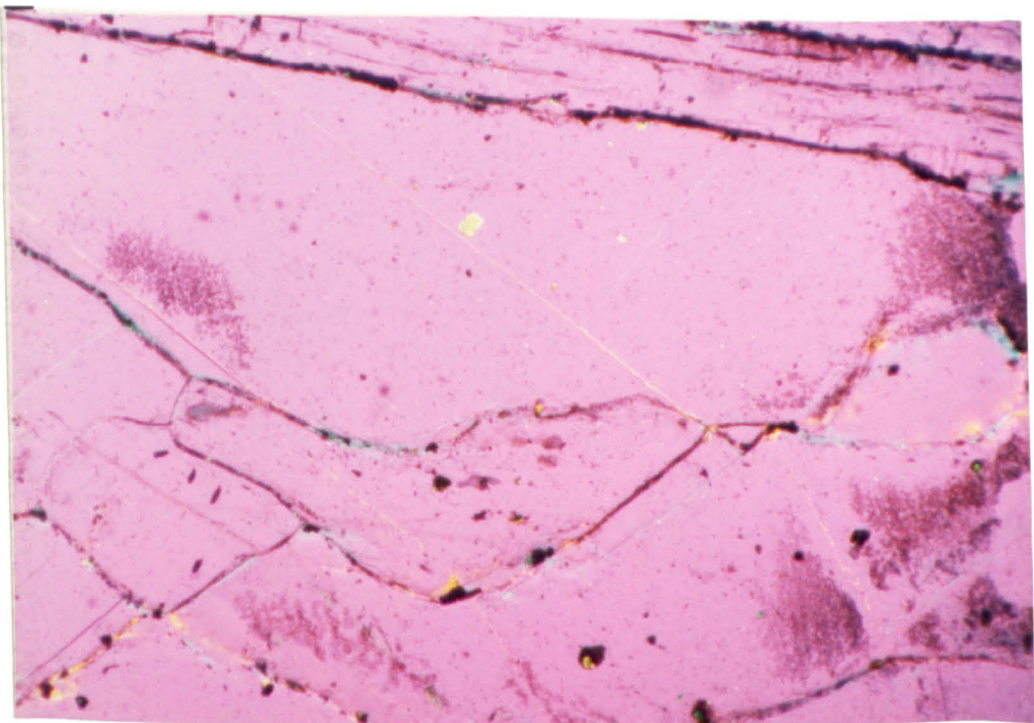
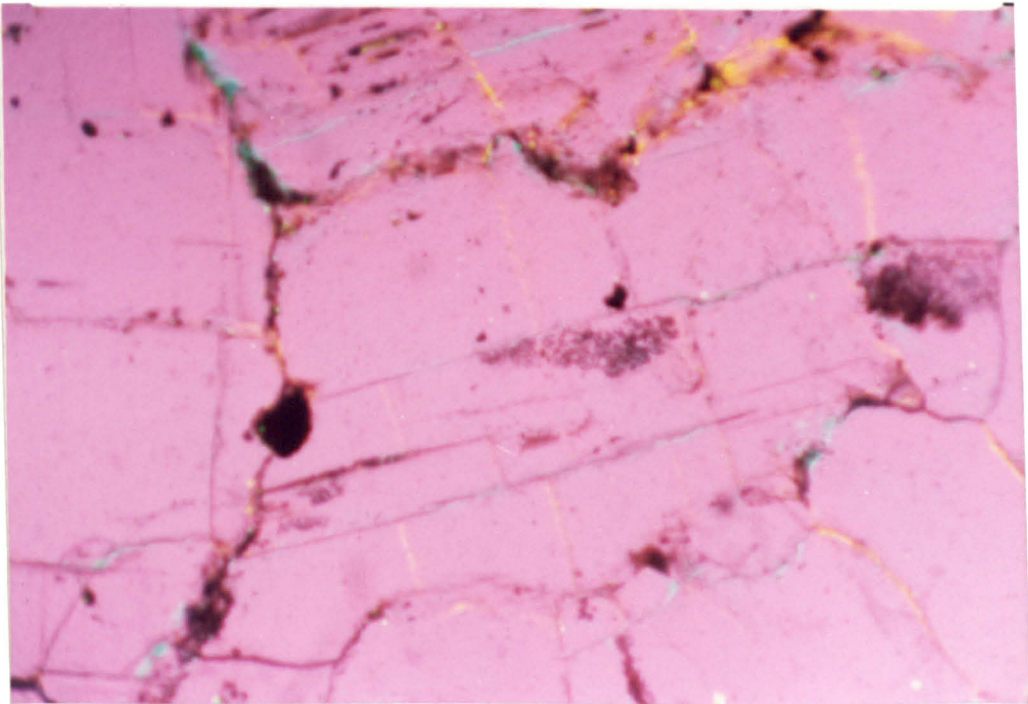
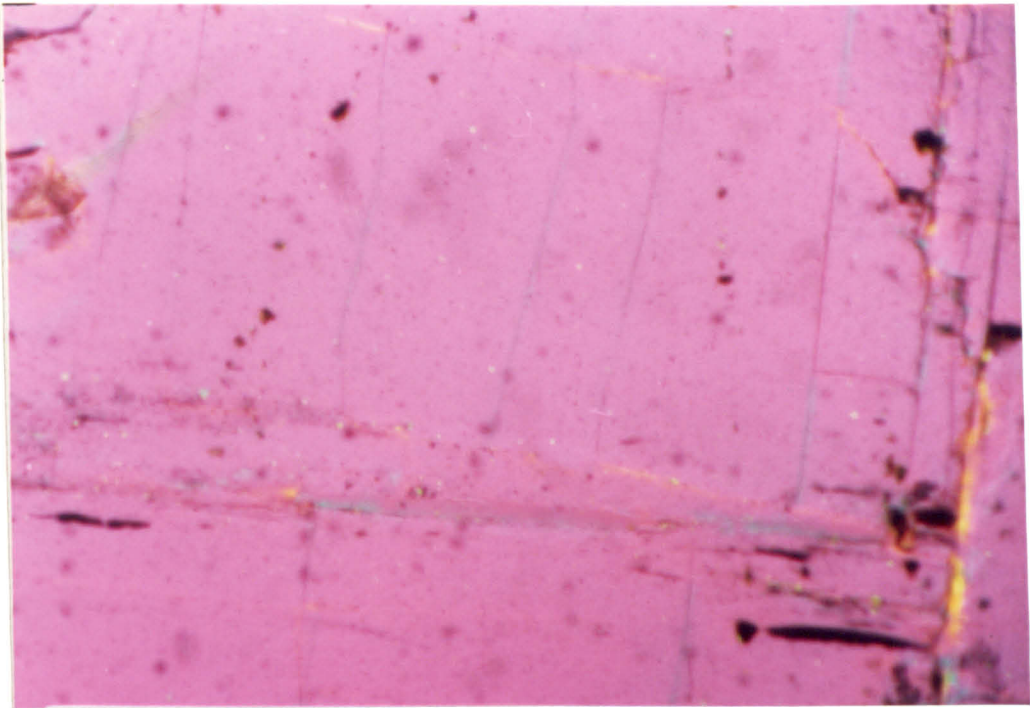


PLATE 8.2

Photomicrograph Specimen No. 4

- A. Section along C_{13} . Note bent grain in the centre of viewfield. Also shearing in vertical plane of photo and at 45° .

- B. Section along C_{23} showing fracturing of rounded centre grain and also dilation of cleavage.

- C. Section along C_{12} showing highly fractured and sheared groundmass.

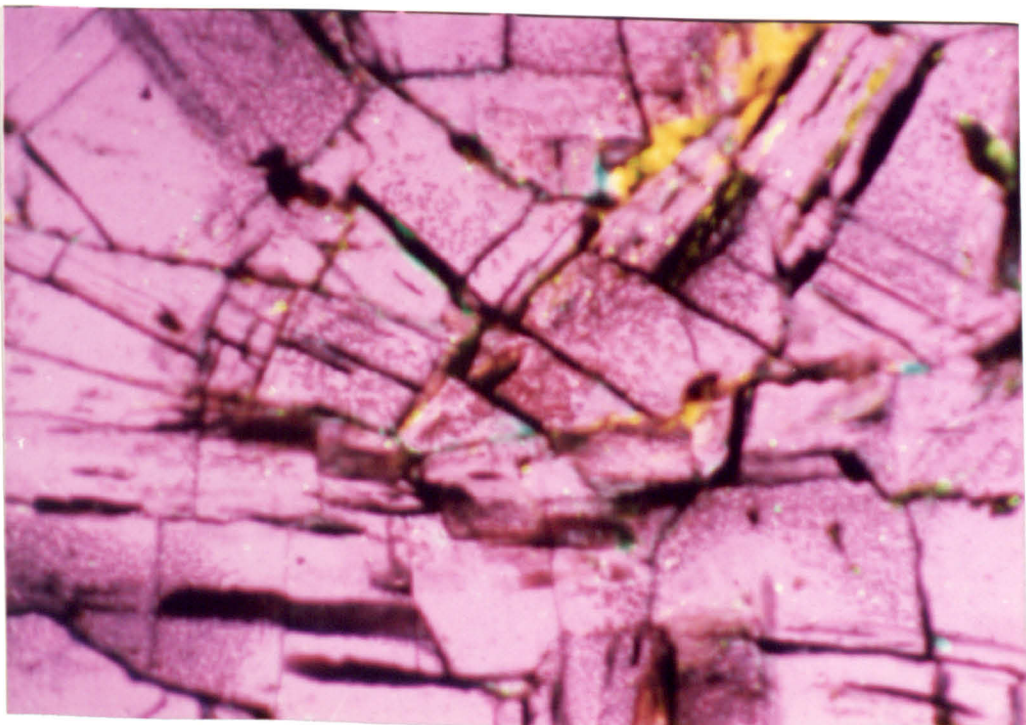
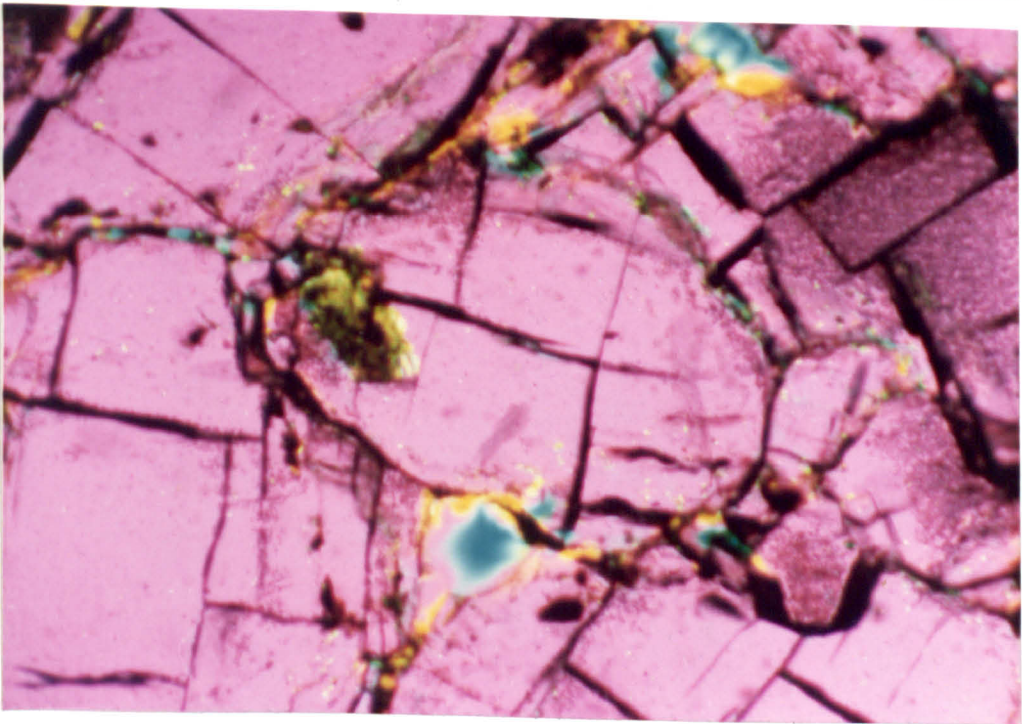
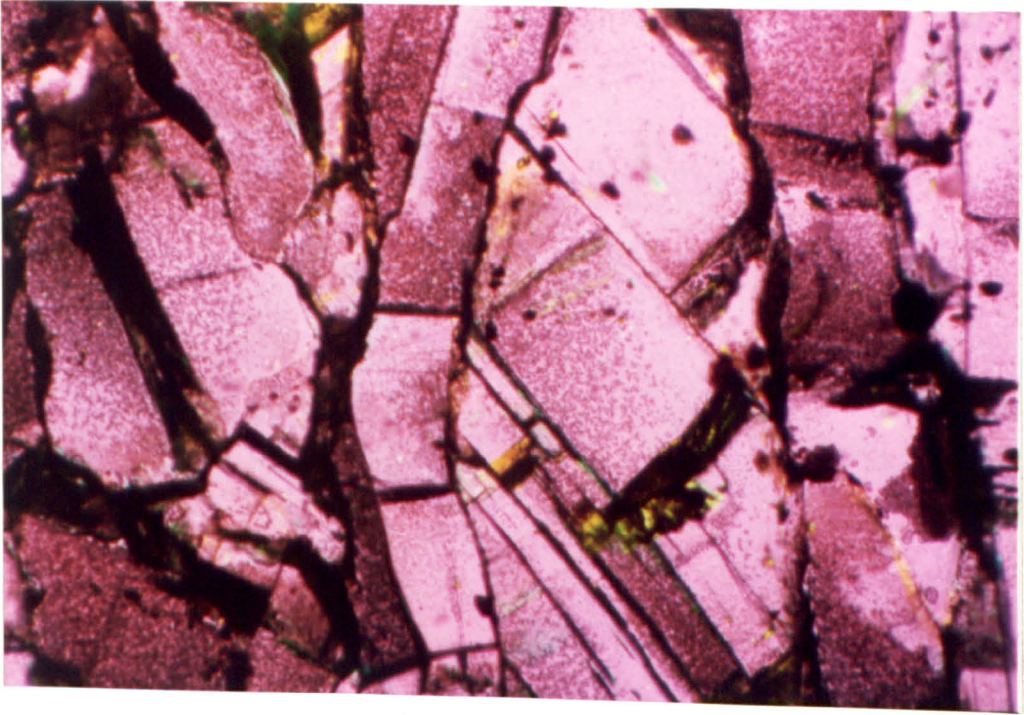


PLATE 8.3

Photomicrograph Specimen No.5

- A. Section along B_{13} showing limited shear and some budding of cleavage fractures.

- B. Section along B_{12} showing fracturing and rotation of grains. Note how fracturing is more intense in this plane than the other two.

- C. Section along B_{23} showing interference colours along cleavage fractures.

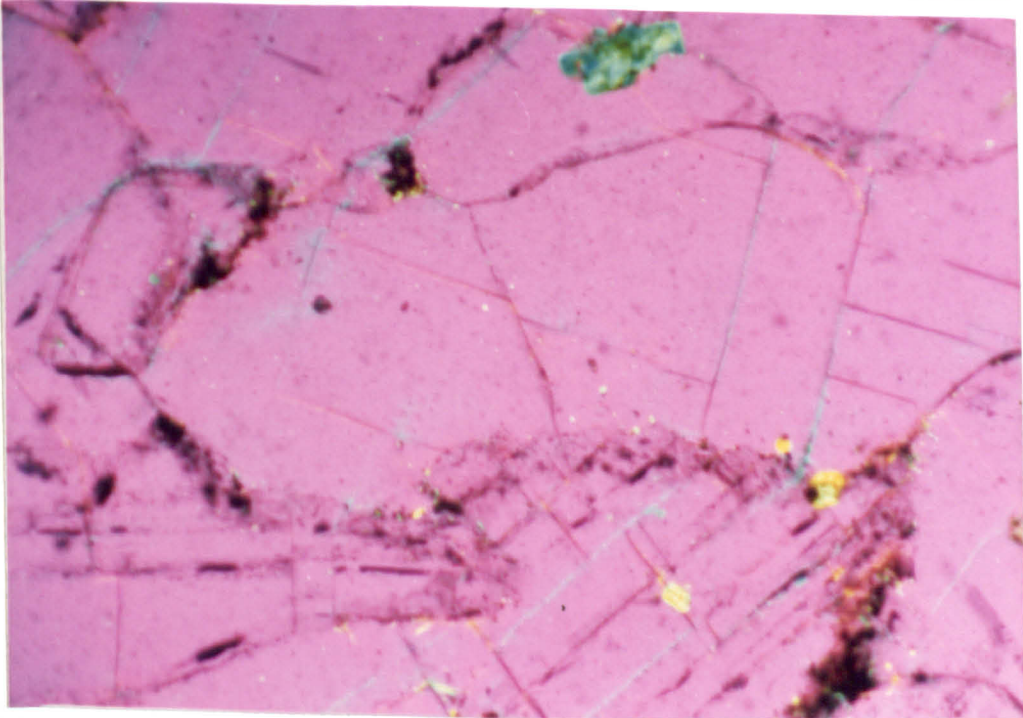
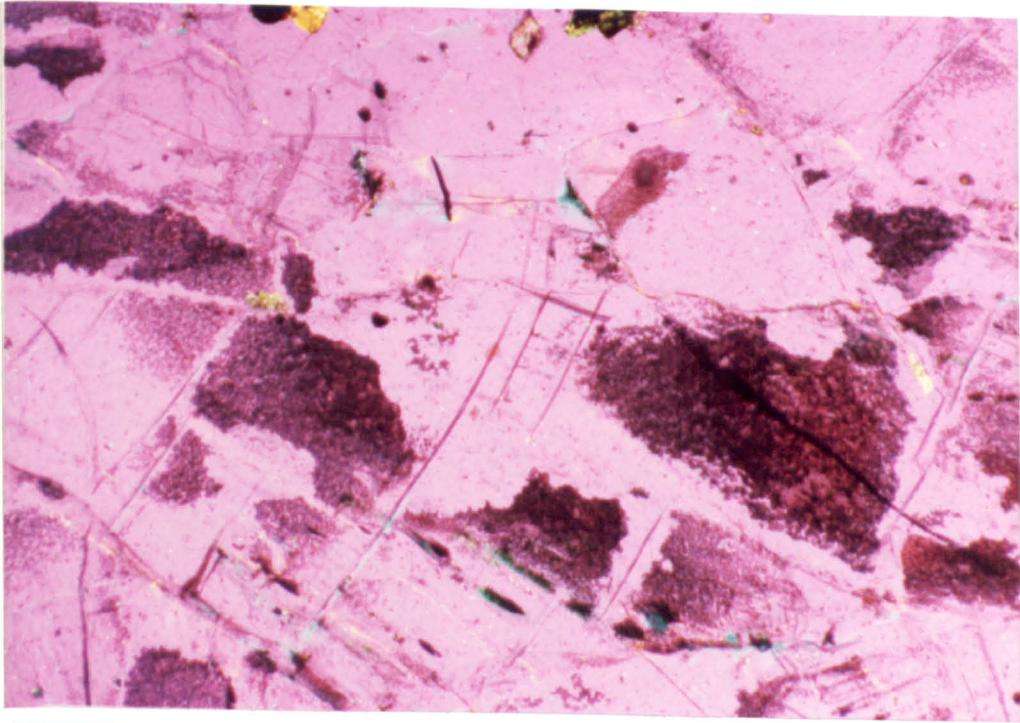
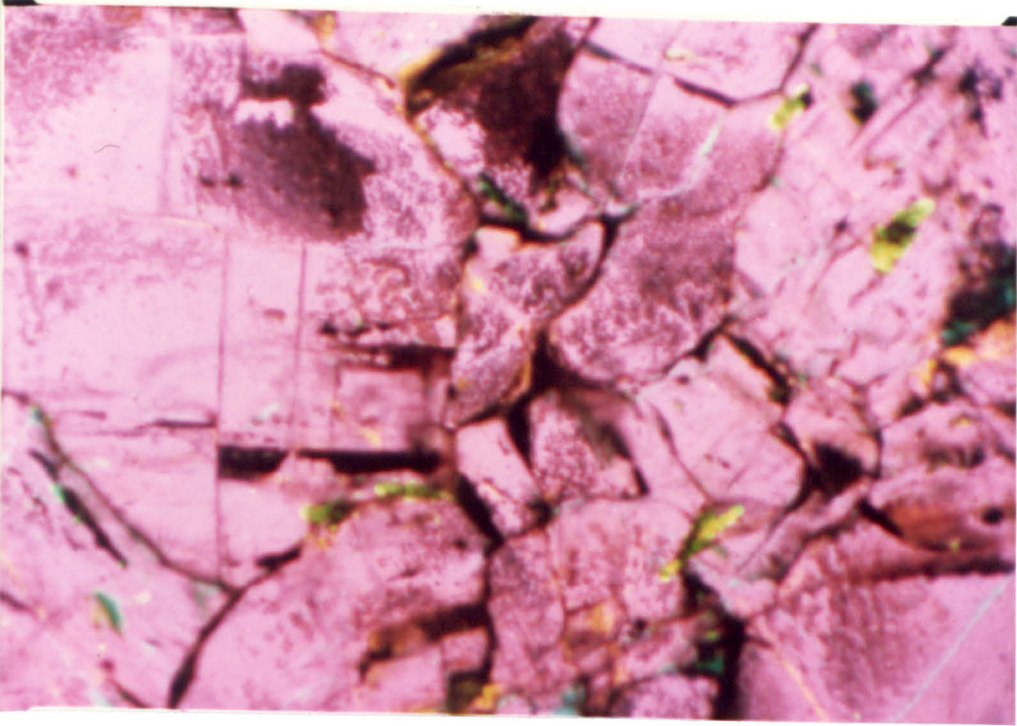


PLATE 8.4

Photomicrograph Specimen No. 6

- A. Section along A23 plane (xy) showing cleavage fracturing and grain boundary shear.

- B. Section along A13 plane showing development of fracturing.

- C. Section along A12 showing the fracturing and breakage of larger grains to smaller units.

Compare with untested specimens.

The background colour variations are due to the effect of varying slide thickness on light transmission and film temperature.

All test loads applied normal to 2 - 3 plane.

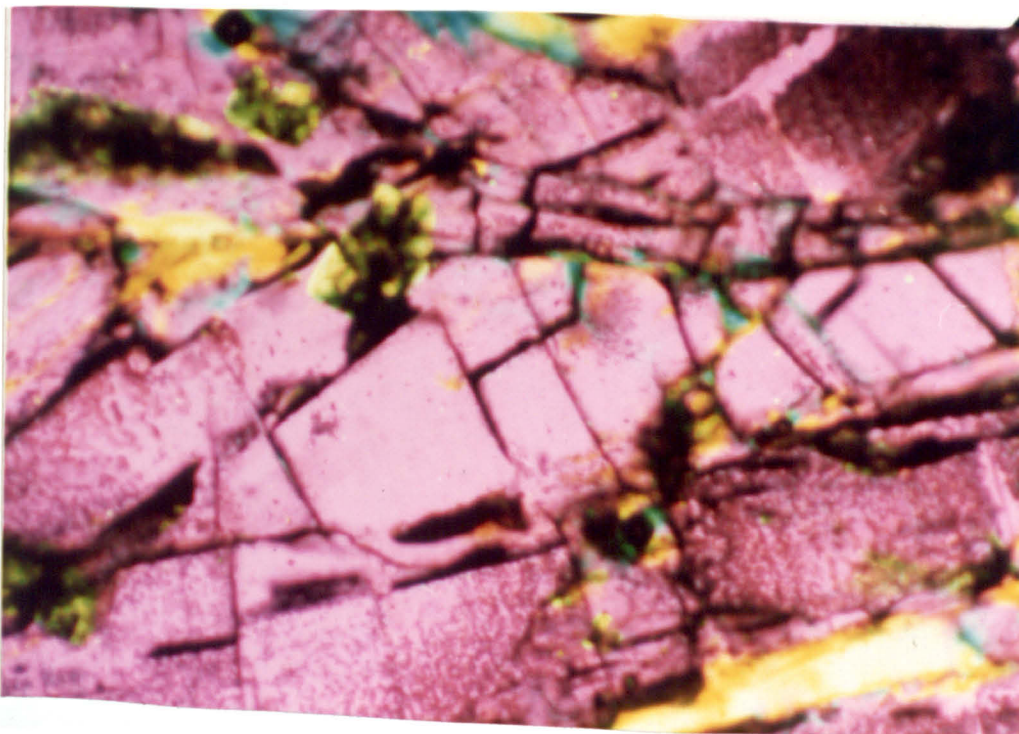
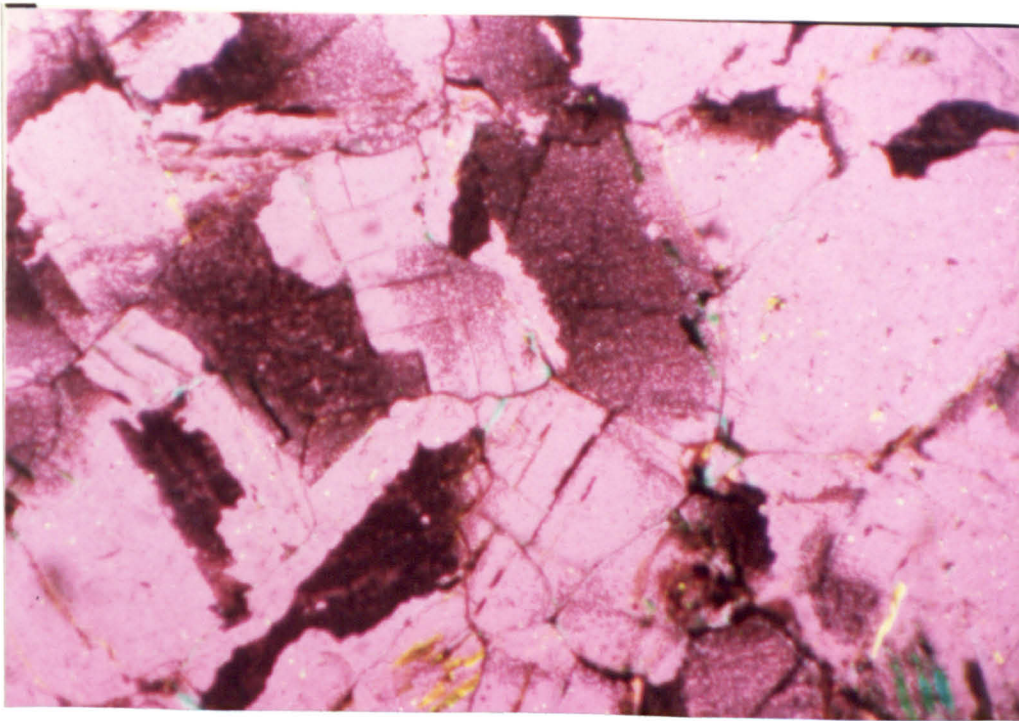
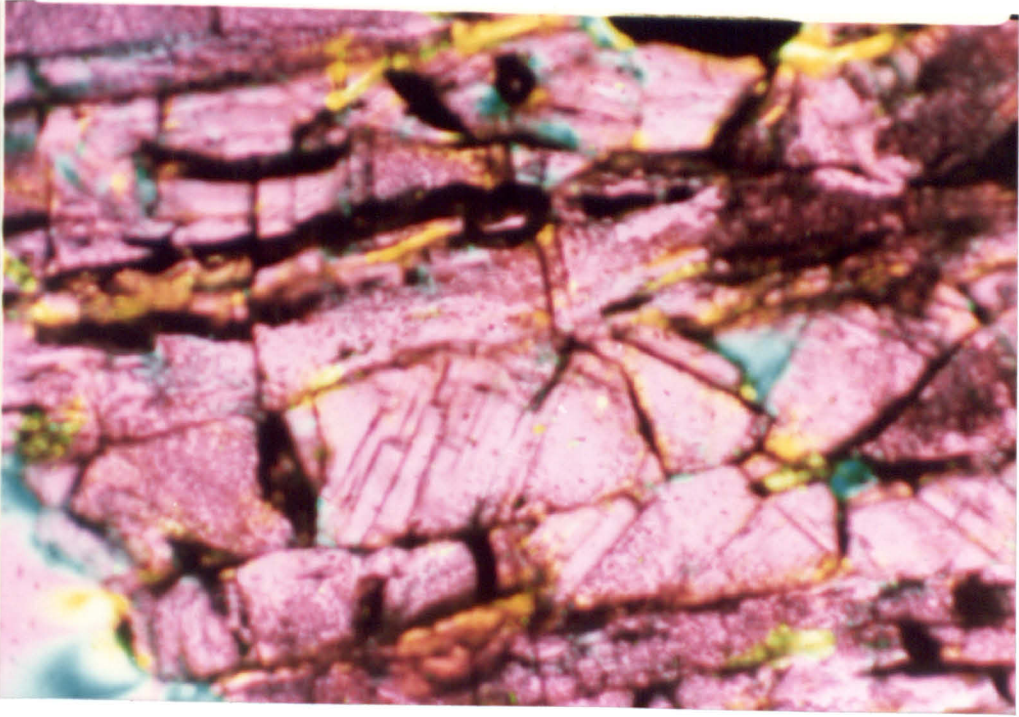


PLATE 8.5

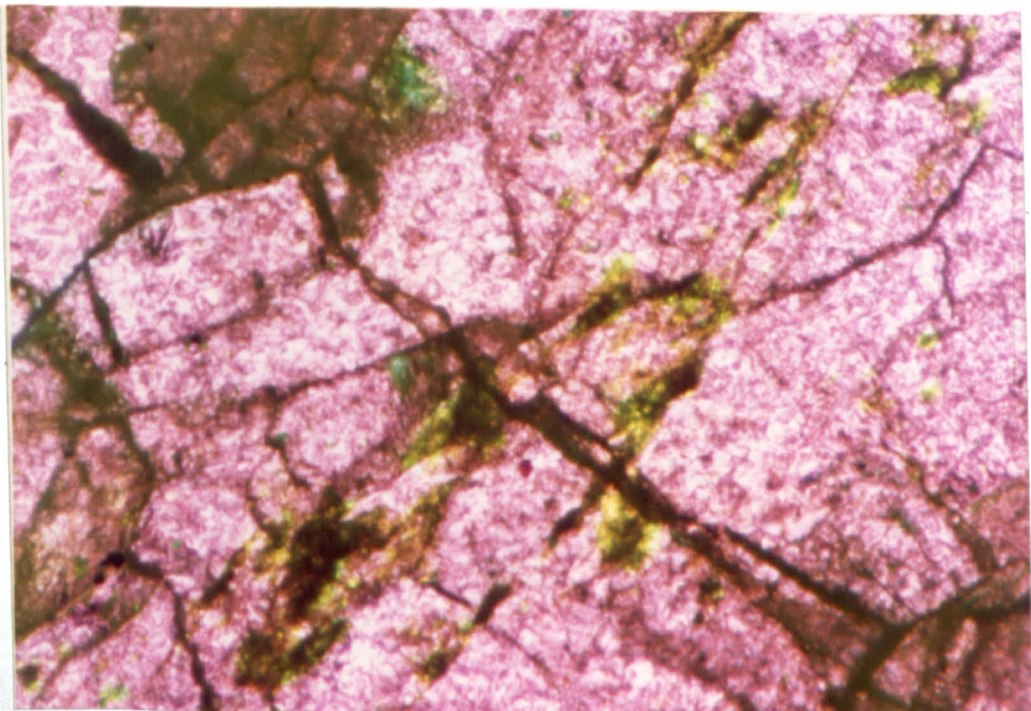
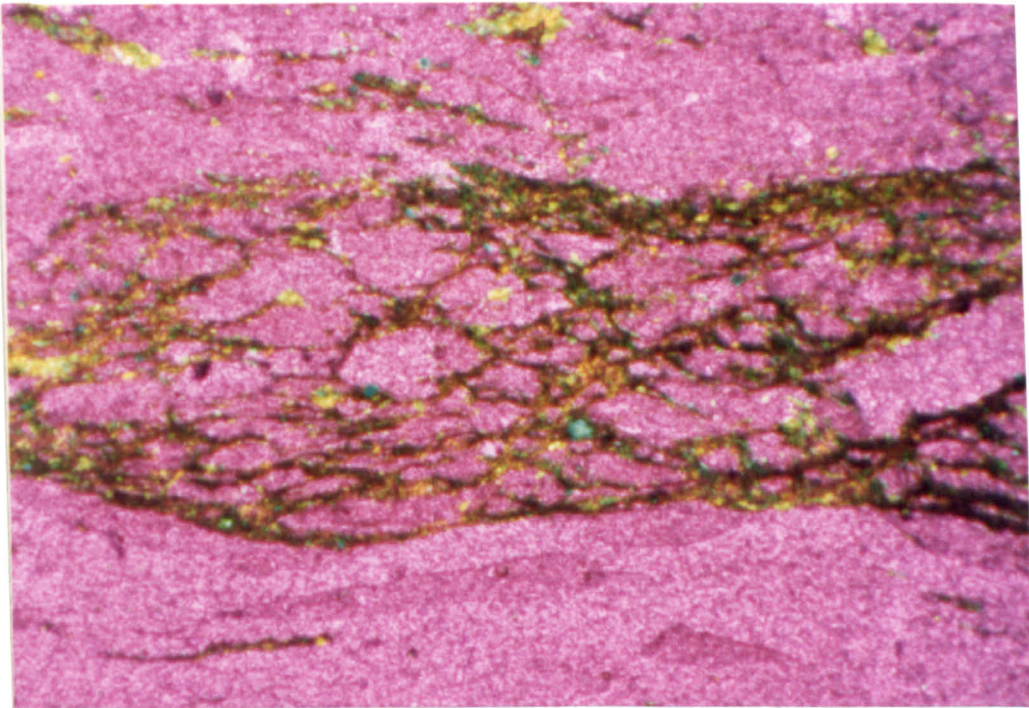
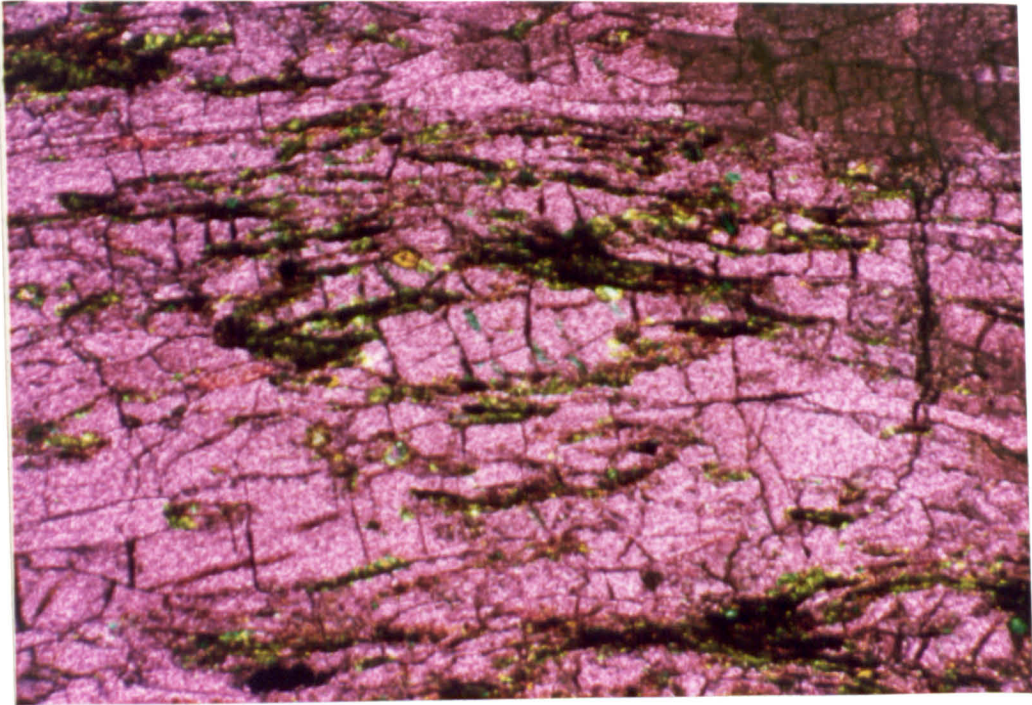
Photomicrograph Potash Specimens

Potash Specimens

- A. General view showing highly fractured ground mass
flattening of clay inclusions and a "pseudo-metamorphic"
appearance.

- B. Showing development of boudinage type structure.
Necking due to load being applied across layers of
dissimilar viscosities.

- C. Grain showing shearing off and rotation at corners
(mag x 75).



8.4 Summary of Conclusions

The laboratory test results show that:

1. Strain hardening occurs, but the effect decreases as the rate of deformation decreases.
2. As the strain rate increases, the load bearing capability of a given W:H ratio specimen decreases.
3. As the strain rate increases, potash and salt rocks are able to withstand greater stresses for the same amount of strain.
4. As the W:H ratio increases, so does the load bearing capability of the rock.
5. Confined cores begin to develop when the W:H ratio reaches about 2:1.
6. Thin section analysis has shown itself a useful technique for investigation of rock properties of evaporite rocks.
7. Deformation in potash and salt results from movement along pre-existing planes of weakness.
8. Salt rocks are stronger when loaded parallel to the direction of any existing direction of crystal alignment, and virtually equally weak in the other two directions.
9. The pre-existing direction of in-situ rock flow appears to be in the E-W direction.

CHAPTER NINE

CONCLUSIONS DRAWN FROM RESULTS OF MEASUREMENTS AND PROPOSED HIGH
EXTRACTION PANEL DEFORMATION MODEL

Chapter Nine

9.0 Introduction

In this chapter the intention was to bring all the measured data together so that general conclusions could be drawn. From these, it was expected to be able to derive a model describing the mechanism of deformation in and around a high extraction panel. This was done, but when it came to setting the results down on paper, certain difficulties arose. It was therefore decided to describe the model, supporting it as required by reference to the results obtained in previous chapters. In many ways this reflects how the investigation developed. After the first high extraction panels had been established, observations of their subsequent behaviour required explanations. From these a picture began to emerge. Other aspects were then sought which would support, controvert or modify the behavioural model which was developing.

9. The Proposed Model

It is instructive at this stage to consider a scale section across a high extraction panel, Figure 9.1. This is a typical 90m wide panel with five entries. Average figures for the thicknesses of roof strata have been assumed. The intuitive feeling is that the presence of a competent bed of relatively strong elastic rock such as the Upper Anhydrite, will exert a considerable influence on the stability or otherwise of the workings below.

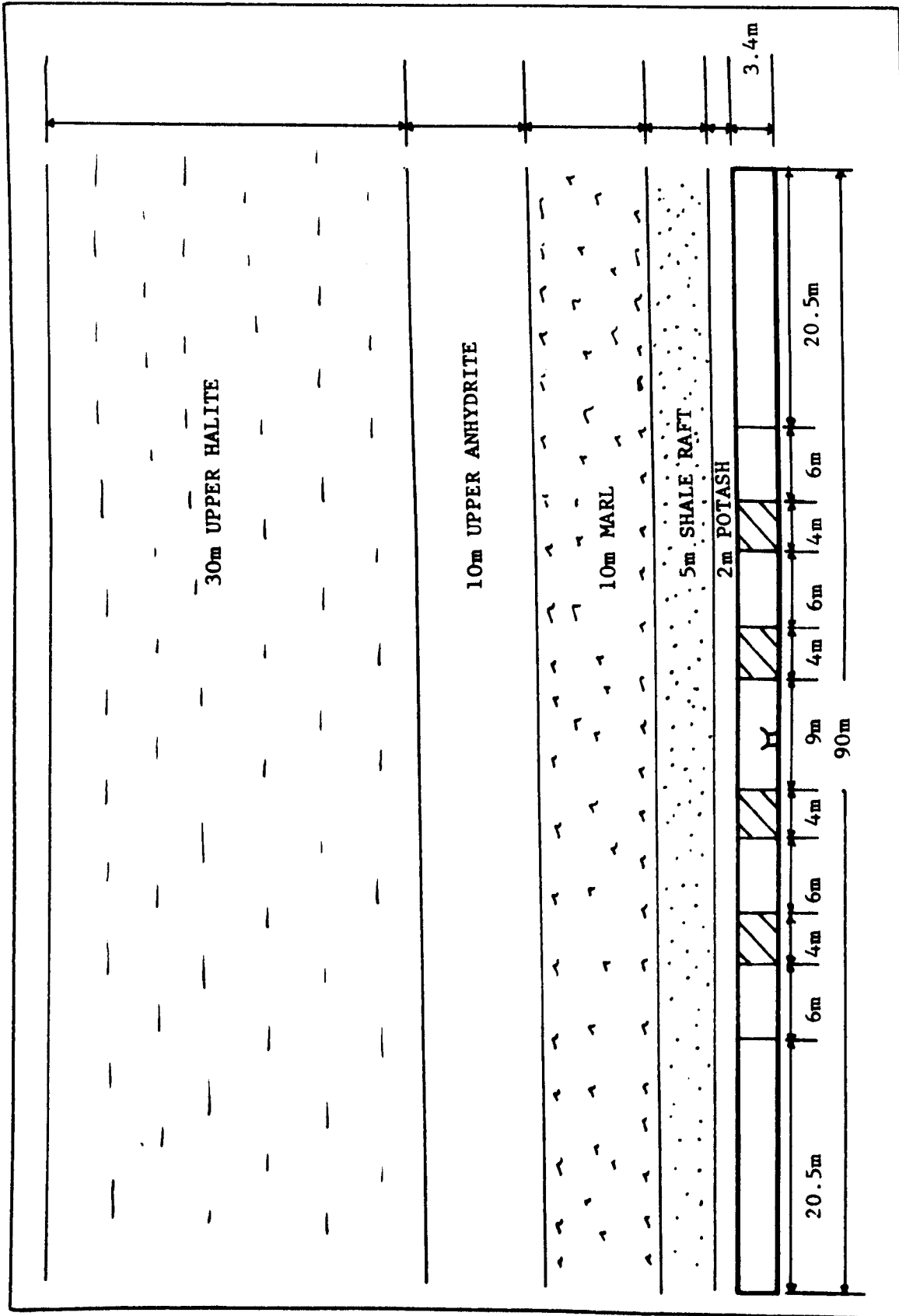


Figure 9.1 Section through No. 10 Panel

In the two dimensional case shown, this anhydrite bed can be expected to behave as a beam, fixed at both ends and sitting on yielding abutments of Carnallite Marl and potash. It is postulated that two mechanisms occur when the excavation is made. These take place simultaneously and immediately; depending on circumstances, one may predominate.

9.1.1 Mechanisms of Plastic Flow of Roof Rock

Firstly, the marl and immediate roof rocks yield and tend to flow in a direction that depends primarily on the deviator stress acting at the point in question. The greatest deviator will initially be located somewhere above the panel abutments. In the perfectly elastic situation, the distribution of deviatoric stress along the roof beam will be similar to that for shear stress, Figure 9.2(a). The actual potash panel situation will differ from this to something like Figure 9.2(b), which is a result of time dependent deformation of the roof rocks. The peak abutment stress will decrease and be diffused over a greater distance. The effect will be further enhanced by the yield of the potash ribside itself. High vertical stresses will be set up in the strata below the Upper Anhydrite beam, these being greatest over the ribsides. Where an outer roadway abuts immediately on to the ribside, i.e. the panel has no stubs, the nett effect of the high deviator stresses in the roof rock is to cause shearing along the abutment edge.

The presence of stubs with yield pillars between them

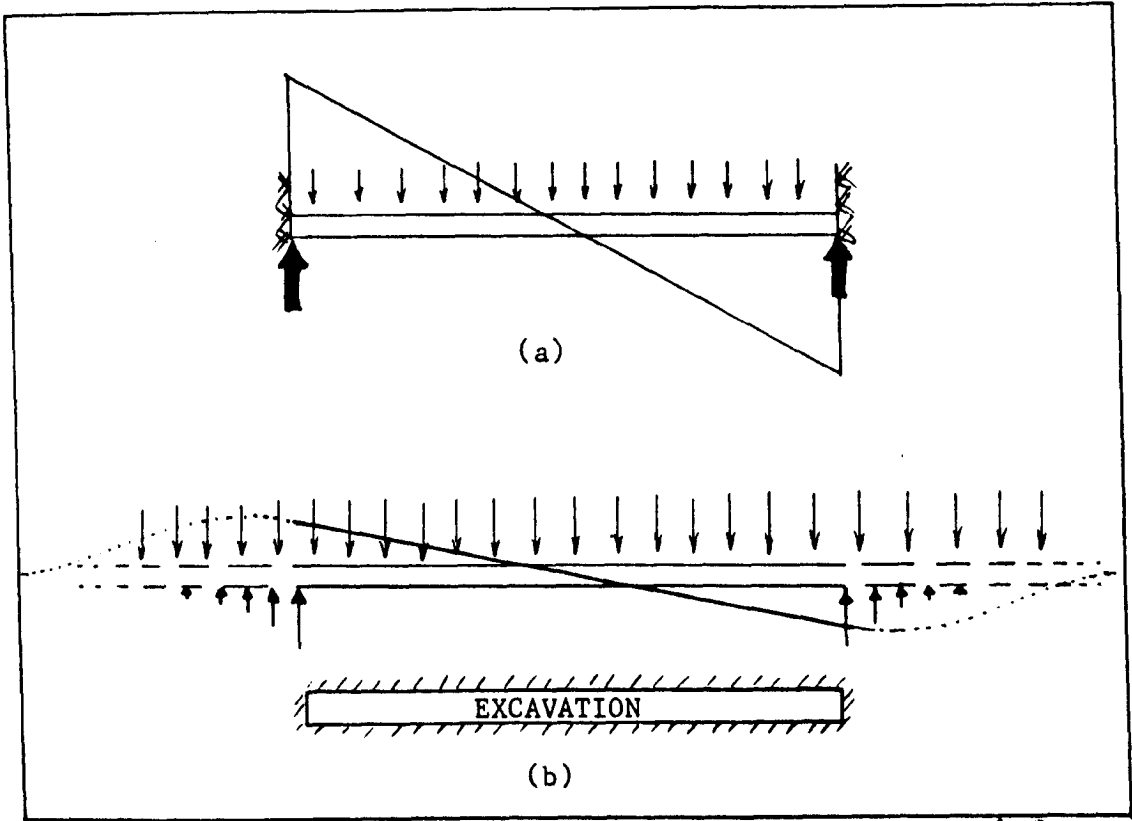


Figure 9.2 Distribution of stresses along a beam (a) theoretical
and (b) actual

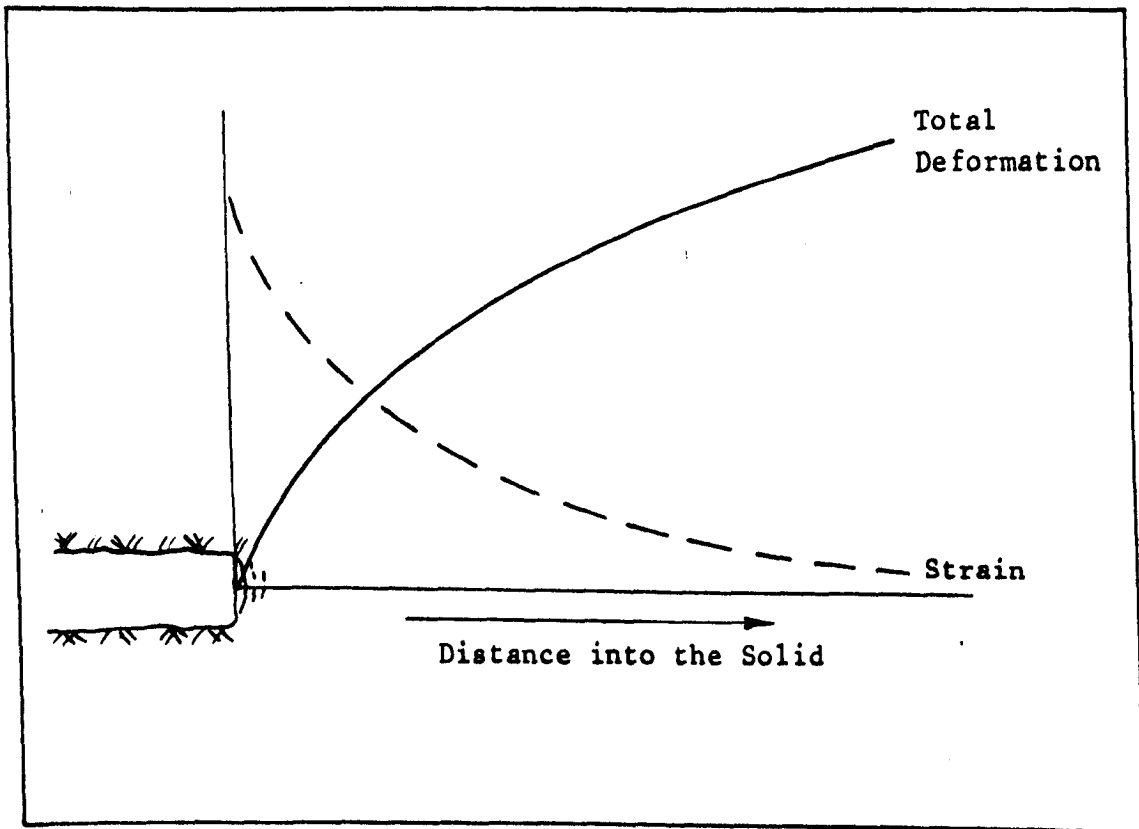


Figure 9.3 Deformation vs. distance into ribside (pillar)

will result in a zone of increasing stiffness towards the panel edge. This exerts a cushioning effect, and as a result shearing does not occur. Observations have borne this out.

9.1.2 The Mechanism of the Deformation of the Upper Anhydrite

The second effect is that which arises from the existence of the anhydrite bed which can be considered to act as a plate. It is assumed that very little or no cohesion exists between the marl and the anhydrite. The plate can also be considered to have a uniformly distributed load and to be clamped all round. It will deflect according to the laws governing the behaviour under load of such structures. Timoshanko and Woinowsky-Krieger⁽⁴⁰⁾ give a full account of the derivation of functional relationships describing the deflections of plates of different types and configurations. No solution has been derived for the case of a thick composite plate, sitting on yielding abutments that undergoes large deflections.

The bending of the plate can be expected to result in increasing deformation towards the centre of the unsupported span. The results from the high extraction panels, Figures 6.10, 6.31, 6.33 and 6.36, do not show that this is occurring. The maximum variation in total closure obtained across one panel is of the order of 150mm, an amount which could easily be explained by the presence of local inhomogeneities. When considered as a whole over the total width of the panels, it is concluded that fairly even roof sag is taking place. The only exception to this appears to be No. 19 Panel where

the centre conveyor road, at G19B, exhibited a significantly lower overall closure rate.

Of great significance too, is the manner and amount that the panel ribsides deform by with time. Hebblewhite et al⁽³⁹⁾ showed that the lateral deformation in salt rocks could be related to their vertical deformation by assuming zero volumetric strain. In applying a zero volumetric strain criterion to the in-situ pillar results, over estimation of vertical strains would result if major fracturing had occurred. On the other hand, it would under-estimate vertical strains if the average volumetric strain was compressive due to the large area of confined pillar material. In view of these opposing effects, a zero volumetric strain criterion would appear to be valid. The vertical strain can therefore be taken as being equal to the lateral strain.

If the results from extensometers RA1 and CEA, BH01, are examined and compared, a number of interesting points emerge. Deformation both laterally and vertically drops off rapidly with distance into the solid. A general picture of deformation with distance into the pillar is given diagrammatically in Figure 9.3.

9.1.3 Combined Mechanism of Panel Deformation

When this picture of ribside deformation is added to that of marl and roof rock flow plus bending of an anhydrite plate, the composite that emerges is shown somewhat exaggerated in Figure 9.4.

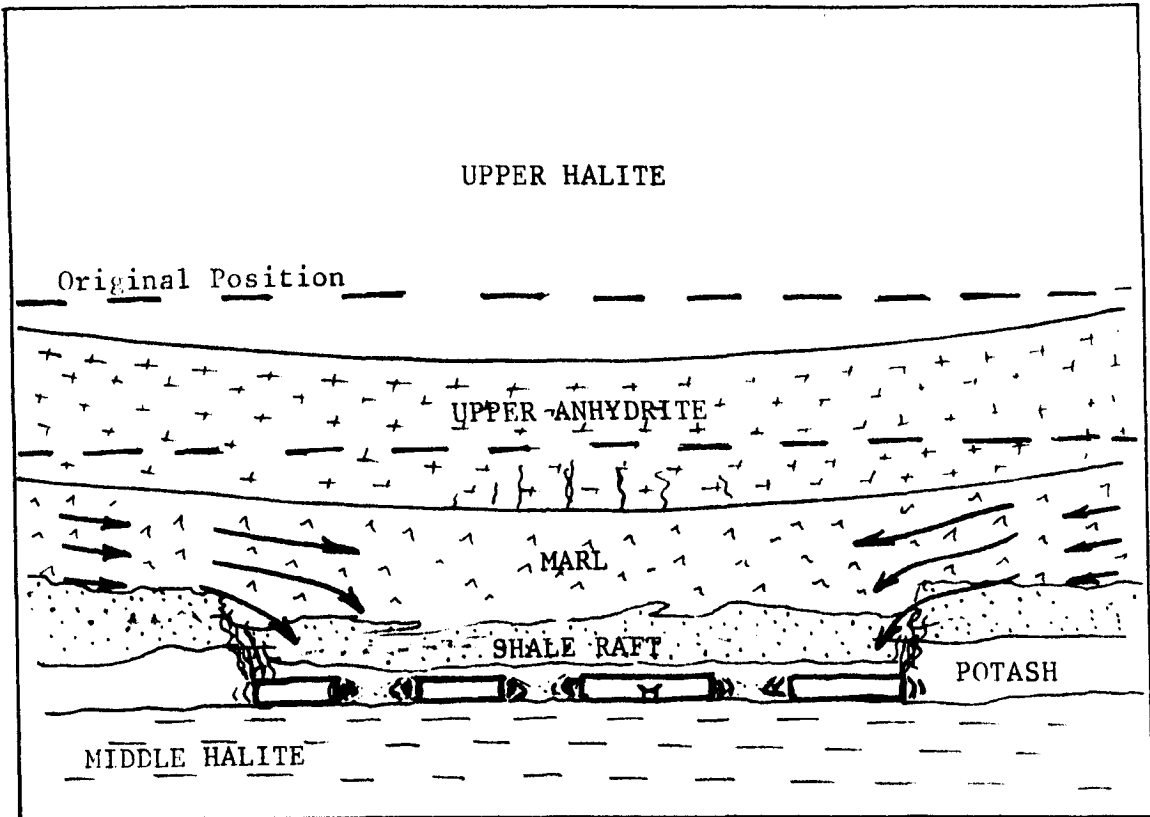


Figure 9.4 Mechanism of Panel Deformation

It should be possible to equate the volume change within the panel and ribside to that produced by the bending of the beam and the flow of roof material. The results from No. 8 Panel extensometers support the picture that is presented, borehole RF8 in particular, as it shows that very little deformation took place between 2m and 9.5m into the roof.

The effect of stubs mined off the outer roads plays an important part in the stability of these roads. Because there is no abrupt abutment with stubs, the roof rocks are more gradually loaded. No. 12 Panel is a good example of the beneficial effect of stubs.

The mechanism described thus far also explains why there is no apparent correlation between panel width or percent extraction and roof to floor closure rate in the high extraction panels.

These have been presented in Table 9.1

TABLE 9.1

Average initial 20-day closure rates, high extraction panels

Panel No.	Width m	Closure Rate		% Extraction
		Range	Average	
8	67	2.1-9.4	6.2	61.6
10, A*	30	2.3-9.9	5.2	73
10, B	90	5-7.8	6.6	73.6
12	80-90	3.6-10.6	7.5	69.5
15	100	4.3-8.7	6.0	65.8
16	85	2.3-8.3	5.3	65
17A	100	N/A	N/A	60
17B	45	1-7	5	73.1
19	75-100	9.4-21.9	13.8	73.6
20	40-70	6.2-6.9	6.6	65.9
21	40	6.8-9.6	8.7	76.9
22	40-75	2.4-19.3	10.9	74.3

* Central section only

The normal 20-day closure rate in roadways in No. 6 Panel, a low extraction panel, was found to be between 5 and 10mm per day.

It would therefore appear that roadway closure rates in a high extraction panel are not significantly different from those experienced in a low extraction panel. One hundred days after mining, the rates are much the same at about 1-3 mm/day.

9.1.4 Change of Slope of Strain/Convergence Rate Curves

Figure 9.5 gives the graph of log of strain rate versus time for 25m and 40m square pillars in low extraction panels. These exhibit two distinct linear relationships; from 0 to about 50 days and from 50 days onwards, there being a fairly well defined change in the slope of the straight line after 50 days.

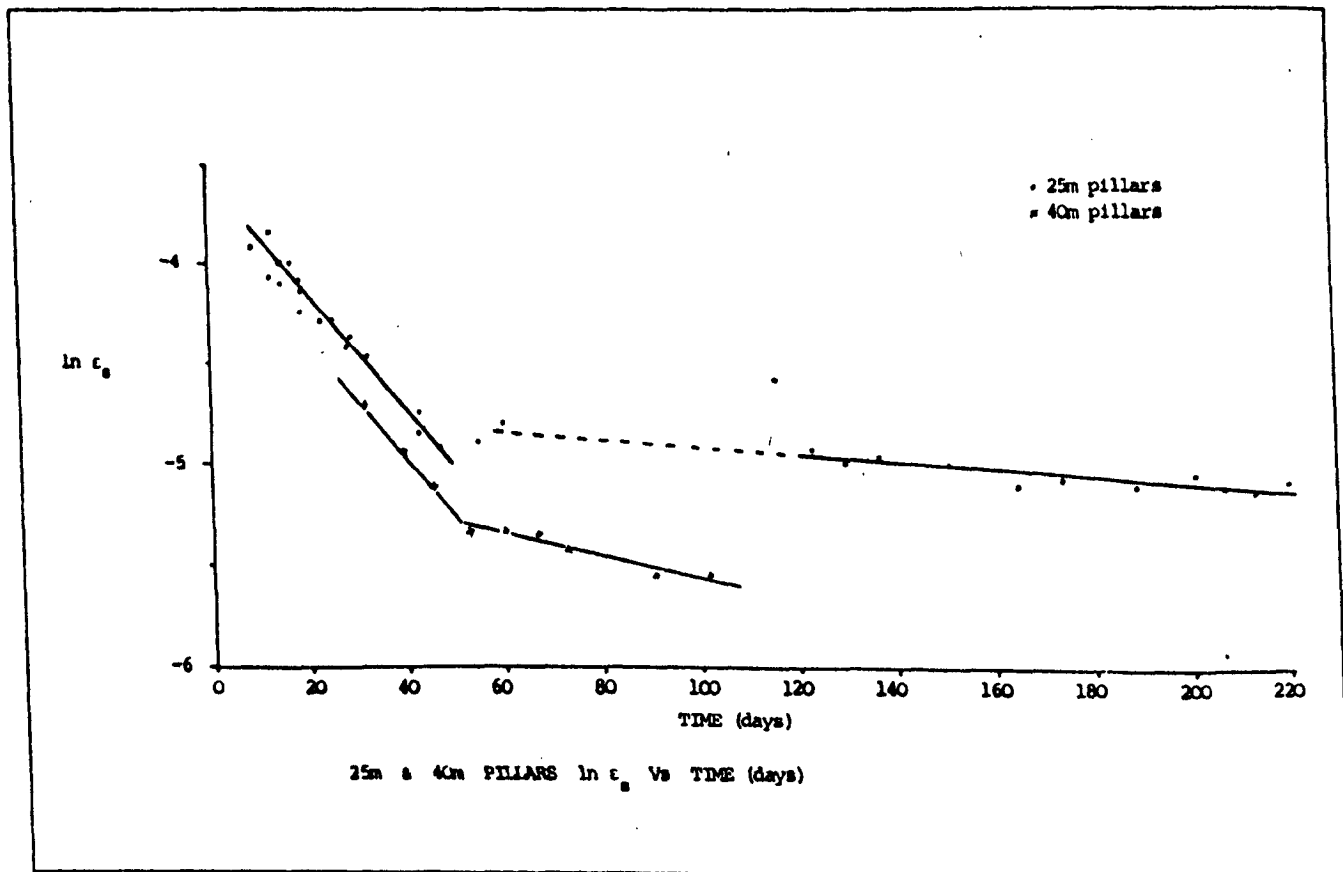


Figure 9.5 Log Strain rate vs. time for 25 & 40m square pillars

A similar effect can be seen in the curves of log of closure rate against time for the 30m wide central section of No. 10 Panel (A section). The relevant curve is shown in Figure 9.6 for C43D

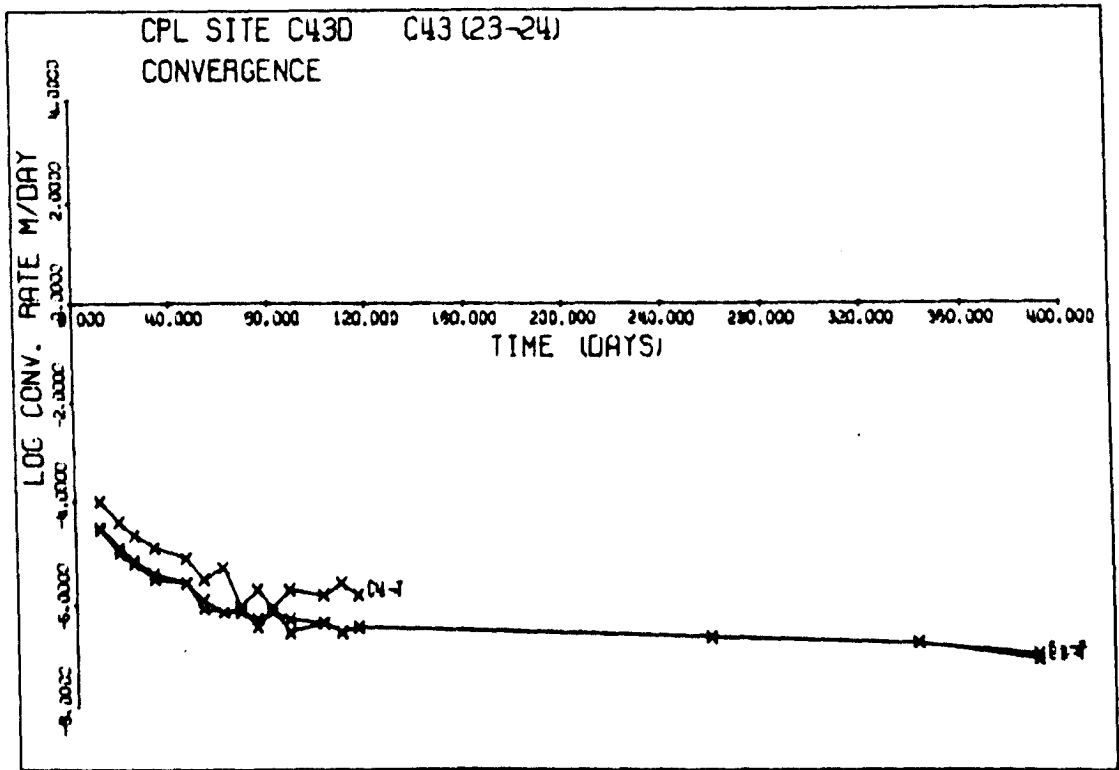


Figure 9.6 No. 10 Panel, A section - Closure rates for 30m wide section

None of the wide high extraction panel closure sites show any sign of this effect. It is therefore suggested that when the width of a high extraction panel gets below a limiting width of between 35 and 40 metres the mechanism causing this phenomenon starts to be significant. It is further postulated that the mechanism responsible is the first one described at the beginning of this chapter. That is, the plastic flow of the roof rock into the excavation, and the

yield of the ribside abutment zone. This results in the initial high decay of closure and strain rate. After 40 to 50 days have passed, the distressed zone reaches the base of the Upper Anhydrite, which then starts to accept load and behave as an elastic beam or plate. The marl continues to deform plastically into the excavation, thus gradually increasing the overall span on the anhydrite. It is this combination of plastic flow and elastic beam response which gives rise to the second slope to the decay of strain and closure rate.

9.1.5 The Upper Anhydrite as an Elastic Plate

In order to describe the behaviour of a high extraction panel, it is necessary to think of the anhydrite bed as a plate of relatively strong elastic material sitting on yielding abutments. The mathematical treatment of this problem is extremely complex and beyond the scope of the present work. Three dimensional finite element analysis appears to offer the best possibilities for solution and work has begun on this.

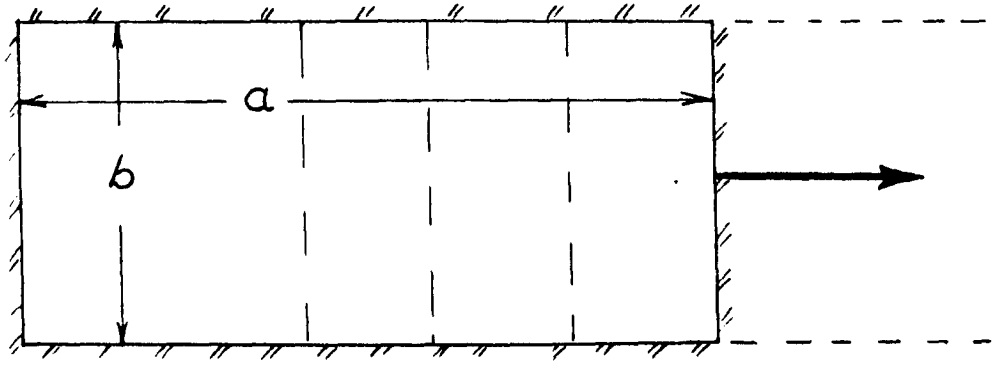
Timoshenko and Woinowsky-Krieger⁽⁴⁰⁾ give a number of solutions for the deformation of rectangular plates with all edges clamped that has been loaded with a uniformly distributed load with different $\frac{b}{a}$ ratios, where a and b are the lengths of the sides. They show that this $\frac{b}{a}$ ratio is an important parameter, and that when the ratio becomes less than about $\frac{2}{3}$ the deflections of the plate are close to those obtained for an infinitely long plate. Plate deflection is a function of:

1. Width.
2. Length.
3. Thickness.
4. Flexural rigidity, which is in turn a function of Young's Modulus and Poisson's Ratio.
5. Applied load (stress).

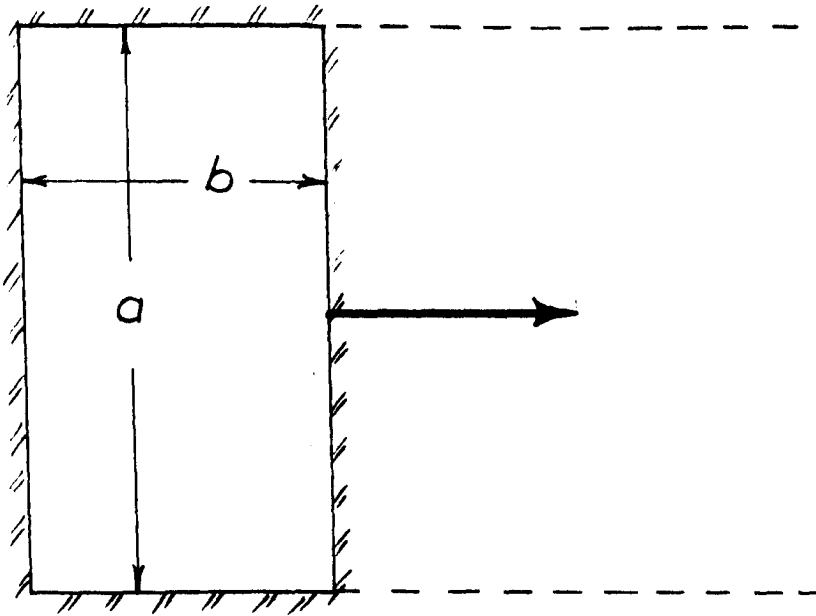
If it is assumed that for any intended mining layout, 3, 4 and 5, above are fixed, and as it is normally desirable to keep the panel width constant, the length of the plate will increase as mining progresses. It therefore follows that as the length of panel mined increases, the $\frac{b}{a}$ ratio alters accordingly.

For a given thickness of roof rock (anhydrite), having a certain flexural rigidity and that is subjected to a given uniformly distributed load (the overburden stress) there will exist a critical $\frac{b}{a}$ ratio for a set panel width, where the plate will fail either in shear or tension. Where the plate is sitting on yielding abutments, this critical ratio may be achieved not when the initial mining geometry is established, but some time later, depending on the amount of yield that takes place.

Two cases can be considered. Figure 9.7(a) depicts the situation where the initial panel width is sub-critical; i.e. no matter what length of panel is mined, the roof plate will be able to sustain the imposed stress. It is argued that this is the case only in certain high extraction panels where the panel width is less than 60m.



(a)



(b)

Figure 9.7 (a) & (b) Sub-critical and Critical Panel Widths

Figure 9.7(b) illustrates the second case where the initial panel width is greater than the critical panel width for the other conditions (plate thickness, flexural rigidity) existing in that area. As the panel is mined the critical $\frac{b}{a}$ ratio is approached and passed. The closure rate experienced in such a panel will be greater than in the former case and failure of the roof due to tension failure or shear failure, or both, will result. Nos. 10 and 19 Panels are regarded as having suffered this fate.

The total mechanism described above would explain why high extraction panels are successful in providing stable roof conditions, to all roadways, not only the inner ones. It also explains why the roof to floor closure rates experienced are so similar; why the horizontal deformations of large pillars and solid ribsides have virtually the same characteristics and why water has entered some panels and not others.

9.1.6 Deformation with distance mined

The graphs of deformation along roadways, Figures 6.4, 6.10, 6.31, 6.33 and 6.36, all show a periodicity where the 20 day convergence increases with distance down the roadway reaching a maximum at about 60m. The indications are that this is followed by a rapid drop and then a build up again. A possible mechanism is given in Figure 9.8. As the panel proceeds, the span increases and so does the closure rate until a span of about 60m is achieved. Most of the high extraction panels have a width of approximately 90m and so at that stage, the $\frac{b}{a}$ ratio is $\frac{60}{90}$ or $\frac{2}{3}$. This ties in with the theory of bending of

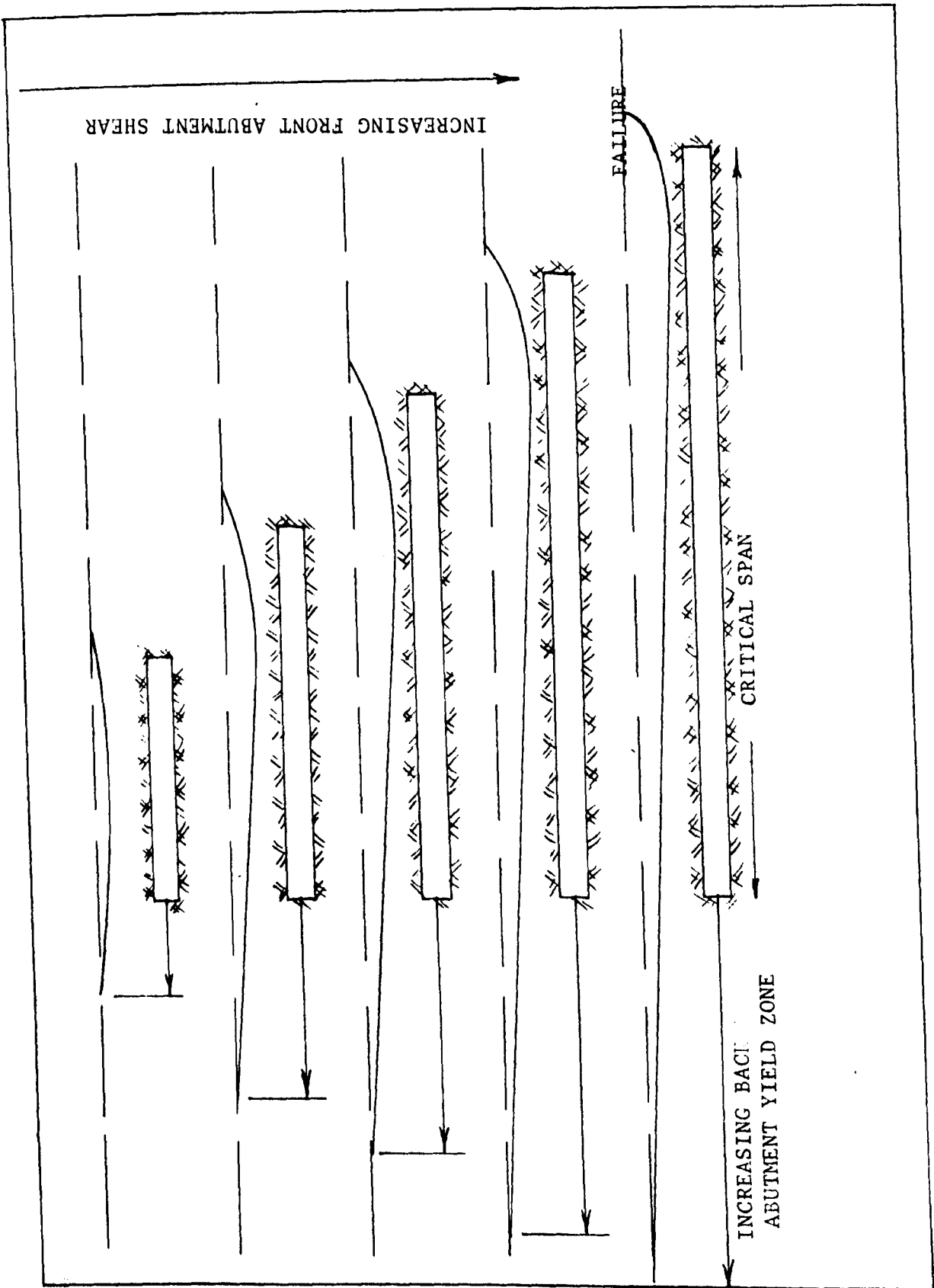


Figure 9.8 Mechanism of deformation along a panel

plates. What happens next is that the plate fails, thus explaining the drop in closure rate and subsequent steady rise as the face line progresses further. The reason why the plate fails at the face line and not at the back, is that at the "back abutment", the plate is sitting on yielding material that has a cushioning effect. At the front abutment, however, there is increasingly severe dynamic loading of the plate with resultant large shear stresses which cannot be diffused by yielding and which ultimately cause failure of the roof material. The process then starts again.

It is realised that this is an over-simplification of what must be an extremely complex interaction of parameters that are varying both spatially and with time. The probability is that the plate is not a simple one, but a compound structure in which the marl, the anhydrite, the Upper Halite and possibly higher strata are all active. However, because of the relative high strength, the elastic nature, and the proximity to the workings of the anhydrite, it is felt that this stratum plays the predominant role in determining the stability of the excavations below.

9.1.7 The Stability of Yield Pillars

Yield pillars with widths varying from 3m to 6m have been used. The indications are that in a 3.5m high roadway, a yield pillar that is wider than 4m will cause vertical shearing in the roof by punching. Three metre pillars on the other hand tended to slab very badly and this has been a problem in many areas. Because the W:H ratio increases as the pillar yields, and a central core forms which then

Plate 9.1

The art of communication



stiffens the pillar, it is felt that 4m should be the maximum width. Experience with the pillar in No. 12 Panel, Plate 4.1 showed that the cross-sectional area remained more or less constant, the pillar merely becoming shorter and wider. Laboratory testing of specimens of different W:H ratios support these findings from in-situ pillar behaviour.

9.1.8. The Water Problem

An explanation of how the water came to enter the workings is given below and it takes full account of the stability mechanism described in section 9.1.

The facts must again be considered. Water inflows have occurred in five panels, previously referred to in Chapter Three. The points of entry were either down the sides of the panels, or in the case of the smaller flows, in the panel centres. In Nos. 10 and 19 Panels, the approach of the water was heralded by an increase in closure rate across the panels, as well as by increased pillar and ribside deformation. Roof extensometers in No. 10 Panel exhibited very little, if any, increase in strain rate, up to 6m into the roof, even though they were fairly close to the point of ingress.

The picture then is one of the yield pillars showing an increase in deformation rate, but not the first 6m of roof strata. This implies that increased deformation was taking place somewhere from the base of the marl upwards. It is felt that the increase in deformation was due to the Upper Anhydrite failing either by shear

or tension, or both. The hydrostatic action of the water acting between the anhydrite and the Upper Halite would enhance this effect. If the plate theory is correct, then what took place was the shearing and/or tensile failure of the roof plate which allowed water to enter the workings. The only bed in the immediate roof succession which could be considered to be a barrier to the migration of water is the Upper Anhydrite. It is suggested that water has collected in certain low points on the top of the anhydrite. These are troughs or basins, the existence of which can be deduced from the variability in the thickness of the Upper Anhydrite bed, see Table 2.2 It is significant that the panels affected by the water all lie along a fairly well defined zone of geologically disturbed ground, probably associated with regional faulting known to exist in the Magnesian Limestone below the Middle Halite.

It is highly probable therefore, that the water now entering the mine is in fact draining from a possibly large, but limited, source.

New workings should avoid being sited in the vicinity of similar disturbed structures such as the salt overfold zone. The new northeast panels appear to have been laid out in just such a zone, and it is to be hoped that they do not encounter similar problems.

9.2 Summary of Conclusions

1. The predominant factors in the stability or otherwise of excavations in the potash seam are the presence and characteristics of the Carnallite Marl and the Upper Anhydrite beds in the roof strata.

2. The Upper Anhydrite can be considered to act as a plate of strong elastic rock which fails when certain criteria are met. These are mainly geometrical.
3. The maximum stable panel width for a high extraction panel is something less than 60m, but greater than 30m.
4. Stress relief as defined by Serata or Baar is not the mechanism that results in good conditions in high extraction panels.
5. The presence of stubs improves the condition of the outer roads because of their "cushioning" effect.
6. At panel widths of less than 30m, the plastic flow of the marl becomes predominant and these panels can be expected to have a shorter working life, particularly in the outer roads.
7. Yield pillars should be no wider than 4m.
8. Water entered No. 10 Panel as a result of failure of the Upper Anhydrite bed.
9. The water is not coming directly from the Bunter formation, but has collected over geological time in troughs and basins above the Upper Anhydrite.
10. Water probably occurs all along geologically disturbed zones such as the salt overfold that passes through No. 10 Panel

and mining adjacent to such structures should be avoided.

11. Mining through a geologically disturbed zone should be with as narrow a panel as possible (of the order of 30m wide) or preferably in the salt below.

CHAPTER TEN

PANEL DESIGN AND LAYOUT

Chapter Ten

10.0 Introduction

The design of any new panel layout should take into account all the experience gained to date, both from a production as well as a ground stability point of view.

Production orientated requirements demand that any layout to be acceptable must have or be:-

1. Regular and repetitive, in order that the men can get used to it and develop techniques and mining sequences that can be optimised.
2. Provide sufficient separate headings so that the operations of drill and blast, cleaning and profiling, supporting and finally probe drilling that are required because of constraints imposed by the Mines' Inspectorate, can be carried out with maximum use of mechanised equipment.
3. Safe, in that adequate cover is maintained between the roof and weak shale or the Carnallite Marl so that immediate roof strata remain intact in areas where men work or travel.
4. A minimum of three roadways and preferably four, must remain open and safe for the economic life of the panel. This is envisaged to be in the region of one year. If problems due to bad roof conditions are encountered, then

it must be possible to get around the affected area without restricting panel advance.

Ground stability considerations require that the layout:-

1. Must provide good roof (and floor) conditions for the expected life of the panel.
2. Prevent the ingress of water, if possible.
3. One panel must not interact detrimentally with another, or with main access ways.
4. Must form part of an overall mine layout that ensures stability of both surface and underground structures. This requires the leaving of adequate barrier pillars, and not exceeding a critical extraction ratio.

10.1 The Concept of Stability

It is imperative to decide on a firmly based criterion of what constitutes stability, related both to pillars and excavations. The problem with excavations in rocks that undergo time dependent deformation is that what is stable today may not be so tomorrow.

Hebblewhite⁽⁷⁾ used a criterion for roadways in low extraction panels that was based on a "stability envelope". This was the curve given by the equation

$$\dot{c} = 34.81 t^{-0.785} \quad \dots 10.1$$

where \dot{c} is the roadway closure rate in mm/day, and t , the time since mining in days. Any measured results falling above the curve indicate instability and below it, stability.

Because the deformation mechanism is so different in a high extraction panel, this stability criterion is of limited use.

It is therefore proposed that a much more general classification of stability be employed. The system is based on the rate of deformation with time as follows:

1. If a pillar or excavation has a deformation rate that is either constant or increasing, then it is unstable.
2. If a pillar or excavation has a deformation rate that is decreasing, then it is stable.

The stability or otherwise can thus be determined by the slope of the curve of log strain (or convergence) rate against time. This curve is generally a straight line, but if not, it is easy to tell by inspection whether the strain rate is increasing or not.

In order to make the classification more useful, it is necessary to define different degrees of stability.

10.1.1. Roadway Stability Criterion

Roadways are characterised by the fact that they exhibit roof-to-floor as well as wall-to-wall closure. These can be combined to give a change in area. There is a minimum area below which normal

mining operations cannot be continued. If the allowable change in area is, say, one fifth of the original area, then the stability of a roadway can be expressed in terms of the time it takes for the roadway to achieve this change in area.

If a roadway has width w , and height h , when mined, and after time t , has elapsed these become w' and h' , then the change in area

$$\Delta A = wh - w'h'$$

$$\text{but, } w' = w - c_w$$

$$\text{and, } h' = h - c_r$$

where c_w and c_r are the wall to wall and roof to floor closures.

$$\Delta A = hc_w - c_w c_r + wc_r$$

But it has been shown (Section 6.3) that c_w and c_r are functions of t of the form

$$c = \frac{1}{A} (e^{At+B} - e^B)$$

Where A and B are the slope and intercept of the log convergence rate/time curve.

Therefore,

$$\begin{aligned} \Delta A = & w \frac{1}{C} (e^{Ct+D} - e^D) \\ & + h \frac{1}{A} (e^{At+B} - e^B) \\ & - \frac{1}{AC} (e^{At+b} - e^B) (e^{Ct+D} - e^D) \end{aligned}$$

where A and B are constants relating to the wall to wall closure and C and D those for roof to floor closure.

The change in area has been calculated for sites H 15 B, C43 B

and J 19 G for different values of t and the results are depicted in Figure 10.1, with A expressed as a percentage of the original area. Table 10.1 lists the time it takes to achieve various amounts of change in area for the three sites, and the difference in stability between the sites is self-evident.

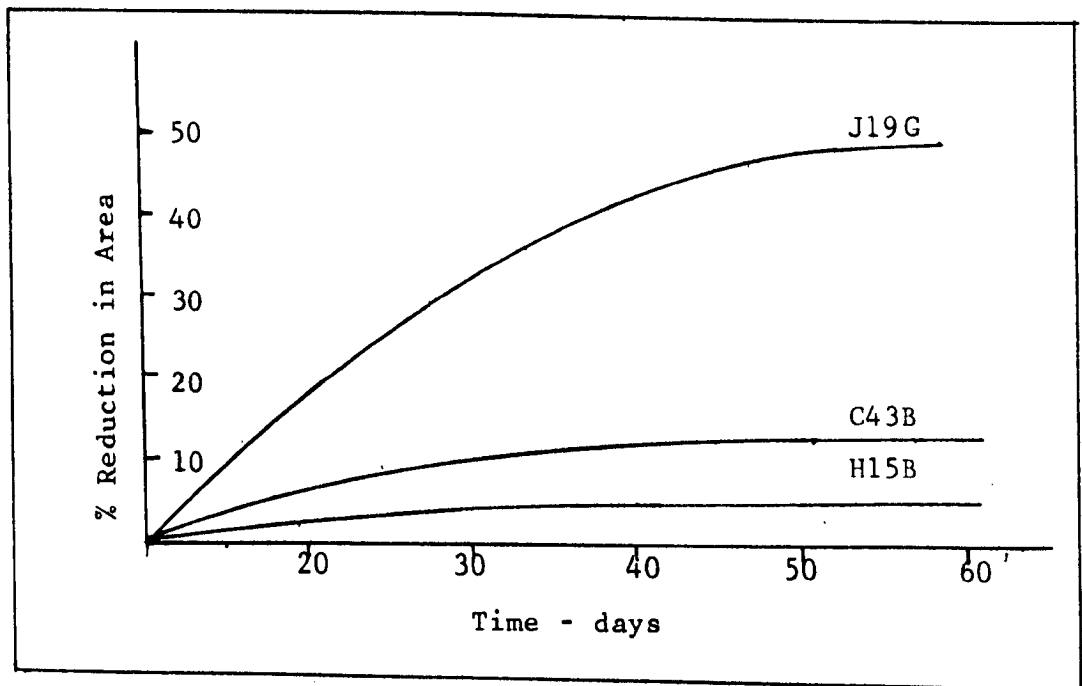


Figure 10.1 Change in roadway area with time

When applied to the average roadway closure conditions for various high extraction panels, the results in Table 10.2 are obtained,

TABLE 10.1

Relationship between change in roadway area and time for various sites

Site	C 43 B	H 15 B	J 19 G
% Area Change	days	days	days
5	49	15	5
10	121	33	10
15	233	181	15
20	>400	>400	24
25			28
30			35
$33\frac{1}{3}$			40
50			87
	Stable	Moderately Stable	Not very Stable

TABLE 10.2

Time to 10% and 20% Area Closure for various high extraction panels

Number	Site	Panel No.	Time	
			10%	20%
1	C42C	10-A	46	>400
2	C43B	10-A	121	>400
3	C44A	10-A	27	70
4	C46B	10-A	23	97
5	C46D	10-A	26	>400
6	PR5A	12	36	100
7	H15B	15	33	>400
8	H16B	16	33	170
9	E17A	17	10	19
10	J19G	19	10	24

This stability criterion is felt to be useful because it takes into account, not only the initial closure rate, but also the decay of strain rate with time.

10.1.2 Pillar Stability Criterion

The assumption of zero volumetric strain referred to in Chapter 9 is held to be true for all pillar and immediate roof rocks in the mine. This means that vertical strain equals the lateral strain.

The initial statement in 10.1 that constant or increasing strain rates in the solid are defined as resulting in unstable conditions is re-iterated. However, as with roadway closures, there is the problem remaining of how to classify relative stable conditions. It is impossible in this context to avoid reference to the existence or otherwise of a "core" in a pillar. This term although frequently used, is not defined. It is loosely used to describe a zone of relatively lower strain rate. There is no doubt that all pillars that have a width to height ratio greater than about 2:1 develop a central zone having relatively lower deformation, although the absolute value of strain may be quite high, say between 5 and 10 per cent.

It appears logical therefore to define the stability of a pillar, or section of a pillar by its average strain. Table 10.3 is a suggested classification of relative stability for pillars which suits the conditions at Boulby. A pillar or section of a pillar having a relative stability of 1 is very stable and 5 is much less stable.

TABLE 10.3

Classification of Pillar Stability

Strain %	Classification Class
0 - 0.1	1
0.1 - 0.5	2
0.5 - 2.0	3
2.0 - 5.0	4
5.0	5

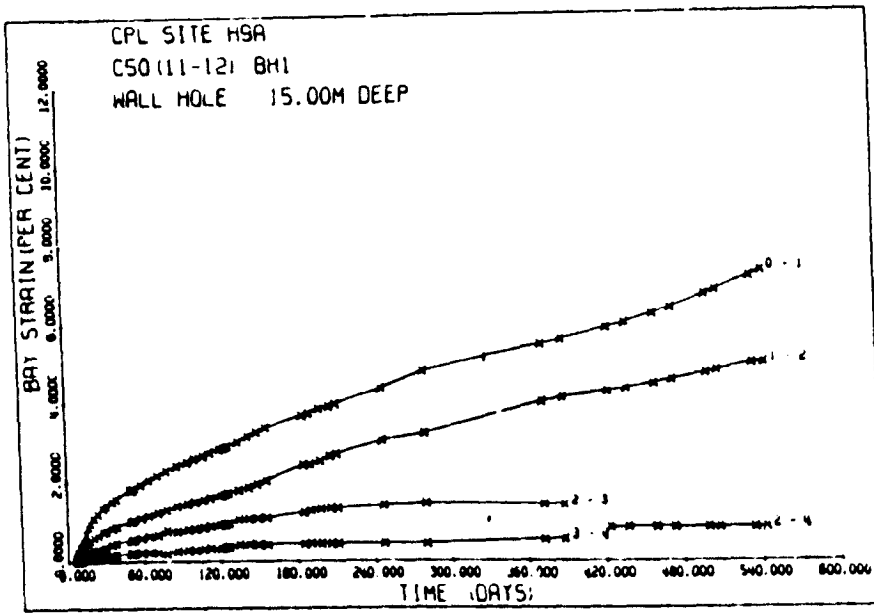
↓
decreasing
stability

The distribution of strain within a 30m square pillar with a W:H ratio of 8.6:1 is given in Figure 10.2. At 100 days after mining, the outer 3.5m can be said to have a relative stability of class 4; from 3.5m to 9m into the pillar, class 3, and the central "core", 11m wide, has a relative stability of class 2. The pillar as a whole is stable since the strain rates are decreasing.

This concept of pillar stability will be used when discussing the stability of the 40m pillar in No. 15 Panel.

10.2 The Design of a Stable Standard High Extraction Panel Layout

The problem of designing a viable high extraction panel was approached by firstly considering the overall production requirements. These were:



Anchor 1 at 3m
2 at 6m
3 at 9m
4 at 15m

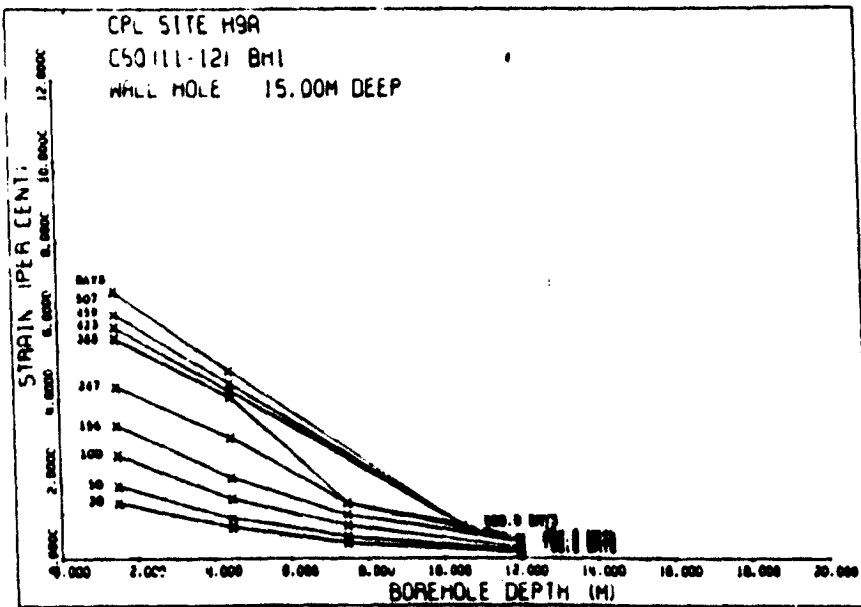


Figure 10.2 Distribution of Strain in 30m Pillar

1. Minimum roadway dimensions were 3.5m high and 6.5m wide.
2. A minimum of three roadways, but preferably four were required.
3. If there was to be a central pillar, there had to be cross-cuts put through at regular intervals of not more than 45m. These had to remain open and safe for at least the time it took to mine a further two cross-cuts.
4. The overall length of the panel had to be at least 500m.

These were in addition to the more general requirements mentioned in Section 10.0.

The rock mechanics aspects that had to be taken into account were:

1. The panel width had to be such that overall stability of the roof strata was assured. This meant keeping it below the critical width at which water might break through.
2. Yield pillars had to be of the correct dimensions so as to yield sufficiently to prevent punching and thus break-up of the immediate roadway roof.
3. The panel layout had to form part of an overall area layout, bearing in mind the overall extraction ratio which had to be not more than 35%.

Having considered these desired pre-conditions, the next step was to look at the possible panel layouts that would meet with the requirements stipulated.

The most important and overriding requirement was that of reducing the panel width in order to prevent the ingress of water. If the description of how the water entered the workings advanced in Chapter Nine was correct, namely that there was general breakdown of the roof strata, and the Upper Anhydrite in particular, then what was required was a mining geometry that would minimise the bending of these strata.

If a single panel was to be considered, it would have to have at least four headings with stubs, or six headings without stubs. This was in order to provide sufficient headings for the sequential mining operations of undercut, drill and blast, mucking out and profiling, supporting, and probe drilling. The two cases mentioned would result in minimum viable panel widths of approximately 60.5m and 61.5m respectively, see Figure 10.3. Because 60m (Chapters 6 & 9) appeared to be a critical dimension at which closure rates were at a maximum, and probably the dimension at which breakdown of the roof rock occurred, this should be avoided as the minimum plan panel dimension; that is, the width, as it was expected that the dimension in the direction of mining would always exceed the panel width. It was for this reason that the idea of a split panel was conceived.

Such a panel would consist of two sub-panels separated by a substantial pillar. This central pillar would have to be fully load

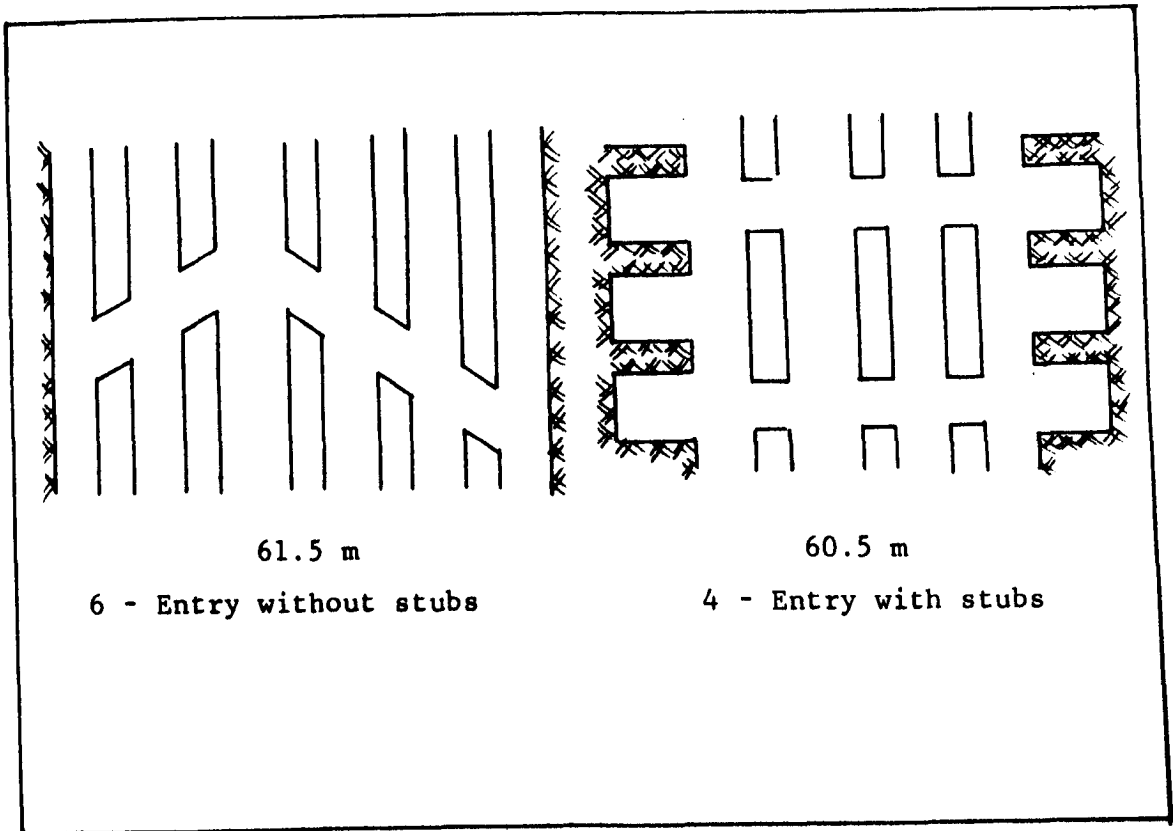


Figure 10.3 Panel layouts with and without stubs

carrying and would in fact serve to break the overall span on the roof rock between the two extreme outer roads. The scheme is shown diagrammatically in Figure 10.4. No. 10 Panel (A section) had been similar to this layout and although certain minor difficulties had arisen, it had been satisfactory from the operations point of view. In order to be viable, the sub-panels would have to have a minimum of three roadways and preferably four. These meant sub-panel widths of 30 or 40 metres respectively, without stubs.

Because the split panel layout appeared to satisfy most of the prerequisites, it was decided to go ahead and investigate it further.

The critical factor in the successful design of a split panel

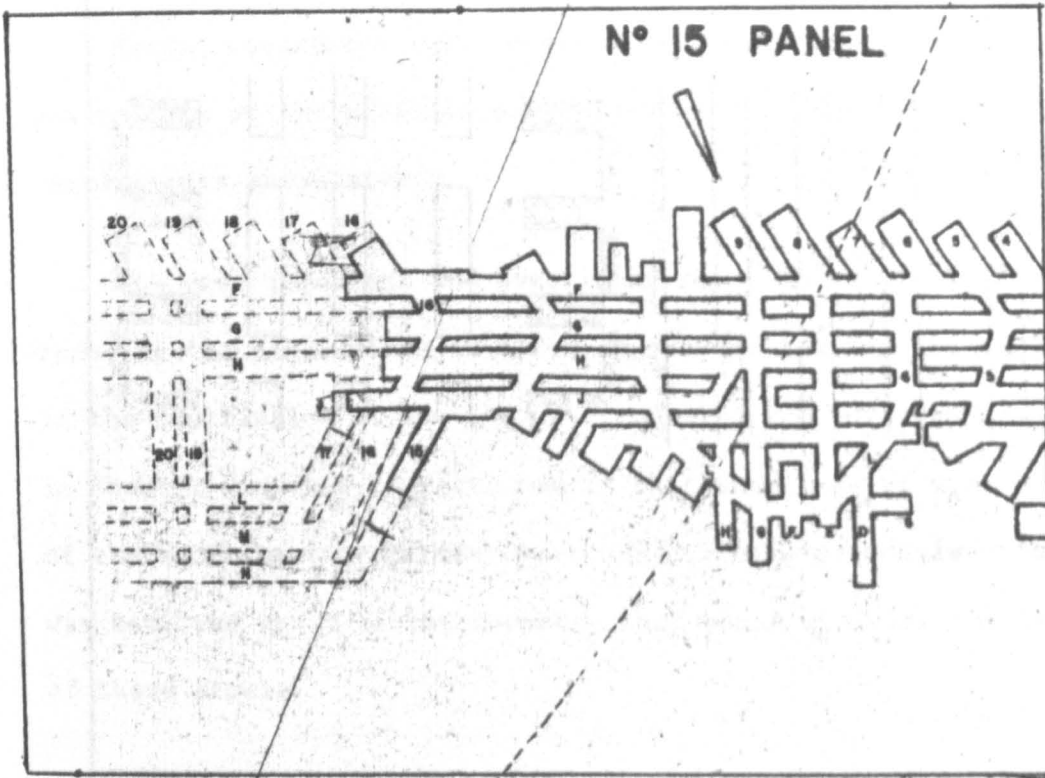


Figure 10.4 Split Panel Layout

would be the stability of the central pillar. This in turn would depend ultimately on the load it would be expected to carry. Figure 10.5 shows diagrammatically how load could be expected to be redistributed around a split panel. It is assumed that there are solid abutments on either side of the overall panel.

If the sub-panel widths are W and the central pillar width is B , then the overburden load per unit length of panel from each sub-panel will be $W\sigma_v$, where σ_v is the vertical virgin stress. The overburden load will be redistributed such that the load carried by the central pillar will be R_B and that on each outer abutment, R_A . At this stage it is assumed that the internal yield pillars carry no load.

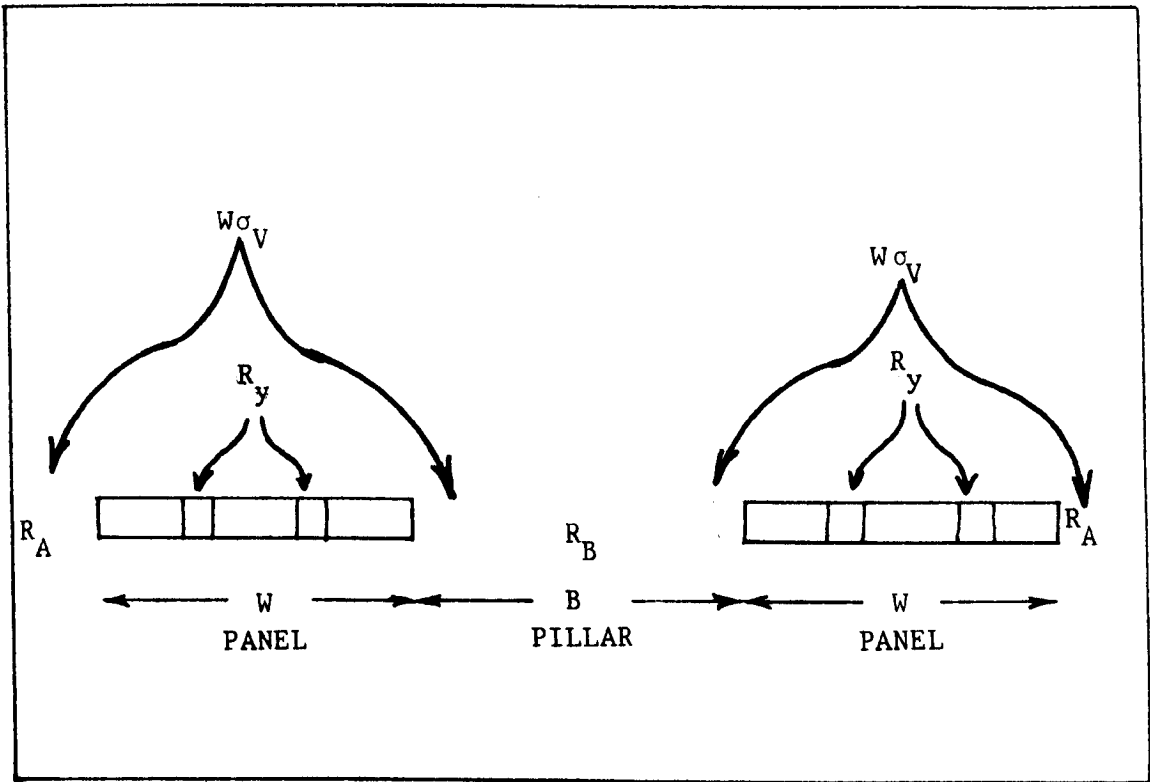


Figure 10.5 Load redistribution around a split panel

If the central pillar were large enough, then it would be logical to assume

$$R_B = 2R_A \quad \dots 10.2$$

then

$$W\sigma_v = 2R_A \quad \dots 10.3$$

or $W\sigma_v = R_B \quad \dots 10.4$

Assuming that R_B gives rise to σ_{R_B} on the pillar, then,

$$\sigma_{R_B} = R_B/B = \frac{W\sigma_v}{B}$$

The total stress on B, $\sigma_B = \sigma_v + \sigma_{R_B}$

$$\text{Therefore, } \sigma_B = \sigma_v + \frac{W\sigma_v}{B} \quad \dots 10.5$$

$$\text{This gives, } \frac{W}{B} = \left(\frac{\sigma_B}{\sigma_v} - 1 \right) \quad \dots 10.6$$

It is possible to obtain a maximum value of σ_B in terms of σ_v , This is done by reference to the minimum pillar size used in the mine that has been found to be stable, i.e. 25m. The average normal stress for a fully loaded 25m square pillar was found by Hebblewhite⁽⁷⁾ to be $1.65\sigma_v$. Substituting this value in equation 10.6 and assuming $\sigma_v = 30 \text{ MPa}$, gives,

$$W = 0.65 B \quad \dots 10.7$$

It can be seen that this relationship would give a pillar width of 61m for a sub-panel width of 40m. This would be an unacceptably large pillar, and therefore the basic assumptions were re-examined to see if any suitable adjustments could be made.

Upon inspection it would appear that the assumption that $R_B = 2R_A$ is not realistic since the sole purpose of the central pillar is to break the overall panel span. As it took load it could be expected to yield, throwing a significant portion of the load onto the extreme abutments.

In addition, the yield pillars would certainly carry some load, and as they yielded and their W:H ratios altered, this yield pillar load could be expected to increase.

The case of $R_B = R_A$ is therefore considered. If the same steps are followed as before, the result:

$$W = 0.975 B \quad \dots 10.7$$

is obtained.

If support provided by the yield pillars is added to the case of $R_B = R_A$ then

$$R_B = \frac{2}{3}W \left[\sigma_v - \sigma_{\max}(1 - e) \right] \quad \dots 10.8$$

where the load supported by the yield pillars is given by

$$R_y = \sigma_{\max}(1 - e)W \quad \dots 10.9$$

where e is the sub-panel extraction ratio and σ_{\max} is the maximum permissible stress on the pillars.

The value of σ_{\max} is obtained from the laboratory testing of specimens of similar W:H ratio to the yield pillars. The maximum yield stress at the strain rate occurring in the mine was found to be 41.5 MPa. However, allowing for fracturing and the fact that this stress acts over a much reduced area (approximately half) in the central core of the pillar, the value of 16 MPa has been assumed.

Substituting this value in equation assuming $e = 0.81$ gives the result

$$W = 1.085 B \quad \dots 10.10$$

Figure 10.6 shows the relationship between the ratio of B/W for different values of R_B/R_A . It also shows the effect of increasing the sub-panel extraction ratio.

The split panel section of No.15 Panel was designed using the assumption that $R_B = R_A$, i.e. an R_B/R_A ratio of 1 and an extraction

ratio of 0.81 which gives the result in equation 10.10.

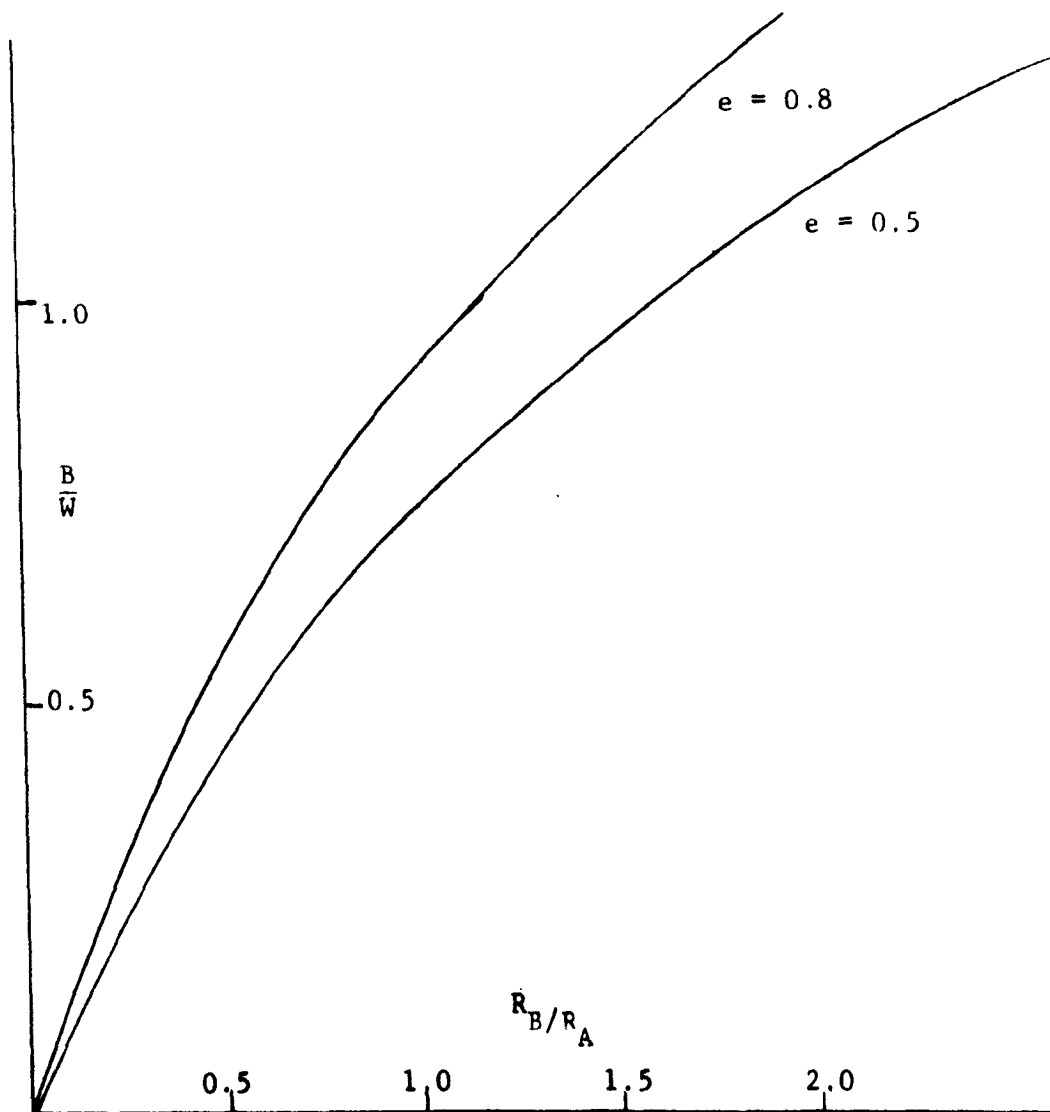


Figure 10.6 Relationship of B/W to R_B/R_A for different extraction ratios

A four roadway system was decided upon because of production requirements, and the sub-panel width that resulted was 40m. Substituting this value in 10.10 gave a pillar width of 37m. It was felt that these dimensions were suitable overall and the mine then changed the existing No.15 Panel layout to follow this design - Figure 10.7

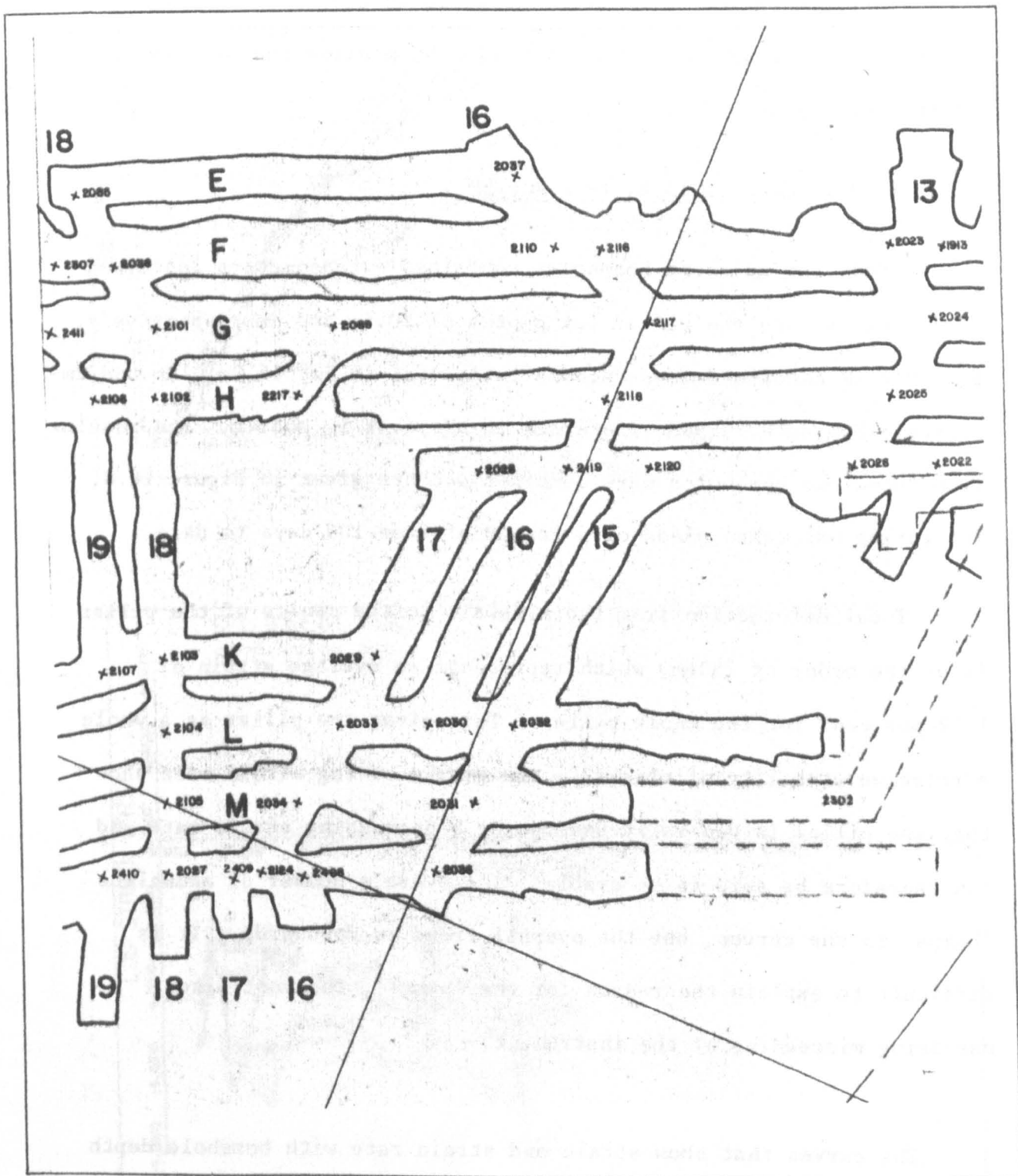


Figure 10.7 No.15 Split Panel Layout

10.3 Monitoring of No.15 Panel (B section) Performance

Instrumentation sites were installed as described in Chapter 6 in the B section of No.15 Panel in order to monitor the performance of the new layout.

10.3.1 Site 17 15 B, BH 2 and BH 3

These two adjacent boreholes contained extensometers installed horizontally into the pillar, at depths of 20.5m and 8m respectively. Borehole Q2 contained four anchors located at 20.5m, 16.0m, 12m and 2m depths. Two anchors were installed in BH 01 at 8m and 4m. The results from these two boreholes were combined and are given in Figure 10.8. Monitoring has taken place of a period of some 100 days to date.

Total deformation from the sidewall to the centre of the pillar is of the order of 250mm, which represents an average strain of 1.22 per cent for the whole pillar. This gives the pillar as a whole a relative stability of class 3. The graphs of log strain rate show that the pillar is generally undergoing a decreasing strain rate and can therefore be said to be stable. There are a number of anomalous 'bumps' in the curves, but the overall trend is downwards. It is difficult to explain the reason for the 'bumps', the most likely one being misreading of the instrument.

The curves that show strain and strain rate with borehole depth indicate that most of the deformation is taking place in the first 6m of the pillar, a similar situation to that observed in other pillars

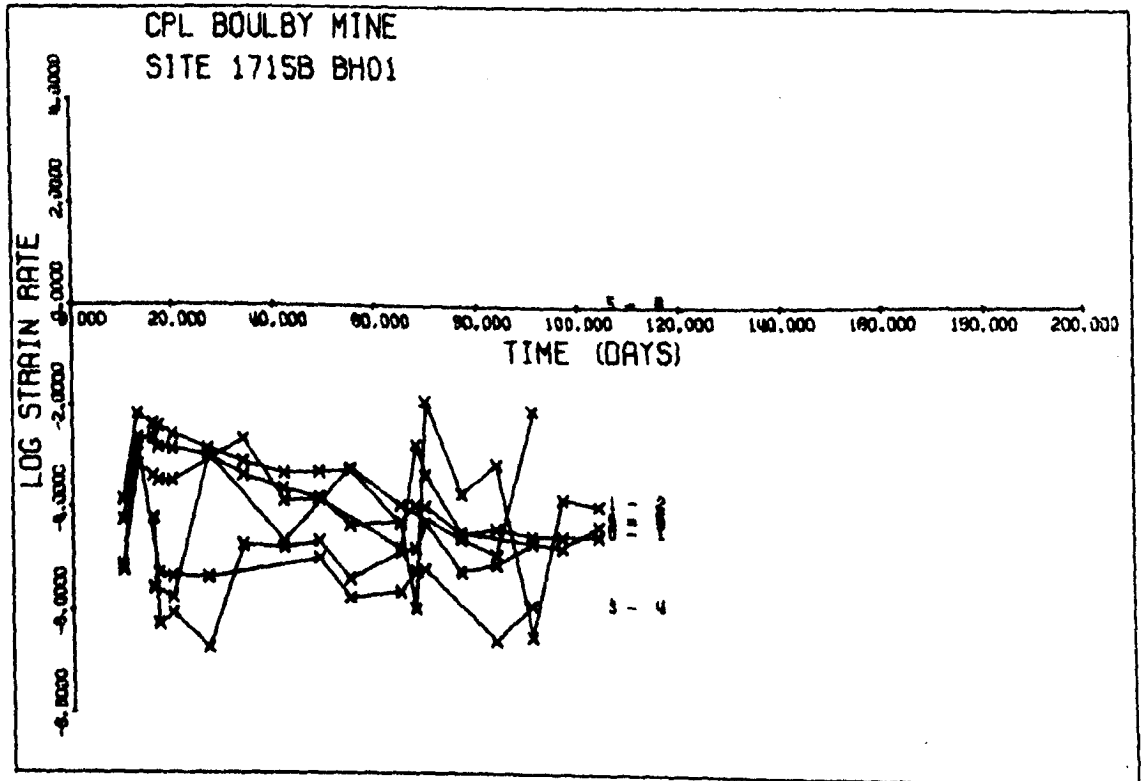
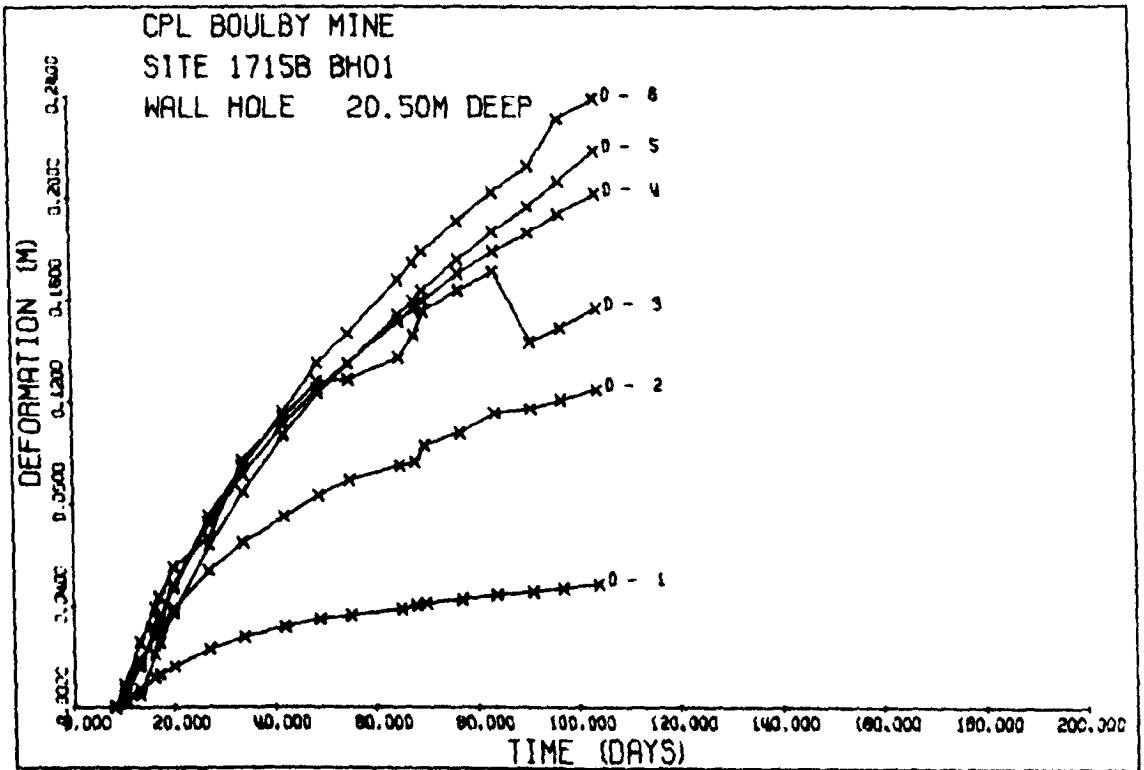


Figure 10.8 Site 17 15 B Extensometer results

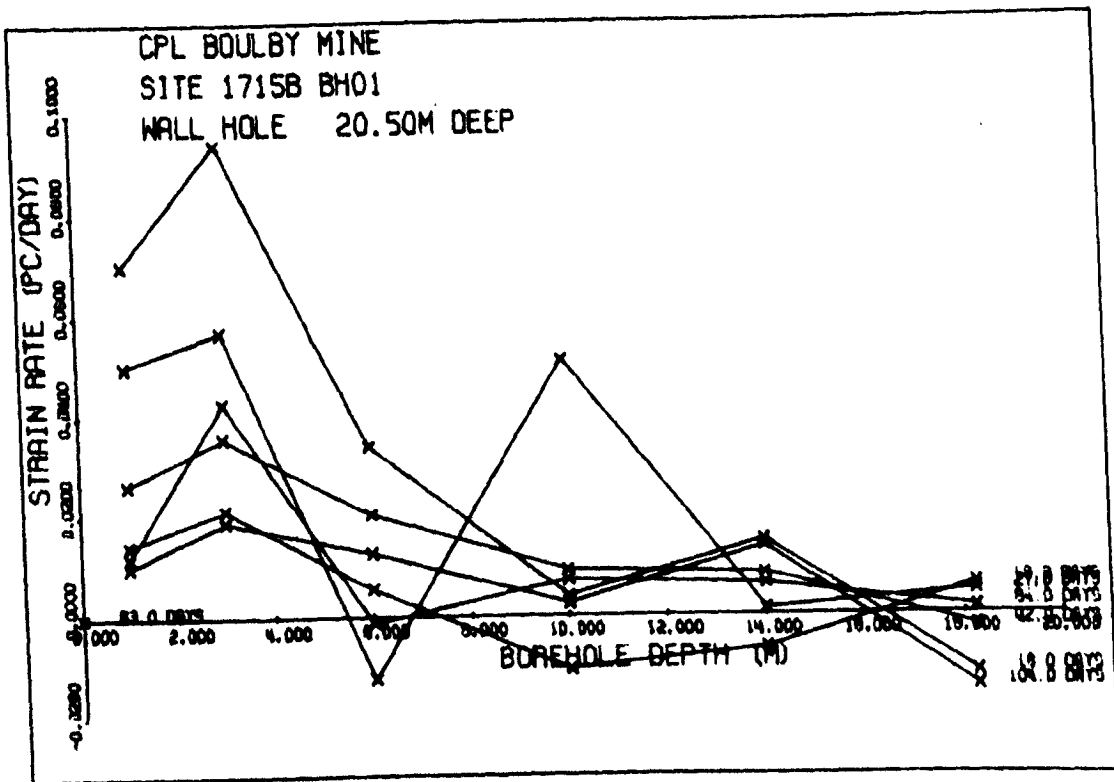
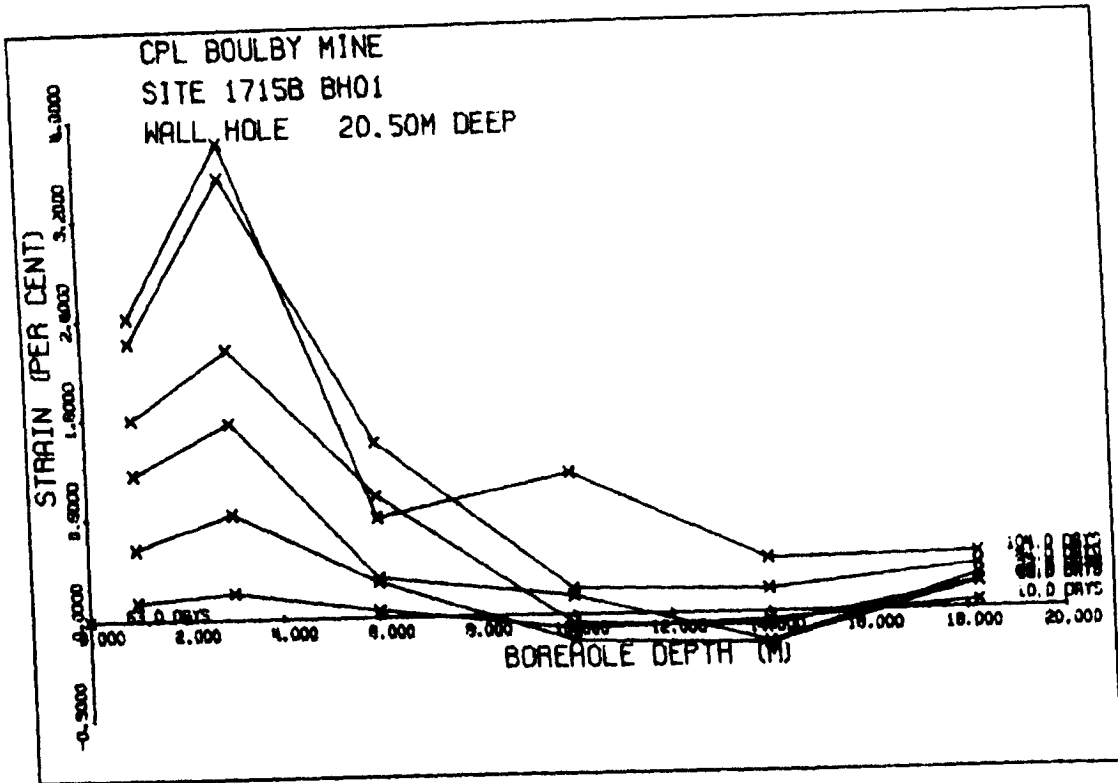


Figure 10.8 Site 17 15 B (Contd.)

and ribsides. Deeper than 6m there is evidence of a stable core forming with the relative stability of the central 24m zone being mainly class 2, which is fairly stable. At the same time the strain rate in this zone is decreasing.

10.3.2 Site H15B, BH 03

This was an extensometer installed horizontally into the 40m pillar with anchors at 19m, 15m 11m and 2m. Figure 10.9 shows the layout of the measuring stations at H15B. The results are given in Figure 10.10.

The average strain after 77 days to the end of the anchor is 0.63% which puts it in the lower range of the class 3 relative stability category. This strain is somewhat lower than that in 17 15B, but this is because fo the shorter time it had been installed. The deformation curves show that something interesting is occurring after 56 days, where there is an increase in the total strains in all bays. Largest increases take place in bays 0-1 and 1-2, .i.e. at depths into the pillar of up to 11m. Although the strains do not appear great enough to represent the formation of slabs, they would appear to indicate incipient slabbing. The curves of log strain rate vs time show an increase in bays 0-1 and 1-2 and an overall decrease in 2-3 and 3-4 after 56 days. The conclusion is therefore made that the outer 11m pillar zone has become unstable, due probably to the formation of slabs. There is an inner core of approximately 16m width that has a relative stability of class 2, bordering on class 1 with a decreasing strain rate. This indicates a stable core. However it is important to watch the future performance of the outer zone.

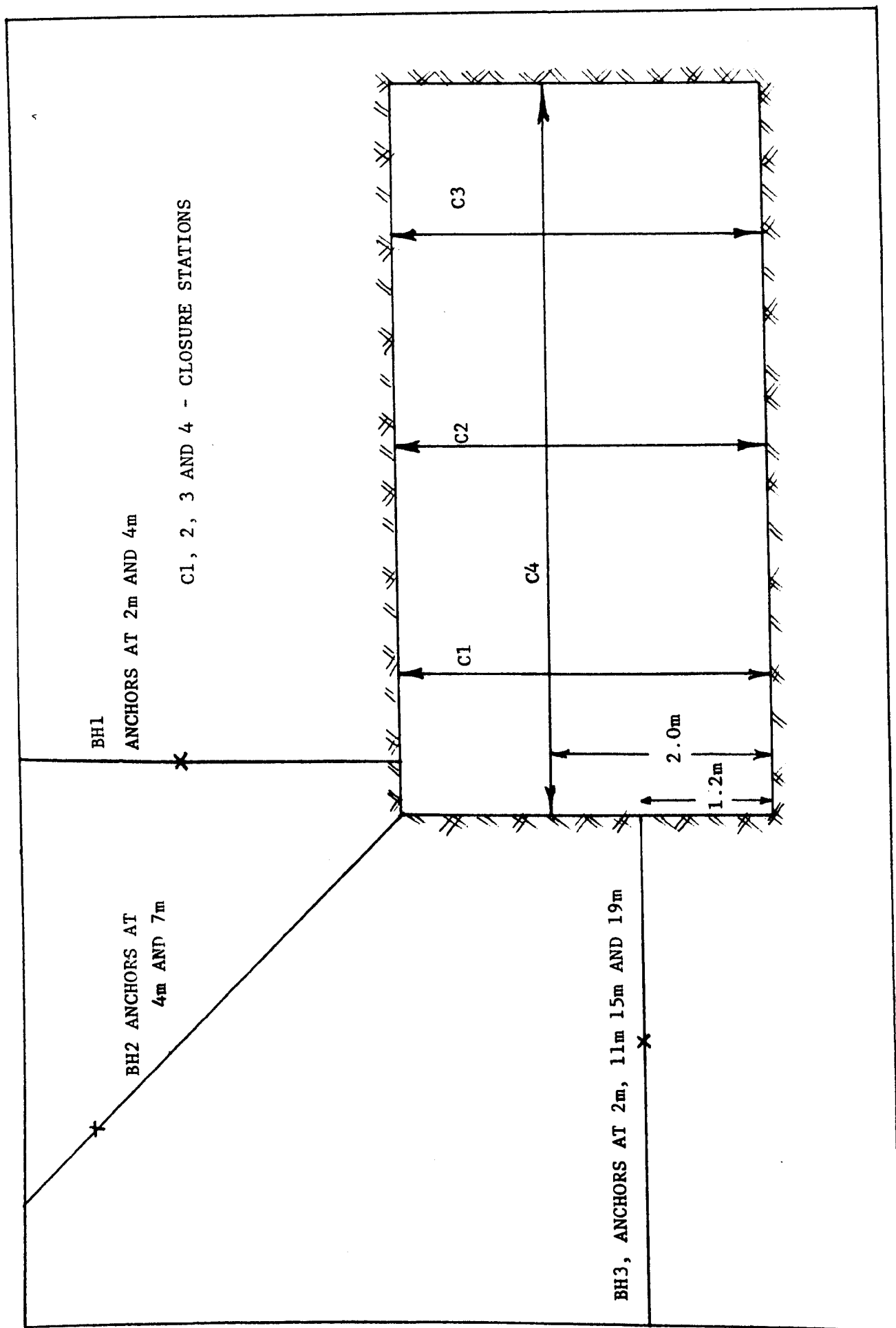


Figure 10.9 Instrumentation Layout at H 15 B

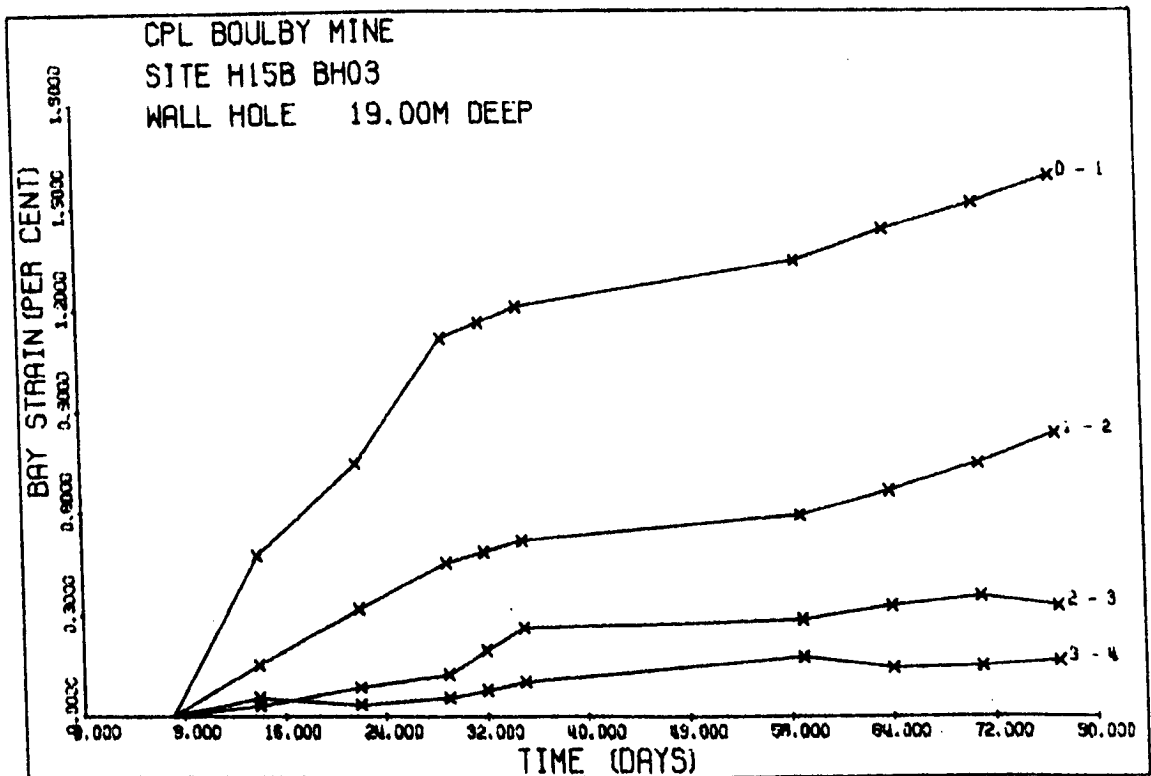
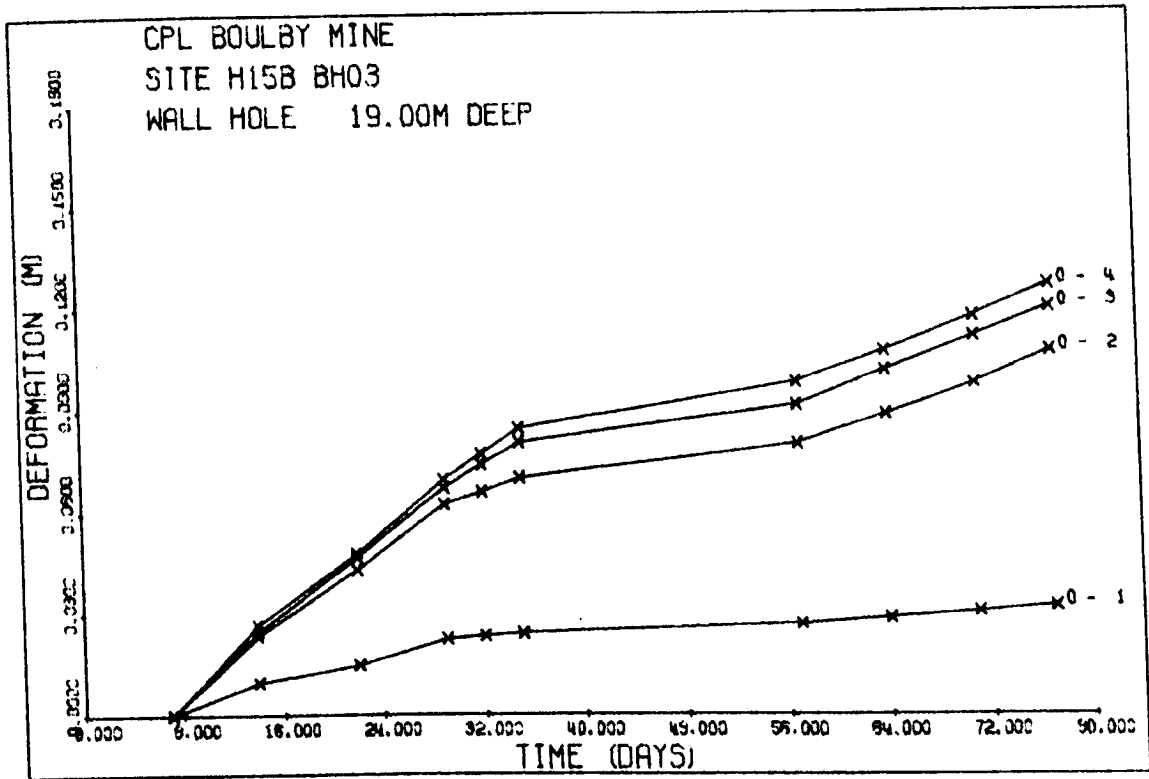


Figure 10.10 Site H 15 B Pillar Extensometer Results

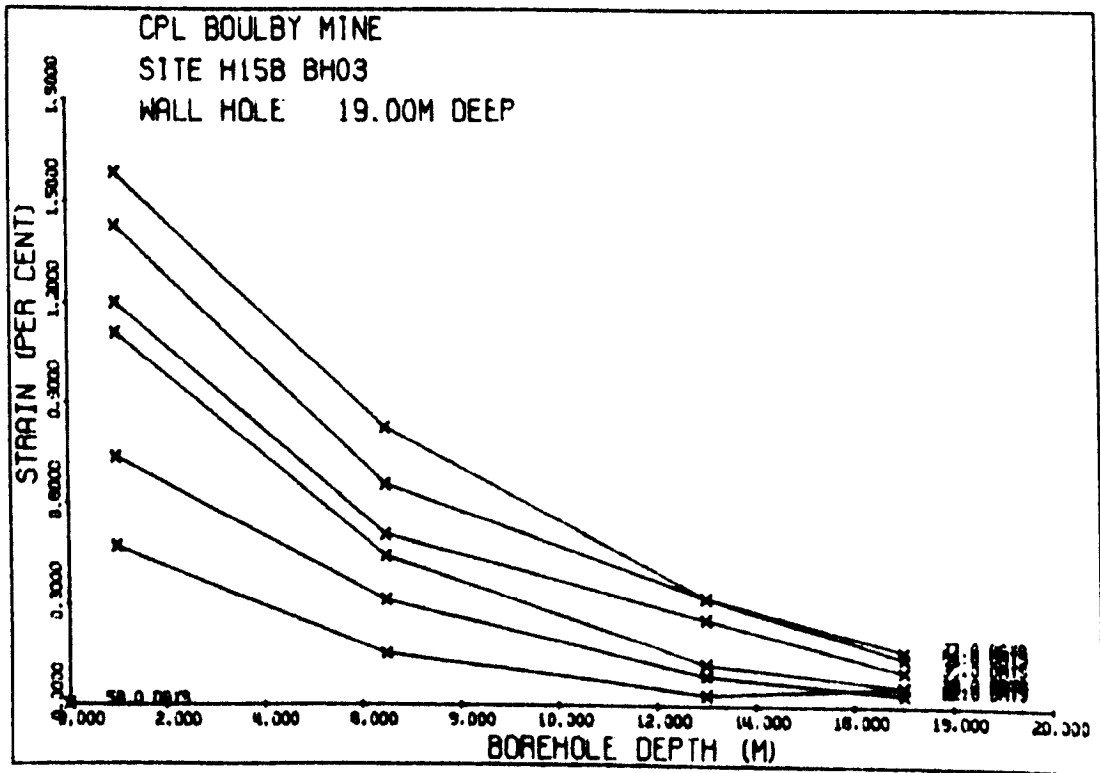
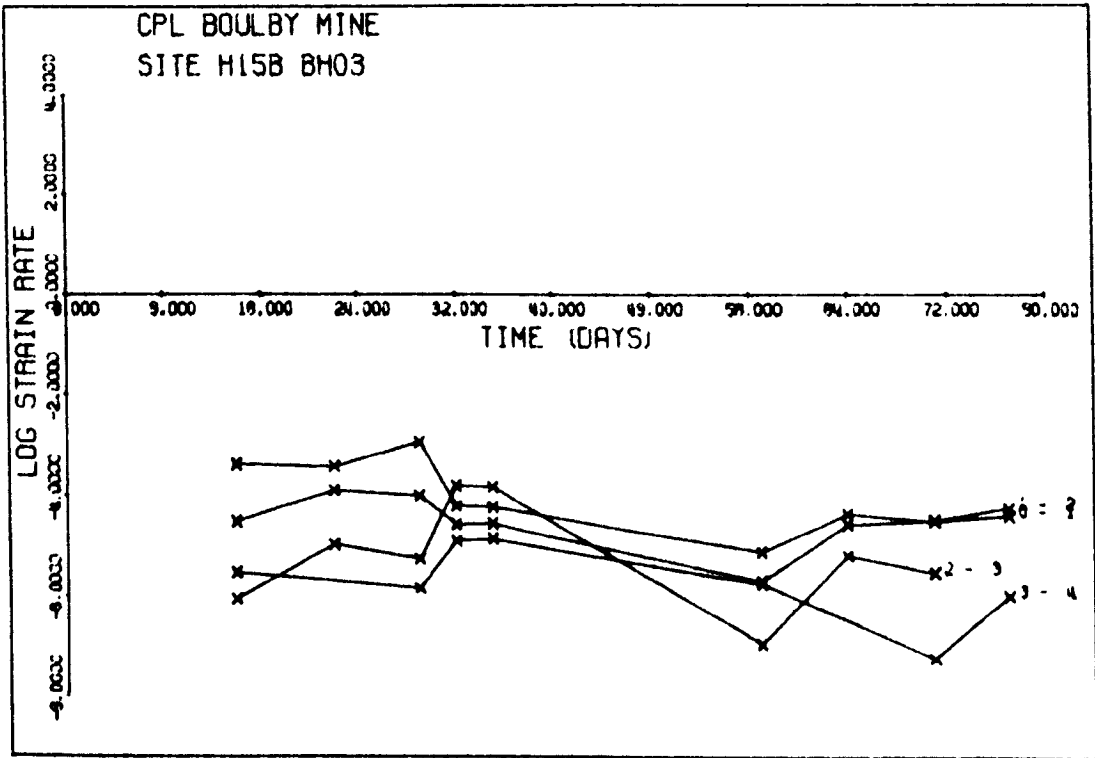


Figure 10.10 H 15 B Pillar Results (Contd.)

10.3.3 Site H15B, BH 01

This is a roof hole with an extensometer that has anchors at 4m and 2m into the roof and the graphical output is given in Figure 10.11. The overall strain after 84 days is 1.125% which puts it into the class 3 category. The log strain rate curves show that the strain rates are decreasing continually, so stability is indicated. Total deformation after 84 days is of the order of 55mm (allowing 10mm after mining and before monitoring began). Total roadway closure at this site after 80 days is 308mm, which means that even if floor heave is contributing 100mm of this total, then more than 70% of the roof deformation is occurring deeper than 4m. What is being measured by the roof extensometer is incipient slabbing taking place within the first 2m. Nearly three times as much movement is occurring beyond the deepest anchor. This anchor is installed as close to the marl as possible, so most of the movement is in the marl or above; again a pointer towards a combination of plastic flow in the marl and bending of the Upper Anhydrite.

10.3.4 Site H15B, BH 02

Borehole 02 was installed with an extensometer with anchors at 7.5m and 4m. Figure 10.9 shows that it was installed at an angle of 45° up over the pillar ribside. The results are given in Figure 10.12. Total deformation after 77 days is about 80mm, giving an overall strain of 1.06%. About twice as much strain is occurring in the first 4m compared with the next 3.5m.

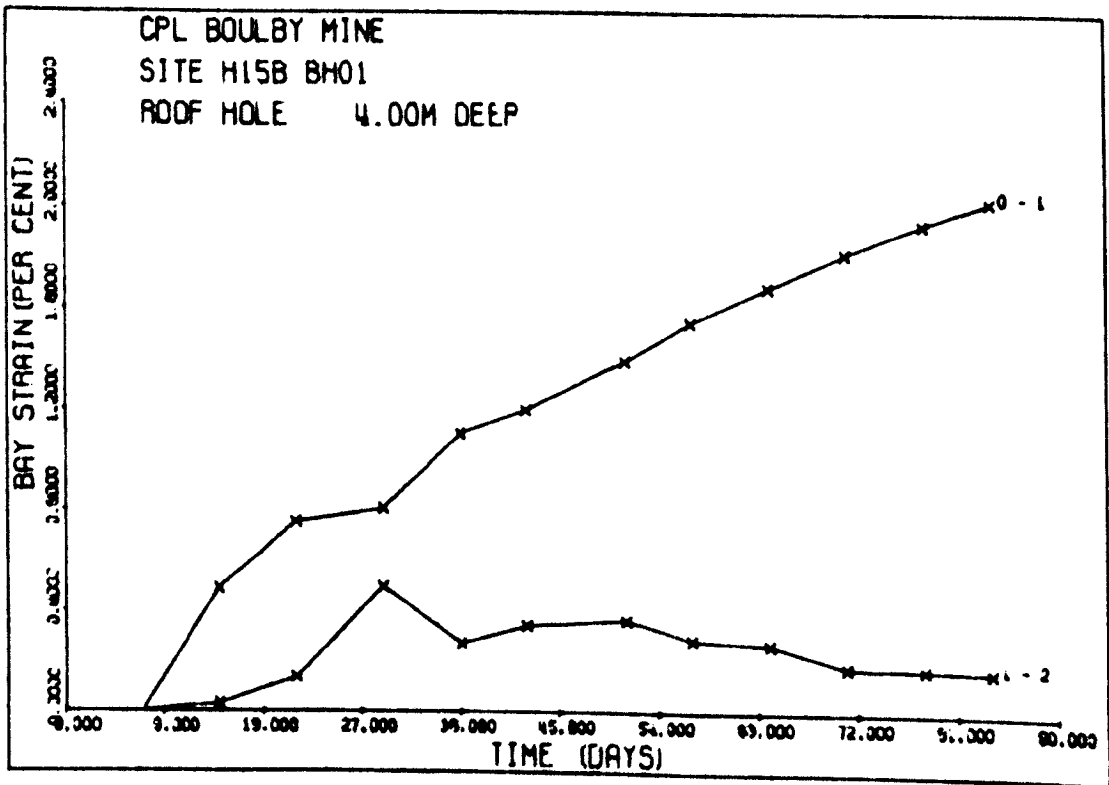
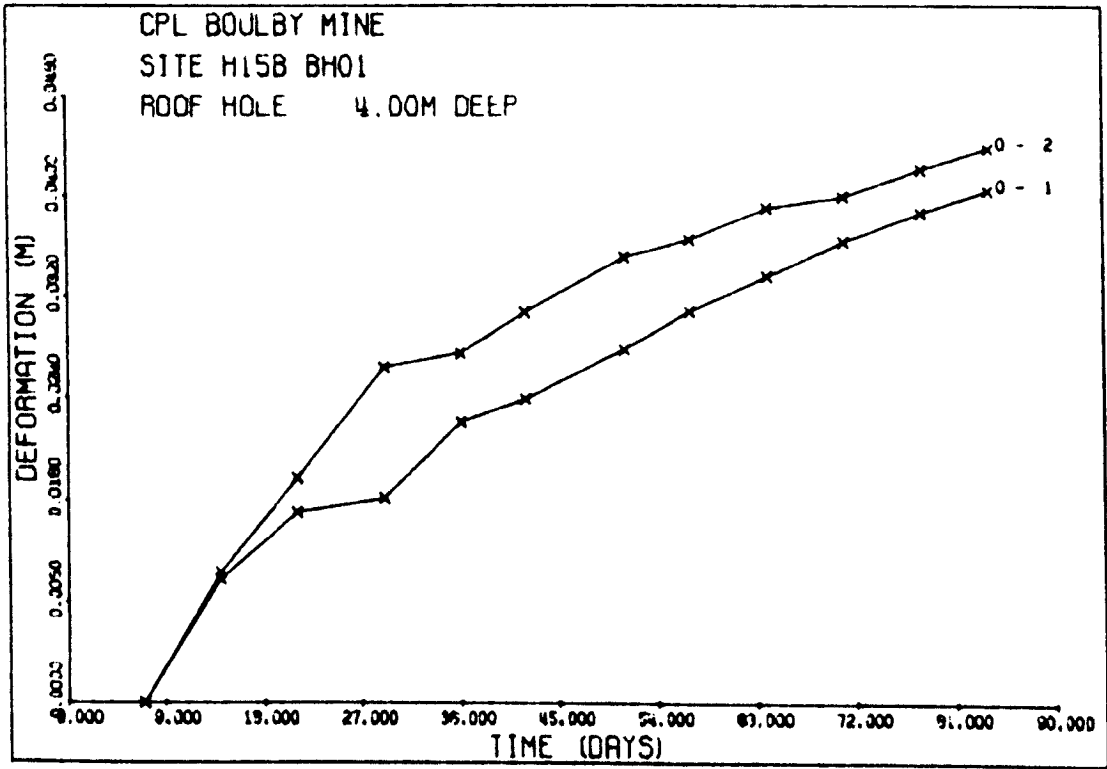


Figure 10.11 Site H 15 B Roof Extensometer Results

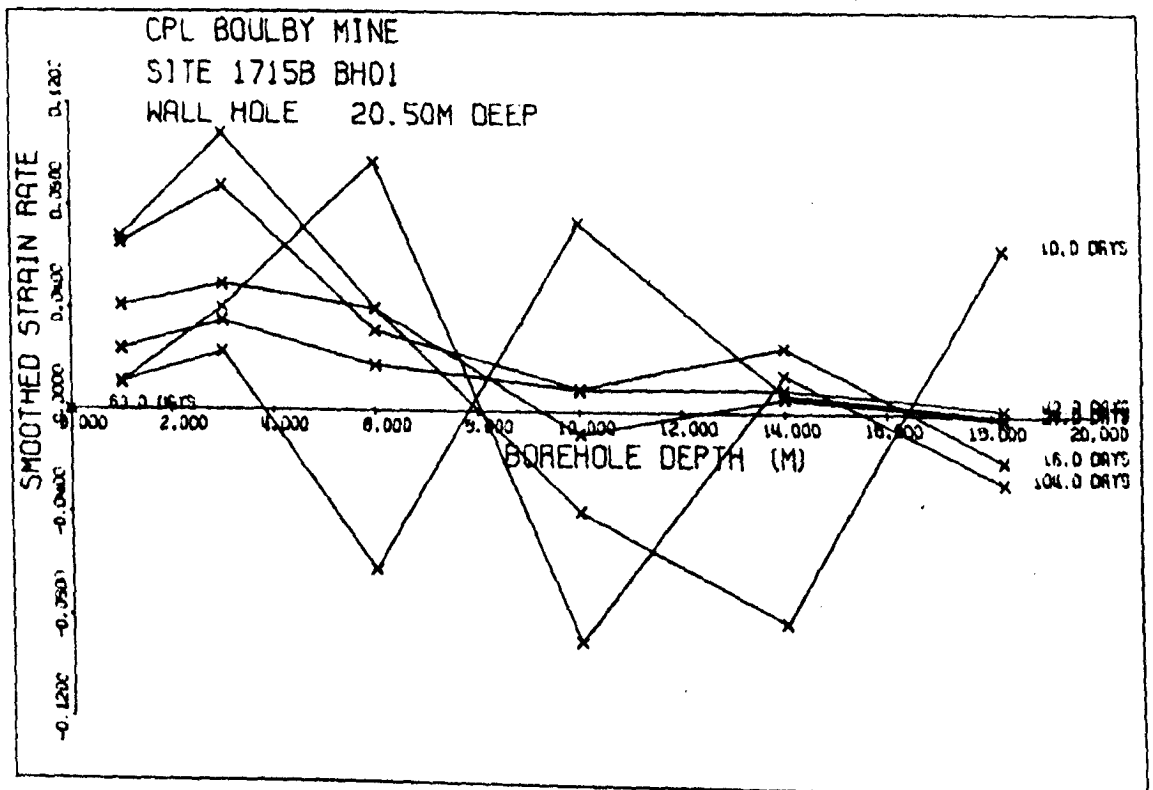
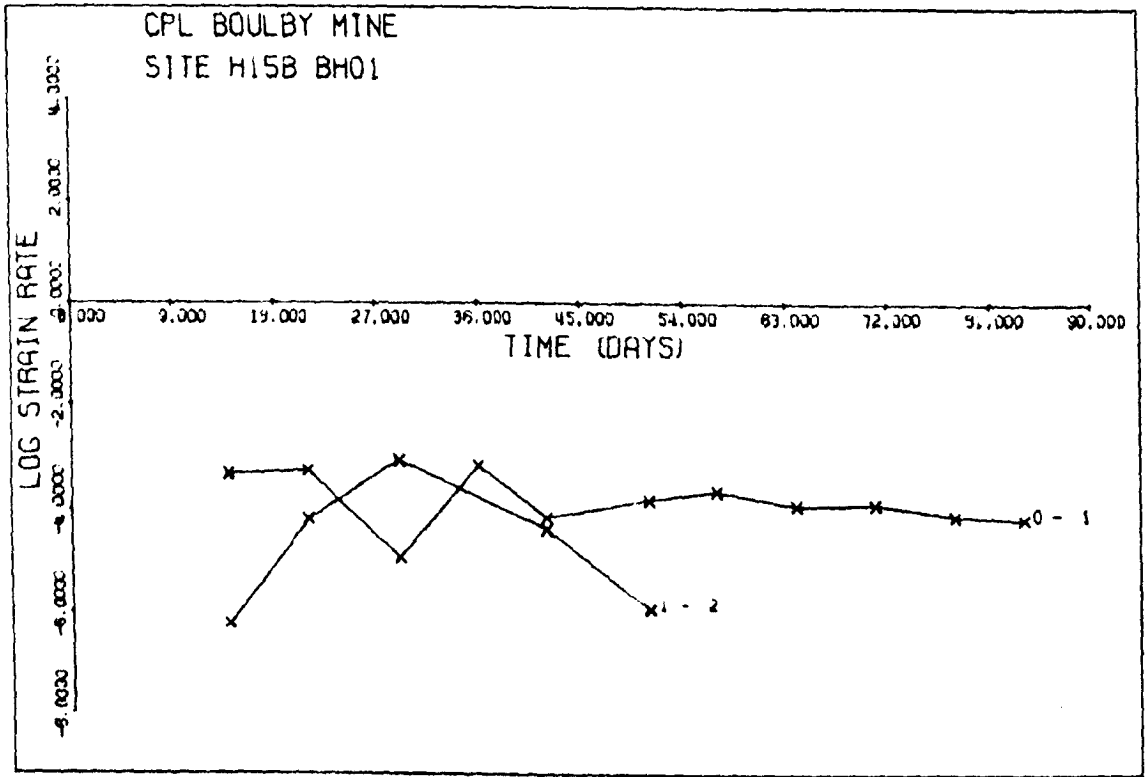


Figure 10.11 Site H 15 B Results (Contd.)

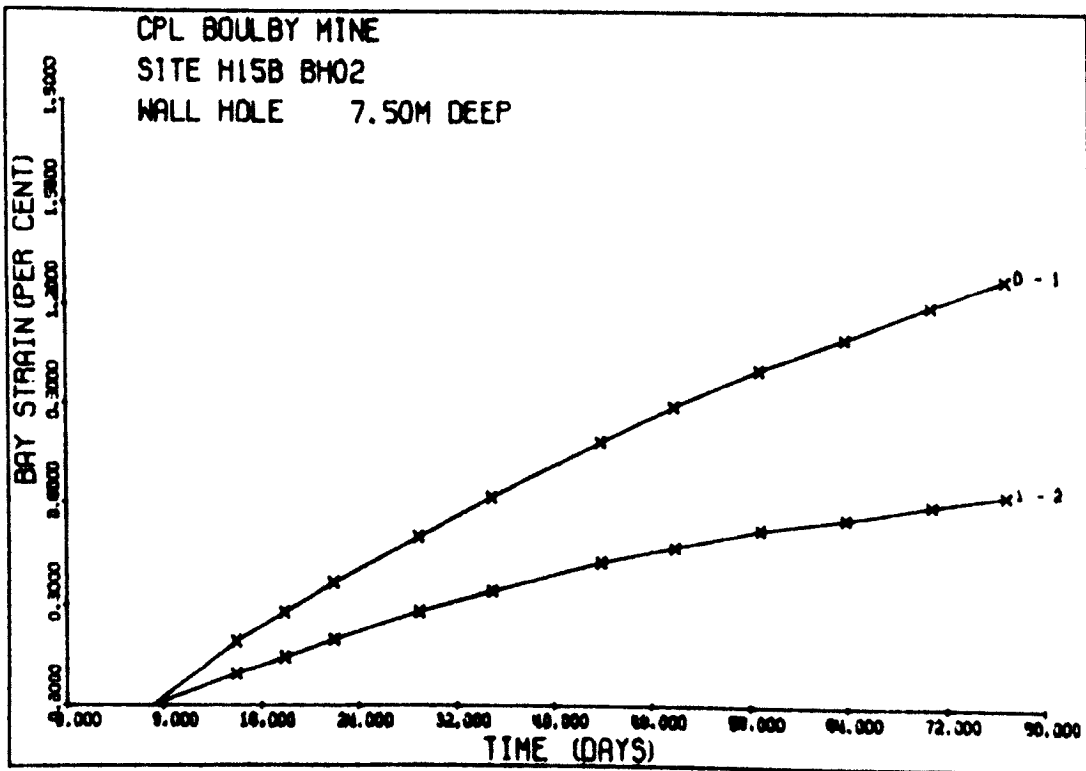
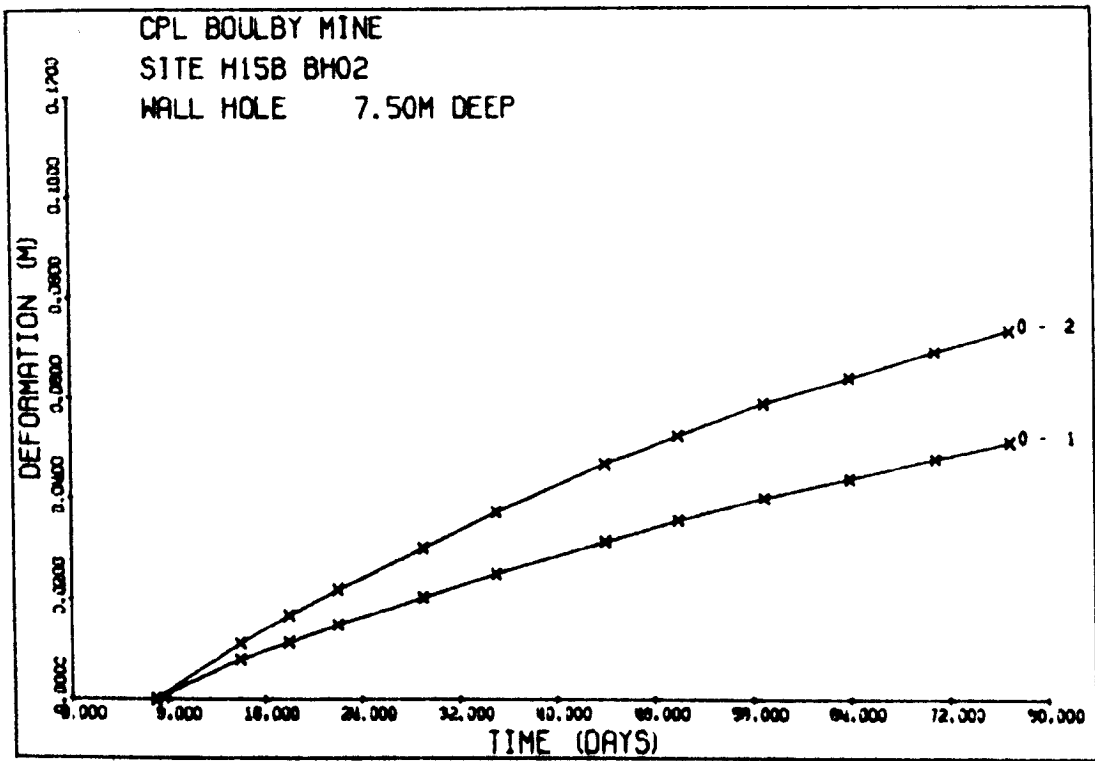


Figure 10.12 Site H 15 B, 45° hole, Extensometer Results

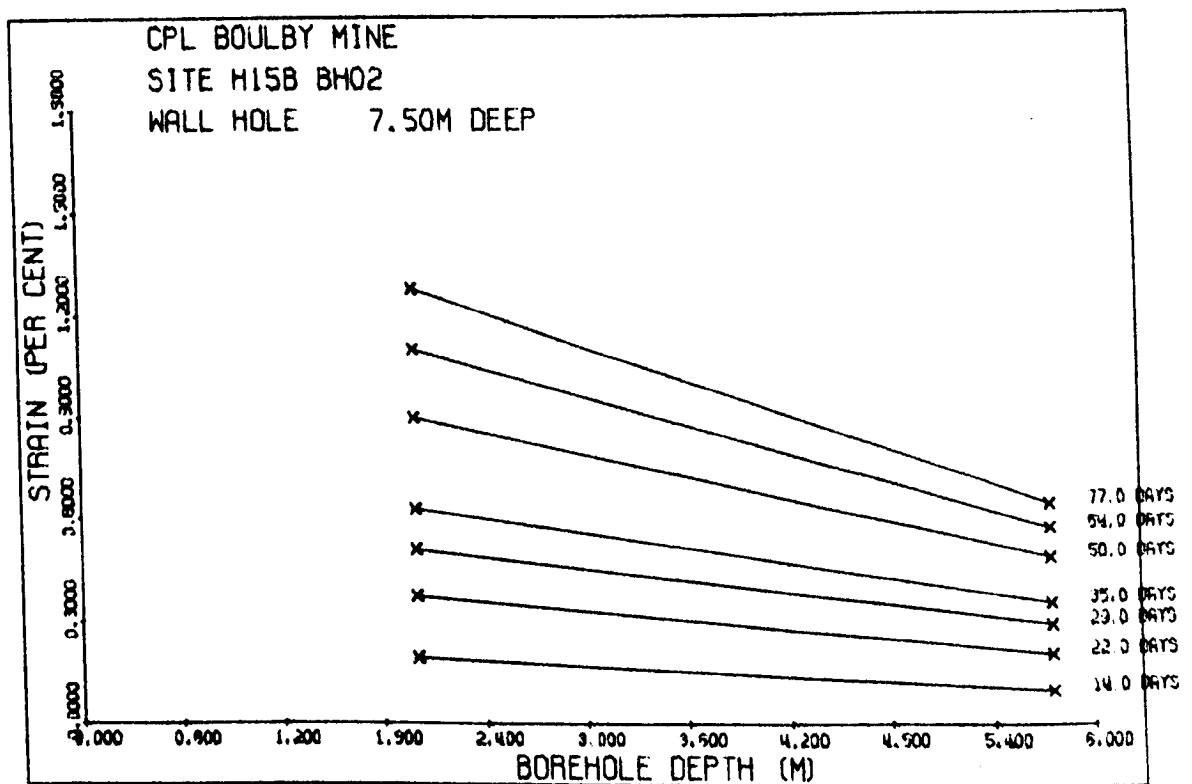
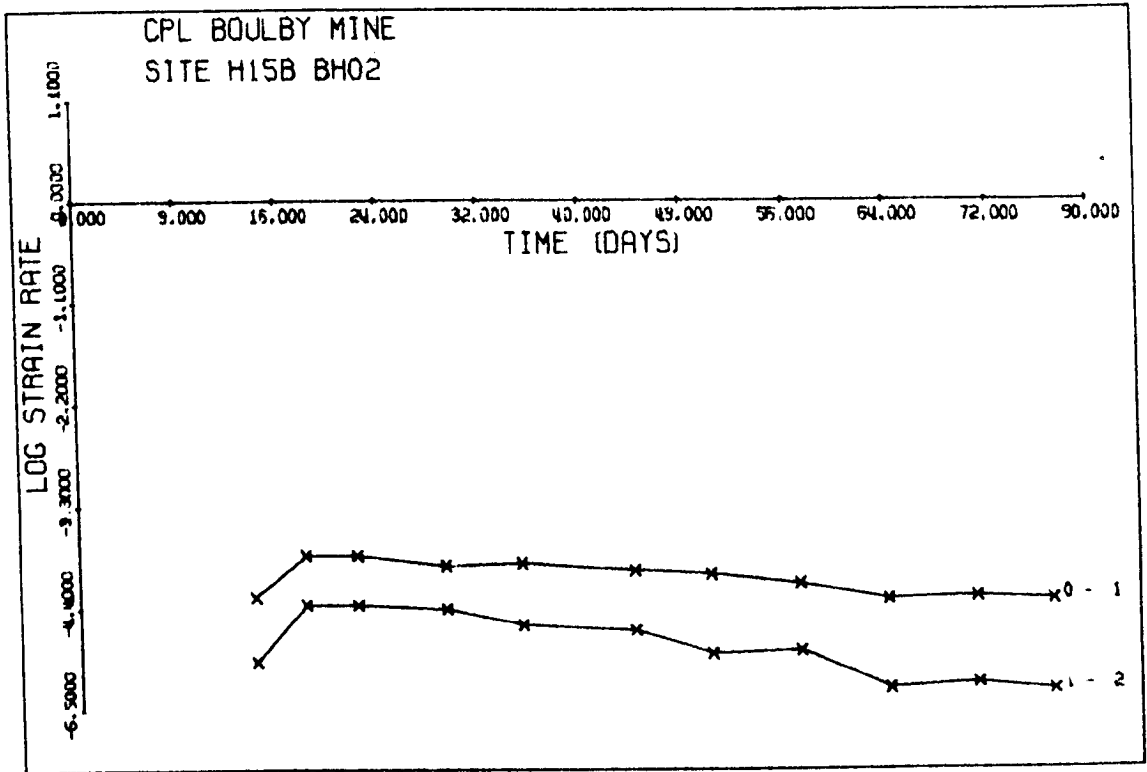


Figure 10.12 Site H 15 B 45° hole (Contd.)

From the graph of log strain rate it can be seen that the strain rates are decreasing up to 56 days after mining following which the rate of decrease slows down and the strain rate eventually increases. This effect also occurred in the pillar borehole O3, and the two are obviously connected.

10.4 Discussion of Pillar Extensometer Results

The results obtained from the pillar extensometers indicate general stability of the 40m central pillar with the development of a stable core. Strain rates are decreasing with the exception of the outer zone adjacent to the roadway. Because the anchors in H15B BH03 in this unstable zone are located at 2m and 11m, the increase in deformation that is occurring could well be taking place not much deeper than 2m. This is certainly the most likely explanation, based on results from other pillars. It also points to the importance of having extensometer anchors spaced evenly along the borehole length.

The 45° borehole, H15B BH 02 has a number of interesting features when compared with the others. The deformation along the length of the hole is much 'smoother', without kinks or bumps. There is not as great a difference between the anchor displacements as there is with the horizontal and vertical holes. This would indicate that there is no slabbing or incipient slabbing taking place at right angles to the line of the hole. The strain rates reflect the evenness of the deformation into the roadway.

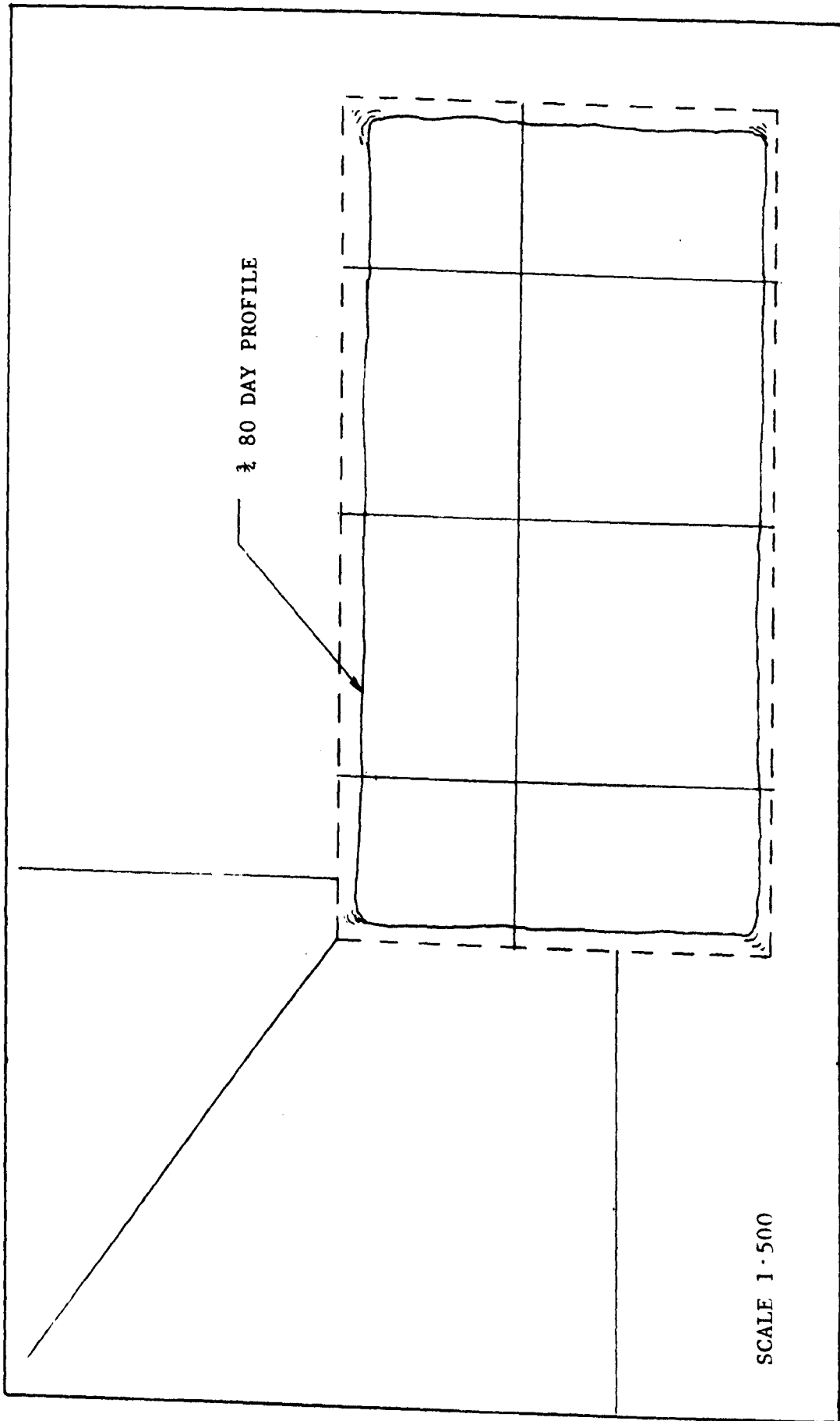


Figure 10.13 Deformation into the roadway at H 15 B

As BHO2 must be located in the zone of high deviator stress what it is exhibiting is almost certainly smooth plastic flow down towards the roadway. Because it does not have a free surface at right angles to it, the formation of failure surfaces is inhibited, thus promoting even further plastic deformation.

An attempt is made in Figure 10.13 to indicate the deformation into the roadway based on the borehole displacements.

10.5 Photography as a Monitoring Aid

Extensive use has been made of photography in this project both to record general conditions as well as to record special features. It says much for the skill of the professional photographer, who obtained his results almost exclusively with the lighting provided by cap lamps. Because of the limitations of space in this thesis the photographs have had to be reduced in size to get them in, and as such it is difficult to observe some of the finer details that are clearly visible in the larger prints. It is felt that there is much scope for the use of photographic techniques in 'photoprofiling', some examples of which are given in Plates 10.1 to 10.2.

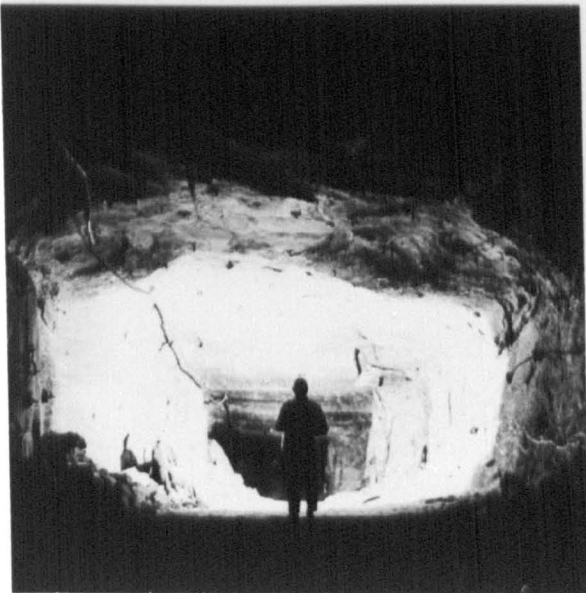
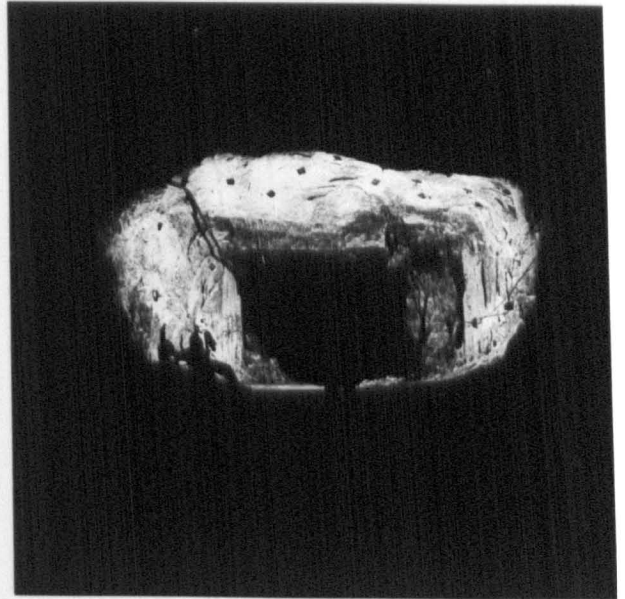
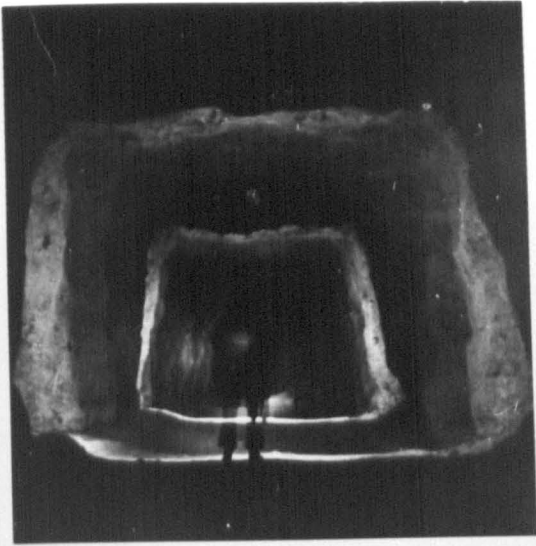
The saying that "one good picture is worth a thousand words" is no more true than when applied to the underground mining situation.

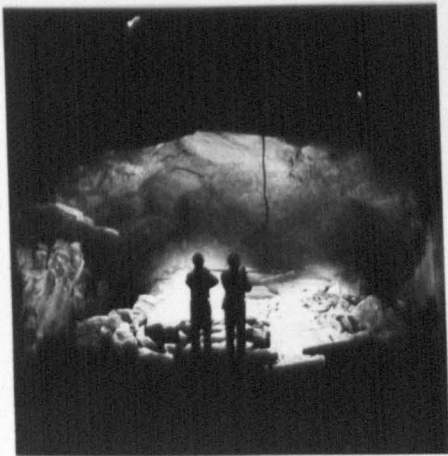
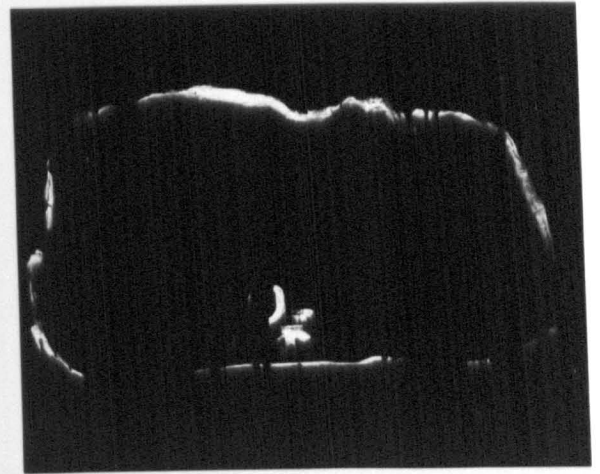
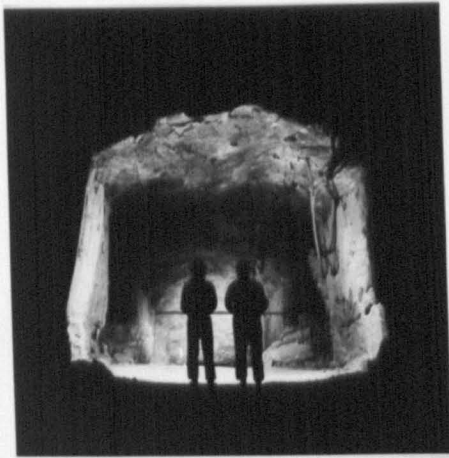
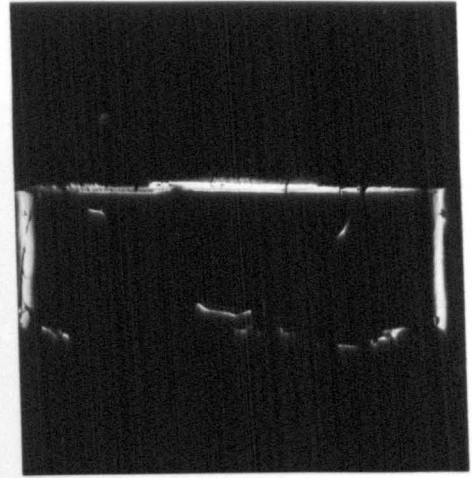
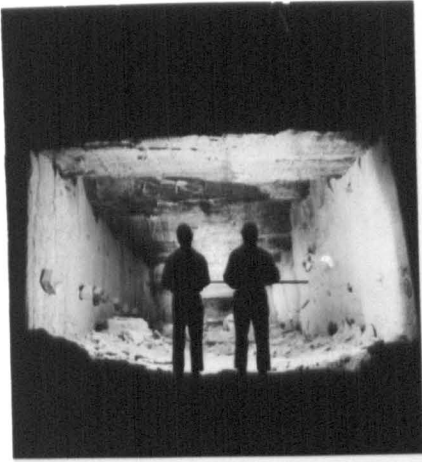
10.6 Finite Element Analysis

A finite element analysis was undertaken using a standard package called Annolin which dealt with the elastic solution only. It is

Plates 10.1 and 10.2

Photoprofiling





unfortunate that access to a programme was not available that could solve the time dependent deformation case. However, an attempt was made to simulate yield by altering the moduli of the rocks where creep was expected. The results are not felt to be particularly informative, but the graphical output does give a picture of the relative magnitude and location of stress concentrations. A split panel system was modelled with a 40m central pillar, but with three roadways instead of four, as this had been the mine's initial intention. Four runs were carried out with different moduli. The contour plots of runs 1 and 4 for vertical, horizontal and deviator stresses are given in Appendix 5. As the split panel system is symmetrical, only one half of the solution is shown.

Table 10.4

Rock strength parameters for finite element model								
	Run 1		Run 4		1st 4m		2nd 4m	
	E(GPa)		E(GPa)		E(GPa)		E(GPa)	
Potash	20.03	0.32	3	0.42	10	0.36	15	0.32
Shale raft	11.03	0.24						
Marl	8.0	0.24						
Anhydrite	25.99	0.20						
Halite	22.06	0.24						

Table 10.4 lists the rock strength parameters that were used in runs 1 and 4. Runs 2 and 3 used intermediate values, but are not included as they do not add materially to the discussion.

10.6.1 Results of Finite Element Analysis

Figures 10.14, 10.15 and 10.16 have been extracted from the contour plots in Appendix 5 and illustrate some of the major differences that occur between runs 1 and 4. They refer to the vertical, the horizontal and the deviator stresses respectively. These results are discussed below in terms of going from run 1 to run 4.

Vertical Stress, σ_v

The results in Figure 10.14 show that there is a reduction in the vertical stress above the panel, with an increase in the size of the distressed zone. Although expected, the effect is not as significant as anticipated. There is however, a very marked increase in the vertical stress on the central pillar and to a somewhat lesser extent on the ribside abutment.

Horizontal Stress, σ_H

There appears to be little change in the horizontal stress below the anhydrite. Above this level there is a very definite increase in the horizontal stress and stress concentration, which points to the protective influence that the Upper Anhydrite exerts on the strata below it. A reduction in σ_H takes place over the central pillar which is a result of the bending of the strata over the panel. The horizontal stress decreases fairly markedly over the roadways.

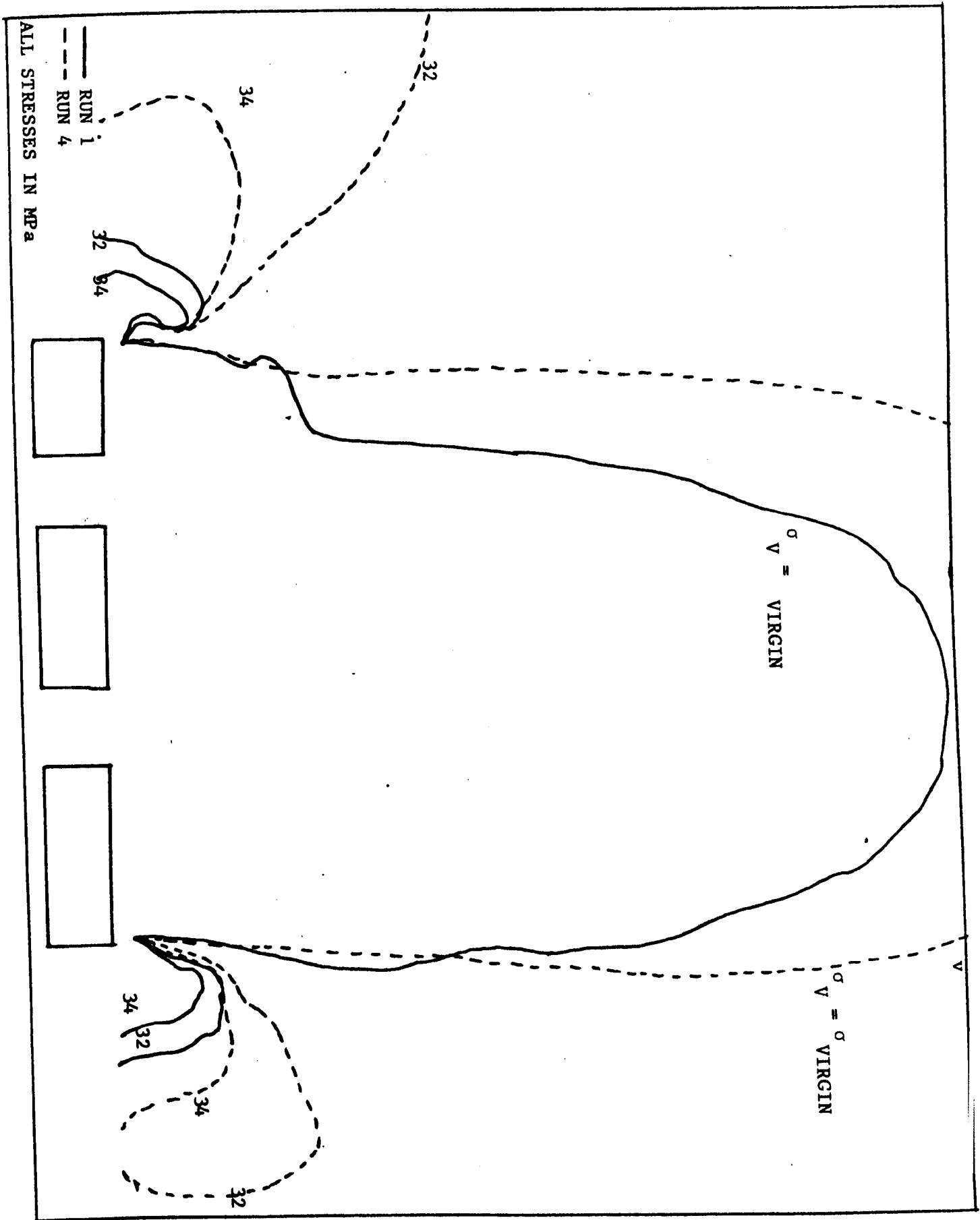


Figure 10.14 Change in Vertical Stress

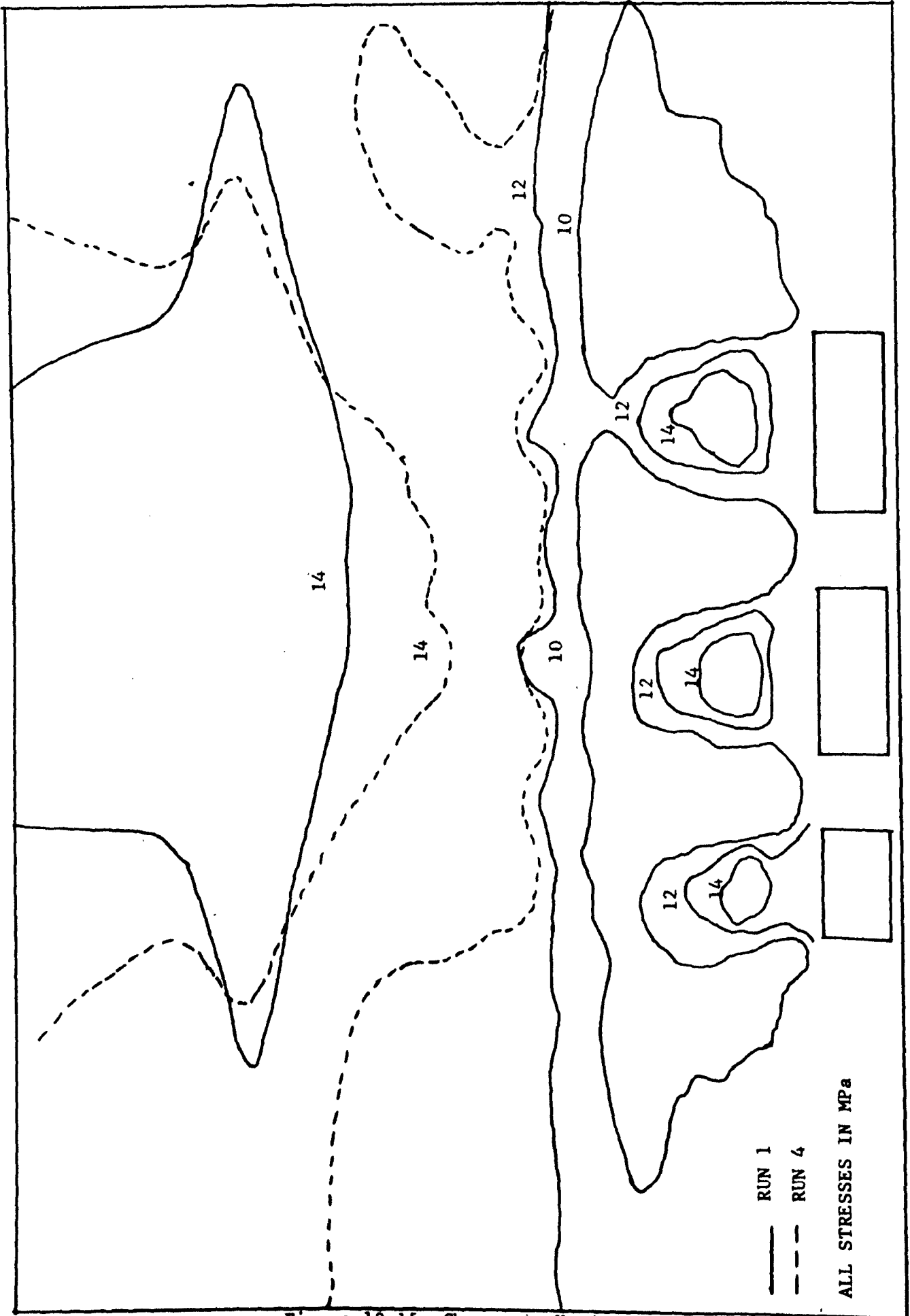


Figure 10.15 Change in Horizontal Stress

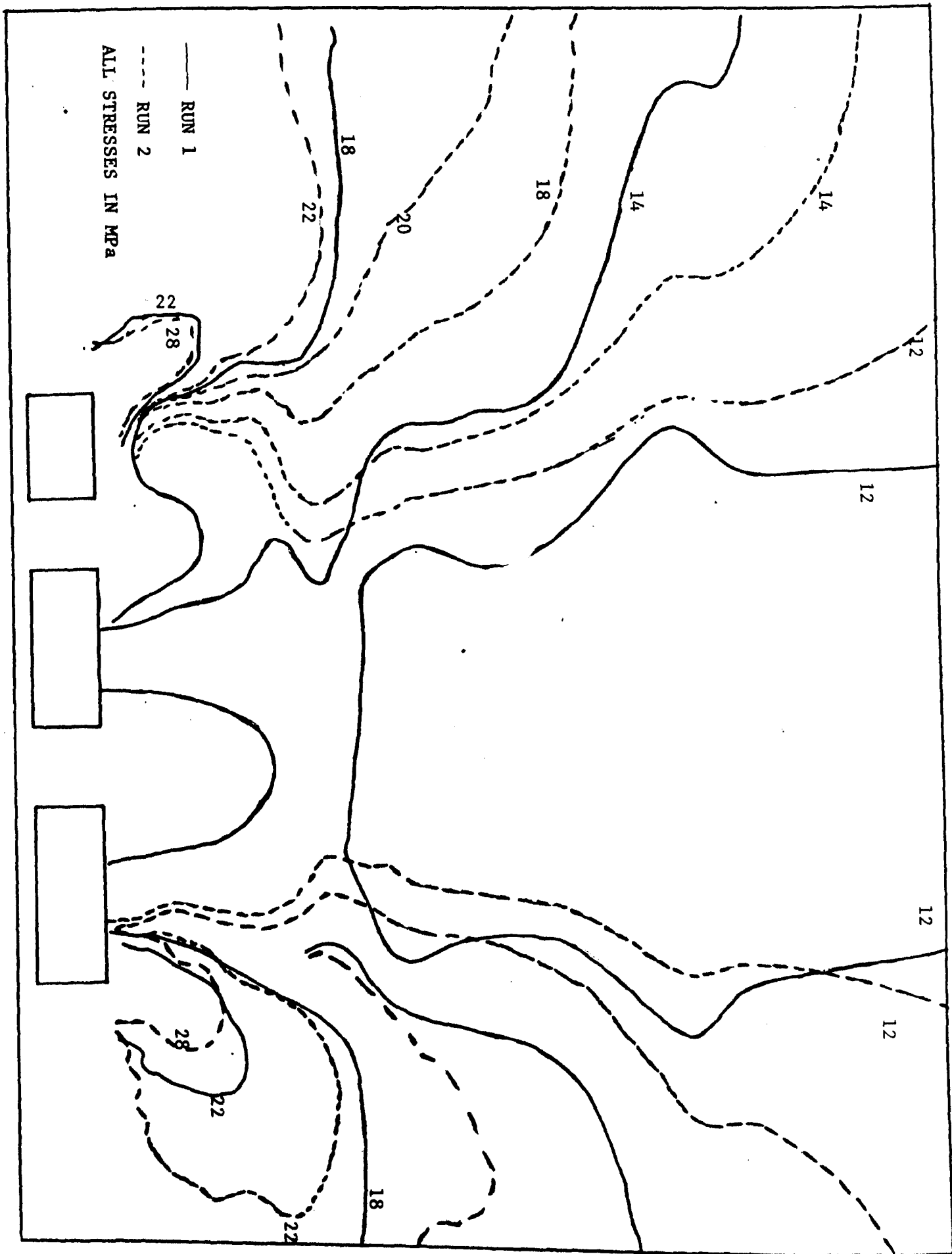


Figure 10.16 Change in Deviator Stress

Deviator Stress, σ_D

These results, Figure 10.16, are probably the most interesting, in that the deviator stresses are the driving force behind creep and time dependent effects.

There is a decrease in the deviator stress over the panel. This is most significant in that the original assymmetric distribution indicates that the roadway adjacent to the central pillar has a more diffuse pattern of deviator stresses in the first 15m of roof. These alter in run 4 and a more symmetrical pattern emerges over the top of the whole panel, but the stress concentration over the central pillar abutment increases.

This effect could help to explain why J roadway in No.19 Panel had much higher closure rates than the other roadways in the panel. The geometry, with No.10 Panel on the other side of the pillar between the two panels, is similar to that modelled.

The initial high deviator stresses in the roof lends weight to the argument of high initial closure rates being influenced by plastic flow arising as a result of these stresses. The picture presented after run 4 is one of the beam (or plate) sitting heavily on the abutments and protecting the zone immediately above the panel. There is a dramatic increase in σ_D over the pillar and solid ribside abutments shown in Figure 10.16.

The σ_D stress contours bulge inwards over the panel in the marl immediately below the anhydrite, suggesting high deviator stresses and thus creep or flow.

10.6.2 General Comments on Finite Element Analysis

The value of finite element analysis in this situation has been its ability to visually demonstrate the relative effect of changing certain parameters around the designed layout. Little reliance can be placed on absolute figures of deformation or stress, particularly when close to the excavation surfaces. Other situations, such as that of increasing the roadway W:H ratio, with and without fill of different characteristics, have been modelled, but because of time and space, are not reported here. They have all been extremely useful in helping to obtain a 'feel' for what is occurring in the rockmass.

The advent of the rheological finite element programme will assist in improving the predictive capability of this type of numerical modelling techniques, by introducing the effect of time on the distribution of stresses and deformations. However, the usefulness of the output from such a programme depends ultimately on how realistic the input is.

10.7 Stress Relief vs High Extraction

The title to this section is somewhat misleading as it implies that stress relief and high extraction mining are independent of one another. They are, in the sense that high extraction can be achieved without stress relief, but not vice-versa. Stress relief can be obtained, but only when enough time has elapsed to allow sufficient plastic deformation of the marl so that the anhydrite and the halite can bridge and protect the panel excavation below.

There is no doubt that this is what is occurring in the old No.7 Panel area where new roadways have mined through pillars that have been standing for periods in excess of 400 days. Plates 10.3 and 3.1 , show conditions in both the old and the new roads in the area.

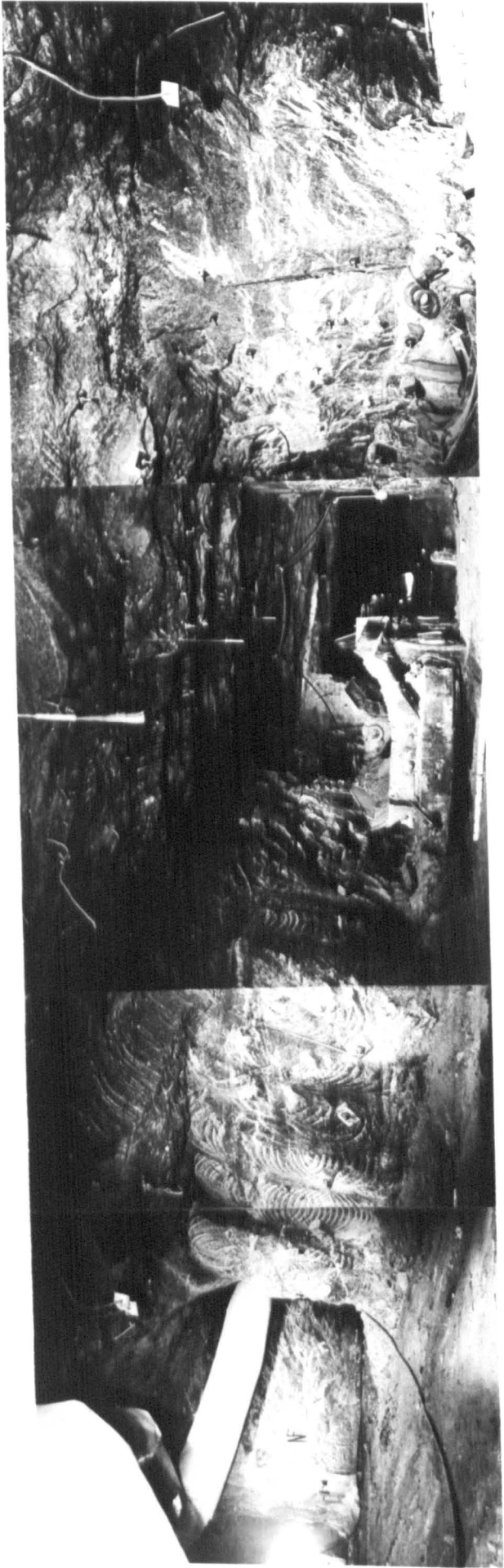
It is therefore advocated that old square pillar areas be re-opened and roadways driven to split the existing pillars, thus creating high extraction conditions. However, it is essential that on either side of the new panels thus formed, areas of low extraction should be left intact in order to stabilise the roof strata.

10.8 Conclusions and Recommendations for mining

- 1 High extraction areas should not exceed 40m in width and should conform to the general pattern of the split panel section of No.15 Panel, where each sub-panel should be limited to a width of 40m.
- 2 The mined height within the high extraction roadways can take the full potash thickness except in the conveyor road where it should remain 3.5m. This will assist in stabilising the conveyor road by deflecting the horizontal stresses further into the solid.
- 3 In order to preserve the overall 35% extraction and to stabilise the high extraction panels, barrier pillars at least 100m wide, should be left between the panels.

Plate 10.3

No.7 Panel - Panoramic view of new high extraction section
created by mining through old pillars.



- 4 At the average closure rates obtained so far in 'stable' high extraction panels, the roadway cross section area can be expected to decrease by 20% in just over a year. The useful life of these roads can thus be 18 months at most. Widening the conveyor road improves this situation, but only marginally. Long life access roads must therefore be driven in salt.
- 5 Mining in or adjacent to geologically disturbed zones such as the salt overfolds should be avoided at all costs. Main production panels should be a minimum of 150m away from these features.

10.9 Recommendations for Rock Mechanics Investigations and Monitoring.

- 1 Closure measurements should be made in all production panels with sites located down and across the panels at frequent intervals. Sites along roadways should be spaced no further than 15m apart, with the lines of sites across being every 40m or so. Only one roadway along the panel need be instrumented.
- 2 It is vital that the closure measurements begin as close to the date of mining as possible. The technique outlined in Chapter 6 can be used to obtain predictive information as well as providing a means for projecting closure curves backwards for deriving total closure.
- 3 Every effort should be made to drill up to the base of the Upper Anhydrite across the width of a panel and in over the

ribsides to discover how and by how much this layer is deforming. Extensometers should be installed in these holes to monitor the deformation of the intervening strata.

Knowledge obtained about the thickness of the Carnalite Marl by these holes will be extremely useful.

- 4 Three-dimensional rheological finite element programmes should be developed to suit the Boulby requirement.

10.10 Concluding Remarks

This thesis has postulated a mechanism for the behaviour of high extraction panels that is felt to be valid, but with the aid of more and better measurements and computer models this behavioural mechanism should be modified and updated. This will lead to a deeper understanding of how the rock behaves as it does and so assist the mine to prevent rather than cure some of the problems it encounters all too frequently.

8. WIGGETT, C.H.
1976
Rock Mechanics investigation associated with roof support and rock properties at Boulby Mine. M.Sc. Thesis University of Newcastle upon Tyne.
9. HEBBLETHWAITE, R.P.B.,
WOODS, P.J.E.
1977
Gas Blow Project Report. Internal Confidential Report, Cleveland Potash Limited.
10. CLEASBY, J.V., PEARSE,
G.E., GRIVES, M.,
THORBURN, G.
1975
Shaft Sinking at Boulby Mine, Cleveland Potash Ltd., Trans. Institn. of Mining and Metallurgy, A7, 1975.
11. BUZDAR, S.A.R.K.
1967
A laboratory investigation into the mechanical properties of some sedimentary rocks with special reference to potash. Ph.D. Thesis, Univ. of Newcastle upon Tyne.
12. COOK, R.F.
1974
Rock mechanics investigations associated with shaft excavations in a deep evaporite deposit. Ph.D. Thesis, University of Newcastle upon Tyne.
13. PEARSE, G.E.,
1975
The selection of mining equipment and the initial operations at Boulby Potash Mine, Cleveland Potash Ltd., The Mining Engineer, V 134. Aug/Sept. 1974.

14. WISE, N., MILLER, H.D.S. Underground instrumentation in the
1978 Experimental Panel (COO56W) at Boulby
Mine. A report to Cleveland Potash
Limited.

15. SERATA, S. Stress Control Technique - An alter-
1976 native to roof bolting. Mining Engrng.
Vol. 28, May.

16. UHLENBECKER, F. Gebirgsmechanische Untersuchungen
auf dem Kaliwerk Hattorf (Werra-Revier)
Kali und Strensalsz, Heft 10/1971 S.
345/359.

17. WISE, N., MILLER, H.D.S., Analysis of measured surface subsid-
POTTS, E.L.J. ence at Boulby Mine. Confidential
1979 report No. 61 - 0779 to Cleveland
Potash Ltd.,

18. SERATA, S. Instrumentation for stress control
1978 design of deep mine entries. 19th
U.S. Rock Mechanics Symposium - Reno,
Nevada.

19. SERATA, S. Continuum theory and model of rock
1966 salt structures. 2nd Symp. on Salt,
Northern Ohio Geological Soc.

20. SERATA, S. The Serata stress control method
1972 of stabilising underground openings.
7th Canadian Rock Mech. Symp., Edmonton.

21. BAAR, C.A.
1977
Applied Salt-Rock Mechanics 1.
Elsevier Scientific Publishing Co.,
Amsterdam.
22. BAAR, C.A.
1975
The deformational behaviour of salt
rocks in-situ: Hypotheses vs. measure-
ments. Bulletin, Int. Assn. of
Engineering Geology. No. 12 p65-72.
23. MRAZ, D.Z.
1972
The theory of flow and its practical
application for pillar design in deep
potash mines. Western Miner.
24. MRAZ, D.Z.
1973
Behaviour of rooms and pillars in
deep potash mines, CIM Trans. Vol.
LXXVI, pp. 138-145.
25. MRAZ, D.Z.
1978
Theoretical predictions confirmed by
in-situ rock behaviour in a deep
potash mine. Proc. 19th U.S. Rock
Mechs. Symp., Reno, Nevada.
26. POTTS, E.L.J.,
HEBBLEWHITE, B.K.
1977
A report on a visit to Potash mines
in Saskatchewan, Canada. Confidential
Report to Cleveland Potash Ltd.
27. MILLER, H.D.S.
1979
Report on a visit to some Canadian
Potash mines. Confidential Report to
Boulby Mine Ltd.

36. HORSEMAN, S.T.
1979
An evaluation of the rheological properties of rock salt for deep storage cavity design. Ph.D. Thesis, University of Newcastle upon Tyne.
37. BUZDAR, S.A.R.K.
1968
A laboratory investigation into the mechanical properties of some sedimentary rocks with special reference to potash. Ph.D. Thesis, Univ. of Newcastle upon Tyne.
38. PEGGS, R.D.
1972
Model roadway studies for the Boulby Mine. Confidential report to Cleveland Potash Ltd.
39. HEBBLEWHITE, B.K.,
MILLER, H.D.S., POTTS,
E.L.J.
1977
A method for predicting time dependent deformations in evaporites around a vertical shaft. Brit. Geotech. Soc. Conf. on Rock Engineering. Newcastle upon Tyne.
40. TIMOSHENKO, S.P.,
WOINOWSKY-KRIEGER, S.
1959
Theory of Plates and Shells. 2nd Ed. McGraw-Hill & Kogakusha. Book Co. Inc., New York & Toronto.

APPENDIX 1

MINING LAYOUTS

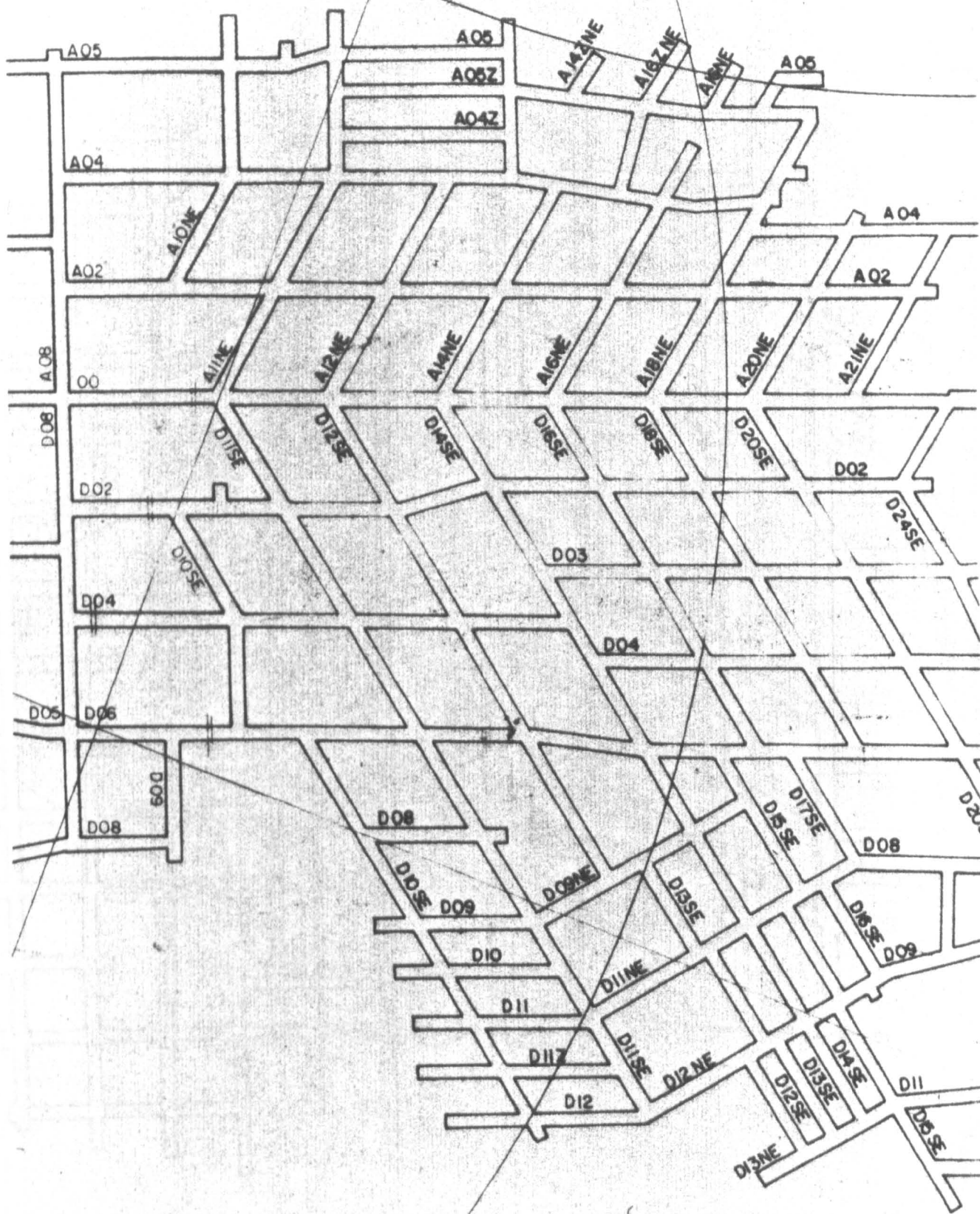


FIGURE 1

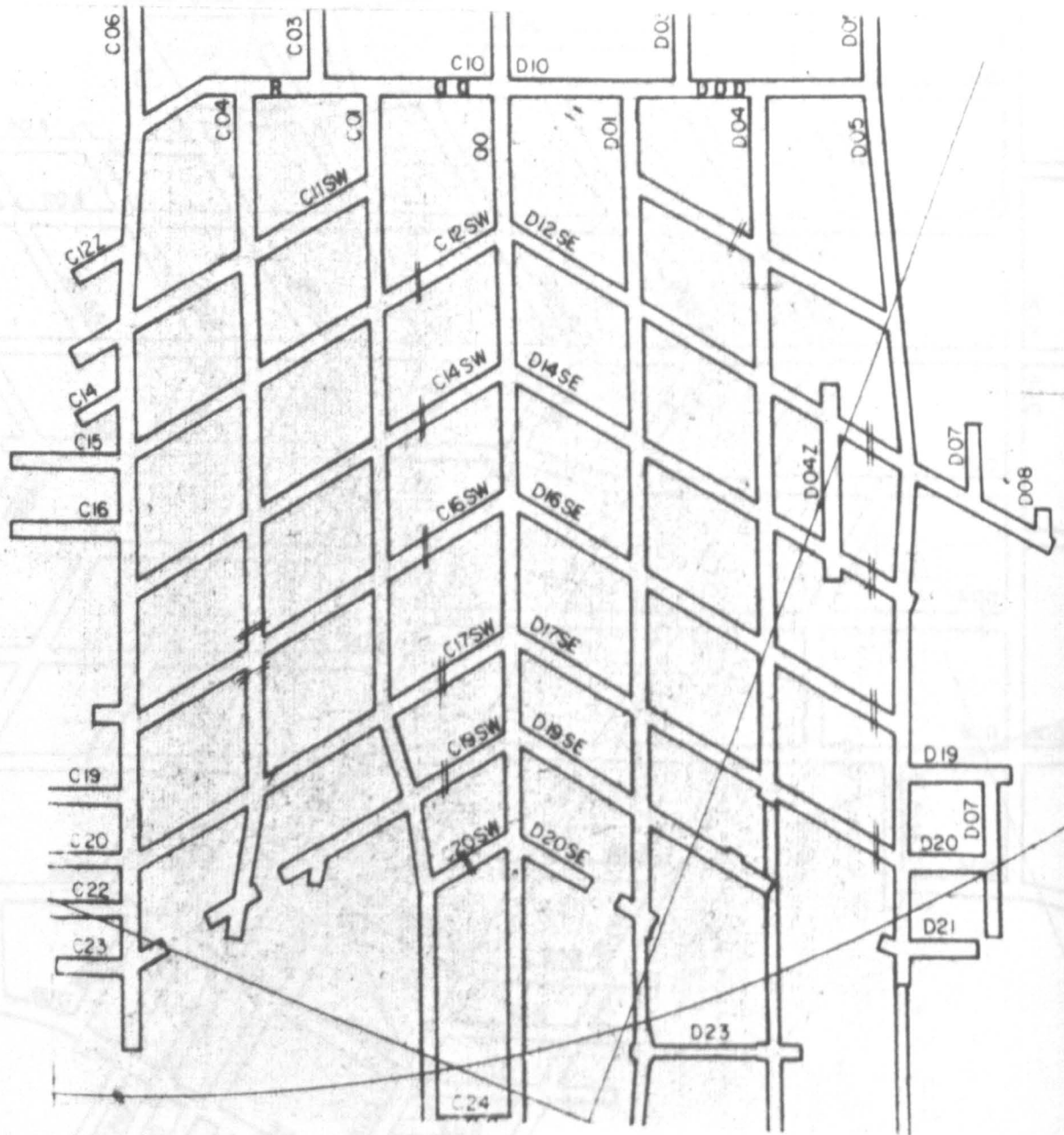


FIGURE 2

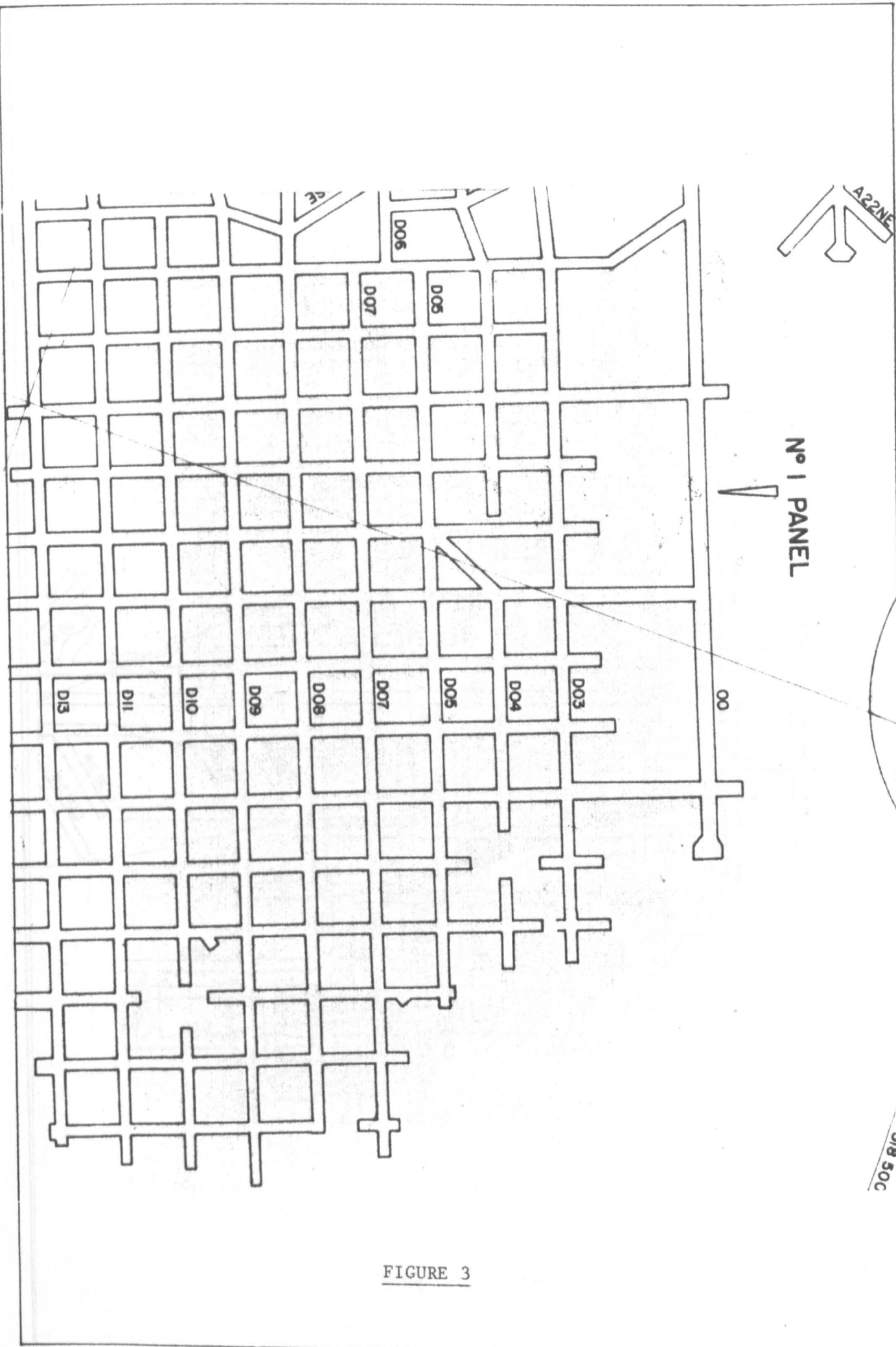


FIGURE 3

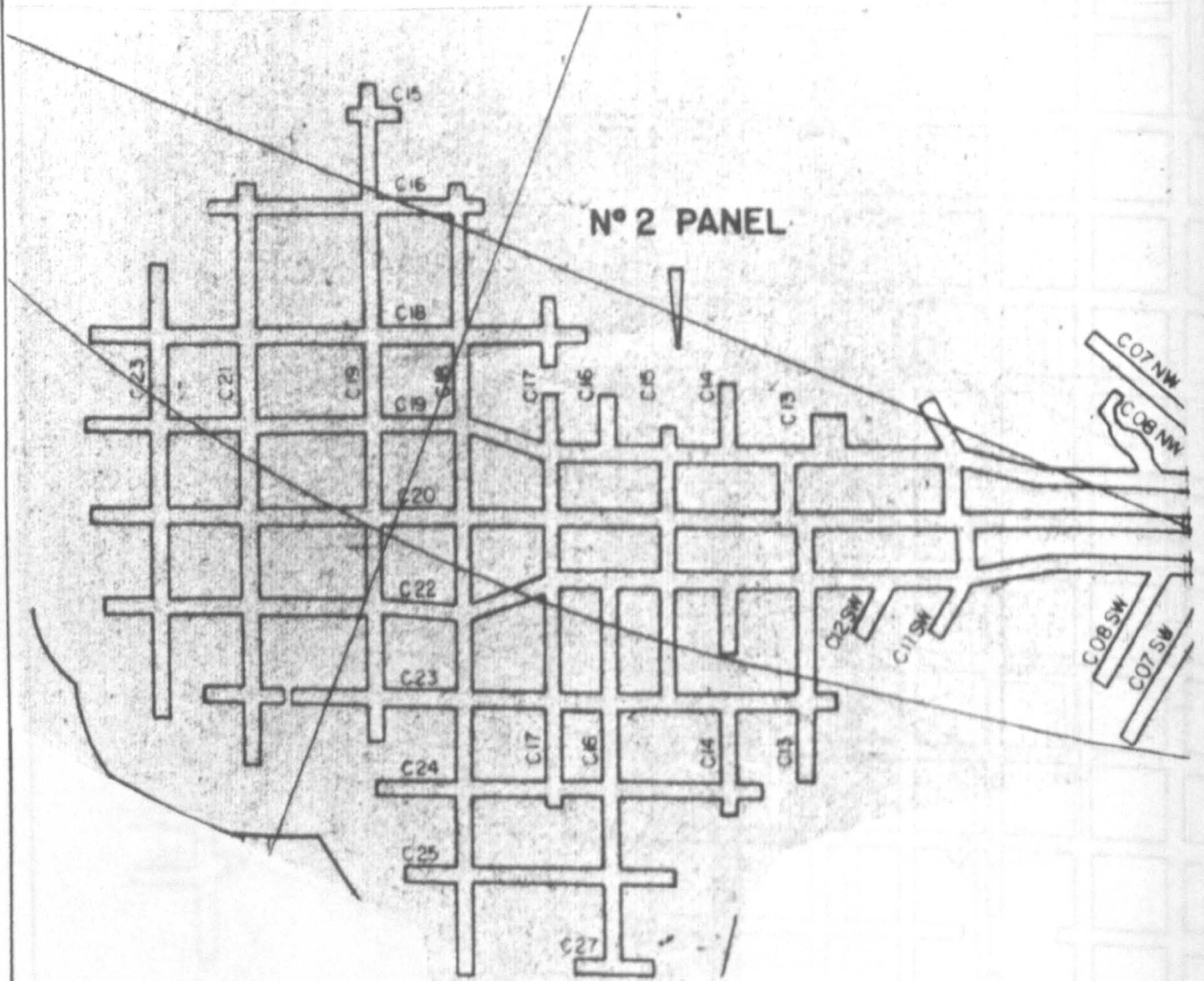


FIGURE 4

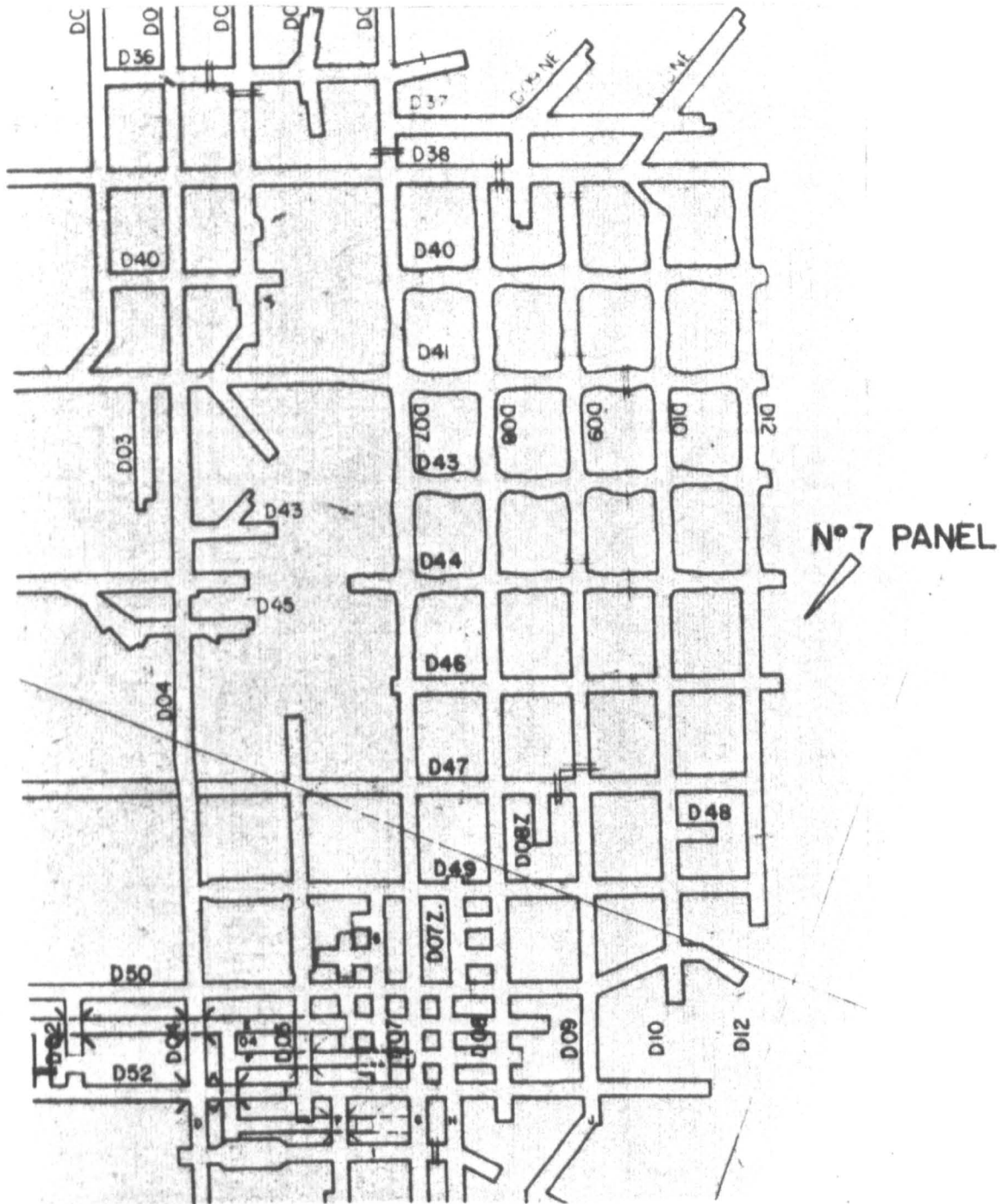


FIGURE 5

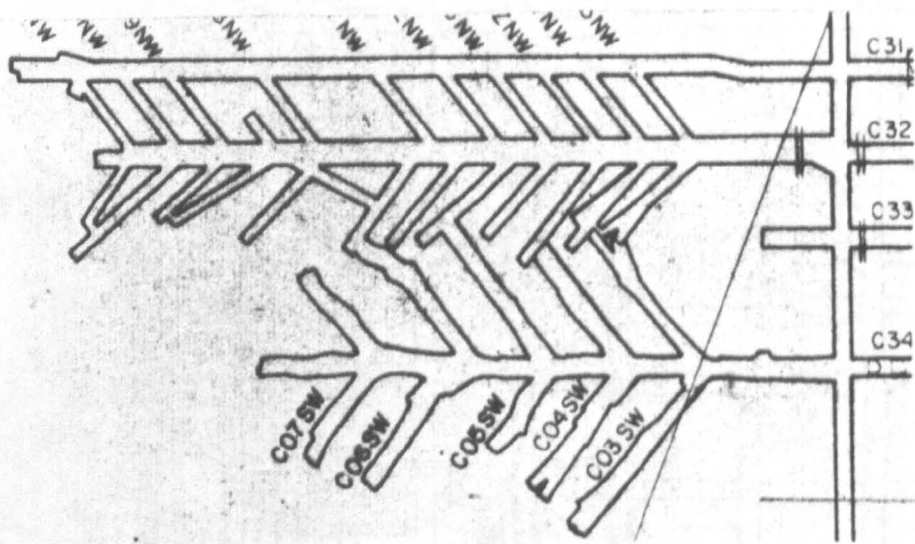


FIGURE 6

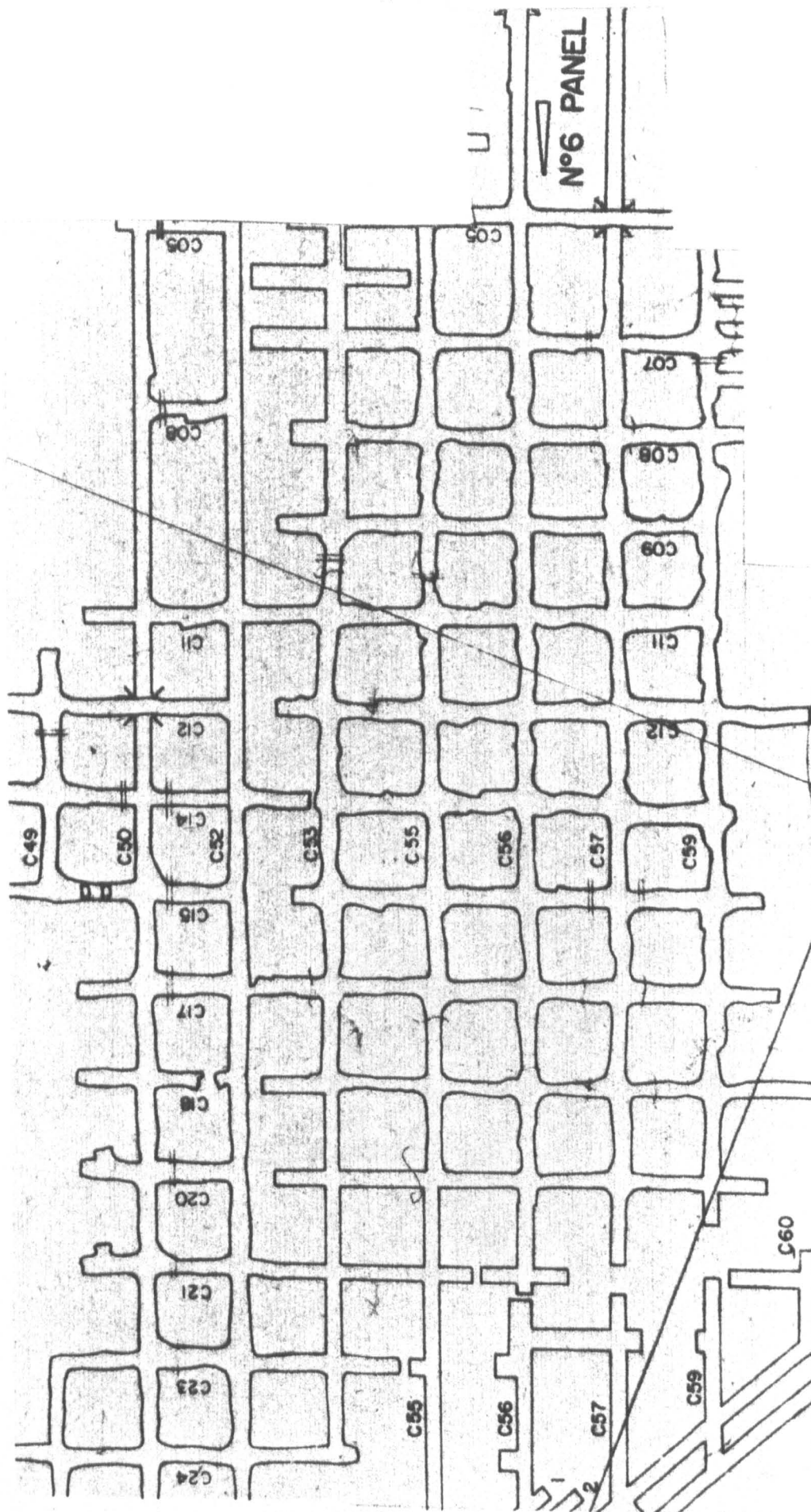


FIGURE 7

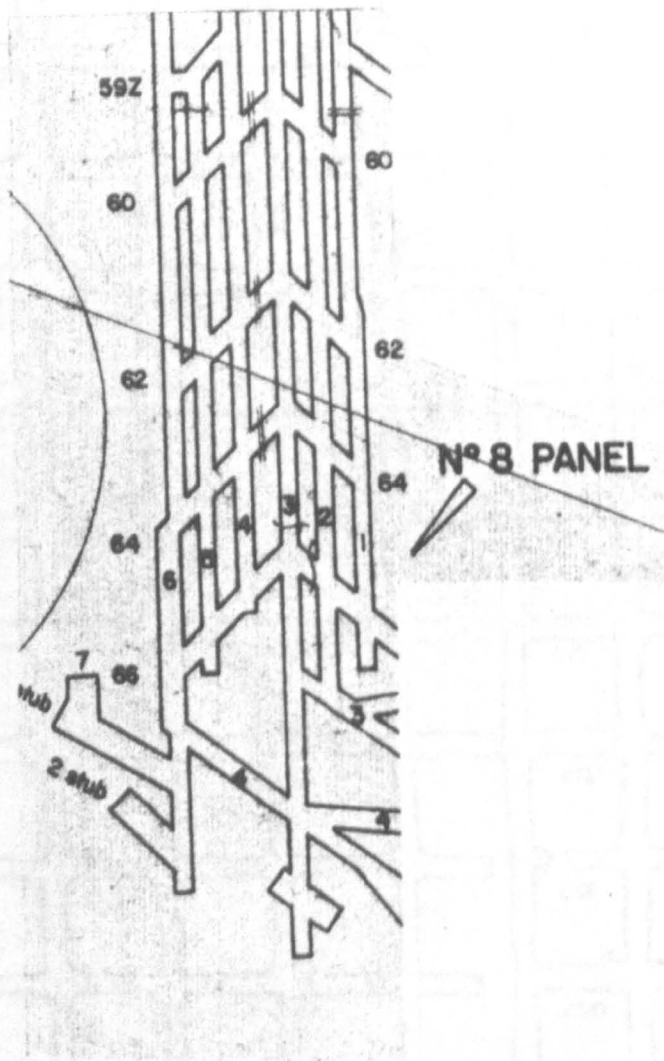


FIGURE 8

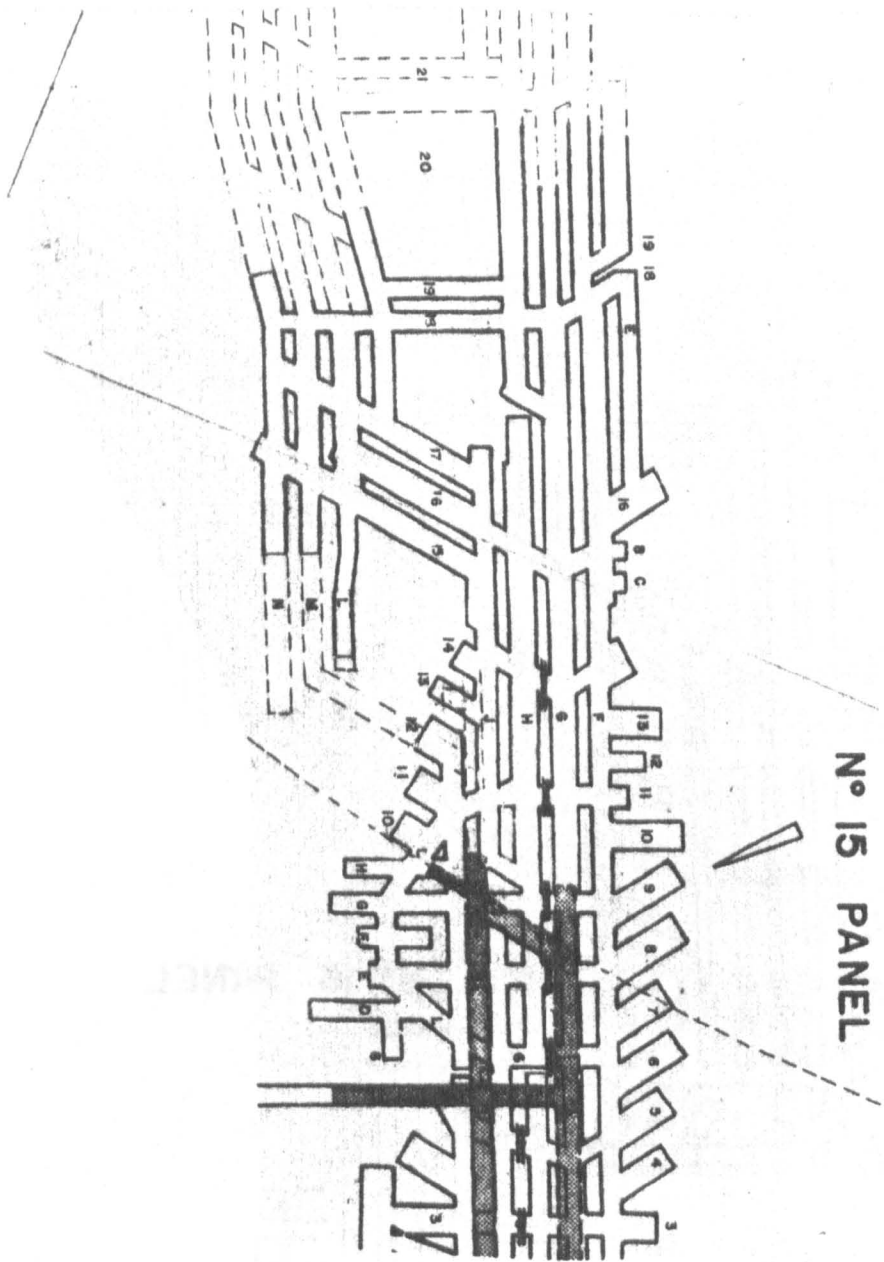
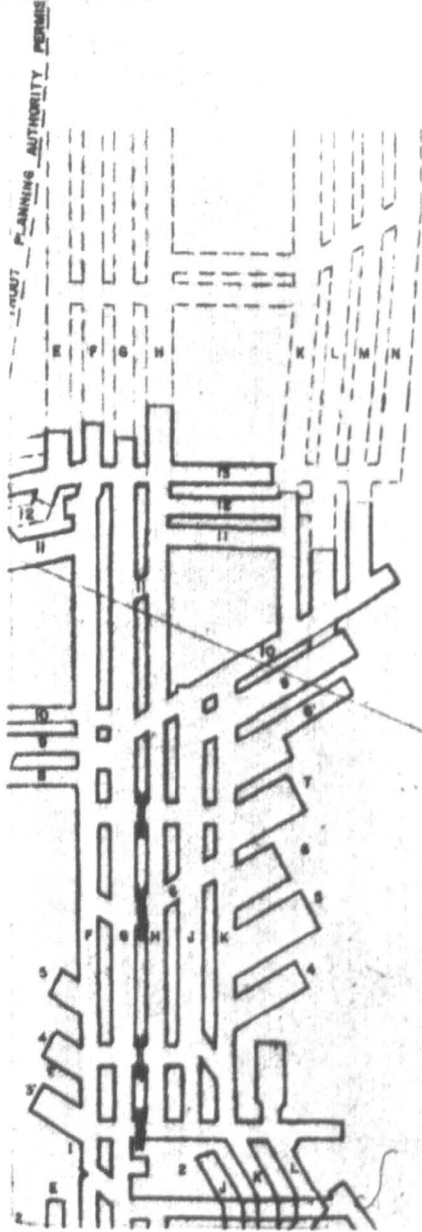


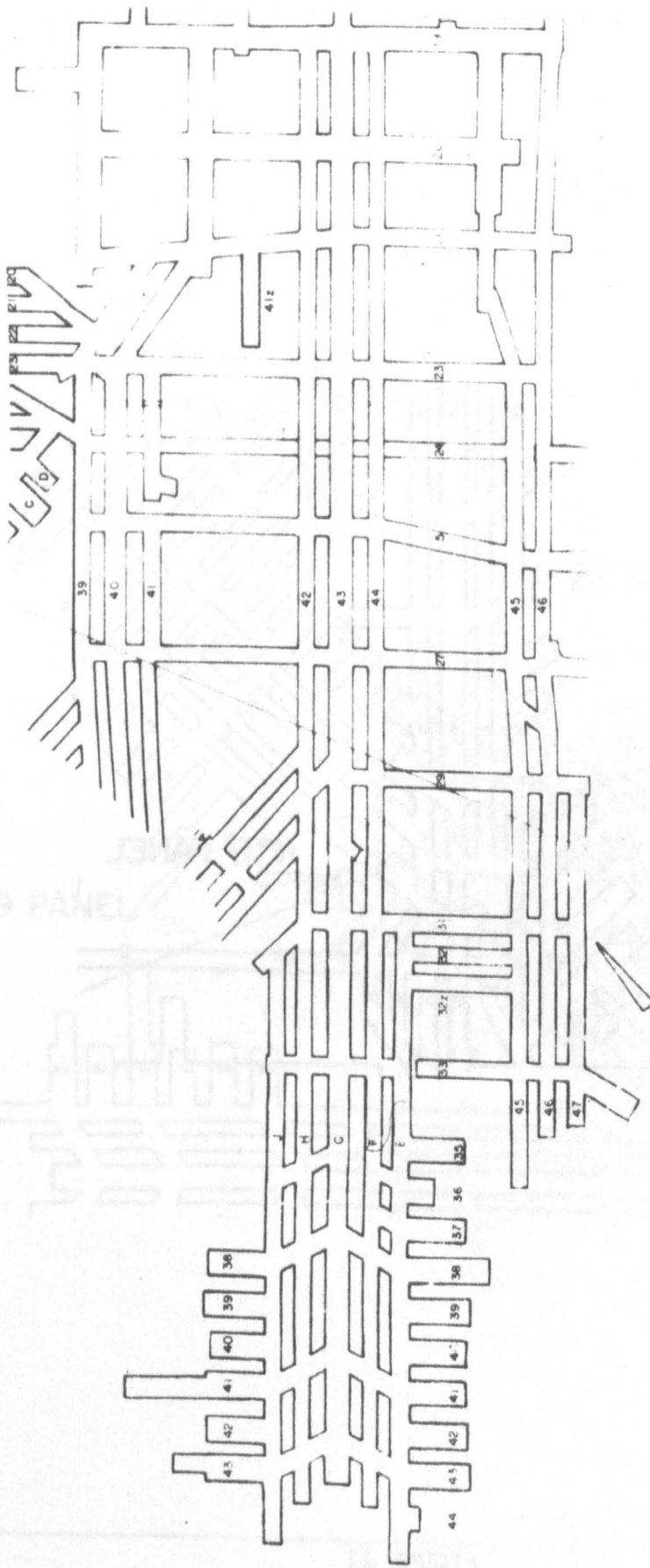
FIGURE 9(a)



N° 16 PANEL



FIGURE 9(b)



N° 10 PANEL

FIGURE 10

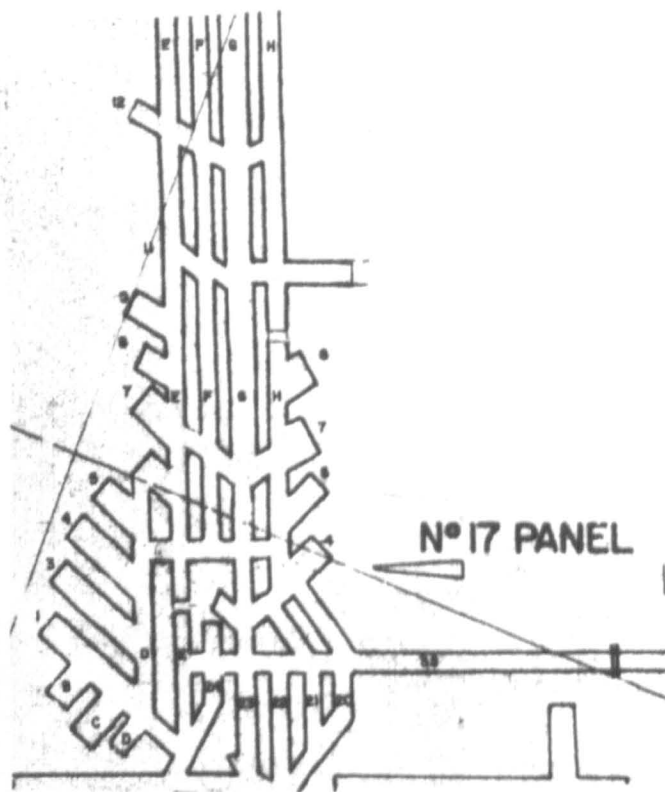


FIGURE 11

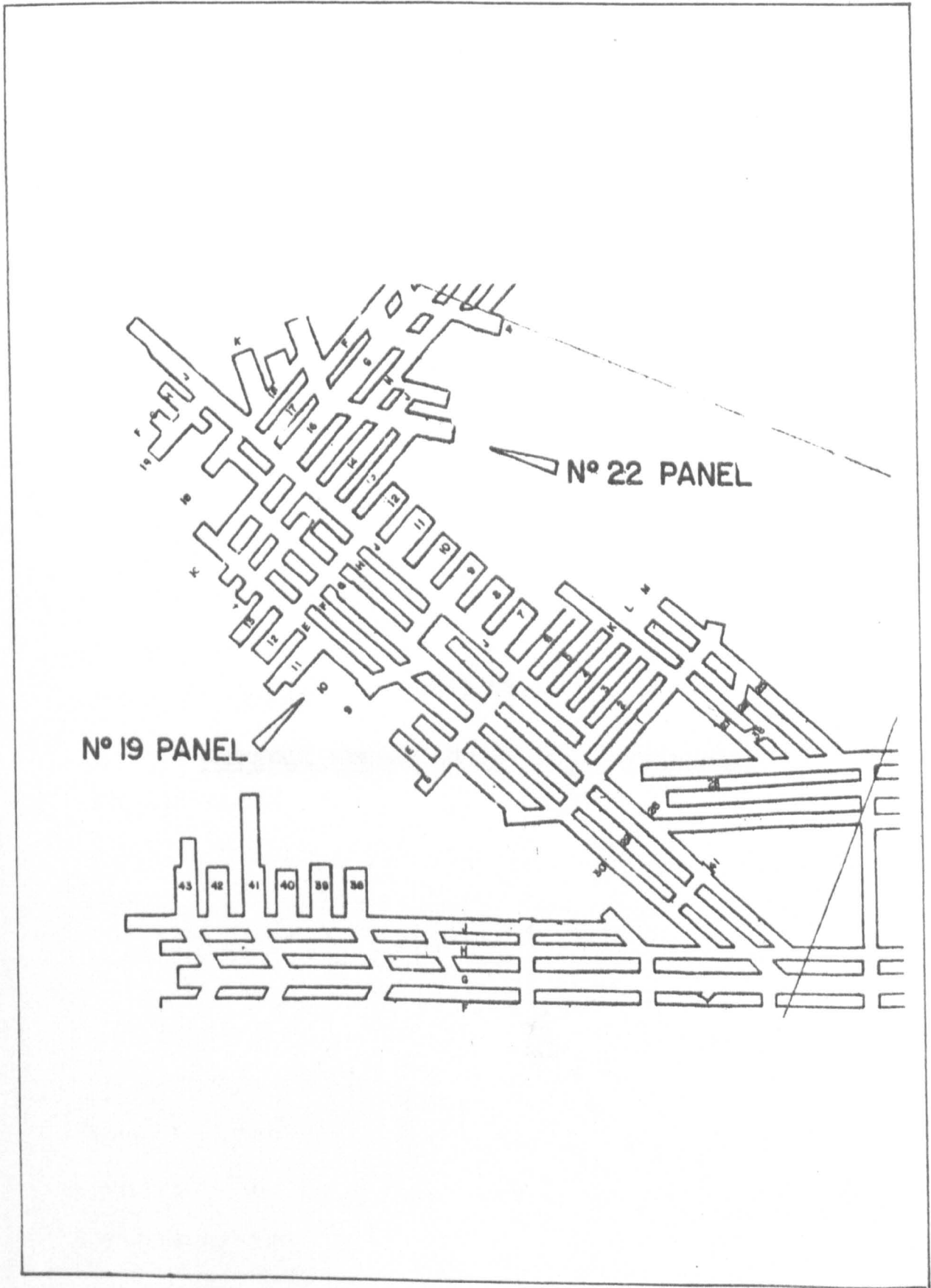


Figure 12 No.19 Panel

APPENDIX 2

GAMMATROL PORTABLE POTASH ASSAYING EQUIPMENT

Description

The equipment consists of two units, a Detector Probe (type PRI 44) and a Control/Indicator Unit (type PRI 43), the two being interconnected by a 3 core cable whose length is selected according to the particular measuring requirements.

The probe houses a radiation detector which is capable of detecting the very small amount of natural gamma radiation emitted by potassium, the intensity of the radiation detected being a function of the amount of potassium within a radius of approximately 0.3m of the probe.

The signal from the radiation detector in the form of voltage pulses is transmitted via the cable to the Indicator Unit where the pulses are counted over a selected period of time (normally 80 or 800 seconds, the longer measuring time being provided for calibration purposes and for greater measuring accuracy if required). The pulse count is displayed on a 4 decade LED (light emitting diode) digital display, the displayed count being a function of the potash concentration in the ore surrounding the probe.

The equipment is self powered from rechargeable batteries contained within the Indicator Unit, battery life being in excess of 5 hours for continuous operation and normally in excess of 10 hours if the digital display is switched on for reading only at the end of each measuring period.

Battery test facilities are provided, discharged batteries being readily recharged by an external charging unit connected via the same socket on the Indicator Unit used for the Probe cable connector. 14 hours charge time will give full recharge of fully discharged batteries.

Operation

In use the Indicator Unit may be held by means of the shoulder/ halter strap provided or left free standing, and the Probe inserted into the test hole at the location where the measurements are required. The Probe is designed for connection to standard extension rods, making it suitable for use in test holes at any angle (35mm diameter, or greater). To obtain an accurate scan the probe is stopped at selected intervals along the length of the test hole and a measure of counts made for each position.

APPENDIX 3

SUMMARY OF RESULTS OF LABORATORY TESTING OF POTASH AND NEAR-SEAM

ROCKS, BOULBY MINE

CLEVELAND POTASH
PROJECT

Summary of Results from
Laboratory Testing Carried out by

- i S. J. Patchet
- ii R. F. Cook
- iii C. H. Wiggett
- iv S. Vutukuri
- v B. K. Hebblewhite
- vi N. Wise

Prepared by

N. Wise
B. K. Hebblewhite

March, 1977

PATCHET

TENSILE STRENGTH

(i) Upper Strata Rock

Material	No. of Tests	Mean Tensile Strength (KN/m ²)	Range (KN/m ²)
Lower Lias I	5	3495.8	2178.8 - 546.8
Lower Lias II	5	4275	2758 - 7081
Rhaetic	6	4247	1027 - 15355
Keuper Marl	3	2765	2179 - 3641
Bunter Sandstone	14	5192	4261 - 6488
Upper Permian Marl I	8	5495	3523 - 7460
Upper Permian Marl II	9	8233	5392 - 9825
Upper Halite	11	1586	1076 - 1986

(ii) Near - Seam Rock

Upper Anhydrite	31	6075	2751 - 12776
Carnallite Marl	13	1241	487 - 1972
Halite Parting	23	2420	1413 - 3385
Middle Potash	70	1793	1055 - 3268
Middle Halite	55	1634	931 - 3696

UNIAXIAL COMPRESSIVE STRENGTH

(i) Upper Strata Rock

Material	No. of Tests	Mean Strength (KN/m ²)	Range (KN/m ²)	Dia/Hei Ratio
Middle Lias	1	37750	-	0.50
Ironstone	2	48127	-	1
Lower Lias I	1	51960	-	0.5
	2	62923	-	1
	3	55739	53078 - 58732	2
Lower Lias II	1	103239	-	0.5
	4	58504	-	1
	1	45583	48058 - 71777	2
Rhaetic	1	51616	-	0.5
	1	56518	-	2
Keuper Marl	1	113037	-	0.5
	6	76079	59980 - 94634	1
Bunter Sandstone	6	59883	48444 - 71315	0.5
	5	95248	84836 - 101198	1
	6	110065	97268 - 123455	2
Upper Permian Marl I	1	75659	-	0.5
	4	76907	67845 - 80258	1
	1	67702	-	2
Upper Permian Marl II	2	90828	-	0.5
	2	122745	24270 - 36502	2
Upper Halite	4	30999	28214 - 39329	0.5
	3	31986	-	1
	2	61634	-	2

(ii) Near Seam Rock

Material	Dia/Height Ratio	No. of Tests	Mean Strength (KN/m ²)	Range (KN/m ²)	
Upper Anhydrite	S6	0.5	9	43976	24898 - 97392
	S11	0.5	5	60324	41542 - 106314
	S6	1	1	108707	-
	S11	1	7	101053	79396 - 119711
Carnallite Marl		0.5	5	14238	13528 - 14955
		0.5	3	15383	6047 - 26856
		1	3	13500	6709 - 20292
		1	5	15838	10694 - 30317
Halite Parting		0.5	6	30579	11921 - 47713
		0.5	3	28869	21961 - 41653
		1	2	32648	-
		1	1	45583	-
Middle Potash		0.5	7	30221	25270 - 39198
		0.5	14	28945	25312 - 30841
		1	3	44721	32096 - 53119
		1	12	33696	31421 - 35875
Middle Halite		0.5	7	29386	22119 - 39198
		0.5	6	23705	19416 - 31331
		2	7	48637	46293 - 52754
		2	4	56732	52222 - 59221

ELASTIC CONSTANTS FOR NORTH YORKSHIRE ROCK

Material	Elastic Mod. $\times 10^6$ KN/m ²	Poissons Ratio
Lower Lias I	8.41	0.37
Lower Lias II	25.86	0.03
Rhaetic	12.96	0.05
Keuper Marl	34.06	0.08
Bunter Sandstone	20.82	0.07
Upper Permian Marl I	18.27	0.09
Upper Permian Marl II	22.27	0.05
Upper Halite	1.86	0.24
Upper Anhydrite S6	16.62	0.18
Upper Anhydrite S11	21.65	0.25
Carnallite Marl S6	5.10	0.16
Carnallite Marl S11	5.03	0.40
Halite Parting S6	10.48	0.10
Halite Parting S11	7.31	-
Middle Potash S6	9.86	0.15
Middle Potash S11	5.03	0.32
Middle Halite S6	3.79	0.21
Middle Halite S11	4.55	0.24

TRIAXIAL COMPRESSIVE STRENGTH

Material	Confining Pressure (KN/m ²)	Ultimate Strength (KN/m ²)
Lower Lias 1	0	51961
	3447	77941
	6895	79761
	10342	91848
Lower Lias II	0	103239
	3447	-
Rhaetic	0	51616
	3447	54698
	6895	101639
	10342	76348
Keuper Marl	0	113037
	6895	159302
Bunter Sandstone (Saturated in brine)	0	58950
	6895	155480
	13790	156860
	20685	185820
	27580	225470
Bunter Sandstone (Air dried)	0	58950
	6895	139280
	13790	167550
	20685	205130
	27580 - 25856	226500
	34475 - 20685	215810

Upper Permian	3447	155880
(Marl I)	6895	159980
	10342	181630
	13790	165450
	17237	186420
Upper Halite	0	30100
	3447	67230
	6895	87570
	10342	104830
	13790	113950
	17237	123520
Upper Anhydrite	0	85390
	3447	122940
	5171	122940
	6895	88390
	10342	132040
	13790	139970
	17237	95700
	31027	195960
	44817	210300
Carnallite Marl	0	20360
	3447	26340
	6205	37100
	8618	55090
	17237	96120
	34475	91360
	51712	136180
Halite Parting	0	22990
	10342	55330
	10342	78260
	10342	82880

Middle Potash	0	30130	
	3447	55990	
	4826	62810	
	6895	74470	
	17237	109560	
	34475	143070	
	51712	121770	? Not typical failure
Middle Halite	0	26870	
	3447	47990	
	4826	64400	
	6895	78470	
	10342	86190	
	20685	143760	
	34475	172380	
	44817	192370	
	55160	198580	
	65502	207880	

UNIAXIAL COMPRESSIVE CREEP

Halite Parting

Specimen No.	D/H Ratio	Applied Stress (KN/m ²)	Steady Creep Rate x10 ⁻⁵ day ⁻¹	Duration Days
S7 - 11C	2.0	18616	0.43	708 C
S5 - 2B	2.0	20685	0.48	204 C
S7 - 11B	2.0	20685	1.90	391
S7 - 15B	2.0	22753	59	228
S7 - 15C	2.0	25856	90	41

Middle Halite

NM - 93A	0.9	17237	1.02	56
NM - 93B	1.2	17237	0.67	0 - 56
		20685	0.87	56 - 337
		27580	1.36	337 - 516
NM - 99A	1.2	24132	1.72	111
S6 - 167	2.0	17237	1.49	626 C
S13 - 75A	2.0	20685	0.22	0 - 286
		27580	1.38	286 - 537
S6 - 164	2.0	20685	0.45	626 C
S13 - 75B	2.0	22753	0.48	0 - 286
		31027	6.1	286 - 537
NM - 99B	2.0	27580	0.72	0 - 115
		34475	1.82	115 - 295
S7 - 50A	2.0	27580	0.58	254 C

c = Currently under test

Middle Potash

NM - 85A	0.7	17237	20	0 - 56
		20685	89	56 - 86
S20 - 9A	0.7	20685	14	31 C
S8 - 16A	1.4	13790	5.3	70 C
	1.4	17237	3.5	0 - 277
		24132	28	277 - 456
		31027	1200	457 - 468
NM - 87B	1.4	17237	6.8	364
S5 - 25A	1.4	20685	310	43
S8 - 16B	1.4	20685	106	126
S5 - 25B	1.4	24132	336	33
NM - 77A	1.4	24132	29	166
S4 - 30A	2.0	13790	3.0	107
S13 - 53A	2.0	13790	2.2	276 C
S8 - 74B	2.0	13790	0.99	276 C
NM - 79C	2.0	17237	10.6	181
S4 - 24B	2.0	17237	6.5	109
S6 - 2	2.0	17237	1.8	181
S6 - 145	2.0	17237	2.3	56
S11 - 105	2.0	17237	4.2	585 C
S6 - 142	2.0	18616	3.1	420
S6 - 4	2.0	18616	6.3	808 C
S11 - 147	2.0	18961	12.6	116
NM - 79B	2.0	20685	43	525
S4 - 30B	2.0	20685	5.0	266
S5 - 15A	2.0	20685	190	161
S6 - 134	2.0	20685	34	479
S8 - 10B	2.0	20685	60	267
S8 - 74A	2.0	20685	75	267
S11 - 76	2.0	20685	1.2	558
S12 - 39B	2.0	20685	15.7	247 C
S10 - 14B	2.0	20685	11.7	276 C
S11 - 134	2.0	20685	7.5	583 C
S6 - 6	2.0	21375	7.2	765
NM - 89C	2.0	22754	30	524
S5 - 15B	2.0	22754	91	156
S6 - 8	2.0	22754	77	230

S7 - 28B	2.0	22754	186	63	
S8 - 34B	2.0	22754	1.67	189	
S10 - 26A	2.0	22754	238	66	
S11 - 121B	2.0	22754	11.9	189	
S12 - 6C	2.0	22754	52	189	
S8 - 97B	2.0	22754	7.0	373	C
NM - 79A	2.0	24132	90	188	
NM - 89B	2.0	24132	45	339	
S4 - 24A	2.0	24132	12.5	47	
S8 - 10A	2.0	24132	122	73	
S8 - 57A	2.0	24132	1.58	73	
S10 - 14A	2.0	24132	178	77	
S11 - 77	2.0	24132	274	62	
S11 - 85	2.0	24132	311	20	
S11 - 146	2.0	24132	174	105	
S12 - 6A	2.0	24132	106	77	
S13 - 53B	2.0	24132	53	92	
NM - 77C	2.0	27580	43	139	
S12 - 44A	2.0	27580	104	92	
NM - 87A	3.0	34475	116	170	
NM - 89A	3.5	24132	12.2	0	- 296
		31027	43	296	- 477
S8 - 43A	3.5	24132	16.0	174	C
NM - 77D	3.5	27580	3.6	0	- 297
		37922	51	297	- 477
S8 - 43B	3.5	31027	84	154	C
S10 - 23B	3.5	34475	51	242	
S8 - 43C	3.5	37922	72	247	

c = Currently under test

SUMMARY OF UNIAXIAL COMPRESSIVE CREEP TESTS ON
MIDDLE POTASH

D/H Ratio	No. of Tests	Applied Stress (KN/m ²)	Average Steady Creep Rate ₁ (x10 ⁻⁵ day ⁻¹)
0.7	1	17237	20
0.7	2	20685	52
1.4	1	13790	5.3
1.4	2	17237	5.1
1.4	2	20685	208
1.4	3	24132	131
1.4	1	31027	1200
2.0	3	13790	2.1
2.0	5	17237	5.1
2.0	2	18616	4.7
2.0	1	18961	12.6
2.0	10	20685	41
2.0	1	21374	7.2
2.0	9	22753	67
2.0	11	24132	124
2.0	2	27580	74
2.0	1	31027	43
3.0	1	34475	116
3.5	2	24132	14.1
3.5	1	27580	3.6
3.5	1	31027	84
3.5	1	34475	51
3.5	2	37922	123

COOK

COMPRESSIVE STRENGTH

Upper Halite

D/H Ratio	No of Tests	Direction of Bedding to axis of specimen	Compressive Strength (KN/m ²)
0.5	1	parallel	29350
0.5	4	perpendicular	31500 mean
0.66	1	parallel	32500
0.66	1	perpendicular	39200
0.66	1	parallel	23500
1.0	3	perpendicular	32500 mean
1.0	1	perpendicular	39000
1.0	1	parallel	41450

Tensile Strength of Upper Halite

Direction of Bedding to Major Failure Plane	Tensile Strength (KN/m ²)
perpendicular	2050
perpendicular	2050
parallel	1390
parallel	1250

UNIAXIAL CREEP TEST ON UPPER HALITE

Specimen No.	D/H	Applied Stress (KN/m ²)	Duration (days)	Strain %	Strain Rate x10 ⁻⁵ day ⁻¹
S20 - 645	2.0	24500	750	5.5	1.7
S20 - 646	2.0	22750	750	6.9	2.0
S20 - 647	2.0	26250	526	13.7	9.2
UM1	0.5	21000	11	1.7	32.0
UM2	0.5	21000	15	2.3	31.0

TRIAXIAL CREEP TEST ON UPPER HALITE

		Axial Stress	Lateral Stress			
UM3	0.5	49000	14000	60	9.4	44
UM4	0.5	49000	21000	42	3.5	6
UM5	0.5	28000	14000	49	1.2	0.4
UM6	0.5	28000	7000	59	0.9	6

UNIAXIAL CREEP TEST ON MIDDLE HALITE

-	0.5	16800	520	2.3	0.6
---	-----	-------	-----	-----	-----

WIGGETT

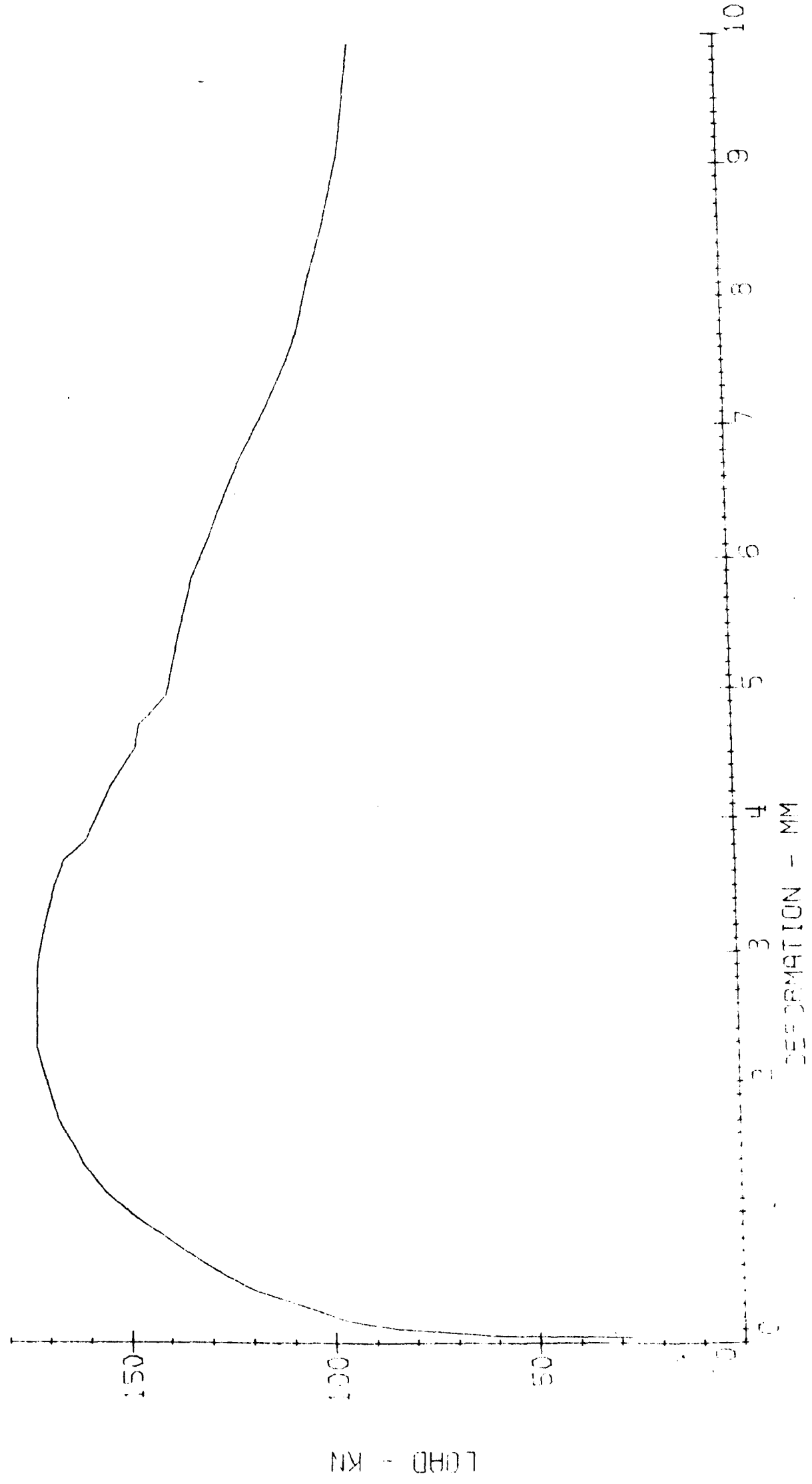
MEAN VALUES FOR MECHANICAL PROPERTIES
OF MIDDLE POTASH

Rock Types	Young's Modulus	Poisson's Ratio	Uniaxial Compressive Strength (KN/m ²)	Tensile Strength (KN/m ²)	Shear Strength (KN/m ²)
Primary Potash	2.428	0.385	41220	-	-
Shaley Potash	1.50	0.320	38100	-	-
Potash Shale	1.142	0.252	10430	1280	10650
Boracitic Shale	1.066	0.276	12280	1100	9970

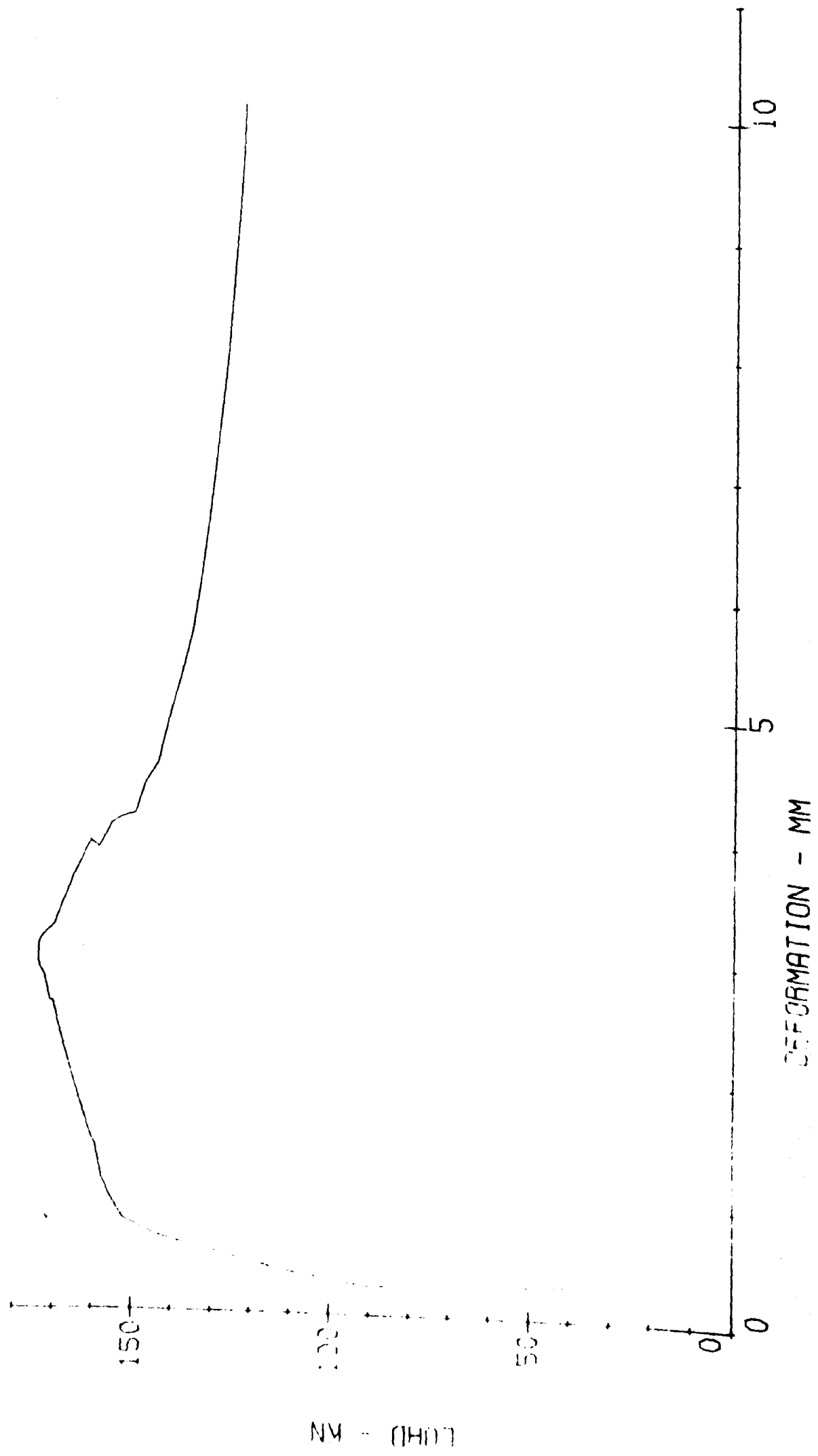
APPENDIX 4

LOAD/DEFORMATION CURVES FOR UNCEMENTED ROCKSALT

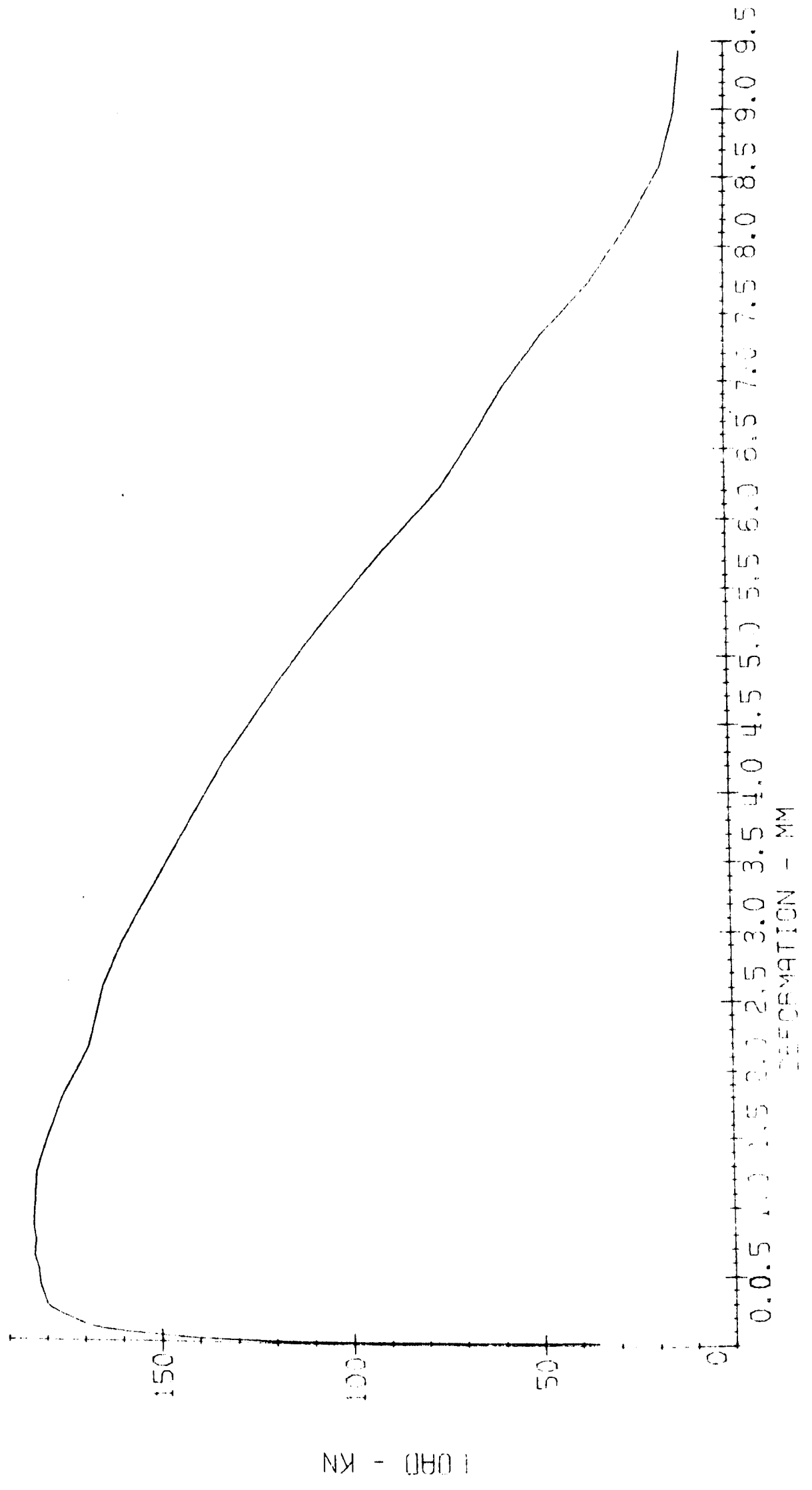
TEST 1. ROCKSALT W₂H=121 SPECIMEN NO.1



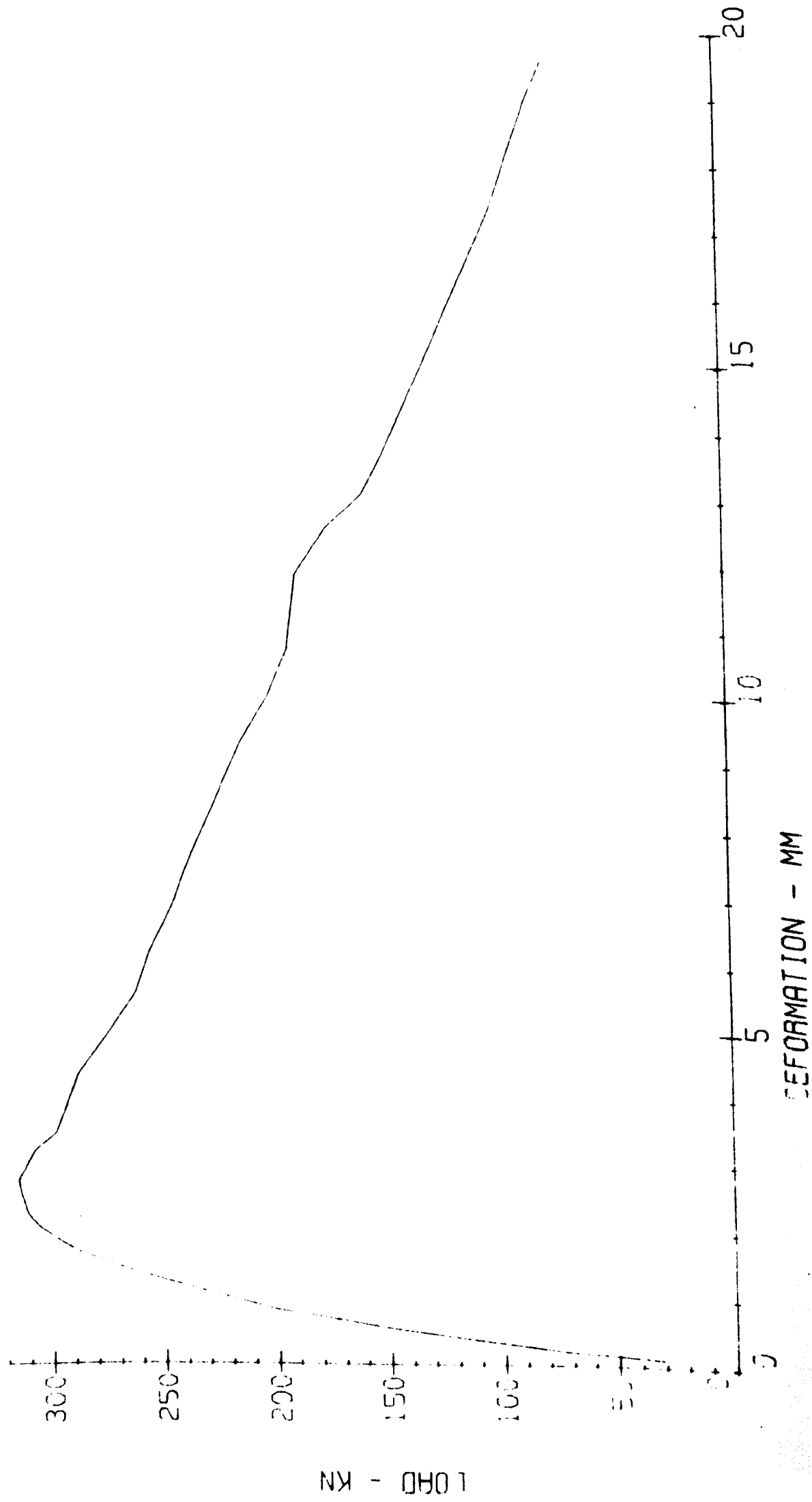
TEST 2. ROCKSALT W: H=1:1 SPECIMEN NO. 2



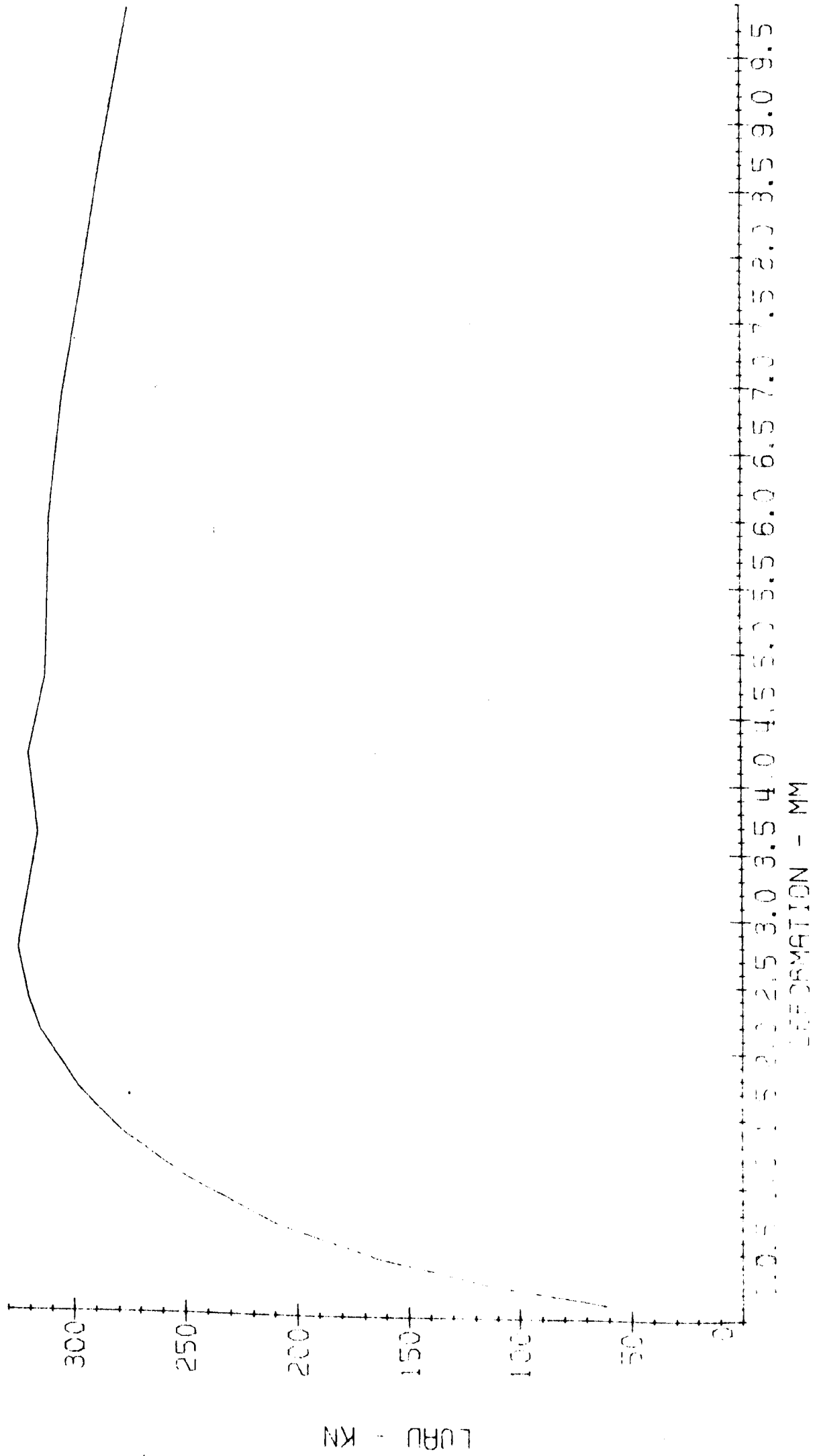
TEST 3. ROCKSALT W: H = 1 : 1 SPECIMEN NO. 3



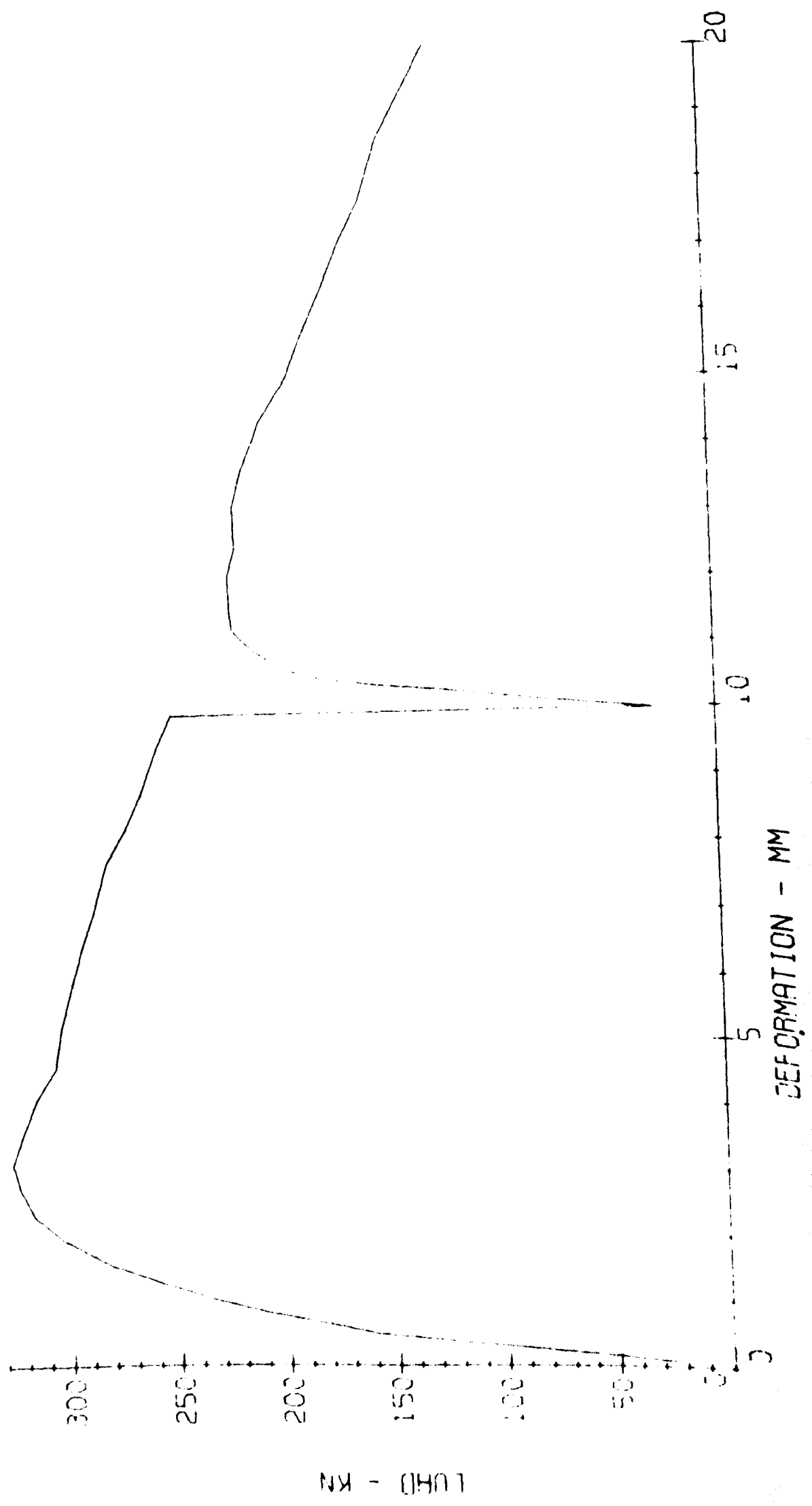
TEST 4. POTASH W:H=1:1 SPECIMEN NO.7



TEST 5. POTASH W: H = 1 : 1 SPECIMEN NO. 8

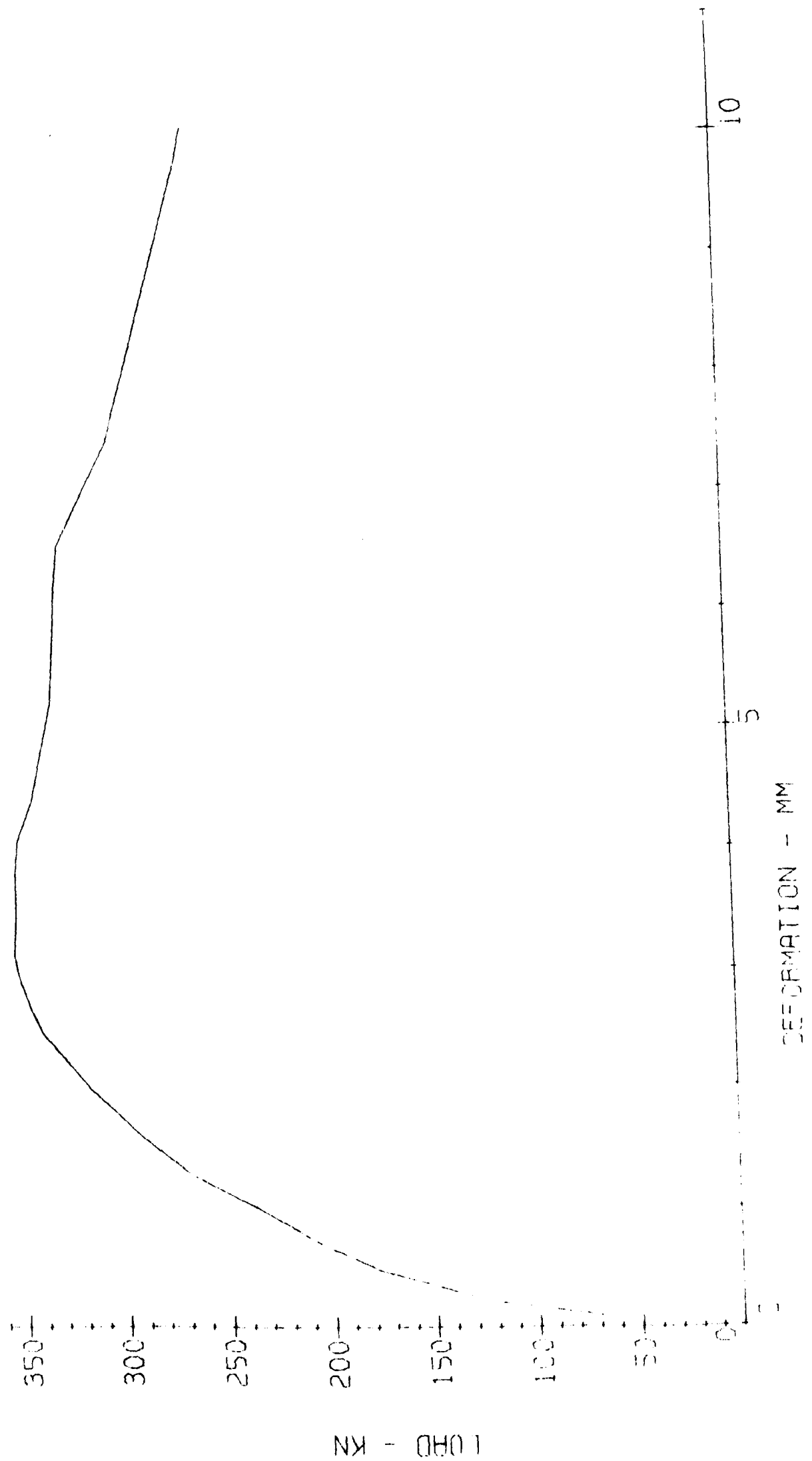


TEST 8. POTAG- W: H=1:1 SPECIMEN NO. 9

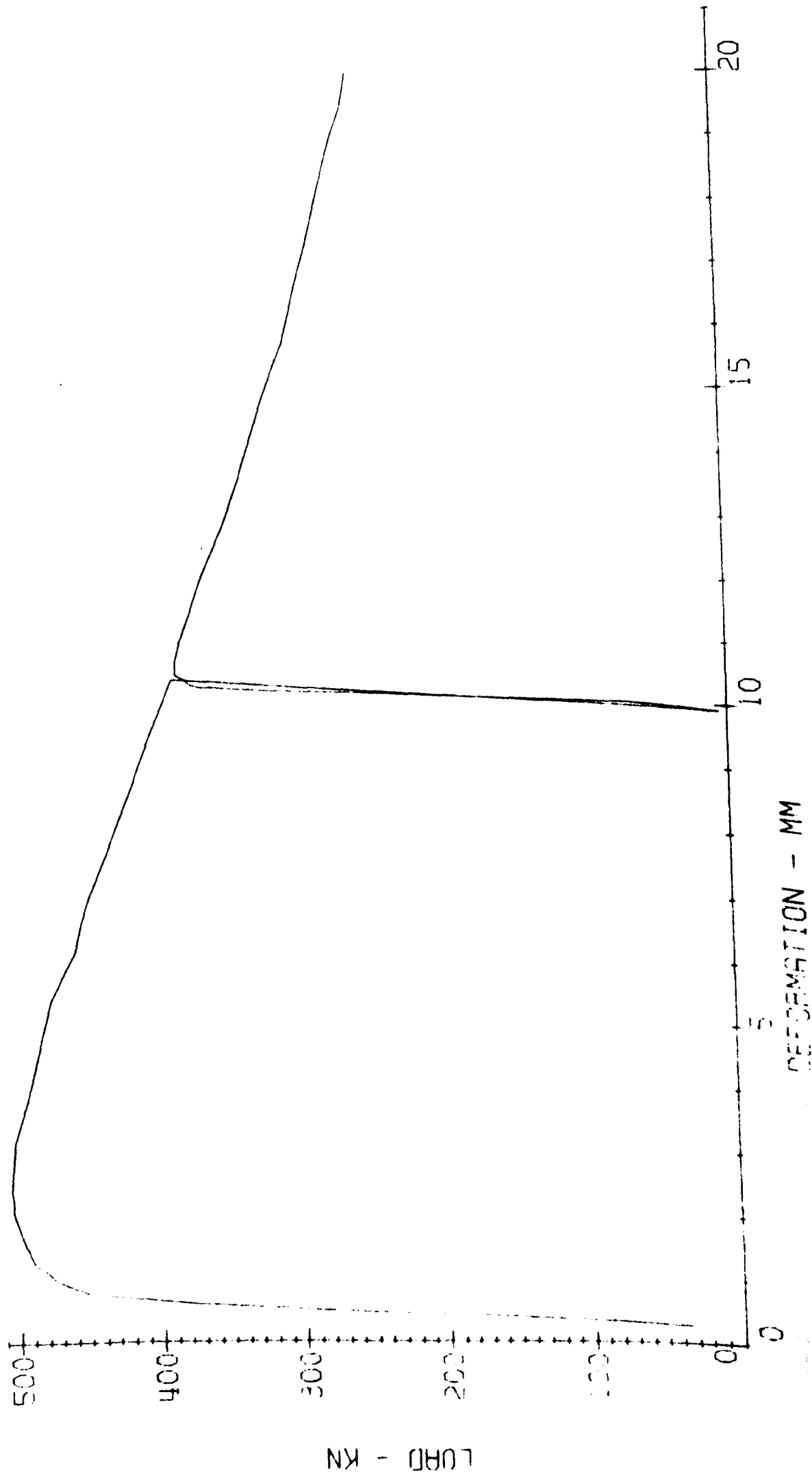


DEFORMATION - MM

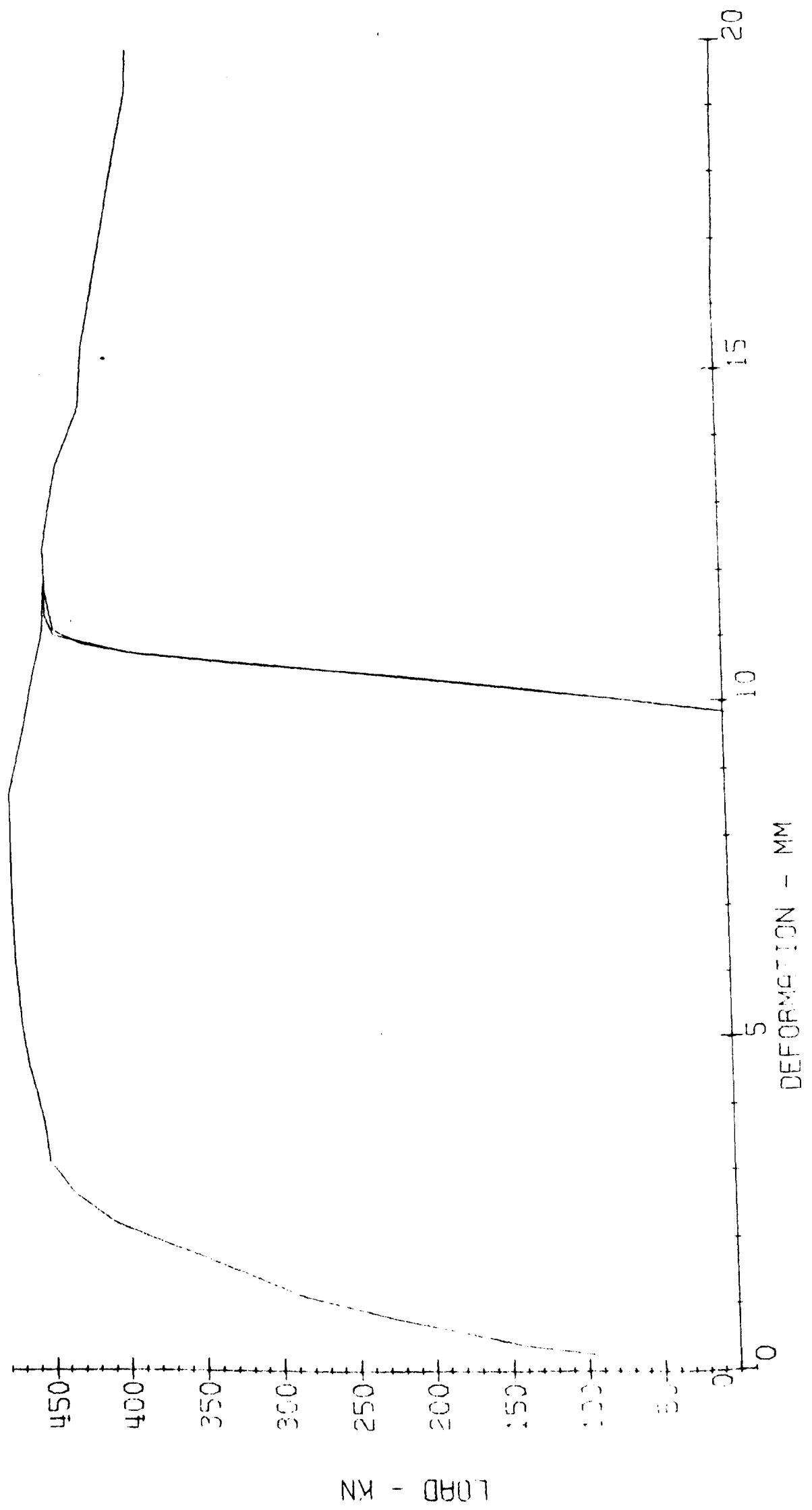
TEST 7. POTASH W: H=1:1 SPECIMEN NO. 10



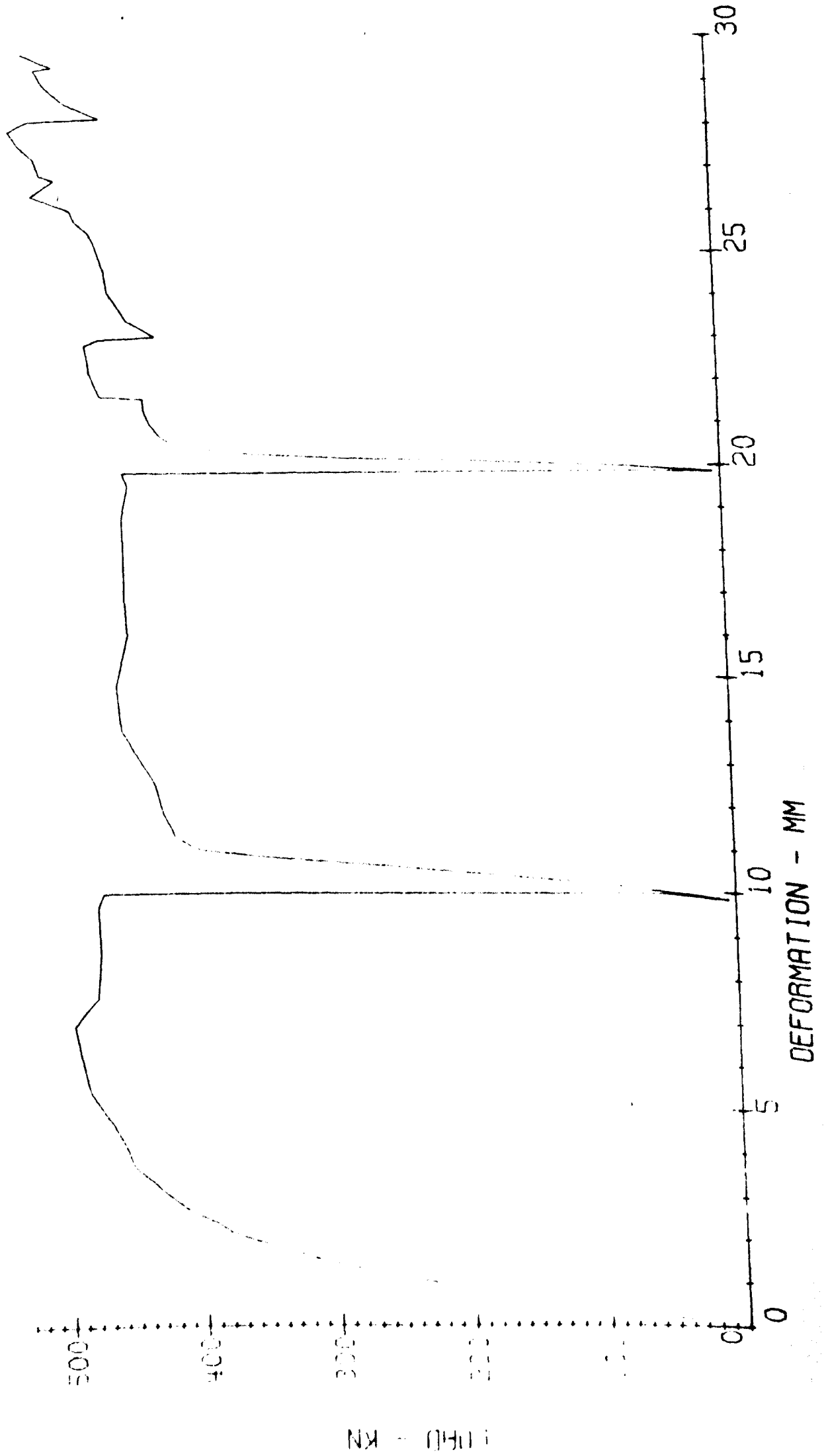
TEST 8. POTASH W: H=2:1 SPECIMEN NO. 12



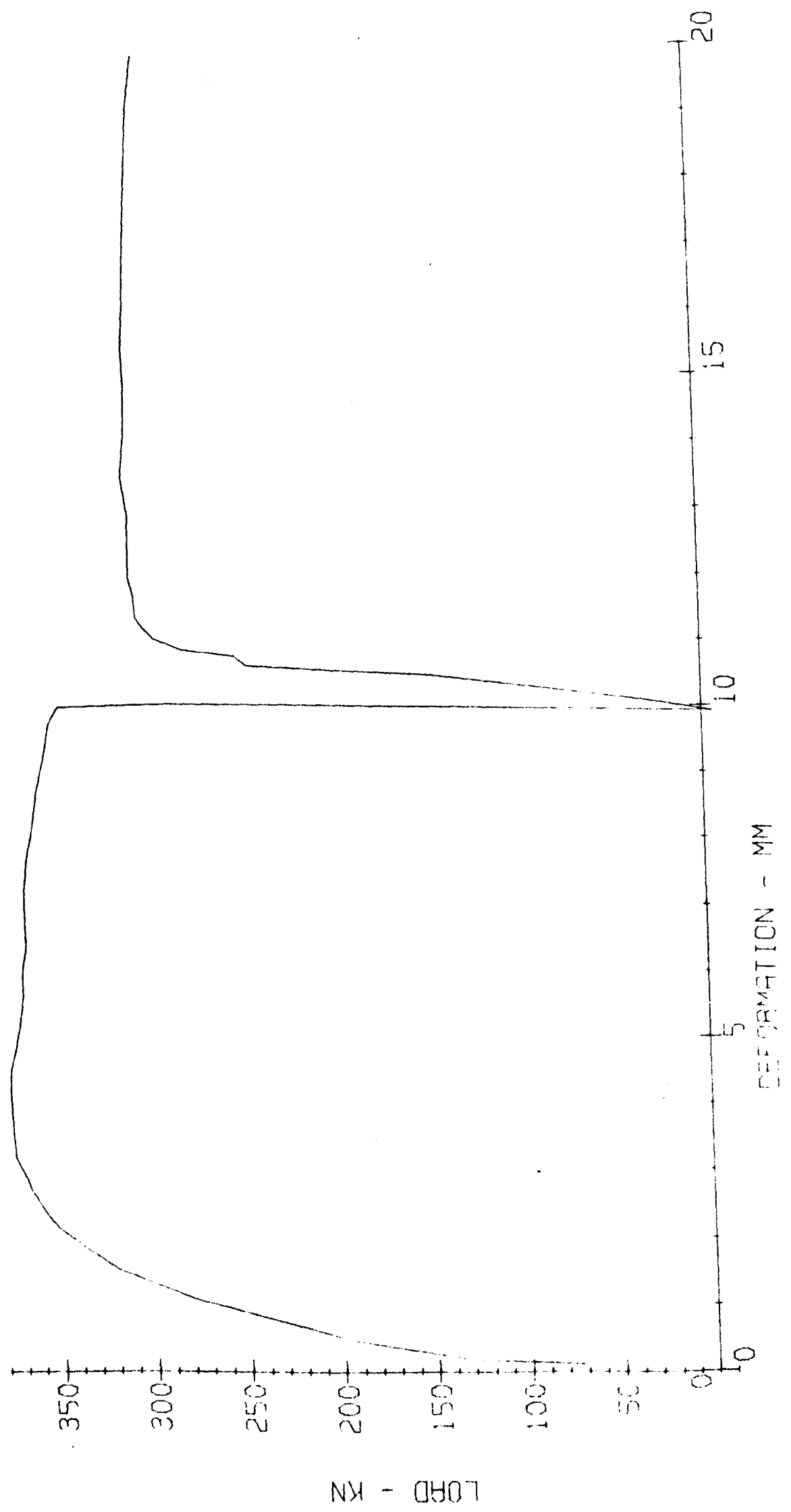
TEST 9. POTASH W:H=2:1 SPECIMEN NO.13



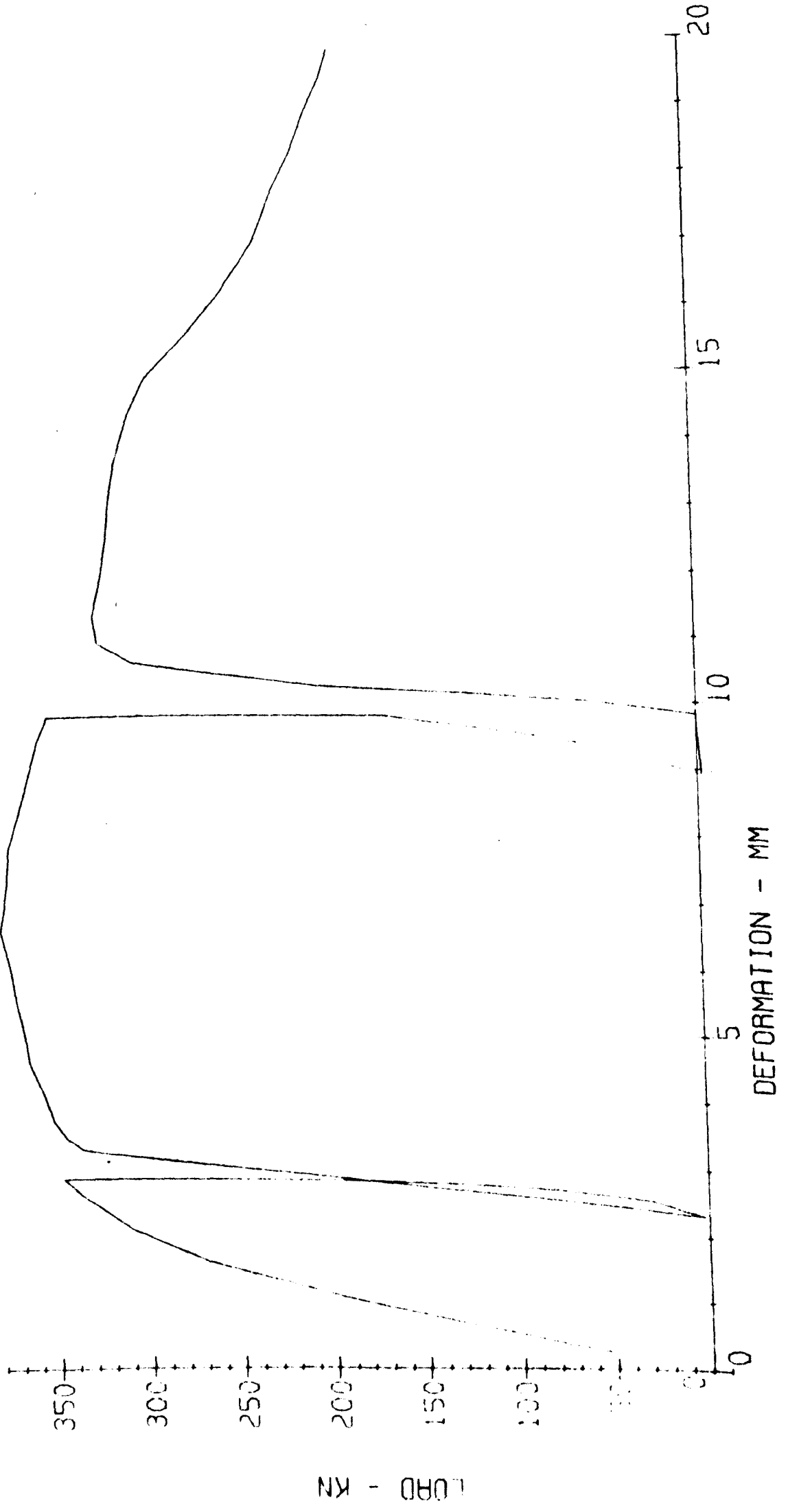
TEST 10. POTASH W:H=2:1 SPECIMEN NO. 14



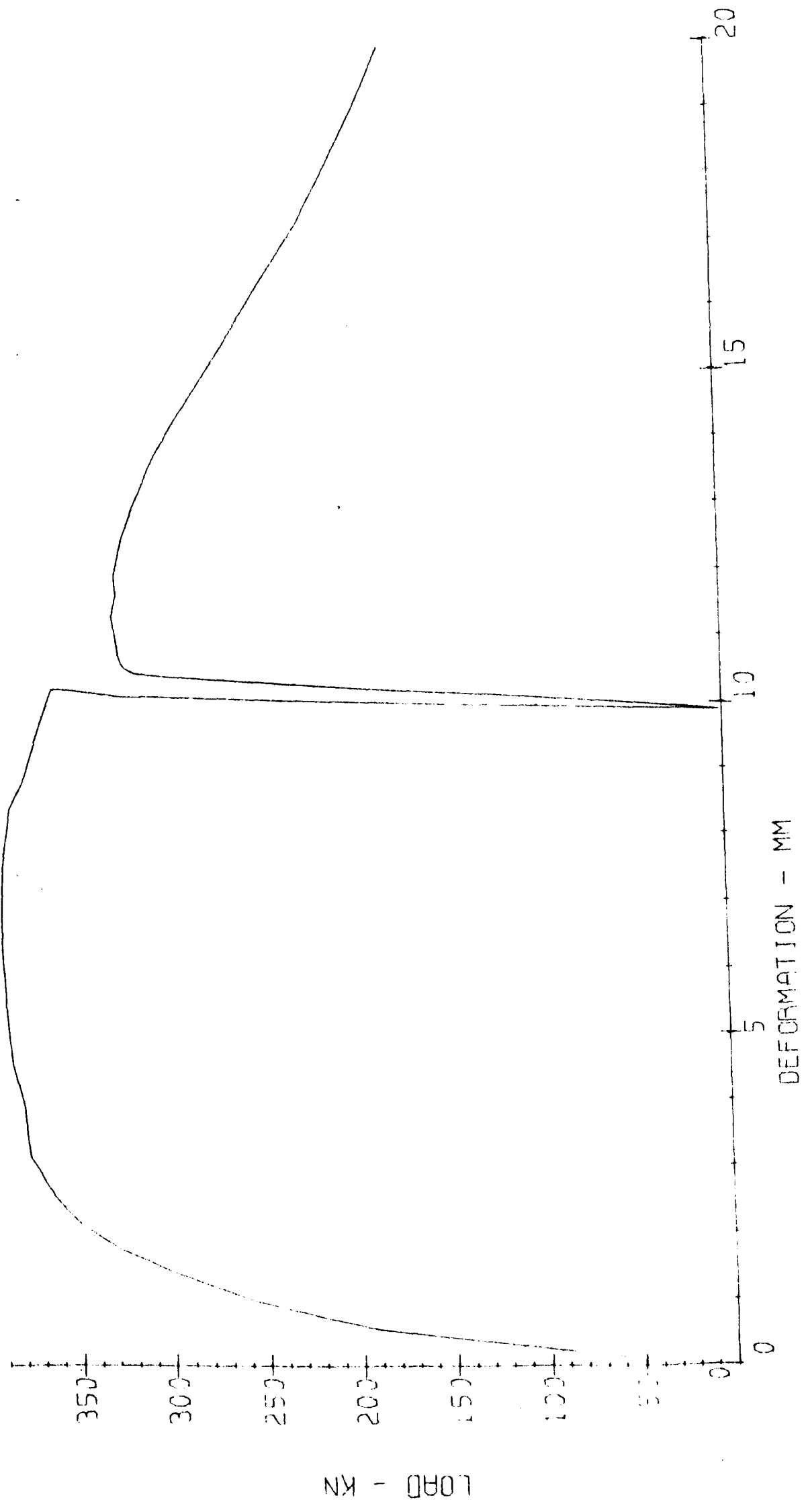
TEST 11. POTASH W:H=1.5:1 SPECIMEN NO. 16



TEST 12. POTASH W: H = 1.5 : 1 SPECIMEN NO. 17

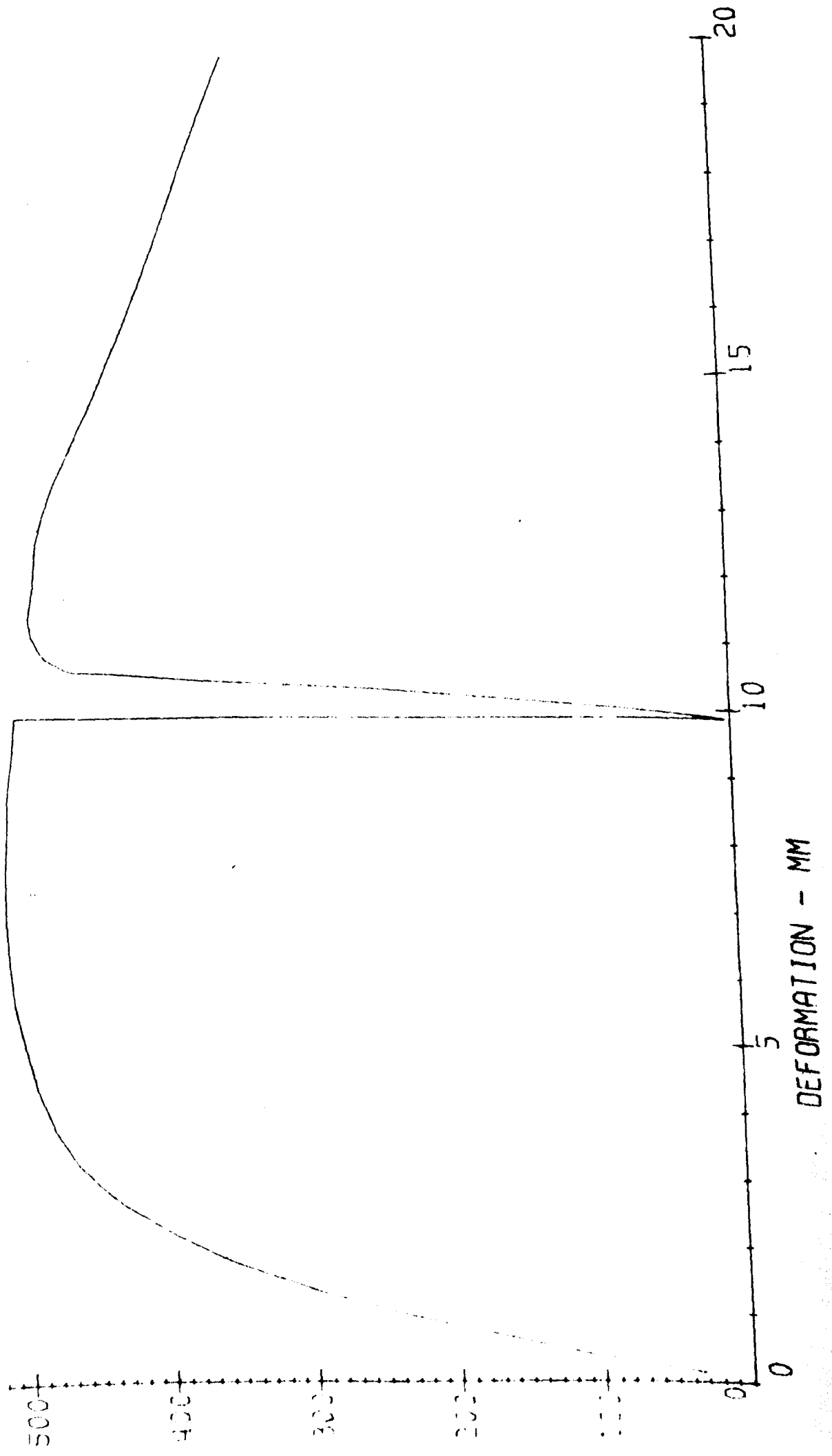


TEST 13. POTASH W: H = 1.5 : 1 SPECIMEN NO. 15



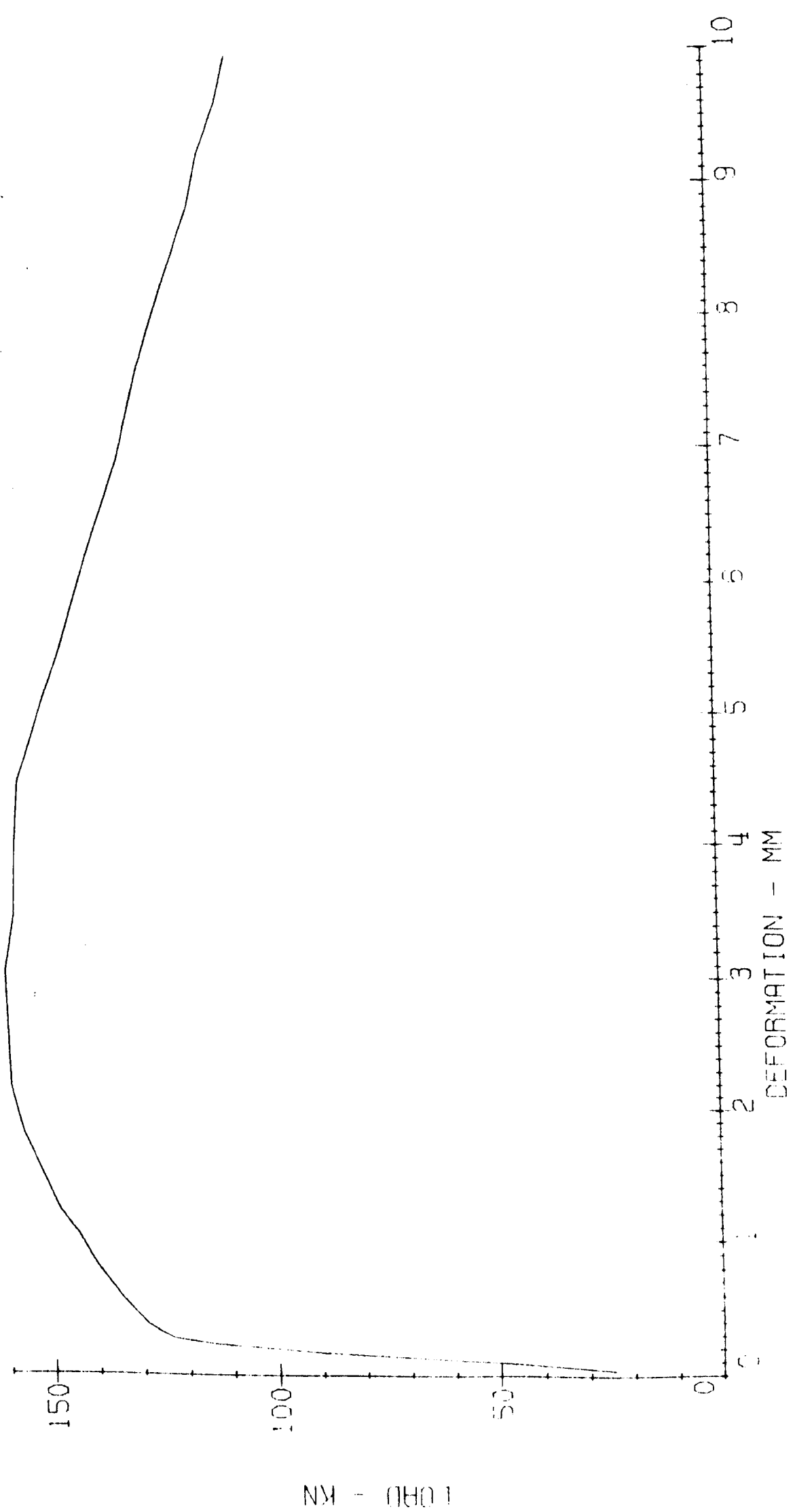
SPECIMEN NO. 11

TEST 14. POTASH W:H=2:1

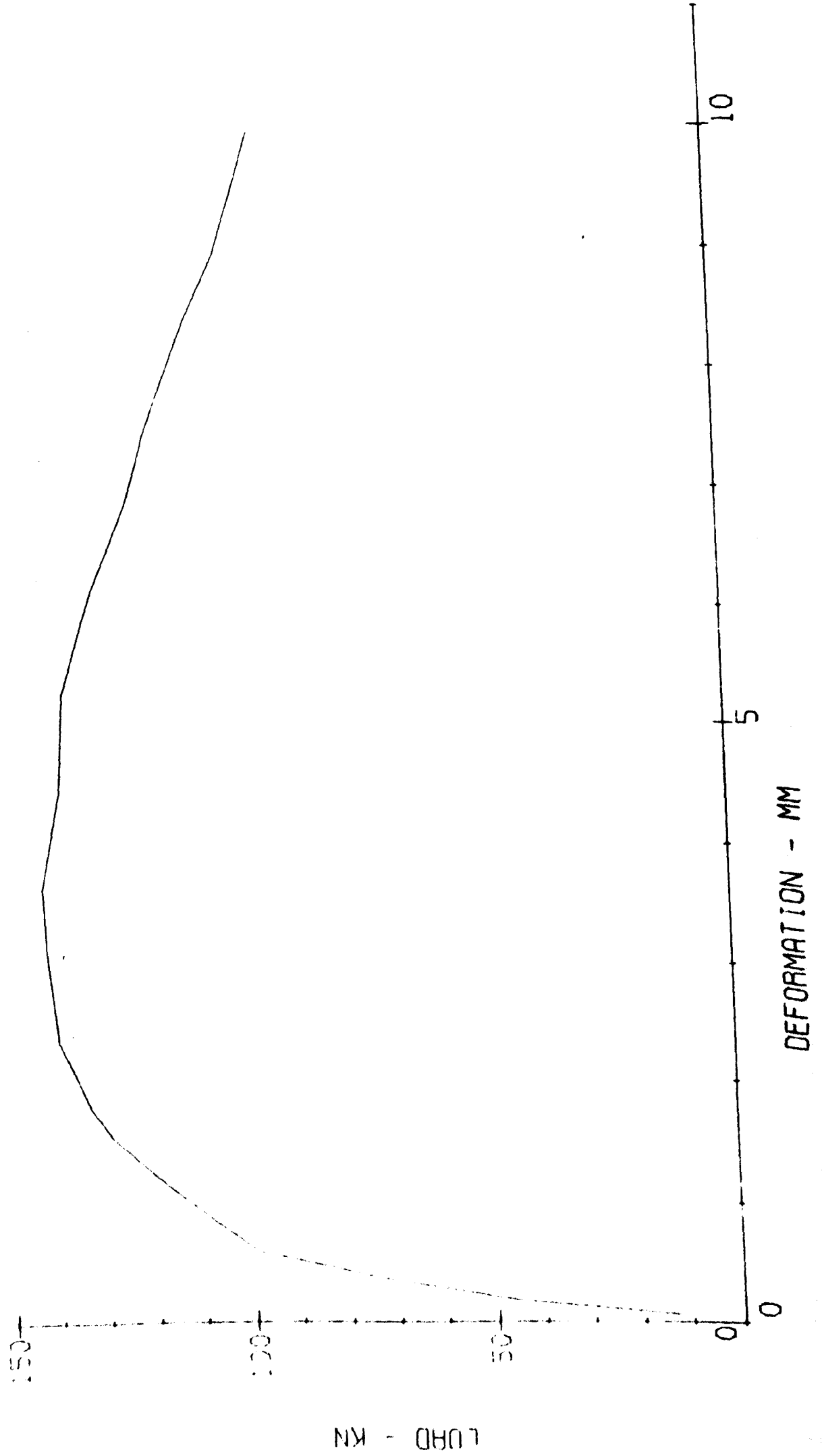


LOAD - KN

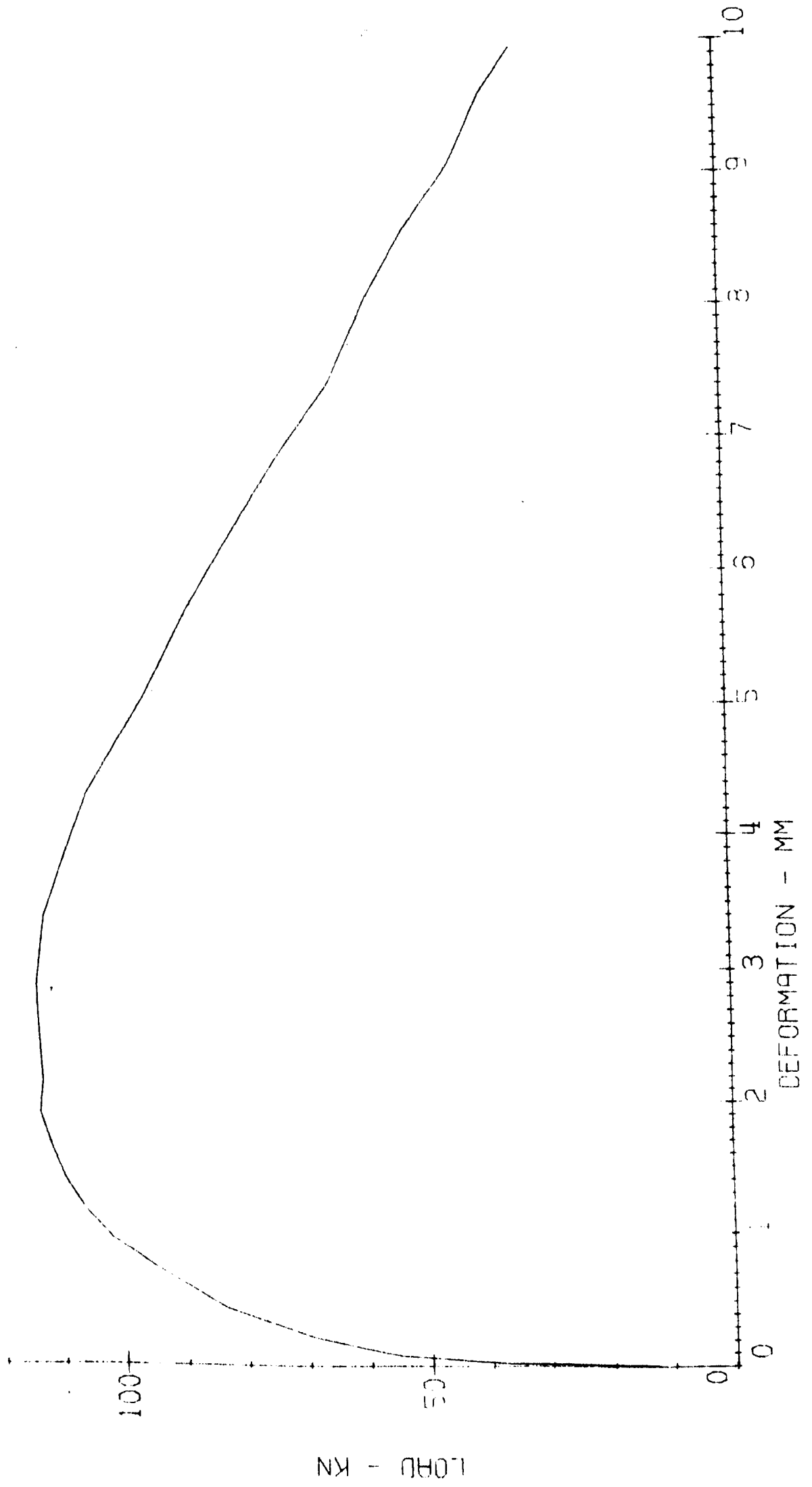
TEST 15. ROCKSALT W: H=1:1 SPECIMEN NO.4



TEST 16. ROCKSALT W: H = 1: 1 SPECIMEN NO. 5



TEST 17. ROCKSALT W: H=1:1 SPECIMEN NO.6

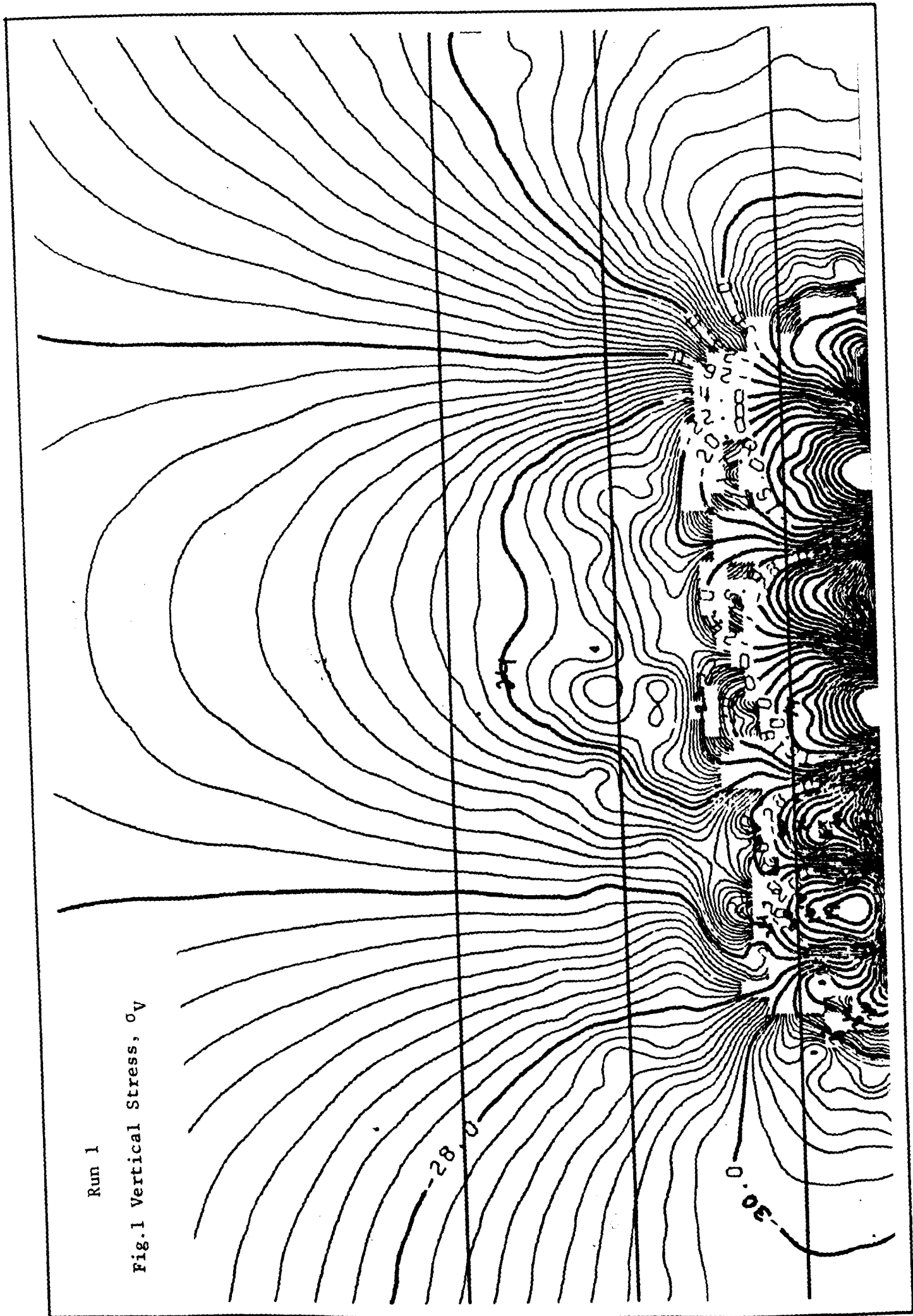


APPENDIX 5

TESTS ON SALTCRETE - MODULUS AND LOADING/UNLOADING

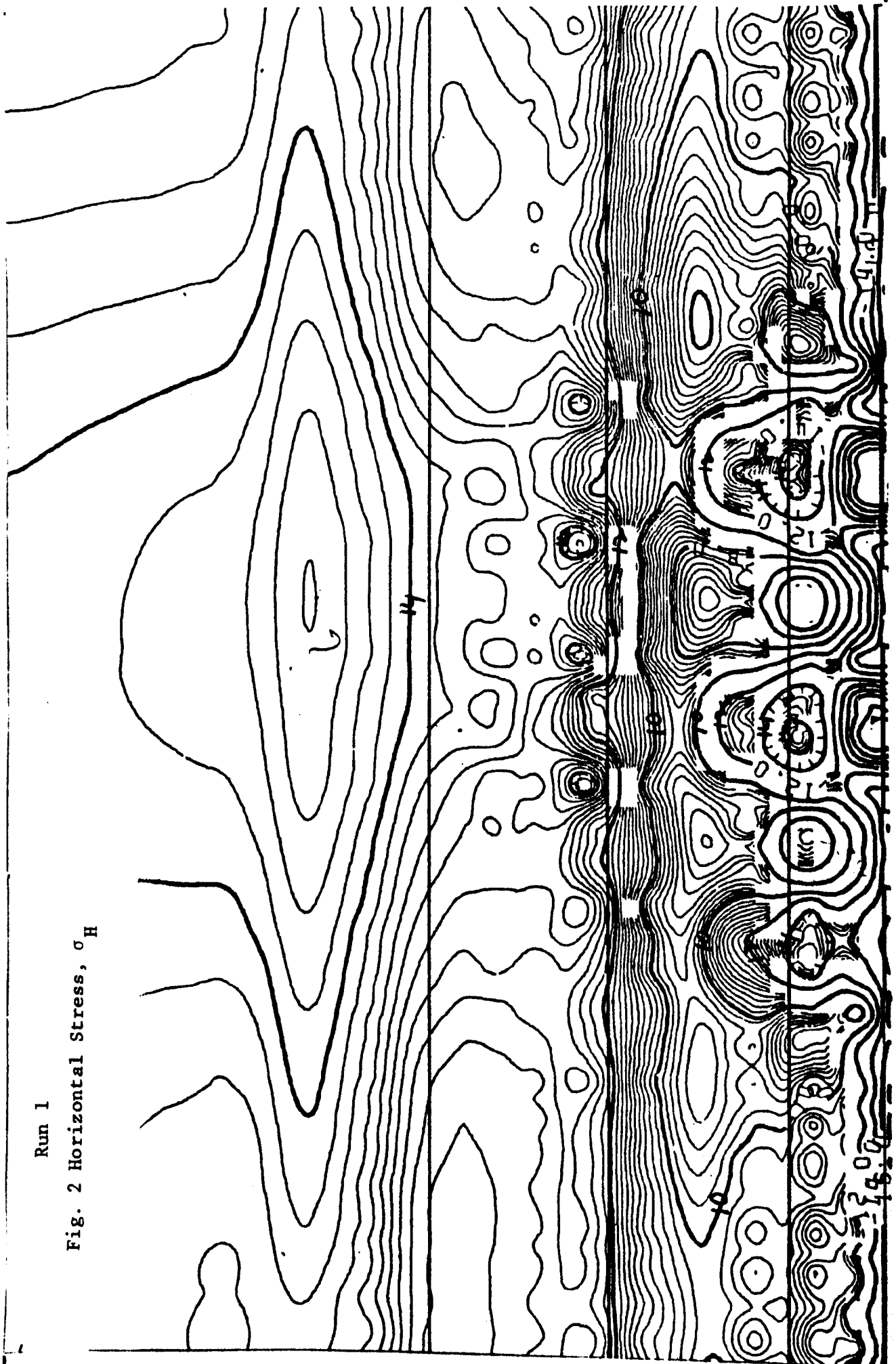
Run 1

Fig. 1 Vertical Stress, σ_v



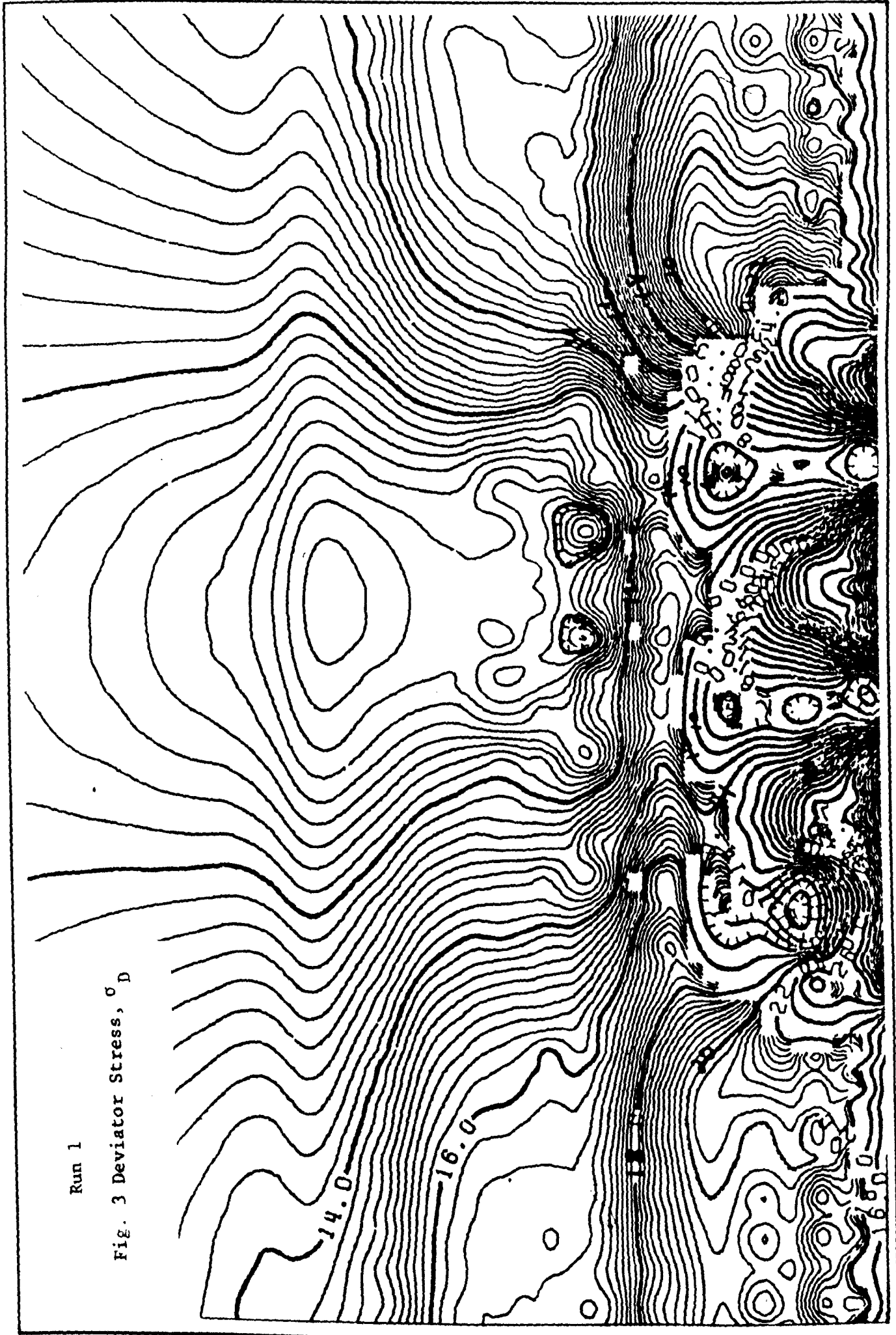
Run 1

Fig. 2 Horizontal Stress, σ_H



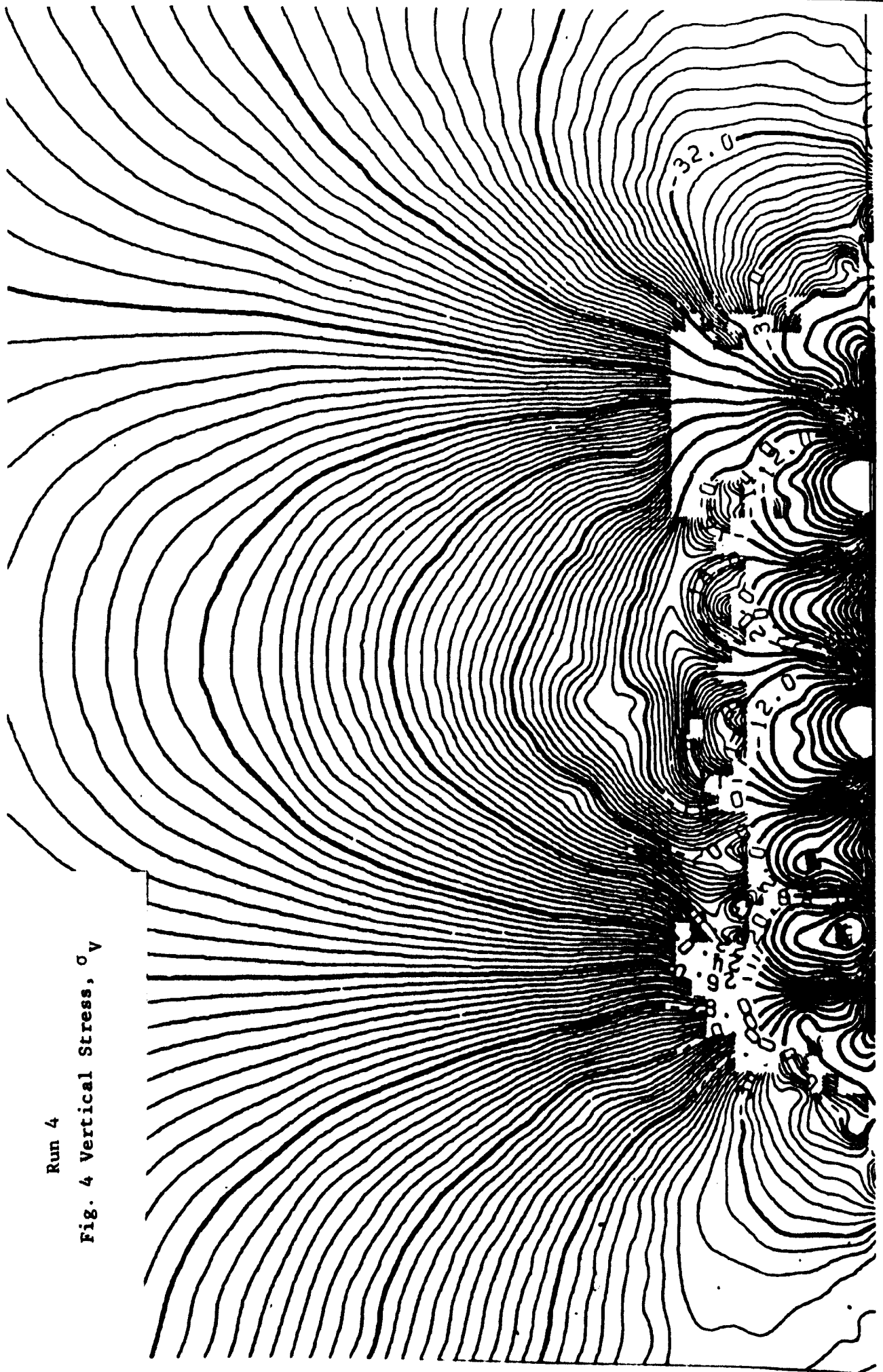
Run 1

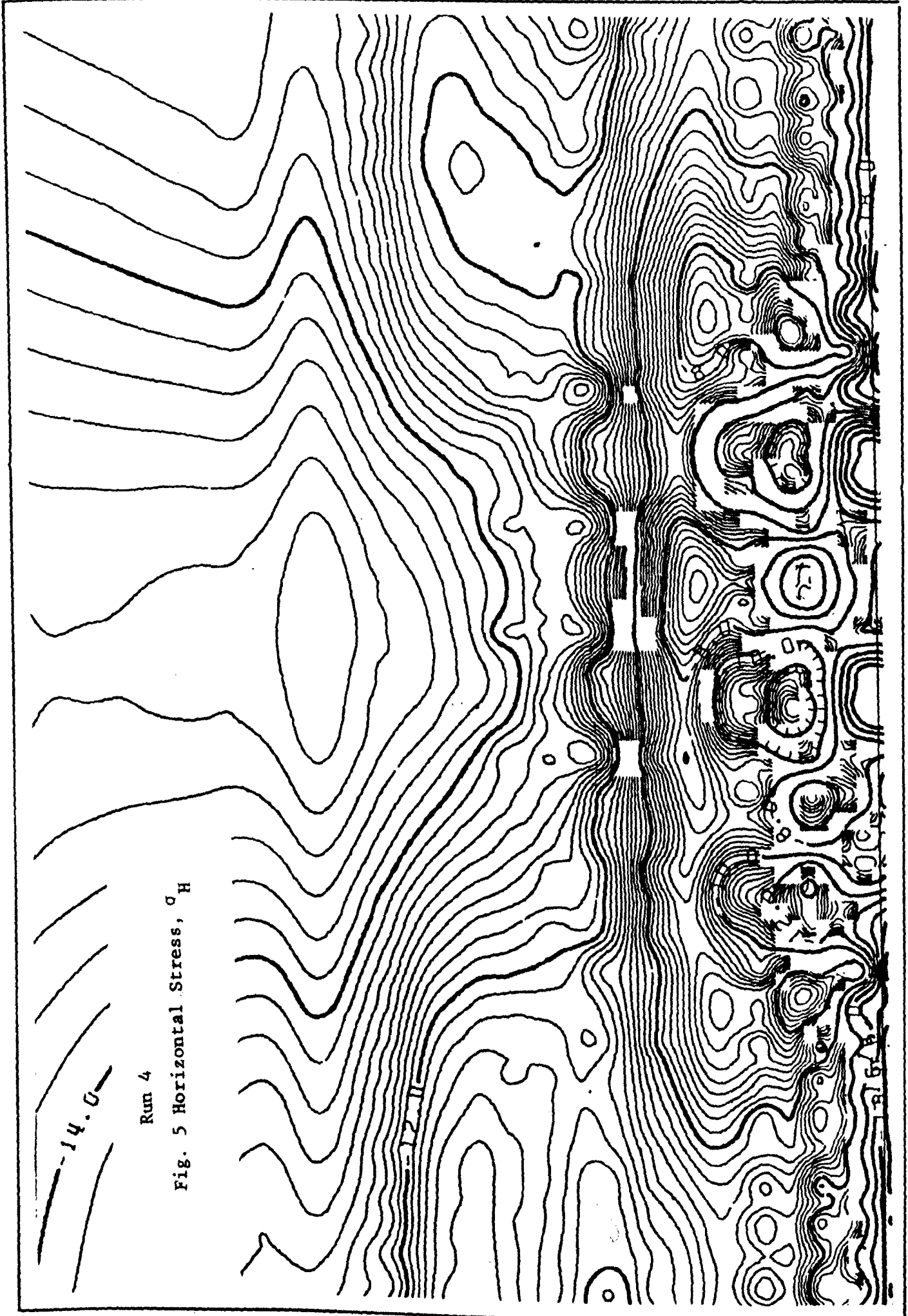
Fig. 3 Deviator Stress, σ_D



Run 4

Fig. 4 Vertical Stress, σ_v



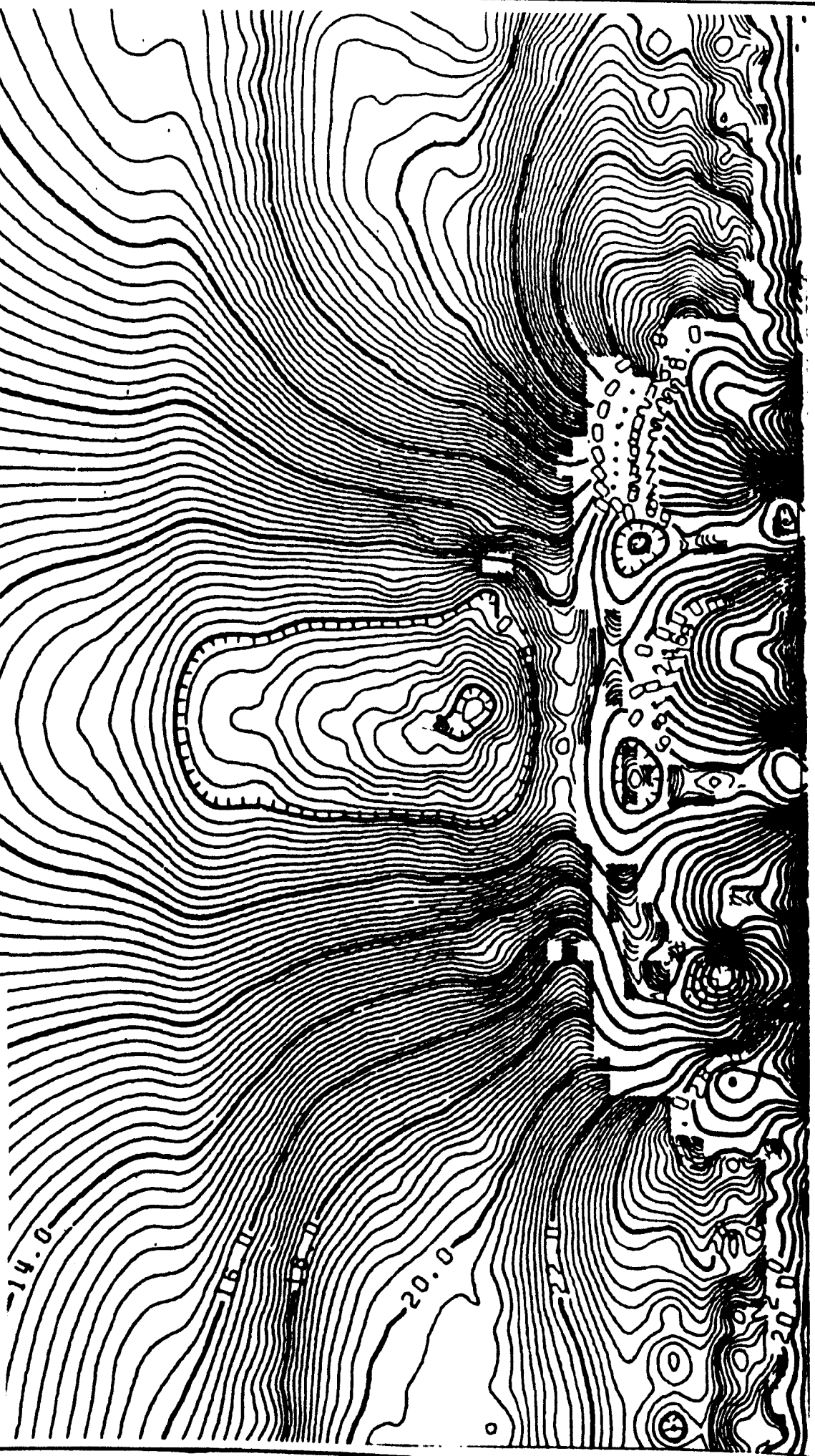


Run 4

Fig. 5 Horizontal Stress, σ_H

Run 4

Fig. 6 Deviator Stress, σ_D



APPENDIX 6

WEEKLY FACE ADVANCES

APPENDIX 6

WEEKLY FACE ADVANCES



Fig.1 No.7 Panel



Fig.2 No.10 Panel

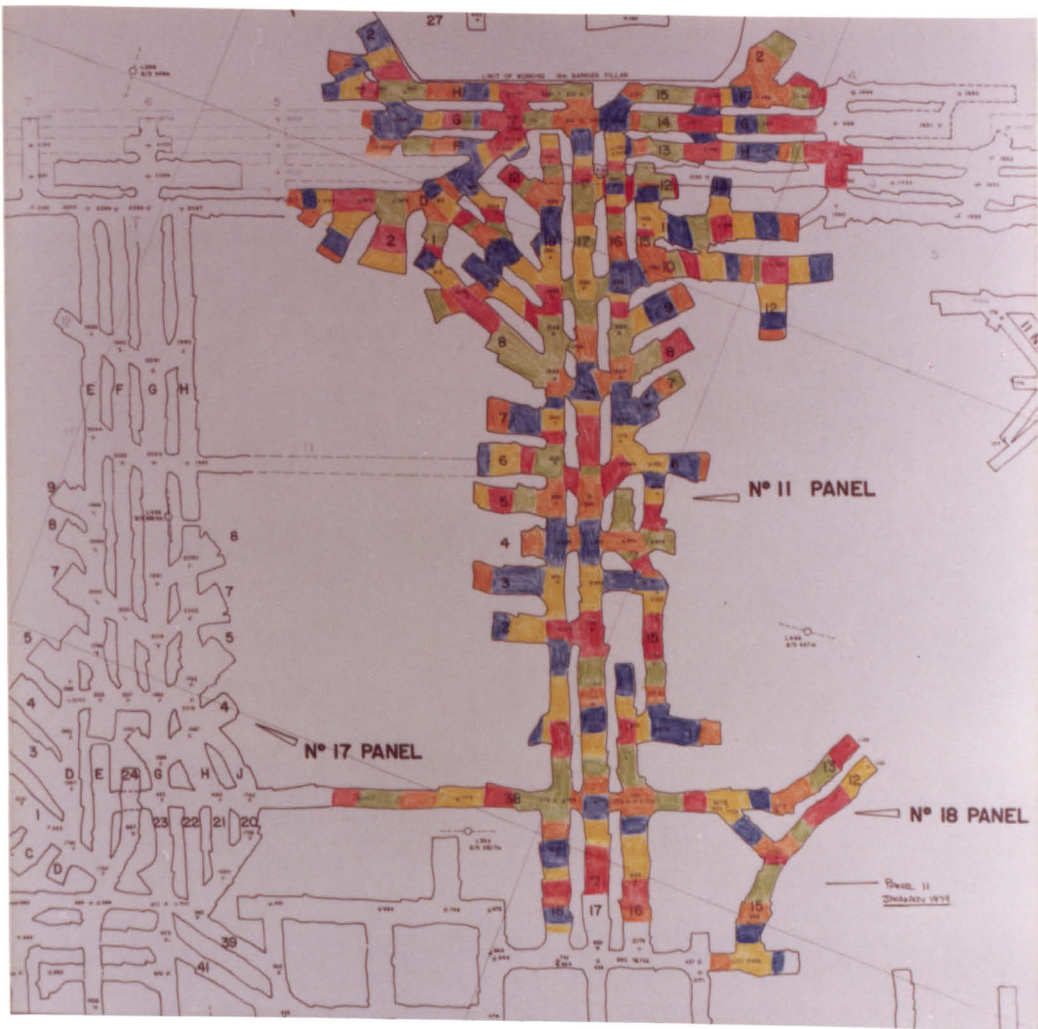


Fig.3 No.11 Panel

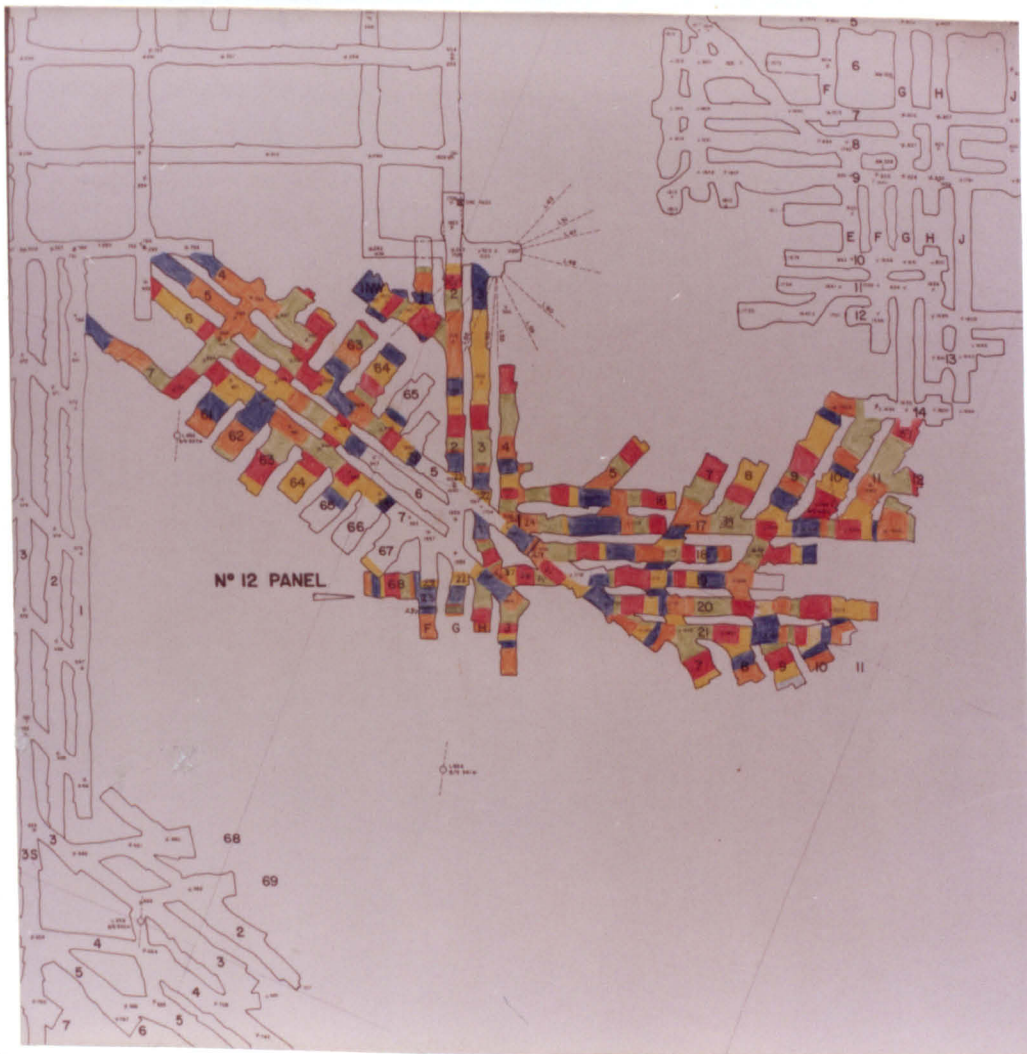


Fig.4 No.12 Panel

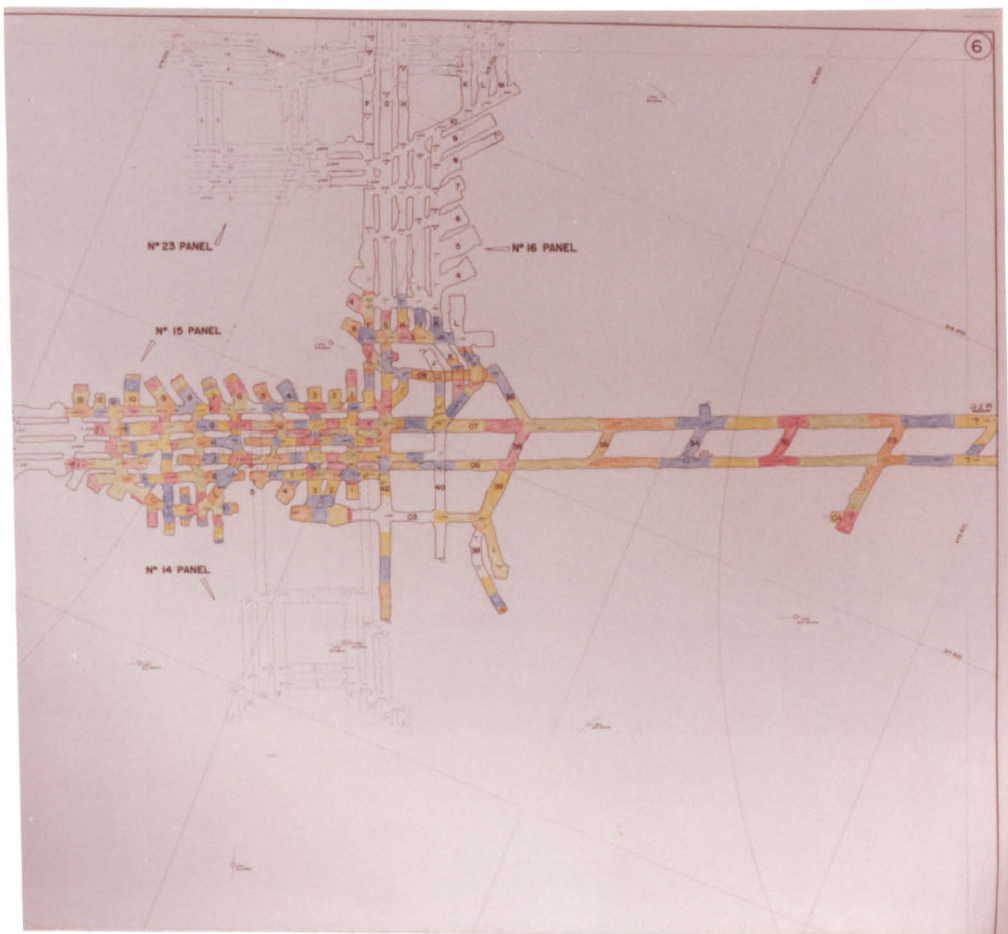


Fig.5 No.15 Panel

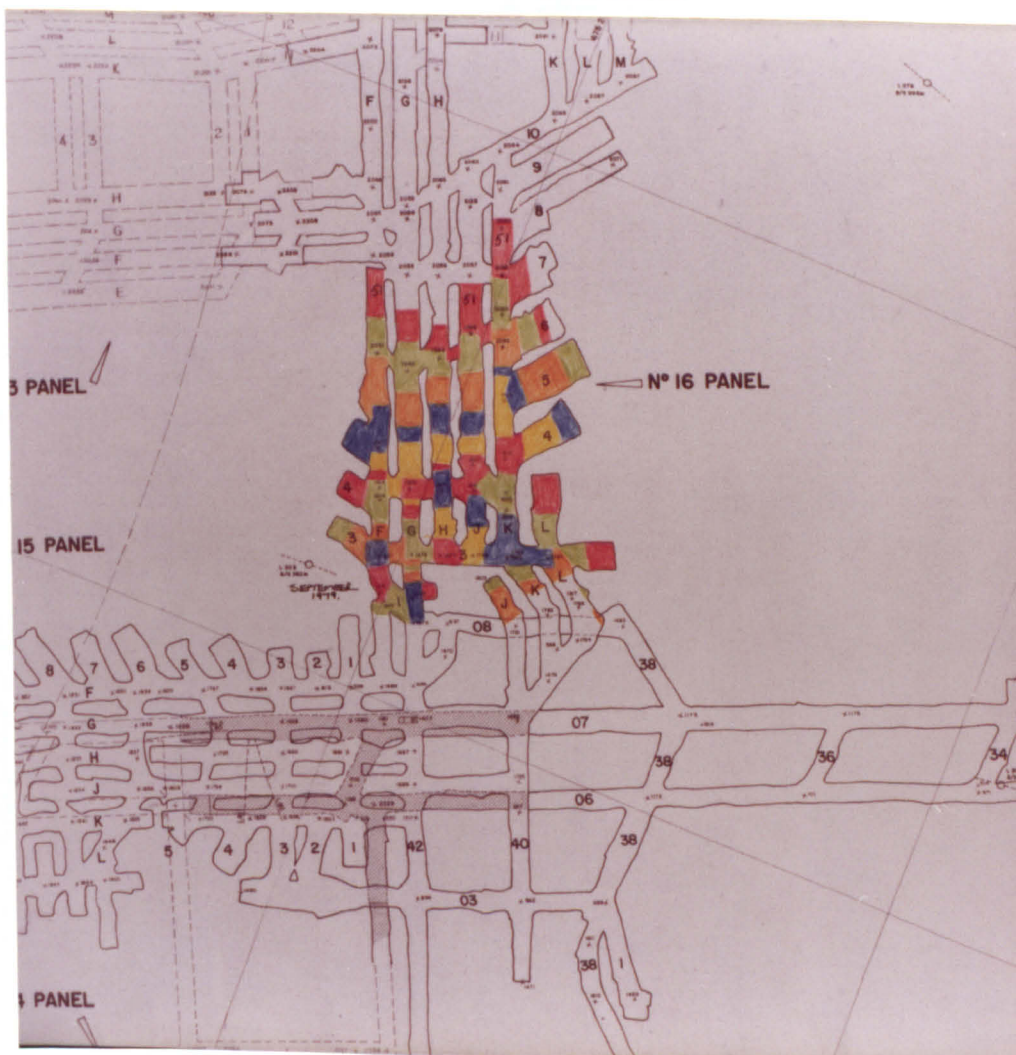


Fig.6 No.16 Panel



Fig.7 No.17 Panel and No.10 Panel
A Section



Fig.8 No.19 Panel